Repurposing a polymer precursor scaffold for medicinal application: Synthesis, characterization and biological evaluation of ferrocenyl 1,3-benzoxazine derivatives as potential antiprotozoal and anticancer agents

A thesis submitted to

Rhodes University

in fulfilment of the requirements for the degree of

Doctor of Philosophy

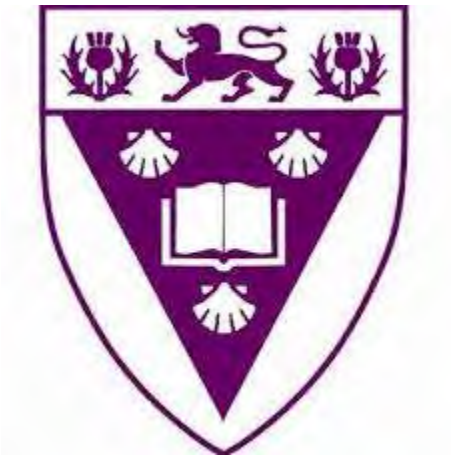

by

Mziyanda Mbaba

December 2019

DEDICATION

I dedicate this thesis to my parents: Mr Fikile Mbaba and the late Mrs Nondzondelelo Mbaba.

To my father:

Thank you for your love.

To my late mother:

I am blessed to be your son.

Ndiyakukhumbula, MaZwane!

ACKNOWLEDGEMENTS

First and above all, I give praise and worship to my Creator, Lord and Saviour: God – The Most High – for the boundless love and mercy He has shown me all my life and continues to do so. I thank the Almighty God for the blessing of strength and providence over the course of my involvement in this research project.

To my supervisor, Professor Setshaba D. Khanye: I cannot thank you enough for the unceasing encouragement and guidance you have been providing throughout my postgraduate studies. Words fall short to express my gratitude for the impact you have made on my development as a researcher. Thank you for molding me into the chemist that I am today!

Equally, I thank my co-supervisor Professor Adrienne L. Edkins for the enlightening engagements and guidance about the biological aspects of the project. I am grateful for your motivation and support, and for providing me with the best opportunity to learn biology. Thank you for being a great teacher!

I also acknowledge present and past members of the labs F22 and G5 for creating a productive working (and social) environment that is conducive for learning. Your invaluable contributions and suggestions in the development of this project are duly noted. I also thank Dr Samuel Jali for his assistance with proof-reading of the thesis.

I would like to thank the technical staff from the Rhodes University Department of Chemistry: Sis' Nomvuyo Mbebe, Mr Dondashe, Bhut' Sandile, Mr Mafani, and the maintenance team: Reuben, Andre and Francis for ensuring uninterrupted progress of this project. *Enkosi Sis' Nomvuyo ngomonde nobuntu!*

I thank Rhodes University and the Rhodes University Department of Chemistry for the research facilities and for affording me an opportunity to further my studies.

The assessment of the compounds for biological activity would not have been accomplished without the help of the colleagues from the Rhodes University Department of Biochemistry and Microbiology, especially the labs of Dr Jo-Anne de la Mare and Professor H.C. Hoppe. I thank the following members of these labs: Laura Dingle, Dr Dustin Laming, Devon Cash and Tarryn Swart who conducted the biological assays. My heartfelt thanks to Laura for her valuable time and contribution to this project!

I also acknowledge Dr Dale Taylor (Division of Clinical Pharmacology, Faculty of Medicine, University of Cape Town), and Dr Marietjie Stander (Central Analytical Facility, University of Stellenbosch) for their help with the Dd2 strain biological evaluation and HRMS analysis of the compounds.

I acknowledge the National Research Foundation (NRF) of South Africa for financial support.

Lastly, I thank my family: *uMama noTat'uMbaba* and my sisters and brothers. I am nothing without you! I also thank the families of Jokweni from *eLinge* and Xhoseni from *eCala* for their support.

ABSTRACT

The benzoxazines are a prominent class of heterocyclic compounds that possess a multitude of properties. To this end, benzoxazine derivatives have been used as versatile compounds for various utilities ranging from biological applications to the fabrication of polymers. Particularly, the 1,3-benzoxazine scaffold has featured in several bioactive compounds showing antimalarial, anticancer and antibacterial activities. Traditionally, it has been employed as a substrate in the synthesis of polymers with appealing physical and chemical properties. Due to the increasing interest in the polymer application of 1,3-benzoxazines, research of the 1,3-benzoxazine motif for polymer synthesis has been prioritized over other applications including its medicinal potential.

The continuous development of resistance to clinical anticancer and antimalarial drugs has necessitated the need for the search of innovative bioactive compounds as potential alternative medicinal agents. To address this, the field of medicinal chemistry is adapting new approaches to counter resistance by incorporating nonconventional chemical moieties such as organometallic complexes, like ferrocene, into bioactive chemical motifs to serve as novel compounds with medicinal benefits. Incorporation of ferrocene into known bioactive chemical moieties has been shown to impart beneficial biological effects into the resultant compounds, which include the introduction of novel, and sometimes varied, mechanistic modalities and enhanced potency. Presented with the benefits of this strategy, the current work aims to design and evaluate the pharmaceutical capacity of novel derivatives containing 1,3-benzoxazine scaffold (traditionally applied in polymer synthesis) hybridized with the organometallic ferrocene unit as bioactive agents.

Abstract

Using a combination of expedient synthetic procedures such as the Burke three-component Mannich-type condensation, Vilsmeier-Haack formylation and reductive amination, four series of ferrocenyl 1,3-benzoxazine derivatives were synthesized and their structures confirmed by common spectroscopic techniques: nuclear magnetic resonance (NMR), infrared spectroscopy (IR) and high-resolution mass spectrometry (HRMS). The target compounds were evaluated *in vitro* for potential antimalarial and anticancer activities against strains of the malaria parasite (*Plasmodium falciparum* 3D7 and Dd2) and the triple-negative breast cancer cell line HCC70. Compounds exhibited higher potency towards the *Plasmodium falciparum* strains with IC_{50} values in the low and sub-micromolar range in comparison to the breast cancer cell line against for which mid-molar activities were observed.

To gain insight into the possible mode of action of ferrocenyl 1,3-benzoxazines, representative compounds showing most efficacy from each series were assessed for DNA binding affinity by employing UV-Vis and fluorescence DNA titration experiments. The selected compounds were found to interact with the DNA by binding to the minor groove, and these findings were confirmed by *in silico* ligand docking studies using a B-DNA structure as the receptor. Compound **3.16c** (IC_{50}: 0.261 μM [3D7], 0.599 μM [Dd2], 11.0 μM [HCC70]), which emerged as the most promising compound, was found to induce DNA damage in HCC70 cancer cells when investigated for effects of DNA interaction. Additionally, compound **3.16c** displayed a higher binding constant (K_b) against DNA isolated from 3D7 *Plasmodium falciparum* trophozoites ($K_b = 1.88\times10^6$ M^{-1}) than the mammalian DNA ($K_b = 6.33\times10^4$ M^{-1}) from calf thymus, thus explaining the preferred selectivity of the compounds for the malaria parasite. Moreover, the investigated compounds demonstrated binding affinity for synthetic hemozoin, β-hematin. Collectively, these data suggest that the compounds possess a dual mode of action for antimalarial activity involving DNA interaction and hemozoin inhibition.

ABBREVIATIONS AND SYMBOLS

rt	Room temperature
eq.	Number of equivalents
aq.	Aqueous
h	Hour(s)
min	Minute(s)
mol%	Mole percentage number
°C	Degrees Celsius
HPLC	High performance liquid chromatography
δ	Chemical shift
ppm	Parts per million
Hz	Hertz
v	Wavenumber
$CDCl_3$	Chloroform-*d*
Me	Methyl
OMe	Methoxy group
Boc	*tert*-Butyloxycarbonyl group
SD	Standard Deviation
Calc	Calculated
m/z	Mass by Charge
HCl	Hydrogen Chloride
NaOH	Sodium Hydroxide
DCM	Dichloromethane
DCE	Dichloroethane

DMSO	Dimethyl sulfoxide
DMF	*N*,*N*-Dimethylformamide
R_f	Retention factor
%T	Percentage transmittance
EWG	Electron-withdrawing group
DEAD	Diethyl azodicarboxylate
PPh_3	Triphenylphosphine
DMF	*N,N*-dimethylformamide
DNA	Deoxyribonucleic acid
UV	Ultraviolet
UV-Vis	Ultraviolet-Visible
AU	Arbitrary fluorescence units
HEPES	4-(2-Hydroxyethyl)-1-piperazineethanesulfonic acid
NP-40	4-Nonylphenyl-polyethylene glycol
$NaHCO_3$	Sodium bicarbonate
$POCl_3$	Phosphorus oxychloride
ADME	Absorption, Distribution, Metabolism, And Excretion
mmol	Millimole
mL	Millilitre
N	Equivalent
M	Molar
µM	Micromolar
nM	Nanomolar
Å	Angstrom
dH_2O	Distilled water

g	Gram
mg	Milligram

TABLE OF CONTENTS

Chapter 1: Introduction

The current project explores the potential biological activity of benzoxazine derivatives bearing the organometallic ferrocene unit against breast cancer, malaria and trypanosomiasis. Thus, this chapter describes the broader scope of the project by providing a brief background on the pathology of the investigated diseases and the current chemotherapeutic drugs employed for their treatment. To understand this, challenges faced in the treatment of these diseases are also addressed along with the mitigating strategies used in drug discovery to manage their impact. Furthermore, application of bioactive compounds based on organometallic scaffolds such as ferrocene and their potential merit as alternative chemotherapeutic drugs are reviewed.

1.1. Brief background on the pathology of cancer, malaria and trypanosomiasis

Cancer is a disease resulting from unprogrammed division of normal cells that have severe and sometimes fatal consequences to normal physiological functions in humans. On the other hand, malaria and trypanosomiasis, also known as the African sleeping sickness, are infectious diseases caused by pathogenic protozoan microorganisms transmitted by the *Anopheles* female mosquito and tsetse fly vectors, respectively. These diseases remain prevalent pathologies for several reasons and are responsible for high mortalities worldwide.

1.1.1. Cancer

Mitosis is a cellular process whereby existing cells divide to produce copies of themselves culminating to formation of new tissues. During cell division, cells make use of a combination of mechanisms to ensure regulation of division of the cells leading to controlled formation of the new tissues.[1] Upon disruption of underlying cell division programming machinery, the cells

can divide uncontrollably resulting in the formation of invasive, malignant tumours which are harmful to normal physiological processes.[1]

Cancer is defined as a disease or collection of diseases that results when cells divide out of control leading to accumulation of malignant tumours. It is a global threat to mankind with one of the highest mortality rates. It is estimated that about 9.6 million deaths in the year 2018 were caused by cancer.[2] One of the leading causes of cancer fatalities is the difficulty in the treatment of the disease and challenges in the early diagnosis of the disease.[3] Treatment of cancer involves the elimination of the unwanted malignant tumours from the body by a combination of procedures including surgery, non-invasive radiation and chemotherapy, among others. The challenge in the treatment of cancer is exacerbated by the limited specificity of therapies in place for the management of the diseases. As endogenous cells, the biology of cancer cells is similar to normal cells.[4] As a result, it is often a challenge for anticancer therapies to distinguish between the unwanted malignant tumours and normal cells.

For many years cancer has been treated by means of chemotherapy making use of chemical compounds that target and kill malignant tumours leading to their elimination from the body and restoration of normal physiological functions.[5] Cancer chemotherapy has been a stronghold for cancer treatment with many successes in reducing fatalities of the disease. Anticancer drugs exhibit activity by targeting biomolecules such as nucleic acids and proteins that are pivotal in the carcinogenesis of tumour cells and propagation of the disease. Antitumour drugs can be classically classified into five major categories, namely: alkylating agents and antibiotics (targeting nucleic acids DNA and RNA), antimetabolites (inhibiting folic acid action), topoisomerase and mitosis inhibitors.[6]

Examples of classical antitumour drugs are shown in **Figure 1.1**. Early anticancer drugs were first developed as alkylating agents, like nitrogen mustards (**1.1a-c**), acting on tumour nucleic

acids DNA and RNA via interactions that alter the structure or disrupt their function to exhibit therapeutic activity, leading to cancer cell death.[7] Evolution of anticancer chemotherapy from alkylating agents led to the discovery of other antitumour drug types such as antifolates (**1.2a-b)** that deprive tumour cells of energy by preventing the action of folic acid, and chemical scaffolds, which block the function of topoisomerases I/II involved in DNA replication (**1.3a-b**).[8] Mitosis of tumour cells is crucial in the pathology of cancer and has emerged as another pathway that could be exploited to combat the disease. By blocking one of the phases of cell division in cancerous cells, taxanes (**1.4a**) and vinca alkaloids (**1.4b**) binding to specific sites on tubulins during the anaphase stage have been developed into anticancer drugs that work by preventing microtubule formation in dividing tumour cells.[9]

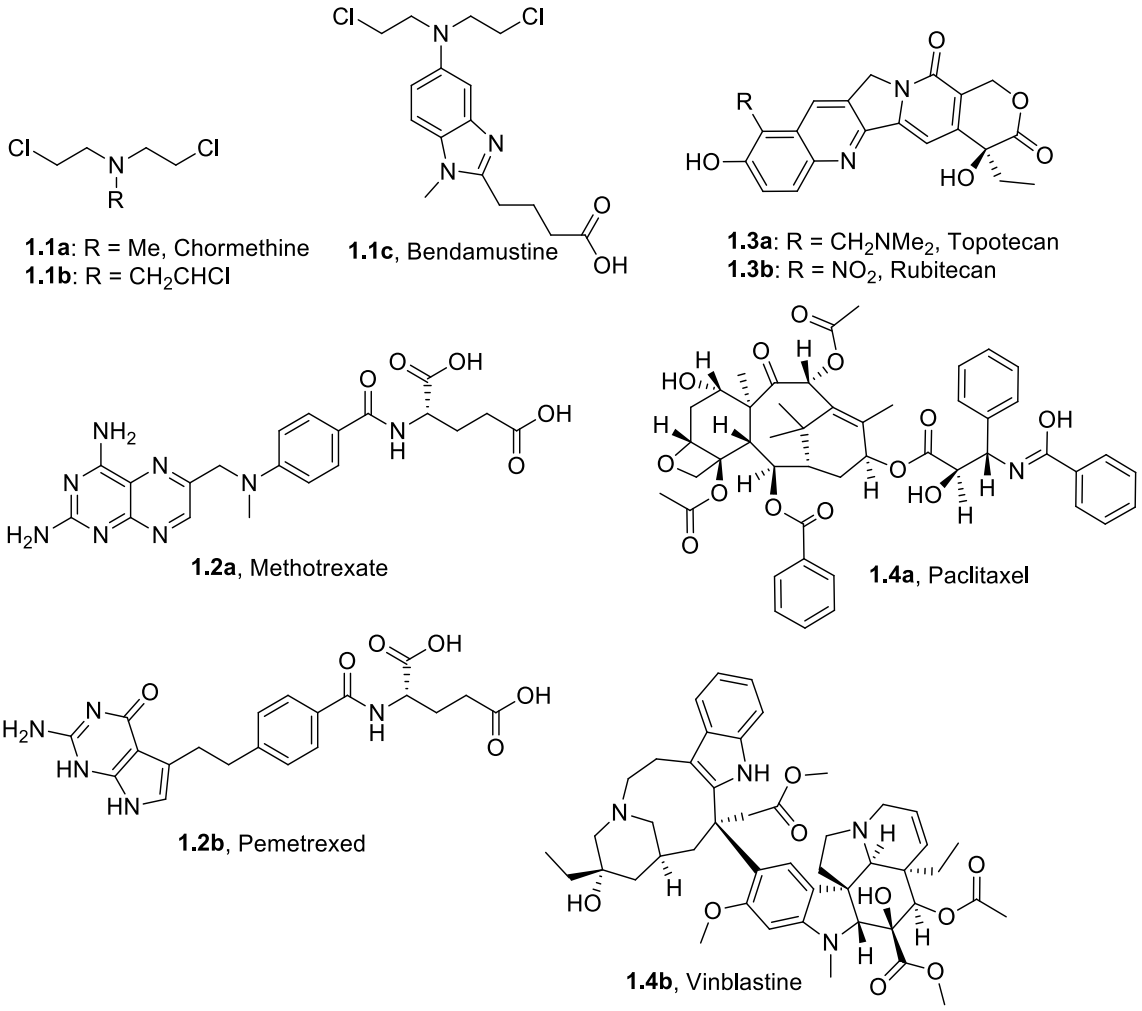

Figure 1.1 Clinically approved anticancer drugs acting on different targets.

Cancer can also arise from genetic mutations that cause the expression of phenotype that renders cells to divide uncontrollably. The endocrine system plays a crucial role in the expression of the oncogenic phenotype.[10] Particularly, steroid hormones such as sex hormones, i.e., androgens and oestrogens, and corticoids bind to specific receptors and proteins involved in the expression of cancerous genes and growth of tumour cells.[11] Due to the dependency of tumour cells on the endocrine system, hormonal therapy has been devised as an alternative method for treatment of cancer by inhibiting the action of these proteins through the blockade of required steroid hormones either via prevention of their production or by competitively binding to their receptors.[12]

The prevention of the production of oestrogens was first demonstrated by surgical oophorectomy as a viable treatment option leading to remission of malignant tumours in women.[13] Ever since this discovery, the endocrine system has been exploited to develop new medicines targeting the endocrine system to treat cancer. Several anticancer drugs that mimic the action of steroid hormones by binding to their receptors on proteins involved in the expression of the oncogenic phenotype have been developed.[14] These drugs are known as hormone antagonists and have been employed to treat cancers such as breast, prostate and endometrial cancer that grow in response to changes in natural growth hormone levels.[14] Examples of clinical drugs used for the treatment of cancer by targeting the endocrine system are shown in **Figure 1.2**.

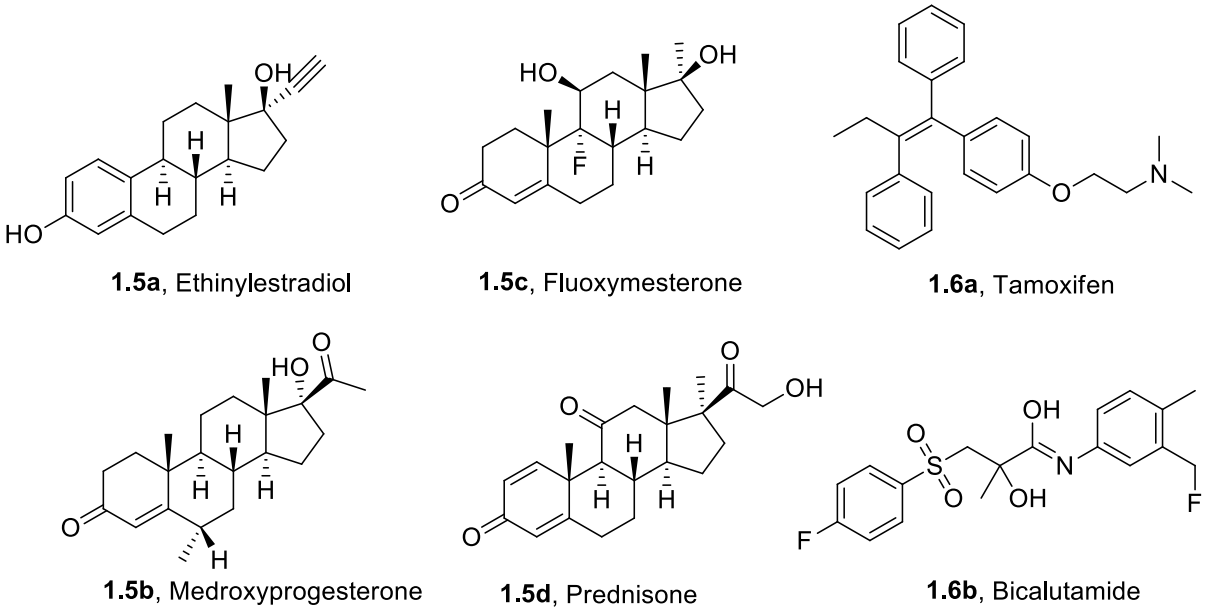

Figure 1.2 Steroid hormones (**1.5a-d**) and antiandrogens (**1.6a-b**) employed as clinical anticancer drugs targeting the endocrine system.

Developments in oncology and cancer research have led to the identification of various other biological targets and new classification of anticancer drugs.[15] Nowadays several anticancer drugs targeting nonclassical therapeutic targets are in clinical use for cancer treatment. Examples of these new-generation anticancer drugs and their therapeutic targets are illustrated in **Table 1.1**.

Table 1.1 New-generation clinical anticancer drugs targeting different tumour cell pathways.

Anticancer drug	Cancer type treated	Target	Reference
Bortezomib	• Multiple myeloma • Mantle cell lymphoma	26S Proteasome	Adams[16]
Imatinib	• Leukemia • Gastrointestinal stromal tumours	Tyrosine Kinase	Boros et al.,[17] Savage and Antman[18]
Bevacizumab	• Colon cancer • Cervical cancer • Lung cancer	VEGF-A[a] NADH dehydrogenase Mitochondrial biogenesis	Xu et al.,[19] Los et al.[20]
Trastuzumab	• HER2 positive breast cancer	HER2/neu receptor[b]	Verma et al.,[21] Cho et al.[22]
Rituximab	• Chronic lymphocytic leukemia • Non-Hodgson lymphoma	CD20[c]	Pavlasova et al.[23]
Lenalidomide	• Multiple myeloma	Celebron	Steward and Keith[24]

[a] Vascular endothelial growth factor A, [b] Human epidermal growth factor receptor 2, [c] B-lymphocyte antigen CD20

1.1.2. Malaria

Malaria is a pathogenic disease caused by species of the *Plasmodium* parasite. It is transmitted through a bite of a female *Anopheles* mosquito carrying the parasite, which enters the blood stream as sporozoites leading to subsequent manifestation of the symptoms of the disease. Once in the blood stream, the parasite undergoes different lifecycle stages involving invasion of the human liver cells (exo-erythrocytic cycle) and red blood cells (erythrocytic cycle) until the formation of *Plasmodium* gametocytes in the blood stream (**Figure 1.3**).[25] The parasite's lifecycle is completed when the female *Anopheles* mosquito is infected by the *Plasmodium*

gametocytes through a bite that undergo fertilisation and maturation into sporozoite in the mosquito host (**Figure 1.3**).

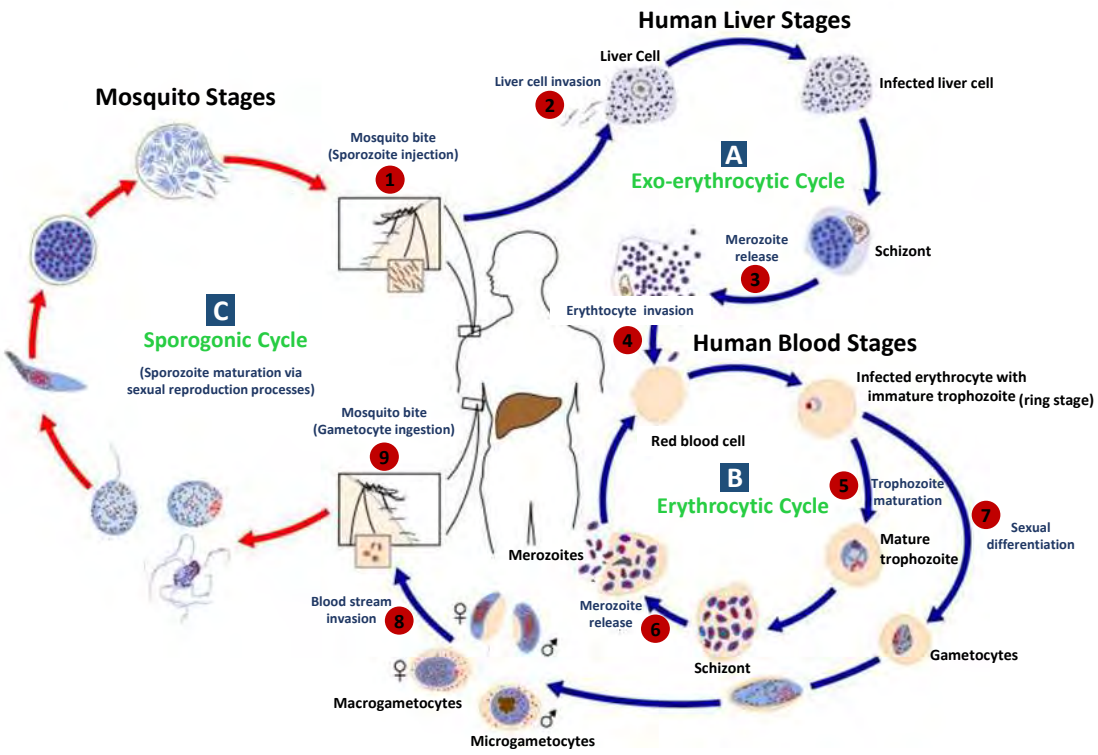

Figure 1.3 Lifecycle of the malaria parasite.[25]

Of the five species of the parasite responsible for malaria, namely: *Plasmodium vivax*, *Plasmodium ovale*, *Plasmodium malariae*, *Plasmodium knowlesi* and *Plasmodium falciparum*, the latter is the most devastating. According to the World Health Organization (WHO) there were estimated 219 million reported incidences of malaria and 430 000 related deaths worldwide in 2018 primarily attributable to the *P. falciparum* parasite.[26] The effective prevention and treatment of malaria dates as far back as the fifteenth century when the indigenous people of Peru discovered a tincture prepared from cinchona tree bark could treat fevers.[27] Despite the significant strides in the development of antimalarial treatment options over the years, malaria remains a global threat due to the emergence of resistant strains of the *Plasmodium* parasites.

Strategies in the control of malaria comprise the prevention of transmission of the disease focused on quelling populations of the *Anopheles* mosquito vector and the treatment of the disease by inhibiting one or more of the lifecycle stages of the parasite. The prevention of malaria transmission relies on the use of insecticides that kill the malaria vector, i.e. *Anopheles* mosquito. WHO implemented two initiatives by which this can be achieved, namely indoor residual spraying (IRS) and use of insecticide-treated nets (ITNs) in endemic areas.[28] **Figure 1.4** shows examples of insecticidal compounds that are used for malaria vector control in prevention of the spread of malaria.[29]

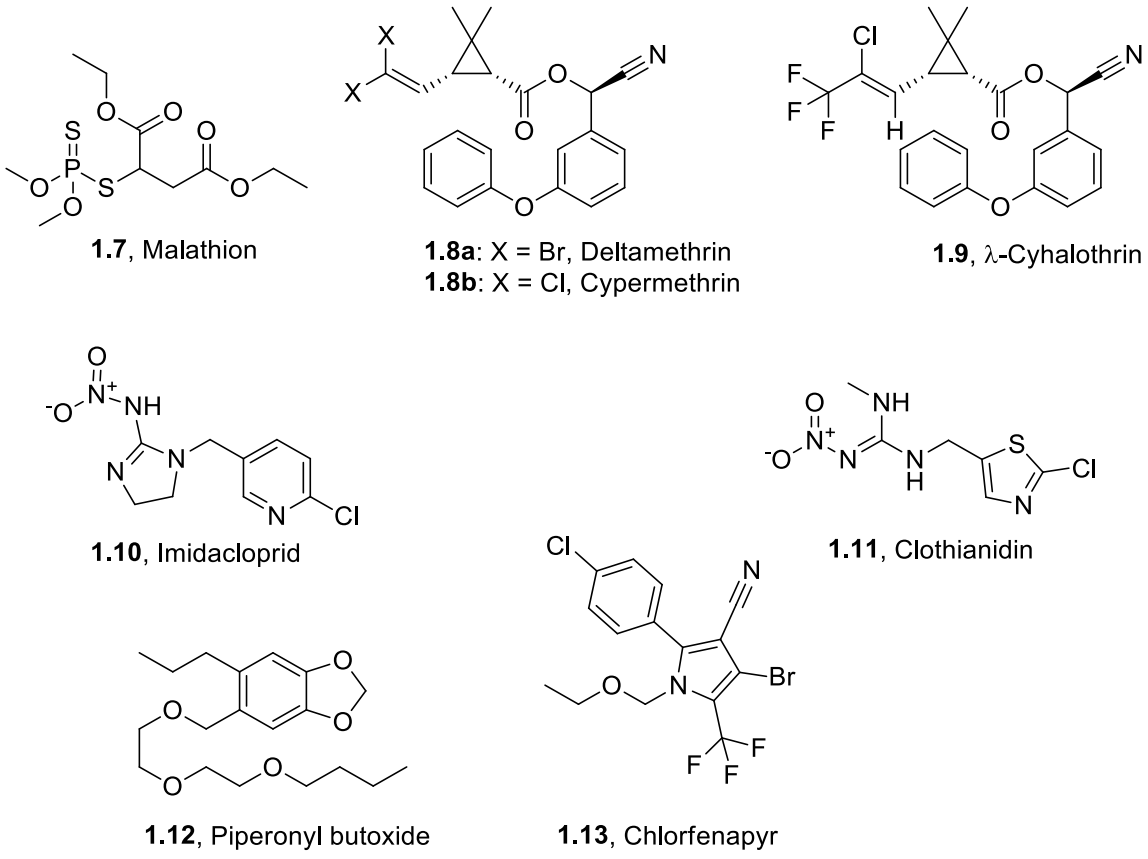

Figure 1.4 Insecticides recommended by WHO for prevention of the spread of malaria by controlling mosquito populations.

The clinical drugs employed in the treatment of malaria act by inhibiting the biological pathways that are crucial in the stages of the lifecycle of the malaria parasite. The hemozoin

synthesis pathway is one of the well-studied pathways that is pivotal in the survival of the *Plasmodium* parasite.[30] Following invasion of the human red blood cells by the trophozoites, the *Plasmodium* parasite digests human haemoglobin for subsistence, resulting in concomitant release of the oxidative heme-complex (α-haematin) that is lethal to the parasite. To prevent damage by this complex, the parasite biocrystallizes the harmful α-haematin into insoluble, non-toxic β-haematin crystals known as hemozoin.[31] This pathway has been exploited to devise drugs that inhibit the detoxification of the harmful heme-complex leading to subsequent death of the parasite by oxidative stress.[32] For instance, a once highly effective antimalarial drug chloroquine (**1.14**) has high affinity to bind to the forming hemozoin to prevent further biocrystalization of the toxic heme-complex, thus killing the parasite due to oxidative stress during the asexual stages (**Figure 1.5**).[33] Based on what is understood of the mechanism of chloroquine (**1.14**), the mode of action of other 4-aminoquinoline antimalarial drugs is postulated to involve hemozoin inhibition.[30] Other examples of clinically approved 4-aminoquinoline drugs thought to target the hemozoin synthesis pathway include primaquine (**1.15**), quinine (**1.16**) and mefloquine (**1.17**) that mainly inhibit the schizont stage in the *Plasmodium* life cycle (**Figure 1.5**).[34]

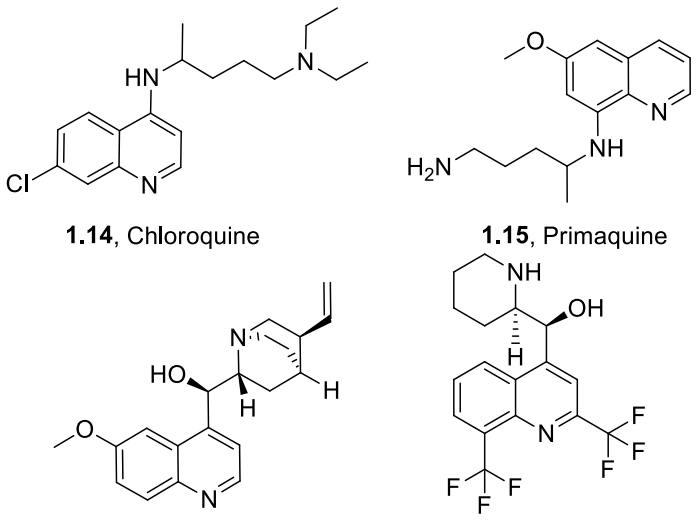

Figure 1.5 4-Aminoquinoline-based drugs associated with inhibition of the hemozoin detoxification pathway.

Although beneficial and still in clinical use for first-line treatment of malaria, the emergence of drug resistance to hemozoin-inhibiting drugs has rendered such drugs less effective. As a result, antimalarial drugs based on other chemical scaffolds with alternative mechanistic modalities, such as antifolate metabolism and generation of reactive oxygens species (ROS), have been discovered and developed. Some examples of antimalarial drugs targeting pathways other than hemozoin formation are illustrated in **Table 1.2**.

Table 1.2 Antimalarial that act on targets other than hemozoin inhibition.

Antimalarial drug	**Mode of action**	**Reference**
Artemisinin based drugs 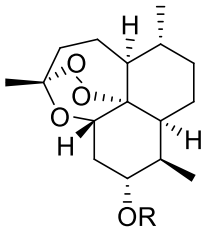 **1.18**: Dihydroartemisinin, R = H **1.19**: Artemether, R = Me **1.20**: Artemotil, R = Et	• Oxidative stress by production of reactive oxygen species	Reviews by: Kamchonwongpaisan and Meshnick,[35] Olliaro et al.[36]
Sulfadoxine 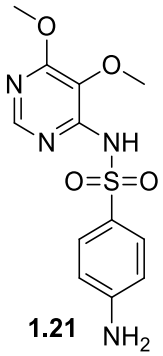 **1.21**	• Blocks folate synthesis through dihydropteroate synthase inhibition	Reviews by: Olliaro,[37] Alam et al.[38]
Atovaquone 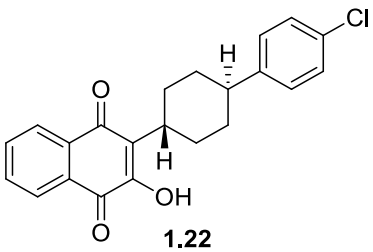 **1.22**	• Inhibition of pyrimidine synthesis by disruption of mitochondrial membrane potential	Hammond et al.[39]

1.1.3. Human African trypanosomiasis

Trypanosomiasis also known as the African sleeping sickness is another type of an insect-borne parasitic disease transmitted through the bite of an infected tsetse fly. The disease is endemic in sub-Saharan Africa and is caused by the protozoan parasite of genus *Trypanosoma*. Two types of the parasite, namely: *Trypanosoma brucei gambiense* and *Trypanosoma brucei rhodesiense*, are responsible for human trypanosomiasis with the former being the most deadly.[40] Like malaria, the symptoms associated with this disease begin with the attack of the haemo-lymphatic system by the parasite characterized by fevers and painful joints at the onset of the disease followed by disruption of the central nervous system symptomatically manifested in the form of confusion and tremor.[40] Although not widespread, African sleeping sickness threatens millions of lives in over 36 countries in sub-Saharan Africa and can be fatal if left untreated.[41]

The incidences of the diseases have seen significant reduction at the turn of the twenty-first century, with no epidemic outbreaks since the late 1990s, as a result of the intensified preventative and treatment collaborative efforts by government and non-government organisations fighting to combat the disease.[42] Currently, there are only two clinical drugs, pentamidine (**1.23**) and suramin (**1.24**), used for first-line treatment of the disease, while melarsoprol (**1.25**), eflornithine (**1.26**) and nifurtimox (**1.27**) are employed to treat more acute, advanced cases of the infection (**Figure 1.6**).[40]

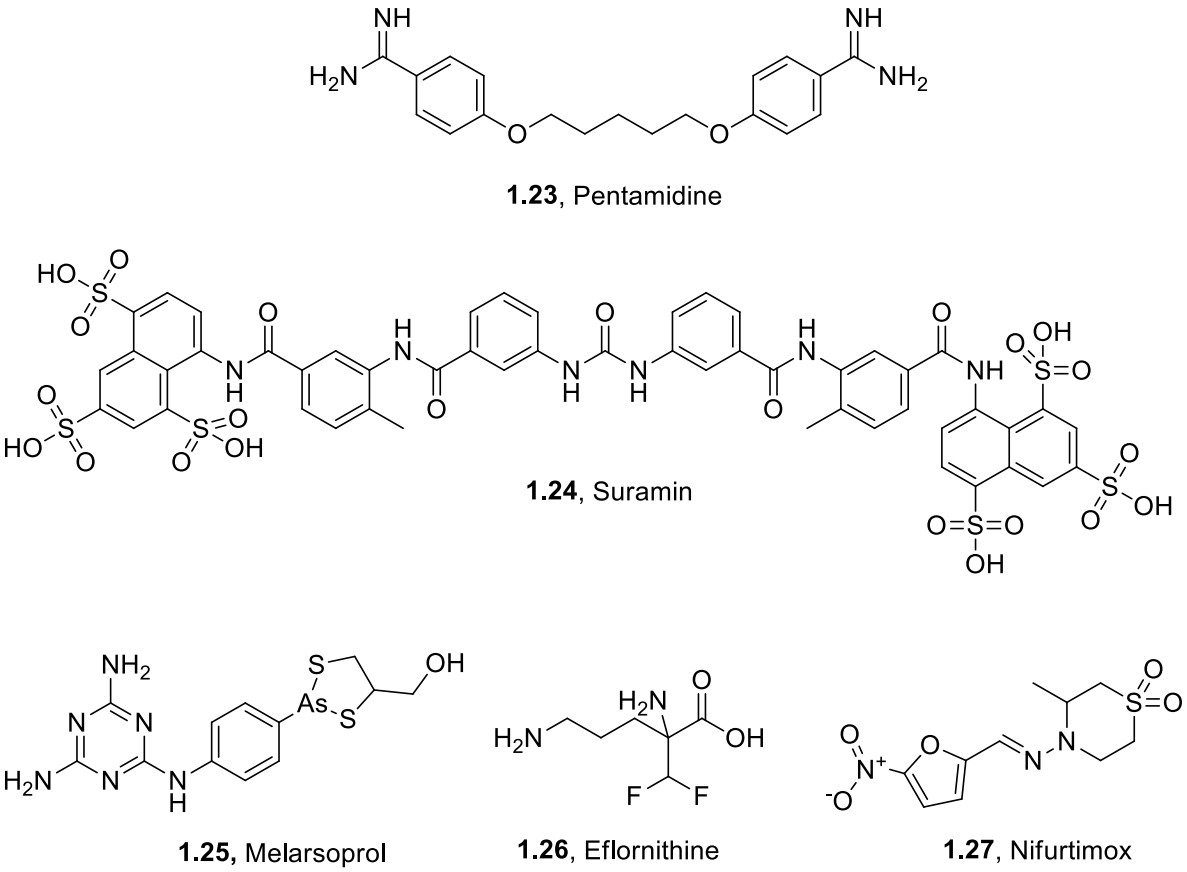

Figure 1.6 Clinical drugs used for treatment of human trypanosomiasis.

Although effective at minimizing incidences of the disease, the limited anti-trypanosomiasis drug arsenal is worrisome especially with the increasing incidences of clinical resistance to drugs used to treat pathogenic diseases.

1.2. Challenges in the treatment of cancer and malaria

The use of chemotherapy in the control and management of cancer, malaria and trypanosomiasis has resulted in significant reduction in incidences of these diseases and mortalities. Despite the successes, current clinical drugs face challenges arising from different factors such as limited selectivity and the emergence of multi-drug resistant tumours and strains of the malaria and trypanosomiasis parasites. However, these challenges present an opportunity to search for innovative therapeutic targets and drug scaffolds to address them.

1.2.1. Challenges in cancer chemotherapy

As the origin of cancer tumours is endogenous, tumour cells share significant biological similarities in cellular composition and biochemical processes with normal cells. Because of the subtle difference between the two cell types, it is often a challenge to devise medicaments that specifically target and destroy the malignant tumours while having no harmful effects on the normal cells.[43] This challenge shows in the form of the development of side effects observed in patients undergoing chemotherapy.[43]

The plight of limited selectivity of anticancer drugs is best represented by the mitotic anticancer agents that exhibit efficacy by targeting tubulins and microtubules in dividing tumour cells. This class of drugs binds to tubulins and destabilises microtubule polymerization during mitosis of tumour cells, thus preventing tumour cell division.[44] Besides the role of driving fission of the dividing cells during mitosis, microtubules are pivotal in sensory functions by serving as tracks for axonal transport and mitochondrial function in neurons.[45] Since the anti-mitotic cancer drugs are not cell specific, they also disrupt microtubule formation in normal cells resulting in neurotoxicity characterized by a neurodegenerative condition called chemotherapy-induced peripheral neuropathy.[46] The occurrence of chemotherapy-induced peripheral neuropathy has also been observed in proteasome antitumour inhibitors such as bortezomib.[47] Another group of drugs facing clinical limitations are the topoisomerase inhibitors such as doxorubicin, which are associated with cardiotoxicity postulated to be caused by oxidative stress and perturbation of protein and nucleic acid synthesis in normal cells among other proposed mechanisms.[48]

The emergence of tenacious malignant tumours that are resistant to treatment by known drugs is arguably one of the most pressing challenge in contemporary oncology. Clinical resistance arises when the targeted tumour cells undergo changes at biochemical level to counteract the

effects of the administered drug.[49] Various proposed hypotheses to explain processes underpinning the mechanisms that initiate and promote anticancer resistance are presented in literature.[49] Succinct reviews by Housman et al.[50] and Nikolaou et al.[51] on the subject give a comprehensive summary of the common mechanisms by which tumoral drug resistance occurs as illustrated in **Figure 1.7**.

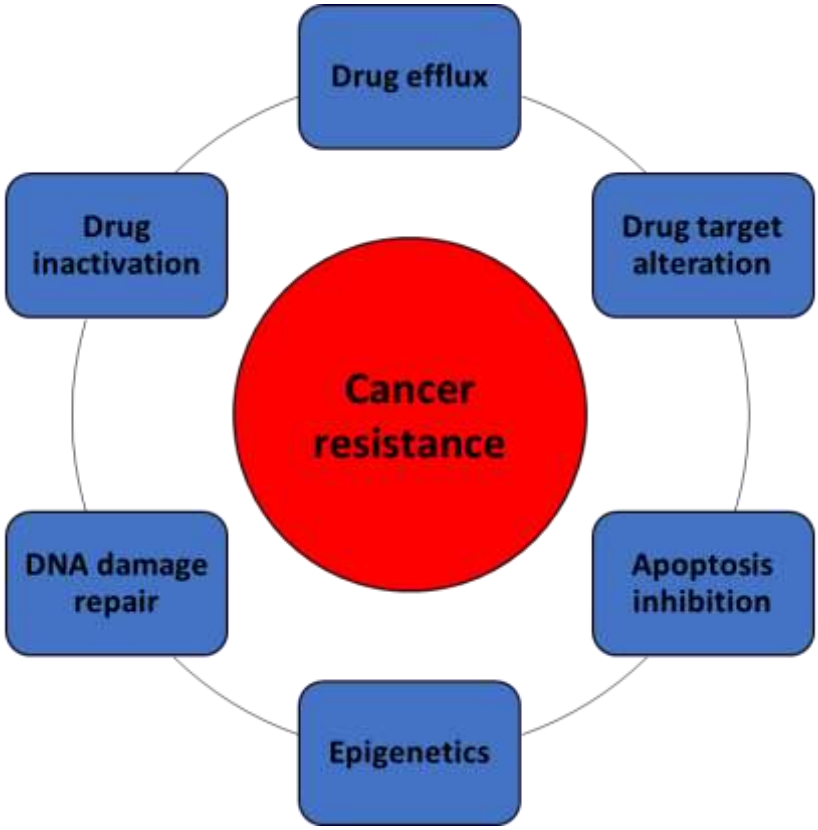

Figure 1.7 Classification of proposed mechanisms that promote anticancer resistance.[50]

Of the presented modes in **Figure 1.7**, drug inactivation and drug efflux are some of the most understood mechanisms of anticancer resistance. These processes involve metabolic deactivation of the drug into non-toxic metabolites via alterations of its metabolic pathway and reducing the accumulation of drug molecules inside the tumour cells through promoting of their efflux by transmembrane proteins, respectively.[50]

Another chemotherapy challenge worth mentioning is the existence of the aggressive breast tumours that grow independently of sex hormones, oestrogen and progesterone, and the human epidermal growth factor protein which are essential in carcinogenesis.[52] Unlike other cancer cell types, these cancers lack the human epidermal growth factor receptor 2 (HER2) and the receptors for both oestrogen and progesterone.[52] These cancers are referred to as triple-negative breast cancers as they test negative for all three receptors and are the most aggressive class of breast cancers that readily spread to other parts of the body.[52] With the lack of the HER2 and hormonal receptors, hormone-based therapies and drugs targeting HER2 are ineffective against triple-negative breast cancers.[53] The challenge in the treatment of this type of cancer is compounded by the fact that triple-negative breast cancer cells resemble normal cells more than any other types of breast cancer, resulting in limited selectivity by alternative anticancer drugs.[54]

1.2.2. Challenges in malaria chemotherapy

As a pathogenic disease, there exists substantial differences in the cellular and biochemical composition of the *Plasmodium* parasite and the human host. Unlike in cancer, these differences make it moderately convenient to target biological processes unique to the malaria parasite leading to its destruction. Therefore, challenges in antimalaria chemotherapy are primarily due to development of clinical resistance by strains of the malaria parasite than the limited selectivity of clinical antimalarial drugs.

The discovery of chloroquine (**1.14**) by Andersag in 1930s revolutionized the treatment of malaria.[55] This synthetic 4-aminoquinoline drug led to significant decrease in the incidences of malaria, saving many lives during the World War II where malaria was most rampant and has ever since continued to do so in tropical regions where the disease is endemic.[55-56] However, in 1950s strains of the *P. falciparum* parasite that showed resistance to treatment by

chloroquine emerged, threatening future use of the drug as an antimalarial agent.[57] Chloroquine has limited mechanistic diversity as it primarily targets hemozoin biosynthesis by the *Plasmodium* parasite to induce plasmocidal effects. The primary mechanism of chloroquine resistance is postulated to occur by drug efflux, whereby the parasite transmembrane proteins mutate in order to expeditiously pump-out drug molecules from the plasmodial digestive vacuole (DV) where the drug acts, thus rendering it ineffective.[58]

As with many predominantly unimodal antimicrobial drugs, when the *Plasmodium* parasite evolved to develop counteractive mechanism to the effects of chloroquine it means that the drug can no longer elicit detrimental action against the parasite. Thus, the lack of mechanistic diversity of the drug is a contributing factor that led to the development of resistance by the *Plasmodium* parasite to the drug.[58] Today several strains of the *P. falciparum* parasite showing full-blown chloroquine resistance exist. Despite this, chloroquine is still used for first-hand intervention in mild cases of malaria infections and is classified as an important drug in the list of essential medicines by WHO.[59] Antimalarial resistance remains a dreadful challenge in endemic areas.

To combat the scourge of clinical resistance, WHO introduced artemisinin-based combination therapies (ACTs) that utilize a combination of mechanistically dissimilar drugs acting on different stages of the *Plasmodium* parasite's lifecycle (**Figure 1.3**).[60] Currently, artemisinin-based drugs, such as dihydroartemisinin (**1.18**), artemether (**1.19**) and artemotil (**1.20**), are some of the most potent antimalarial drugs currently on the market for the treatment of malaria (**Table 1.2**).[36] Unlike chloroquine, they elicit multiple modes of action against the malaria parasite, including the generation of lethal reactive oxygen species (ROS).[36] The ingenuity of ACTs is based on the application of a dual drug cocktail comprised of a short-lived fast-acting, highly potent artemisinin-based drug that will significantly reduce the majority of parasitemia in the blood stages and a long-lived drug partner, e.g., mefloquine (**1.17**), acting on the liver

stages to completely eliminate any remaining parasites that may have survived the effects of the former antimalarial agent.[60] ACTs have been an effective strategy to contain the disease and its success is attested by the decline in reported mortalities of the disease since its implementation in 2001 (**Figure 1.8**).[26]

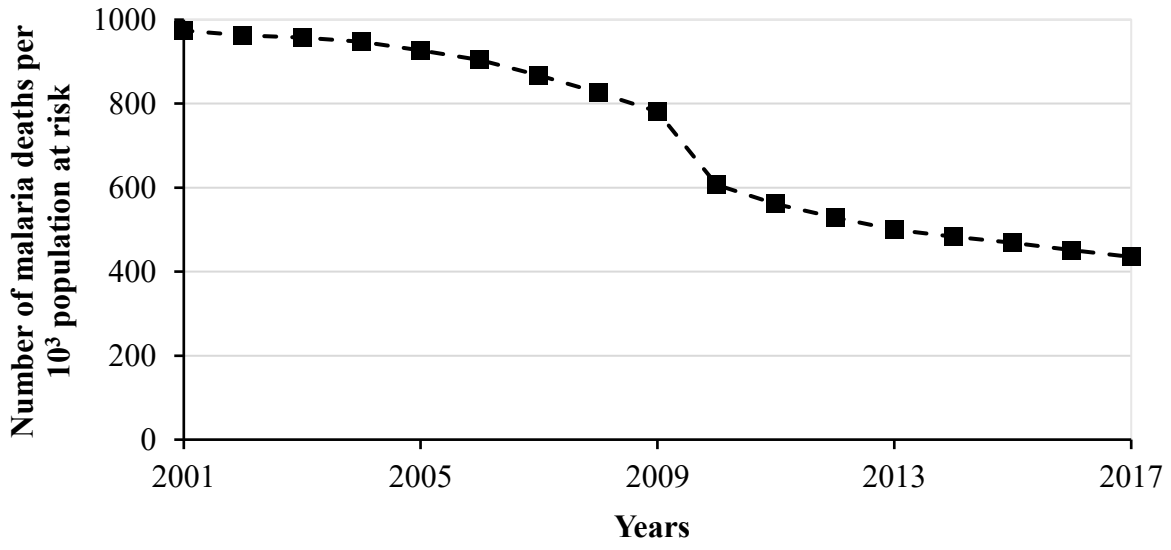

Figure 1.8 Graph illustrating the decline of malaria mortalities between 2001 and 2017.[26,61]

The outlook of artemisinin-based drugs is being threatened by the emergence of artemisinin-resistant *P. falciparum* strains that was first reported in Southeast Asia in 2010.[62] The incidence of these strains poses a great hazard to the great successes of ACTs that have been achieved so far, and if not acted upon with expediency may result in full-blown resistance. Thus, there is a great need to expand the antimalarial drug arsenal by searching for novel drug scaffolds and innovative therapeutic targets to address clinical resistance. One of the ways to achieve this is to turn to "nonconventional scaffolds" such as structural motifs not traditionally considered in medicinal chemistry for adaptation in antimalarial drug discovery. The Medicines for Malaria Venture (MMV) is a non-profit organization that has made substantial contributions in the discovery of innovative antimalarial drug scaffolds and the promising hits have been deposited in their open-access MMV Malaria Box database.[63] Some examples of bioactive scaffolds from

the MMV Malaria Box showing promise as new-generation antimalarial agents (**1.28-1.31**) including "nonconventional" organometallic-based scaffolds **1.28-1.29** are illustrated in **Figure 1.9**.[64]

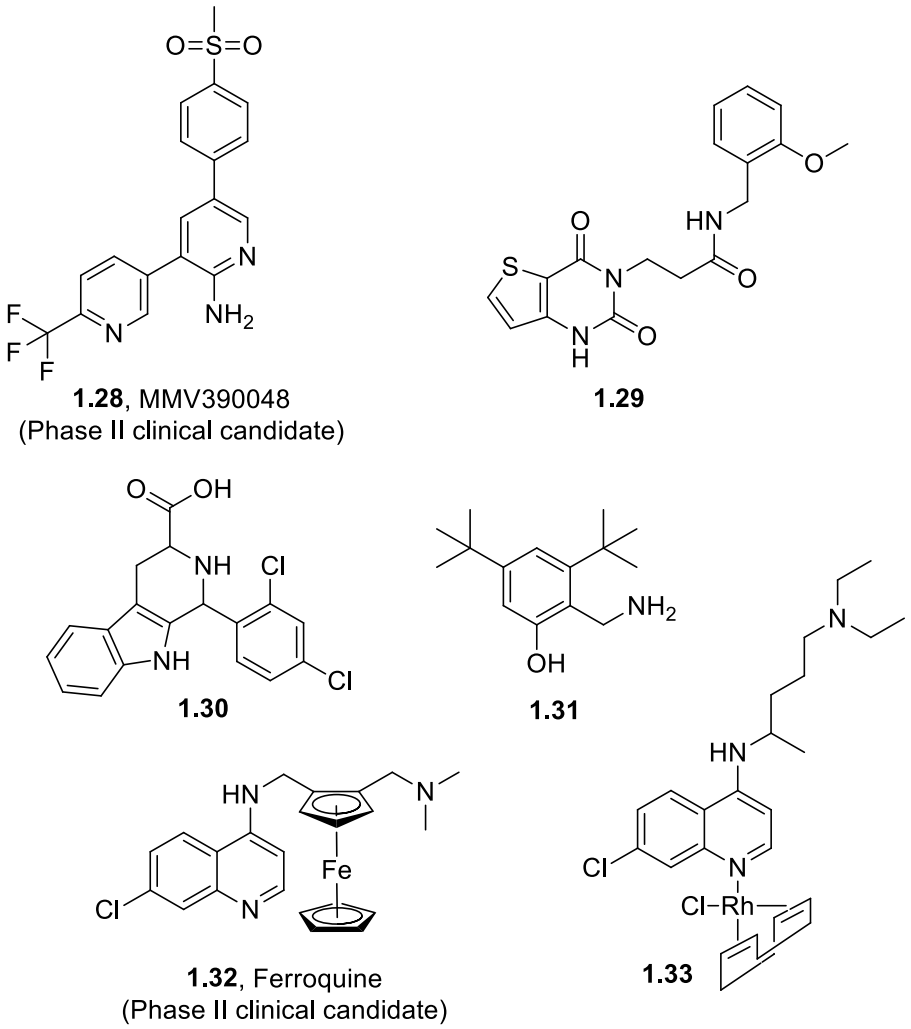

Figure 1.9 Chemical structures of novel bioactive compounds investigated as antimalarial agents based on innovative scaffolds.

1.3. Strategies for generation of innovative bioactive scaffolds: An overview

As demonstrated in the previous sections, clinical drugs are facing a menacing threat of resistance. The need to search for novel drug scaffolds acting on innovative therapeutic targets is necessary to address resistance by circumventing or delaying its development. Traditionally,

the generation of bioactive compounds in drug discovery is mainly achieved through structure-based design directed towards blockade of a known biomolecule, repurposing of known drugs for application in other diseases and amalgamation of bioactive structural motifs from different drugs into novel bioactive compounds. These approaches are briefly reviewed in this section ending with the introduction of organometallic compounds as an emerging strategy for the development of novel bioactive compounds as potential drugs.

1.3.1. Structure-based drug design

Structure-based drug design also known as target-based drug design involves conceptualization and development of a molecule that can disrupt the function of an identified biomolecule, such as proteins and nucleic acids (DNA and RNA), that is essential for the survival of the targeted disease. This requires in-depth knowledge of the shape and chemical composition of the binding site of the targeted biomolecule to allow the design of a molecule that can act as an inhibitor (antagonist) or activator (agonist) of its function in a manner that will elicit overall damage to the targeted pathogen.[65] Enzymes and surface receptors are common biological targets of this approach.[65]

Classical target-based drug design was achieved by experimental screening of the compound for affinity against the isolated biological target biomolecule using relevant biochemical assays, which can be subjected to further structural modification to optimize the interaction.[66] Modern practice of the approach takes advantage of the technological advances in X-ray crystallography, nuclear magnetic resonance (NMR) and computation used in structural determination of biomolecules. Using designated computer programs, lead compounds are easily identified by docking a library of proposed drug molecules to the targeted site of an established or homology model of the intended biomolecule, and the affinity results are statistically analyzed with appropriate computer algorithms.[67] The antiviral drugs amprenavir

(**1.34**) and viracept (**1.35**) originally designed as inhibitors of HIV protease are the first success stories of computer-aided structure-based drug design to get approval for clinical use (**Figure 1.10**).[68]

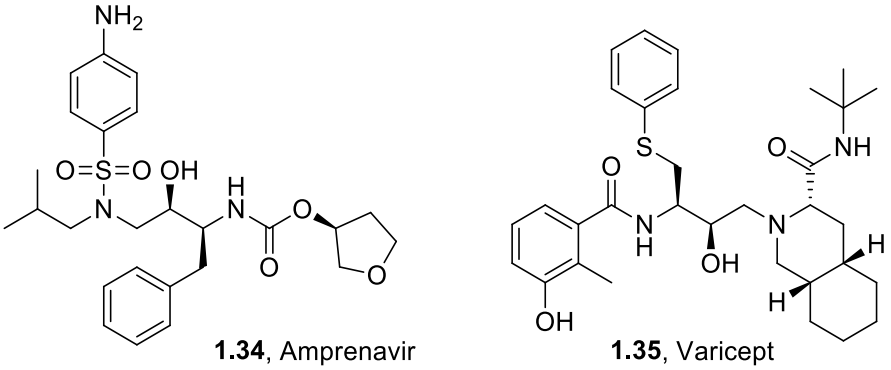

Figure 1.10 First clinically approved antiviral drugs discovered by target-based drug design as HIV protease inhibitors.

1.3.2. High-throughput screening

An alternative approach to structure-based design is the high-throughput screening (HTS) strategy. The HTS is an automated process whereby a large library of selected molecules is screened in vitro for biological activity as inhibitors or activators against a biological target.[69] Unlike structure-based drug design, the primary objective of HTS is to identify hit or lead compounds that can be structurally optimized and developed into therapeutic drugs. HTS offers an inexpensive and expeditious generation of multiple leads from a large library of compounds, thus reducing the cost and time of an otherwise laborious process.[69] The HTS approach has contributed several clinical drugs on the market, such as dasatinib (**1.36**), tipranavir (**1.37**) and ambrisentan (**1.38**) (**Figure 1.11**).[70]

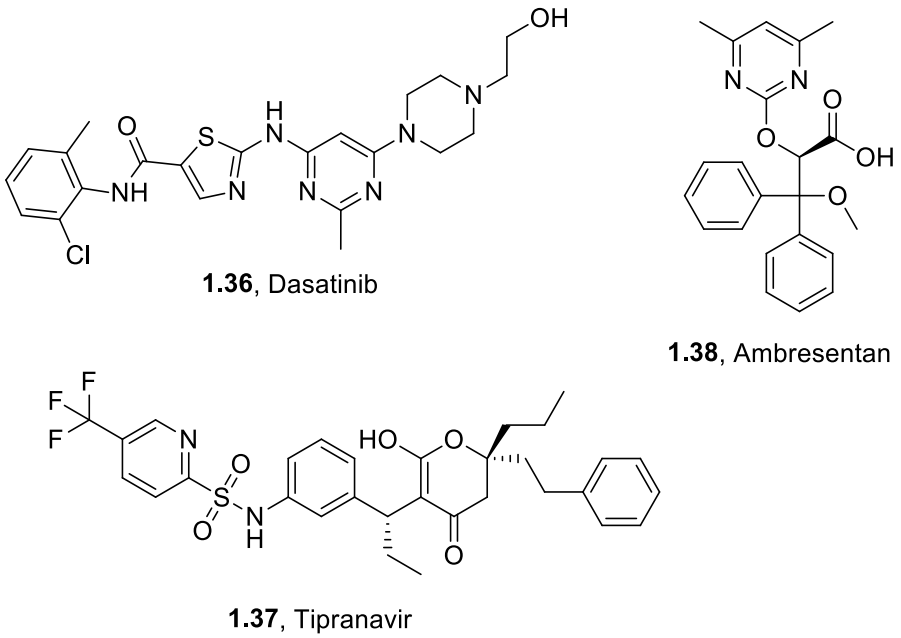

Figure 1.11 Clinically approved anticancer (**1.36**), anti-HIV (**1.37**) and antihypertensive (**1.38**) drugs discovered through HTS.

The limitation of HTS is that it does not address the pharmacokinetic and pharmacodynamic properties of the generated hit compounds.[69] Additionally, it is impossible to know if the identified compounds will only interact with the determined target and not other similar biomolecules in the human body.[69] To address the issue of target specificity, sophisticated HTS programs involve cross-screening of the library against the intended therapeutic target like HIV protease and a related human biomolecule, e.g., cellular aspartyl protease, for which the screened compounds may have binding affinity.[69] A desirable hit will selectively target the intended therapeutic target and not the related human biomolecule. Advances in statistical and computational technology have permitted adaptation of the HTS *in silico*. With the availability of highly resolved structures of many biomolecules, it is possible to employ computational programs to virtually screen a large library of compounds against computer-generated, high resolution 3D models of the therapeutic target to identify hits with promising affinity. This

process is also known as virtual screening and coincides with computer-aided structure-based design.[71]

1.3.3. Drug repurposing

Drug repurposing or repositioning is an approach for finding new clinical applications for established, approved or investigational drugs.[72] With the pharmacological aspects of the existing drug already addressed during its clinical development for the original application, the drug repositioning strategy offers many advantages[72-73] with regard to clinical development compared to other drug design approaches:

(i) The time-frame for clinical development of repurposed drugs is shortened since most aspects of clinical trials of the drug will already have been addressed in the original clinical assessment of the dug.

(ii) The expenditure associated with the developmental costs of the repurposed drug for new application are reduced owing to existing clinical knowledge of the drug.

(iii) Repurposed drugs have a lower risk of clinical failure as the preclinical evaluation and toxicity assessment of the drug will have been established.

(iv) With current clinical drugs facing the inevitable threat of clinical resistance by pathogenic diseases which may render them obsolete as medicines, the drug repositioning strategy offers an opportunity to keep drugs facing resistance in clinical use by finding them new uses, thus expanding the drug arsenal of the diseases for which they are repurposed.

Repurposed drugs are showing great promise in anticancer and antimicrobial chemotherapy.[74] Using repurposing approaches such as pharmacological and retrospective clinical analysis, analgesic and anti-osteoporosis drugs, aspirin (**1.39**) and raloxifene (**1.40**), respectively, have

been approved as anticancer drugs, while new antimalarial drug leads (**1.41-1.42**) have been identified from drugs not previously used for malaria treatment (**Figure 1.12**).[75]

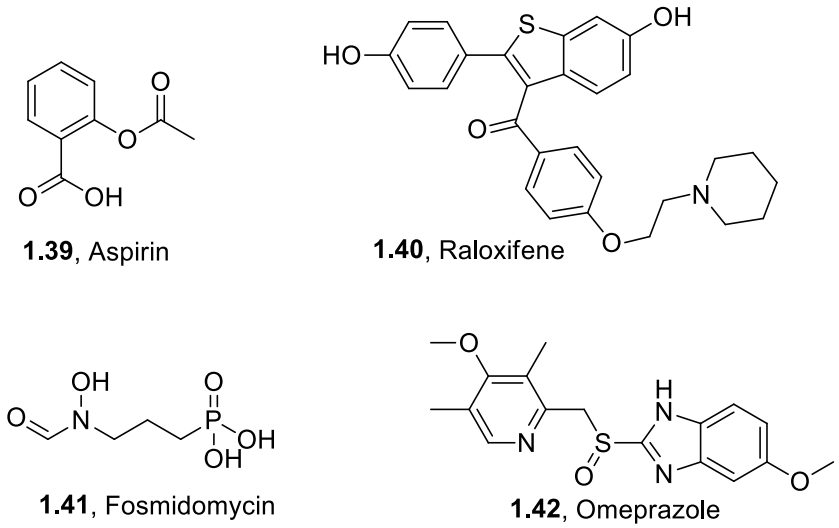

Figure 1.12 Chemical structures of repurposed drugs for anticancer (**1.39-1.40**) and antimalarial (**1.41-1.42**) treatment.

1.3.4. Drug hybridization

Similar to HTS, the goal of drug hybridization is to generate lead compounds with potential medicinal benefits that can be developed into clinical drugs. The concept of molecular hybridization is about combining pharmacophoric motifs from different scaffolds of bioactive molecules into a single drug prototype through structural fusion, merging, or conjugation with a suitable linker.[76] By the virtue of combining different pharmacophoric units from bioactive compounds with distinct modes of action into one, the merit of the drug hybridization strategy is the potential to produce drug prototypes displaying multiple or dual mechanistic modalities through targeting different biomolecules.[76a,b] As a fairly recent development in the discipline of drug discovery, the drug hybridization strategy has not yet yielded clinical drugs that have reached the market. However, the concept of generating polypharmacophoric compounds through drug hybridization has been successfully demonstrated by numerous studies in

literature[76c,77] as attested by a highly potent antibiotic, cefiderocol (**1.45**, S-649266), in phase III clinical development for treatment of multi-resistant Gram-negative bacteria.[78] Cefiderocol (**1.45**) is an efficacious sideromycin antibiotic that resulted from the conjugation of an antibacterial β-lactam pharmacophoric unit and an iron-chelating siderophore motif, catechol (**Figure 1.13**).[79]

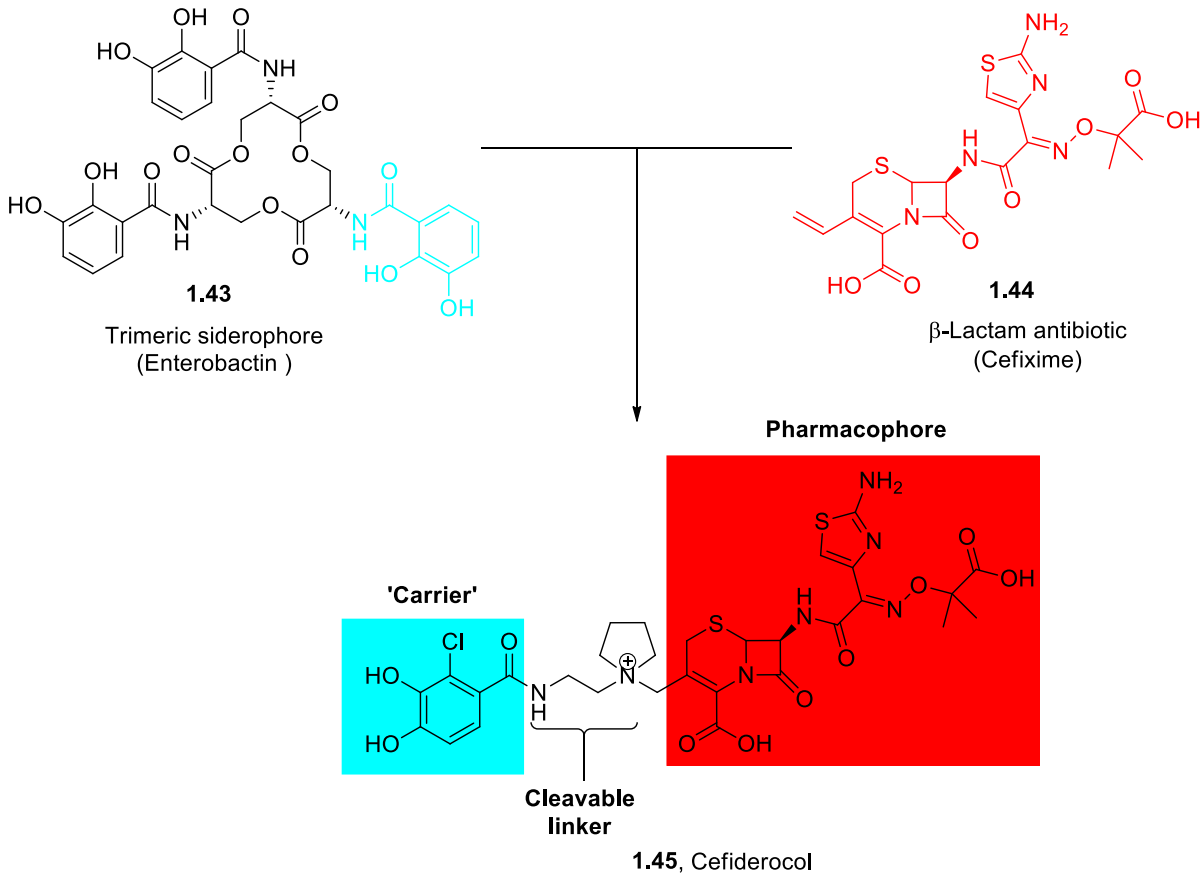

Figure 1.13 Hybridization strategy in cefiderocol.

A bacterium requires iron to support its biochemical processes. To meet this need, bacterial cells secrete iron-chelating compounds known as siderophores that can cross the bacterial cell wall to acquire iron from the surroundings into the cell in the form of iron-complexes via ferric transporters on the cell wall.[80] The rationale in the discovery of cefiderocol exploits this concept by merging a cell wall-permeating motif, siderophore, with an antibacterial β-lactam pharmacophoric unit into a single molecule using a biodegradable linker (**Figure 1.13**). This

approach confers the resulting compound with both antibacterial activity and ability to cross the bacterial cell wall, a feat most antibiotics lack. Once inside the cell, the linker gets cleaved releasing the β-lactam antibiotic unit from the siderophore moiety to kill the bacterium.

Rationally designed polypharmacophoric drug leads possess numerous potential advantages over drugs comprised of only single pharmacophoric units targeting singular targets.[76a] Having several pharmacophoric units that act on more than one target, multitargeting drugs are suitable for treatment of multifactorial diseases, like cancer, that are regulated by different biological pathways. As demonstrated by synthetic sideromycins, this strategy could replace combination therapies comprising several drugs targeting different biological pathways and bears the potential of addressing clinical resistance.[81] Furthermore, clinical development of hybrid drugs promises an economic advantage as it is less expensive to develop a single multitargeting drug compared to many drugs targeting different pathways for a disease.

1.3.5. Organometallic complexes in drug design: An emerging field of bioorganometallic chemistry

Despite the successes of strategies for designing innovative and effective drugs previously discussed, drugs based on organic scaffolds still face the threat of clinical resistance. Additionally, most clinical drugs on the market tend to contain unvaried pharmacophoric units displaying uniform mechanistic modalities. Lack of mechanistic diversity renders the drug vulnerable to development of clinical resistance. The challenges presented by the threat of development of resistance to clinical drugs necessitates the need for the establishment of innovative bioactive molecules as potential pharmaceuticals. To this end, the field of medicinal chemistry is undergoing a paradigm shift, adapting non-traditional approaches to impart structural variability and mechanistic diversity to medicinal compounds with therapeutic potential.[82]

The application of metallic complexes in medicine is an appealing strategy for the design of novel therapeutic and diagnostic agents.[82] The platinum complex, cisplatin (**1.46**) is the first metal-based drug to be approved for cancer treatment. Its mode of action involves DNA damage by cross-linking the DNA strands in tumour cells through binding to the DNA guanine bases to induce cell death.[83] Despite its high efficacy in eradicating tumour, cisplatin suffers from many side effects and is facing resistance by malignant cancers.[84] Other platinum-based clinically drugs such as carboplatin (**1.47**), oxaliplatin (**1.48**) and the second generation nedaplatin (**1.50**) have been developed for better efficacy and toxicological profile (**Figure 1.14**).[84]

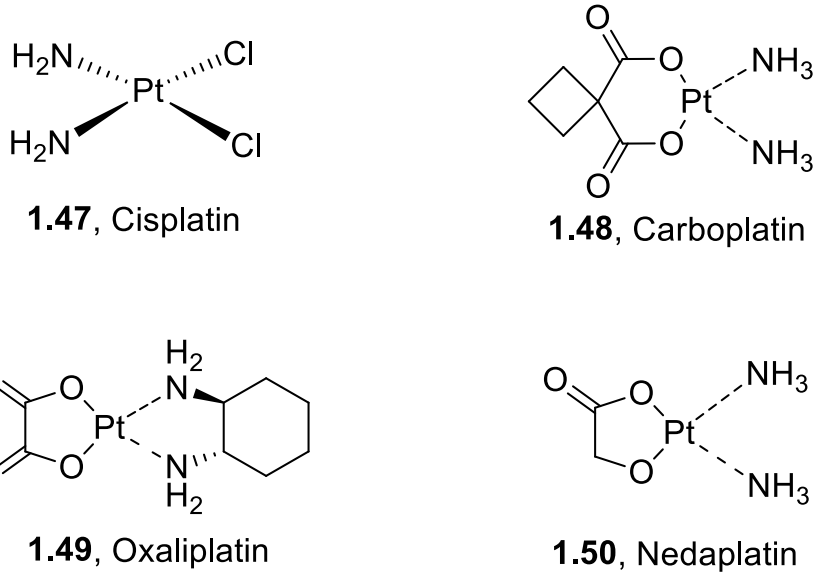

Figure 1.14 Metal-based platinum complexes used in cancer chemotherapy.

Exploitation of nonconventional chemotypes such as organometallic complexes, which have been extensively applied in catalysis, in drug discovery has gained immense attention in medicinal chemistry.[85] Unlike the classical inorganic metal complexes, organometallic complexes contain at least one bond between the metallic center and a carbon atom from an organic structural unit, like benzene and cyclopentadiene, acting as a ligand. Incorporation of organometallic complexes to existing drug molecules is a promising avenue for designing

novel drug leads.[85] Many organometallic complexes such as ferrocene possess several medicinal properties, namely: low human toxicity, high lipophilicity, reversible redox activity and ability to produce reactive oxygen species.[85b] For these reasons, organometallic compounds have gained interest as promising candidates for designing innovative bioactive agents with novel modes of action and better pharmacological profiles.[85b] Indeed, organometallic-based compounds have been demonstrated to possess novel and sometimes multiple mechanisms of action, particularly against cancer (**Table 1.3**).[86] The evaluation of organometallic complexes, metallocene dichlorides such as, like titanocene dichloride (**1.51**), against selected cancer cell lines by Köpf-Maier and colleagues in 1981 was arguably the most influential undertaking in highlighting the potential of organometallic complexes in medicinal application.[87] Though subsequently withdrawn, titanocene dichloride (**1.51**) identified from these studies entered to clinical trials as an anticancer drug and was also found to possess a mechanism that was distinct from that of cisplatin.[88]

Table 1.3 Organometallic complexes with potential biological activity.

Complex	Disease targeted	Mode of action	Reference
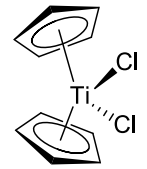 **1.51**	Cancer	• Inhibits nucleotide biosynthesis	Köpf-Maier[88]
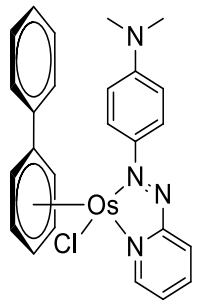 **1.52**	Cancer	• DNA binding • Oxidative stress by ROS	Fu et al.[89]
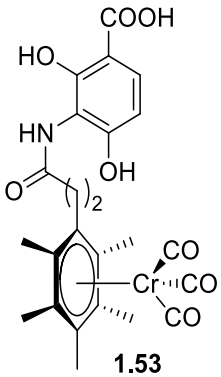 **1.53**	Bacterial infections	• Bacteriolysis	Wenzel et al.[90]
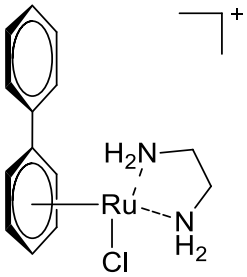 **1.54**	Cancer	• DNA binding • Oxidative stress by ROS	Wang et al.[91]

By the late 1990s, the research groups of Jaouen and Biot had revolutionized the field of drug design and discovery by adopting an ingenious strategy of incorporating an organometallic complex, ferrocene, into known drug motifs to produce novel prototype drugs possessing better anticancer and antimalarial potencies, respectively.[92] These developments sprouted a number of bioactive organometallic-based compounds, including those of other metallic centers, like osmium, chromium and ruthenium with distinct modes of action as shown in **Table 1.3**.

1.4. Ferrocenyl compounds in medicinal chemistry

Of all the organometallic complexes investigated in medicinal chemistry, ferrocene-containing bioactive agents are the most represented in literature owing to their encouraging medicinal potential. This section highlights the medicinal attributes of ferrocene and its application in drug design and discovery.

1.4.1. Medicinal attributes of ferrocene

Ferrocene is a metallocene comprised of an iron metallic center sandwiched between two cyclopentadienyl rings. It was discovered by accident in 1951 when Kealy and Pauson attempted a new synthetic method to prepare bicyclopentadienylidene, i.e., fulvalene (**1.55**), from cyclopentadiene magnesium bromide (**1.55**) in the presence of iron(III) chloride ($FeCl_3$) as a catalyst, which led to formation of ferrocene (**5.57**) as the major product (**Scheme 1.1**).[93] Ferrocene has unique physicochemical properties. These include high aromaticity, high chemical stability, reversible redox behaviour, ability to form reactive oxygen species (ROS) and lack of cytotoxicity in human cells.

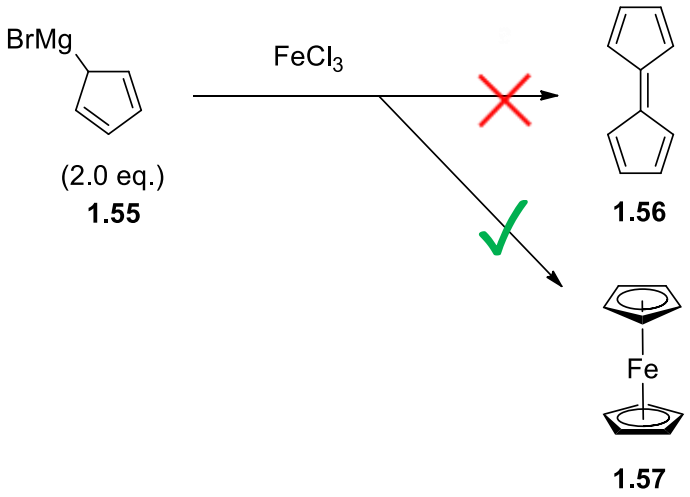

Scheme 1.1 Serendipitous formation of ferrocene (**1.57**) from attempted synthesis of fulvalene (**1.55**) from cyclopentadiene magnesium bromide (**1.55**) reported by Kealy and Pauson.[93]

High aromaticity of ferrocene and its low aqueous solubility confer the complex with favourable lipophilic properties, which are desirable features in bioactive compounds. It has a redox potential of –0.59 V and undergoes reversible anodic oxidation facilitated by strong Brønsted and Lewis acids or halogens.[94] In biological systems, ferrocene similarly exhibits peroxidative reversible oxidation that generates ROS, most notably the hydroxyl ($OH^{\bullet}$) radicals.[95] This is attributed to the ability of the central Fe(II) atom in ferrocene to oxidize to Fe(III), leading to formation of the ferrocenium ion and concomitant production of $OH^{\bullet}$ radicals via a Fenton-type reaction, as exemplified by ferroquine (**1.32**) (**Figure 1.15**).[96] Production of ROS plays a crucial role in the mechanism of action of ferrocene-containing bioactive derivatives. The generated $OH^{\bullet}$ radicals cause irreversible damage to the parasite, resulting in its death.[95-96] Owing to these properties, ferrocene and derivatives are appealing in medicinal chemistry for the generation of novel scaffolds with biological activity, and have been extensively investigated for various diseases.

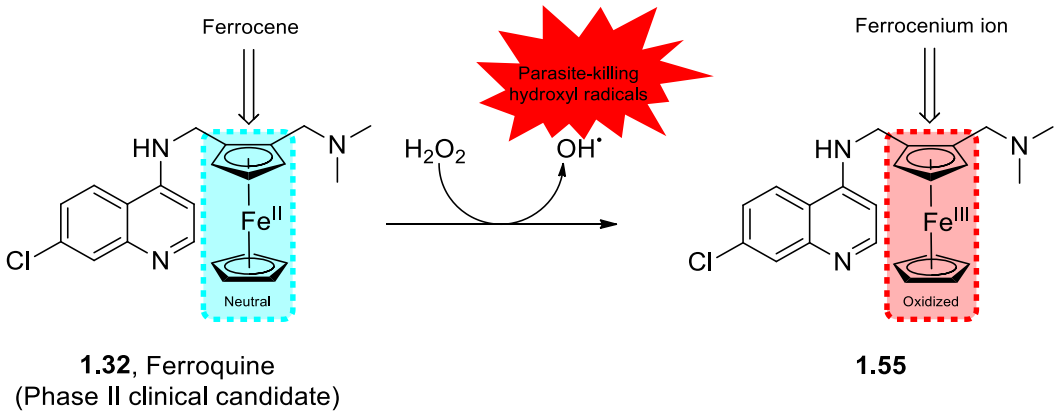

1.32, Ferroquine
(Phase II clinical candidate)

1.55

Figure 1.15 Proposed mechanism of ferroquine for production of hydroxyl radicals via Fenton-type mechanism inside the digestive vacuole of the *Plasmodium* parasite.

1.4.2. Ferrocene-based compounds as potential drugs

The discovery of ferrocene as the first synthetic metallocene led to investigation of several metallocenes and their derivatives. Since the adaptation of organometallic complexes for biological applications,[97] investigation of ferrocene and other metallocenes, like **1.52-1.54** (**Table 1.3**), as well as their derivatives as potential anticancer agents accented the field of bioorganometallic chemistry.[98]

In 1996, Jaouen and coworkers rationally designed a new class of anticancer compounds as inhibitors of the estrogen receptor (ER) by incorporating the organometallic unit, ferrocene, into the structural framework of a known ER-targeting anticancer drug, tamoxifen (**1.6a**) (**Figure 1.2**).[92a] The rationale of the study was premised on synergizing the anticancer properties of tamoxifen and the ferrocenium ion by hybridizing their structural motifs into a single unit. The prepared ferrocene-tamoxifen hybrids showed moderate binding affinity for the ER and higher toxicity against the MCF7 ATCC breast cancer cell line containing estrogen receptors than the parent hydroxytamoxifen compound. Most interestingly, the prepared ferrocenyl compound exhibited DNA damage in the micromolar concentrations which the

parent compound lacked. These findings demonstrated that the presence of the ferrocene unit resulted in anticancer agents showing potential mechanistic duality targeting the ER and inducing DNA damage. Later investigations of the identified hits from the study led to the development of potent anticancer agents that came to be known as ferrocifens (**1.57a-e**), targeting not only the ER but also showing novel modes of mechanism to elicit biological activity including production of ROS (**Table 1.4**).[99]

Subsequently, Biot and colleagues reported a novel class of antimalarial agents by introducing the ferrocene unit into the basic aliphatic side chain of chloroquine (**1.14**).[92b] This culminated in a state-of-the-art antimalarial drug, ferroquine (**1.32**), with enhanced bioactivity lacking the drawbacks of chloroquine and novel modes of action. Chloroquine resistance is proposed to result when the membrane of the digestive vacuole (DV) of the *Plasmodium* parasite where the drug acts evolves to cause quick removal of the drug molecules by drug efflux shortening the time required by the drug to prevent hemozoin formation.[58] The bulkiness of the ferrocene unit in ferroquine endows the molecule with improved hydrophobic and lipophilic character, allowing better interaction with hematin and lipid structures in the DV target site, thus ensuring its prolonged accumulation in the target site.[58] Indeed, ferroquine has been demonstrated to lack the resistance suffered by chloroquine in isolated *P. falciparum* strains and its activity has been shown to be independent of polymorphism in transport protein genes associated with chloroquine resistance.[100] Similar to ferrocifens, ferroquine produces ROS which contribute to the eradicating the parasite in addition to hemozoin inhibition.[101]

It is clear from the above representative studies that ferrocene is a worthy organometallic scaffold possessing superior medicinal properties with great potential in drug design and discovery. These attributes have been accentuated by the subsequent development of ferrocene-containing bioactive agents based on other chemical moieties for application against a

multitude of diseases. Representative examples of bioactive agents containing ferrocene highlighting its role in the biological activity are presented in **Table 1.4**.

Table 1.4 Role of ferrocene in biologically active ferrocenyl compounds.

Bioactive agent	Disease	Biological role of ferrocene	References
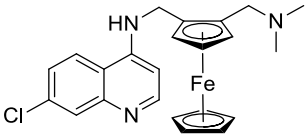 **1.32**, Ferroquine (Phase II clinical candidate)	Malaria	• Improves antimalarial activity • Allows the compound to easily cross the parasitic DV membrane • Produces ROS • Retains compound in the DV	Dive and Biot;[102] review by Dubar et al.[101]
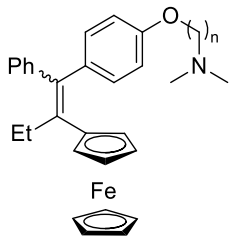 **1.57a-e:** n = 2 - 6	Cancer	• Improves anticancer activity • Allows DNA interaction • Allows the compound to easily cross the membrane in tumour cells • Produces ROS • Retains compound in the target site	Review by Jaouen et al.[99]
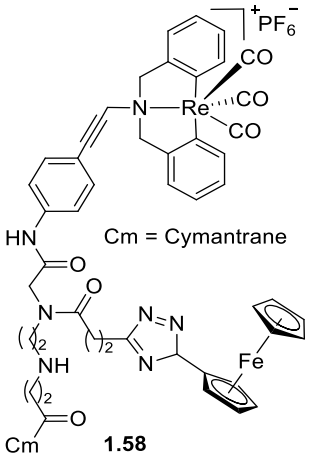 Cm = Cymantrane **1.58**	Bacterial infections	• Production of ROS • Allows compound to accumulate in the bacterial membrane to facilitate membrane function disruption	Wenzel et al.[103]
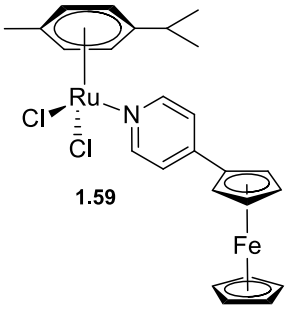 **1.59**	Bacterial infections and cancer	• Confers antibacterial activity to the compound by ROS production	Mu et al.[104]

1.5. Motivation for the current study

The emergence of resistance to clinical drugs is a dreadful threat that has intensified the need to search for novel biological agents as potential pharmaceuticals drugs. To devise novel bioactive scaffolds with structural variability and mechanistic diversity, the field of medicinal chemistry is undergoing a paradigm shift by adapting non-traditional approaches in drug design and discovery. Exploitation of nonconventional chemotypes such as organometallic complexes is a promising avenue to conceptualize compounds that can potentially delay or avert clinical resistance due to structural and mechanistic novelty. This approach has made significant contributions in malaria research and oncology.[105] Contemporary perspectives in drug design propose the incorporation of the organometallic unit, ferrocene, into known drug molecules as a promising strategy for the generation of potentially multi-modal drug molecules with intrinsic capacity to delay or avert resistance owing to its medicinal attributes.[106]

Presented with the attractive medicinal benefits of ferrocene and the merits of the drug hybridization and repurposing strategies, the present study aims to explore the potential benefits of incorporating the organometallic unit, ferrocene, by conjugation to a known chemical scaffold, 3,4-dihydro-2*H*-1,3-benzoxazine, that has been primarily employed in polymer applications.[107] The benzoxazine framework has also been demonstrated in literature to possess biological activity against a spectrum of diseases.[108] Despite the medicinal characteristics of ferrocene and the proved pharmaceutical potential of the benzoxazine moiety, as far as we know, the medicinal potential of ferrocene-based benzoxazine conjugates remains unexplored. It is noteworthy to mention that at the time of undertaking the current research only two accounts of ferrocenyl 3,4-dihydro-2*H*-1,3-benzoxazines had been reported in literature for polymer applications.[109] However, none of the reported ferrocenyl 1,3-benzoxazines have been investigated for the medicinal benefits of hybridizing the ferrocene and benzoxazine units.

References

(1) Ames, B. N.; Gold, L. S.; Willett, W. C. *Proc. Natl. Acad. Sci. U.S.A.* **1995**, *92*, 5258.

(2) (a) World Health Organization. Cancer, https://www.who.int/news-room/fact-sheets/detail/cancer, Accessed: 16 October 2019; (b) Ismail, R. S.; Baldwin, R. L.; Fang, J.; Browning, D.; Karlan, B. Y.; Gasson, J. C.; Chang, D. D. *Cancer Res.* **2000**, *60*, 6744.

(3) Ebert, M. P.; Korc, M.; Malfertheiner, P.; Röcken, C. *Journal of proteome research* **2006**, *5*, 19.

(4) Zhang, L.; Zhou, W.; Velculescu, V. E.; Kern, S. E.; Hruban, R. H.; Hamilton, S. R.; Vogelstein, B.; Kinzler, K. W. *Science* **1997**, *276*, 1268.

(5) DeVita, V. T.; Chu, E. *Cancer Res.* **2008**, *68*, 8643.

(6) Espinosa, E.; Zamora, P.; Feliu, J.; Barón, M. G. *Cancer Treat. Rev.* **2003**, *29*, 515.

(7) (a) Ward Jr, K. *J. Am. Chem. Soc.* **1935**, *57*, 914; (b) Berenblum, I. *J. Pathol. Bacteriol.* **1935**, *40*, 549.

(8) (a) Meyer, L. M.; Miller, F. R.; Rowen, M. J.; Bock, G.; Rutzky, J. *Acta Haematol.* **1950**, *4*, 157; (b) Burchenal, J. H.; Karnofsky, D. A.; Kingsley-Pillers, E. M.; Southam, C. M.; Myers, W. L.; Escher, G. C.; Craver, L. F.; Dargeon, H. W.; Rhoads, C. P. *Cancer* **1951**, *4*, 549; (c) Holden, J. A. *Curr. Med. Chem. Anti-Cancer Agents* **2001**, *1*, 1.

(9) (a) Wall, M. E.; Wani, M. C. *Cancer Res.* **1995**, *55*, 753; (b) Rowinsky, M., Eric K *Annu. Rev. Med.* **1997**, *48*, 353; (c) Noble, R. L. *Biochem. Cell Biol.* **1990**, *68*, 1344.

(10) Birnbaum, L. S.; Fenton, S. E. *Environ. Health Perspect.* **2003**, *111*, 389.

(11) (a) Lippert, T. H.; Seeger, H.; Mueck, A. O. *Steroids* **2000**, *65*, 357; (b) Key, T. J. *Mutat. Res-Fund. Mol. M.* **1995**, *333*, 59.

(12) (a) Muss, H. B. *Breast Cancer Res. Treat.* **1992**, *21*, 15; (b) Evans-Storms, R. B.; Cidlowski, J. A. *J. Steroid Biochem. Mol. Biol.* **1995**, *53*, 1.

(13) Beatson, G. T. *Tr. Med. Chir. Soc. Edinburgh* **1896**, *15*, 153.

(14) (a) Ponzone, R.; Biglia, N.; Jacomuzzi, M. E.; Mariani, L.; Dominguez, A.; Sismondi, P. *Ann. N.Y. Acad. Sci.* **2006**, *1089*, 143; (b) Parczyk, K.; Schneider, M. R. *J. Cancer Res. Clin. Oncol.* **1996**, *122*, 383.

(15) Wu, X.-Z. *Med. Hypotheses* **2006**, *66*, 883.

(16) Adams, J. *Cancer cell* **2004**, *5*, 417.

(17) Boros, L. G.; Lee, W.-N. P.; Cascante, M. *N. Engl. J. Med.* **2002**, *347*, 67.

(18) Savage, D. G.; Antman, K. H. *N. Engl. J. Med.* **2002**, *346*, 683.

(19) Xu, J.; Wang, J.; Xu, B.; Ge, H.; Zhou, X.; Fang, J.-Y. *Mol. Cancer Ther.* **2013**, *12*, 717.

(20) Los, M.; Roodhart, J. M.; Voest, E. E. *Oncologist.* **2007**, *12*, 443.

(21) Verma, S.; Miles, D.; Gianni, L.; Krop, I. E.; Welslau, M.; Baselga, J.; Pegram, M.; Oh, D.-Y.; Diéras, V.; Guardino, E. *N. Engl. J. Med.* **2012**, *367*, 1783.

(22) Cho, H.-S.; Mason, K.; Ramyar, K. X.; Stanley, A. M.; Gabelli, S. B.; Denney Jr, D. W.; Leahy, D. J. *Nature* **2003**, *421*, 756.

(23) Pavlasova, G.; Borsky, M.; Svobodova, V.; Oppelt, J.; Cerna, K.; Novotna, J.; Seda, V.; Fojtova, M.; Fajkus, J.; Brychtova, Y. *Leukemia* **2018**, *32*, 2028.

(24) Stewart, A. K. *Science* **2014**, *343*, 256.

(25) Centers for DIsease Control and Prevention. Centers for DIsease Control and Prevention. Malaria Lifecycle, https://www.cdc.gov/malaria/about/biology/, Accessed: 16 October 2019.

(26) World Health Organization, World Malaria Report 2018, http://apps.who.int/iris/bitstream/handle/10665/275867/9789241565653-eng.pdf?ua=1, Accessed: 10 October 2019.

(27) Jaramillo-Arango, J. *Bot. J. Linn. Soc.* **1949**, *53*, 272.

(28) World Health Organization, Guidelines for malaria vector control, https://www.who.int/malaria/publications/atoz/9789241550499/en/, Accessed: 10 October 2019.

(29) World Health Organization. Vector control products, https://www.who.int/pq-vector-control/prequalified-lists/en/, Accessed: 10 October 2019.

(30) Coronado, L. M.; Nadovich, C. T.; Spadafora, C. *Biochim. Biophys. Acta* **2014**, *1840*, 2032.

(31) Sullivan, A.; Meshnick, S. *Parasitol. Today* **1996**, *12*, 161.

(32) Foley, M.; Tilley, L. *Pharmacol. Ther.* **1998**, *79*, 55.

(33) Slater, A. F. *Pharmacol. Ther.* **1993**, *57*, 203.

(34) Kumar, A.; Katiyar, S.; Agarwal, A.; Chauhan, P. *Curr. Med. Chem.* **2003**, *10*, 1137.

(35) Kamchonwongpaisan, S.; Meshnick, S. R. *Gen. Pharmacol.* **1996**, *27*, 587.

(36) Olliaro, P. L.; Haynes, R. K.; Meunier, B.; Yuthavong, Y. *Trends Parasitol.* **2001**, *17*, 122.

(37) Olliaro, P. *Pharmacol. Ther.* **2001**, *89*, 207.

(38) Saifi, M. A.; Beg, T.; Harrath, A. H.; Altayalan, F. S. H.; Al Quraishy, S. *Afr. J. Pharm. Pharmacol.* **2013**, *7*, 148.

(39) Hammond, D. J.; Burchell, J. R.; Pudney, M. *Mol. Biochem. Parasitol.* **1985**, *14*, 97.

(40) Brun, R.; Blum, J.; Chappuis, F.; Burri, C. *Lancet.* **2010**, *375*, 148.

(41) Simarro, P. P.; Cecchi, G.; Franco, J. R.; Paone, M.; Diarra, A.; Ruiz-Postigo, J. A.; Fèvre, E. M.; Mattioli, R. C.; Jannin, J. G. *PLOS Negl. Trop. Dis.* **2012**, *6*, e1859.

(42) Simarro, P. P.; Diarra, A.; Postigo, J. A. R.; Franco, J. R.; Jannin, J. G. *PLOS Negl. Trop. Dis.* **2011**, *5*, e1007.

(43) (a) Lindley, C.; McCune, J. S.; Thomason, T. E.; Lauder, D.; Sauls, A.; Adkins, S.; Sawyer, W. T. *Cancer Pract.* **1999**, *7*, 59; (b) Love, R. R.; Leventhal, H.; Easterling, D. V.; Nerenz, D. R. *Cancer* **1989**, *63*, 604.

(44) van Vuuren, R. J.; Visagie, M. H.; Theron, A. E.; Joubert, A. M. *Cancer Chemother. Pharmacol.* **2015**, *76*, 1101.

(45) Baas, P. W.; Vidya Nadar, C.; Myers, K. A. *Traffic* **2006**, *7*, 490.

(46) Staff, N. P.; Grisold, A.; Grisold, W.; Windebank, A. J. *Ann. Neurol.* **2017**, *81*, 772.

(47) Argyriou, A. A.; Iconomou, G.; Kalofonos, H. P. *Blood* **2008**, *112*, 1593.

(48) Chatterjee, K.; Zhang, J.; Honbo, N.; Karliner, J. S. *Cardiology* **2010**, *115*, 155.

(49) (a) Baguley, B. C. *Mol. Biotechnol.* **2010**, *46*, 308; (b) Gottesman, M. M. *Annu. Rev. Med.* **2002**, *53*, 615.

(50) Housman, G.; Byler, S.; Heerboth, S.; Lapinska, K.; Longacre, M.; Snyder, N.; Sarkar, S. *Cancers* **2014**, *6*, 1769.

(51) Nikolaou, M.; Pavlopoulou, A.; Georgakilas, A. G.; Kyrodimos, E. *Clin. Exp. Metastasis* **2018**, *35*, 309.

(52) Foulkes, W. D.; Smith, I. E.; Reis-Filho, J. S. *N. Engl. J. Med.* **2010**, *363*, 1938.

(53) Manna, S.; Bostner, J.; Sun, Y.; Miller, L. D.; Alayev, A.; Schwartz, N. S.; Lager, E.; Fornander, T.; Nordenskjöld, B.; Jane, J. Y. *Clin. Cancer. Res.* **2016**, *22*, 1421.

(54) Liedtke, C.; Mazouni, C.; Hess, K. R.; André, F.; Tordai, A.; Mejia, J. A.; Symmans, W. F.; Gonzalez-Angulo, A. M.; Hennessy, B.; Green, M. *J. Clin. Oncol.* **2008**, *26*, 1275.

(55) Coatney, G. R. *Am. J. Trop. M. Hyg.* **1963**, *12*, 121.

(56) Krafts, K.; Hempelmann, E.; Skórska-Stania, A. *Parasitol. Res.* **2012**, *111*, 1.

(57) Payne, D. *Parasitol. Today* **1987**, *3*, 241.

(58) Krogstad, D. J.; Gluzman, I. Y.; Kyle, D. E.; Oduola, A.; Martin, S. K.; Milhous, W. K.; Schlesinger, P. H. *Science* **1987**, *238*, 1283.

(59) World Health Organization, World Health Organization Model List of Essential Medicines, https://www.apps.who.int/iris/bitstream/handle/10665/325771/WHO-MVP-EMP-IAU-2019.06-eng.pdf?ua=1, Accessed: 15 October 2019.

(60) Ashley, E. A.; White, N. J. *Curr. Opin. Infect. Dis.* **2005**, *18*, 531.

(61) World Health Organization, World Malaria Report 2010, https://www.who.int/malaria/world_malaria_report_2010/worldmalariareport2010.pdf?ua=1, Accessed: 10 October 2019.

(62) World Health Organization, Status report on artemisinin resistance, http://www.who.int/malaria/publications/atoz/status_rep_artemisinin_resistance_sep2014.pdf, Accessed: 15 October 2019.

(63) (a) Medicines for Malaria Venture. Malaria Box supporting information, https://www.mmv.org/mmv-open/malaria-box/malaria-box-supporting-information, Accessed: 10 October 2019; (b) Spangenberg, T.; Burrows, J. N.; Kowalczyk, P.; McDonald, S.; Wells, T. N.; Willis, P. *PloS One* **2013**, *8*, e62906.

(64) (a) Navarro, M.; Castro, W.; Biot, C. *Organometallics* **2012**, *31*, 5715; (b) Paquet, T.; Le Manach, C.; Cabrera, D. G.; Younis, Y.; Henrich, P. P.; Abraham, T. S.; Lee, M. C.; Basak, R.; Ghidelli-Disse, S.; Lafuente-Monasterio, M. J. *Sci. Transl. Med.* **2017**, *9*, eaad9735.

(65) Anderson, A. C. *Chem. Biol.* **2003**, *10*, 787.

(66) Roberts, N. A.; Martin, J. A.; Kinchington, D.; Broadhurst, A. V.; Craig, J. C.; Duncan, I. B.; Galpin, S. A.; Handa, B. K.; Kay, J.; Krohn, A. *Science* **1990**, *248*, 358.

(67) Rahman, M. M.; Karim, M. R.; Ahsan, M. Q.; Khalipha, A. B. R.; Chowdhury, M. R.; Saifuzzaman, M. *Int. J. Pharm. Life Sci.* **2012**, *1*.

(68) (a) Clark, D. E. *Expert Opin. Drug Dis.* **2006**, *1*, 103; (b) Kaldor, S. W.; Kalish, V. J.; Davies, J. F.; Shetty, B. V.; Fritz, J. E.; Appelt, K.; Burgess, J. A.; Campanale, K. M.; Chirgadze, N. Y.; Clawson, D. K. *J. Med. Chem.* **1997**, *40*, 3979.

(69) Broach, J. R.; Thorner, J. *Nature* **1996**, *384*, 14.

(70) Macarron, R.; Banks, M. N.; Bojanic, D.; Burns, D. J.; Cirovic, D. A.; Garyantes, T.; Green, D. V.; Hertzberg, R. P.; Janzen, W. P.; Paslay, J. W. *Nat. Rev. Drug Discov.* **2011**, *10*, 188.

(71) Kitchen, D. B.; Decornez, H.; Furr, J. R.; Bajorath, J. *Nat. Rev. Drug Discov.* **2004**, *3*, 935.

(72) Ashburn, T. T.; Thor, K. B. *Nat. Rev. Drug Discov.* **2004**, *3*, 673.

(73) Pushpakom, S.; Iorio, F.; Eyers, P. A.; Escott, K. J.; Hopper, S.; Wells, A.; Doig, A.; Guilliams, T.; Latimer, J.; McNamee, C. *Nat. Rev. Drug Discov.* **2019**, *18*, 41.

(74) (a) Bertolini, F.; Sukhatme, V. P.; Bouche, G. *Nat. Rev. Clin. Oncol.* **2015**, *12*, 732; (b) Pazhayam, N. M.; Chhibber-Goel, J.; Sharma, A. *Drug Discov. Today* **2019**, *24*, 263.

(75) (a) U.S. Preventive Services Task Force. Final Recommendation Statement. Aspirin Use to Prevent Cardiovascular Disease and Colorectal Cancer: Preventive Medication., https://www.uspreventiveservicestaskforce.org/Page/Document/RecommendationStatementFinal/aspirin-to-prevent-cardiovascular-disease-and-cancer, Accessed: 11 October 2019; (b) Tatar, O.; Ilhan, N.; Ilhan, N.; Susam, S.; Ozercan, I. H. *J. Biochem. Mol. Toxicol.* **2019**, e22371; (c) Skinner-Adams, T.; Davis, T. *Antimicrob. Agents Chemother.* **1999**, *43*, 1304.

(76) (a) Proschak, E.; Stark, H.; Merk, D. *J. Med. Chem.* **2018**, *62*, 420; (b) Fraga, C. A. M. *Expert Opin. Drug Dis.* **2009**, *4*, 605; (c) Morphy, R.; Rankovic, Z. *J. Med. Chem.* **2005**, *48*, 6523.

(77) Lazar, C.; Kluczyk, A.; Kiyota, T.; Konishi, Y. *J. Med. Chem.* **2004**, *47*, 6973.

(78) (a) Kohira, N.; West, J.; Ito, A.; Ito-Horiyama, T.; Nakamura, R.; Sato, T.; Rittenhouse, S.; Tsuji, M.; Yamano, Y. *Antimicrob. Agents Chemother.* **2016**, *60*, 729; (b) Zhanel, G. G.; Golden, A. R.; Zelenitsky, S.; Wiebe, K.; Lawrence, C. K.; Adam, H. J.; Idowu, T.; Domalaon, R.; Schweizer, F.; Zhanel, M. A. *Drugs* **2019**, *79*, 271; (c) NIH U.S. National Library of Medicine Clinical Study of S-649266 for the Treatment of Nosocomial Pneumonia Caused by Gram-negative Pathogens (APEKS-NP), https://www.clinicaltrials.gov/ct2/show/NCT03032380?term=649266, Accessed: 16 October 2019.

(79) Choi, J. J.; McCarthy, M. W. *Expert Opin. Investig. Drugs* **2018**, *27*, 193.

(80) Möllmann, U.; Heinisch, L.; Bauernfeind, A.; Köhler, T.; Ankel-Fuchs, D. *Biometals* **2009**, *22*, 615.

(81) (a) Liu, R.; Miller, P. A.; Vakulenko, S. B.; Stewart, N. K.; Boggess, W. C.; Miller, M. J. *J. Med. Chem.* **2018**, *61*, 3845; (b) Wencewicz, T. A.; Long, T. E.; M llmann, U.; Miller, M. J. *Bioconjugate Chem.* **2013**, *24*, 473.

(82) (a) Franz, K. J.; Metzler-Nolte, N. *Chem. Rev.* **2019**, *119*, 727; (b) Guo, Z.; Sadler, P. J. *Angew. Chem. Int. Ed.* **1999**, *38*, 1512.

(83) Todda, R. C.; Lipparda, S. J. *J. Inorg. Biochem.* **2010**, *104*, 902.

(84) Dilruba, S.; Kalayda, G. V. *Cancer Chemother. Pharmacol.* **2016**, *77*, 1103.

(85) (a) Jaouen, G.; Beck, W.; McGlinchey, M. J. In *Bioorganometallics: Biomolecules, Labeling, Medicine*; Jaouen, G., Ed.; Wiley-VCH Verlag GmbH & Co. KGaA: Wiley

Online Library 2006; (b) Gasser, G.; Metzler-Nolte, N. *Curr. Opin. Chem. Biol.* **2012**, *16*, 84.

(86) (a) Casini, A.; Hartinger, C. G.; Nazarov, A. A.; Dyson, P. J. *Top. Organomet. Chem.* **2010**, *32*, 57; (b) Bergamo, A.; Dyson, P. J.; Sava, G. *Coord. Chem. Rev.* **2018**, *360*, 17.

(87) Köpf-Maier, P.; Wagner, W.; Köpf, H. *Cancer Chemother. Pharmacol.* **1981**, *5*, 237.

(88) Köpf-Maier, P.; Köpf, H. *Naturwissenschaften* **1980**, *67*, 415.

(89) Fu, Y.; Habtemariam, A.; Pizarro, A. M.; van Rijt, S. H.; Healey, D. J.; Cooper, P. A.; Shnyder, S. D.; Clarkson, G. J.; Sadler, P. J. *J. Med. Chem.* **2010**, *53*, 8192.

(90) Wenzel, M.; Patra, M.; Albrecht, D.; Chen, D. Y.-K.; Nicolaou, K. C.; Metzler-Nolte, N.; Bandow, J. E. *Antimicrob. Agents Chemother.* **2011**, *55*, 2590.

(91) Wang, F.; Xu, J.; Habtemariam, A.; Bella, J.; Sadler, P. J. *J. Am. Chem. Soc.* **2005**, *127*, 17734.

(92) (a) Top, S.; Tang, J.; Vessières, A.; Carrez, D.; Provot, C.; Jaouen, G. *Chem. Commun.* **1996**, 955; (b) Biot, C.; Glorian, G.; Maciejewski, L. A.; Brocard, J. S.; Domarle, O.; Blampain, G.; Millet, P.; Georges, A. J.; Abessolo, H.; Dive, D. *J. Med. Chem.* **1997**, *40*, 3715.

(93) Kealy, T.; Pauson, P. *Nature* **1951**, *168*, 1039.

(94) Wilkinson, G.; Rosenblum, M.; Whiting, M.; Woodward, R. *J. Am. Chem. Soc.* **1952**, *74*, 2125.

(95) Salas, P. F.; Herrmann, C.; Orvig, C. *Chem. Rev.* **2013**, *113*, 3450.

(96) Chavain, N.; Vezin, H.; Dive, D.; Touati, N.; Paul, J.-F.; Buisine, E.; Biot, C. *Mol. Pharm.* **2008**, *5*, 710.

(97) Jaouen, G.; Beck, W.; McGlinchey, M. J. In *Bioorganometallics: Biomolecules, Labeling, Medicine*; Jaouen, G., Ed.; Wiley-VCH Verlag GmbH & Co. KGaA: Weinheim, 2006.

(98) Hartinger, C. G.; Dyson, P. J. *Chem. Soc. Rev.* **2009**, *38*, 391.

(99) Jaouen, G.; Vessières, A.; Top, S. *Chem. Soc. Rev.* **2015**, *44*, 8802.

(100) (a) Kreidenweiss, A.; Kremsner, P. G.; Dietz, K.; Mordmueller, B. *Am. J. Trop. M. Hyg.* **2006**, *75*, 1178; (b) Henry, M.; Briolant, S.; Fontaine, A.; Mosnier, J.; Baret, E.; Amalvict, R.; Fusaï, T.; Fraisse, L.; Rogier, C.; Pradines, B. *Antimicrob. Agents Chemother.* **2008**, *52*, 2755.

(101) Dubar, F.; Khalife, J.; Brocard, J.; Dive, D.; Biot, C. *Molecules* **2008**, *13*, 2900.

(102) Dive, D.; Biot, C. *Curr. Top. Med. Chem.* **2014**, *14*, 1684.

(103) Wenzel, M.; Patra, M.; Senges, C. H. R.; Ott, I.; Stepanek, J. J.; Pinto, A.; Prochnow, P.; Vuong, C.; Langklotz, S.; Metzler-Nolte, N. *ACS Chem. Biol.* **2013**, *8*, 1442.

(104) Mu, C.; Prosser, K. E.; Harrypersad, S.; MacNeil, G. A.; Panchmatia, R.; Thompson, J. R.; Sinha, S.; Warren, J. J.; Walsby, C. J. *Inorg. Chem.* **2018**, *57*, 15247.

(105) (a) Schatzschneider, U.; Metzler-Nolte, N. *Angew. Chem. Int. Ed.* **2006**, *45*, 1504; (b) Biot, C.; Dive, D. In *Medicinal Organometallic Chemistry*; Jaouen, G., Metzler-Nolte, N., Eds.; Springer Berlin Heidelberg: Berlin, Heidelberg, 2010.

(106) Patra, M.; Gasser, G. *Nat. Rev. Chem.* **2017**, *1*, 0066.

(107) (a) Ishida, H. In *Handbook of Benzoxazine Resins*; Ishida, H., Agag, T., Eds.; Elsevier: Amsterdam, 2011; (b) Kiskan, B. *React. Funct. Polym.* **2018**, *129*, 76.

(108) (a) Urbański, T.; Radzikowski, C.; Ledochowski, Z.; Czarnocki, W. *Nature* **1956**, *178*, 1351; (b) March, L.; Romanchick, W.; Bajwa, G.; Joullie, M. *J. Med. Chem.* **1973**, *16*, 337; (c) Gemma, S.; Camodeca, C.; Brindisi, M.; Brogi, S.; Kukreja, G.; Kunjir, S.; Gabellieri, E.; Lucantoni, L.; Habluetzel, A.; Taramelli, D. *J. Med. Chem.* **2012**, *55*,

10387; (d) Kamble, R. D.; Hese, S. V.; Meshram, R. J.; Kote, J. R.; Gacche, R. N.; Dawane, B. S. *Med. Chem. Res.* **2015**, *24*, 1077; (e) Desai, N.; Bhatt, N.; Joshi, S. B.; Vaja, D. V. *Synth. Commun.* **2017**, *47*, 2360.

(109) (a) Li, W.; Chu, J.; Heng, L.; Wei, T.; Gu, J.; Xi, K.; Jia, X. *Polymer* **2013**, *54*, 4909; (b) Li, W.; Wei, T.; Gao, Y.; Xi, K.; Jia, X. *Polymer* **2012**, *53*, 1236.

Chapter 2: Benzoxazine scaffold as a bioactive template

Benzoxazines are a class of heterocyclic compounds comprised of a benzene ring annulated to an oxazine unit. There are six sub-classes of benzoxazines. Several types of the benzoxazine scaffold are prominently featured in literature and possess a spectrum of properties making them versatile for different applications. This chapter looks at the different classes of the benzoxazine scaffold with particular focus on the medicinal application of compounds bearing the 3,4-dihydro-2*H*-1,3-benzoxazine motif.

2.1. Background

Depending on the position of the constituent oxygen and nitrogen heteroatoms in the benzoxazine scaffold, six common, parental classes of benzoxazines result, namely: 1,3-benzoxazine (**A**), 3,1-benzoxazine (**B**) and 1,4-benzoxazine (**C**), 1,2-benzoxazine (**D**), 2,1-benzoxazine (**E**) and 2,3-benzoxazine (**F**) (**Figure 2.1**).[1]

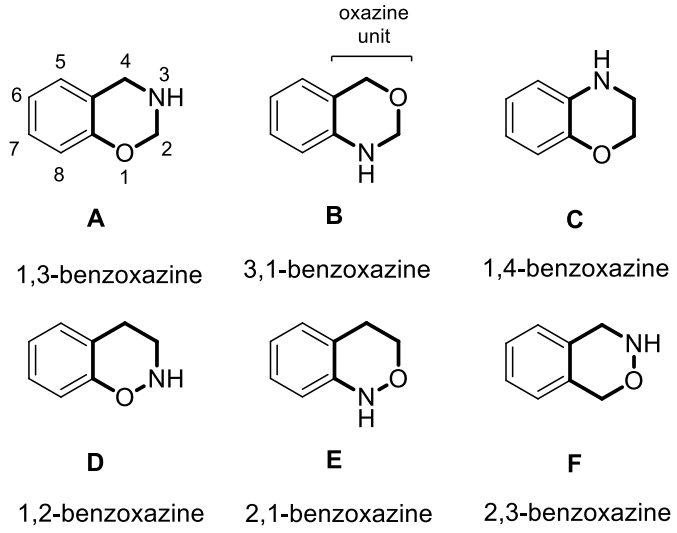

Figure 2.1 Structures of six primary classes of the benzoxazine scaffold.

According to the IUPAC naming convention, the numbering is assigned in such a way that the oxygen atom precedes the nitrogen in the naming as exemplified by the 1,3-benzoxazine structure (**A**) in which the oxygen and nitrogen atoms occupy positions 2 and 3, respectively (**Figure 2.1**). Since the original benzoxazine structure contained a double bond, the term "dihydro" is often incorporated in the IUPAC name of benzoxazines such as the ones in **Figure 2.1** to indicate the saturated carbon atoms in the oxazine unit (bold).[1] Thus, the IUPAC name of structure **A** in **Figure 2.1** is 3,4-dihydro-2*H*-1,3-benzoxazine. The structures of the indicated benzoxazine sub-classes have proven as versatile templates for generation of novel compounds with a myriad of physicochemical properties for various applications, ranging from medicinal potential to polymer synthesis. Since their discovery, either as parental moieties or by grafting to other biologically active chemical motifs, several compounds based on the benzoxazine scaffold have been developed and demonstrated to possess a multitude of biological activities, including anticancer, antibacterial and antifungal activities.[2] Lately, the 3,4-dihydro-2*H*-1,3-benzoxazine subclass **A** has found new applications particularly in the field of polymer synthesis owing to the chemically labile O-CH_2-N oxazine connection that is amenable to polymerization by cationic ring-opening.[1,3] As a result, research endeavours in this new application of the 1,3-benzoxazines have been prioritized over medicinal investigations.

2.1.1. Anticancer activity of benzoxazines

The history of benzoxazines as potential anticancer agents dates as early as the 1950s. The research team of Urbański was among the first to investigate the potential antineoplastic potential of simple 1,3-benzoxazines (**Scheme 2.1**).[2a] The study was motivated by the findings of their earlier investigations of related 1,3-oxazines that showed inhibitory activity *in vitro* against *Mycobacterium tuberculosis*.[4] Having been shown to be a bioactive scaffold, similar 1,3-benzoxazines were investigated for potential anti-neoplastic efficacy *in vivo*. By employing

the three-component Mannich-type condensation procedure by Burke,[5] Urbański and colleagues prepared a tailored series of three 1,3-benzoxazine derivatives from phenols or 2-napthhol and relevant amines in the presence of formaldehyde (**Scheme 2.1**).

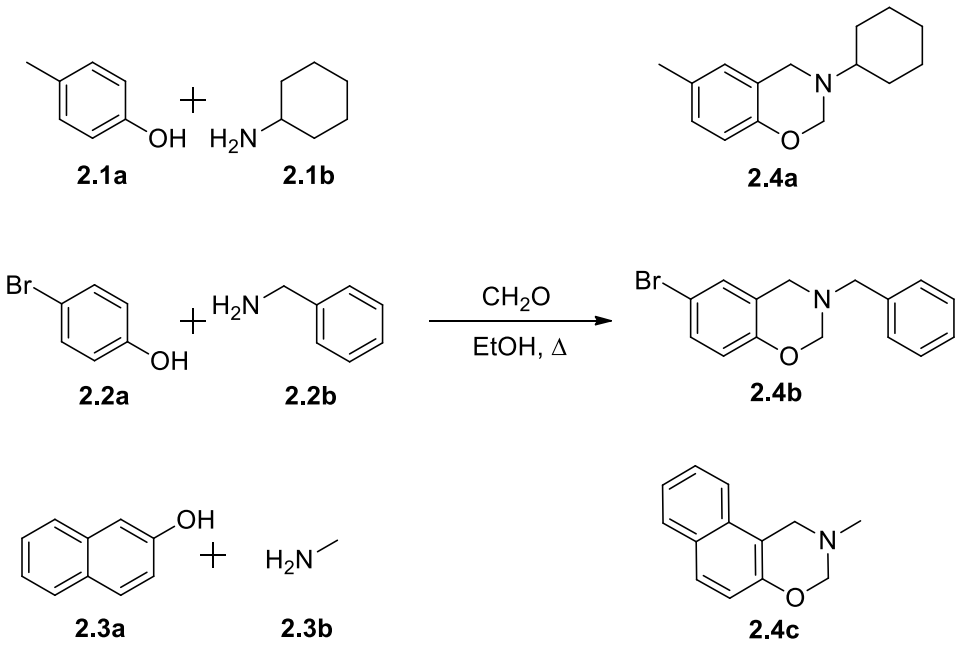

Scheme 2.1 Burke condensation procedure for the synthesis of 1,3-benzoxazine analogues evaluated for anticancer activity by Urbański et al.

The compounds exhibited promising anticancer activity *in vivo* against tumours caused by the Crocker Sarcoma virus with the 6-brominated benzoxazine **2.4b** and the naphthalenyloxazine derivative **2.4c** possessing the most efficacy. The activity of these compounds was attributed to the labile O-CH_2-N oxazine linkage as previously postulated in the studies of other bioactive 1,3-oxazine derivatives.[6] Subsequent to these findings, various derivatives bearing the 1,3-benzoxazine motif with other structural units were investigated for anticancer activity.

In 1962, Kuehne and colleagues incorporated the 1,3-benzoxazine motif into the aromatic steroidal scaffolds to assemble a novel class of estrogenic 1,3-oxazine derivatives (**Figure 2.2**).[7] Motivated by the carcinostatic properties of the 1,3-benzoxazine compounds and the importance of hormonal therapy in the treatment of hormone-dependent tumours, Kuehne et

al. proposed that combining the steroidal skeleton with the benzoxazine unit would result in potent estrogenic anticancer molecules.[7] By following the Burke protocol, steroidal derivatives bearing the steroid units fused with the 1,3-oxazine moiety were synthesized similarly to the benzoxazines reported by Urbański et al.[5,7] The steroidal 1,3-benzoxazines were accessed by condensing primary amines and phenolic steroids, equilenin **2.5a** and ethinylestradiol **2.5b**, in the presence of formaldehyde. The steroidal derivatives were tested for estrogenic activity, i.e., estrogen agonism, and *in vivo* anticancer activity against experimental adenocarcinoma E0771 tumours in mice. Except for the *N*-benzyl derivative (**2.6a**) that showed only minor estrogenic activity, none of the compounds from the equilenin series (**2.6a-d**) showed any estrogenic or significant antitumour activity.[7] On the contrary, all of the ethinylestradiol derivatives (**2.7a-c** and **2.8a-c**) displayed estrogenic activity at high doses and significant antitumour activities were observed for the *N*-cyclohexyl (**2.7c**) and *N*-benzyl (**2.8a**) analogues.

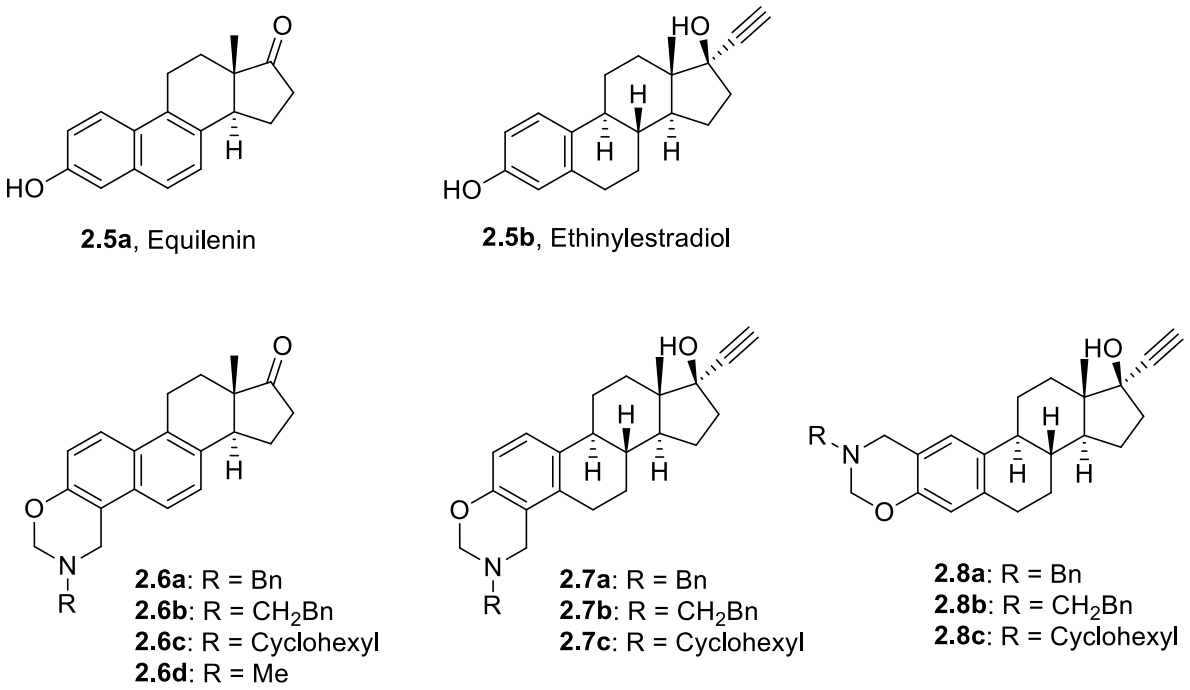

Figure 2.2 Steroidal 1,3-benzoxazine derivatives possessing *in vivo* anticancer activity.

Taking advantage of advances in drug design approaches, such as the targeted drug design and drug hybridization strategies, Garg and co-workers rationally designed flavone-benzoxazine

hybrids targeting the epidermal growth factor receptor (EGFR) using computer-aided ligand docking simulations.[8] The compounds were found to bind to the narrow hydrophobic pocket of the *N*-terminal chain in the ATP binding site of the EGFR in a similar fashion as the anticancer drug, erlotinib. Unlike the previous examples, the flavone-benzoxazine hybrids were assembled via sodium borohydride-promoted reductive amination of the salicylimine intermediates (**2.10a-b**) formed from substituted salicyaldehydes (**2.10**) and 6- or 7-aminoflavone (**2.9a-b**). Subsequent cyclisation with formaldehyde led to formation of the oxazine moiety (**Scheme 2.2**).

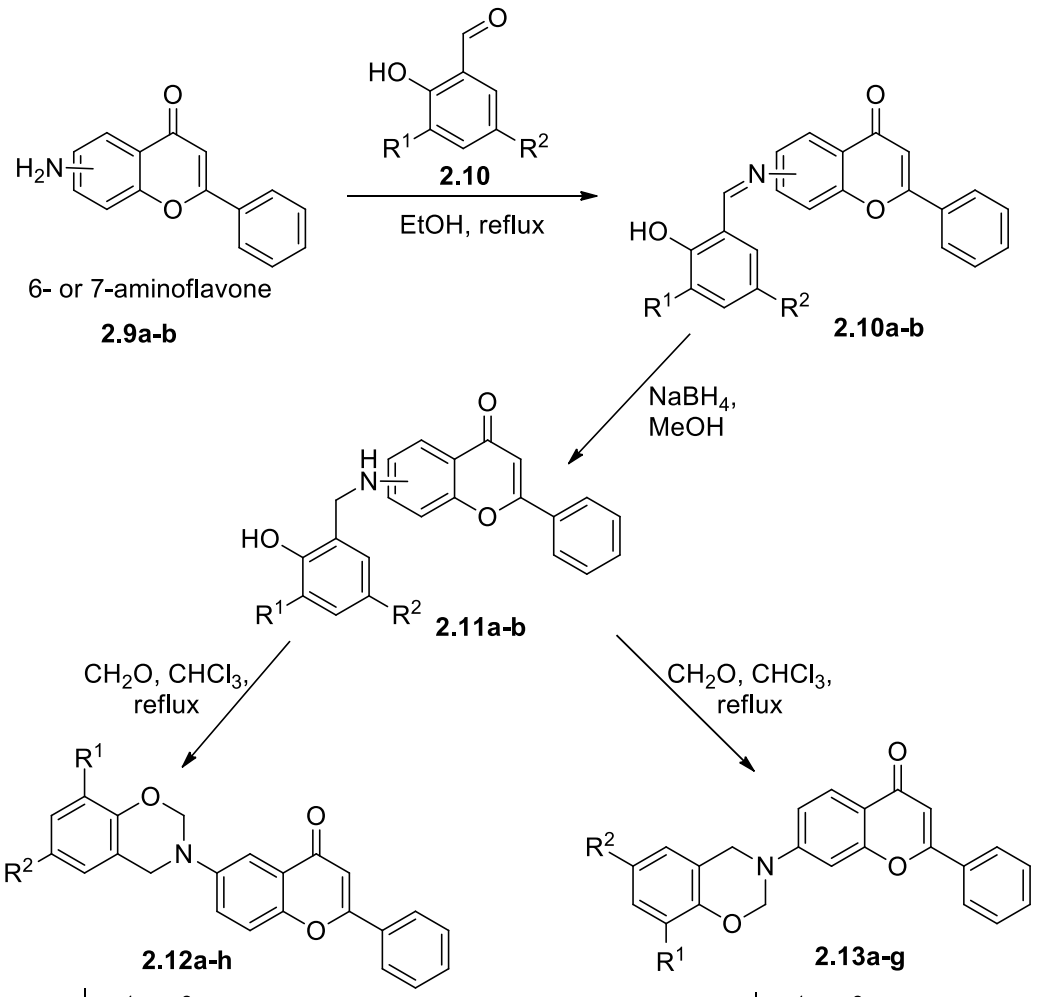

	R^1	R^2	IC_{50} (μM)
a	H	H	27.48
b	Br	H	19.60
c	Cl	Cl	12.03
d	NO_2	H	28.43
e	Me	H	14.30
f	H	Me	29.80
g	OMe	H	17.01
h	OMe	OMe	8.01

	R^1	R^2	IC_{50} (μM)
a	H	H	na
b	Br	H	na
c	Cl	Cl	44.5
d	NO_2	H	na
e	Me	H	14.9
f	H	Me	61.89
g	OMe	H	12.1

Scheme 2.2 Synthesis of flavonyl 1,3-benzoxazine hybrids reported by Garg et al.[8]

The anticancer activity of the compounds was investigated on the MCF-7 breast cancer cell line against which they displayed moderate activity in mid-micromolar IC_{50} range (**Scheme 2.2**). The 6-flavonyl dimethoxy hybrid **2.12h** had the highest predicted inhibition constant (K_i) against the EGFR and was the most active in the series.

Other derivatives of benzoxazines belonging to the other sub-classes have also been demonstrated to possess anticancer activity. For example, antibiotic FR900482 (**2.14**) is a naturally occurring aziridine-containing 1,2-benzoxazine derivative isolated from *Streptomyces sandaensis* displaying activity against a variety of tumours in mice (**Table 2.1**).[9] Nagarapu and colleagues rationally designed and synthesized 1,4-benzoxazines coupled to [1,2,3]-triazoles in four steps.[10] When evaluated for potential antiproliferative activity against cervical (HeLa), pancreatic (MIAPACA) and breast (MDA-MB-231) cancer cell lines, compounds **2.15** and **2.16** emerged as the most active across all four cell lines, while compound **2.17** exhibited significant activity against the MDA-MB-231 breast cancer cell line (**Table 2.1**).[10] Compound **2.18** belonging to the 3,1-benzoxazine sub-class was identified as one of the lead compounds by Bharathkumar et al. from a series of 3,1-benzoxazine derivatives designed as anticancer agents targeting methionyl-tRNA synthetase (MRS).[11] The compound exhibited potent inhibitory activity against human MRS and suppressed the proliferation of lung (A549) and colon (HCT116) cancer cell lines.

Table 2.1 Anticancer activity of benzoxazine derivatives belonging to the 1,2- and 1,4-benzoxazine sub-classes.

Compound	Anticancer activity	References
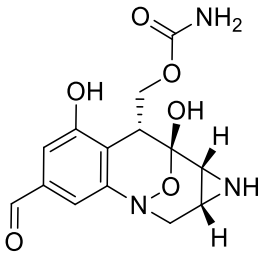 **2.14**, FR900482	• Antiproliferative activity against murine tumours: P388, AH130, L1210 and Ehrlich	Itsuo et al.,[9a] Shimomura et al.[9b]
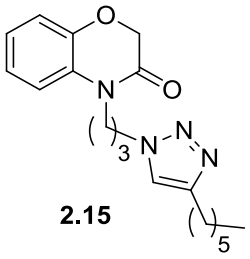 **2.15**	• Cervical cancer: IC_{50} (HeLa) = 0.1 ± 0.3 µM • Breast cancer: IC_{50} (MDA-MB-231) = 1.1 ± 0.08 µM • Pancreatic cancer: IC_{50} (MIAPACA) = 1.1 ± 0.15 µM	Bollu et al.[10]
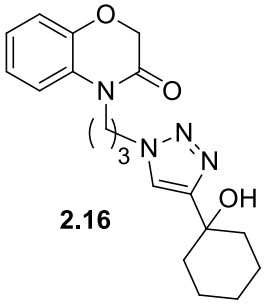 **2.16**	• Cervical cancer: IC_{50} (HeLa) = 2.0 ± 0.5 µM • Breast cancer: IC_{50} (MDA-MB-231) = 1.2 ± 0.1 µM • Pancreatic cancer: IC_{50} (MIAPACA) = 2.5 ± 0.5 µM	Bollu et al.[10]
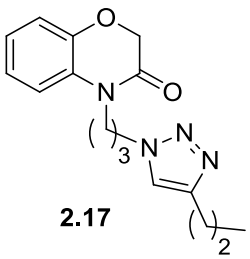 **2.17**	• Cervical cancer: IC_{50} (HeLa) = 23.2 ± 0.6 µM • Breast cancer: IC_{50} (MDA-MB-231) = 1.1 ± 0.04 µM • Pancreatic cancer: IC_{50} (MIAPACA) = 2.6 ± 0.3 µM	Bollu et al.[10]
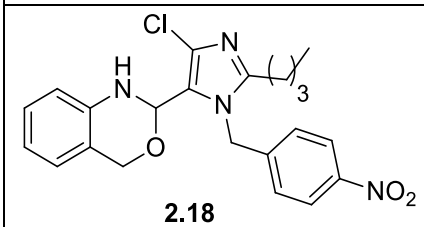 **2.18**	• Lung cancer: IC_{50} (A549) = 41.9 ± 5.7 µM • Colon cancer: IC_{50} (HCT116) = 19.8 ± 4.9 µM	Bharathkumar et al.[11]

2.1.2. Antiplasmodial activity of benzoxazines

Since their discovery, the pharmaceutical application of benzoxazine compounds has predominantly been focused on their anticancer activity. Early studies of compounds featuring the benzoxazine scaffold for antimalarial activity were first reported by the research group of Joullié in the early 1970s.[2b,12] Recently, the benzoxazine moiety has attracted revived attention in malaria research and has been incorporated into bioactive motifs to produce novel compounds possessing antiplasmodial efficacy.[13]

Motivated by the promising antimalarial activity of bis-α-aminomethylnaphthols (**2.21a-b**) reported by Duffin and Rollo that were synthesized via hydrolysis of bis-naphthoxazines as intermediates (**2.20a-b**),[14] in 1972 Joullié and co-workers introduced the 1,3-oxazine unit into the naphthalene nucleus to produce bis-1,3-naphthaloxazines like **2.22** as a new class of antimalarial agents (**Scheme 2.3**).[12] Given the chemically labile nature of the 1,3-oxazine unit due to its propensity to hydrolyse into corresponding aminoalcohol derivatives under low pH, the rationale of the study was that the bis-naphthoxazines are the active drug substrates of the antimalarial α-aminomethylnaphthols. Thus, it was proposed that the napthoxazines would produce *in vivo* antimalarial activity comparable to the corresponding α-aminomethylnaphthols reported by Duffin and Rollo (**Scheme 2.3**).

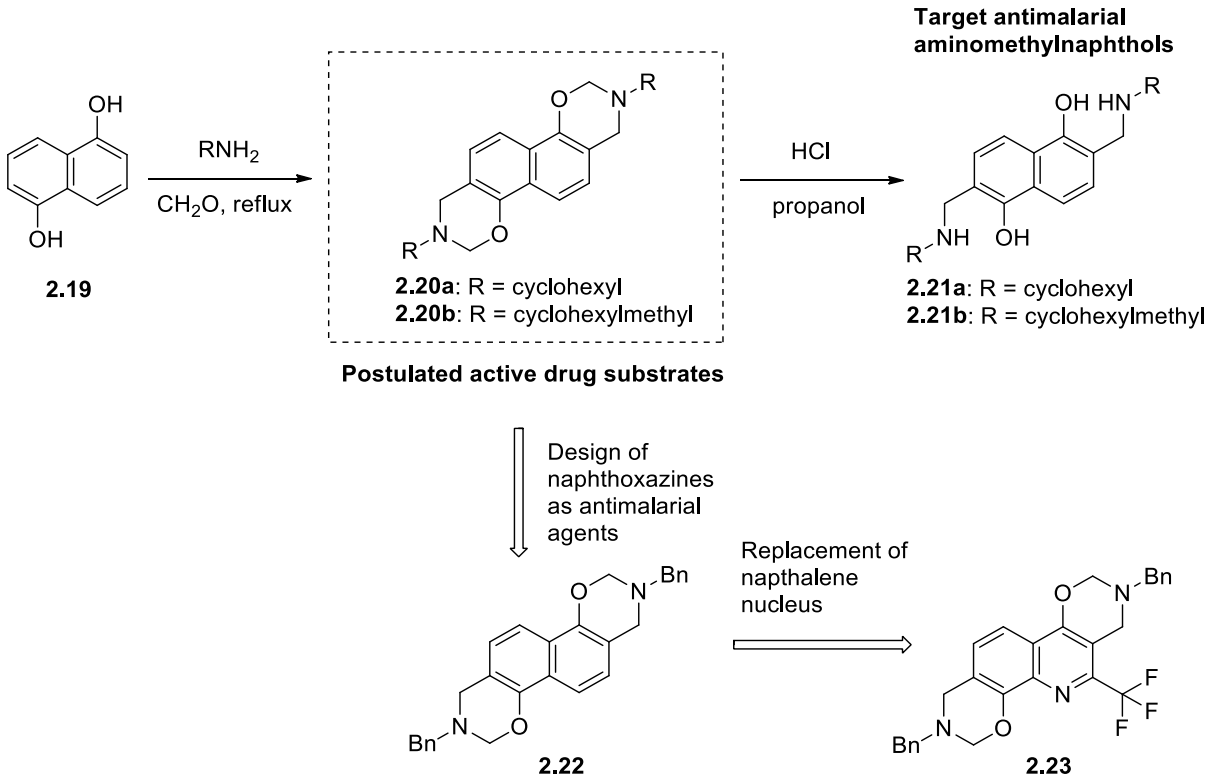

Scheme 2.3 Design and synthesis of naphthalene and quinoline derivatives featuring the benzoxazine unit.

Indeed, the resultant bis-napthoxazines exhibited antimalarial activity similar to their respective α-aminomethylnaphthols in mice infected with *Plasmodium gallinaceum* and *Plasmodium berghei* parasites.[12,14] By replacing the naphthalene ring system with the antimalarial quinoline nucleus, Joullié et al. produced a novel class of 1,3-quinoxazines and 1,3-pyridobenzoxazine such as **2.23** with improved the antimalarial efficacy (**Scheme 2.3**).[2b,12]

In a study published in 2012 that aimed to mimic the internal hydrogen bonding in clinical 4-aminoquinoline antimalarial agents, amodiaquine (**2.24a**) and isoquine (**2.24b**), Campiani and colleagues replaced the α-aminocresol side chain in position 4 with 1,3-benzoxazine substituents, producing 4-aminoquinolinyl benzoxazine hybrids (**Figure 2.3**).[13a] The resultant compounds exhibited *in vitro* antimalarial activity in the low nanomolar range against both chloroquine-sensitive (D10) and resistant (W2) strains of the *P. falciparum* parasite, with

2.25a-b exerting higher potency than their parental antimalarial drugs **2.24a-b** against the sensitive D10 strain (**Figure 2.3**). These findings suggested that the presence of the internal hydrogen bond mimicking the O-CH_2-N linkage in the benzoxazine unit was favourable for antimalarial activity.

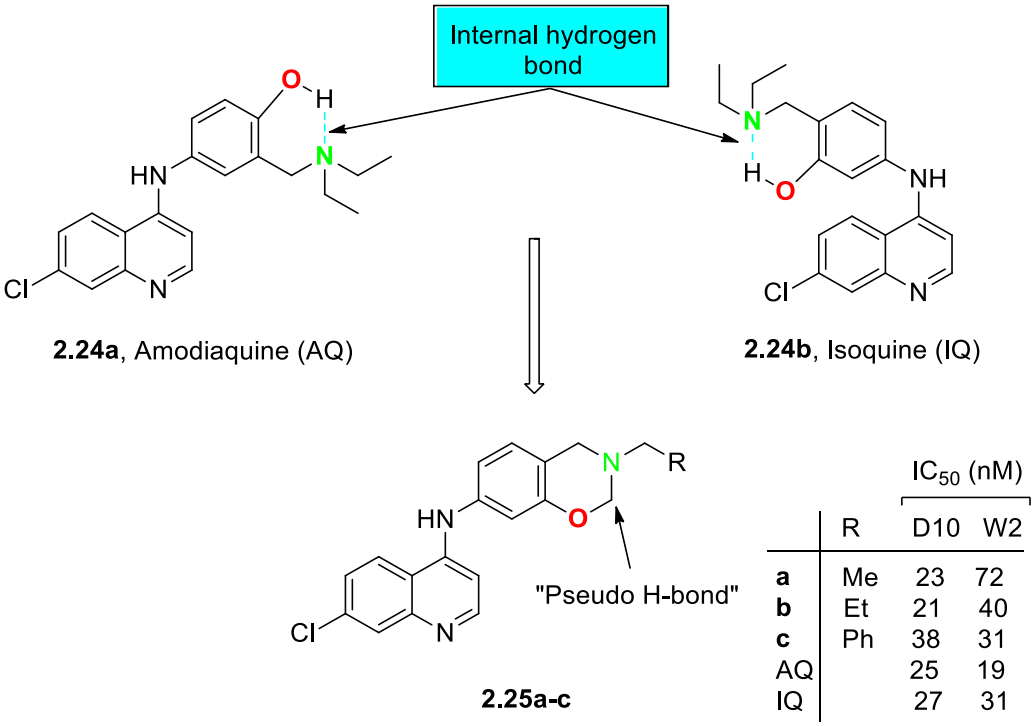

Figure 2.3 Design of the internal hydrogen bond mimicking 4-aminoquinolinyl benzoxazine compounds possessing potent antimalarial activity.

Recently, Sharma et al. derivatized bioactive phytophenols, eugenol (**2.26a**) and isoeugenol (**2.26b**) into their corresponding 1,3-benzoxazine analogues **2.27a-b** with 2-furanmethylamine and formaldehyde via the Mannich-type Burke condensation (**Scheme 2.4**).[13b] The resultant eugenyl- and isoeugenyl-benzoxazine derivatives showed IC_{50} values of 22.0 and 17.54 µM when assessed for potential antimalarial activity against the 3D7 *P. falciparum* strain, respectively. Additionally, the antimalarial activity of these compounds was attributed to the perturbation of sodium homeostasis and mitochondrial depolarisation of the *P. falciparum* parasite by binding to the plasma membrane P-type cation translocating ATPase protein

(*Pf*ATP4) responsible for the regulation of sodium ions in the parasite, which is an established antimalarial target.[15] Although not extensively studied, the above studies demonstrate the promising pharmacological significance of 1,3-benzoxazines in malaria research.

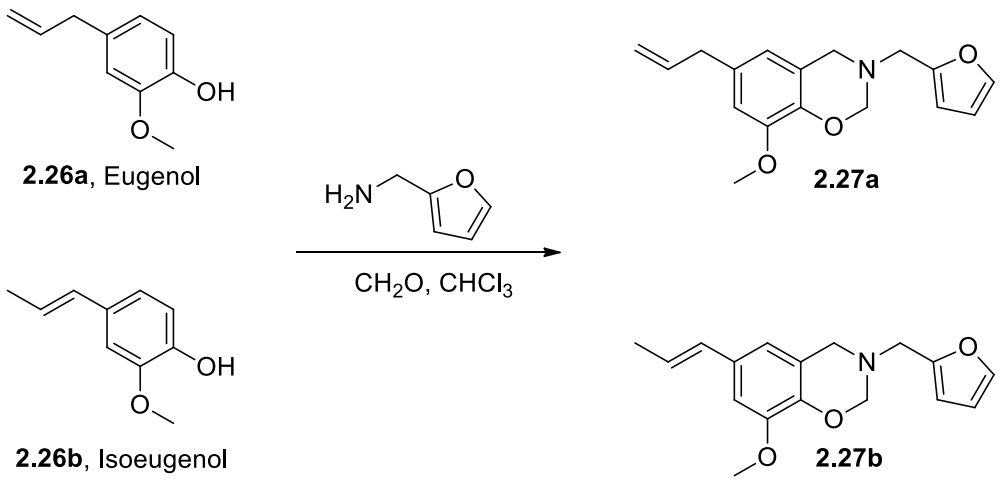

Scheme 2.4 Synthesis of antimalarial benzoxazine analogues of phytophenols, eugenol and isoeugenol.

2.1.3. Antibacterial activity of benzoxazines

The benzoxazine framework is a versatile template for the design of bioactive compounds with wide spectrum of biological activities. Besides the anticancer and antimalarial efficacy as previously described, benzoxazines have also been demonstrated to be active against a variety of bacterial strains including *Mycobacterium tuberculosis*, which is responsible for causing tuberculosis (TB). In fact, early 1,3-benzoxazines were originally studied for antituberculotic activity.[4] Examples of simple 1,3-benzoxazines possessing antibacterial activity are shown in **Figure 2.4**.[2c,16] The relevance of the benzoxazine scaffold in the treatment of bacterial infections is attested by the clinical fluoroquinolone-type antibiotics, ofloxacin (**2.33**) and pazufloxacin (**2.34**), featuring the 1,4-benzoxazine framework grafted in positions N1 and C8 of the quinolone nucleus.[17]

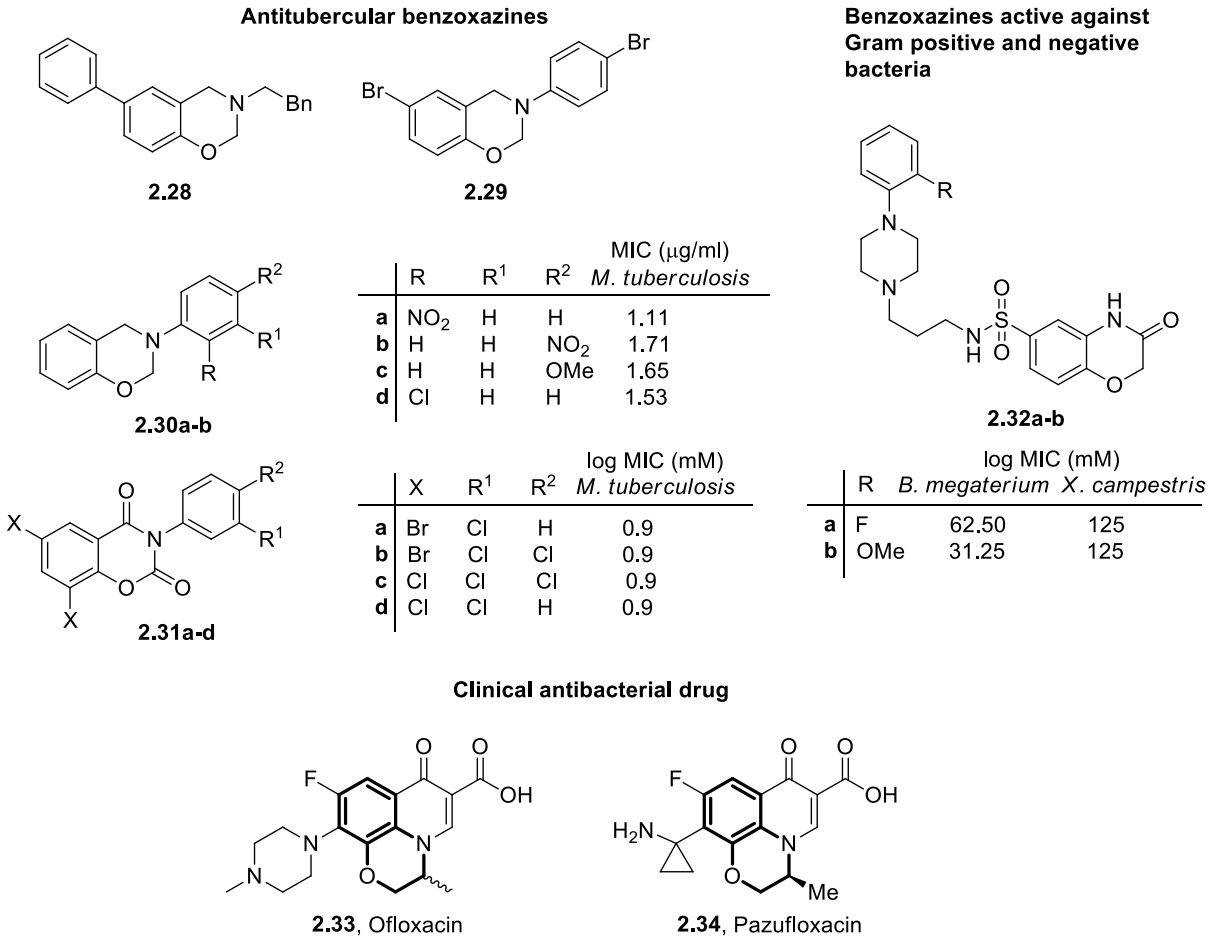

	R	R^1	R^2	MIC (μg/ml) *M. tuberculosis*
a	NO_2	H	H	1.11
b	H	H	NO_2	1.71
c	H	H	OMe	1.65
d	Cl	H	H	1.53

	X	R^1	R^2	log MIC (mM) *M. tuberculosis*
a	Br	Cl	H	0.9
b	Br	Cl	Cl	0.9
c	Cl	Cl	Cl	0.9
d	Cl	Cl	H	0.9

	R	log MIC (mM) *B. megaterium*	*X. campestris*
a	F	62.50	125
b	OMe	31.25	125

Figure 2.4 Structures of benzoxazine derivatives possessing antibacterial activity.

2.1.4. Antifungal activity of benzoxazines

By combining the coumarin and 2-oxopyridine moieties with the benzoxazine motif, the research groups of Zhang and Desai synthesized novel classes of benzoxazine derivatives showing inhibitory activity against a variety of fungal strains.[18] The above studies were inspired by the antifungal activities of the coumarin- and 2-oxopyridine-based compounds like osthol (**2.35**) and ciclopirox (**2.36**), respectively.[19] Using drug hybridization strategies, the benzoxazine unit was conjugated to the coumarin and 2-oxopyridine templates to generate novel 1,3-benzoxazine analogues with enhanced antifungal activities. Compounds **2.35a-c** and **2.36a-c** exhibited the most promising activity against the tested fungal strains (**Figure 2.5**).

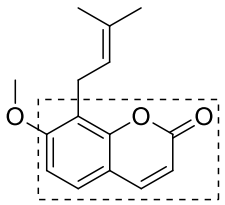

2.35, Osthol

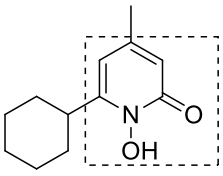

2.36, Ciclopirox

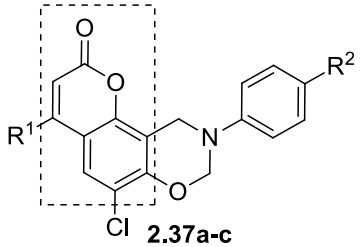

2.37a-c

			MIC (μg/ml)	
	R^1	R^2	*B. cinrea*	*R. solani*
a	Me	H	16	65
b	NMe_2	NMe_2	2.1	2.1
c	H	OMe	3.0	n.d.

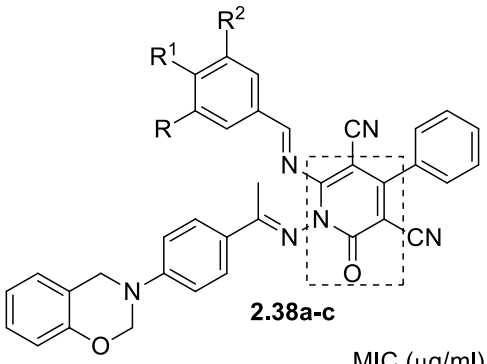

2.38a-c

				MIC (μg/ml)	
	R	R^1	R^2	*A. niger*	*A. clavatus*
a	OMe	OMe	OMe	50	50
b	NMe_2	NMe_2	NMe_2	100	25
c	H	OMe	H	25	100

Figure 2.5 Chemical structures of benzoxazine-containing compounds **2.37a-c** and **2.38a-c** based on coumarin (**2.35**) and 2-oxopyridine (**2.36**) showing antifungal activities.

2.2. Non-pharmacological application of benzoxazines: Polymer synthesis

The benzoxazine skeleton forms a class of versatile heterocyclic compounds owing to their appealing physicochemical properties. Besides the medicinal attributes of benzoxazine scaffold, compounds belonging to the 1,3-benzoxazine class have been extensively applied in the fabrication of polymers, known as polybenzoxazines.[1,3] The chemically labile nature of the O-CH_2-N connection in the oxazine unit allows polymerization of the 1,3-benzoxazines via thermal cationic ring-opening as illustrated in **Scheme 3.5**.[20] Polymerisation between benzoxazine monomers occurs between the activated methylene of the O-CH_2-N oxazine linkage and the unsubstituted C8 of the benzene ring of the 1,3-benzoxazine scaffold.[20] For this reason, only derivatives belonging to the 1,3-benzoxazine class are amenable to polymerisation as they are the only group fitting this structural criterion.[3]

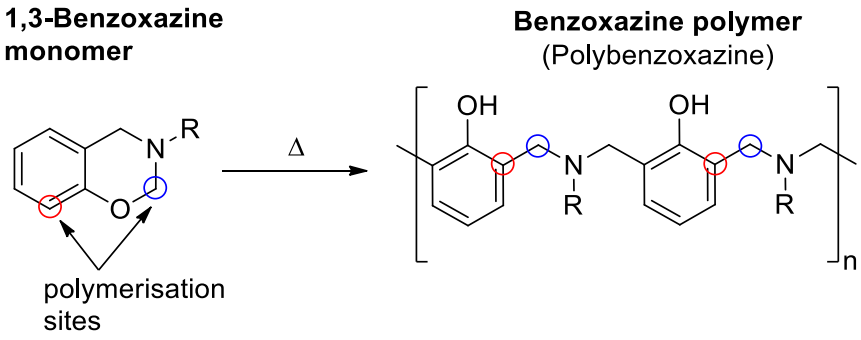

Scheme 2.5 Fabrication of polymers from 1,3-benzoxazines as monomers.

Polybenzoxazines possess superior physical, mechanical, chemical and electrochemical attributes, which have rendered them vital in many industrial applications, such as electronic and aerospace sectors.[21] These properties can be fine-tuned by introducing various functional groups into the benzoxazine monomers or already formed polybenzoxazine to elicit the desired characteristics.

Due to the chemical and physical stability and heat retardance of the organometallic unit, ferrocene, 1,3-benzoxazine derivatives bearing this unit in position 3 have been synthesized by the research group of Jia to attain polymers possessing high mechanical rigidity and thermal stability as exemplified in **Scheme 2.6**.[22] The synthesized ferrocenyl polybenzoxazines had lower ring-opening temperatures and exhibited improved thermal stability and storage capacity than the typical organic counterparts, which was attributed to the electronic effects of ferrocene. Additionally, these ferrocenyl benzoxazines displayed reversible redox behaviour similar to ferrocene-containing compounds.

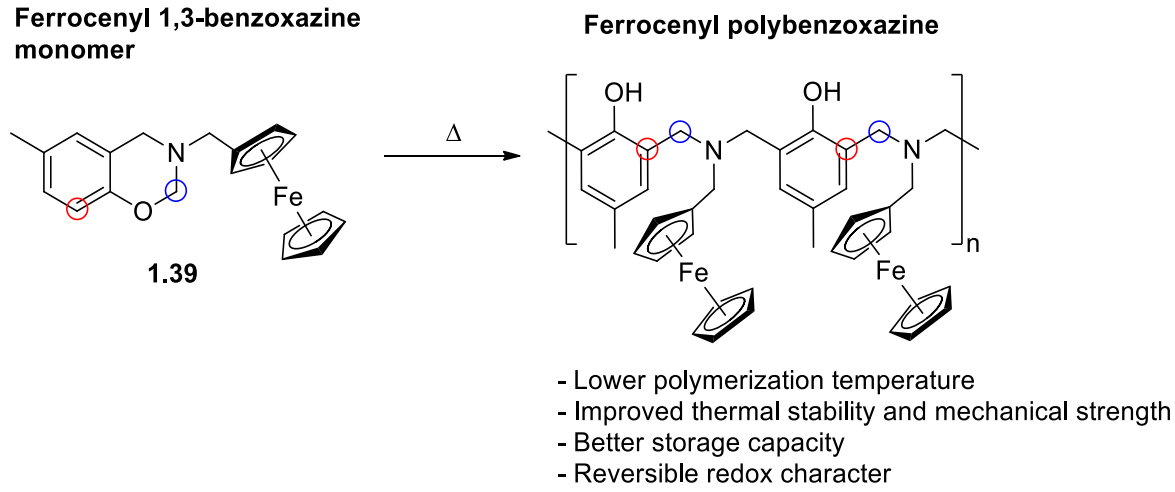

Scheme 2.6 Example of a ferrocene-based polybenzoxazine assembled from a ferrocenyl 1,3-benzoxazine monomer.

2.3. Aims and objectives of the current study

Ever since the discovery of polybenzoxazines and their remarkable qualities, research involving 1,3-benzoxazines for polymer applications has received high priority over their medicinal investigation.[3,23] Additionally, only two accounts of ferrocenyl 1,3-benzoxazines are reported in literature for polymer applications.[22] Considering these observations and the biological activity of the 1,3-benzoxazine scaffold together with the benefits of incorporating ferrocene into bioactive chemical scaffolds as demonstrated above and in **Chapter 1**, the current study explores the pharmaceutical potential of the ferrocenyl 1,3-benzoxazine derivatives, which have so far only been investigated for polymer applications. Thus, the aims and objectives of the current study are described below.

Overall aim:

The underlying question of the current research is to investigate whether it is possible to generate a focused library of biologically active compounds employing scaffold repurposing and molecular hybridization approaches by conjugating the ferrocene unit into the 1,3-

benzoxazine framework. Thus, the overall aim of the research project is to investigate the pharmaceutical potential of 1,3-benzoxazine derivatives containing the ferrocene unit.

Specific objectives:

(i) To synthesize and determine the structural identity of ferrocenyl 1,3-benzoxazine derivatives using relevant spectroscopic characterization techniques.

(ii) To pharmacologically evaluate the target ferrocenyl 1,3-benzoxazine compounds for potential *in vitro* anticancer and antiparasitic activity against the HCC70 triple-negative breast cancer cell line and selected strains of the malaria parasite, *P. falciparum*, and causative agent of African sleeping sickness, *T. b. brucei*.

(iii) To probe the possible mode of action of the active compounds employing appropriate biochemical assays and computer-aided ligand docking simulations.

References

(1) Ishida, H. In *Handbook of Benzoxazine Resins*; Ishida, H., Agag, T., Eds.; Elsevier: Amsterdam, 2011.

(2) (a) Urbański, T.; Radzikowski, C.; Ledochowski, Z.; Czarnocki, W. *Nature* **1956**, *178*, 1351; (b) March, L.; Romanchick, W.; Bajwa, G.; Joullie, M. *J. Med. Chem.* **1973**, *16*, 337; (c) Konda, S.; Raparthi, S.; Bhaskar, K.; Munaganti, R. K.; Guguloth, V.; Nagarapu, L.; Akkewar, D. M. *Bioorg. Med. Chem. Lett.* **2015**, *25*, 1643.

(3) Kiskan, B. *React. Funct. Polym.* **2018**, *129*, 76.

(4) Urbański, T.; Gürne, D.; Eckstein, Z.; ŚLopek, S. *Bull. Acad. Polon. Sci. Cl* **1955**, *3*, 397.

(5) Burke, W. *J. Am. Chem. Soc.* **1949**, *71*, 609.

(6) Urbański, T.; Gürne, D.; Šlopek, S.; Mordarska, H.; Mordarski, M. *Nature* **1960**, *187*, 426.

(7) Kuehne, M.; Konopka, E.; Lambert, B. *J. Med. Chem.* **1962**, *5*, 281.

(8) Garg, V.; Kumar, A.; Chaudhary, A.; Agrawal, S.; Tomar, P.; Sreenivasan, K. *Med. Chem. Res.* **2013**, *22*, 5256.

(9) (a) Uchida, I.; Takase, S.; Kayakiri, H.; Kiyoto, S.; Hashimoto, M.; Tada, T.; Koda, S.; Morimoto, Y. *J. Am. Chem. Soc.* **1987**, *109*, 4108; (b) Shimomura, K.; Hirai, O.; Mizota, T.; Matsumoto, S.; Mori, J.; Shibayama, F.; Kikuchi, H. *J. Antibiot.* **1987**, *40*, 600.

(10) Bollu, R.; Palem, J. D.; Bantu, R.; Guguloth, V.; Nagarapu, L.; Polepalli, S.; Jain, N. *Eur. J. Med. Chem.* **2015**, *89*, 138.

(11) Bharathkumar, H.; Mohan, C. D.; Rangappa, S.; Kang, T.; Keerthy, H.; Fuchs, J. E.; Kwon, N. H.; Bender, A.; Kim, S.; Rangappa, K. S. *Org. Biomol. Chem.* **2015**, *13*, 9381.

(12) Bajwa, G. S.; Hartman, K. E.; Joullie, M. M. *J. Med. Chem.* **1973**, *16*, 134.

(13) (a) Gemma, S.; Camodeca, C.; Brindisi, M.; Brogi, S.; Kukreja, G.; Kunjir, S.; Gabellieri, E.; Lucantoni, L.; Habluetzel, A.; Taramelli, D. *J. Med. Chem.* **2012**, *55*, 10387; (b) Sharma, V.; Amarnath, N.; Shukla, S.; Ayana, R.; Kumar, N.; Yadav, N.; Kannan, D.; Sehrawat, S.; Pati, S.; Lochab, B. *Bioorg. Med. Chem. Lett.* **2018**, *28*, 1629.

(14) Duffin, W.; Rollo, I. *Br. J. Pharmacol.* **1957**, *12*, 171.

(15) Spillman, N. J.; Kirk, K. *Int. J. Parasitol. Drugs Drug Resist.* **2015**, *5*, 149.

(16) (a) Chylińska, J.; Janowiec, M.; Urbański, T. *Br. J. Pharmacol.* **1971**, *43*, 649; (b) Waisser, K.; Hladuvková, J.; Gregor, J.; Rada, T.; Kubicová, L.; Klimešová, V.; Kaustová, J. *Arch. Pharm.* **1998**, *331*, 3; (c) Kamble, R. D.; Hese, S. V.; Meshram, R. J.; Kote, J. R.; Gacche, R. N.; Dawane, B. S. *Med. Chem. Res.* **2015**, *24*, 1077.

(17) Proudfoot, J. R. In *Analogue-based Drug Discovery*; Fischer, J., Ganellin, C. R., Eds.; WILEY-VCH Verlag GmbH & Co. KGaA: Weinheim, 2006.

(18) (a) Desai, N.; Bhatt, N.; Joshi, S. B.; Vaja, D. V. *Synth. Commun.* **2017**, *47*, 2360; (b) Zhang, M.-Z.; Zhang, R.-R.; Yin, W.-Z.; Yu, X.; Zhang, Y.-L.; Liu, P.; Gu, Y.-C.; Zhang, W.-H. *Mol. Divers.* **2016**, *20*, 611.

(19) Shi, Z.; Wang, F.; Zhou, W.; Zhang, P.; Fan, Y. *Int. J. Mol. Sci.* **2007**, *8*, 1001.

(20) Hamerton, I.; McNamara, L. T.; Howlin, B. J.; Smith, P. A.; Cross, P.; Ward, S. *Macromolecules* **2013**, *46*, 5117.

(21) (a) Kiskan, B.; Ghosh, N. N.; Yagci, Y. *Polym. Int.* **2011**, *60*, 167; (b) Rimdusit, S.; Ishida, H. *Polymer* **2000**, *41*, 7941; (c) Ruilian, L. W. S. S. Y.; Zhihai, Y. C. F. *Aerospace Mater. Technol.* **2004**, *2*, 003.

(22) (a) Li, W.; Wei, T.; Gao, Y.; Xi, K.; Jia, X. *Polymer* **2012**, *53*, 1236; (b) Li, W.; Chu, J.; Heng, L.; Wei, T.; Gu, J.; Xi, K.; Jia, X. *Polymer* **2013**, *54*, 4909.

(23) Kiskan, B.; Yagci, Y. In *Thermosets: Structure, Properties, and Applications*; 2 ed.; Guo, Q., Ed.; Elsevier, 2018.

Chapter 3: Design, synthesis, characterization and biological evaluation of ferrocenyl 3,4-dihydro-2*H*-1,3-benzoxazine derivatives

This chapter presents the synthesis and characterization of ferrocenyl 3,4-dihydro-2*H*-1,3-benzoxazine derivatives using various characterization techniques. In line with the aims and objectives of the current study, the targeted compounds were investigated for potential *in vitro* anticancer, antimalarial and antitrypanosomiasis activity using the HCC70 triple-negative breast cancer cell line and strains of the malaria parasite, *Plasmodium falciparum*, and the causative agent of trypanosomiasis, *Trypanosoma brucei brucei*, respectively.

3.1. Rationale

As of the writing of the thesis, only two accounts of ferrocenyl 1,3-benzoxazines had been reported in literature for the fabrication of polymers, i.e. ferrocenyl polybenzoxazines.[1] Despite the appealing pharmaceutical potential of the 3,4-dihydro-2*H*-1,3-benzoxazine scaffold and the beneficial medicinal attributes of ferrocene, the biological activity of compounds featuring these two structural units remains unexplored. Given the appeal of drug design strategies such as the repurposing of established scaffolds for new biological applications and the incorporation of ferrocene into bioactive motifs, we hypothesized that 3,4-dihydro-2*H*-1,3-benzoxazine compounds bearing the organometallic ferrocene unit in position 3 would elicit beneficial biological activity. Thus, this chapter explores the medicinal potential of ferrocenyl 1,3-benzoxazine derivatives assembled by facile synthetic methods.

3.2. Synthesis of ferrocenyl 3,4-dihydro-2*H*-1,3-benzoxazines

The simplicity of the 3,4-dihydro-2*H*-1,3-benzoxazine scaffold allows straightforward access to the target compounds. Synthesis of 3,4-dihydro-2*H*-1,3-benzoxazine is predominantly performed via two synthetic protocols: i) the three-component, one-pot Mannich-type Burke condensation and ii) stepwise reductive amination of salicyaldehydes (**3.5**) followed by cyclization of the resultant salicylamine intermediates (**3.6**) with formaldehyde (**3.3**) (**Scheme 3.1**).[2]

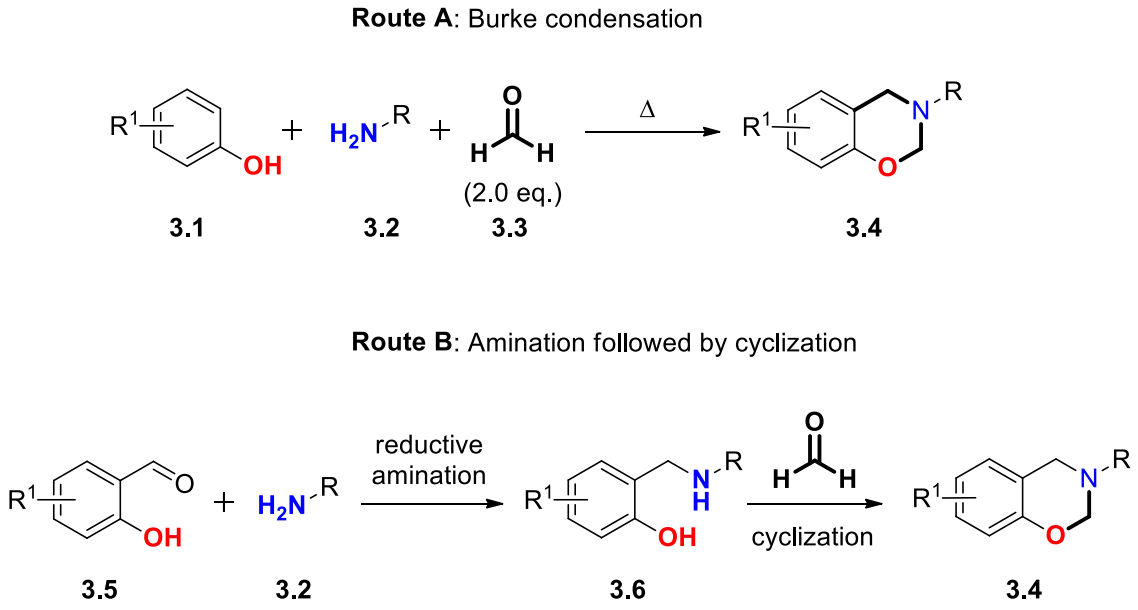

Scheme 3.1 Common synthetic routes for accessing 3,4-dihydro-2*H*-1,3-benzoxazines.

Each method has its own merits and applicability depending on the nature of substrates used and the desired 1,3-benzoxazine product. By refluxing phenols (**3.1**) and primary amines (**3.2**) in the presence of two equivalents of formaldehyde (**3.3**), the classical Burke condensation offers an expedient, single step route to the benzoxazine product (**3.4**) in high yields and purity with only a simple workup of washing with dilute sodium hydroxide solution.[2a] However, the method has limited substrate scope as some starting materials may not be compatible with the reaction conditions of the procedure.[2b] For example, the reaction of phenolic amines under

Burke conditions leads to polymerization or gelation of substrates instead of the target benzoxazine product.[2b] This challenge is not an issue with the stepwise reductive amination route.[2c] Despite the ability to produce benzoxazines from substrates that are not compatible with the Burke procedure, another advantage of the second method is ability to access unsymmetrical benzoxazine products in high yields from suitable salicyaldehydes (**3.5**).[2b,3] The major drawback of the stepwise procedure is the number of steps required to get to the final compound, which may slow down the expediency of the synthesis. Thus, despite the limited substrate scope, the classical Burke protocol is usually preferred for synthesis of benzoxazines due to its simplicity.

Alternative methods to the synthetic routes described above for the synthesis of 1,3-benzoxazines are reported in literature. Katritzky and co-workers reported alternative approach for the synthesis of 3,4-dihydro-2*H*-1,3-benzoxazines involving activation by *ortho*-lithiation of a phenol followed by cyclization of the dilithiated intermediate (**3.7**) with *N,N*-bis[(benzotriazol-1-yl)methyl]amine (**3.8**) (**Scheme 3.2**).[4] Similar to the stepwise reductive amination route above, this method also allows synthesis of unsymmetrical benzoxazine products by selecting appropriate substrates. However, the procedure was found to give poor product yields compared to the classical Burke protocol.

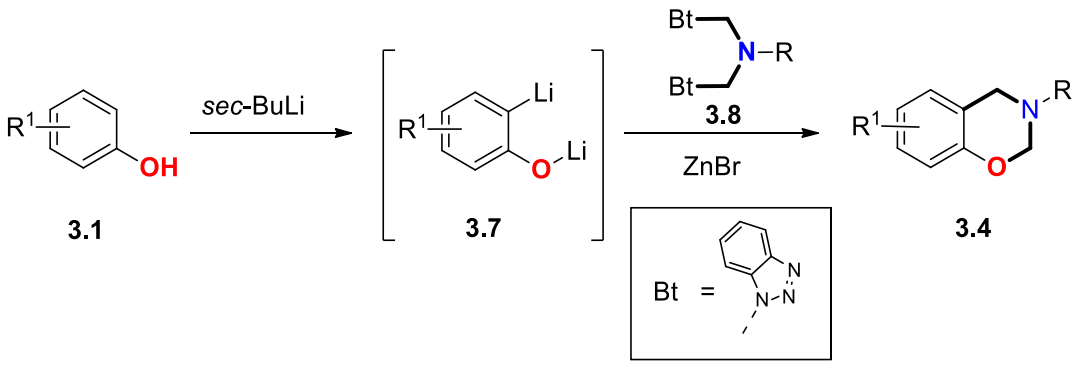

Scheme 3.2 Synthesis of 1,3-benzoxazines via *ortho*-lithiation of phenols.

Ishida and colleagues described a stepwise synthesis of 1,3-benzoxazines from triazines and phenols. In this method, a triazine is first prepared by reacting a primary amine (**3.2**) and formaldehyde (**3.3**) in 1:1 ratio which is then treated with a phenol (**3.1**) at high temperatures to furnish the desired 1,3-benzoxazine product (**Scheme 3.3**).[5] The number of steps in this procedure makes it unattractive to use for facile synthesis of 1,3-benzoxazine compounds.

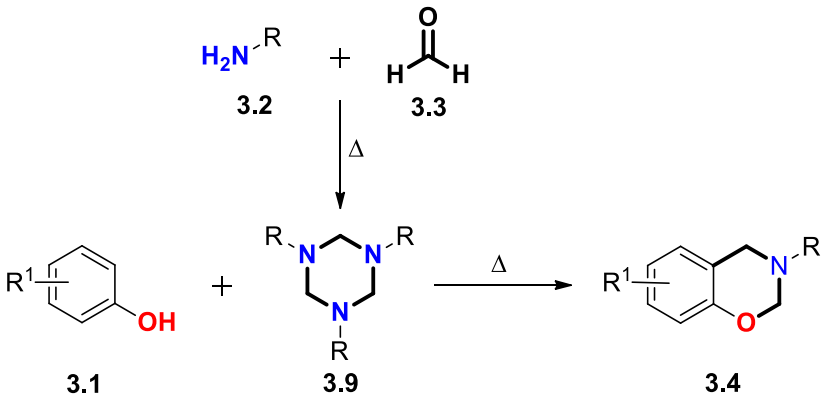

Scheme 3.3 Synthesis of 1,3-benzoxazines from triazines.

3.2.1. Synthesis and characterization of ferrocenyl 3,4-dihydro-2*H*-1,3-benzoxazine derivatives

The classical Burke protocol offers many advantages for the synthesis of 3,4-dihydro-2*H*-1,3-benzoxazines. This multi-component reaction protocol couples all three starting materials, i.e. phenol, primary amine and formaldehyde, in 1:1:2 ratio into the final compound in a single step by reflux. The product is achieved within hours in good yields, usually with no additional purification steps required. Thus, the target compounds were prepared following the Burke protocol with appropriate phenolic substrates and ferrocenyl amines.

Initially, simplified ferrocenyl 1,3-benzoxazines resembling compound **3.13b** (see **Scheme 3.7** ahead) reported in literature for polymer applications were prioritized for synthesis.[1b] The phenolic substrates required in the reaction to form the target products were readily available.

However, ferrocenyl methylamine **3.12a** was prepared from commercially available ferrocene carboxaldehyde **3.10a**. Ferrocene carboxaldehyde **3.10a** was converted into its oxime variant **3.11a** by refluxing with hydroxylamine, which was followed by reduction with $LiAlH_4$ to furnish the desired amine **3.12a** as a brown viscous oil in 85% yield under a nitrogen atmosphere (**Scheme 3.4**).[6]

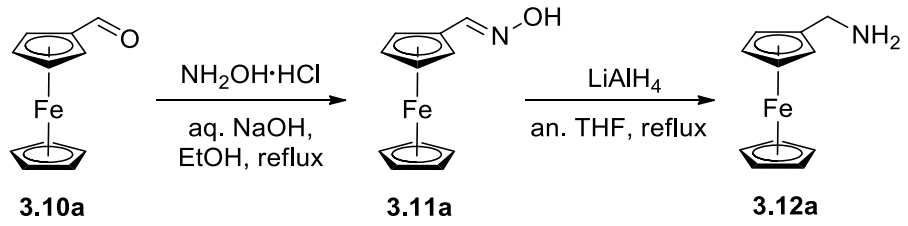

Scheme 3.4 Synthesis of ferrocene methylamine from carboxaldehyde **3.12a**.

With the ferrocenyl amine **3.12a** at hand, the Burke protocol was utilized to synthesize the target benzoxazine derivatives.[2a] In an initial attempt, the original procedure reported by Burke in 1949 was followed unmodified by refluxing equimolar amounts of unsubstituted phenol **3.1a** with amine **3.3a** in the presence of two equivalents of the formaldehyde solution in 1,4-dioxane (**Scheme 3.5**).[2a] The progress of the reaction was monitored by thin-layer chromatography (TLC). To our disappointment, the TLC revealed noticeable formation of the product only after 5 hours of reflux in small amounts as judged by the intensity of the newly formed spot. The reaction was left to reflux for another 5 hours at which time no significant change in the intensity of the spot was observed.

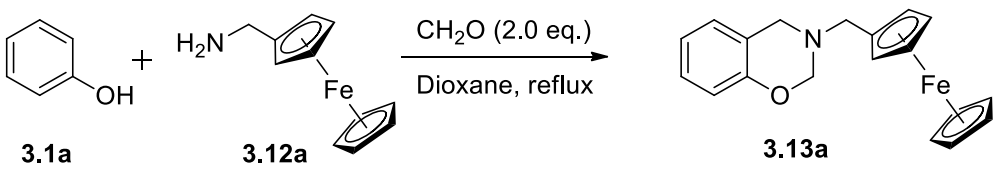

Scheme 3.5 Synthesis of ferrocenyl 1,3-benzoxazine **3.13a** via unmodified Burke protocol.

The reaction was terminated after 48 hours following checking of the reaction progress with TLC, which suggested improved the formation of the product but with the spots of the starting materials still visible. Extraction of the product with chloroform ($CHCl_3$) and successive washing with 1N NaOH solution and brine only removed the phenol, leaving the product in the organic phase. Thus, the crude product was purified by silica gel column chromatography to furnish the pure benzoxazine compound **3.13a** in a yield of 30%.

The structural identity of compound **3.13a** was confirmed by spectroscopic techniques: proton and carbon-13 nuclear magnetic resonance (^1H and ^{13}C NMR), infra-red (IR) and high-resolution mass spectroscopy (HRMS). From the ^1H NMR spectrum of **3.13a**, the distinctive oxazine methylene protons of the benzoxazine scaffold were observed at δ 4.84 ppm (H-2) and δ 3.99 ppm (H-4) as broad singlets while the signals for the benzene ring and the ferrocene unit appeared in the typical regions with those of ferrocene being upfield of those for the benzene ring (**Figure 3.1**).[1b] Furthermore, the methylene oxazines were confirmed by the DEPT-135 NMR spectrum, which revealed two oxazine methylene carbon signals and the ferrocenyl CH_2 (C-3′) with chemical shifts similarly observed by Li et al. for a ferrocenyl 1,3-benzoxazine compound synthesized for polymer applications.[1b] These data suggested that compound **3.13a** was successfully synthesized using the classical Burke protocol. Despite producing the desired compound in good purity with a less laborious workup, the low product yields and long reaction times of the procedure were not ideal for the synthesis of the remainder of the ferrocenyl 1,3-benzoxazine derivatives.

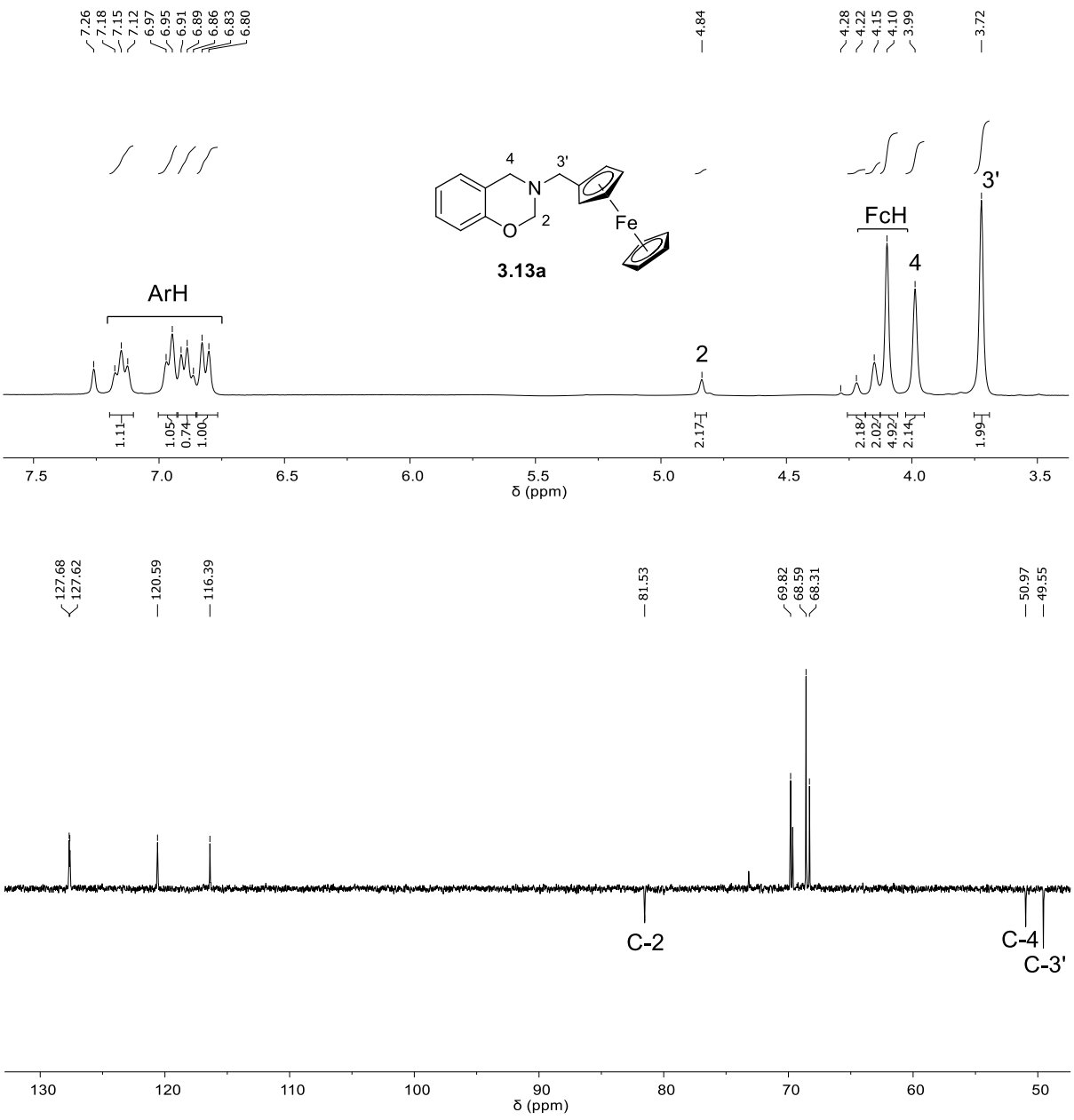

Figure 3.1 ^{1}H and DEPT-135 NMR spectra of compound **3.13a** in $CDCl_3$.

In efforts to improve the product yields of the reaction, the influence of the solvent on the formation of the product and reaction times was investigated. Protic solvents, methanol (MeOH), ethanol (EtOH) and propanol (*n*-PrOH), and aprotic solvents; tetrahydrofuran (THF), toluene and $CHCl_3$, were employed in the investigations. In the solvent optimization study, the substrates were reacted in similar equivalents as the classical Burke protocol and 1,4-dioxane was replaced with the solvents above. The formaldehyde solution was replaced with solid

paraformaldehyde ($(CH_2O)_n$) to push the reaction equilibrium forward by minimizing the presence of water in the reaction medium. Six reactions were run in parallel for a period of 48 hours monitoring the progress with TLC in five-hour intervals.

Observations similar to the classical Burke protocol were made for the alcoholic solvents MeOH, EtOH and *n*-PrOH. For all three solvents, the TLC plate showed only faint spots of the product after 5 hours of refluxing. Improvement in the formation of the product (TLC) was perceived at 10 hours, however, no significant changes were seen at the termination of the reaction after 48 hours. The resultant yields from MeOH, EtOH and *n*-PrOH were comparable to 1,4-dioxane with 18, 28 and 35%, respectively (**Table 3.1**). Aprotic solvents THF and toluene gave inferior results and product yields with respect to the protic solvents MeOH, EtOH and *n*-PrOH. In both cases, the presence of the product was only visible on the TLC after 20 hours of the reaction. Furthermore, unidentified side products (TLC) were noticed in the reaction with THF and toluene on termination of the reaction, which complicated the purification of products. The product yields are presented in **Table 3.1**. Chloroform emerged as the most desirable solvent from the study. Formation of the product with $CHCl_3$ was observed after 5 hours of the reaction with a significant improvement (intense TLC spot) at 10 hours and the product was obtained in 48% yield at end of the reaction (**Table 3.1**).

Table 3.1 Yields of the solvent optimization study for the synthesis of **3.13a**.

Solvent	Yield (%)
1,4-Dioxane	30
MeOH	18
EtOH	25
n-PrOH	35
THF	12
Toluene	20
$CHCl_3$	48

Having identified $CHCl_3$ as a promising solvent from the solvent optimization study, the next step was to shorten the reaction times. There was no significant change in the TLC spot intensity of the product between 10 and 48 hours with $CHCl_3$ during solvent optimization studies. Based on this observation, the reaction was repeated with $CHCl_3$ and terminated after 10 hours. A product yield of 45% was attained, which was comparable to the yield obtained when the reaction was ran for 48 hours. Thus, it was decided to synthesize the remaining compounds using $CHCl_3$ conditions, thereby reducing the reaction times to 10 hours.

At mechanistic level, the Burke protocol is a stepwise Mannich type-condensation mediated by the formation of an iminium ion intermediate formed from the primary amine and one equivalent of formaldehyde (**Scheme 3.6**).[7] The iminium ion intermediate reacts with the phenolic substrate via electrophilic aromatic substitution followed by ring-closure of the resultant salicylamine intermediate with a formaldehyde equivalent to produce the final benzoxazine product (**Scheme 3.6**).[7] Electronic aromatic substitution is an important reaction with wide applicability in organic synthesis. The mechanism of the reaction involves formation of an electrophile that replaces one of the aromatic hydrogen atoms. This process is facilitated by addition of a Lewis acid catalyst, which increases the reactivity of the electrophile and lowers the reaction times.[8] Based on this fact, we investigated the effect of adding Lewis acid catalysts to the reaction medium in an effort to improve the product yields and reaction times using $CHCl_3$ as a solvent.

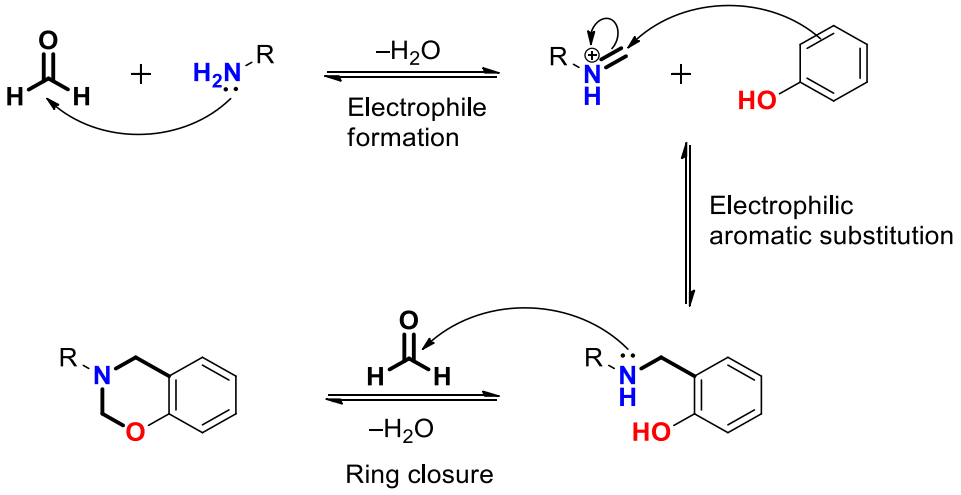

Scheme 3.6 Reaction mechanism of the formation of 1,3-benzoxazines.[7]

The acids that were investigated were aluminium trichloride ($AlCl_3$), iron chloride ($FeCl_3$) and *p*-toluenesulphonic acid (PTSA). Mole percent equivalents of 5, 10, 20, 30, and 50 mol % of each acid were employed in each reaction. To our disappointment, none of the investigated acids produced any beneficial effects on the reaction at the tested mole percent equivalents. Instead, a complex mixture of unedified products was immediately observed after one hour of refluxing (TCL). This not only complicated the purification process but also led to lower product yields (9 – 14%) than when no acid was added to the reaction solution. Consequently, it was decided that the remaining ferrocenyl 1,3-benzoxazine derivatives would be synthesized following the Burke protocol with $CHCl_3$ as the solvent.

To access the target benzoxazine compounds, phenols **3.1b-i** with suitable substituents were refluxed with ferrocenyl amine **3.12a** and paraformaldehyde in 1:1:2 ratio in $CHCl_3$. The synthesis was limited to phenolic substrates substituted in the *meta* and *para* positions (**Scheme 3.7**). To allow facile access to the target compounds, the reactions were refluxed for 10 hours based on the previous test run for synthesis of **3.13a** with $CHCl_3$ as a solvent. The workup and purification of the products were performed as described for the synthesis of **3.13a** above. The reaction of the *para* phenolic substrates (**3.1b-f**) exclusively furnished 6-substituted

benzoxazine products (**3.13b-f**), whereas the *meta* phenols (**3.1g-i**) afforded 7-functionalized products (**3.13h-i**) in yield ranging between 19 and 66% along with their corresponding 5-substituted counterparts (**3.13j-k**) as minor products (yields: 15 and 26%) (**Scheme 3.7**).

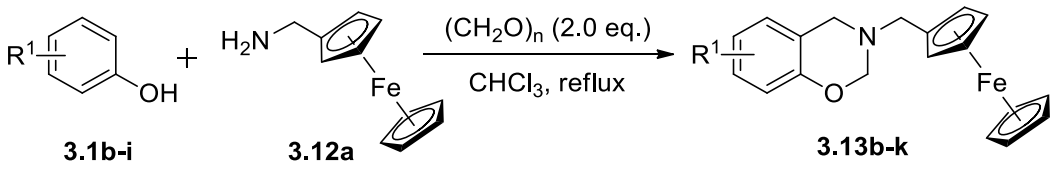

3.1b-i **3.12a** **3.13b-k**

	R^1	Isolated yield (%)
3.13b	6-Me	37
3.13c	6-Cl	66
3.13d	6-Br	37
3.13e	6-OMe	42
3.13f	6-NO_2	19
3.13g	7-Me	59
3.13h	7-Br	41
3.13i	7-F	56
3.13j	5-Br	26
3.13k	5-F	15

Scheme 3.7 Synthesis of functionalized ferrocenyl 1,3-benzoxazine derivatives **3.13a-k**.

Formation of two isomers was expected since the *meta*-functionalized phenols have two reaction sites at C-2 and C-6 in the *ortho* positions of the hydroxyl group, resulting in 5- and 7-isomeric products (**Scheme 3.8**). However, the reaction of 3-methylphenol (**3.1g**) with amine **3.12a** exclusively gave the 7-methyl benzoxazine product (**3.13g**) in 59% yield with no indication of the 5-methyl isomer.

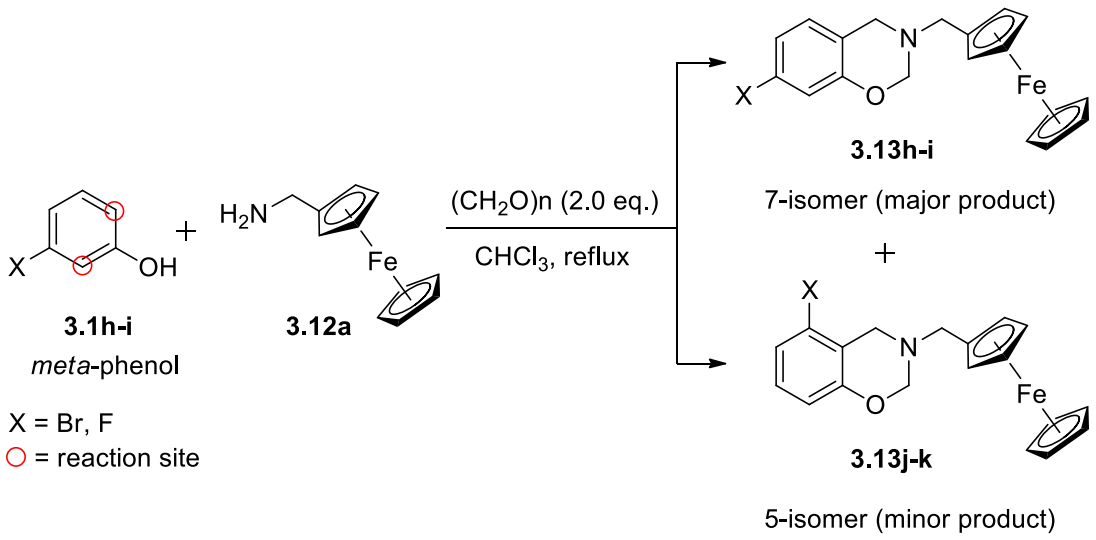

Scheme 3.8 Formation of 5- and 7-isomers from the reaction of *meta*-substituted phenols.

The structures of the synthesized compounds were confirmed by common spectroscopic techniques (NMR and HRMS) as was done for compound **3.13a**. In all instances, the characteristic oxazine methylene protons of the benzoxazine scaffold were observed around δ 4.80 (H-2) and δ 4.00 ppm (H-4) in the ^{1}H NMR spectra of the compounds as seen in literature, while the ferrocene (Fc) and benzene units appeared in their typical regions at δ 4.50 – 4.00 ppm and δ 8.00 – 6.50 ppm, respectively. The oxazine unit resonated around δ 81.5 ppm for C-2 and from δ 50.0 – 43.0 ppm for C-4 in the ^{13}C NMR spectra of the compounds. Compounds **3.13i** and **3.13k** contain a fluorine atom at C-7 and C-5, respectively. Since fluorine (^{19}F) has an odd nuclear spin (½) as a proton (^{1}H) and carbon (^{13}C), it couples with the neighbouring proton and carbon nuclei in a molecule, which is shown by the splitting of the proton and carbon signals in the ^{1}H and ^{13}C NMR spectra of a compound containing a fluorine atom, respectively.[9] Considering this fact, the 5-isomer of the fluorinated product was easily distinguished from its 7-congener (**3.13i**) by analysis of the C-4 signal of the oxazine ring in the ^{13}C NMR spectrum of **3.13k**. Due to the proximity the fluorine atom on C-5 to C-4, the signal of the carbon in position 4 of the benzoxazine scaffold was observed as a doublet with

a *J*-coupling constant of 3.7 Hz, typical of a three-bond $^{13}C - {}^{13}F$ coupling (**Figure 3.2**).[9a] This was not the case in the ^{13}C NMR spectrum of the 7-isomer **3.13i**.

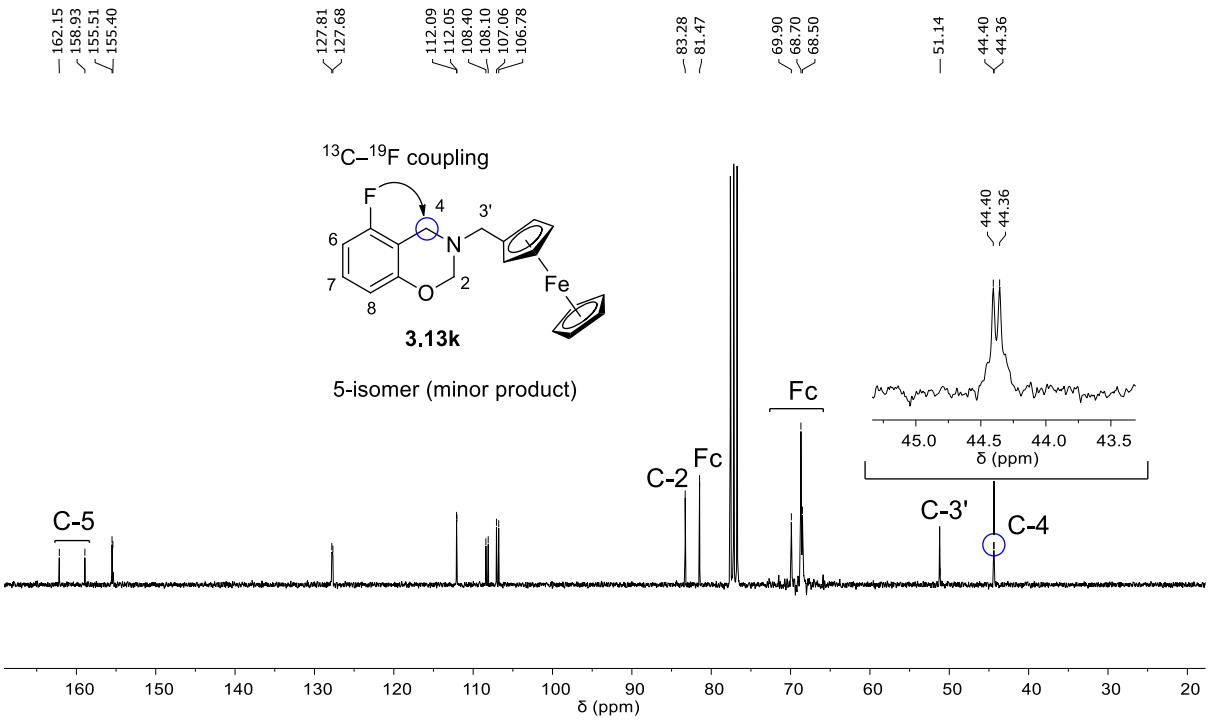

Figure 3.2 ^{13}C NMR spectrum of **3.13k** in $CDCl_3$.

The assignment of protons was achieved by multiplet analysis of proton signals in the ^{1}H NMR spectra of the compounds and two-dimensional NMR (2D NMR) techniques, as illustrated in **Figure 3.3** showing the HSQC NMR spectrum of compound **3.13k**.

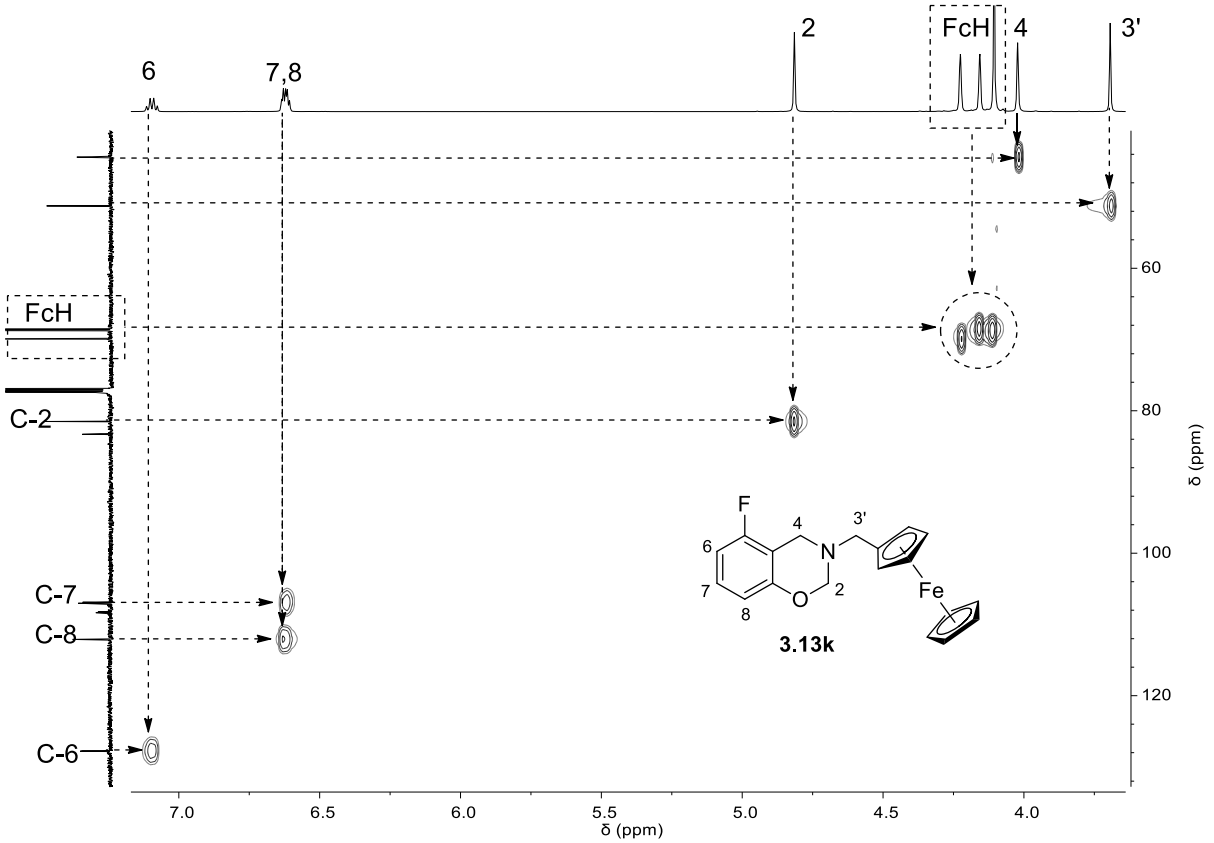

Figure 3.3 HSQC NMR spectrum of compound **3.13k** in $CDCl_3$.

The NMR data was corroborated by HRMS spectra of the compounds, which were acquired using the electrospray ionization (ESI) method set to the positive ionization mode. In all cases, the experimental mass of the compounds matched the predicted values. Data from HRMS are presented in **Table 3.2**.

Table 3.2 HRMS data of target compounds **3.13a-k**.

Compound	Calculated mass $[M]^+$	Observed mass $[M]^+$
3.13a	333.0816	333.0797
3.13b	347.0973	347.0950
3.13c	368.0426	368.0505
3.13d	410.9921	410.9891
3.13e	363.0922	363.0894
3.13f	379.0745[a]	379.0745[a]
3.13g	348.1051[a]	348.1051[a]
3.13h	410.9921	410.9889
3.13i	352.0800[a]	352.0800[a]
3.13j	411.9921[a]	411.9922[a]
3.13k	352.0800[a]	352.0800[a]

[a] Masses of the compounds were obtained as $[M+H]^+$ ions.

Having obtained and performed structural characterization of this novel series of ferrocenyl 1,3-benzoxazines carrying assorted electronic and structural substituents on the benzene ring and a plain ferrocene unit in moderate yields at appreciable reaction times, the next step in the study was to introduce modifications to the ferrocene unit while keeping the benzene substituents intact.

3.3. Modifications of the ferrocene unit

As per aims and objectives of the study, modifications of the ferrocene unit would allow comprehensive examination of the overall effects of the structural units on the biological activity of the investigated scaffold. Additionally, the reaction conditions for the formation of benzoxazine products had been optimized to permit expeditious synthesis. Thus, to simplify the synthetic route for the preparation of the next series of benzoxazine derivatives containing a modified ferrocene unit, ferrocenyl amines already carrying the desired functional groups were prepared separately and subjected to the optimized reaction conditions as amine **3.12a** for the synthesis of **3.13a-k**.

The choice of structural moieties to append to the ferrocene unit was inspired by the pioneering work of Biot and co-workers in which they reported a tailored series of chloroquine-ferrocene hybrid compounds as antiplasmodial compounds, which culminated in a phase II clinical candidate, ferroquine (**1.35**, FQ), for treatment of malaria.[6,10] In the study, the presence of the *N,N*-(dimethylamino)methyl (CH_2NMe_2) moiety in position 2 of the ferrocene unit was found to be conducive for the biological activity of the resulting compounds.[6] Additionally, this structural feature plays a crucial role in the antimalarial activity of FQ.[11] Mechanistically, it allows accumulation of the drug in the target site, i.e., the plasmodial digestive vacuole (DV), by forming an internal hydrogen bond with the quinolinyl NH at C-4 of protonated FQ (**3.14a**, FQ A) by the "hydrogen bond flip-flop" mechanism (**Figure 3.4**).[11] This causes the FQ molecule to assume a highly hydrophobic closed conformation (**3.14b**, FQ B) with strong affinity for the lipid structures in the DV, thus retaining the molecule in the active site for longer times.[11] Furthermore, studies such as the ones reported by the research groups of Smith and Blackie found this moiety to impart beneficial biological effects to ferrocenyl azines and phenylequine-type antiplasmodial compounds, respectively.[12]

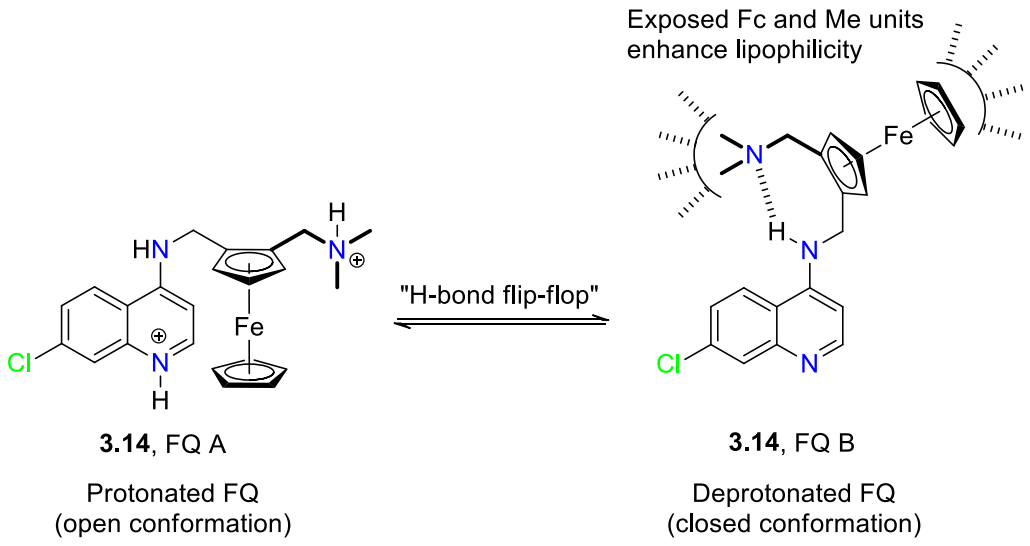

Figure 3.4 Role of the ferrocenyl CH_2NMe_2 moiety (bold) in the hydrogen bond flip-flop mechanism in ferroquine.[11]

3.3.1. Synthesis and characterization of 2-((*N*,*N*-dimethylamino)methyl)ferrocenemethyl-3,4-dihydro-2*H*-1,3-benzoxazines

Ferrocenyl amine **3.12b** bearing the CH_2NMe_2 motif in position 2 was synthesized from the commercially available *N,N*-dimethylaminomethylferrocene (**3.15a**) following literature methods (**Scheme 3.9**).[6,13] The *N,N*-dimethylaminomethylferrocene (**3.15a**) was formylated via *ortho*-lithiation with *tert*-butyllithium (*t*-LiBu) under nitrogen atmosphere followed by addition of anhydrous *N,N*-dimethylformamide (DMF) to furnish the corresponding ferrocene carboxaldehyde **3.10b** as a brown viscous oil in 85% yield.[13]

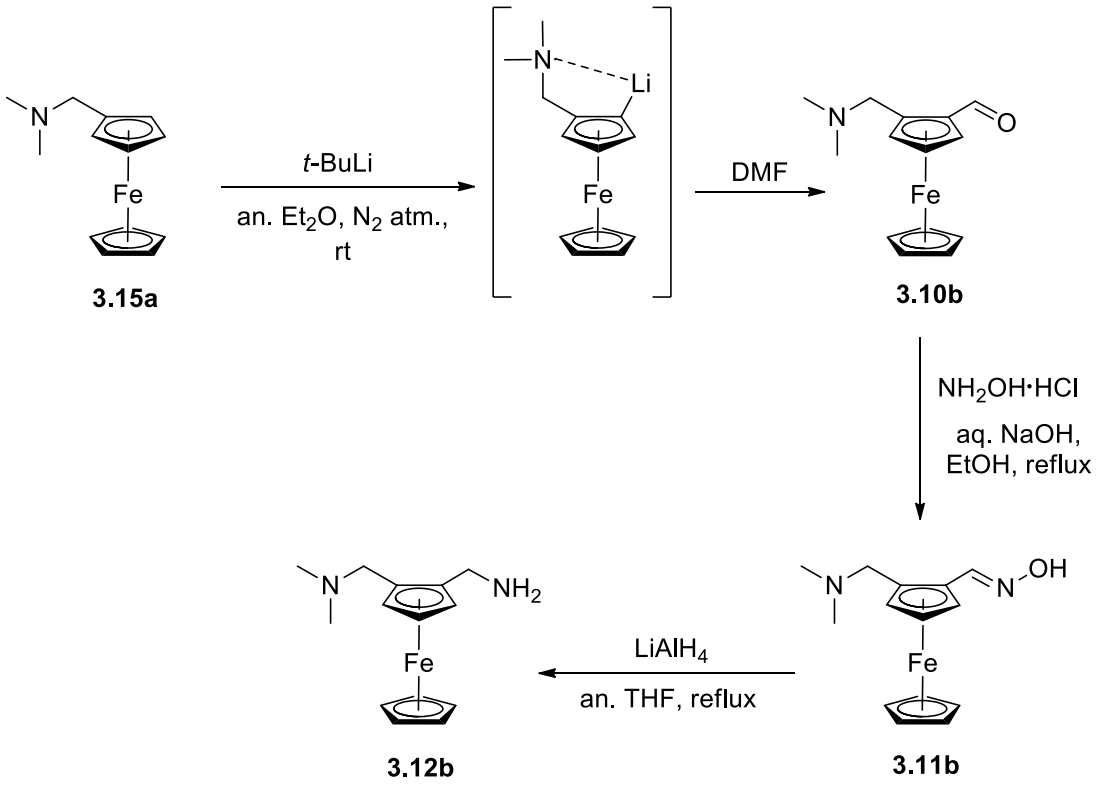

Scheme 3.9 Synthesis of *N,N*-dimethylaminomethylferrocene amine **3.12b**.

Formation of ferrocene carboxaldehyde **3.10b** was confirmed by the appearance of carbonyl signals in both ^1H and ^{13}C NMR spectra of the compound at δ 10.08 and 193.3 ppm, respectively (**Figure 3.5**), consistent with literature observations.[6] Interestingly, the splitting of

the diastereotopic methylene protons of the CH_2NMe_2 chain into two 1H doublets at δ 3.82 (1′a) and 3.53 (1′b) ppm with a *J*-coupling constant of 13.0 Hz was also observed in the ^1H NMR spectrum of **3.10b** (**Figure 3.5**), which is consistent with literature.[6] The splitting of the methylene protons is due to the fact that, like all 1,2-substitued metallocenes, ferrocene exhibits planar chirality.[14] Normally, methylene protons like 1′ in **3.10b** would appear as a 2H singlet in a non-chiral environment. However, because of the difference in the environments occupied by the top and bottom cyclopentadienyl (Cp) rings of ferrocene, one of the methylene protons (1′) in **3.10b** is in closer proximity to the iron centre than the other one.[15] Hence, these protons experience different magnetic fields resonating at different chemical shifts and couple with each other, i.e., geminal coupling.

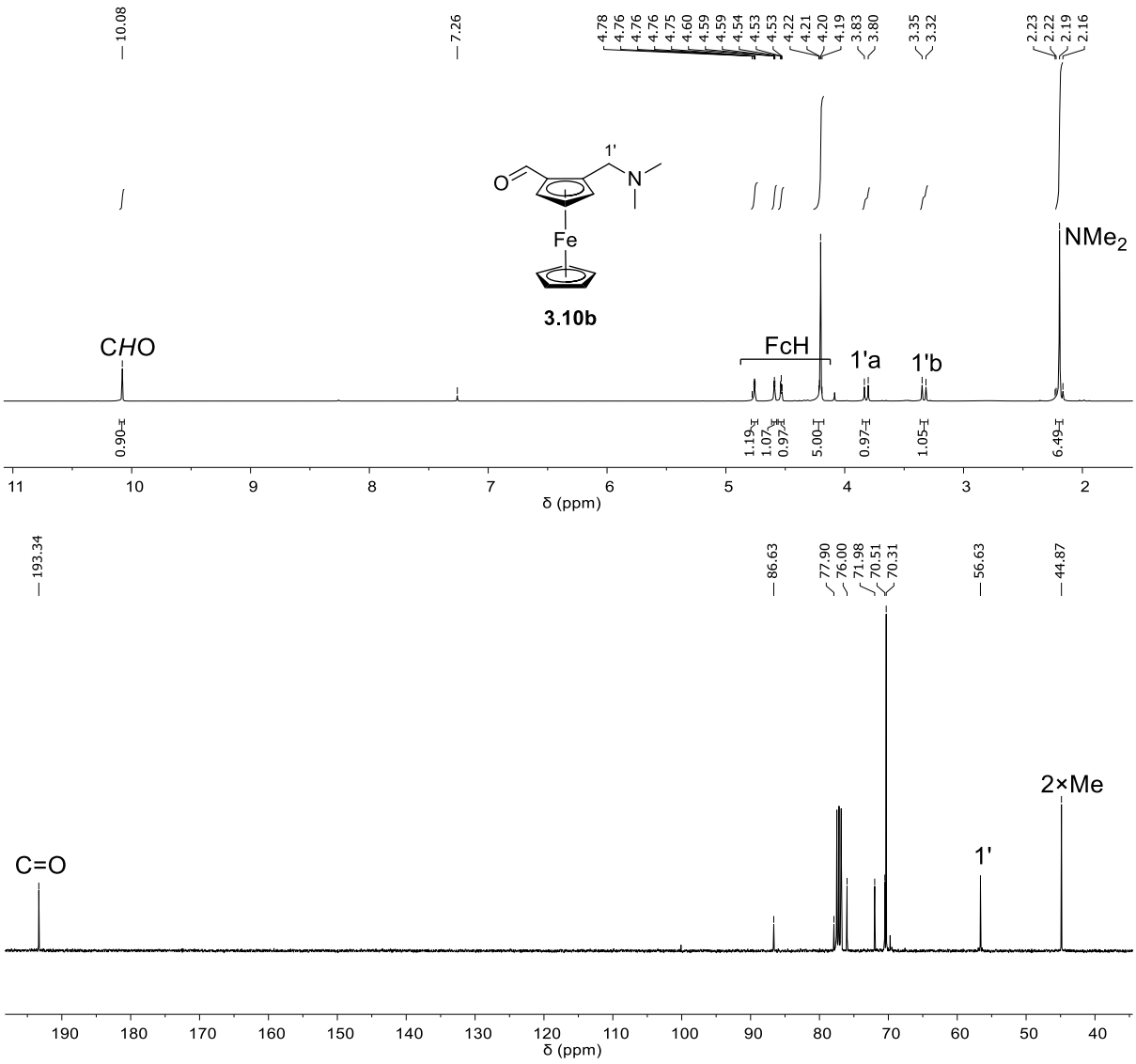

Figure 3.5 ^{1}H and ^{13}C NMR spectra of ferrocenyl carboxaldehyde **3.10b** in $CDCl_3$.

Once the ferrocene carboxaldehyde was attained, it was readily converted to its oxime variant (**3.11b**) as previously described for oxime **3.11a** and was obtained in more than 90% yield.[6] The oxime **3.11b** was then refluxed with lithium aluminium hydride ($LiAlH_4$) in anhydrous THF under an inert atmosphere to produce the desired amine **3.12b** in an excellent yield of 94%.[6] Similar to the methylene protons in carboxaldehyde **3.10a**, the newly generated methylene protons of amine **3.12b** were diastereotopic and appeared as doublets integrating for 1H each with *J*-coupling constants of 13.7 and 14.0 Hz in the ^{1}H NMR spectrum of **3.12b**.

With the ferrocene amine **3.12b** bearing the desired CH_2NMe_2 side chain successfully prepared, the synthesis of a second series of 1,3-benzoxazines with a modified ferrocene unit was pursued. The reaction conditions for the expeditious synthesis of 1,3-benzoxazines were already optimized with amine **3.12a** above. Thus, ferrocenyl amine **3.12b** was subjected to the same conditions using various phenolic substrates (**3.1a-i**) as before to access the target basic benzoxazine derivatives **3.16a-k** (**Scheme 3.10**). The boc-protected *p*-aminophenol **3.1j** and 2,3,5-trichlorophenol **3.1k** were also included in the synthesis to interrogate the biological effect of attaching a bulky functional group (6-NHBoc) and multiple electron-withdrawing groups (three Cl atoms) to the benzene ring, respectively.

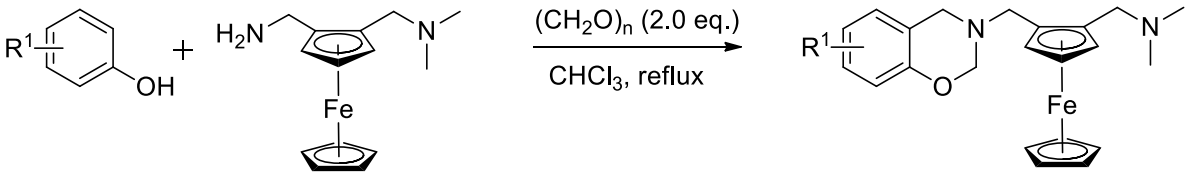

3.1a-k **3.12b** **3.16a-o**

R^1	Isolated yield (%)
3.16a : H	43
3.16b : 6-Me	30
3.16c : 6-Cl	50
3.16d : 6-Br	50
3.16e : 6-OMe	35
3.16f : 6-NO_2	66
3.16g : 7- / 5-Me*	30
3.16h : 7-Br	11
3.16i : 7-F	13
3.16j : 5-Br	23
3.16k : 5-F	13
3.16l : 6-NHBoc	39
3.16m : 5,7,8-Cl	46
3.16n : 6-Cl**	6
3.16o : 6-NO_2**	7

Scheme 3.10 Synthesis of basic ferrocenyl 1,3-benzoxazines bearing the CH_2NMe_2 moiety. *Product was obtained as a mixture of 5- and 7-methyl isomers. **Deaminated side products lacking the NMe_2 moiety.

As before, the reaction of the *para* phenols **3.1b-f** exclusively furnished the 6-substituted benzoxazine products (**3.16b-f**), while the *meta* phenols gave both 7- and 5-functionalized products (**3.16h-k**). However, 3-methylphenol **3.1g** was converted into an inseparable mixture of both 7- and 5-methylated isomers of product **3.16g** in a 2:3 ratio based on the HPCL (**Figure 3.6**) and ^{1}H NMR data. Interestingly, the synthesis of 6-Cl (**3.16c**) and 6-NO_2 (**3.16f**) benzoxazines from their corresponding phenols (**3.1c** and **3.1f**) led to concomitant formation of side products **3.16n-o** devoid of the basic *N*,*N*-dimethylamine (NMe_2) moiety in poor yields (**Scheme 3.10**). This process is likely to have occurred via a mechanism described by Winter and Wolmershäuser for the fragmentation of *N,N*-ferrocenylmethyldimethylamine in chlorinated solvents.[16]

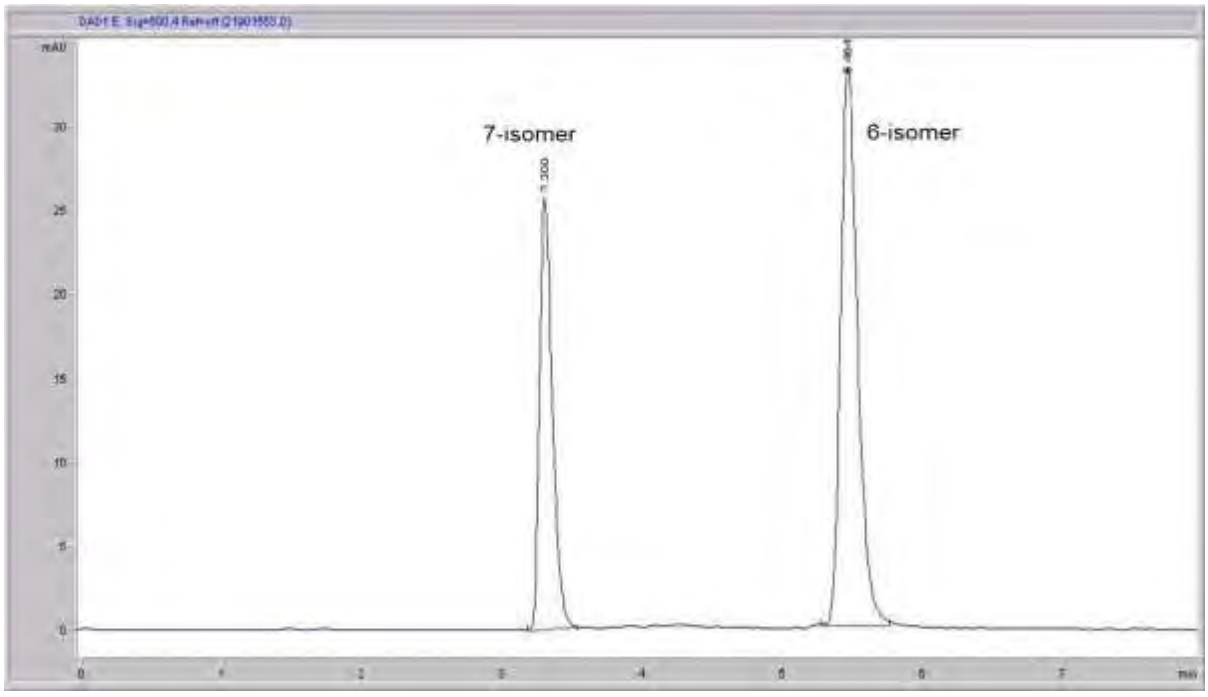

Figure 3.6 HPLC chromatogram of compound **3.16g** showing the 7- and 5-methylbenzoxazine isomers.

The target compounds were characterized by NMR, IR and HRMS spectroscopic techniques. Using benzoxazine **3.16j** as a representative compound, the protons were assigned by multiplet

analysis of signals from the ^{1}H NMR spectra as well as 2D NMR techniques: COSY, HMBC and HSQC. From the ^{1}H NMR spectrum of **3.16j**, the dimethylamine (NMe_2) protons were easily identified as a singlet integrating for 6H at δ 2.17 ppm and the ferrocene protons (FcH) were observed between δ 4.27 and 4.00 ppm, corresponding to the top and bottom cyclopentadienyl (Cp) rings (**Figure 3.7**). Multiplet analysis of the aromatic signals allowed the proton on C-7 to be readily assigned to the triplet signal at δ 7.01 ppm. Protons 6 and 7 were distinguished by 2D NMR techniques as will be described later.

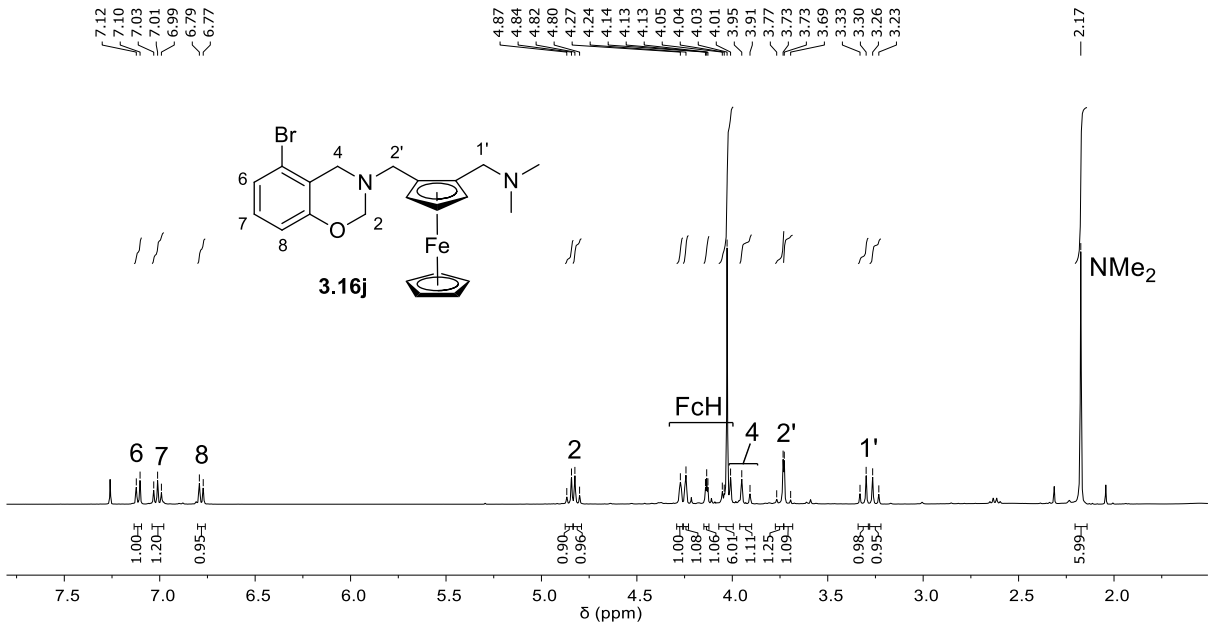

Figure 3.7 ^{1}H NMR spectrum of benzoxazine **3.16j** in $CDCl_3$.

Importantly, the characteristic oxazine methylene protons on C-2 and C-4 of the benzoxazine scaffold appeared at the expected chemical shifts at δ 5.00 – 4.80 ppm and δ 4.10 – 3.90 ppm, respectively, as was observed for the previous series (**3.13a-k**) bearing an unsubstituted ferrocene unit. However, the oxazine protons attached to the same methylene carbon in the ferrocenyl CH_2NMe_2 series appeared as doublets for the majority of the compounds as illustrated in the ^{1}H NMR spectrum of **3.16j** (**Figure 3.7**). This can be explained by examining the structural conformation of the 3,4-dihydro-2*H*-1,3-benzoxazine scaffold. Due to the

presence of unsaturated methylene carbons, the non-flat oxazine ring unit assumes a chair conformation in the 1,3-benzoxazine scaffold (**Figure 3.8**).[17]

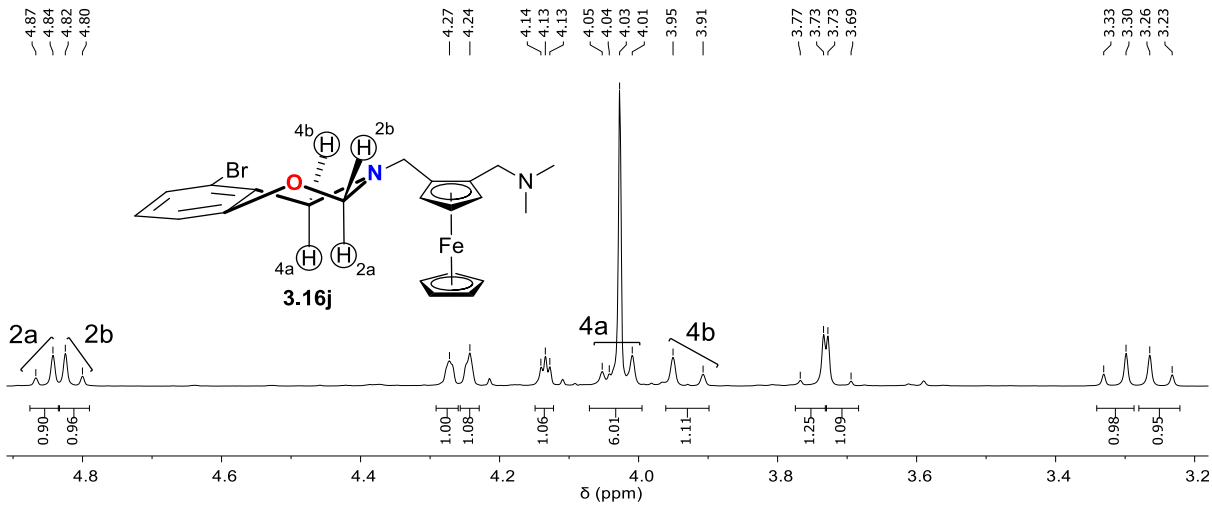

Figure 3.8 Truncated ^{1}H NMR spectrum of **3.16j** in $CDCl_3$ showing the aliphatic region with the oxazine protons in chair conformation.

Because of the chair conformation, protons of the same methylene carbon occupy magnetically different environments, i.e., axial and equatorial positions, as illustrated in **Figure 3.8**. As a result, the methylene protons attached to the same carbon will resonate at distinguishable chemical shifts and couple with one another. Hence, the protons on C-2 (2a and 2b) appeared as 1H doublets with a *J*-coupling constant of 9.9 Hz at the expected chemical shifts typical of position 2 of the 1,3-benzoxazine moiety at δ 4.78 – 4.80 ppm.[1b] Likewise, protons 4a and 4b showed as 1H doublets (J = 17.3 Hz) at δ 4.03 (overlapping with ferrocene) and 3.93 ppm, respectively. The splitting of the oxazine protons could also be attributed to the shielding effects of the ferrocene unit. Because of the environmental differences above and below the top Cp ring, the oxazine protons oriented above or below the axis of this ring will experience distinct magnetic fields, leading to shielding of the equatorial oxazine protons in the vicinity of the iron centre.[15]

It is important to note that the oxazine protons of the previous series (**3.13a-k**) with an unmodified ferrocene unit did not exhibit this phenomenon. This could be due to the fact that the ferrocene unit of this series is mono-substituted and achiral, and thus does not exhibit diastereotopicity. Also, because it lacks a bulky functional group (CH_2NMe_2) in position 2, the movement of the chair conformation of the oxazine unit is more dynamic, leading to the splitting of the methylene protons being indistinguishable. Hence, protons in positions 2 and 4 in this series each appeared as broad 2H singlets in the ^{1}H NMR spectra of the compounds as seen in **Figure 3.1**.

The assignment of protons to signals in the ^{1}H NMR spectra of the compounds was facilitated by COSY, HMBC and HSQC 2D NMR techniques. From the COSY spectrum of **3.16j** showing the aromatic region, protons 6 and 8 were assigned to the 1H doublets at δ 7.11 and 7.88 ppm, respectively (**Figure 3.9**).

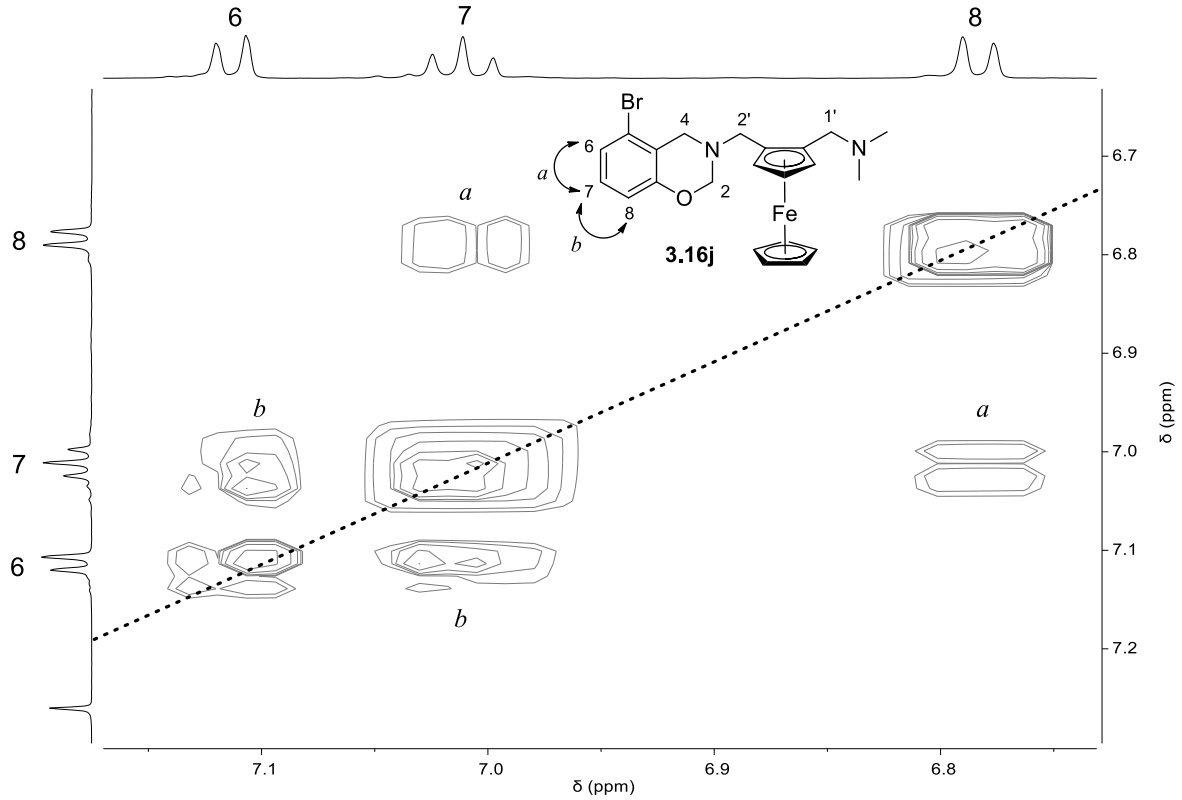

Figure 3.9 COSY NMR spectrum of **3.16j** in $CDCl_3$ showing the aromatic region.

Both HMBC and HSQC NMR were invaluable for the definitive assignment of protons. Based on the C – H correlations in HMBC NMR spectra of the target compounds, the signals were assigned as shown in **Figure 3.10** for compound **3.16j**. Assignment of proton 8 was further corroborated by the HMBC data as shown by its correlation with the phenoxy C-1a carbon atom, i.e., correlation *h* (**Figure 3.10**). The methylene protons on C-1′ were distinguished from protons at C-2′ by their correlation (*f*) with the vicinal NMe_2 carbons at cross-peak [3.27, 45.4] ppm (**Figure 3.10**).

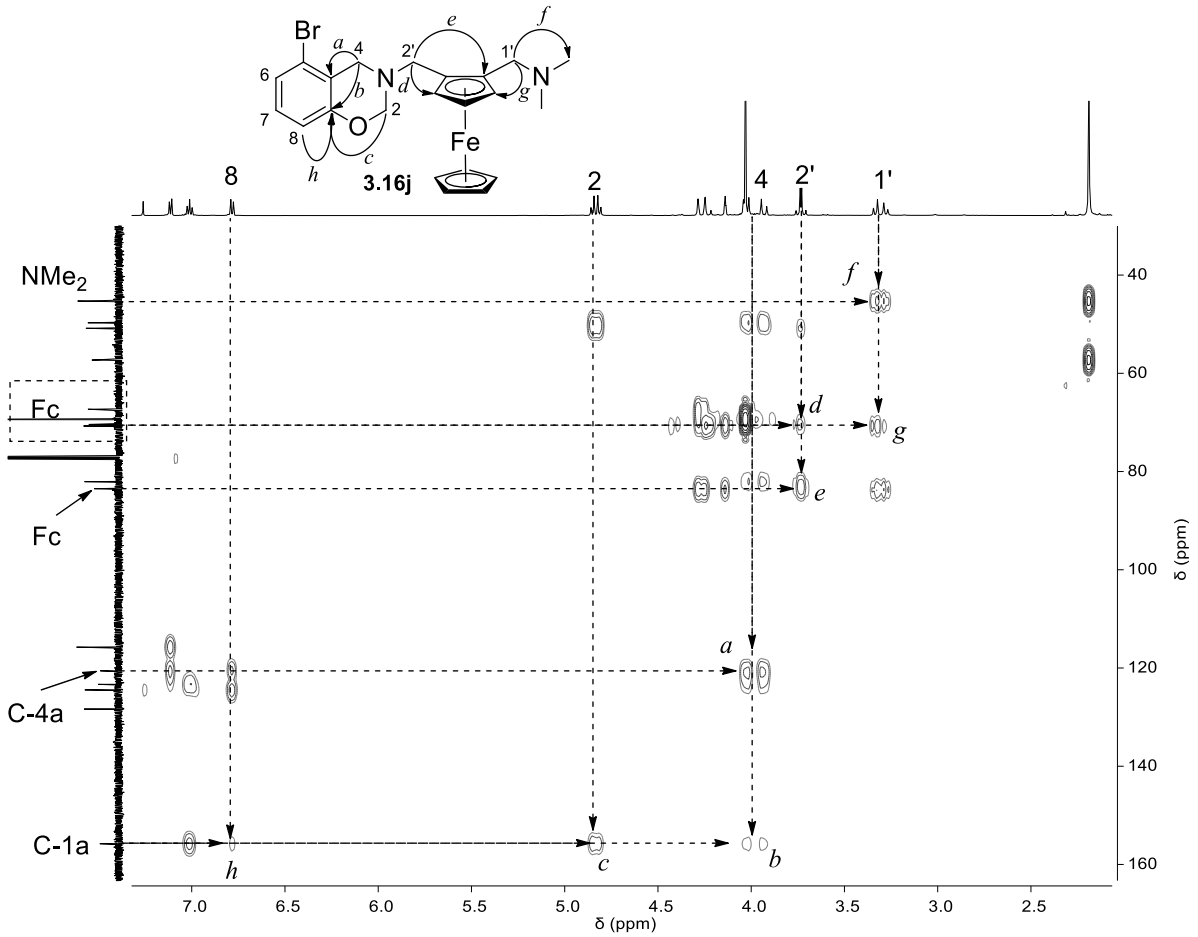

Figure 3.10 HMBC NMR spectrum of compound **3.16j** in $CDCl_3$.

Carbons carrying hydrogens were readily assigned to their respective protons by HSQC (**Figure 3.11**). These assignments were in agreement with the ^{1}H NMR and HMBC data as previously described. This was the case for all the CH_2NMe_2 ferrocenyl 1,3-benzoxazine derivatives in the series.

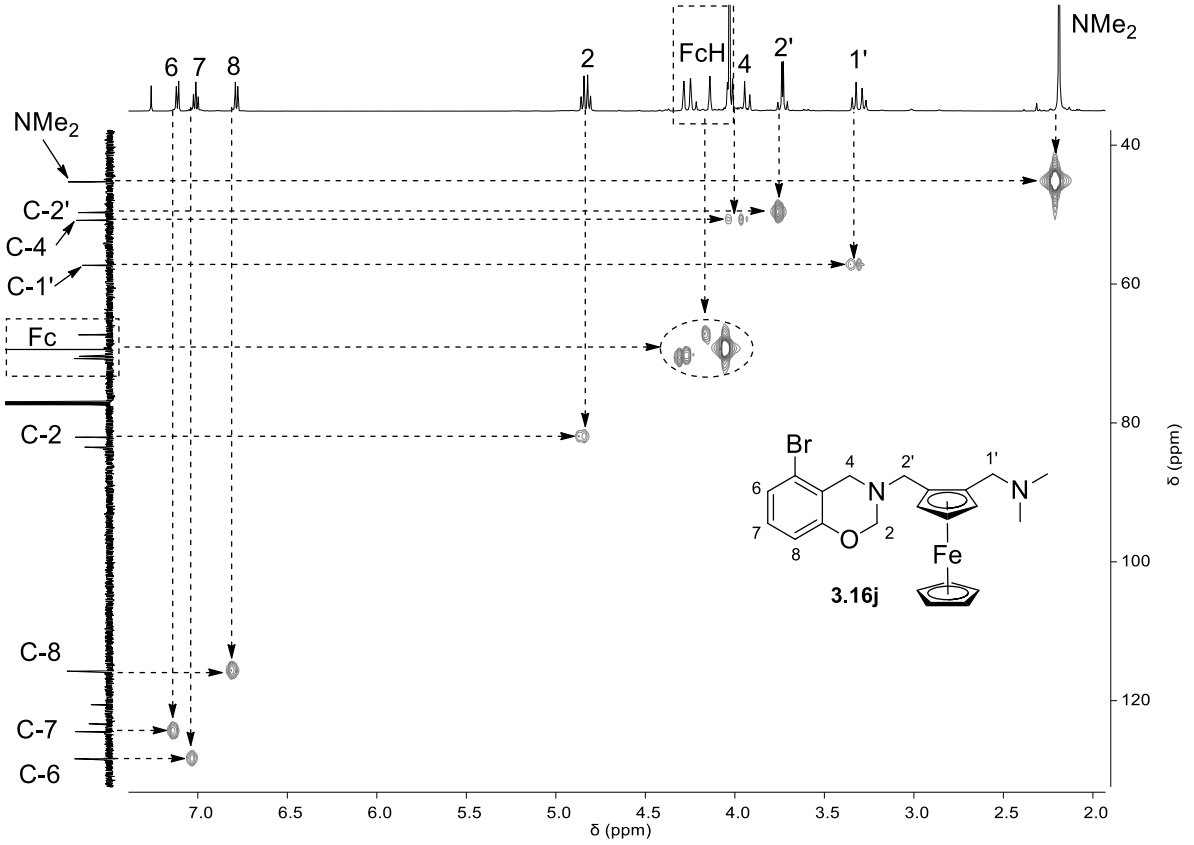

Figure 3.11 HSQC NMR spectrum of compound **3.16j** in $CDCl_3$.

The characterization with NMR techniques above was supported by the HRMS data. As with the unsubstituted ferrocenyl series (**3.13a-j**), the calculated masses of compounds **3.16a-l** correlated with the experimental values. Full details of the characterization of the compounds are presented in the experimental section in **Chapter 9**.

Interestingly, upon monitoring the reaction progress (TLC) of 4-methylphenol **3.1b** and 4-nitrophenol **3.1f**, new prominent spots were noticed in addition to those of the forming products. These were isolated during purification by silica gel column chromatography and identified to be *N,N*-bis(2-hydroxybenzyl)ferrocenemethylamines **3.16p-q** (**Scheme 3.11**). These products were also observed by Burke and co-workers under similar conditions for the condensation of *para*-substituted phenols with formaldehyde and primary amines.[18] In our case, these products were only observed for 4-methylphenol **3.1b** and 4-nitrophenol **3.1f**.

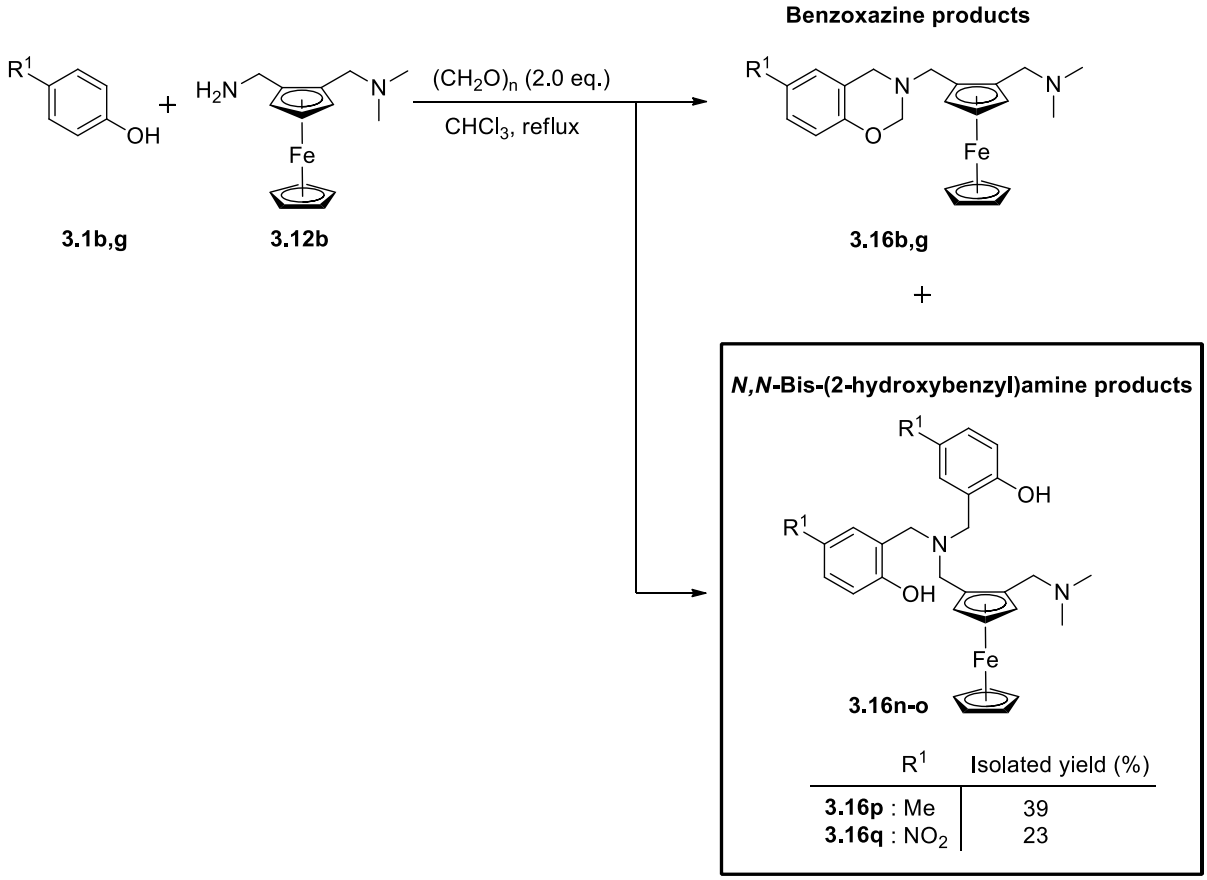

Scheme 3.11 Formation of *N,N*-bis(2-hydroxybenzyl)ferrocenemethylamines **3.16p-q**.

Mechanistically, the formation of *N,N*-bis(2-hydroxybenzyl)ferrocenemethylamines **3.16p-q** could be explained as illustrated in **Scheme 3.12** below. The O-CH_2-N linkage of the benzoxazine scaffold is chemically labile. To this end, open-ring iminium zwitterionic conformers (e.g., **3.16b′**) of ferrocenyl 1,3-benzoxazine derivatives were also observed by Li et al.[1b] As an electrophilic species, this open-ring conformer (**3.16b′**) can undergo electrophilic aromatic substitution with an unreacted phenolic substrate (**3.1b**) in the reaction medium, leading to formation of the *N,N*-bis(2-hydroxybenzyl)ferrocenemethylamine product **3.16p**. This mechanism is similar to the one proposed by Li et al. for the thermal polymerization of 1,3-benzoxazines by ring-opening.[1b]

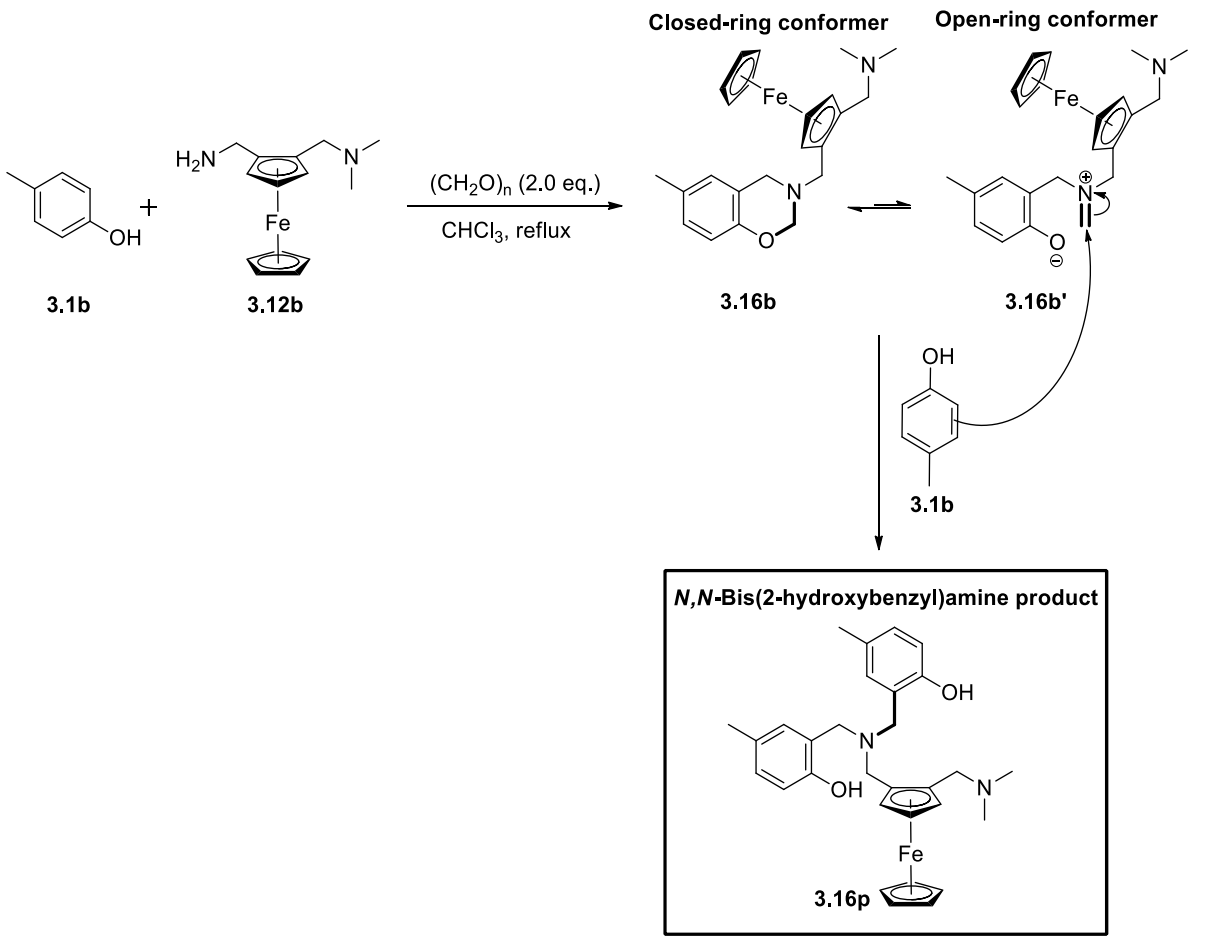

Scheme 3.12 Possible mechanism for the formation of *N,N*-bis(2-hydroxybenzyl)amine products **3.16p-q**.

The structures of the *N,N*-bis(2-hydroxybenzyl)ferrocenemethylamines **3.16p-q** were confirmed similarly to their benzoxazine counterparts. The protons of **3.16p** were readily assigned as shown in the ^{1}H NMR spectrum in **Figure 3.12**. The diastereotopic methylene protons (1′ and 2′) attached to the ferrocene unit were also observed as 1H doublets with *J*-coupling constants between 12.5 and 14.0 Hz as previously seen for the benzoxazine analogues.

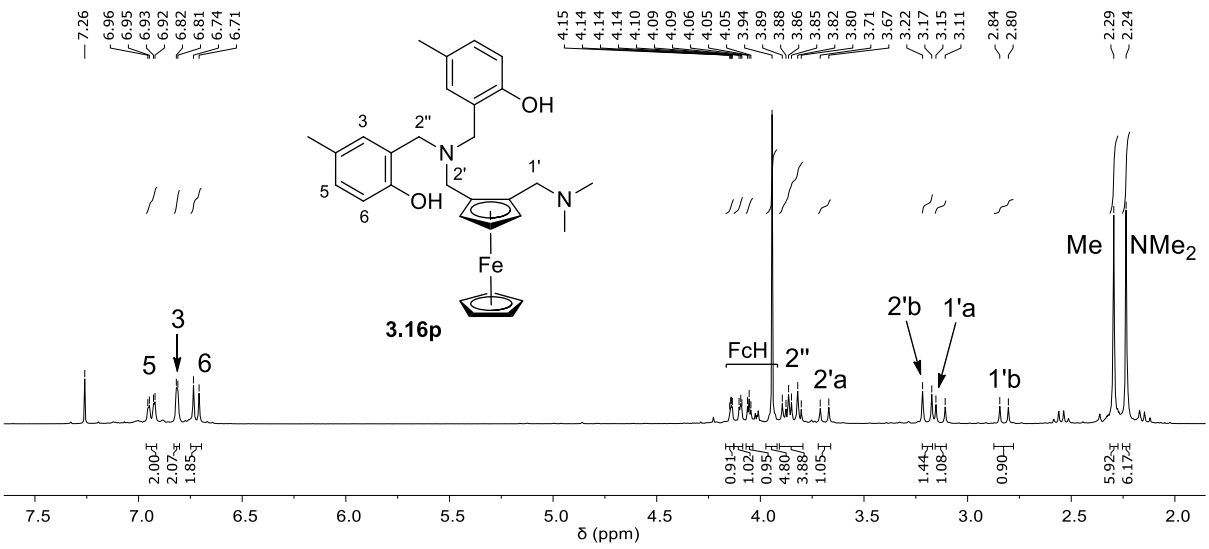

Figure 3.12 ^{1}H NMR spectrum of compound **3.16p** in $CDCl_3$.

Structural determination by NMR was corroborated by HRMS data as shown by the HRMS spectrum of compound **3.16p** in **Figure 3.13**. The base peak (*m/z*: 513.2208 a.u.) corresponding to the protonated molecular ion of the compound (*m/z*: 512.2126 a.u.) together with the deaminated fragment (*m/z*: 468.1624 a.u.) were easily identified as the prominent peaks in the HRMS spectrum of **3.16p** (**Figure 3.13**).

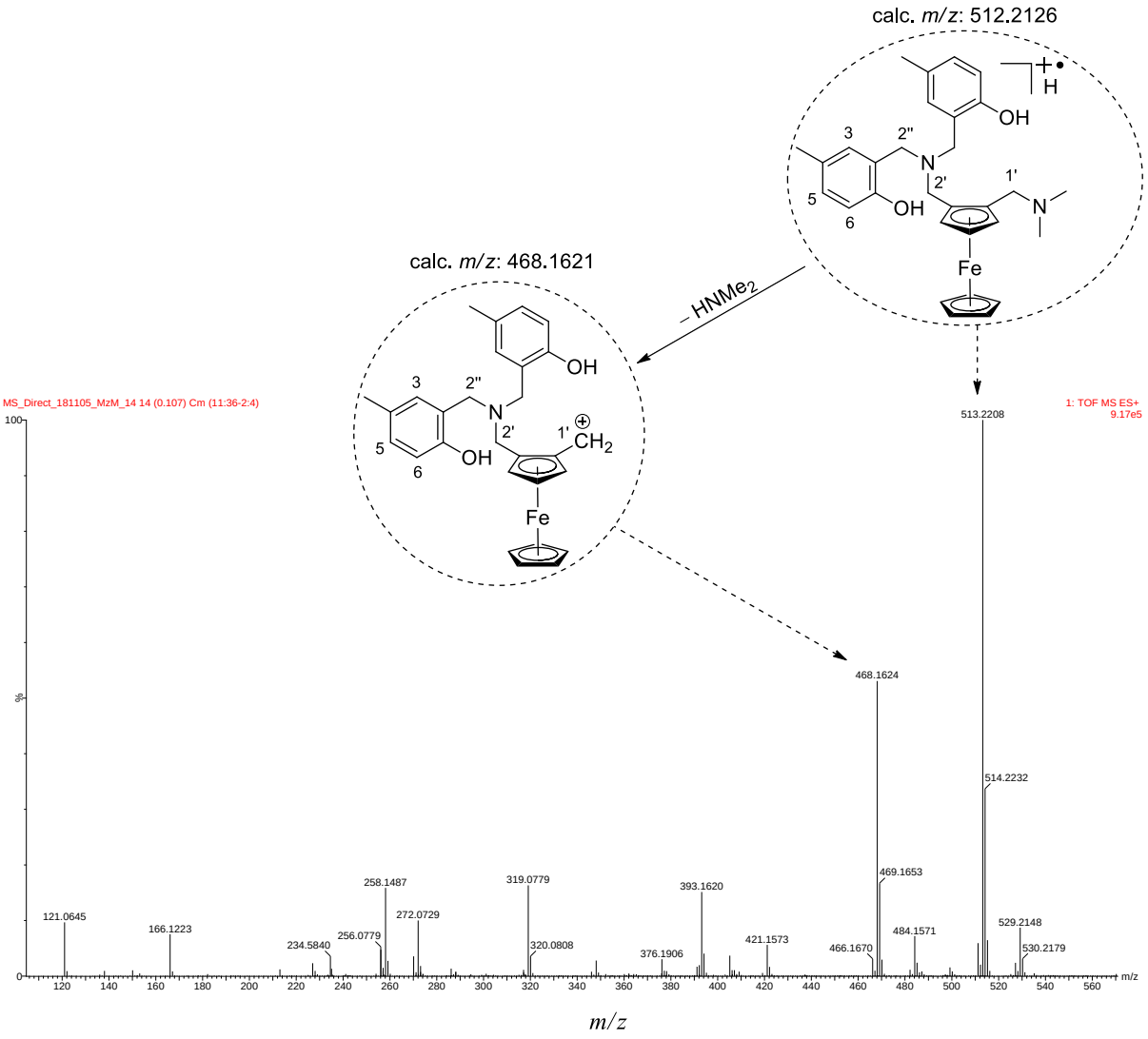

Figure 3.13 HRMS spectrum of compound **3.16p**.

3.3.2. Synthesis and characterization of 2-((*N*,*N*-diethylamino)methyl)ferrocenemethyl-3,4-dihydro-2*H*-1,3-benzoxazines

To further probe the biological effects of modifying the ferrocene unit, diethylamine (CH_2NEt_2) congeners of the CH_2NMe_2 ferrocenyl derivatives above were synthesized. As above, the approach to this new series involved preparation of the ferrocenyl amine carrying the CH_2NEt_2 group followed by the Burke protocol. Since *N,N*-diethylaminomethylferrocene (**3.15b**) is not commercially available, it was prepared from relevant ferrocenyl substrates. Initially, the proposed synthesis of this amine involved diethylation of ferrocenemethyl amine **3.12a** by

adapting a dimethylation procedure for the synthesis of methylated amines with excess formaldehyde reported by da Silva et al.[19] In our synthesis, formaldehyde was replaced with acetaldehyde (**3.17**) to incorporate the ethyl group in the final amine (**Scheme 3.13**). In an alternative route, ferrocenyl amine **3.12a** was reacted with 2.0 equivalents of ethylbromide (**3.18**) under basic conditions as shown in the bottom reaction in **Scheme 3.13**.[20] Disappointingly, none of the attempted synthetic routes yielded the desired product. With the abundance of alternative methods in literature, these approaches were abandoned without further interrogation.

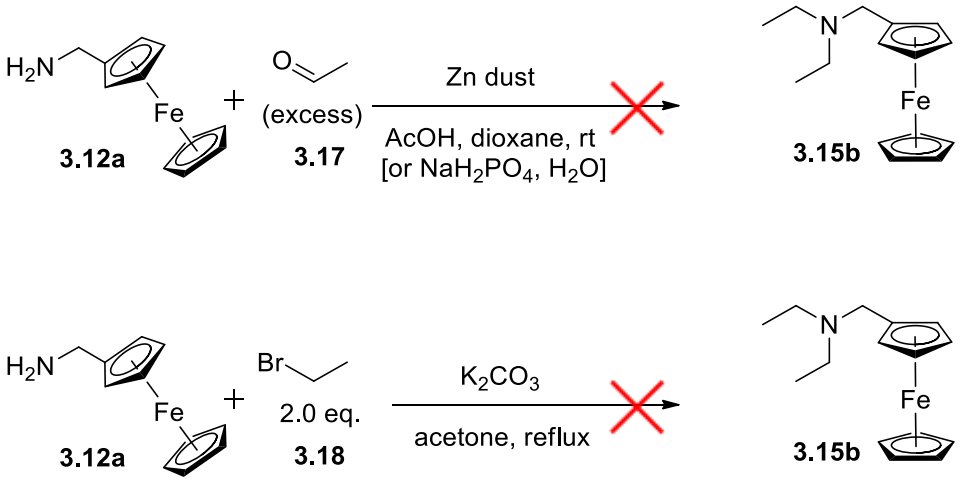

Scheme 3.13 Attempted synthesis of *N,N*-diethylaminoethylferrocene **3.15b** from ferrocene methylamine **3.12a**.

It was proposed that instead of attaching ethyl electrophiles to amine **3.12a** as the nucleophile, it would be prudent to reverse the electronic roles of the reagents by reacting an electrophilic ferrocenyl variant of **3.12a** with diethylamine (**3.19**) acting as a nucleophile (**Scheme 3.14**). Thus, the selected ferrocenyl electrophiles were ferrocene carboxaldehyde (**3.10a**) and ferrocene methyl halides (**3.20a-b**) (**Scheme 3.14**). In the first instance, ferrocene carboxaldehyde (**3.10a**) was subjected to reductive amination with diethylamine (**3.19**), employing sodium triacetoxyborohydride ($Na(OAc)_3BH$) as the reductant in dichloroethane

(DCE) under inert conditions.[21] On the other hand, synthesis with ferrocene methyl halides (**3.21a-b**) required the conversion of ferrocene carboxaldehyde **3.10a** to ferrocene methanol (**3.20**) via reduction with sodium borohydride ($NaBH_4$) followed by substitution of the hydroxyl group with a relevant halide. Both ferrocene methyl chloride **3.19a** and bromide **3.19b** were prepared *in situ* with thionyl chloride ($SOCl_2$) and phosphorus tribromide (PBr_3) under a nitrogen atmosphere.[22] Again, none of these approaches furnished the desired amine.

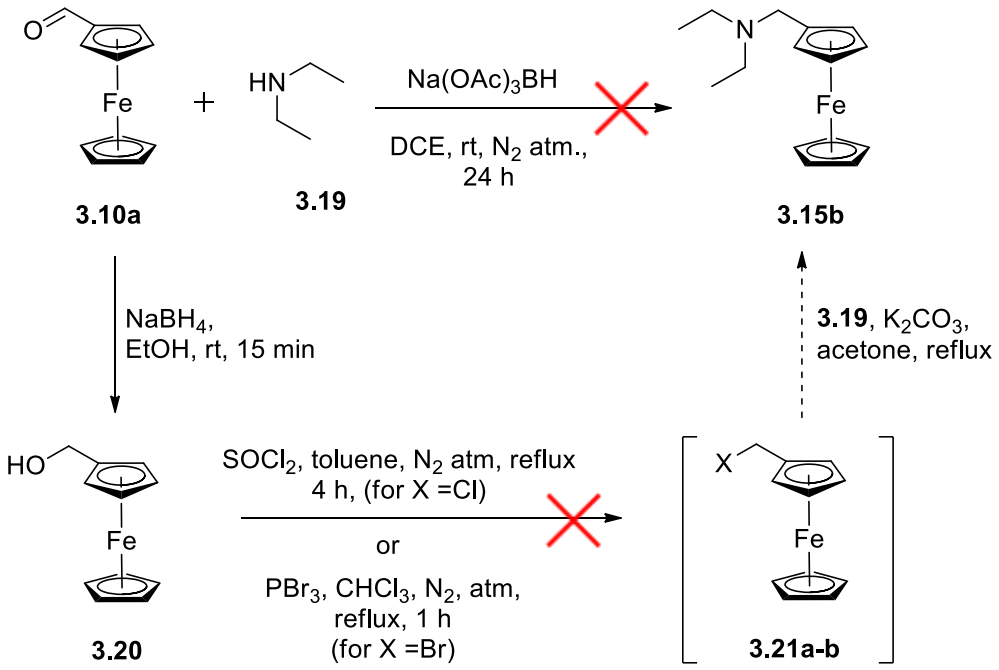

Scheme 3.14 Attempted synthesis of amine *N,N*-diethylaminomethylferrocene **3.15b** from ferrocene carboxaldehyde **3.10a**.

In the second instance, ferrocene methyl halides are known to be unstable.[23] It was then hypothesized that the lack of stability may have caused ferrocene methyl halides (**3.21a-b**) to revert back to ferrocene methanol **3.20** during removal of the volatiles under reduced pressure following completion of the reaction (TLC). Indeed, the presence **3.20** was noticed on the TLC during monitoring of the amination step (**Scheme 3.14**).

To circumvent the formation of these unstable methyl halides **3.21a-b**, excess diethylamine **3.19** was directly alkylated with ferrocene methanol **3.20**, utilizing $AlCl_3$ as an alkylating agent (**Scheme 3.15**).[24] This route successfully yielded the desired amine **3.15b** in an excellent yield of 82% within 6 hours after a simple workup. The workup was performed by quenching of untreated $AlCl_3$ with water followed by extraction of the product with dichloromethane (DCM). After the removal of DCM *in vacuo*, the crude product was dissolved in pentane and washed with water to yield the pure amine **3.15b** without further purification.

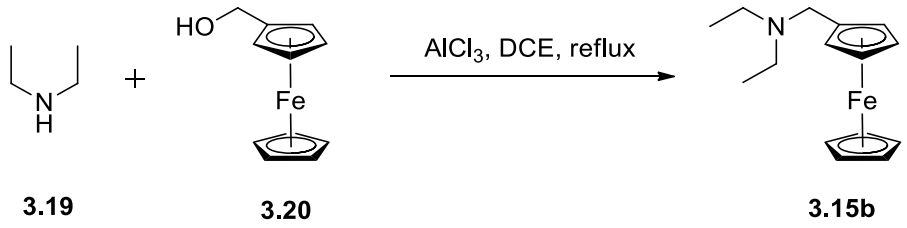

Scheme 3.15 Synthesis of *N,N*-diethylaminomethylferrocene **3.15b** by direct alkylation of diethylamine **3.19** with ferrocene methanol **3.20**.

As before, the structure of amine **3.15b** was confirmed by ^{1}H and ^{13}C NMR spectroscopy (**Figure 3.14**). The protons were easily assigned by multiplet analysis. The diethyl chain appeared as a 4H quartet and 6H triplet at δ 2.24 and 1.03 ppm corresponding to the methylene and methyl groups, respectively, while the 2H singlet of the methylene group attached to the ferrocene unit was further downfield at δ 3.50 ppm. The ferrocene protons (FcH) showed in the typical ferrocene region (δ 4.20 – 4.00 ppm) as two 2H triplets of the top Cp ring flanking the 5H singlet of the bottom Cp unit (**Figure 3.14**). The observed number of signals in ^{13}C NMR spectrum were in agreement with the skeletal structure of the compound.

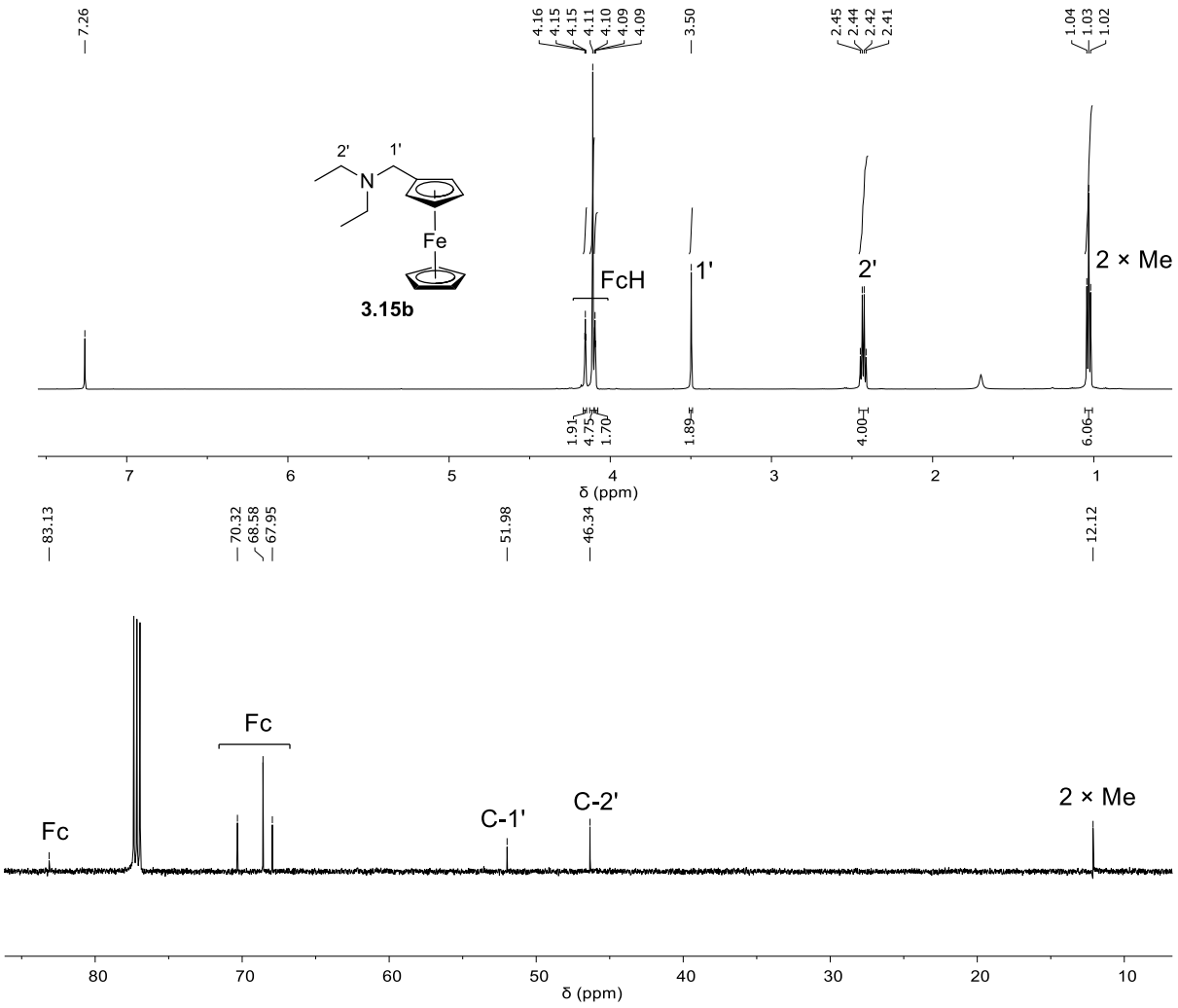

Figure 3.14 ^{1}H and ^{13}C NMR spectra of *N,N*-diethylaminomethylferrocene **3.15b** in $CDCl_3$.

Having synthesized the precursor **3.15b** for the synthesis of ferrocenyl 1,3-benzoxazine containing the CH_2Et_2 group on the ferrocene unit, amine **3.12c** required for the Burke protocol was prepared by subjecting *N,N*-diethylaminomethylferrocene **3.15b** to the conditions described in **Scheme 3.9** without any modifications. The desired amine was acquired as a brown viscous oil in a lower yield of 75% relative to amine **3.12a** (yield: 93%). A focused series of six representative compounds was prepared from this newly synthesized amine using phenols indicated in **Scheme 3.16**. An improvement in the yield (> 50%) was observed for the synthesis of the CH_2NEt_2 ferrocenyl 1,3-benzoxazine congeners.

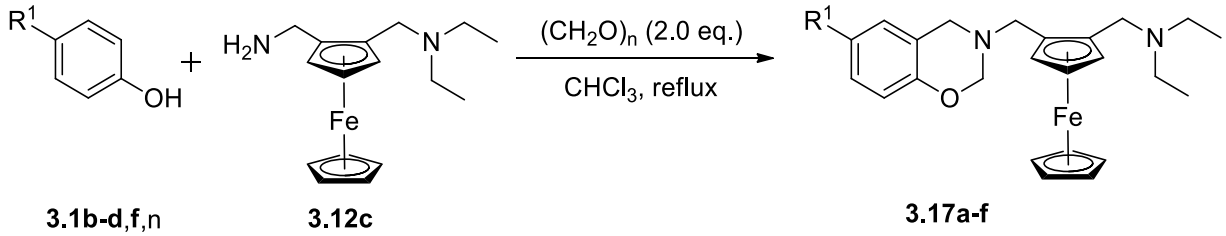

3.1b-d,**f**,n **3.12c** **3.17a-f**

R^1	Isolated yield (%)
3.17a : Me	52
3.17b : OMe	65
3.17c : Cl	79
3.17d : Br	50
3.17e : F	54
3.17f : NO_2	46

Scheme 3.16 Synthesis of 1,3-benzoxazine derivatives bearing a ferrocenyl CH_2NEt_2 side chain.

Characterization of these compounds was performed in a similar manner to the previous series. Both the oxazine and methylene protons attached to the ferrocene unit appeared as separate pairs of doublets with each doublet integrating for 1H as previously observed for the CH_2NMe_2 series above. This is illustrated by the ^{1}H NMR spectrum of compound **3.17a** in **Figure 3.15**.

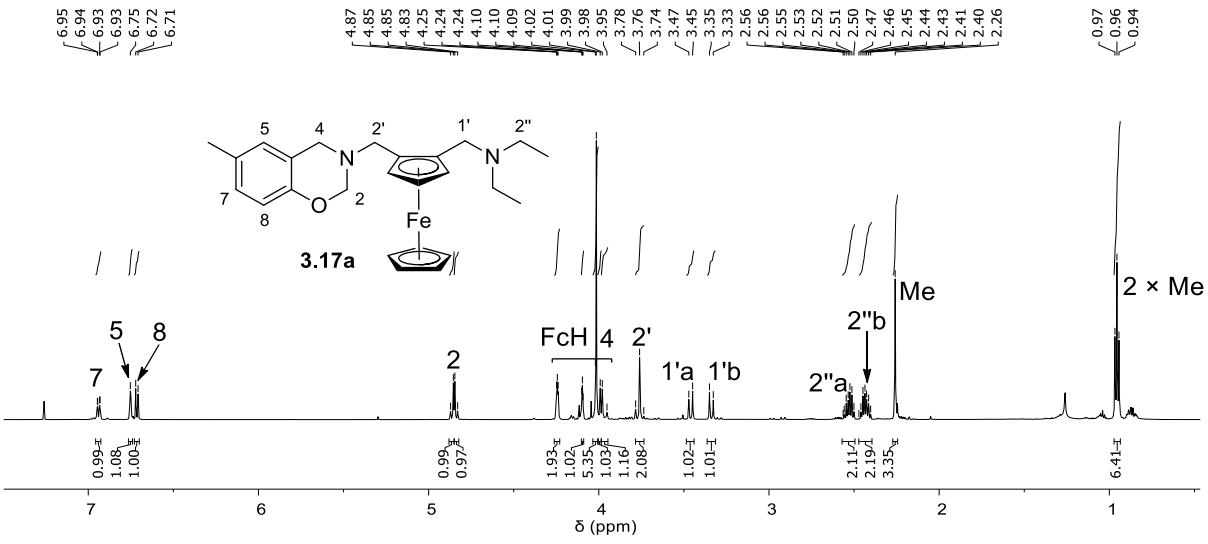

Figure 3.15 ^{1}H NMR spectrum of compound **3.17a** in $CDCl_3$.

The confirmatory HRMS data of the compounds is presented in the experimental section in **Chapter 9**.

3.4. Biological evaluation results

As per aims and objectives of the study, the target ferrocenyl 1,3-benzoxazine derivatives were investigated for potential biological activity by screening them *in vitro* against the triple-negative HCC70 breast cancer cell line and strains of the malaria parasite, *Plasmodium falciparum*, and the causative agent of trypanosomiasis, *Trypanosoma brucei brucei*. The chloroquine-sensitive (3D7) and resistant (Dd2) strains of the *P. falciparum* parasite were utilized to evaluate the antiplasmodial activity of the compounds, while the 427 *Trypanosoma brucei brucei* strain was used for antitrypanosomal evaluation. Lastly, the compounds were tested for general toxicity effects on HeLa cells.

3.4.1. Antiplasmodial activity of ferrocenyl 1,3-benzoxazine derivatives

Known antimalarial drugs, chloroquine and artemisinin, were used as positive controls in the assays. The compounds displayed high potency against both chloroquine-sensitive (3D7) and resistant (Dd2) strains with IC_{50} values in the low and sub-micromolar range (**Table 3.2**). In general, the compounds showed some selectivity for the Dd2 resistant strain over the sensitive 3D7 strain. The basic CH_2NMe_2 ferrocenyl chain is known to augment the bioactivity of chloroquine-based ferrocenyl derivatives.[6] Indeed, this moiety seemed to enhance the antiplasmodial activity of the compounds as evidenced by the higher potency of the series carrying this side chain (**3.16a-k**) compared to the CH_2Et_2 functionalized congeners (**3.17a-f**) followed by the unsubstituted derivatives (**3.13a-k**).

Table 3.2 *In vitro* antiplasmodial activity of ferrocenyl 1,3-benzoxazines against 3D7 and Dd2 *P. falciparum* strains.

Compound	[a]IC_{50} (µM)		[b]R.I.	Compound	[a]IC_{50} (µM)		[b]R.I.
	3D7	Dd2			3D7	Dd2	
3.13a	1.7	>10	>5.0	**3.16a**	1.09	2.36	2.2
3.13b	1.3	>10	>10.0	**3.16b**	1.58	0.577	0.3
3.13c	4.6	2.12	0.5	**3.16c**	0.261	0.599	2.3
3.13d	1.1	1.57	1.4	**3.16d**	0.402	0.512	1.3
3.13e	1.3	>10	>10.0	**3.16e**	0.407	1.87	4.6
3.13f	13.4	0.252	0.07	**3.16f**	na	nd	–
3.13g	3.5	0.229	0.07	**3.16g**	0.25	nd	–
3.13h	3.0	0.152	0.05	**3.16h**	0.321	0.152	0.5
3.13i	1.5	0.982	0.7	**3.16i**	0.114	0.652	5.7
3.13j	na	2.36	<1.0	**3.16j**	0.292	0.305	1.0
3.13k	na	1.92	<1.0	**3.16k**	0.162	0.365	2.3
3.17a	0.99	nd	–	**3.16l**	0.05	nd	–
3.17b	na	nd	–	**3.16m**	na	nd	–
3.17c	0.55	nd	–	**3.16n**	43.4	0.599	0.01
3.17d	0.22	nd	–	**3.16o**	1.41	3.34	2.4
3.17e	0.63	nd	–	**3.16p**	0.393	1.44	3.7
3.17f	4.86	nd	–	**3.16q**	0.35	4.06	11.6
Chloroquine	0.03	0.188	6.3	Artemisinin	–	0.006	–

[a]IC_{50} = half maximal inhibitory concentration, values are a mean of $n \geq 2$ experiments. In all cases, the standard deviation (±SD) was below 1.0. [b]R.I. = resistance index, defined as the ratio of antiplasmodial activity against the resistant strain Dd2 to the sensitive strain 3D7 [IC_{50}(Dd2)/IC_{50}(3D7)]. na = not active, which was assessed as compounds producing a cell viability of ≥ 50% in a single point cytotoxicity assay at 25 µM. nd = not determined.

The benzene ring substituents revealed no immediate overall trend in terms of the activity of the compounds. However, closer inspection of benzene substituents for the plain ferrocene series (**3.13a-k**) suggests that position 6 (**3.13b**, **3.13d**) is the most favourable for activity against the 3D7 strain, followed by positions 7 (**3.13g-i**) and 5 (**3.13j-k**), respectively. This

order was reversed for the series bearing the basic ferrocenyl CH_2NMe_2 moiety, i.e., 5 (**3.16j**) > 7 (**3.16g**) > 6 (**3.16d**) (**Table 3.2**). With the exception of the nitro group (NO_2), the electron-withdrawing groups (EWGs) generally imparted higher efficacy with F > Cl > Br > OMe > Me ≈ H regardless of the position of substitution for the plain (**3.13a-k**) and CH_2Me_2-substituted ferrocenyl series (**3.16a-k**) against the 3D7 sensitive strain. The halogenated derivatives (**3.17c-f**) of the CH_2Et_2 series exhibited higher activity than the electron-donating counterparts (**3.17a-b**). Within the halogenated variants (**3.17c-e**) of this series, the antiplasmodial activity seemed to increase with the atomic size of the halogen: Br (**3.17d**, IC_{50} = 0.22 μM) > Cl (**3.17c**, IC_{50} = 0.55 μM) > F (**3.17e**, IC_{50} = 0.63 μM). Replacement of the halogen substituents with the OMe (**3.17b**) and NO_2 (**3.17f**) groups was less favourable for activity as shown by the impotence of **3.17b** and lower activity of **3.17f** (IC_{50} = 4.86 μM) (**Table 3.2**).

Notwithstanding the above observations, incorporation of the bulky NHBoc group to C-6 imparted beneficial antiplasmodial effects to compound **3.16l** (IC_{50} = 0.05 μM), while the presence of the Cl group at positions 5, 7 and 8 in compound **3.16m** (IC_{50} = na) was detrimental for activity (**Table 3.2**). The 6-NHBoc derivative **3.16l** was the most active against the sensitive 3D7 *P. falciparum* strain in the three series. This observation seems to suggest that the combination of the steric bulk and NH and O functional groups, which can participate in hydrogen-bonding, of the NHBoc group are important for the activity of the ferrocenyl 1,3-benzoxazine compounds. Given that the compounds carrying halogens at C-5 (**3.16j-k**) and C-7 (**3.16h-i**) were active against the 3D7 strain, the lack of activity of the 5,7,8-trichlorinated benzoxazine (**3.16m**) could imply that either substitution at C-8 is not ideal for activity or antiplasmodial activity is only attained if one of the 5, 7 and 8 positions is substituted, but not all three.

For the Dd2 chloroquine-resistant *P. falciparum* strain, substitution at C-7 exerted enhanced antiplasmodial activity compared to positions 5 and 8, respectively, for the non-basic ferrocenyl benzoxazines (**3.13a-k**), while the order for favoured substitution pattern was 5 > 7 > 6 for the basic CH_2NMe_2 ferrocenyl congeners (**3.16a-l**). A general trend delineating the electronic and lipophilic effects of substituents on the antiplasmodial activity of the compounds against the Dd2 strain was not immediately obvious from the obtained data (**Table 3.2**). However, the halogenated variants (F, Cl, Br) were generally more potent than derivatives carrying electron-releasing substituents (H, Me, OMe), with the bromine atom being the most favourable for activity in the series (**Table 3.2**).

The antiplasmodial activity of the 6-Cl deaminated side product (**3.16n**) lacking the dimethylamine (NMe_2) moiety seemed to assert the biological significance of the basic ferrocenyl side chain (CH_2NMe_2 or CH_2NEt_2). This is illustrated by the lower activity of this compound (**3.16n**, IC_{50} = 43.4 μM) with respect to its CH_2NMe_2 and CH_2NEt_2 counterparts (**3.16c** and **3.17c**) against the 3D7 strain. However, the activity of this compound against the resistant strain was comparable to its basic congener **3.16c**. These observations were reversed for the 6-NO_2 deaminated derivative (**3.16o**) when compared to its basic variants (**3.16f** and **3.17f**). Collectively, the overall lower activity of the unsubstituted ferrocenyl series (**3.13a-k**) *vis-à-vis* its basic congener series (**3.16a-k** and **3.17a-k**) together with the observations made for the 6-Cl deaminated compound (**3.16n**) and its basic derivatives (**3.16c** and **3.17c**) strongly support the pharmacological importance of appending basic CH_2NMe_2 and CH_2Et_2 chains to position 2 of the ferrocene unit.

Interestingly, the *N,N*-bis(2-hydroxybenzyl)ferrocenemethylamines **3.16p-q** displayed activity that was analogous to that of the targeted ferrocenyl 1,3-benzoxazines (**3.16a-k**, **3.16a-m** and **3.17a-f**) against both tested strains (**Table 3.2**). However, these compounds were less selective for the Dd2 resistant strain as shown by the resistance indices above 1.0. Encouraged by this

promising activity, synthesis of tertiary amines resembling the scaffold of these compounds was explored in **Chapter 6**.

3.4.2. Antitrypanosomal activity of ferrocenyl 1,3-benzoxazine derivatives

To investigate the antitrypanosomal activity of the target compounds, the synthesized ferrocenyl 1,3-benzoxazines were pharmacologically screened for *in vitro* growth inhibitory effects against the 427 *Trypanosoma brucei brucei*. In the assay, varying concentrations of the compounds were incubated with the 427 *Trypanosoma brucei brucei* trypomastigotes for 24 hours and the inhibitory effects were quantified as IC_{50} values using the fluorescent assay.[25] The results for the tested compounds are presented in **Table 3.3**. A clinical antitrypanosomal drug, pentamidine, was used as the positive control in the assay.

Table 3.3 *In vitro* antitrypanosomal activity of ferrocenyl 1,3-benzoxazines against the 427 *Trypanosoma brucei brucei* strain.

Compound	[a]IC_{50} (µM)	Compound	[a]IC_{50} (µM)
3.13a	22.9	**3.16a**	1.2
3.13b	27.4	**3.16b**	0.8
3.13c	37.0	**3.16c**	1.3
3.13d	38.6	**3.16d**	1.2
3.13e	na	**3.16e**	1.6
3.13f	na	**3.16h**	5.4
3.13g	10.1	**3.16i**	1.1
3.13h	na	**3.16j**	4.5
3.13i	36.6	**3.16k**	0.15
3.13j	na	**3.16p**	1.4
3.13k	24.4	**3.16q**	1.9
3.16n	na	Pentamidine	0.014
3.16o	na		

[a]IC_{50} = half maximal inhibitory concentration, values are a mean of $n \geq 2$ experiments ($\pm SD \leq 1.0$). na = not active, which was assessed as compounds producing a cell viability of ≥ 50% in a single point cytotoxicity assay at 25 µM.

The antitrypanosomal efficacies of the tested compounds were active in the low and mid-micromolar range (**Table 3.3**). Particularly, the unsubstituted ferrocenyl compounds (**3.13a-k**) exhibited efficacies between 10 and 40 µM, whilst the basic *N*,*N*-dimethylaminomethylferrocene congeners (**3.16a-k**) possessed low micromolar activities with two compounds (**3.16b** and **3.16k**) active in the sub-micromolar range (**Table 3.3**). The methyl ferrocene congeners **3.16n** and **3.15n** were not toxic against the parasite, implying that the replacement of the CH_2NMe_2 ferrocenyl side chain with a methyl group is undesirable for antitrypanosomal activity. As observed for antimalarial efficacy (**Table 3.2**), this observation suggests that the basic CH_2NMe_2 side chain on the ferrocene unit is beneficial for the biological activity of the compounds with more than 20 times increase in potency (**Table 3.3**). For both series **3.13a-k** and **3.16a-k**, electron-donating groups (H, Me and OMe) were generally more

conducive for activity in comparison to the halogen counterparts. Within the halogenated compounds, the activity increased with the electron-withdrawing capacity of the substituent (**Table 3.3**). This could also be an influence of lipophilicity since, a lesser lipophilic NO_2 congener **3.13f** was not active against the 427 strain of *T. b. brucei*.

3.4.3. Anticancer activity of ferrocenyl 1,3-benzoxazine derivatives

The anticancer activity of the compounds was assessed on the HCC70 triple-negative breast cancer cell line *in vitro*. The cells were incubated with the test compounds for 72 hours and the activity of each compound was assessed after this period in at least three replicates. A known anticancer drug, paclitaxel, was employed as a positive control in the assay. Anticancer evaluation results are presented as IC_{50} values in **Table 3.4**. Only data for the active compounds are shown in **Table 3.4** and the inactive compounds are not included.

Table 3.4 *In vitro* anticancer activity of target compounds against HCC70 breast cancer cell line.

Compound	[a]IC_{50} (µM)
3.16b	25.9
3.16c	11.0
3.16d	14.6
3.16g	30.5
3.16h	16.5
3.16i	22.3
3.16j	27.6
3.16k	15.8
3.16l	25.6
3.16n	25.0
3.16p	111.3
3.17b	43.9
3.17c	16.0
3.17d	19.0
3.17e	39.1
Paclitaxel	0.0025

From the anticancer data in **Table 3.4**, only compounds in series **3.16** and **3.17** containing the basic CH_2NMe_2 and CH_2NEt_2 ferrocenyl side chain showed potency against the cell line with IC_{50} values in the range of 11.0 and 31.0 µM, making these moieties crucial for anticancer activity. For the CH_2NMe_2 derivatives, substitution at C-6 (**3.16b-d**) was generally more tolerated for activity compared to positions 7 (**3.16h-i**) and 5 (**3.16j-k**), respectively, with potency increasing with stronger EWGs. Similarly, the halogenated compounds (**3.17c-e**) belonging to the ferrocenyl CH_2NEt_2 series were more active than their 6-OMe (**3.17b**) and 6-NO_2 (**3.17f**) derivatives (**Table 3.4**). From both series (**3.16** and **3.17**), the 6-Cl variants **3.16c** and **3.17c** were the most active with IC_{50} values of 11.0 and 16.0 µM, respectively. This suggests that the chlorine group in position 6 was the most favoured substituent for anticancer

activity in the ferrocenyl 1,3-benzoxazine derivatives investigated in the study. Interestingly, these compounds were among the most active against the chloroquine-sensitive 3D7 *P. falciparum* strain in the antimalarial evaluation study (**Table 3.2**).

Interestingly, although lower than its basic congener **3.16c** (IC_{50} = 11.0 μM) ferrocenyl methyl compound **3.16n** (IC_{50} = 25.0 μM) exhibited activity analogous to most CH_2NMe_2 and CH_2NEt_2 derivatives in the series (**Table 3.4**). This observation appears to be partly influenced by lipophilicity than electronic effects due to the 6-Cl group, since a lesser lipophilic, albeit stronger electron-withdrawing, 6-NO_2 group, elicited no activity in the respective compound **3.16f**. Additionally, the NO_2 derivative **3.16q** of the *N,N*-bis(2-hydroxybenzyl)ferrocenemethylamines was not active against the cell line while its more lipophilic methyl congener **3.16p** (IC_{50} = 111.3 μM) showed modest activity. From these observations, it appears that lipophilic and electron-withdrawing substituents on the benzene ring are important for activity. On the other hand, the 6-NHBoc derivative (**3.16l**) displayed lower efficacy with an IC_{50} value of 25.6 μM despite being the most active compound against the 3D7 *P. falciparum* strain. This, together with the general lower toxicity of the compounds against the mammalian HCC70 triple-negative cancer cell line relative to the malaria and trypanosomiasis parasites, seems to imply the investigated derivatives possess higher selectivity for parasitic infections.

3.4.4. General toxicity evaluation using the HeLa cell line

The biological evaluation results above revealed that the investigated ferrocenyl 1,3-benzoxazine derivatives are more selective for the parasitic strains of *P. falciparum* and *T. b. brucei* than the mammalian HCC70 cancer cell line. To further probe the selectivity and general toxicity effects of the derivative, the investigated compounds were evaluated for growth inhibitory effects against the mammalian HeLa cell line. Although cancerous (cervical

carcinoma), the cells have been extensively employed in literature as a first-line preliminary measure to gauge the selectivity of antiparasitic compounds.[26] All the tested compounds showed negligible toxicity against the HeLa cell line at the tested concentration of 25 μM with more than 70% cell viability often observed (**Figure 3.16**). The data seemed to indicate that these compounds possess higher selectivity for the *P. falciparum* and *T. b. brucei* parasites over mammalian cells, thus corroborating the previous observations.

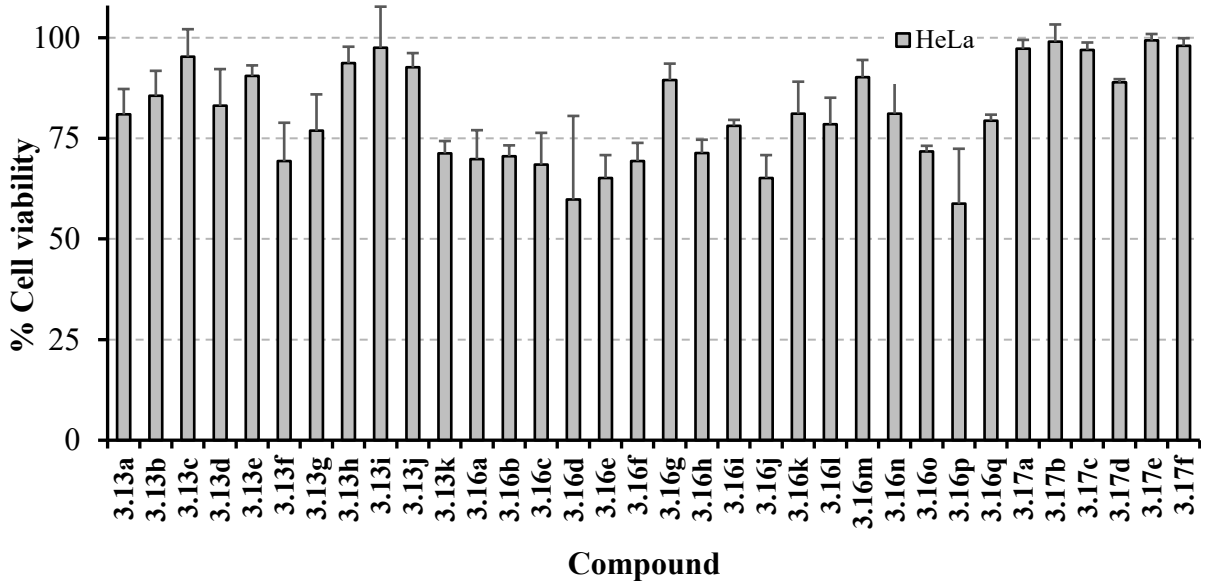

Figure 3.16 Screening of compounds for general human cytotoxicity. The bars indicate percentage cell viability (±SD) of HeLa cells incubated with the test compounds at a fixed concentration of 25 μM for 48 hours.

3.5. Preliminary structure-activity relationship (SAR) analysis

To study the influence of substituents on the biological activity of the investigated compounds, various substituents (Fl, Cl, Br, H, Me, OMe, NO_2, NHBoc) were introduced to the benzene ring to produce electronically and structurally diverse ferrocenyl 1,3-benzoxazine derivatives. Furthermore, the basic aminoalkyl chains, i.e., CH_2NMe_2 and CH_2NEt_2, were incorporated in position 2 of the ferrocenyl unit as part of structure-activity relationship (SAR) studies. The

side products, **3.16n-o** bearing a Me group instead of CH_2NMe_2 or CH_2NEt_2 on C-2 of the ferrocene unit served as further structural congeners in the study. By examining the activity of the derivatives with various benzene substituents and the ferrocenyl side chains, it was possible to assemble a preliminary SAR model for anticancer and antiparasitic activity of the compounds (**Figure 3.15**).

Compounds containing the CH_2NMe_2 ferrocenyl side chain (series **3.16**) possessed the highest activity against the investigated diseases, followed by the CH_2NEt_2 ferrocenyl series **3.17**. The plain ferrocenyl series **3.13** was the least active in the *in vitro* assays. Although compound **3.16n** containing the Me group in place of CH_2NMe_2 and CH_2NEt_2 ferrocenyl chains was active against the cancer cell line, this compound and its 6-NO_2 congener were not toxic against *T. b. brucei* strains and generally had lower antiplasmodial activity compared to their CH_2NMe_2 and CH_2NEt_2 ferrocenyl variants. The influence of the benzene substituents and favoured substitution positions on the biological activity was not immediately obvious. However, with the exception of the 6-NHBoc and 5,7,8-trichloro benzoxazines (**3.16l-m**), the presence of lipophilic and EWG groups (e.g., halogens) was generally conducive for the biological activity of the studied compounds. These observations are summarized in **Figure 3.15** using compound **3.16c**, which showed favourable activity across all three investigated diseases, as an example.

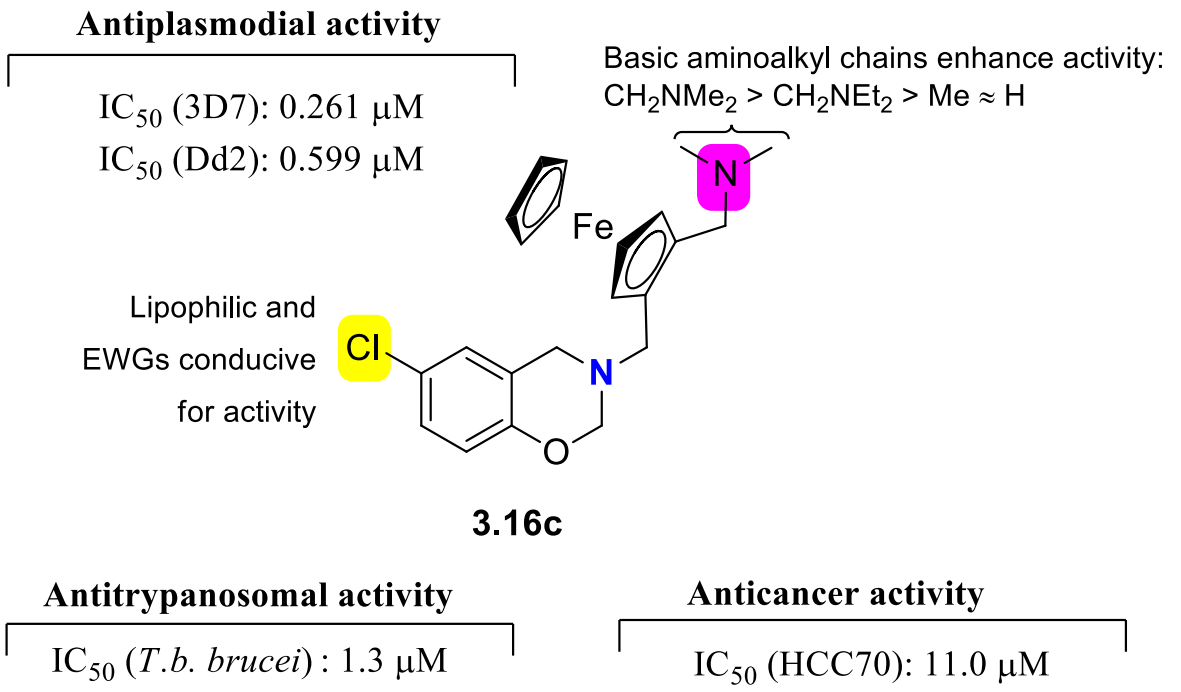

Figure 3.15 Preliminary SAR analysis of ferrocenyl 1,3-benzoxazines exemplified by compound **3.16c**.

3.6. Overall summary and conclusions

By adapting a polymer precursor, ferrocenyl 1,3-benzoxazine derivatives were synthesized using the classical Mannich-type Burke protocol and their structures confirmed by various spectroscopic techniques: NMR, IR and HRMS. The potential biological activity of the compounds was investigated *in vitro* against the aggressive triple-negative HCC70 cancer cell line and the *P. falciparum* parasite strains (3D7 and Dd2) and the causative agent of the African sleeping sickness, *T. b. brucei*.

The attained compounds, i.e., series **3.13**, **3.16** and **3.17**, which showed higher selectivity for the resistant strain, were efficacious against both chloroquine-sensitive (3D7) and resistant (Dd2) strains of the *P. falciparum* parasite in the low to sub-micromolar range. While series **3.13** devoid of the basic side chain displayed moderate activity against *T. b. brucei*, the majority of compounds from the basic CH_2NMe_2 series **3.16** showed superior antitrypanosomal activity

with IC_{50} values between 0.15 and 6.6 μM without major toxic side effects as measured by the mammalian HeLa cell line assay. With the exception of the ferrocenyl methyl side product **3.16n**, only compounds containing the basic ferrocenyl chains, CH_2NMe_2 and CH_2Et_2, exhibited anticancer activity against the HCC70 cancer cell line and none from the plain ferrocenyl series **3.13** were active at the maximum tested concentration. More importantly, none of the compounds showed toxic side effects when investigated for general cytotoxicity on the HeLa cell line, suggesting selectivity for the investigated diseases.

Thus, by repurposing a polymer precursor we have developed a novel class of compounds and demonstrated their biological potential via *in vitro* pharmacological assessment against the HCC70 cancer cell line and the 3D7 and Dd2 chloroquine-sensitive and resistant *P. falciparum* strains, respectively, and *T. b. brucei*. This chemical class of compounds holds great scope for further study and development as anticancer and parasiticidal agents, particularly against the malaria parasite, *P. falciparum*.

References

(1) (a) Li, W.; Chu, J.; Heng, L.; Wei, T.; Gu, J.; Xi, K.; Jia, X. *Polymer* **2013**, *54*, 4909; (b) Li, W.; Wei, T.; Gao, Y.; Xi, K.; Jia, X. *Polymer* **2012**, *53*, 1236.

(2) (a) Burke, W. *J. Am. Chem. Soc.* **1949**, *71*, 609; (b) Kiskan, B.; Yagci, Y. In *Thermosets*; Elsevier, 2018; (c) Andreu, R.; Ronda, J. *Synth. Commun.* **2008**, *38*, 2316.

(3) Imran, M.; Kiskan, B.; Yagci, Y. *Tetrahedron Lett.* **2013**, *54*, 4966.

(4) Katritzky, A. R.; Xu, Y.-J.; Jain, R. *J. Org. Chem.* **2002**, *67*, 8234.

(5) Brunovska, Z.; Liu, J. P.; Ishida, H. *Macromol. Chem. Phys.* **1999**, *200*, 1745.

(6) Biot, C.; Glorian, G.; Maciejewski, L. A.; Brocard, J. S.; Domarle, O.; Blampain, G.; Millet, P.; Georges, A. J.; Abessolo, H.; Dive, D. *J. Med. Chem.* **1997**, *40*, 3715.

(7) M. Ribeiro, F. W.; Rodrigues-Oliveira, A. F.; C. Correra, T. *J. Phys. Chem. A* **2019**, *123*, 8179.

(8) Taylor, R. *Electrophilic aromatic substitution*; John Wiley & Sons: Hoboken, New Jersey, 1990.

(9) (a) Roberts, J. D.; Weigert, F. J. *J. Am. Chem. Soc.* **1971**, *93*, 2361; (b) Williamson, K. L.; Hsu, Y.-F. L.; Hall, F. H.; Swager, S.; Coulter, M. S. *J. Am. Chem. Soc.* **1968**, *90*, 6717.

(10) U.S. National Library of Medicine, To Evaluate the Efficacy of a Single Dose Regimen of Ferroquine and Artefenomel in Adults and Children With Uncomplicated Plasmodium Falciparum Malaria (FALCI), https://clinicaltrials.gov/ct2/show/NCT02497612, Accessed: 17 August 2019.

(11) Biot, C.; Dive, D. In *Medicinal Organometallic Chemistry*; Jaouen, G., Metzler-Nolte, N., Eds.; Springer Berlin Heidelberg: Berlin, Heidelberg, 2010.

(12) (a) Jacobs, L.; de Kock, C.; de Villiers, K. A.; Smith, P. J.; Smith, V. J.; van Otterlo, W. A.; Blackie, M. A. *ChemMedChem* **2015**, *10*, 2099; (b) Stringer, T.; Guzgay, H.;

Combrinck, J. M.; Hopper, M.; Hendricks, D. T.; Smith, P. J.; Land, K. M.; Egan, T. J.; Smith, G. S. *J. Organomet. Chem.* **2015**, *788*, 1.

(13) Picart-Goetgheluck, S.; Delacroix, O.; Maciejewski, L.; Brocard, J. *Synthesis* **2000**, *2000*, 1421.

(14) Marquarding, D.; Klusacek, H.; Gokel, G.; Hoffmann, P.; Ugi, I. *J. Am. Chem. Soc.* **1970**, *92*, 5389.

(15) Blackie, M. A. Doctoral Thesis, University of Cape Town, 2002.

(16) Winter, R. F.; Wolmershäuser, G. *J. Organomet. Chem.* **1998**, *570*, 201.

(17) Heydenreich, M.; Koch, A.; Klod, S.; Szatmári, I.; Fülöp, F.; Kleinpeter, E. *Tetrahedron* **2006**, *62*, 11081.

(18) (a) Burke, W.; Smith, R. P.; Weatherbee, C. *J. Am. Chem. Soc.* **1952**, *74*, 602; (b) Burke, W. J.; Glennie, E. M.; Weatherbee, C. *J. Org. Chem.* **1964**, *29*, 909.

(19) da Silva, R. A.; Estevam, I. H.; Bieber, L. W. *Tetrahedron Lett.* **2007**, *48*, 7680.

(20) Beteck, R. M.; Seldon, R.; Jordaan, A.; Warner, D. F.; Hoppe, H. C.; Laming, D.; Legoabe, L. J.; Khanye, S. D. *MedChemComm* **2019**, *10*, 326.

(21) Abdel-Magid, A. F.; Carson, K. G.; Harris, B. D.; Maryanoff, C. A.; Shah, R. D. *J. Org. Chem.* **1996**, *61*, 3849.

(22) (a) Xu, F.; Simmons, B.; Reamer, R. A.; Corley, E.; Murry, J.; Tschaen, D. *J. Org. Chem.* **2008**, *73*, 312; (b) Wong, Y.-L.; Mak, C.-Y.; Kwan, H. S.; Lee, H. K. *Inorg. Chim. Acta* **2010**, *363*, 1246.

(23) (a) Hausser, C. R.; Lindsay, J. K. *J. Org. Chem.* **1957**, *22*, 1246; (b) Dyachenko, V.; Peregudov, A.; Anan'ev, I.; Antipin, M. Y.; Nekrasov, Y. S.; Sokolov, V.; Igumnov, S. *Russ. Chem. Bull.* **2011**, *60*, 764.

(24) (a) Sturm, T.; Weissensteiner, W.; Spindler, F.; Mereiter, K.; López-Agenjo, A. M.; Manzano, B. R.; Jalón, F. A. *Organometallics* **2002**, *21*, 1766; (b) Weißenbacher, M.;

Sturm, T.; Kalchhauser, H.; Kratky, C.; Weissensteiner, W. *Monatsh. Chem.* **2002**, *133*, 991.

(25) Beteck, R. M.; Legoabe, L. J.; Isaacs, M.; Khanye, S. D.; Laming, D.; Hoppe, H. C. *Medicina* **2019**, *55*, 206.

(26) (a) Kumar, K.; Pradines, B.; Madamet, M.; Amalvict, R.; Benoit, N.; Kumar, V. *Eur. J. Med. Chem.* **2014**, *87*, 801; (b) Mundra, S.; Thakur, V.; Bello, A. M.; Rathore, S.; Asad, M.; Wei, L.; Yang, J.; Chakka, S. K.; Mahesh, R.; Malhotra, P. *Bioorg. Med. Chem.* **2017**, *25*, 5662.

Chapter 4: Synthesis, characterization and *in vitro* evaluation of ferrocenyl 1,3-benzoxazinone derivatives and their non-cyclic analogues

Inspired by the appealing *in vitro* biological activities of the ferrocenyl 1,3-benzoxazine derivatives discussed in **Chapter 3**, the current chapter further explores the structural features that are significant for the biological activity of this class of compounds. The scaffold of the studied compounds comprises three structural units, namely: the benzene ring, the oxazine unit and the ferrocene moiety appended via a methylene linker. To comprehensively examine the influence of each unit on the biological activity, it is prudent to consider the influence of each structural motif individually. Modifications of the ferrocene unit by introduction of basic aminoalkyl chains in position 2 and influence of benzene substituents had been studied in the preceding chapter, and a preliminary SAR model was proposed. Herein, attention is given to modifying the oxazine unit and its effect on the biological activity of the ferrocenyl 1,3-benzoxazine derivatives.

4.1. Rationale: Modification of the oxazine unit

The oxazine unit is an important structural motif featured in several bioactive compounds possessing a multitude of biological activities.[1] In the present case, the O-CH_2-N oxazine linkage is known to be crucial for the biological activity of 1,3-benzoxazine derivatives such as the compounds pursued in current study.[2] In fact, Urbański and colleagues attributed the antitumour activity of 1,3-benzoxazines to this moiety.[2a] To interrogate the pharmacophoric importance of this unit in the 1,3-benzoxazine scaffold of the target compounds, non-cyclic derivatives devoid of the oxazine methylene linkage (O-CH_2-N), i.e., α-amino-*o*-cresols,

together with their cyclic carbamate analogues (i.e., 1,3-benzoxazin-2-ones) containing O-CO-N in place of O-CH_2-N, were synthesized and assessed for biological activity.

4.1.1. Synthesis and characterisation of non-cyclic ferrocenyl 1,3-benzoxazine analogues: α-amino-*o*-cresols and salicylamides

The α-amino-*o*-cresols are an eminent class of phenolic compounds and have been demonstrated to possess antiplasmodial activities (**Figure 4.1**).[3] Furthermore, several α-aminocresols such as compounds **4.3** and **4.4a-b** are featured in the open-source MMV malaria box.[4]

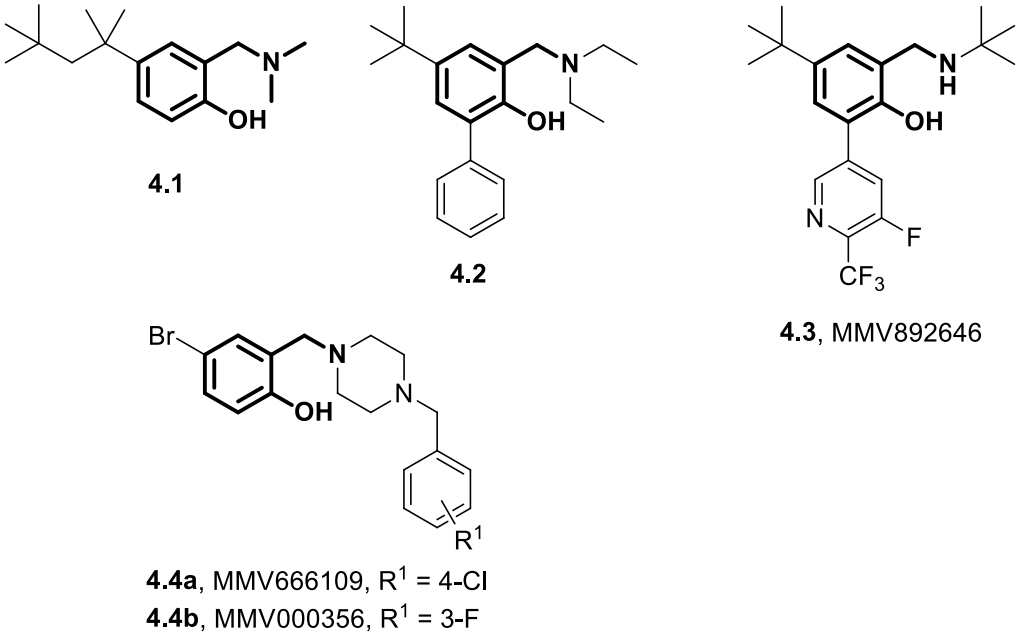

Figure 4.1 Chemical structures of α-amino-*o*-cresols possessing antiplasmodial activity.

Also, we could not find any reports on the biological activity of ferrocenyl α-amino-*o*-cresols when we performed a literature search on these compounds at the time of conducting the present study, despite the appealing strategy of incorporating ferrocene into biologically active chemical scaffolds for the generation of innovative bioactive agents.

Incidentally, the reaction of 4-bromophenol **3.1d** with ferrocenyl amine **3.12b** under Burke conditions for the synthesis of the 6-Br 1,3-benzoxazine product **3.16d** in **Chapter 3** led to concomitant formation of the side product, 4-bromo-α-amino-*o*-cresol **4.6c** in 13% yield (**Scheme 4.1**). This was not discussed in **Chapter 3** until this stage. When assessed for biological activity, this compound displayed potency that was comparable to its benzoxazine analogue, compound **3.16d** (**Scheme 4.1**).

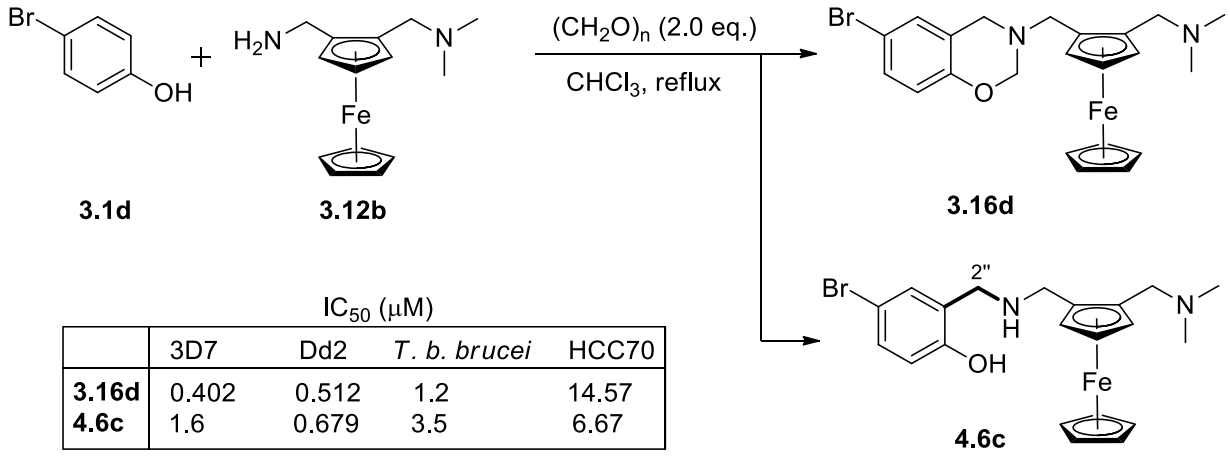

3.1d **3.12b** **3.16d** **4.6c**

IC_{50} (μM)

	3D7	Dd2	*T. b. brucei*	HCC70
3.16d	0.402	0.512	1.2	14.57
4.6c	1.6	0.679	3.5	6.67

Scheme 4.1 Synthesis of benzoxazine **3.16d** resulting in formation of its α-amino-*o*-cresol analogue, **4.6c**.

These observations further strengthened the argument for the modification of the 1,3-oxazine unit by removal of the O-CH_2-N linkage in the investigated compounds. To further elaborate the pharmacological profile of these novel ferrocenyl α-amino-*o*-cresols, amide derivatives of this class of compounds, i.e., ferrocenyl salicylamides, were prepared and subjected to pharmacological evaluation.

4.1.1.1. Synthesis and characterization of α-amino-*o*-cresols

Based on the formation of the α-amino-*o*-cresol **4.6c** containing one unit from formaldehyde (C-2‴) as illustrated in **Scheme 4.1**, the synthesis of α-amino-*o*-cresols was attempted by

Mannich condensation of suitably substituted phenols **3.1a-d** with ferrocenyl amine **3.12b** and paraformaldehyde in equimolar ratios, 1:1:1, under conditions similar to the Burke protocol employed to access the 1,3-benzoxazine derivatives in **Chapter 3**.[5] It was proposed that using one formaldehyde equivalent would exclusively furnish the non-cyclic Mannich product, α -amino-*o*-cresol, instead of the 1,3-benzoxazine product requiring two formaldehyde equivalents. However, regardless of this precaution, this approach exclusively yielded the undesired 1,3-benzoxazine almost for phenol **3.1c**, while the desired α-amino-*o*-cresol products were only achieved in less than 10% yield phenols **3.1a-b**,**d**. To overcome this challenge, an alternative stepwise route making use of a suitably substituted salicyaldehyde (**4.5a-i**) by reductive amination with amines **3.12a-b** and $NaBH_4$ as the reductant was employed to access the desired α-amino-*o*-cresol compounds (**Scheme 4.2**).[6] The first step of this route involves the formation of an imine intermediate, i.e., ferrocenyl salicylimine (**4.6a′-i′**, **4.7a′-e′**), *in situ* followed by reduction with $NaBH_4$ to produce the final product (**4.6a-i**, **4.7a-e**). The synthesis was focused on the CH_2NMe_2 ferrocenyl salicylamines (**4.6a-i**) prepared from amine **3.12b** since their benzoxazine variants showed the most promising activity in the biological screening assays. The unsubstituted ferrocenyl salicylamines (**4.7a-e**) from amine **3.12a** were included in the study for comparison.

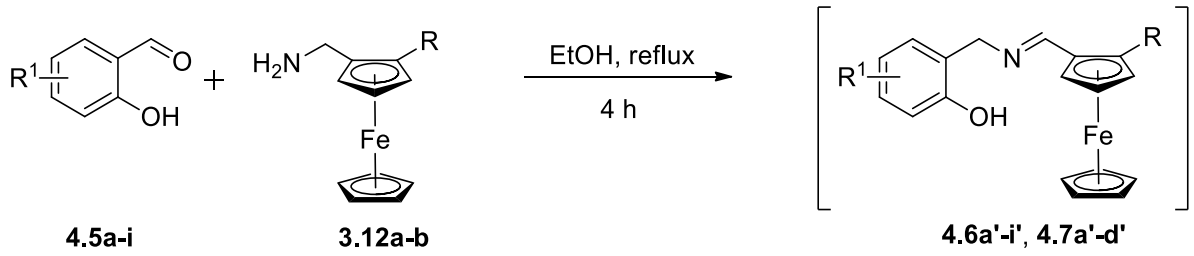

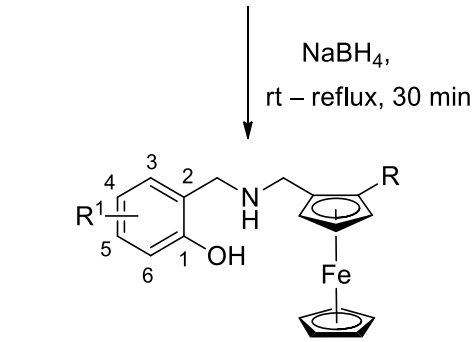

	R^1	Isolated yield (%)
R = CH_2NMe_2	**4.6a** : H	63
	4.6b : 4-Me	38
	4.6c : 4-Br	41
	4.6d : 4-OMe	50
	4.6e : 4-NO_2	35
	4.6f : 6-OMe	76
	4.6g : 6-NO_2	38
	4.6h : 4,6-Br	43
	4.6i : 4-Br, 6-NO_2	23
R = H	**4.7a** : H	98
	4.7b : 4-Br	97
	4.7c : 6-NO_2	96
	4.7d : 4,6-Br	71
	4.7e : 4-Br, 6-NO_2	82

Scheme 4.2 Synthesis of α-amino-*o*-cresols by reductive amination.

Despite being limited by the less availability of salicylaldehyde substrates relative to phenols, reductive amination offered direct access to the final compound in modest to excellent yields (23 – 98%) within two hours. The workup involved extracting the product into the aqueous phase with 2N HCl solution followed by washing with ethyl acetate (EtOAc). The product was recovered by neutralization with 1N NaOH solution and extraction with DCM to produce the target compound often in high purity in most cases without the need for further purification after removal of the solvent *in vacuo*. Where necessary, the product was purified by column chromatography on basic alumina.

As before, the structural identity of each compound was determined by spectroscopic techniques: NMR, IR and HRMS. From the representative ^{1}H NMR spectrum of **4.6f** presented in **Figure 4.2**, the benzene and ferrocene (FcH) protons were easily identified in the aromatic

and aliphatic regions as observed for the 1,3-benzoxazine derivatives in **Chapter 3**. The methylene protons of the cresol moiety (2″) together with the two ferrocenyl CH_2 groups (1′ and 2′) each appeared as two 1H doublets with *J*-coupling constants of 6.0, 12.7 and 14.0 Hz, respectively, as was observed for the benzoxazine analogues. As before, this could be explained by the anisotropic effects induced by the planar chirality of the ferrocene unit, which causes the protons attached to same carbon atom to resonate at different chemical shifts and couple each with other, i.e., to become diastereotopic.[7]

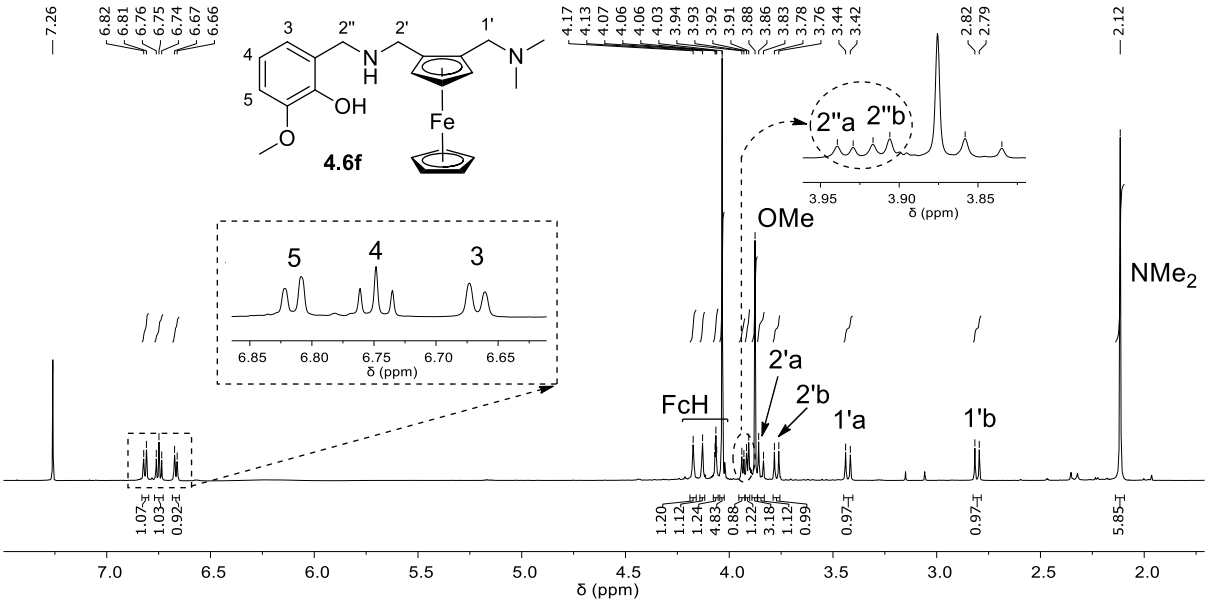

Figure 4.2 ^{1}H NMR spectrum of compound **4.6f** in $CDCl_3$.

To interrogate the influence of the hydroxyl group (OH) on the potential biological activity of this class of compounds, this functional group was removed (H) and replaced with OMe, NO_2 and NH_2 groups to produce non-cresol ferrocenyl benzylamines **4.9a-d** prepared from respective benzaldehydes **4.8a-c** and amine **3.12b** under similar reductive amination conditions in good yields (58 – 64%) (**Scheme 4.3**). The 2-aminobenzylamine **4.9d** was achieved by reduction of its 2-NO_2 congener (**4.9c**) with acidic zinc dust (Zn/H^+) in the presence of excess ammonium chloride (NH_4Cl) in 78% yield (**Scheme 4.3**).[8]

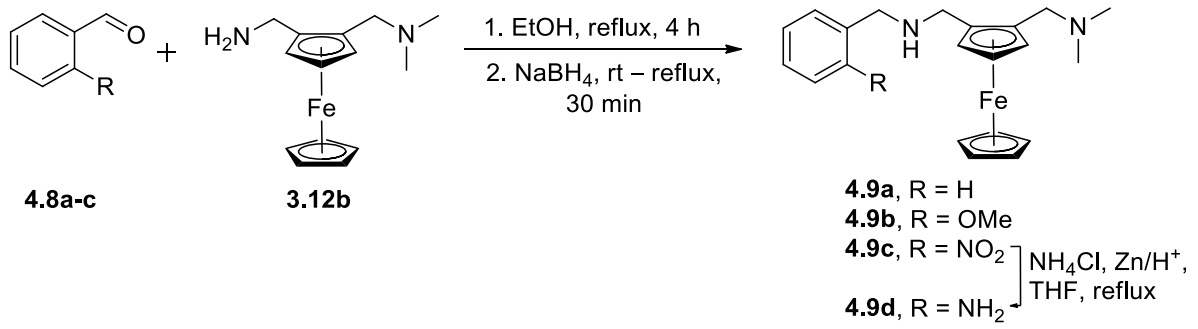

Scheme 4.3 Synthesis of non-cresol ferrocenyl benzylamine analogues **4.9a-d**.

The structures of the compounds were confirmed as previously described. For example, the presence of the electron-withdrawing NO_2 group in compound **4.9c** was verified by the deshielding of the benzene protons, which appeared below δ 7.40 ppm as two 1H doublets and two 1H triplets that were readily assigned by multiplet analysis as shown in **Figure 4.3**.

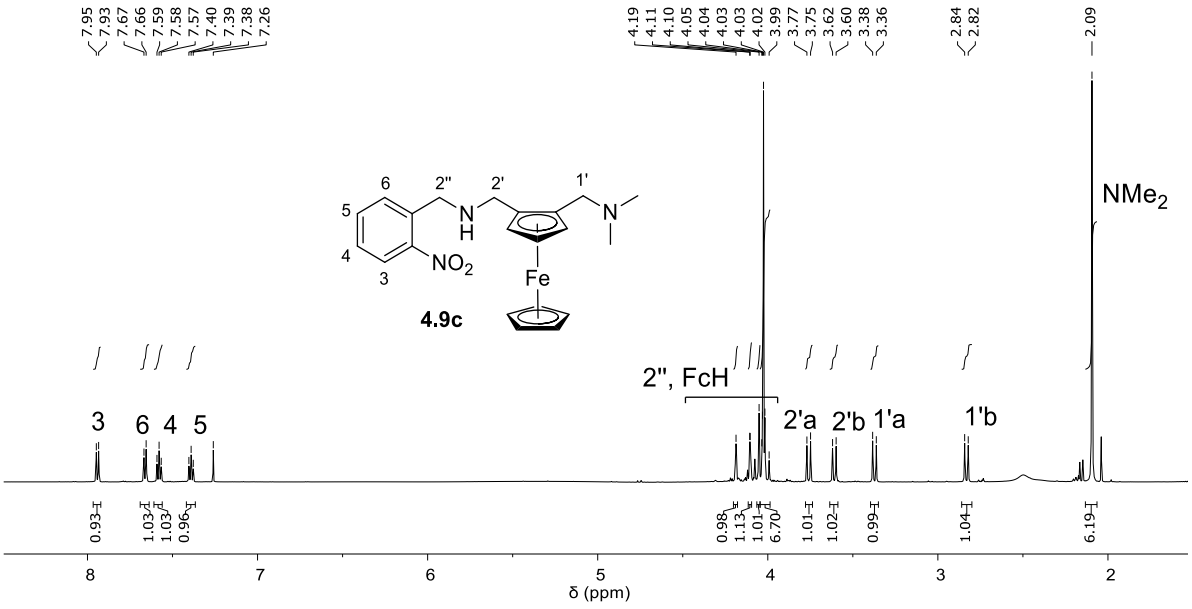

Figure 4.3 ^{1}H NMR spectrum of compound **4.9c**.

The NMR characterization data was supported by HRMS data. For all the ferrocenyl α-amino-*o*-cresols (**4.6a-i** and **4.7b-e**) and benzylamines (**4.9a-d**), the observed molecular masses were in agreement with the expected values (**Table 4.1**).

Table 4.1 HRMS results of ferrocenyl α-amino-*o*-cresols (**4.6a-i** and **4.7a-e**) and benzylamines (**4.9a-d**).

Compound	Predicted mass $[M]^+$	Found mass $[M+H]^+$
4.6a	379.1465	379.1467
4.6b	393.1631	393.1632
4.6c	456.0578	457.0573
4.6d	407.1858	407.1864
4.6e	423.1245	423.1986
4.6f	409.1578	409.1581
4.6g	424.1324	424.1324
4.6h	534.9683	534.9680
4.6i	502.0418	502.0420
4.7a	322.0889	322.0900
4.7b	399.9994	399.9661
4.7c	367.0745	367.0753
4.7d	477.9105	477.9099
4.7e	444.9845	444.9872
4.9a	363.1524	363.1527
4.9b	393.1622	393.1623
4.9c	408.1367	408.1369
4.9d	378.1633	378.1629

4.1.1.2. Synthesis of ferrocenyl salicylamides

To complete the investigation of the influence of structural modifications of the ferrocenyl α-amino-*o*-cresols on the biological activity of the compounds, the cresol -CH_2NH- motif was replaced with a carbonyl amide -CONH- by synthesizing five salicylamide analogues of the cresol compounds as representatives for comparison. Numerous compounds containing the salicylamide unit are vastly presented in literature and possess a myriad of biological activities, ranging from analgesic (**4.10**), antibacterial (**4.11**), anticancer (**4.12**) and antimalarial (**4.13**) activity (**Figure 4.4**).[9] This significantly strengthened the argument for the pursuit of ferrocenyl salicylamides for the SAR analysis of α-amino-*o*-cresols.

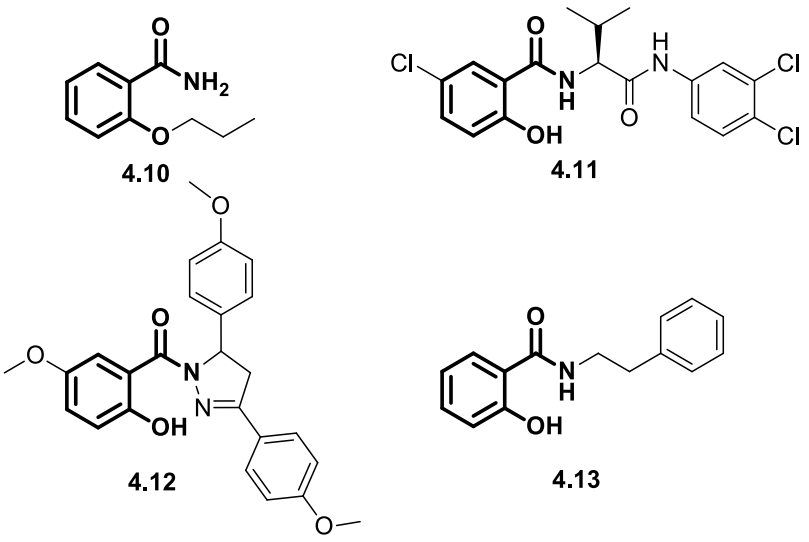

Figure 4.4 Salicylamide derivatives possessing biological activity.

Starting from salicylic acids **4.14a-e**, the target salicylamides **4.15a-e** were accessed via amidation with amine **3.12b**. Initially, salicylic acid **4.14a** was coupled to amine **3.12a** employing a one-pot procedure that proceeds via formation of the salicyloyl chloride *in situ* making use of phosphorus trichloride (PCl_3) as the chlorinating agent at 125 °C in chlorobenzene (**Scheme 4.4**).[10] The product (**4.15a**) was obtained in a low yield of 9%, possibly due to the harsh reaction conditions of this procedure, following a tedious workup involving difficult removal of the chlorobenzene and complicated purification by silica gel column chromatography.

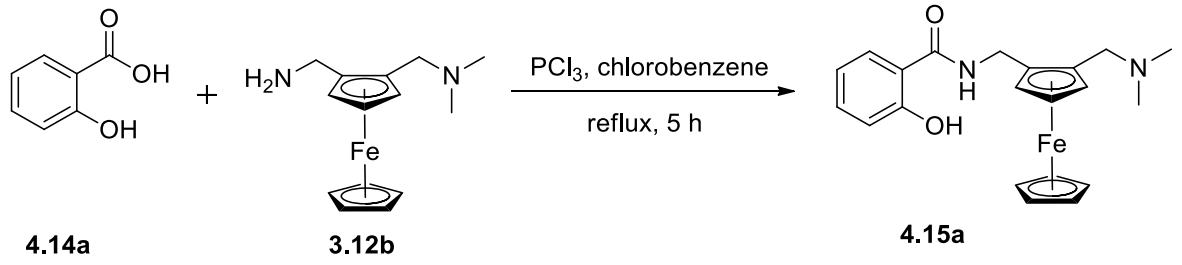

Scheme 4.4 Formation of salicylamide **4.15a** by amidation with PCl_3.

To avoid the harsh reaction conditions, amidation via formation of a salicyloyl chloride intermediate using chlorinating agents such as thionyl chloride ($SOCl_2$) or oxalyl chloride was

abandoned in favour of milder alternatives.[11] Thus, application of a coupling agent to lessen the energy demands of the reaction was imminent. The amidation coupling agents, 1-ethyl-3-(3-dimethylaminopropyl)carbodiimide hydrochloride (EDCI•HCl) and *N,N'*-dicyclohexylcarbodiimide (DCC) were screened for the coupling of salicylic acid **4.14a** with amine **3.12b** at room temperature in 30% pyridine/DCM solution and in pyridine, respectively (**Scheme 4.5**).[12] The progress of each reaction was monitored by TLC as before.

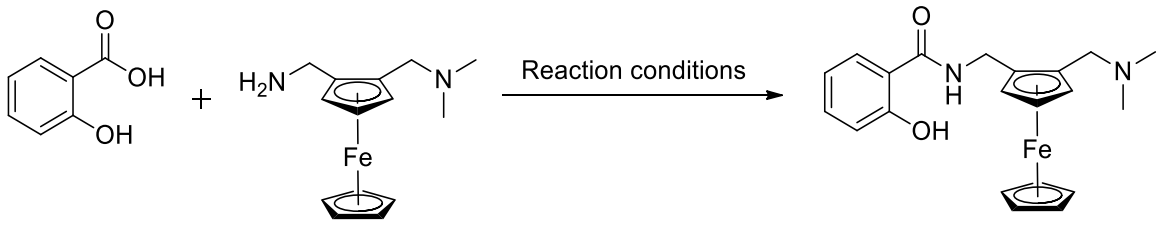

4.14a **3.12b** **4.15a**

Reaction condtions	Yield (%)
EDCI•HCl, 30% pyridine/DCM, rt	0
DCC, pyridine, rt	48

Scheme 4.5 Synthesis of salicylamide **4.15a** using coupling agents, EDCI•HCl and DCC.

Amidation with EDCI•HCl failed to give the desired amide product after 48 hours of stirring, whereas coupling with DCC showed complete conversion of the substrates to the target compound only after 24 hours of the reaction time. Despite the appeal of DCC, removal of the formed urea precipitate side product from the formed amide products proved challenging. After termination of the reaction, the reaction mixture was diluted with EtOAc and filtered through a pad of celite for several times to afford the crude product after removal of the solvent *in vacuo*. The crude product was then subjected to silica gel chromatography to afford the desired compound **4.15a** in 48% yield. In some instances, trace amounts of the urea side product were noticed on the ^{1}H NMR spectrum of the purified product, necessitating further purification.

Given the complex purification of the salicylamide synthesized with DCC, which was time-consuming, it was necessary to optimize the amidation protocol to allow expedient access to

the rest of the target compounds. Thus, the reaction with DCC was performed by microwave irradiation at 80 °C and the product was purified as above. This shortened the reaction time from 24 to 2 hours. The rest of the salicylamides **4.15b-e** were synthesized under these conditions and obtained in good to excellent yields in high purity. A 2-hydroxypyridinyl derivative (**4.15e**) of salicylamide **4.15a** was included in the study to further investigate the pharmacological effect of replacing the benzene unit with its isosteric pyridine ring.

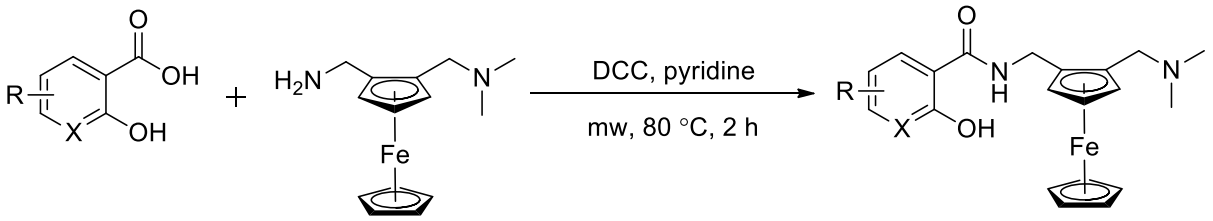

	R	Isolated yield (%)
X = CH	**4.15a** : H	92
	4.15b : 5-Cl	95
	4.15c : 5-NO_2	78
	4.15d : 4-F	82
X = N	**4.15e** : H	69

Scheme 4.6 Synthesis of ferrocenyl salicylamides **4.15a-e** by microwave irradiation using DCC.

The NMR, IR and HRMS spectral data of the compounds confirmed their structural identity. Importantly, a new carbonyl band was observed in the representative IR spectra of the target salicylamide derivative **4.15a** around *v*: 1586 cm^{-1}, which was absent in the IR spectra of the corresponding α-amino-*o*-cresol **4.6a**, confirming successful formation of the amide bond as illustrated in **Figure 4.5**.

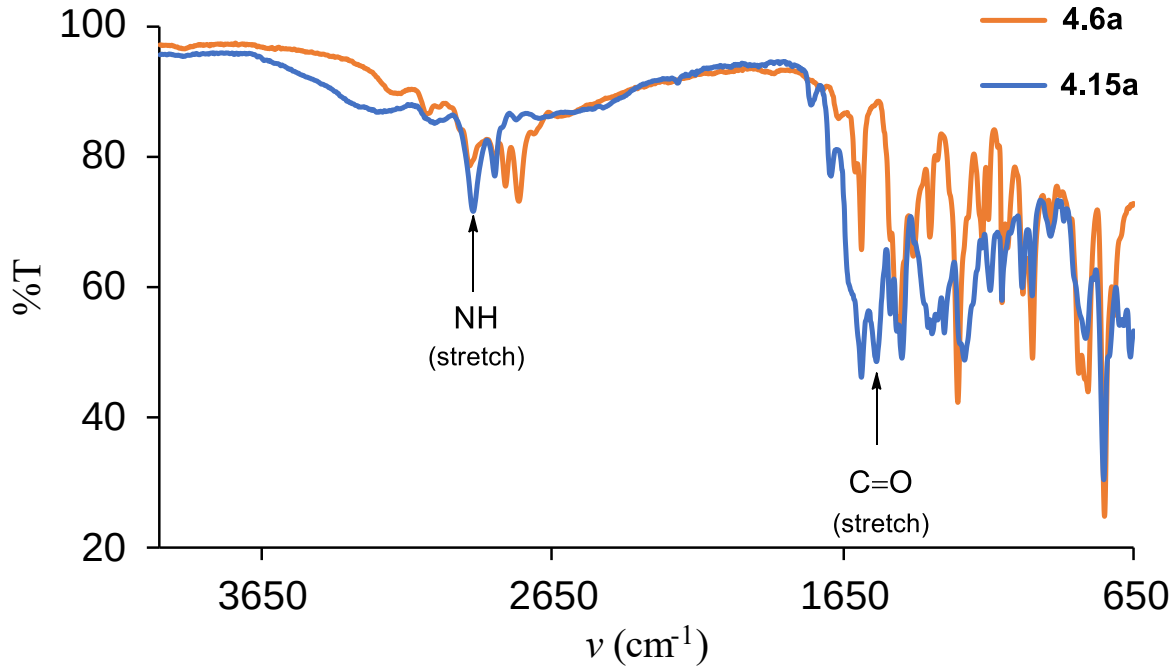

Figure 4.5 IR spectra of the salicylamide **4.15a** and its α-amino-*o*-cresol **4.6a**.

The formation of the amide bond was further confirmed by the splitting of the anisotropic methylene protons (2′) at δ 4.49 and 4.31 ppm into two 1H doublets of doublets (dd) with *J*-coupling constants of 15.0 and 4.7 Hz due to correlation with the NH group in the ^{1}H NMR spectrum of the pyridinyl amide **4.15e**. This was corroborated by the H – H correlation of these protons (correlation *a*) shown in the COSY spectrum of compound **4.15e** (**Figure 4.6**).

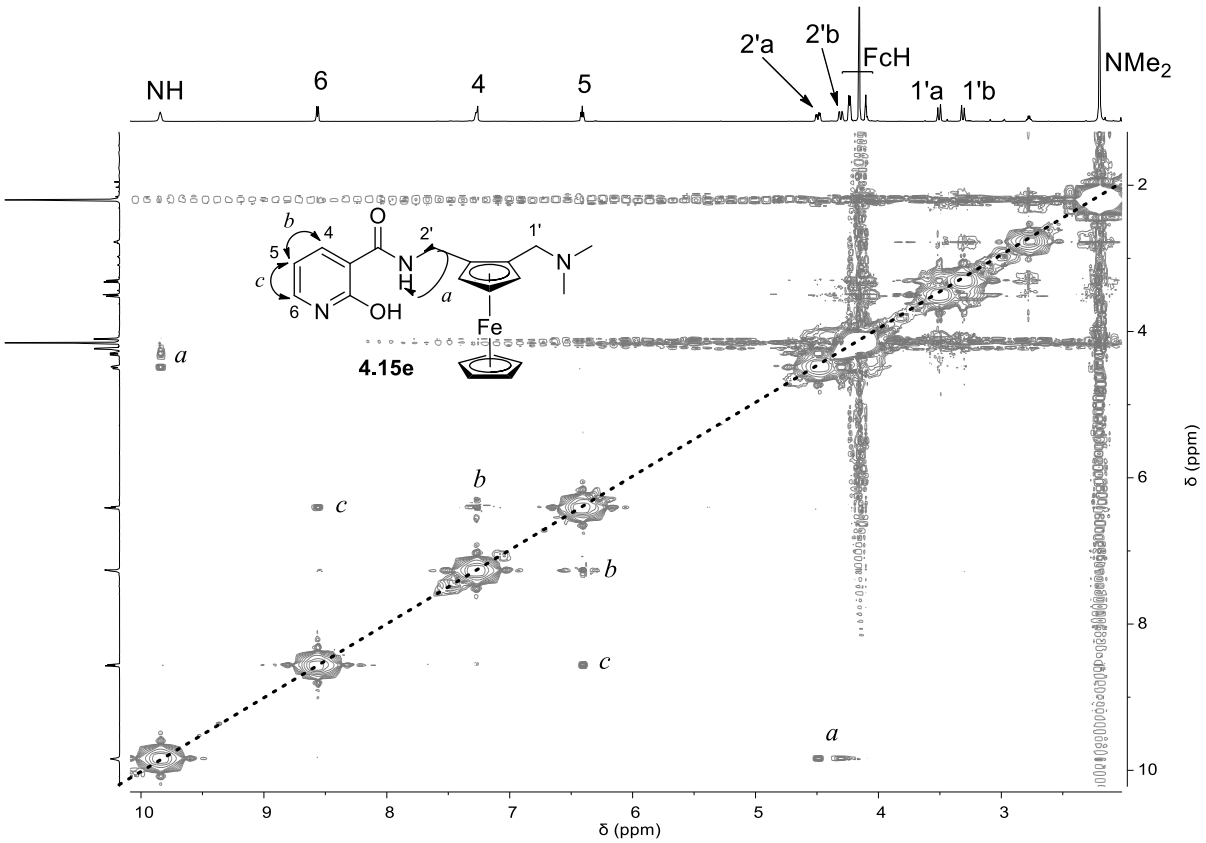

Figure 4.6 COSY spectrum of compound **4.15e** in the $CDCl_3$.

Unsubstituted ferrocenyl analogues of **4.15a**, i.e., *N*-ferrocenemethylsalicylamide **4.16a** and its thiol variant **4.16b**, were also prepared from the corresponding amine **3.12a** to support the SAR analysis. The methylene protons (1′) were observed as a 2H doublet in the aliphatic region in the ^{1}H NMR spectrum of compound **4.16a** due to coupling with the NH group at δ 12.37 ppm (J = 5.1 Hz) (**Figure 4.6**). The splitting of these protons was not observed in the spectrum of the thiol derivative **4.16b**, possibly due to the signal of the exchangeable NH proton not being visible in the spectrum (**Figure 4.7**). Additionally, the presence of the thiol group (2-SH) resulted in the deshielding of the benzene protons when compared to the salicylamide (2-OH) congener **4.16a**.[13]

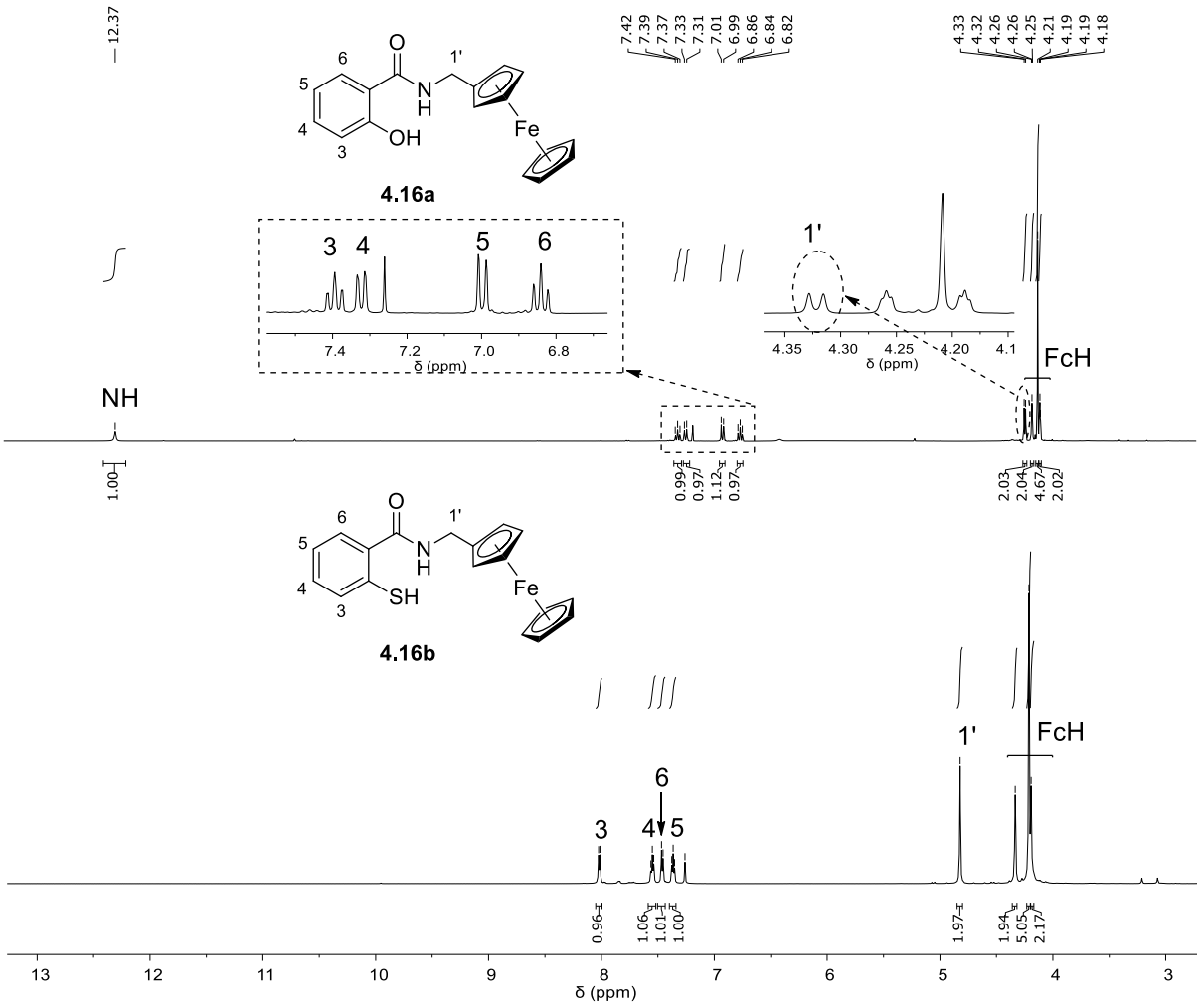

Figure 4.7 ^{1}H NMR spectra of salicylamide **4.16a** and its thiol analogue **4.16b** in $CDCl_3$.

The calculated masses of the ferrocenyl salicylamides (**4.15a-e** and **4.16a-b**) corresponded to the experimental values obtained by HRMS (**Table 4.2**).

Table 4.2 HRMS data of ferrocenyl salicylamides (**4.15a-e** and **4.16a-b**).

Compound	Predicted mass $[M+H]^+$	Found mass $[M+H]^+$
4.15a	392.1187	393.1265
4.15b	426.0797	427.0874
4.15c	437.1038	438.1120
4.15d	409.1015	409.1015[a]
4.15e	394.1218	394.1221
4.16a	335.0609	335.0601[b]
4.16b	351.0380	351.0269[b]

[a]Mass was observed in negative ionization mode as $[M]^-$ ion. [b]Masses were observed as $[M]^+$ ions.

4.1.2. Synthesis and characterization of ferrocenyl 1,3-benzoxazinone derivatives: 1,3-benzoxazin-2-ones and 1,3-benzoxazin-2,4-diones

Having removed the O-CH_2-N oxazine linkage in the ferrocenyl 1,3-benzoxazine compounds under investigation by synthesizing their non-cyclic α-amino-*o*-cresols and salicylamides, attention was directed towards the replacement of this unit with its carbamate variant, O-CO-N, to produce the 1,3-benzoxazin-2-one analogues. Preparation of 1,3-benzoxazn-2,4-diones was also performed by cyclization of salicylamides.

4.1.2.1. Synthesis of ferrocenyl 1,3-benzoxazin-2-one derivatives

The α-amino-*o*-cresols were converted to their corresponding benzoxazine-2-ones by cyclisation with 1,1'-carbonyldiimidazole (CDI) in DCM by stirring at room temperature for 1 – 2 hours (**Scheme 4.7**).[14] This transformation was initially performed with triphosgene under basic conditions but later abandoned due to difficulties in purification and low yields.[12b]

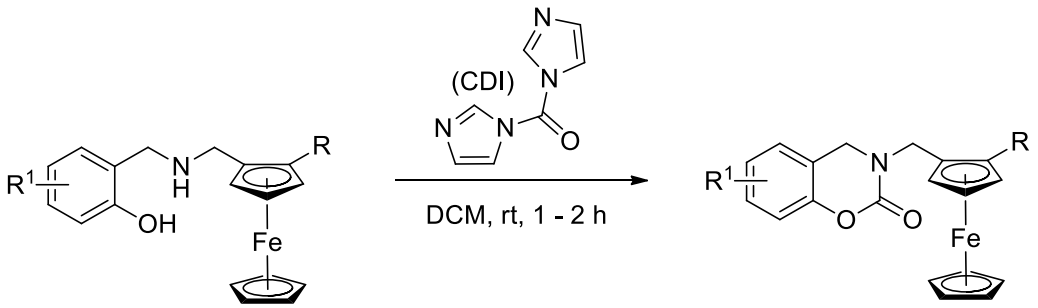

4.6, **4.7** **4.17a-d**, **4.18a-e**

	R^1	Isolated yield (%)
R = CH_2NMe_2	**4.17a** : H	60
	4.17b : 6-Br	45
	4.17c : 6,8-Br	65
	4.17d : 8-OMe	81
R = H	**4.18a** : H	76
	4.18b : 6-Br	66
	4.18c : 6,8-Br	71
	4.18d : 8-OMe	89
	4.18e : 8-NO_2	71

Scheme 4.7 Synthesis of ferrocenyl 1,3-benzoxazin-2-one derivatives.

Synthesis with CDI involving stirring a relevant α-amino-*o*-cresol with CDI in 1:1.2 molar ratios in DCM for 1 hour at room temperature, followed by a simple workup of washing the formed product successively with 0.5N NaOH solution and water allowed convenient access to the target carbamate product often with no need for further purification. Where necessary, the product was purified by column chromatography with basic alumina. Only a representative series of this class of compounds was prepared due to their modest biological activity when evaluated against the targeted diseases.

The formation of the carbamate product was confirmed with IR and other spectral data. The disappearance of the O–H bend at ν 1477 cm^{-1} and the appearance of a new C=O stretch at ν 1694.0 cm^{-1} in the representative IR spectra of α-amino-*o*-cresol **4.7b** and its 1,3-benzoxazin-2-one counterpart **4.18b**, respectively, substantiated successful cyclization (**Figure 4.8**).

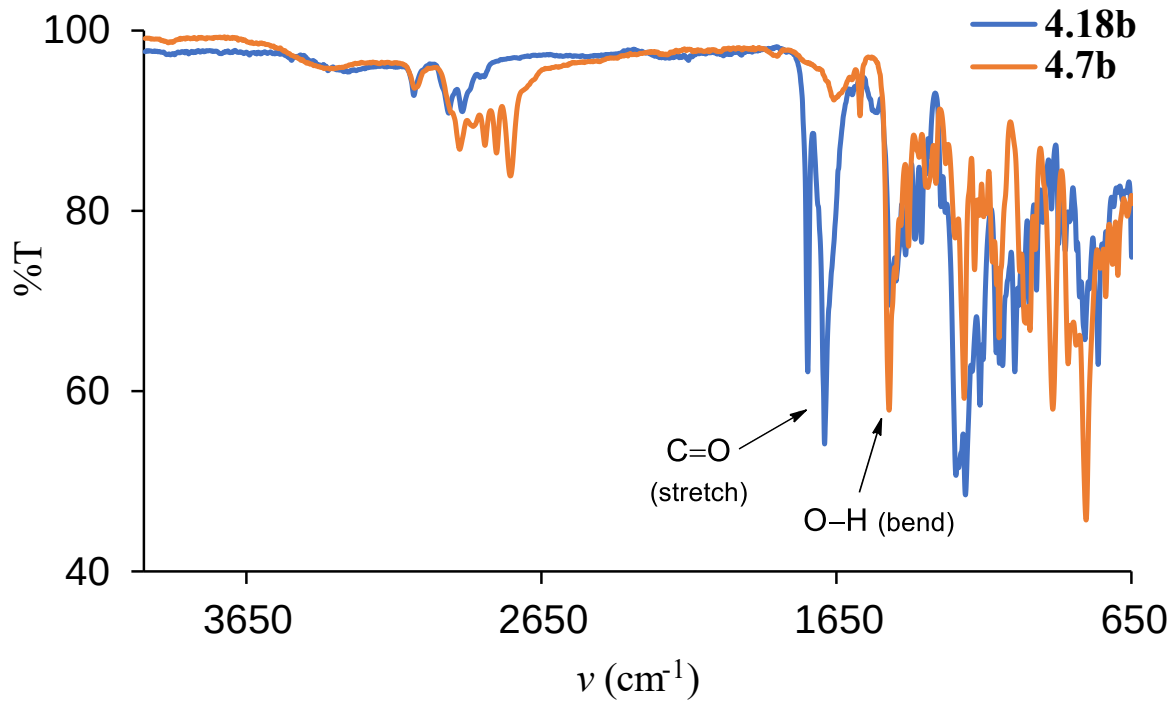

Figure 4.8 IR spectrum of compound **4.18b** with its non-cyclic α-amino-*o*-cresol analogue **4.7b**.

The appearance of a new carbonyl peak δ 148.0 ppm in the ^{13}C NMR spectra of the prepared cyclic ferrocenyl 1,3-benzoxazin-2-ones (**4.17a-d** and **4.18a-e**) confirmed the newly formed carbamate unit (O-CO-N). The aligned ^{13}C NMR spectra of the 8-methoxy-1,3-benzoxazin-2-one (**4.17d**) with its non-cyclic analogue (**4.16f**) illustrate the formation of the carbamate (**Figure 4.9**).

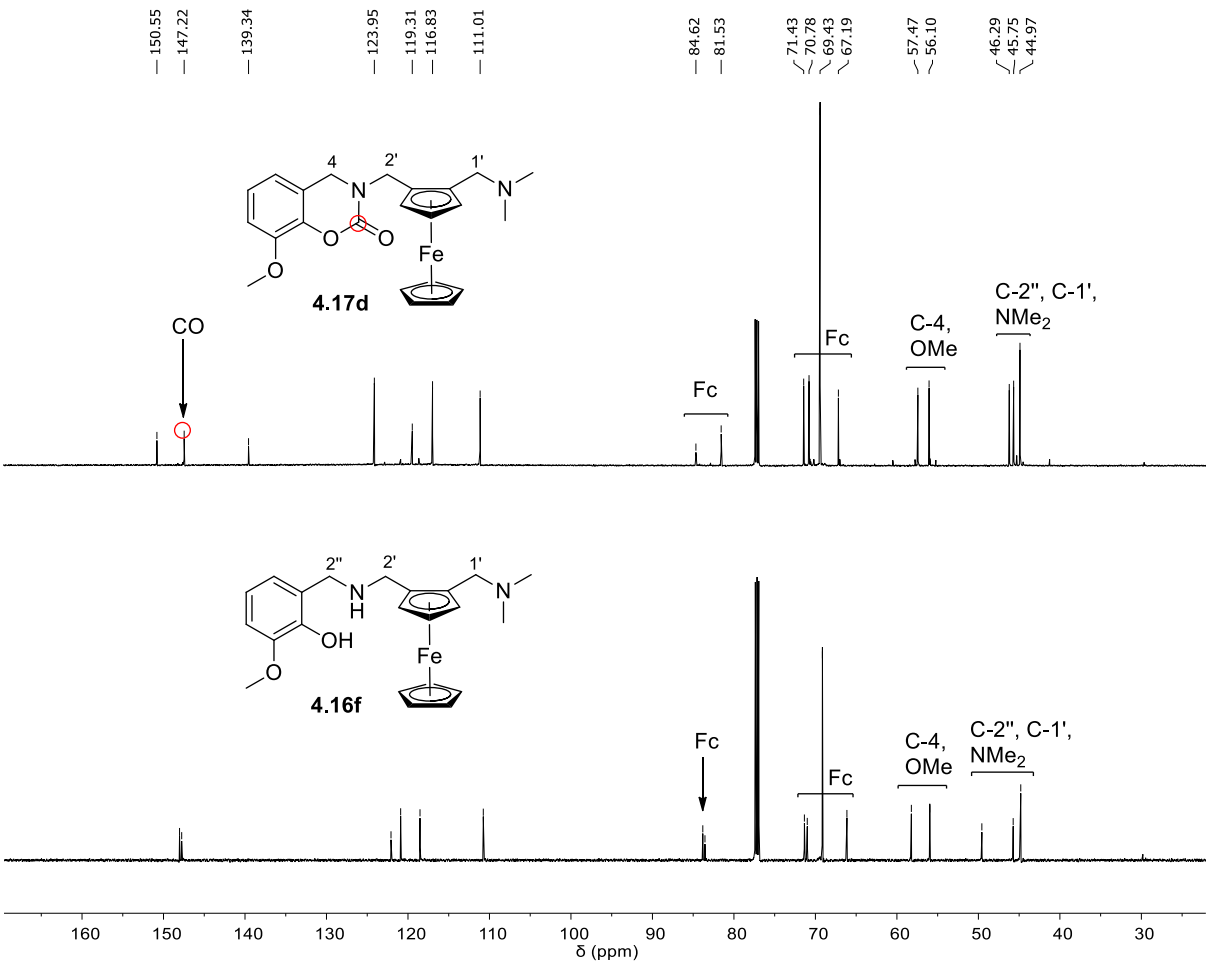

Figure 4.9 ^{13}C NMR spectra of 1,3-benzoxazin-2-one **4.17d** and its α-amino-*o*-cresol derivative **4.16f** in $CDCl_3$.

Furthermore, the HRMS data of 1,3-benzoxazines were in agreement with the predicted results. The masses of the cyclized target compounds (**4.17a-d** and **4.18a-e**) were higher than those of the aminocresols (**4.6a-i** and **4.7a-e**) by approximately mass units equivalent to the CO group, as shown in the HRMS spectra of HRMS spectra of 1,3-benzoxazin-2-one **4.17a** and its α-amino-*o*-cresol substrate **4.6a** (**Figure 4.10**). Full structural characterization details of the compounds are provided in **Chapter 8**.

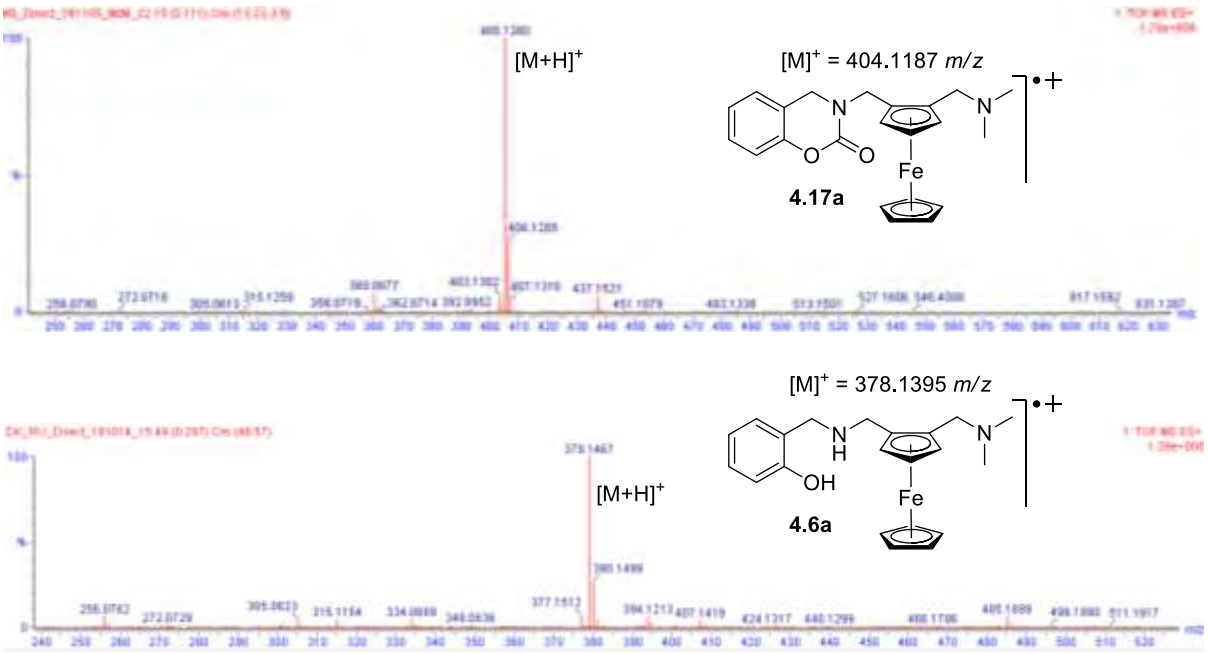

Figure 4.10 HRMS spectra of 1,3-benzoxazin-2-one **4.17a** and its α-amino-*o*-cresol analogue **4.6a**.

4.1.2.2. Synthesis and characterization of ferrocenyl 1,3-benzoxazin-2,4-dione derivatives

To synthesize the 1,3-benzoxazine derivatives of salicylamides, the acyclic analogues **4.15a-e** and **4.16a-b** were subjected to similar reaction conditions as the α-amino-*o*-cresols to produce ferrocenyl 1,3-benzoxazin-2,4-dione derivatives. Benzoxazin-2,4-diones and their thioxo derivatives have been extensively studied by the research group of Waisser as bioactive agents against strains of *Mycobacterium tuberculosis*.[10,15] Examples of chemical structures of 1,3-benzoxazin-2,4-diones and their thioxo variants possessing antitubercular activity are shown in **Figure 4.11**.[10,15] Interestingly, there were no literature reports on the organometallic derivatives of these compounds at time this study was undertaken. This provided further motivation to pursue ferrocenyl derivatives of these compounds.

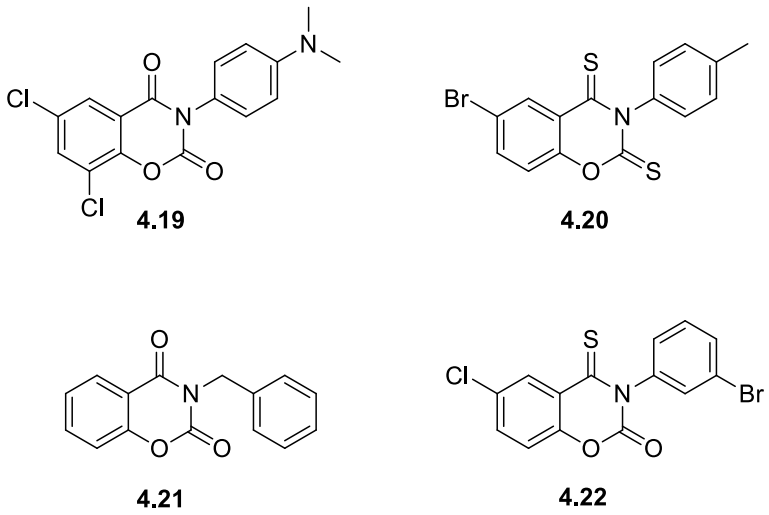

Figure 4.11 Chemical structures of organic 1,3-benzoxazin-2,4-diones and their thioxo derivatives possessing antitubercular activity.

The cyclization of salicylamides was conducted similarly to the synthesis of 1,3-benzoxazin-2-ones **4.17a-d** and **4.18a-e** with CDI (**Scheme 4.8**). To our surprise, only the unsubstituted ferrocenyl salicylamide **4.16a** was successfully converted to its benzoxazine analogue **4.24a** under these conditions.

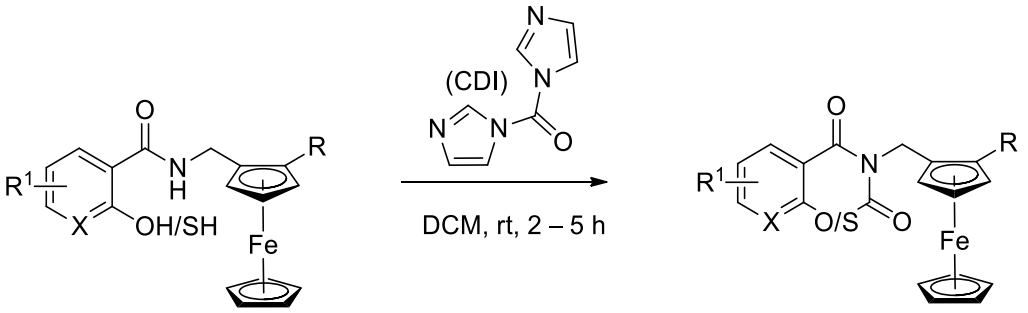

4.15a-e, **4.16a-b** **4.23a-e**, **4.24a-b**

		R^1	R	Isolated yield (%)
X = CH	**4.23a**	H	CH_2NMe	0
	4.23b	6-Cl	CH_2NMe	0
	4.23c	6-NO_2	CH_2NMe	0
	4.23d	7-F	CH_2NMe	0
X = N	**4.23e**	H	CH_2NMe	0
X = CH	**4.24a**	H	H	41
	4.24b*	H	H	0

Scheme 4.8 Synthesis of ferrocenyl 1,3-benzoxazin-2,4-diones with CDI. **4.42b*** = unsuccessful 1,3-benzothiazine product from the reaction of thiosalicylamide **4.16b**.

Even salicylamide **4.15a**, differing from the successfully cyclized congener **4.16a** only by the ferrocenyl side chain, could not be transformed into the desired benzoxazin-2,4-dione **4.23a**. Thus, it was hypothesized that failure to cyclize the basic CH_2NMe_2 ferrocenyl salicylamides **4.15a-e** could have been caused by the influence of the CH_2NMe_2 side chain. This seemed plausible since this is the only structural difference between the two salicylamides. Moreover, Geffken did not encounter similar challenges in his cyclization of *N*-phenylsalicylamide to its 1,3-benzoxzin-2,4-dione devoid of any basic side chain.[16] Consideration of the mechanism of cyclization by CDI may provide justification to illustrate the possible effect of the CH_2NMe_2 in preventing ring-closure of the salicylamides. According to Geffken, the reaction proceeds via formation of an isoimide **4.27**, which undergoes rearrangement under basic conditions in DCM to produce the benzoxazine-2,4-dione product **4.28** (**Scheme 4.9**).[16]

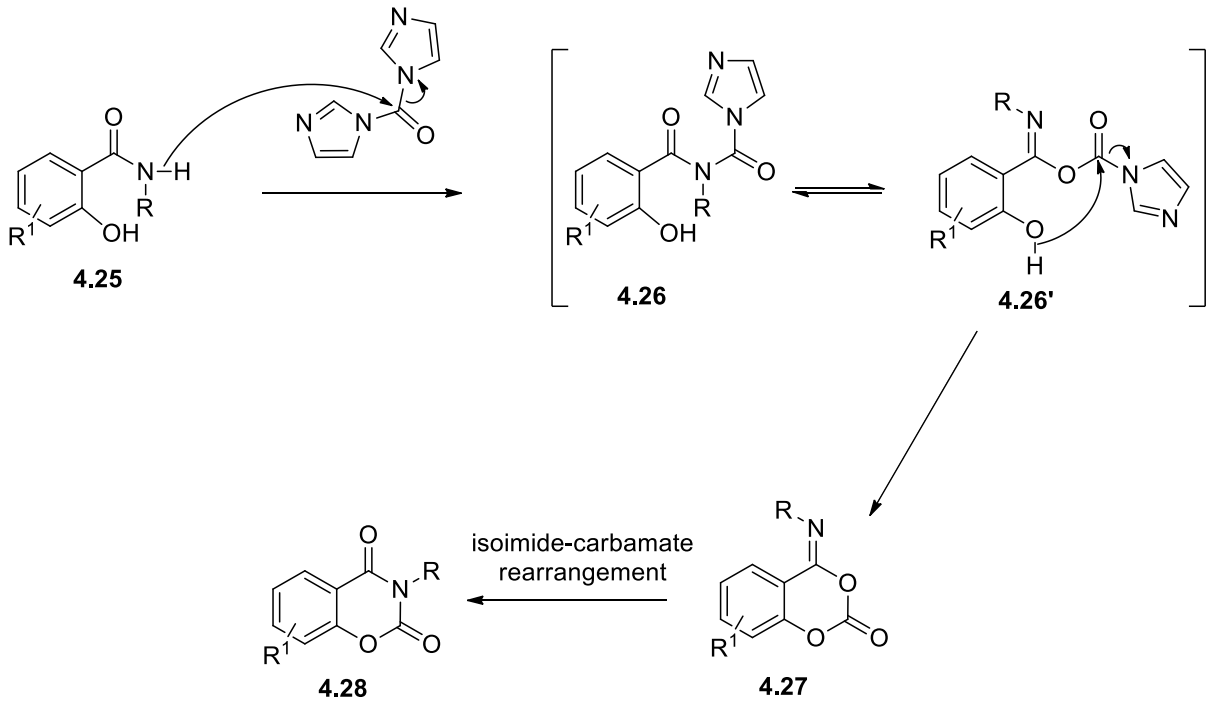

Scheme 4.9 Possible mechanism for formation of 1,3-benzoxazin-2,4-diones by cyclization of salicylamides with CDI.[16]

The reaction is initiated by substitution of one imidazole unit from CDI, resulting in an open chain intermediate (**4.26**/**4.26′**). The ring-closure step is achieved when the phenolic OH group attacks the carbonyl group of the CDI, thus replacing the second imidazole unit to yield the isoimide intermediate **4.27**, which rearranges to the 1,3-benzoxazin-2,4-dione product **4.28**. In the case of cyclization of CH_2NMe_2 ferrocenyl salicylamides, it is proposed that the basic nitrogen atom of the CH_2NMe_2 chain forms a strong intramolecular hydrogen bond with the phenolic OH group in the isoimide intermediates **4.49a′-e′**, preventing attack of the imidazolyl carbonyl to produce the benzoxazine-2,4-dione products **4.23a-e** (**Scheme 4.10**). Indeed, intramolecular hydrogen bonding is known to prevent some reactions from taking place, even in biological systems, as documented in literature.[17]

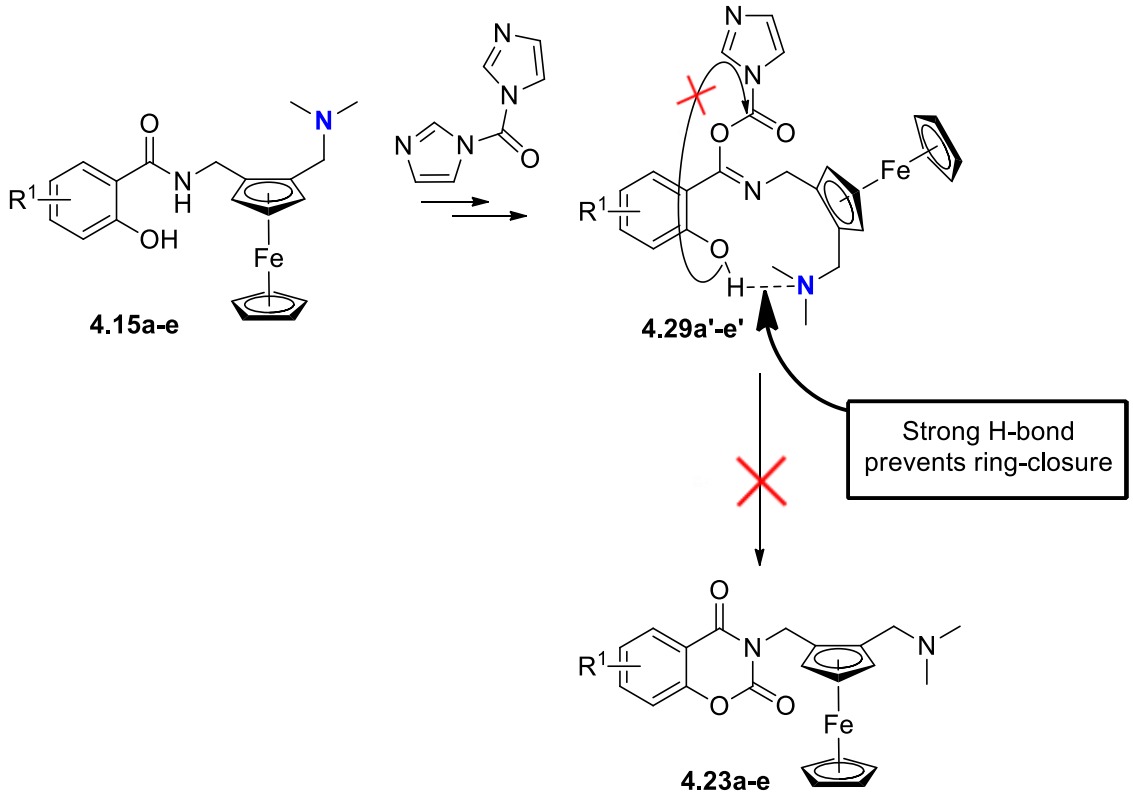

Scheme 4.10 Proposed explanation for the failure of cyclization of salicylamides **4.15a-e** into corresponding 1,3-benzoxazin-2,4-diones **4.23a-e** by CDI.

Furthermore, the monitoring (TLC) of the cyclization of salicylamides **4.15a-e** revealed formation of new spots (R_f: 0.53 – 0.65) above that of the starting material (R_f: 0.42 – 0.46). Regrettably, after washing the reaction mixture with 0.5N NaOH solution and water only the salicylamide spot was visible. This led us to conclude that the workup could be responsible for the hydrolysis of the product back to the salicylamide substrate. To overcome this challenge, the reaction solution was only washed with distilled water, dried (Na_2SO_4) and the solvent removed *in vacuo*. The obtained material was immediately subjected to ^{1}H NMR analysis for identification. The NMR revealed the compound to be an acyclic isoimide intermediate (**4.29a′-e′**). This is better illustrated by the cyclization of the 5-Cl salicylamide **4.15b** (**Figure 4.12**). Formation of the isoimide was confirmed by the appearance of the imidazole protons at δ 7.61 and 7.04 ppm as 1H and 2H singlets, respectively (**Figure 4.12B**). This was further

supported by the deshielding of the 2′a proton of methylene group attached to the amide N atom.

The stability of this material was monitored with NMR for 2 hours in 30-minute intervals.

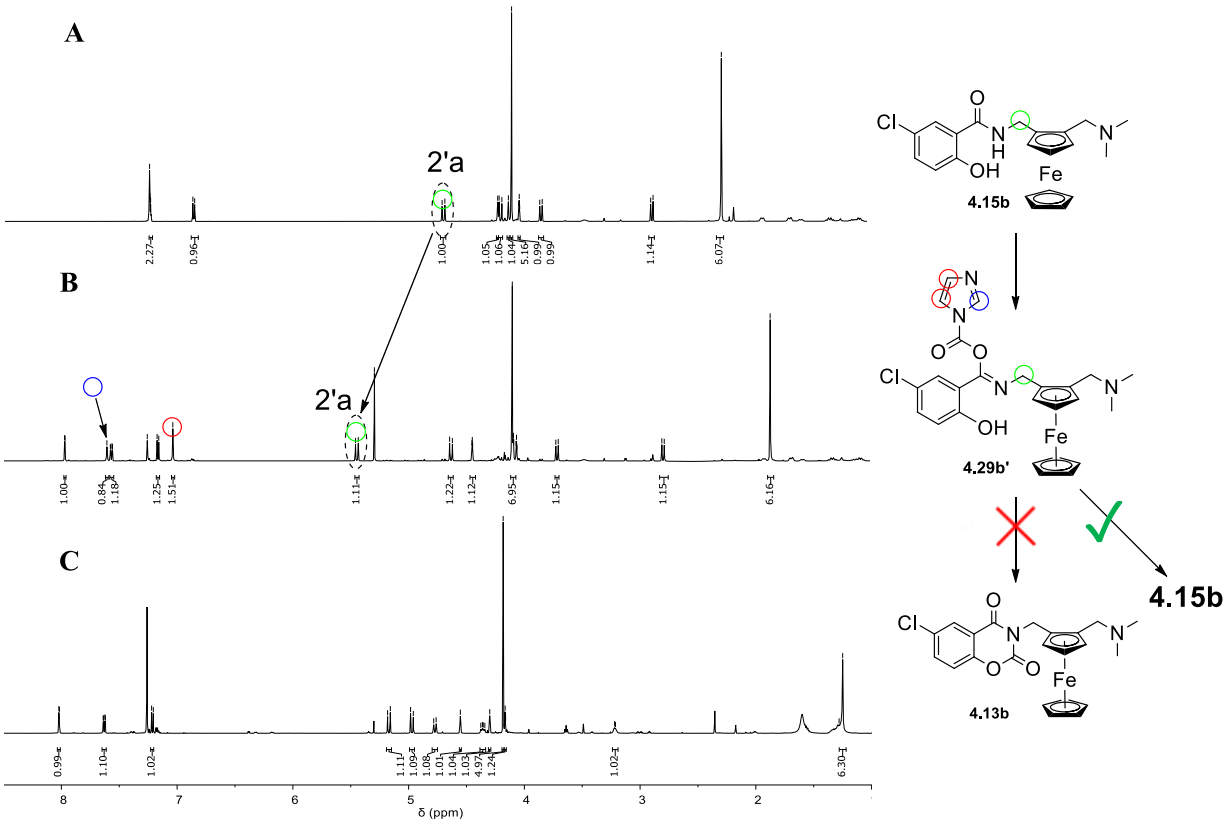

Figure 4.12 Cyclization of salicylamide **4.15b** monitored by NMR. (**A**) ^{1}H NMR spectrum of unreacted **4.15b**. (**B**) ^{1}H NMR spectrum of the isolated isoimide **4.29b′**. (**C**) ^{1}H NMR spectrum of the isoimide sample acquired after 1 hour.

Notwithstanding the proposed explanation for unsuccessful cyclization due to possible intramolecular hydrogen bonding of the ferrocenyl CH_2NMe_2 side chain and phenolic OH, the electronic factors of the benzene substituents are crucial in many chemical transformations. Particularly, the benzene substituents of phenolic compounds, such as the investigated salicylamides, influence the acidity and nucleophilicity of the OH group.[18] Since the OH acts as a nucleophile in the ring-closure step of the reaction (**Scheme 4.9**), we considered it prudent to interrogate the electronic effects of benzene substituents on the reaction. A 5-Cl

unsubstituted ferrocenyl salicylamide (**4.16c**) carrying a chlorine group on the benzene ring was synthesized according to conditions in **Scheme 4.6** and characterized as shown in **Figure 4.13**.

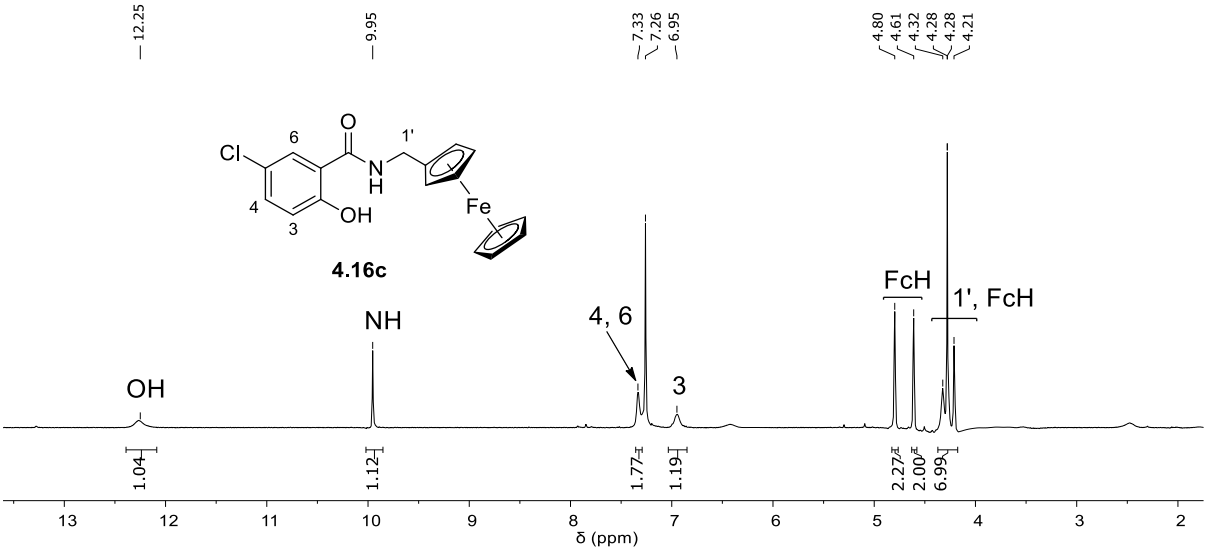

Figure 4.13 ^{1}H NMR spectrum of 5-Cl salicylamide **4.16c** in $CDCl_3$.

When subjected to the cyclization conditions with CDI (**Scheme 4.8**), the compound failed to give the corresponding 1,3-benzoxazin-2,4-dione product. This suggested that the presence of EWGs, particularly halogens, on the benzene ring of salicylamides might be unfavourable for cyclization with CDI, possibly due to deactivation of the phenolic OH via electronic induction.[19]

In attempts to overcome the challenges encountered with CDI cyclization, alternative carbamate cyclization procedures that are not mediated by the formation of an isoimide intermediate were explored. Among the investigated cyclization alternatives were procedures that employ the use of chloroformates (MeOOCCl, EtOOCCl, BnOOCCl and PhOOCl), triphosgene, oxalyl chloride ($(COCl)_2$), carbon dioxide (CO_2) and isocyanate salts as sources of the carbonyl carbamate functionality (**Scheme 4.11**).[10,20]

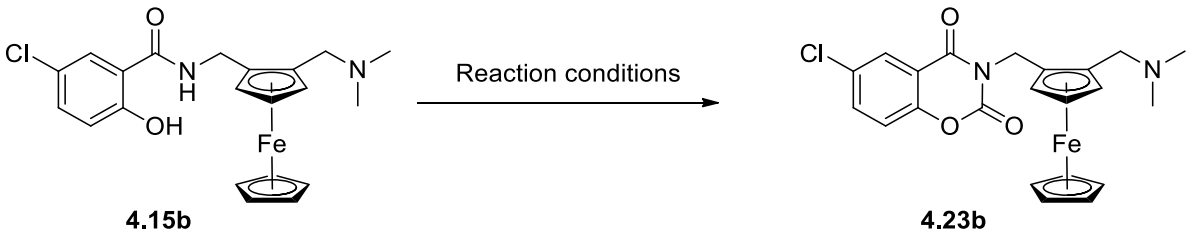

4.15b **4.23b**

Reaction condtions	Isolated yield (%)
MeOOCCl or EtOOCCl or BnOOCCl or PhOOCCl, pyridine, reflux	0
Triphosgene, pyridine, reflux	0
$(COCl)_2$, toluene, reflux	8
CO_2, DEAD, PPh_3, DMSO, Δ	0
NaOCN or KOCN, F_3CCOOH, rt	0

Scheme 4.11 Cyclization of salicylamide **4.15b** by alternative procedures.

Despite the poor product yield (8%), cyclization with oxalyl chloride was the only method that furnished the desired 1,3-benzoxazin-2,4-one product **4.23b**.[20b] The obtained amount of the product was just adequate for NMR characterization. The ^{13}C NMR was invaluable to unambiguously confirm successful formation of the product. A new carbonyl signal was observed in the ^{13}C NMR spectrum of compound **4.23b**, confirming successful cyclization of salicylamide **4.15b** (**Figure 4.14**).

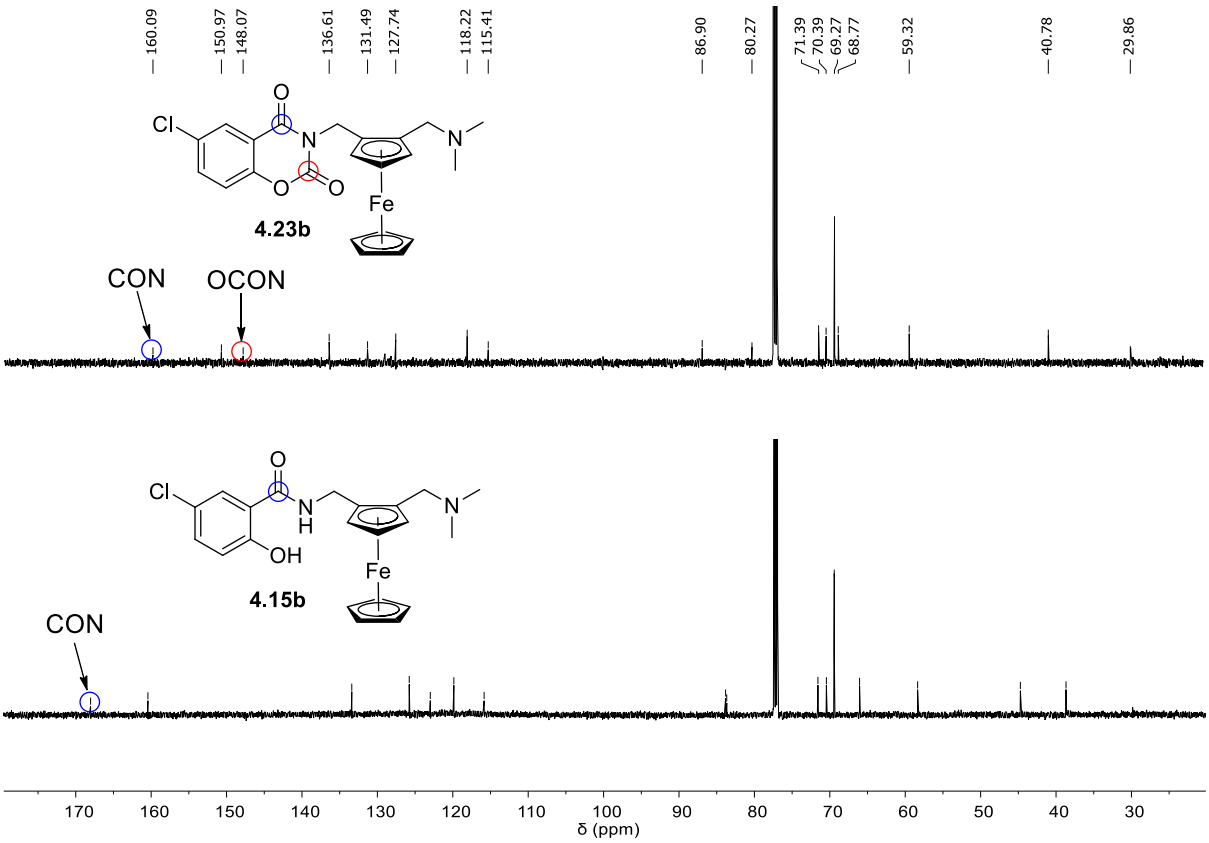

Figure 4.14 ^{13}C NMR spectrum of 1,3-benzoxazin-2,4-dione **4.23b** with its acyclic salicylamide analogue **4.15b** in $CDCl_3$.

Due to time constraints and scope of the project, the cyclization conditions with oxalyl chloride were not optimized and used to pursue 1,3-benzoxazin-2,4-one derivatives.

4.1.2.3. Synthesis of a representative ferrocenyl quinazoline derivative

By merging the 1,3-benzoxazine moiety to the 4-amino-7-chloroquinoline nucleus at C4, Gemma et al. generated a series of highly potent novel compounds with *in vitro* antimalarial activity superior to chloroquine against D10 and W2 *P. falciparum* strains.[21] To further explore the SAR analysis of these compounds, isosteric quinazoline congeners of the 1,3-benzoxazine unit were synthesized and evaluated for biological efficacy. Motivated by this study and in line with the aims and objectives of the current project, especially in relation to modification of the oxazine unit, a representative quinazoline analogue **4.30** of the ferrocenyl 1,3-benzoxazine

derivative **3.16a** and its 2-carbamate variant **4.17a** was prepared as a representative for biological evaluation to support SAR analysis.

Synthesis of ferrocenyl quinazoline **4.30** was achieved by neat cyclization of the ferrocenyl 2-aminobenzylamine **4.9d** with triethyl orthoformate ($CH(OEt)_3$) catalysed by PTSA (**Scheme 4.12**).[21] The product was isolated in 22% yield by silica gel chromatography following a simple workup of successive washing of the reaction solution in EtOAc with 1N NaOH and distilled water.

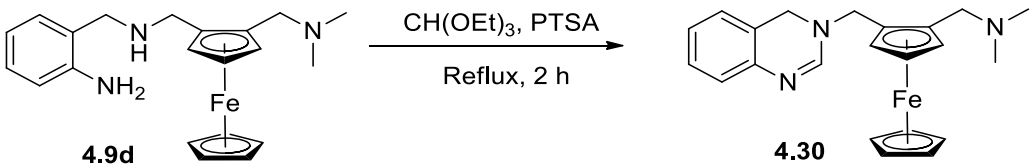

Scheme 4.12 Synthesis of quinazoline **4.30** by cyclization of 2-aminobenzylamine **4.9d** with triethyl orthoformate.

Successful cyclization of **4.9d** into quinazoline **4.30** was confirmed by the appearance of the pyrimidinyl imine (2) and methylene (4a and 4b) protons at δ 7.52 and 4.59 – 4.48 ppm as 1H singlet and two 1H doublets, respectively as shown in **Figure 4.15**. This is supplemented by the δ [7.52, 150.5] ppm cross-peak (H-2, C-2) of the pyrimidinyl CH.

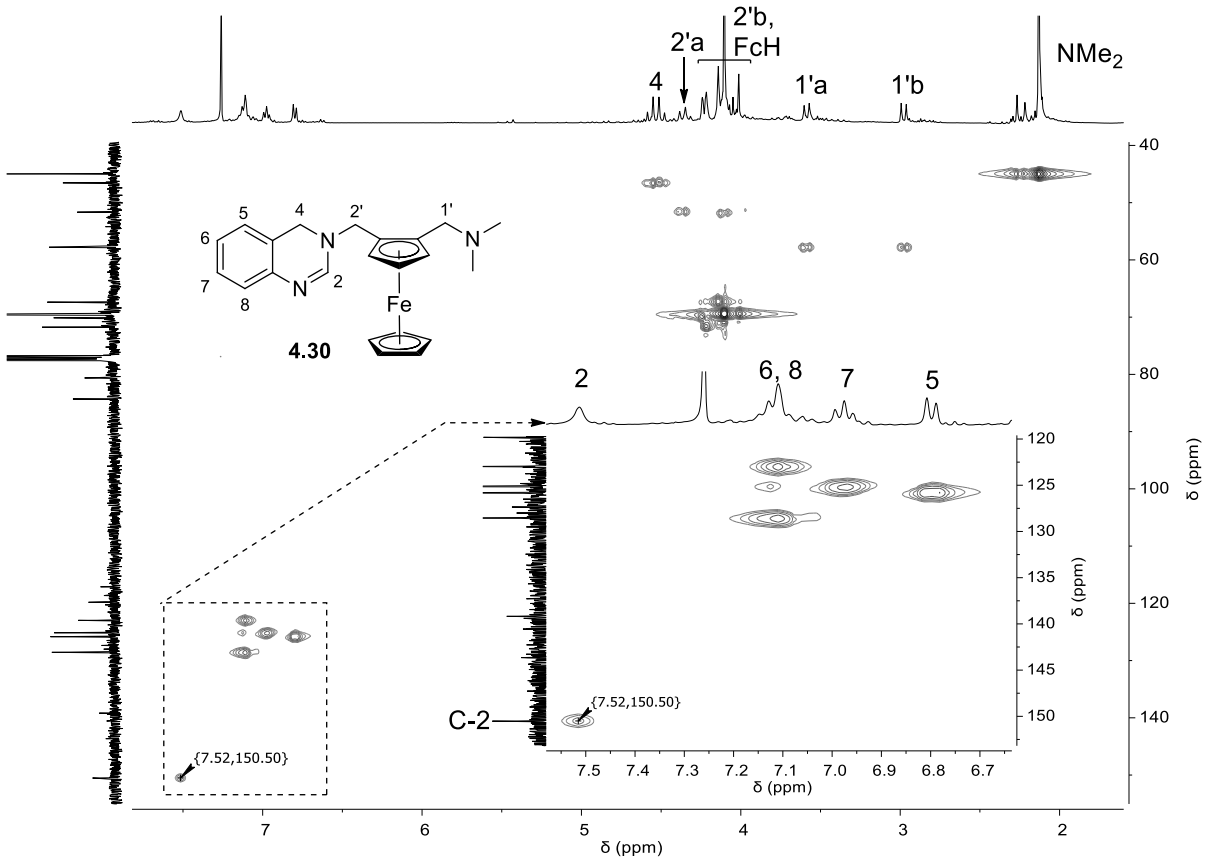

Figure 4.15 HSQC NMR spectrum of quinazoline **4.30** in $CDCl_3$.

As a representative compound, the biological evaluation data of this quinazoline analogue was adequate for comparison purposes and SAR profiling, and no additional quinazolines were pursued.

4.2. Biological evaluation results

In line with the rationale of the study, the ferrocenyl 1,3-benzoxazinones and their acyclic derivatives were synthesized to investigate the influence of modifying the oxazine unit of the 1,3-benzoxazine scaffold on the biological activity of the compounds being studied. Similar to the parental ferrocenyl 3,4-dihydro-2*H*-1,3-benzoxazines (**3.13a-k**, **3.16a-o** and **3.17a-f**), the synthesized analogues with a modified oxazine unit were investigated for potential biological activity by *in vitro* evaluation against the HCC70 cancer cell line, 3D7 and Dd2 *P. falciparum* strain and the 427 *T. b. brucei* parasites.

4.2.1. *In vitro* antiplasmodial activity

The antiplasmodial activity of the compounds was assessed on the chloroquine-sensitive 3D7 *P. falciparum* strain and the activities were reported as a mean of IC_{50} values obtained from duplicate experiments for each compound. In all cases the standard deviation (SD) was below 0.3. The antiplasmodial data of the ferrocenyl acyclic 1,3-benzoxazine derivatives devoid of the O-CH_2-N oxazine linkage are presented in **Table 4.3**. Known antimalarial drugs, chloroquine (CQ) and artemisinin (Art) were used as positive controls in the biological evaluation assays. The biological activity of the 1,3-benzoxazin-2-one compounds containing the carbamate O-CO-N unit in lieu of the O-CH_2-N motif is discussed later.

From the antiplasmodial evaluation results, the α-amino-*o*-cresol series **4.6a-i** and **4.7a-e** was generally the most potent among the screened compounds followed by benzylamines **4.9a-d** and salicylamides (**4.15a-e** and **4.16a-b**) against the 3D7 *P. falciparum* strain, respectively. Within the CH_2NMe_2 ferrocenyl series **4.6a-i**, the activity electron-donating groups (EDGs) imparted higher efficacy with Me > OMe > Br > NO_2 irrespective of the position of substitution on the benzene ring. For instance, compounds bearing the electron-releasing methoxy group (**4.6d** and **4.6f**) exhibited higher activity than their nitro-containing counterparts (**4.6e** and **4.6g**) by approximately 2-folds. These observations appeared to be in contrasted with the apparent trend noticed for the 3,4-dihydro-2*H*-1,3-benzoxazines in **Chapter 3**, where EWGs were favourable for activity (**Table 3.2**). Again, this could be an influence of lipophilicity since the EDGs (Me and OMe) tested in the series are more lipophilic than the EWG, NO_2.[22] Substitution at C-4 of the benzene ring (**4.6b-g**) was the most favourable position for the antiplasmodial activity of the α-amino-*o*-cresols.

Table 4.3 *In vitro* antiplasmodial activity of ferrocenyl α-amino-*o*-cresols, benzylamines and salicylamides against the 3D7 and Dd2 *P. falciparum* strains.

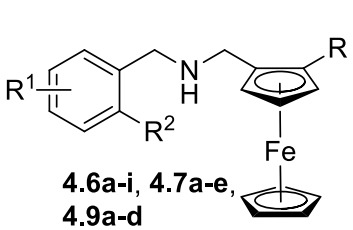

4.6a-i, **4.7a-e**, **4.9a-d**

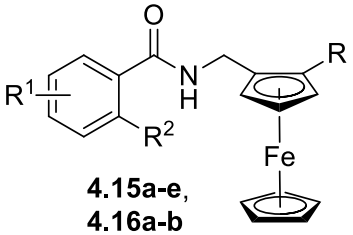

4.15a-e, **4.16a-b**

Compound	R	R^1	R^2	IC_{50} (μM)		[a]R.I.
				3D7	Dd2	
4.6a	CH_2NMe_2	H	OH	2.23	nd	–
4.6b	CH_2NMe_2	4-Me	OH	**0.92**	nd	–
4.6c	CH_2NMe_2	4-Br	OH	1.6	**0.689**	0.4
4.6d	CH_2NMe_2	4-OMe	OH	1.4	nd	–
4.6e	CH_2NMe_2	4-NO_2	OH	1.88	nd	–
4.6f	CH_2NMe_2	6-OMe	OH	4.7	6.61	1.4
4.6g	CH_2NMe_2	6-NO_2	OH	12.3	nd	–
4.6h	CH_2NMe_2	4,6-Br	OH	1.1	**0.943**	0.9
4.6i	CH_2NMe_2	4-Br, 6-NO_2	OH	5.52	nd	–
4.7a	H	H	OH	nd	nd	–
4.7b	H	4-Br	OH	2.3	1.68	0.7
4.7c	H	6-NO_2	OH	nd	nd	–
4.7d	H	4,6-Br	OH	4.3	3.87	0.9
4.7e	H	4-Br, 4-NO_2	OH	nd	>10	–
4.9a	CH_2NMe_2	H	H	2.99	nd	–
4.9b	CH_2NMe_2	H	OMe	4.78	nd	–
4.9c	CH_2NMe_2	H	NO_2	3.13	nd	–
4.9d	CH_2NMe_2	H	NH_2	4.49	nd	–
4.15a	CH_2NMe_2	H	OH	9.64	nd	–
4.15b	CH_2NMe_2	5-Cl	OH	20.85	nd	–
4.15c	CH_2NMe_2	5-NO_2	OH	12.83	nd	–
4.15d	CH_2NMe_2	4-F	OH	na	nd	–
[b]**4.15e**	CH_2NMe_2	H	OH	21.87	nd	–
4.16a	H	H	OH	na	nd	–
4.16b	H	H	SH	na	nd	–
Chloroquine	–	–	–	0.03	0.188	6.3
Artemisinin	–	–	–	–	0.006	–

[a]R.I. = resistance index. [b]Pyridine congener nd = not determined. na = not active.

The inferior activity of the ferrocenyl α-amino-*o*-cresols **4.7b** (IC_{50} = 2.3 μM) and **4.7d** (IC_{50} = 4.3 μM) devoid of the CH_2NMe_2 side chain with respect to their variants **4.6b** (IC_{50} = 0.92 μM) and **4.6d** (IC_{50} = 1.1 μM) with this moiety corroborated the previous observations about the beneficial biological effects of incorporating basic aminoalkyl chains into position 2 of the ferrocene unit on the biological activity of the ferrocenyl 1,3-benzoxazines (**Figure 3.15**). The research groups of Biot and Smith made similar observations regarding the significance of the CH_2NMe_2 ferrocenyl moiety for their reported ferrocene-based 4-aminoquinoline and azine compounds, respectively, as antiplasmodial agents.[23]

The removal (**4.9a**) and replacement of the OH group of the α-amino-*o*-cresols with OMe (**4.9b**), NO_2 (**4.9c**) and NH_2 (**4.9d**) was not beneficial for the biological activity as suggested by the lower efficacy of the benzylamines (**4.9a-d**) compared to their α-amino-*o*-cresol derivative **4.7a**. Looking at the influence of each replacement substituent for the OH group, the order of tolerance for activity was H > NO_2 > NH_2 > OMe (**Table 4.3**). These observations seem to suggest that the presence of the OH group is beneficial for the antiplasmodial activity of the studied ferrocenyl α-amino-*o*-cresols.

On the other hand, the ferrocenyl salicylamides **4.15a-e** were the least active in the entire acyclic series with IC_{50} values in the mid-micromolar range, while the salicylamide **4.16a** lacking the CH_2NMe_2 side chain and its 2-thio isosteric congener **4.16b** were not active against the 3D7 strain (**Table 4.3**). The latter observation further asserts the importance of the basic CH_2NMe_2 moiety for antiplasmodial activity as previously noted. The primary difference between the less active salicylamides (**4.15a-e**) and the α-amino-*o*-cresols (**4.6a-i**) is the basicity of the NH group due to the presence of the amide in compounds **4.15a-e**. Thus, the superior activity of the α-amino-*o*-cresols (**4.6a-i**) to the salicylamides (**4.15a-e**), by ~ 5-fold, suggests that the basic NH group is crucial for the antiplasmodial activity of the compounds

against the 3D7 *P. falciparum* parasite. Chinnapattu et al. made similar findings regarding the pharmacological importance of the basicity of the NH group in their adamantane-based α-amino-*o*-cresols.[24] The activity of the pyridine congener **4.15e** (IC_{50} = 21.87 μM) was lower than its benzene counterpart **4.15a** (IC_{50} = 9.64 μM), but comparable to other members in the salicylamide series (**Table 4.3**). It is apparent from this observation that the replacement of the benzene ring with pyridine is tolerable for activity for the non-cyclic 1,3-benzoxazine analogues.

Lastly, with the exception of compound **4.6f**, all the α-amino-*o*-cresols (**4.6c**, **4.6h**, **4.7b** and **4.7d**) evaluated against the chloroquine-resistant Dd2 *P. falciparum* parasites were more active on this strain than the sensitive 3D7 variant with efficacies in the low and sub-micromolar range. This selectivity is further proved by the favourable resistance index (R.I. < 1.0) as with was noted for the ferrocenyl 3,4-dihydro-2*H*-1,3-benzoxazines in **Chapter 3**.

Having established the antiplasmodial activity of the non-cyclic 1,3-benzoxazine derivatives, the biological significance of replacing the O-CH_2-N benzoxazine motif was investigated by screening the antiplasmodial activity of the cyclic O-CO-N congeners (**4.17a-d** and **4.18a-e**). The antiplasmodial data of these carbamate derivatives is shown in **Table 4.4**. Only the CH_2NMe_2 derivatives (**4.17a-d**) were active against the sensitive 3D7 strain, whereas compounds **4.18a-e** lacking this chain were inactive against both strains tested. Thus, these data affirm the biological importance of the basic CH_2NMe_2 side chain as previously observed.[23] The antiplasmodial activity of these O-CO-N congeners is significantly lower than that of both the parental 3,4-dihydro-2*H*-1,3-benzoxazines in **Chapter 3** and acyclic α-amino-*o*-cresols above (**Tables 3.4** and **4.3**).

The O-CH_2-N moiety is essential for the biological activity of 1,3-oxazine derivatives such as the ferrocenyl 1,3-benzoxazine compounds pursued in this study.[2] The importance of this

moiety is best illustrated by considering the plasmocidal activity of the brominated congeners **3.13d**, **4.7b** and **4.18b**.

Table 4.4 *In vitro* antiplasmodial activity of ferrocenyl 1,3-benzoxazin-2-ones against the 3D7 and Dd2 *P. falciparum* strains.

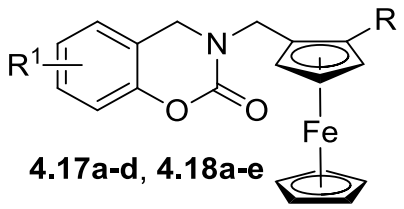

4.17a-d, **4.18a-e**

Compound	R	R^1	IC_{50} (μM)		[a]R.I.
			3D7	Dd2	
4.17a	CH_2NMe_2	H	16.9	>10	–
4.17b	CH_2NMe_2	6-Br	3.7	3.38	0.9
4.17c	CH_2NMe_2	6,8-Br	2.8	nd	–
4.17d	CH_2NMe_2	8-OMe	13.0	nd	–
4.18a	H	H	na	>10	–
4.18b	H	6-Br	na	>10	–
4.18c	H	6,8-Br	na	>10	–
4.18d	H	8-OMe	na	>10	–
4.18e	H	8-NO_2	na	>10	–
[b]**4.24a**	H	H	na	>10	–
[c]**4.30**	–	–	2.7	nd	–
Chloroquine	–	–	0.03	0.188	6.3
Artemisinin	–	–	–	0.006	–

[a]R.I. = resistance index. [b]**4.24a** = 1,3-benzoxazin-2,3-dione derivative. [c]**4.30** = quinazoline analogue. nd = not determined. na = not active.

Although the benzoxazine analogue **3.13d** (IC_{50} = 1.1 μM) was more potent than its α-amino-*o*-cresol equivalent **4.7** (IC_{50} = 2.3 μM) lacking the O-CH_2-N motif, i.e. C-4, by approximately 2-fold against the sensitive strain (3D7), both compounds showed similar activity against the Dd2 resistant strain with IC_{50} values of 1.57 (**3.13d**) and 1.68 μM (**4.7b**), respectively (**Tables 3.4** and **4.3**). Furthermore, plasmocidal efficacy of the non-basic 1,3-benzoxazin-2-one

analogue **4.18b** was completely lost upon replacement of the O-CH_2-N unit with an O-CO-N carbamate linkage (**Table 4.4**). The loss of activity by the carbamate variant **4.18b** lacking the basic nitrogen atom in the oxazine ring relative to the potency of its basic derivatives (**3.13d** and **4.7b**) could be attributed to the reduced basicity of the oxazine nitrogen atom. This is further supported by inferior activity of the salicylamides **4.15a-e** and **4.16a-b** containing an even less basic amide NH group (**Table 4.3**). This confirms the pharmacological importance of the basic nitrogen atom for activity. Furthermore, the isosteric quinazoline **4.30** (IC_{50} = 2.7 μM) containing an N=CH-N linkage was twice as active as its acyclic 2-aminobenzylamine **4.9d** (IC_{50} = 4.49 μM) against the strain. Collectively, these observations seem to suggest that the basic nitrogen atom is required for the antiplasmodial activity of the investigated ferrocenyl 1,3-benzoxazine compounds, whilst the O-CH_2-N oxazine connection is crucial for these biological effects.

4.2.2. *In vitro* antitrypanosomal activity

As before, the antitrypanosomal activity of the ferrocenyl acyclic and benzoxazinone compounds was evaluated using the 427 *T. b. brucei* trypomastigotes. The data of the *in vitro* antitrypanosomal activity data of these compounds are presented in **Table 4.5**. The rest of the compounds had not been evaluated for trypanocidal effects at the time of compiling the thesis.

As before, the compounds containing the basic ferrocenyl CH_2NMe_2 ferrocenyl chain were more active than the analogues lacking this motif for both the α-amino-*o*-cresol (**4.6** and **4.7**) and benzoxzin-2-one (**4.17** and **4.18**) series. All the derivatives with this moiety (R = CH_2NMe_2) exhibited activity in the low and mid-micromolar range, whereas only two compounds (**4.7b** and **4.18b**) devoid of the basic ferrocenyl chain (R = H) were active against the strain. This further underscores the importance of this unit for biological activity.[23]

Table 4.5 *In vitro* antitrypanosomal activity of ferrocenyl α-amino-*o*-cresols, benzylamines, salicylamides and 1,3-benzoxazin-2-ones against the 427 *T. b. brucei* strain.

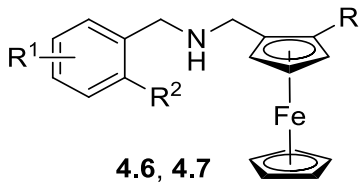

4.6, **4.7**

Compound	R	R^1	R^2	IC_{50} (μM)
				427 *T. b. brucei*
4.6c	CH_2NMe_2	4-Br	OH	3.5
4.6f	CH_2NMe_2	6-OMe	OH	9.7
4.6g	CH_2NMe_2	6-NO_2	OH	9.8
4.6h	CH_2NMe_2	4,6-Br	OH	8.9
4.7b	H	4-Br	OH	6.6
4.7d	H	4,6-Br	OH	[a]na

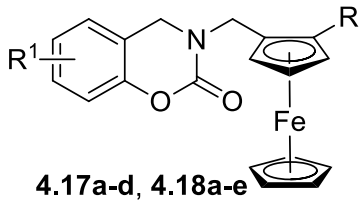

4.17a-d, **4.18a-e**

	R	R^1	
4.17a	CH_2NMe_2	H	9.6
4.17b	CH_2NMe_2	6-Br	12.7
4.17c	CH_2NMe_2	6,8-Br	7.0
4.17d	CH_2NMe_2	8-OMe	18.0
4.18a	H	H	na
4.18b	H	6-Br	na
4.18c	H	6,8-Br	8.1
4.18d	H	8-OMe	na
4.18e	H	8-NO_2	na
Pentamidine	–	–	0.014

na = not active.

The non-cyclic α-amino-*o*-cresols (**4.6c**, **4.6f**, **4.g**, **4.6h**, **4.7b** and **4.7d**) generally showed higher efficacy than the benzoxazine-2-ones (**4.17a-d** and **4.18a-e**) containing a less basic oxazine nitrogen (**Table 4.5**). This emphasizes the previous observations about the pharmacological importance of the basicity of the nitrogen atom of the oxazine unit.[24] When viewed in line with the trypanocidal activity of the ferrocenyl 3,4-dihydro-2*H*-1,3-benzoxazines in **Chapter 3** which were active in the low to sub-micromolar concentrations (**Table 3.6**), it is apparent that the methylene (CH_2) unit of the O-CH_2-N oxazine linkage (in 3,4-dihydro-2*H*-1,3-benzoxazines, e.g. **3.16d**: IC_{50} = 1.2 μM) is crucial for biological activity, while its removal (in α-amino-*o*-cresols, e.g. **4.6c**: IC_{50} = 3.5 μM) may be tolerated. Evidently, the replacement of the oxazine O-CH_2-N (e.g., **3.16d**: IC_{50} = 1.2 μM) with carbamate O-CO-N (e.g., **4.17b**: IC_{50} = 12.7 μM) is detrimental for trypanocidal efficacy of the investigated ferrocenyl 1,3-benzoxazine derivatives, as previously noted for antiplasmodial activity.

4.2.3. *In vitro* anticancer activity

As previously noted for the ferrocenyl 3,4-dihydro-2*H*-1,3-benzoxazines (**Table 3.5**), the non-cyclic α-amino-*o*-cresol and 1,3-benzoxazin-2-one derivatives were less selective for the mammalian HCC70 breast cancer cell line (**Table 4.6**).

For all the non-cyclic analogues, only three α-amino-*o*-cresols (**4.6b**, **4.6c** and **4.i**) carrying the ferrocenyl CH_2NMe_2 and the *O*-methyl α-amino-*o*-cresol **4.9b** were active against the cell line with IC_{50} values between 6.67 and 56.2 μM (**Table 4.6**), highlighting the importance of the CH_2HMe_2 motif as before. The activity was lost upon removal of the *ortho* oxygen atom of the α-amino-*o*-cresol template (**4.9a**). Likewise, decreasing the basicity of the cresolyl NH atom in salicylamides (**4.15a-e** and **4.16a-b**) was detrimental for the anticancer activity of the compounds (**Table 4.6**). This corroborates the patterns noted in the evaluation of these non-

cyclic compounds for antiparasitic activity as observed by Chinnapattu et al. for plasmocidal adamantane-based α-amino-*o*-cresols.[24]

Table 4.6 *In vitro* anticancer activity of non-cyclic ferrocenyl α-amino-*o*-cresols, benzylamines and salicylamides evaluated against triple-negative HCC70 breast cancer cell line.

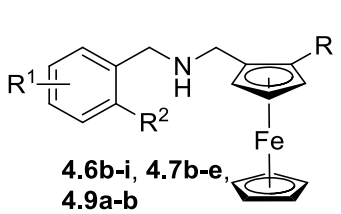

4.6b-i, **4.7b-e**, **4.9a-b**

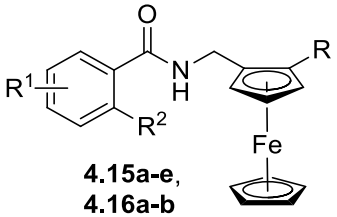

4.15a-e, **4.16a-b**

Compound	R	R^1	R^2	IC_{50} (μM)
				HCC70
4.6b	CH_2NMe_2	4-Me	OH	28.4
4.6c	CH_2NMe_2	4-Br	OH	6.67
4.6e	CH_2NMe_2	4-NO_2	OH	na
4.6f	CH_2NMe_2	6-OMe	OH	na
4.6h	CH_2NMe_2	4,6-Br	OH	na
4.6i	CH_2NMe_2	4-Br, 6-NO_2	OH	56.2
4.7b	H	4-Br	OH	na
4.7c	H	6-NO_2	OH	na
4.7d	H	4,6-Br	OH	na
4.7e	H	4-Br, 4-NO_2	OH	na
4.9a	CH_2NMe_2	H	H	na
4.9b	CH_2NMe_2	H	OMe	20.9
4.15a	CH_2NMe_2	H	OH	na
4.15b	CH_2NMe_2	5-Cl	OH	na
4.15c	CH_2NMe_2	5-NO_2	OH	na
4.15d	CH_2NMe_2	4-F	OH	na
[c]4.15e	CH_2NMe_2	H	OH	na
4.16a	H	H	OH	na
4.16b	H	H	SH	na
Paclitaxel	–		–	0.0025

na = not active. [a]**4.15e** = Pyridine analogue.

With the exception of **4.18c** (IC_{50} = 8.1 μM), only 1,3-benzoxazin-2-ones (**4.17b-d**) bearing the CH_2NMe_2 ferrocenyl chain were active against the HCC70 cell line (**Table 4.7**). Interestingly, the less basic 1,3-benzoxazin-2-one carbamate variants (**4.17a-d**) exhibited higher anticancer efficacy than their more basic α-amino-*o*-cresol (**4.6b-i**), 3,4-dihydro-2*H*-1,3-benzoxazine (**3.16b-l**) and quinazoline (**4.30**) derivatives (**Tables 3.5**, **4.4** and **4.5**).

Table 4.7 *In vitro* anticancer activity of ferrocenyl 1,3-benzoxazin-2-ones evaluated against triple-negative HCC70 breast cancer cell line.

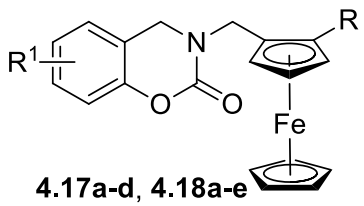

4.17a-d, **4.18a-e**

Compound	R	R^1	IC_{50} (μM)
			HCC70
4.17a	CH_2NMe_2	H	9.6
4.17b	CH_2NMe_2	6-Br	12.7
4.17c	CH_2NMe_2	6,8-Br	7.0
4.17d	CH_2NMe_2	8-OMe	18.0
4.18a	H	H	na
4.18b	H	6-Br	na
4.18c	H	6,8-Br	8.1
4.18d	H	8-OMe	na
4.18e	H	8-NO_2	na
[b]**4.24a**	H	H	na
[c]**4.30**	–	–	33.8
Pentamidine	–	–	0.014

na = not active. [b]**4.24a** = 1,3-benzoxazin-2,4-diones. [c]**4.30** = Quinazoline.

It is evident from these findings that the replacement of the O-CH_2-N unit (**3.16b-l**) with the O-CO-N carbamate moiety (**4.17a-d**) is favourable for anticancer activity, which is in contrast with the trends for antiparasitic efficacy. Notwithstanding, this could still be attributed to the

basicity of the cresolyl NH group as the least basic salicylamides (**4.15a-e** and **4.16a-b**) were inactive against the cell line (**Table 4.6**). Also, the high propensity of the carbamate functionality for hydrolysis could play an important role in the anticancer activity of the compounds, explaining the superior activity of the 1,3-benzoxazin-2-ones *vis-à-vis* the non-cyclic and 3,4-dihydro-2*H*-1,3-benzoxazine equivalents.[25] Indeed, the hydrolysis of carbamates is essential in the biological activity of carbamate-based drugs and prodrugs .[26]

4.2.4. Refined structure-activity relationship (SAR) analysis

Having demonstrated the biological activity of repurposed polymer precursors, ferrocenyl 3,4-dihydro-2*H*-1,3-benzoxazines, in **Chapter 3**, correlations between activity and structural features ferrocene unit and benzene substituents of the compounds were preliminarily drawn (**Figure 3.15**). According to Urbański and colleagues, the O-CH_2-N linkage of 1,3-oxazine compounds is indispensable for biological efficacy of 1,3-oxazine derivatives, such as the ones pursued in this project.[2] To study the influence of this linkage on the investigated compounds, non-cyclic and carbamate benzoxazin-2-one derivatives were prepared and evaluated for biological activity.

Examination of the structural features of these compounds and their influence on biological activity revealed that the basic oxazine nitrogen atom is crucial for both antiparasitic and anticancer activity of the 1,3-benzoxazine compounds. Removal (non-cyclic analogues) and replacement of the O-CH_2-N unit with O-CO-N (1,3-benzoxazin-2-ones) led to reduced activity of the compounds, suggesting the pharmacological significance of this motif for activity as proposed by Urbański et al.[2] Also, the benzene substitution with EDGs (Me > OMe > Br > NO_2) was conducive for antiplasmodial activity of acyclic analogues. On the contrary, the replacement of O-CH_2-N oxazine linkage with carbamate O-CO-N was preferred for anticancer activity against the triple-negative HCC70 breast cancer cell line.

Thus, the SAR analysis was revised as summarised in **Figure 4.14**.

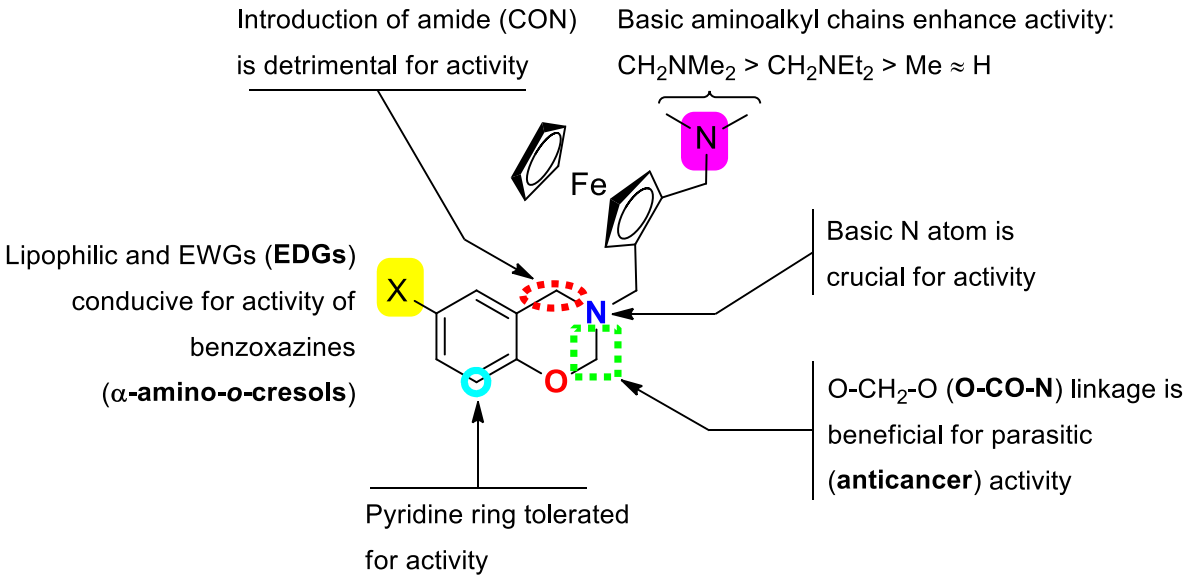

Figure 4.16 Revised SAR analysis of ferrocenyl 1,3-benzoxazine scaffold.[27]

4.2.5. Overall summary and conclusions

Encouraged by the impressive activity of the ferrocenyl 3,4-dihydro-2*H*-1,3-benzoxazine derivatives, a novel class of non-cyclic ferrocenyl α-amino-*o*-cresol and salicylamides, and 1,3-benzoxazin-2-one analogues were designed, synthesized and fully characterized by various spectroscopic techniques: NMR, IR and HRMS. These compounds were evaluated for biological activity and the SARs examined to delineate the influence of modifying the 1,3-oxazine ring of the 1,3-benzoxazine scaffold on the biological activity of the compounds. Generally, the α-amino-*o*-cresols were more active for antiplasmodial and antitrypanosomal activity compared to the salicylamides and carbamate 1,3-benzoxazin-2-ones. However, these compounds were less potent than their respective 3,4-dihydro-2*H*-1,3-benzoxazine derivatives presented in **Chapter 3** for antiparasitic activity. On the other hand, the carbamate 1,3-benzoxazin-2-ones were superior in activity relative to both the parental 3,4-dihydro-2*H*-1,3-benzoxazines and the acyclic aminocresols and salicylamides for anticancer activity in the mid-

micromolar range. The findings of this study together with the data of compounds in **Chapter 3** are summarized in the refined SAR model presented in **Figure 4.16**.

References

(1) Zinad, D. S.; Mahal, A.; Mohapatra, R. K.; Sarangi, A. K.; Pratama, M. R. F. *Chem. Biol. Drug Des.* **2019**.

(2) (a) Eckstein, Z.; Urbański, T. *Adv. Heterocycl. Chem.* **1979**, *23*, 1; (b) Urbański, T.; Gürne, D.; Šlopek, S.; Mordarska, H.; Mordarski, M. *Nature* **1960**, *187*, 426.

(3) (a) Burckhalter, J.; Tendick, F.; Jones, E. M.; Holcomb, W.; Rawlins, A. *J. Am. Chem. Soc.* **1946**, *68*, 1894; (b) Schmidt, L.; Crosby, R. *Antimicrob. Agents Chemother.* **1978**, *14*, 672.

(4) (a) Ullah, I.; Sharma, R.; Mete, A.; Biagini, G. A.; Wetzel, D. M.; Horrocks, P. D. *J. Antimicrob. Chemother.* **2019**; (b) Medicines for Malaria Venture. 2019. Developing antimalarials to save lives. Malaria Box Research, https://www.mmv.org/mmv-open/malaria-box/malaria-box-research, Accessed: 19 November 2019.

(5) Burke, W. *J. Am. Chem. Soc.* **1949**, *71*, 609.

(6) Abdel-Magid, A. F.; Carson, K. G.; Harris, B. D.; Maryanoff, C. A.; Shah, R. D. *J. Org. Chem.* **1996**, *61*, 3849.

(7) Blackie, M. A. Doctoral Thesis, University of Cape Town, 2002.

(8) Saikia, B. *Synlett* **2011**, *17*, 2597.

(9) (a) Bavin, E.; Macrae, F. J.; Seymour, D.; Waterhouse, P. D. *J. Pharm. Pharmacol.* **1952**, *4*, 872; (b) Kushkevych, I.; Kollar, P.; Ferreira, A. L.; Palma, D.; Duarte, A.; Lopes, M. M.; Bartos, M.; Pauk, K.; Imramovsky, A.; Jampilek, J. *J. Appl. Biomed.* **2016**, *14*, 125; (c) Li, Q.-S.; Lv, X.-H.; Zhang, Y.-B.; Dong, J.-J.; Zhou, W.-P.; Yang, Y.; Zhu, H.-L. *Bioorg. Med. Chem. Lett.* **2012**, *22*, 6596; (d) Fritzson, I.; Bedingfield, P. T.; Sundin, A. P.; McConkey, G.; Nilsson, U. J. *MedChemComm* **2011**, *2*, 895.

(10) Waisser, K.; Hladuvková, J.; Gregor, J.; Rada, T.; Kubicová, L.; Klimešová, V.; Kaustová, J. *Arch. Pharm.* **1998**, *331*, 3.

(11) Montalbetti, C. A.; Falque, V. *Tetrahedron* **2005**, *61*, 10827.

(12) (a) Mbaba, M.; Mabhula, A. N.; Boel, N.; Edkins, A. L.; Isaacs, M.; Hoppe, H. C.; Khanye, S. D. *J. Inorg. Biochem.* **2017**, *172*, 88; (b) Mu, F.; Lee, D. J.; Pryor, D. E.; Hamel, E.; Cushman, M. *J. Med. Chem.* **2002**, *45*, 4774.

(13) Glidewell, C.; Rankin, D.; Sheldrick, G. *T. Faraday Soc.* **1969**, *65*, 2801.

(14) D'Addona, D.; Bochet, C. G. *Tetrahedron Lett.* **2001**, *42*, 5227.

(15) (a) Waisser, K.; Gregor, J.; Dostál, H.; Kuneš, J.; Kubicová, L.; Klimešová, V.; Kaustová, J. *Il Farmaco* **2001**, *56*, 803; (b) Waisser, K.; Gregor, J.; Kubicová, L.; Klimešová, V.; Kuneš, J.; Macháček, M.; Kaustová, J. *Eur. J. Med. Chem.* **2000**, *35*, 733; (c) Waisser, K.; Peřina, M.; Kuneš, J.; Klimešová, V.; Kaustová, J. *Il Farmaco* **2003**, *58*, 1137; (d) Waisser, K.; Petrlíková, E.; Peřina, M.; Klimešová, V.; Kuneš, J.; Palát Jr, K.; Kaustová, J.; Dahse, H.-M.; Möllmann, U. *Eur. J. Med. Chem.* **2010**, *45*, 2719.

(16) Geffken, D. *Liebigs Ann. Chem.* **1981**, *1981*, 1513.

(17) (a) Wang, W.; Gong, S.; Chen, Y.; Meng, L. *Supramol. Chem.* **2006**, *18*, 311; (b) Oberth, A. E.; Bruenner, R. S. *J. Phys. Chem.* **1968**, *72*, 845; (c) Jez, J. M.; Bowman, M. E.; Noel, J. P. *Biochemistry* **2002**, *41*, 5168.

(18) Pross, A.; Radom, L.; Taft, R. W. *J. Org. Chem.* **1980**, *45*, 818.

(19) McMurry, J. *Organic Chemistry. A biological approach*; Thomson Higher Education: Belmont, CA, United Sates, 2007.

(20) (a) Cotarca, L.; Delogu, P.; Nardelli, A. *Synthesis* **1996**, *5*, 553; (b) Hernandez, A. G.; Grooms, G. M.; El-Alfy, A. T.; Stec, J. *Synthesis* **2017**, *49*, 2163; (c) Chaturvedi, D.; Mishra, N.; Mishra, V. *Monatsh. Chem.* **2007**, *138*, 57; (d) Loev, B.; Kormendy, M. F. *J. Org. Chem.* **1963**, *28*, 3421.

(21) Gemma, S.; Camodeca, C.; Brindisi, M.; Brogi, S.; Kukreja, G.; Kunjir, S.; Gabellieri, E.; Lucantoni, L.; Habluetzel, A.; Taramelli, D. *J. Med. Chem.* **2012**, *55*, 10387.

(22) Sagawa, N.; Shikata, T. *Phys. Chem. Chem. Phys.* **2014**, *16*, 13262.

(23) (a) Biot, C.; Glorian, G.; Maciejewski, L. A.; Brocard, J. S.; Domarle, O.; Blampain, G.; Millet, P.; Georges, A. J.; Abessolo, H.; Dive, D. *J. Med. Chem.* **1997**, *40*, 3715; (b) Stringer, T.; Guzgay, H.; Combrinck, J. M.; Hopper, M.; Hendricks, D. T.; Smith, P. J.; Land, K. M.; Egan, T. J.; Smith, G. S. *J. Organomet. Chem.* **2015**, *788*, 1.

(24) Chinnapattu, M.; Sathiyanarayanan, K. I.; Iyer, P. S. *Bioorg. Med. Chem. Lett.* **2015**, *25*, 952.

(25) (a) Dittert, L. W.; Higuchi, T. *J. Pharm. Sci.* **1963**, *52*, 852; (b) Armstrong, V.; Farlow, D.; Moodie, R. *J. Chem. Soc. B* **1968**, 1099.

(26) Ghosh, A. K.; Brindisi, M. *J. Med. Chem.* **2015**, *58*, 2895.

(27) Mbaba, M.; Dingle, L. M. K.; Cash, D.; de Lamare, J.-A.; Laming, D.; Taylor, D.; Hoppe, H. C.; Edkins, A. L.; Khanye, S. D. Repurposing of a polymer precursor: Synthesis and in vitro medicinal potential of ferrocenyl 1,3-benzoxazine derivatives, Accepted manuscript: *Eur. J. Med. Chem*. **2019**, DOI: https://doi.org/10.1016/j.ejmech.2019.111924

Chapter 5: Design, synthesis, characterization and evaluation of ferrocenyl naphthoxazines, sesamyl- and coumarin-1,3-oxazines

By adapting contemporary drug design strategies such as drug hybridization and repurposing chemical scaffolds for novel medicinal application, ferrocenyl 1,3-benzoxazines based on the scaffold of a polymer precursor have been synthesized, characterized and investigated for *in vitro* biological activity. The influence of structural featured of the ferrocenyl 1,3-benzoxazine scaffold on the biological activity were probed by modifying the ferrocene (**Chapter 3**) and the oxazine unit (**Chapter 4**). In order to fully examine the pharmacological role of the structural features of the compounds under investigation, the current chapter presents the synthesis of ferrocenyl 1,3-benzoxazines with an annulated benzene ring unit.

5.1. Rationale: Benzene ring annulation of the ferrocenyl 1,3-benzoxazine scaffold

To modify the benzene ring by annulation, the benzene unit was replaced with expanded ring systems such as naphthalene, benzodioxole (sesamol) and coumarin to produce a series of novel ferrocenyl 1,3-oxazine compounds. The rationale for modifying the benzene ring with these structural moieties stems from the documented beneficial biological effect of incorporating these motifs into chemical scaffolds of bioactive compounds.[1] Likewise, by fusing these units into the framework of the investigated ferrocenyl compounds, we hypothesized that this would impart favorable effects to the biological activity of the resultant 1,3-oxazine compounds. These modifications are summarized in **Figure 5.1**.

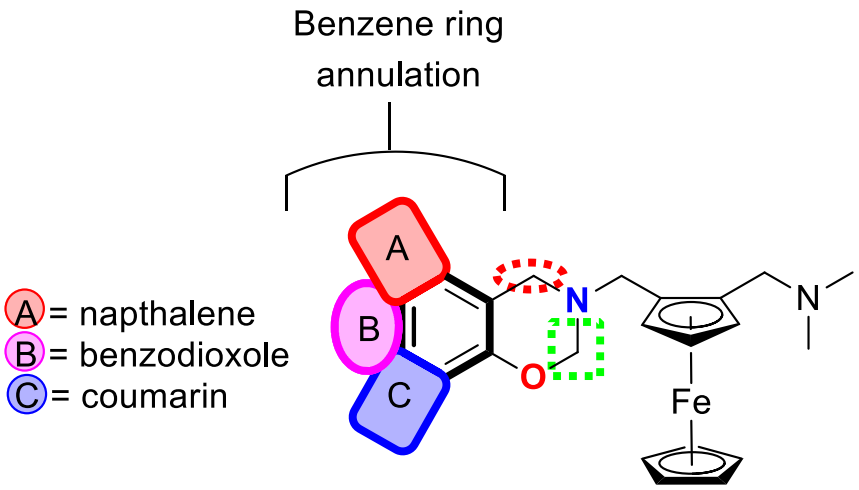

Figure 5.1 Annulation of the benzene ring of ferrocenyl 1,3-benzoxazines.

5.1.1. Synthesis and characterization of naphthoxazines and sesamyl-1,3-oxazine

A considerable number of naphthoxazines are reported in literature. Several naphthoxazines, including the 1,3-oxazine derivatives, have been demonstrated to possess promising anticancer (**2.4c**) and antiparasitic activities including antiplasmodial (**2.20a-b**, **2.22**), antifungal and antibacterial (**2.23**) efficacies (**Figure 5.2**).[2]

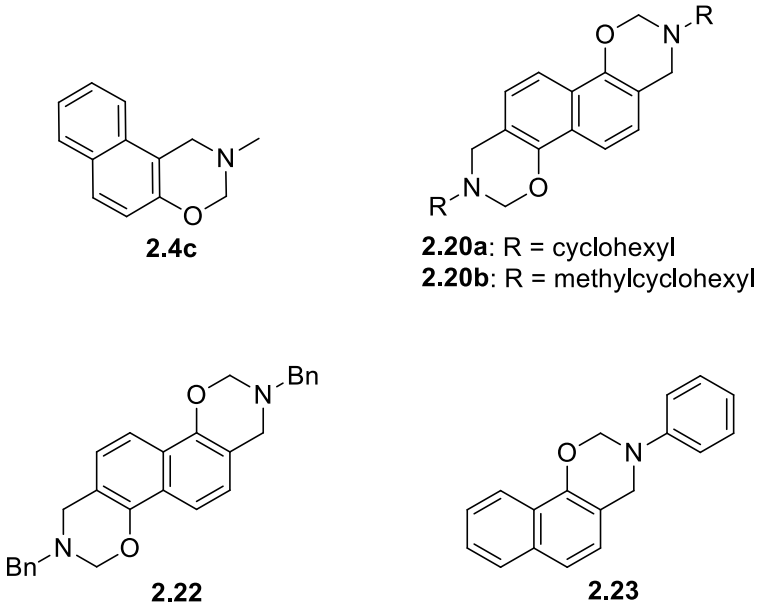

Figure 5.2 Naphthoxazine derivatives possessing biological activity.

As per rationale of the current study and given the biological activity of naphthoxazines, ferrocenyl naphthoxazines (**5.2a-b**) were conveniently synthesized by following the Burke condensation conditions using 2-naphthol (**5.1**) as a phenolic substrate and ferrocenyl amines **3.12a-b** (**Scheme 5.1**). The naphthoxazine product from the CH_2NMe_2 ferrocenyl amine **3.12b** was achieved in 22% yield, while the plain ferrocenyl amine **3.12a** furnished the product in a good yield of 71%.

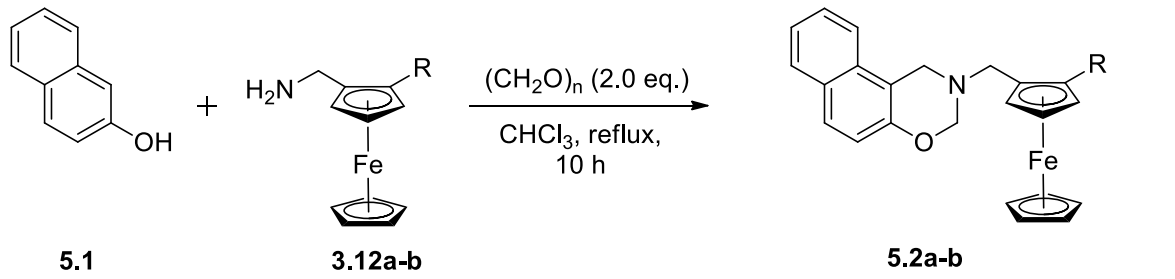

5.1 **3.12a-b** **5.2a-b**

R	Isolated yield (%)
5.2a : CH_2NMe_2	22
5.2b : H	71

Scheme 5.1 Synthesis of ferrocenyl naphthoxazines **5.2a-b**.

The structural identity of the product was confirmed by spectroscopic techniques: NMR, IR and HRMS. In ^{1}H NMR spectra of the comdpounds, the signals of the ferrocene and oxazine units resonated in the regions similar to the 1,3-benzoxazines presented in the previous chapter with the exception of the appearance of additional peaks in the aromatic region corresponding to the naphthalene ring (**Figure 5.3**). For the chiral naphthoxazine **5.2a**, geminal coupling was easily noticed for the diastereotopic methylene protons (3, 1, 2′, 1′) with *J*-coupling constants in the range: 4.6 – 12.9 Hz (**Figure 5.3**).[3] However, proton 2′ appeared as a singlet without indication of geminal coupling.

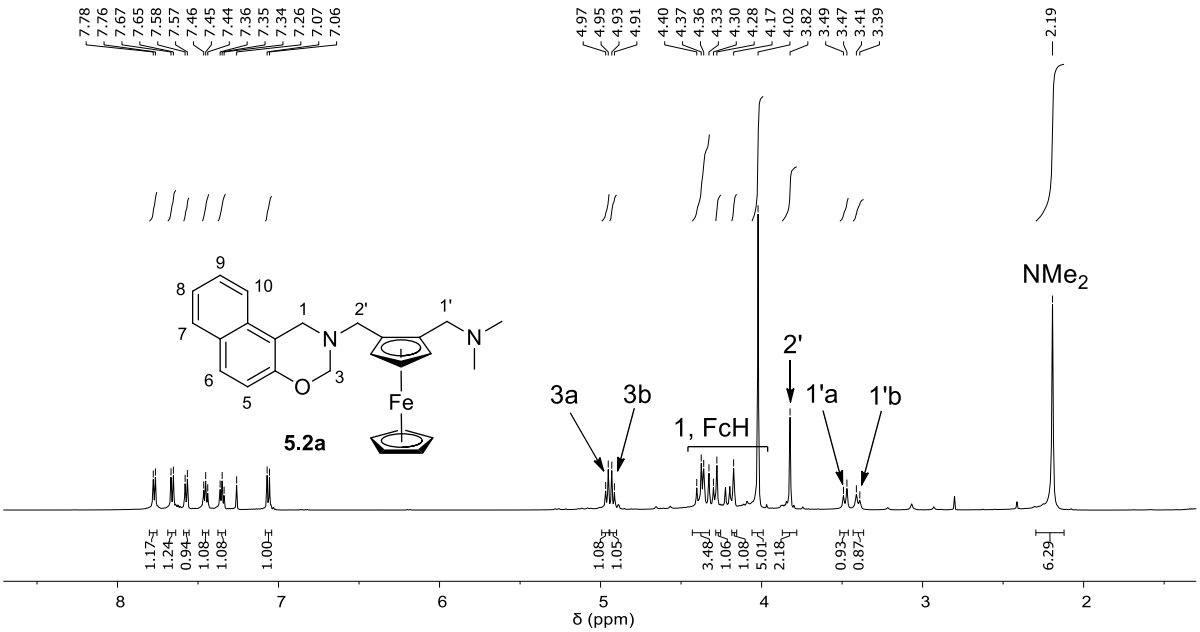

Figure 5.3 ^{1}H NMR spectrum of ferrocenyl naphthoxazine **5.2a** in $CDCl_3$.

Similarly, the carbon signals of the ferrocene and oxazine units of the naphthoxazine derivatives were observed as previously seen for the 1,3-benzoxazines in the ^{13}C NMR spectra of the products (**Figure 5.4**). Application of DEPT-135 NMR allowed ease of differentiation of between methyl (NMe_2), methylene (CH_2) and quaternary carbon signals on the ^{13}C NMR spectrum of the products (**Figure 5.4**).

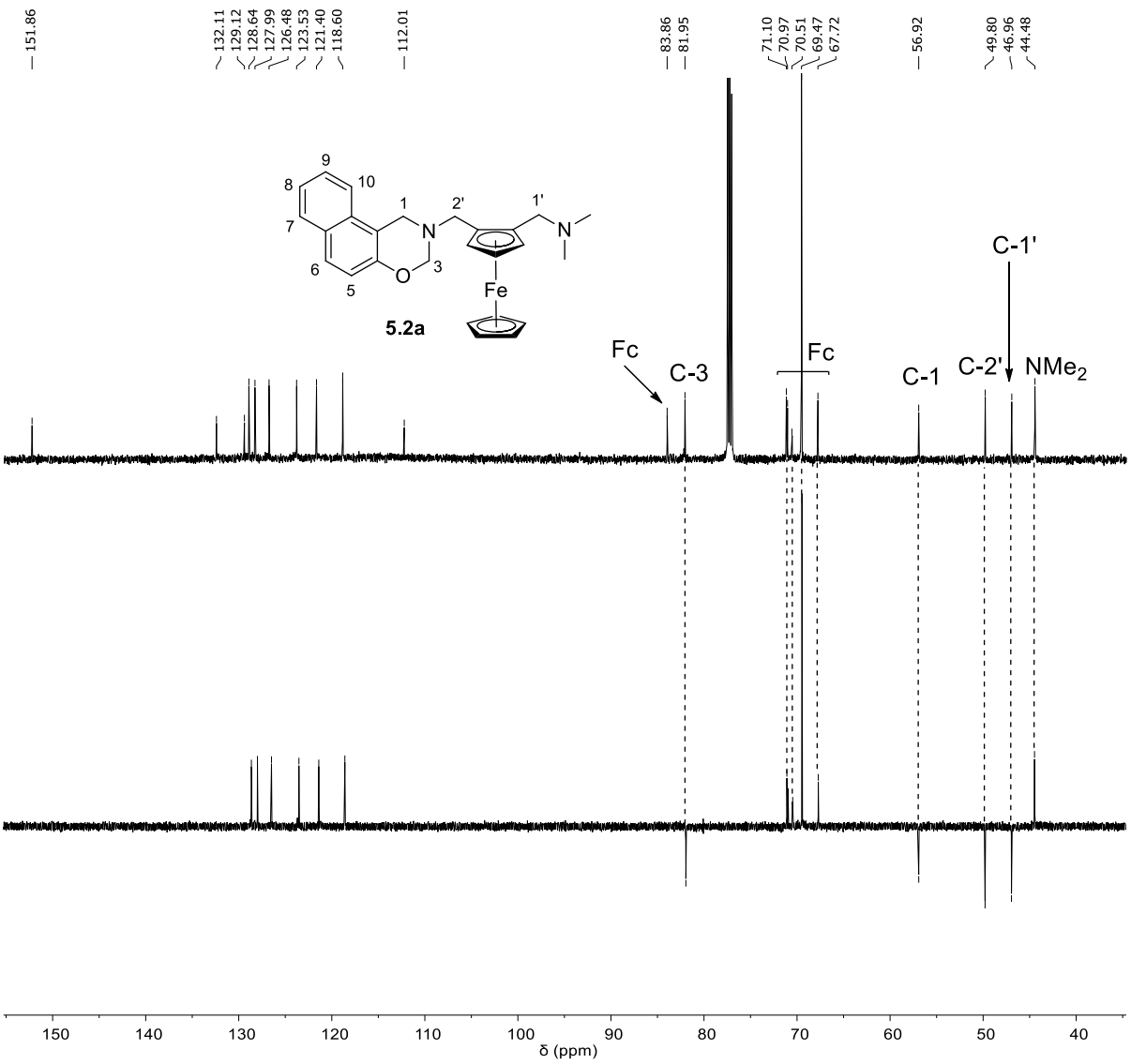

Figure 5.4 ^{13}C NMR and DEPT-135 spectra of ferrocenyl naphthoxazine **5.2a**.

Assignment of aromatic protons was facilitated by 2D COSY NMR (**Figure 5.5**). From the COSY NMR spectrum of compound **5.2b**, protons 5 and 6 were easily identified by their correlation (*a*) at the cross-peak around δ [7.68, 7.08] ppm (**Figure 5.5**).

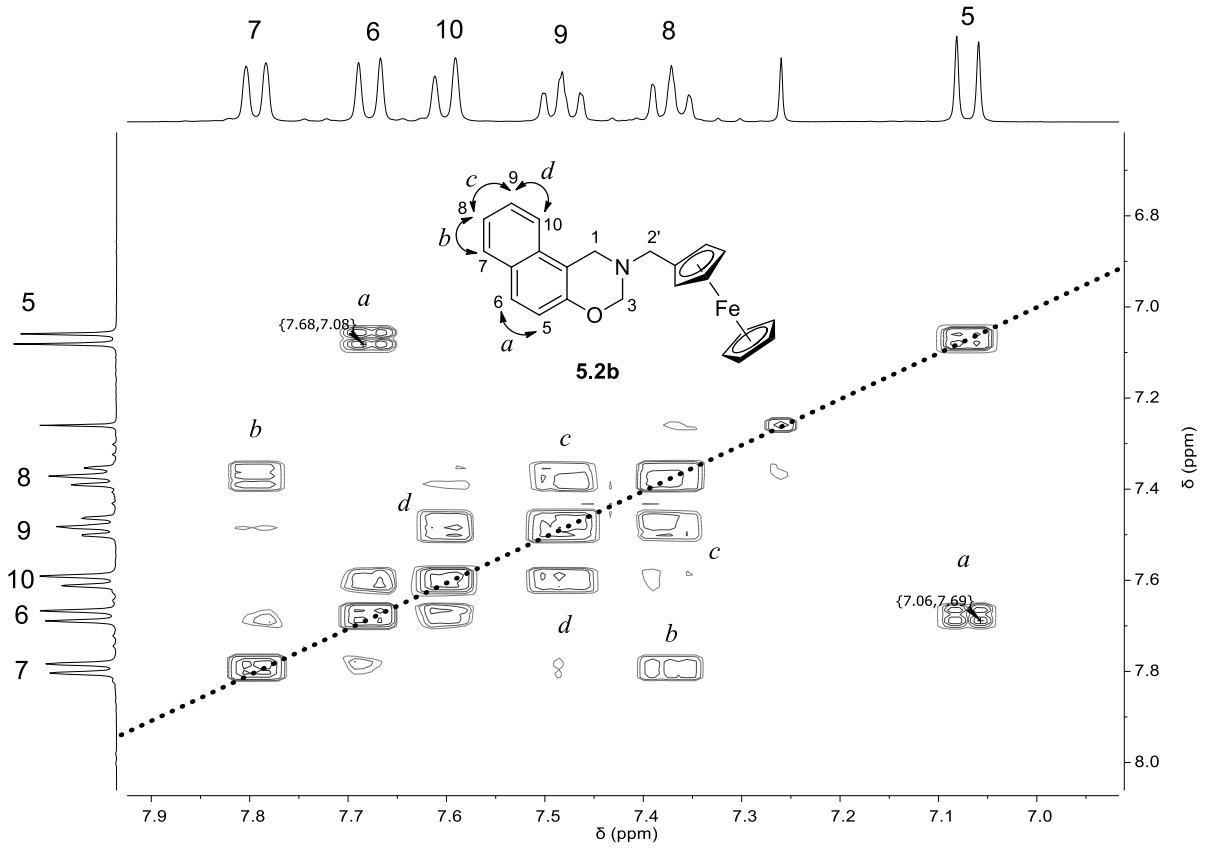

Figure 5.5 COSY NMR spectrum of ferrocenyl naphthoxazine **5.2b**.

On the other hand, HSQC NMR enabled full structural determination of the products as illustrated in **Figure 5.6**.

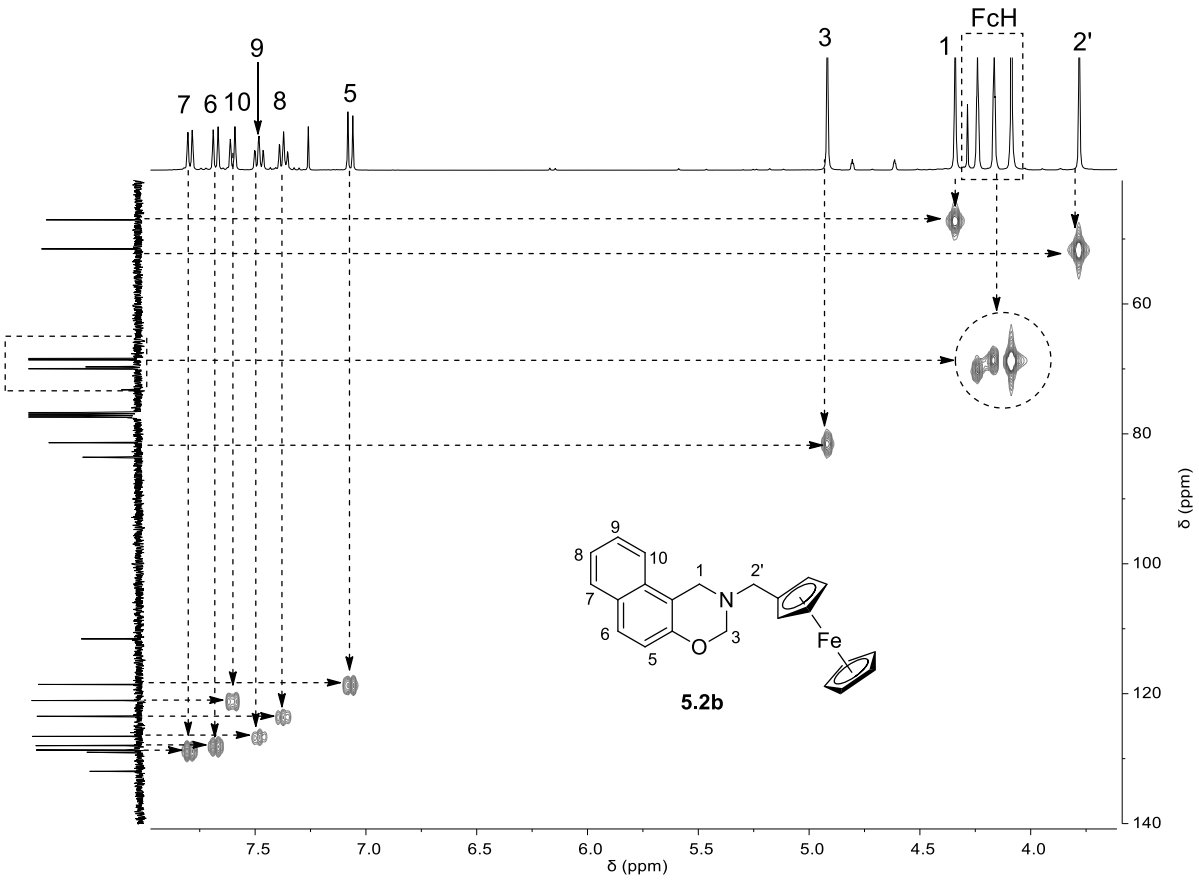

Figure 5.6 HSQC NMR spectrum of naphthoxazine **5.2b** in $CDCl_3$.

Employing the same conditions for the synthesis of naphthoxazines **5.2a-b**, sesamol (**5.3**) was converted to its benzoxazine derivative (**5.4**) with amine **3.12b** (**Scheme 5.2**). The product was obtained in an excellent yield of 85% with no need for purification with silica gel column chromatography.

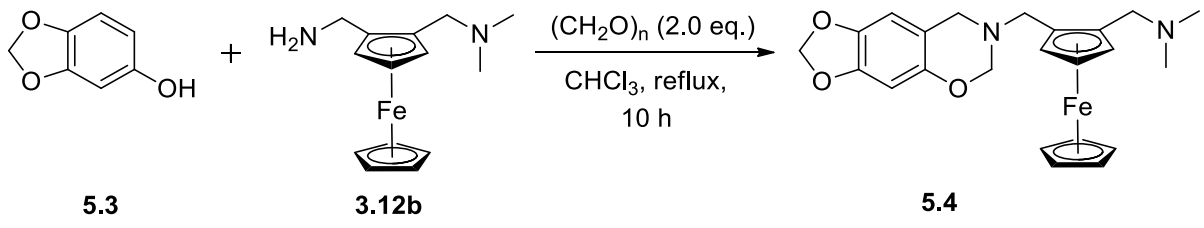

Scheme 5.2 Synthesis of sesamyl-1,3-oxazine by Burke condensation.

The ^{1}H NMR spectral data of the sesamyl-1,3-oxazine **5.4** was similar to those of benzoxazines with the appearance of a new methylene group (O-CH_2-O) at δ 5.87 ppm belonging to the dioxole ring as a 2H singlet (**Figure 5.7**).

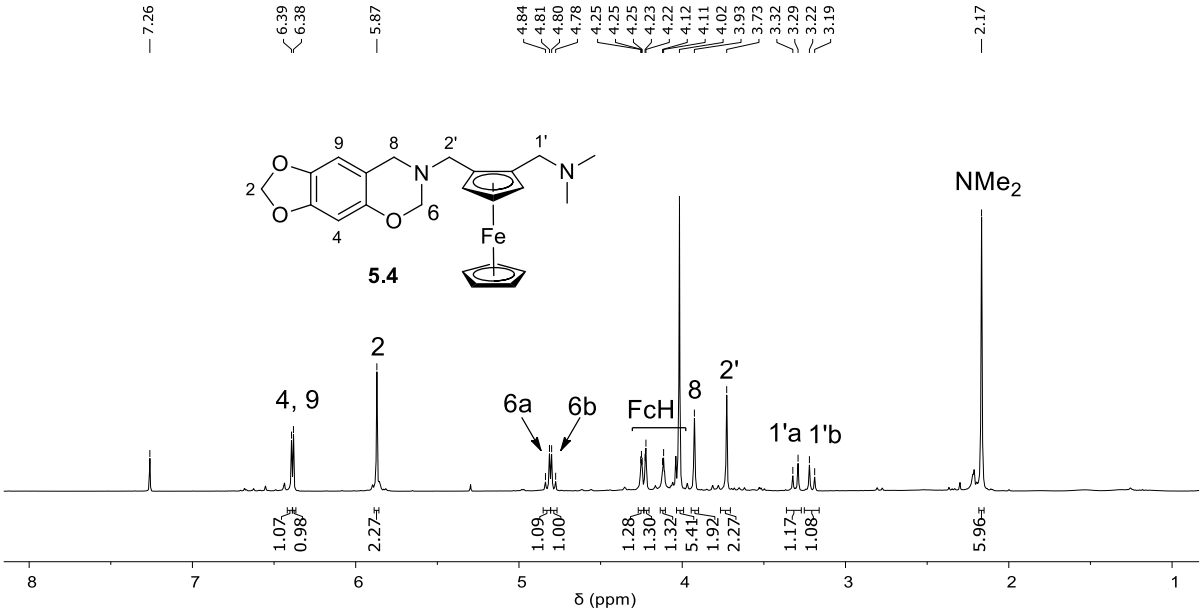

Figure 5.7 ^{1}H NMR spectrum of ferrocenyl sesamyl-1,3-oxazine **5.4** in $CDCl_3$.

The ^{1}H NMR data was further corroborated with DEPT-135 NMR, which confirmed the presence of an additional de-shielded methylene carbon corresponding to the dioxole unit at δ 100.8 ppm in the aromatic region, consistent with literature (**Figure 5.8**).[4] The de-shielding of the dioxole methylene carbon to its attachment to the two electronegative oxygen atoms in the dioxole ring.[4]

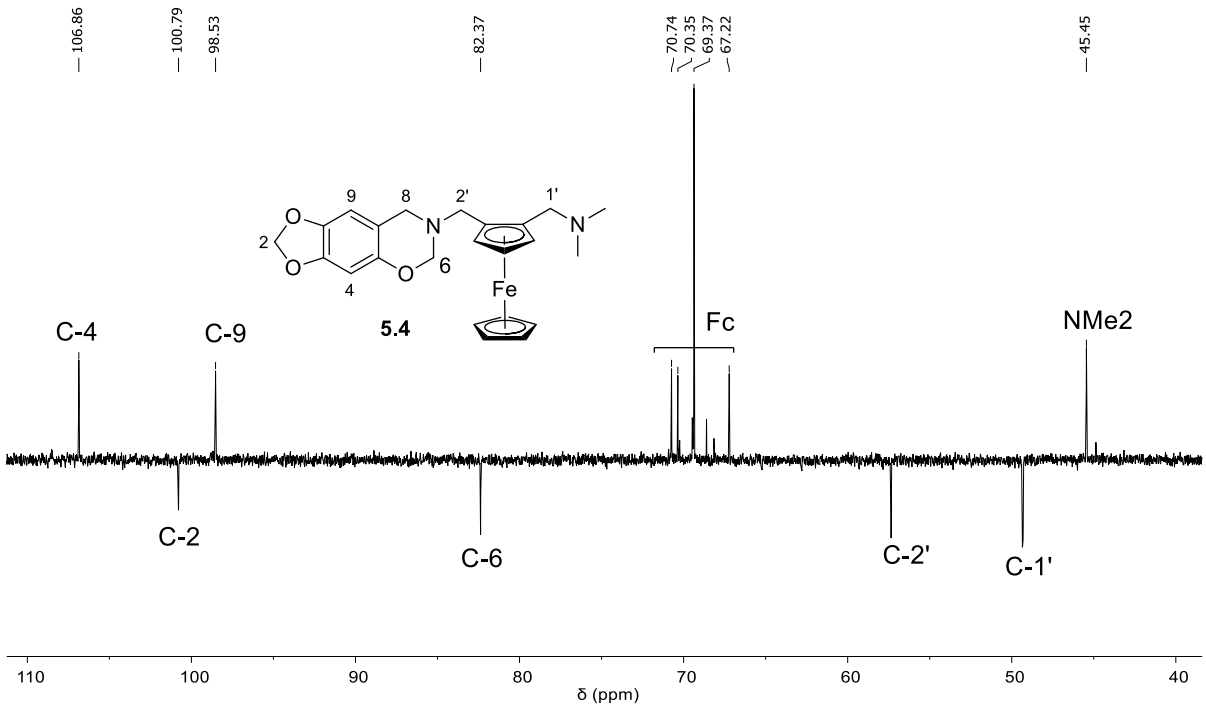

Figure 5.8 DEPT-135 NMR spectrum of ferrocenyl sesamyl-1,3-oxazine **5.4** in $CDCl_3$.

The structural identity of the compounds confirmed by NMR techniques was supported by HRMS data, which was consistent with the expected values (**Table 5.1**).

Table 5.1 HRMS data of ferrocenyl naphthoxazines (**5.2a-b**) and sesamyl-1,3-oxazine **5.4**.

Compound	Predicted mass	Found mass $[M+H]^+$
5.2a	441.1465	441.1465
5.2b	384.1051	384.1025
5.4	435.1366	435.1370

5.1.2. Synthesis and characterization of ferrocenyl coumarin-1,3-oxazines

Coumarins are prominent heterocyclic compounds endowed with a spectrum of biological activities.[1d,e] In the context of compounds that are the subjects of the study, i.e., ferrocenyl 1,3-benzoxazines, examples of compounds bearing the coumarin scaffold fused to the 1,4- and 1,3-oxazine units to produce coumarin-1,3-oxazines with demonstratable biological activities have

been fairly presented in literature (**Figure 5.9**).[5] In 2014, Mathew et al. reported synthesis of a novel class of coumarin-1,3-oxazine-type compounds by grafting the 1,3-oxazine into 2-thioxocoumarin scaffold at positions 7 and 8 to produce antibacterial agents (**5.5a-b**) active against a selection of bacterial strains.[5d] Subsequently, the research groups of Zhang and Kariyappa investigated series of coumarin-1,3-oxazine compounds (**5.6a-b** and **5.7a-b**) of similar structural architecture assembled via microwave-assisted Burke condensation and a two-step cyclization strategy, respectively, for antimicrobial potency using both bacterial and fungal strains.[5b,c]

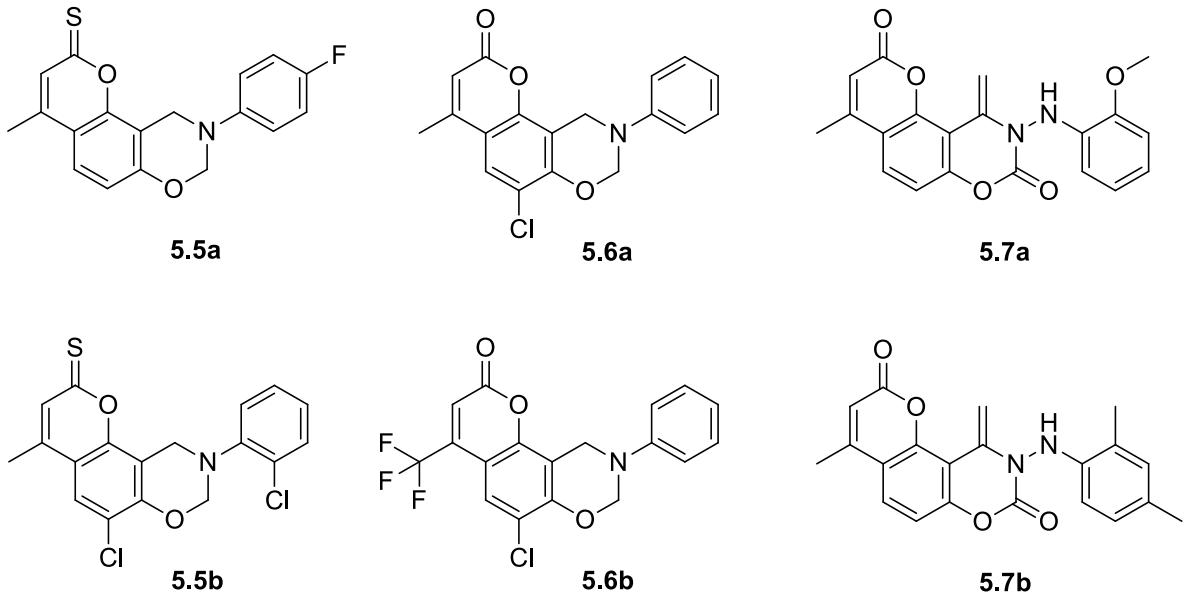

Figure 5.9 Coumarin-1,3-oxazine compounds with antimicrobial activity.

Prior to these developments, Nofal and co-workers prepared a representative series of coumarin-1,4-oxazine derivatives by appending the 1,4-oxazine ring into positions 7 and 8 (**Figure 5.10**).[5a] When assessed for potential *in vitro* antitumour activity, these compounds were disappointingly ineffective at inhibiting proliferation of tumour cells at the tested concentration (100 μg/mL).

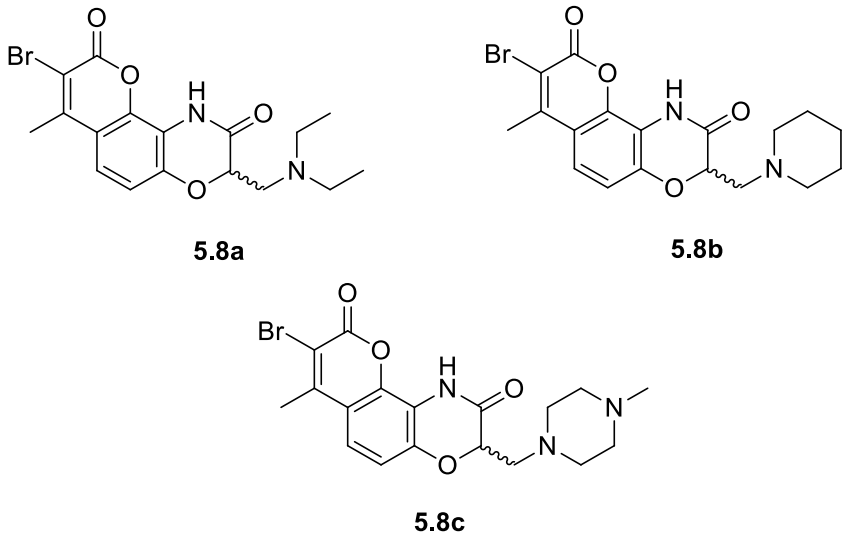

Figure 5.10 Coumarin-1,4-oxazine compounds investigated for anticancer activity.

The attractive pharmacological properties of the coumarin moiety together with the demonstrated biological activity of coumarin-1,3-oxazines as potential antimicrobial agents provided further motivation to replace the benzene ring with the coumarin nucleus in the ferrocenyl 1,3-benzoxazine scaffold under investigation.[1d,e,5a-c] To the best of our knowledge, a majority of coumarin-1,3-oxazines reported in literature for biological application are annulated with the oxazine unit on the benzene ring at C-7 and C-8 of the coumarin nucleus.[5a-c] By the time of the commencement of the current study, only one account of coumarin-1,3-oxazine analogues bearing the oxazine unit on the pyrone sub-ring had been reported.[6] However, the investigation of these congeners for potential biological agents was not reported. Most importantly, besides our previous work reporting the biological activity of coumarin-based ferrocenyl novobiocin analogues, there are no other accounts on the medicinal investigation of ferrocenyl derivatives of coumarins presented in literature, despite the medicinal attributes of both ferrocene and coumarin structural units.[7]

In line with the objectives of the study, we undertook to develop a novel class of bioactive ferrocenyl coumarin-1,3-oxazines by grafting the 1,3-oxazine moiety to the pyrone unit of the coumarin nucleus at C-3 and C-4 (**Figure 5.11**). Thus, the benzene ring of the ferrocenyl 1,3-

benzoxazine scaffold would be replaced with a coumarin unit, resulting in novel ferrocenyl coumarin-1,3-oxazines modified on the pyrone unit.

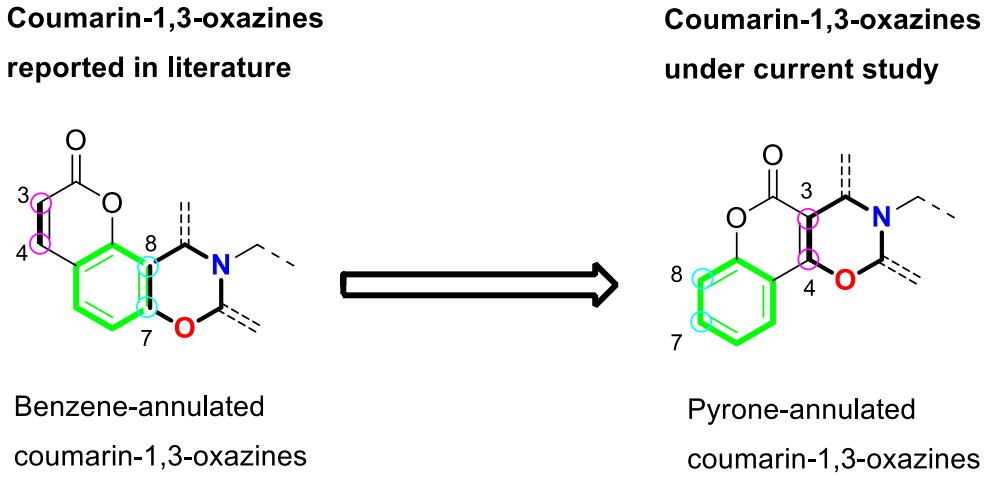

Figure 5.11 Design of pyrone-annulated coumarin-1,3-oxazines for biological activity.

To undertake synthesis of coumarin-1,3-oxazines resembling the structural architecture of the parental ferrocenyl 1,3-benzoxazines from **Chapter 3**, phenolic variants of coumarin, i.e., 3- or 4-hydroxycoumarins, were required as primary substrates in the synthesis. Given the expensive nature of 3-hydroxycoumarins (1 g = 456 ZAR, Merck South Africa) and limited procedures for their synthesis, 4-hydroxycoumarins were prioritized in the study due to their commercial affordability (100 g = 426 ZAR, Merck South Africa) and abundance of their synthetic methods.[8]

In a pilot study to prepare target ferrocenyl coumarin-1,3-oxazines, 4-hydoxy coumarin was subjected to the Burke conditions with amine **3.12a** and paraformaldehyde (**Scheme 5.3**). The reaction was refluxed for the duration 48 hours and progress monitored by TLC. To our disappointment, the reaction showed no indication of the formation of the desired product at any point during monitoring. Even when the reaction time was extended to three days, the product did not form. Switching amine **3.12a** with more basic amine **3.12b** failed to give the desired product, either.

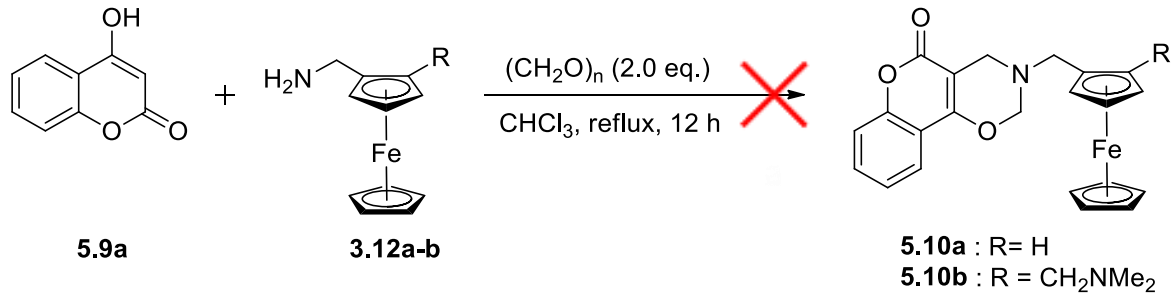

5.9a **3.12a-b**

5.10a : R= H
5.10b : R = CH_2NMe_2

Scheme 5.3 Attempted synthesis of coumarin-1,3-oxazines via the Burke protocol.

As discussed earlier (**Chapter 3**), being a Mannich-type condensation, the formation of 1,3-oxazine product by the Burke protocol proceeds via electrophilic aromatic substitution requiring availability of an aromatic pi-bond (π-bond) to the carbon atom carrying the hydrogen atom being substituted.[9] Thus, failure to form the desired product under these conditions seemed justified due to the non-aromaticity of the pyrone subring, which is less amenable to electrophilic attack by the iminium ion intermediate (**3.12a′-b′**) via electrophilic aromatic substitution (**Scheme 5.4**). Moreover, the non-aromaticity of the pyrone pi-bond of **5.9a** is further demonstrated by its propensity to undergo keto-enol tautomerism.[10]

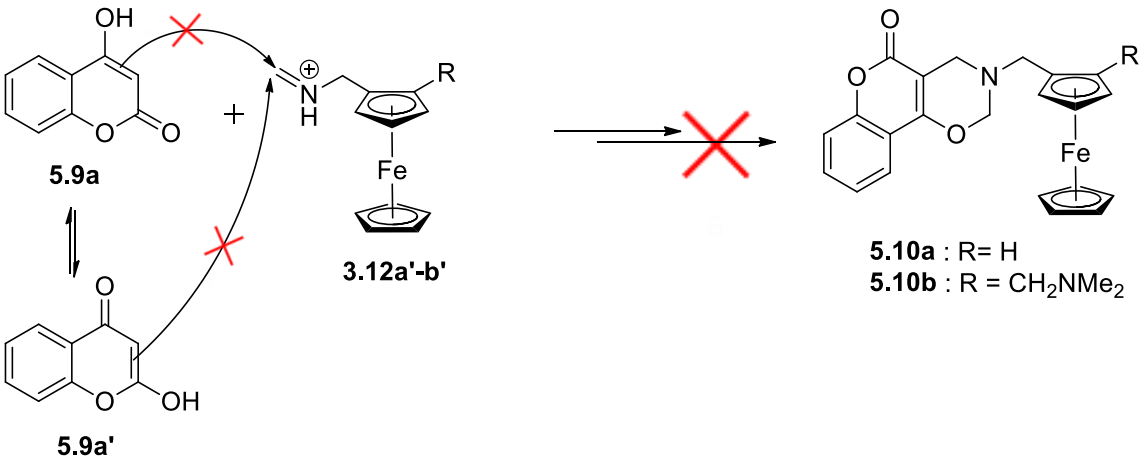

Scheme 5.4 Possible explanation for the failure of formation of coumarin-1,3-oxazine via Burke condensation.

Since addition of Lewis acids is known to facilitate aromatic electrophilic substitution,[9] Lewis acids, $AlCl_3$ and $FeCl_3$, and PTSA were screened under similar conditions, but to no avail. This further suggested the incompatibility of the 4-hydroxycoumarin with the Burke condensation.

By this time towards the end of 2018, Lohar et al. reported a new synthesis of similar organic pyrone-amended coumarin-1,3-oxazine compounds from 4-hydroxy coumarins making use of Lewis acid catalysts in 10% aqueous sodium dodecyl sulfate (SDS) (**Scheme 5.5**).[11]

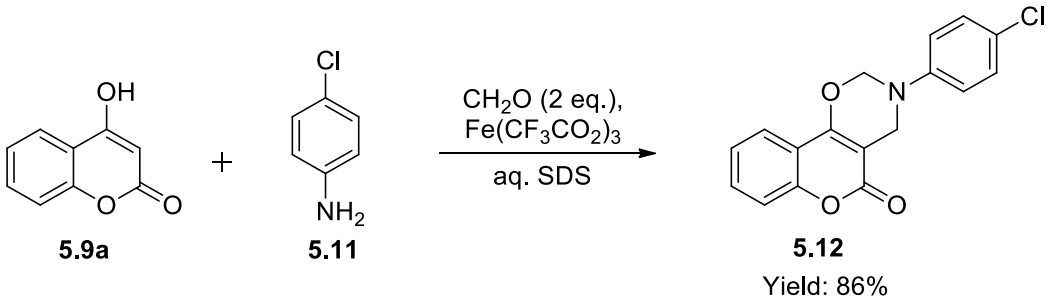

Scheme 5.5 Synthesis of pyrone-annulated coumarin-1,3-oxazines with $Fe(CF_3CO_2)_3$ in aqueous SDS reported by Lohar et al.[11]

Accordingly, we adapted their conditions without modification, except for the replacement of their preferred iron(III) trifluroacetate ($Fe(CF_3CO_2)_3$) with $FeCl_3$ due to reagent unavailability

in our lab. The use of $FeCl_3$ was logical since the researchers also performed synthesis of coumarin-1,3-oxazines with $FeCl_3$, which were obtained in high yields, during their optimization studies.[11] Again, application of these conditions proved unsuccessful in attaining the product, possibly due to the same factors affecting the Burke protocol.

To overcome the challenge of the non-aromaticity of the pyrone subring and the consequent failure of the iminium ion intermediate (**3.12a′-b′**) to couple to C-3 of the 4-hydroxycoumarin (**Scheme 5.4**), we redesigned the synthetic route to the desired coumarin-1,3-oxazines as shown by retrosynthetic analysis of the target compounds (**5.13a-b**) in **Scheme 5.6**. By first forming a 3-aminomethylcoumarin-4-ol (**5.13a-b**) already containing a methylamine at C-3 followed by cyclization with formaldehyde, electrophilic aromatic substitution could be evaded. This is similar to the stepwise synthesis of 1,3-benzoxazines by cyclization of salicylamine intermediates with formaldehyde (Route B, **Scheme 3.1**).[12]

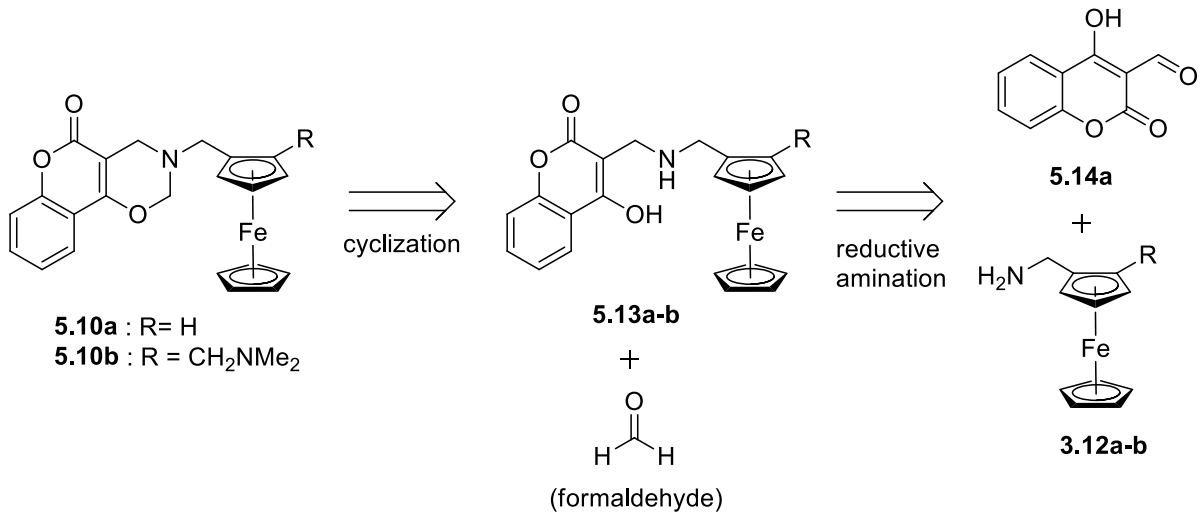

Scheme 5.6 Retrosynthetic analysis of target ferrocenyl coumarin-1,3-benzoxazines for alternative synthesis.

In order to form the appropriate 3-aminomethylcoumarin-4-ol, a relevant 3-formylcoumarin-4-ol is required. Unsubstituted 3-formylcoumarin-4-ol (**5.14a**) was effectively prepared by Vilsmeier-Haack formylation of 4-hydroxycoumarin with phosphorus oxychloride ($POCl_3$)

and DMF overnight (**Scheme 5.7**).[13] The hydroxyl group at C-4 that was substituted with a chlorine atom under these conditions was recovered by basic hydrolysis of the resultant 4-chloro-3-formylcoumarin (**5.15**) with potassium carbonate (K_2CO_3) followed by an acidic workup.[14] The chlorinated formylcoumarin (**5.15**) was refluxed in 5% aqueous K_2CO_3 for 1 hour and then allowed to cool to room temperature. The formed suspension was acidified with HCl to produce a precipitate that was filtered, washed (H_2O) and air-dried to furnish the desired 3-formyl-coumarin-4-ol product as an off-white solid.

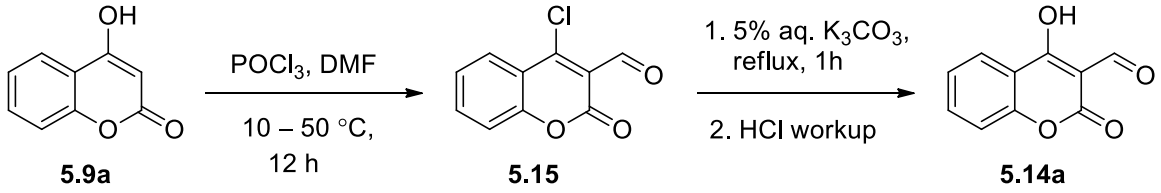

Scheme 5.7 Formylation of 4-hydroxycoumarin via Vilsmeier-Haack formylation.

Successful formylation of 4-hydroxycoumarin was confirmed by the disappearance of the 1H singlet at δ 5.59 ppm (corresponding to the proton in position 3 of 4-hydroxycoumarin) and the appearance of the 1H singlet signal at δ 10.04 ppm, typical of a peak of the aldehyde proton (**Figure 5.12**).[14]

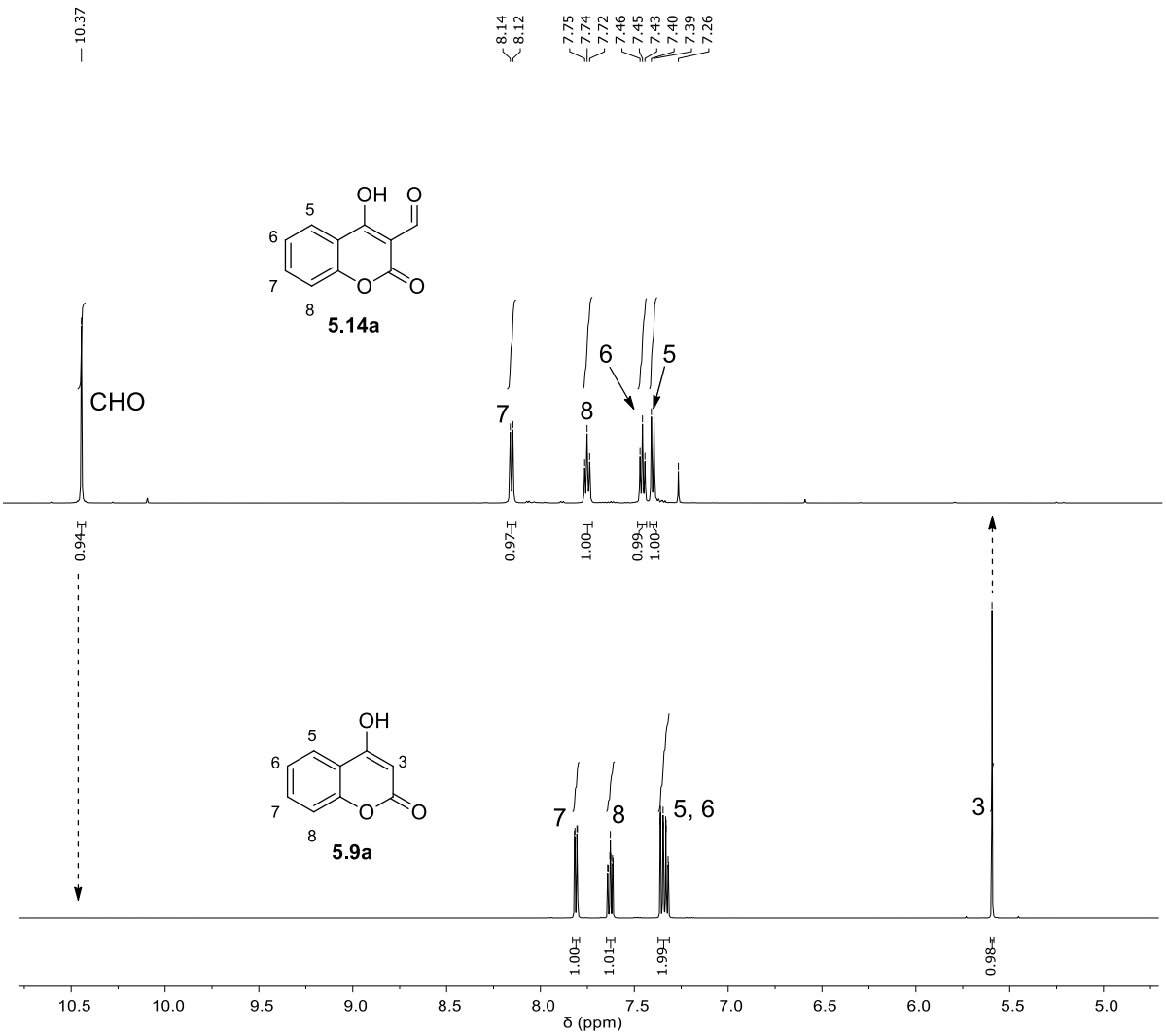

Figure 5.12 ^{1}H NMR spectra of 3-formyl-coumarin-4-ol (**5.14a**) and 4-hydroxycoumarin (**5.9a**) in $CDCl_3$ and DMSO-d_6, respectively.

With the right aldehyde substrate at hand, ferrocenyl 3-aminomethylcoumarin-4-ol (**5.13a**) was conveniently prepared via stepwise reductive amination of 3-formyl-coumarin-4-ol (**5.14a**) with ferrocenyl amines **3.12a-b** and $NaBH_4$ as the reducing agent (**Scheme 5.8**).[13,15] First, the 3-formyl-coumarin-4-ol (**5.14a**) and amines **3.12a-b** were coupled into the imine intermediates (**5.13a′-b′**) *in situ* by refluxing the two reagents in EtOH for 4 – 5 hours.[13] After completion of the reaction (TLC), the reaction was cooled to room temperature and $NaBH_4$ was added. The temperature was slowly raised to reflux with stirring to effect complete reduction of the imine intermediates **5.13a′-b′** into the products (**5.13a-b**).[15]

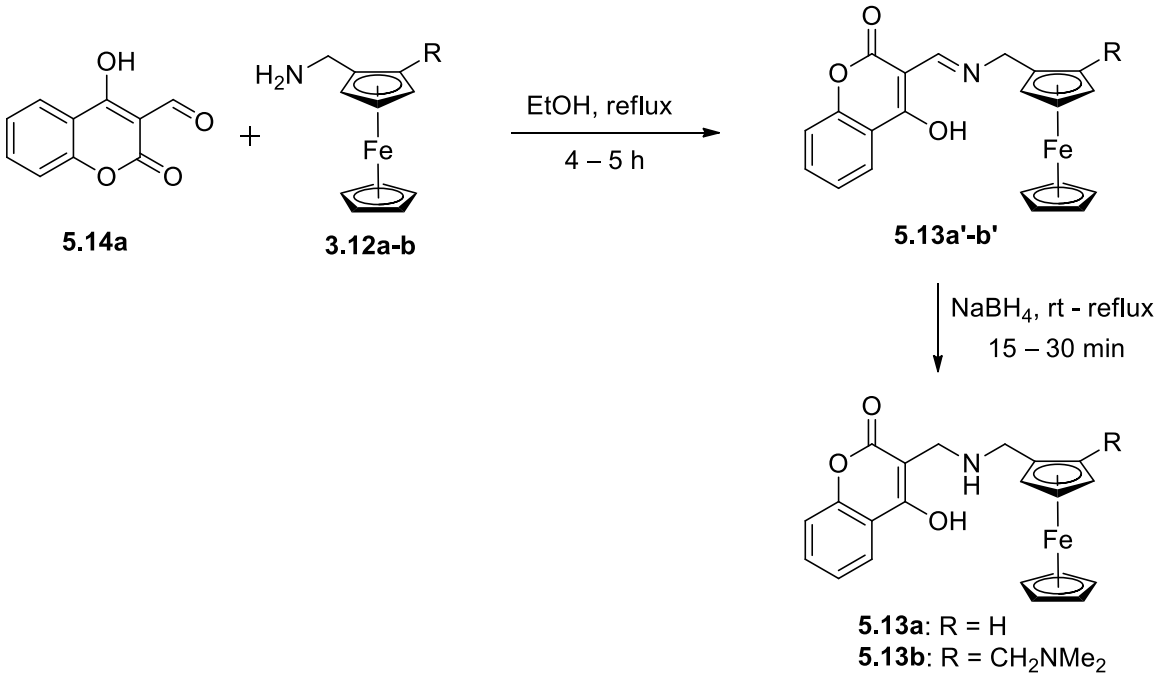

Scheme 5.8 Synthesis of the ferrocenyl 3-aminomethylcoumarin-4-ols (**5.13a-b**) by reductive amination.

Following termination of the reaction, the products (**5.13a-b**) were isolated in a similar manner as the α-amino-*o*-cresols (**Chapter 4**) in 68 – 86 % yields. The plain ferrocenyl product **5.13a** and its basic congener **5.13b** were both obtained as light brown semi-solids in high purity with no need of additional purification.

The products were characterized by spectroscopic techniques. Generally, the NMR spectral data of the formed ferrocenyl 3-aminomethylcoumarin-4-ol derivatives (**5.13a-b**) were similar to those of the ferrocenyl α-amino-*o*-cresols in **Chapter 4**, except for the presence of pyrone carbon signals of the coumarin nucleus in the ^{13}C NMR spectra. From the ^{1}H NMR spectrum of the basic ferrocenyl 3-aminomethylcoumarin-4-ol **5.13b**, the ferrocene (FcH) and aliphatic protons (NMe_2, 1′, 2′ and 3′) resonated in the expected regions as was observed for aminocresol derivatives (**4.6a-i**) with similar splitting patterns (**Figure 5.13**).

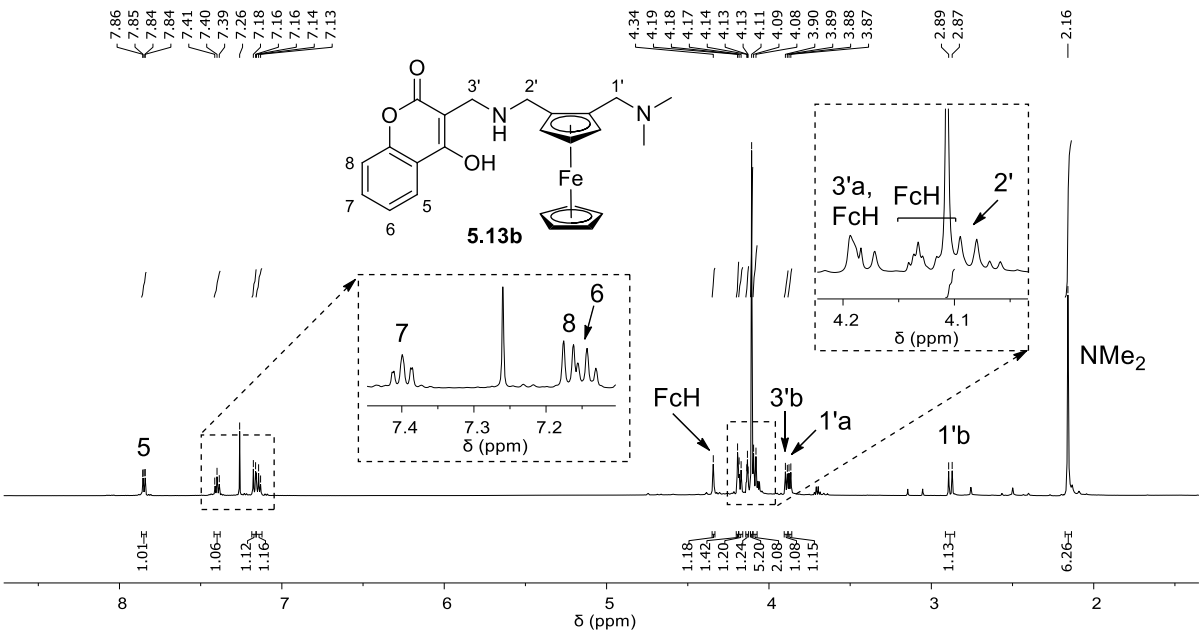

Figure 5.13 ^{1}H NMR spectrum of ferrocenyl 3-aminomethylcoumarin-4-ol **5.13b** in $CDCl_3$.

The benzene protons were assigned by multiplet analysis and were consistent with literature.[10,13] Proton 5 was the most de-shielded proton in the spectrum resonating downfield at δ 7.85 as a well-resolved doublet of doublets (dd) integrating to 1 proton due ortho- and meta-coupling with protons 6 and 7, respectively.[10] On the other hand, protons 6 and 7 were more shielded, appearing a δ 7.40 and 7.14 ppm as 1H triplets. Although not as well-resolved as proton 5, proton 8 was seen at δ 7.17 ppm as a 1H doublet with a *J*-coupling constant of 7.7 Hz confirming its coupling to proton 7, which had a similar first *J*-coupling constant (**Figure 5.13**).

Successful conjugation of ferrocenyl amine **3.12b** to the coumarin nucleus was further validated by the presence of nine carbon signals in the aromatic region and the methylene (CH_2) carbon signal at δ 58.1 ppm linking the two units in the ^{13}C NMR spectrum of **5.13b** (**Scheme 5.14**.

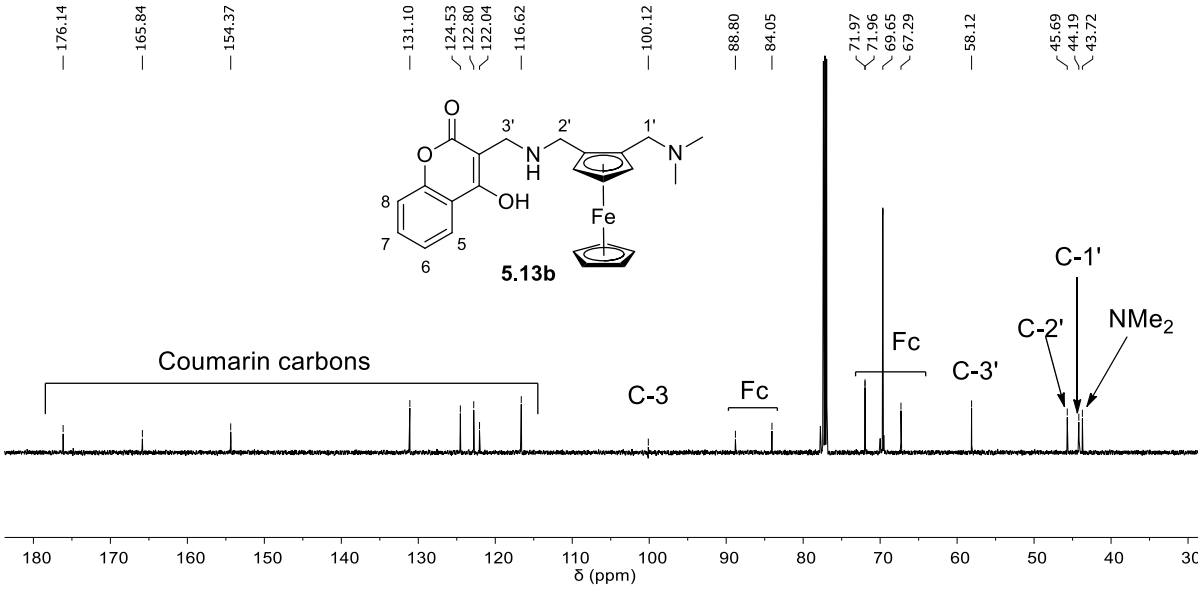

Figure 5.14 ^{13}C NMR spectrum of ferrocenyl 3-aminomethylcoumarin-4-ol **5.13b** in $CDCl_3$.

At this point it is important to highlight the structural similarities between the ferrocenyl 3-aminomethylcoumarin-4-ol and the ferrocenyl α-amino-*o*-cresols in **Chapter 4**. Considering the intended structural modifications in this study, ferrocenyl 3-aminomethylcoumarin-4-ols can be viewed as ring-annulated derivatives of the ferrocenyl α-amino-*o*-cresols in **Chapter 4** containing a coumarin ring in lieu of the benzene ring. The aminomethylhydroxy moiety (bold) is retained in both classes of compounds (**Figure 5.15**).

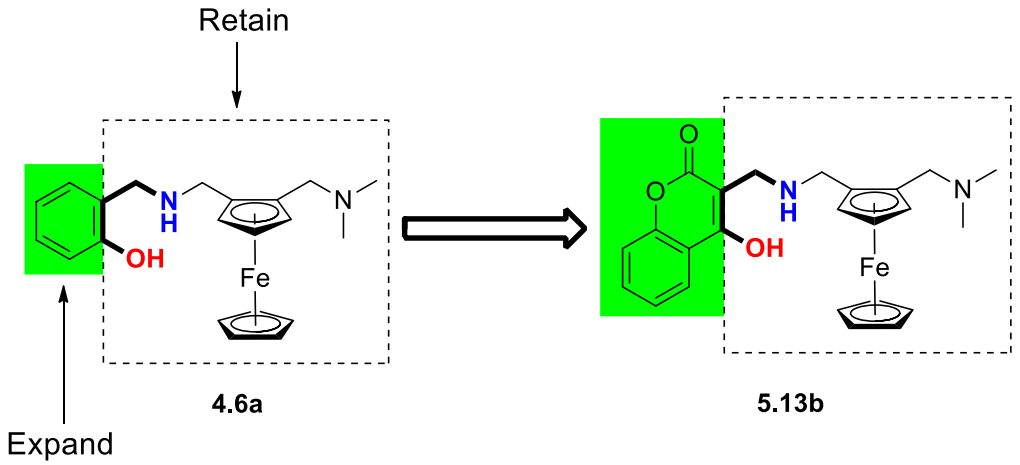

Figure 5.15 Structural similarities between ferrocenyl α-amino-*o*-cresols (**4.6a**) and 3-aminomethylcoumarin-4-ols (**5.13b**).

Consequently, a series of ferrocenyl 3-aminomethylcoumarin-4-ols substituted at C-6 of the coumarin nucleus with halogens F, Cl and Br was prepared for biological evaluation to elucidate the SAR profile of these compounds. Chlorine and fluorine were based on the SAR analysis of the ferrocenyl 3,4-dihydro-2*H*-1,3-benzoxazine derivatives, which suggested that lipophilic and electron-withdrawing benzene substituents were generally conducive for activity (**Figure 4.16**). Due to the expensive nature of both 6-fluoro- and 6-chloro-4-hydroxycoumarins, these reactants had to be synthesized from less costly reagents. There is a plethora of synthetic protocols in literature for synthesis of 4-hydroxycoumarins.[8] The two most common procedures involve cyclization of phenolic substrates: phenols and 2′-hydroxyacetophenones.[16]

Synthesis of 4-hydroxycoumarins from phenols is achieved by heating a substituted phenol (**3.1**) with malonic acid (**5.16**) in the presence of zinc chloride ($ZnCl_4$) and $POCl_3$ or with Meldrum's acid (**5.17**) followed by internal cyclization facilitated by Eaton's reagent (**Scheme 5.9**).[16a,b]

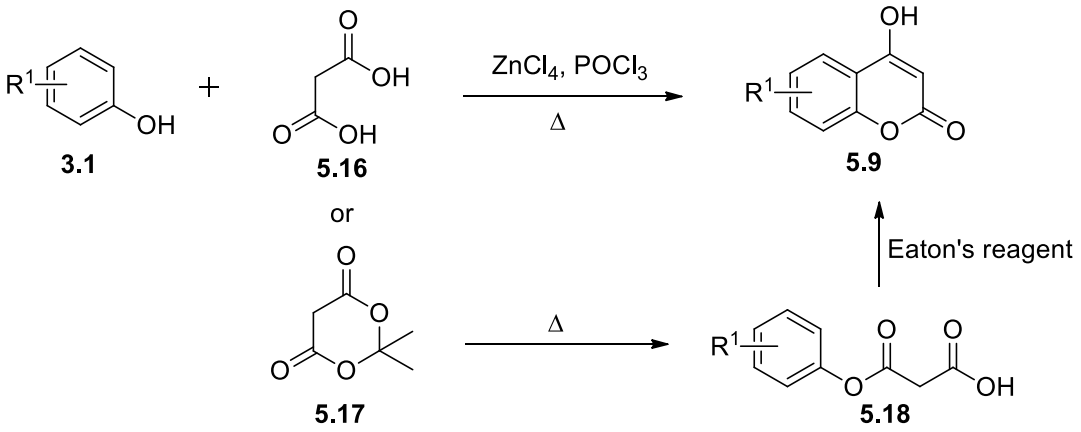

Scheme 5.9 Synthesis of 4-hydroxycoumarins from phenols.

Synthesis with 2′-hydroxyacetophenones (**5.19**) is performed in one step in the presence of a base with acylating agents such as diethyl carbonate or phosgene that couple the acetyl and phenolic OH group to form the 4-hydroxycoumarin product (**Scheme 5.10**).[16c]

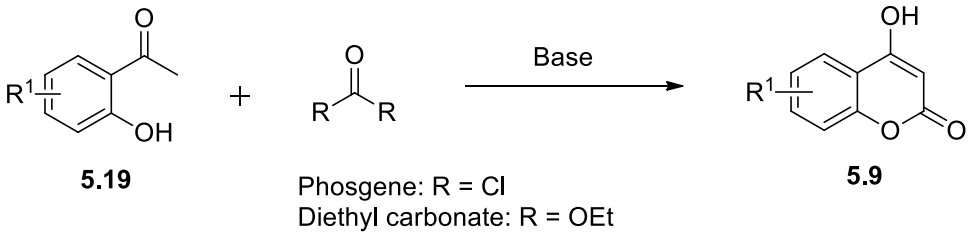

Scheme 5.10 Synthesis of 4-hydroxycoumarins from 2′-hydroxyacetophenones.

With these two alternative procedures at our disposal, it was possible to synthesize desired substrates for the preparation of 6-Cl and 6-F ferrocenyl 3-aminomethylcoumarin-4-ols. Synthesis of 6-fluoro- and 6-chloro-4-hydroxycoumarins by heating 4-chloro and 4-fluorophenols with malonic acid following the conditions in **Scheme 5.9** failed to furnish the desired coumarins.[16a] Preparation with Meldrum's acid was not attempted due to unavailability of Eaton's reagent. Thus, cyclization of 2′-hydroxyacetophenones with acylating agents was the only viable choice. However, the desired 2′-hydroxyacetophenones containing chlorine and fluorine at the desired positions were not available and had to be prepared from scratch.

These substrates were easily accessed by acylation of 4-chloro (**3.1c**), 4-bromo (**3.1d**) and 4-fluorophenol (**3.1l**) with acetic anhydride (Ac_2O) followed by Fries rearrangement of the acetylated products (**5.20a-c**) with $AlCl_3$ (neat) to produce the desired 2′-hydroxyacetophenones **5.19a-b** (**Scheme 5.11**).[17]

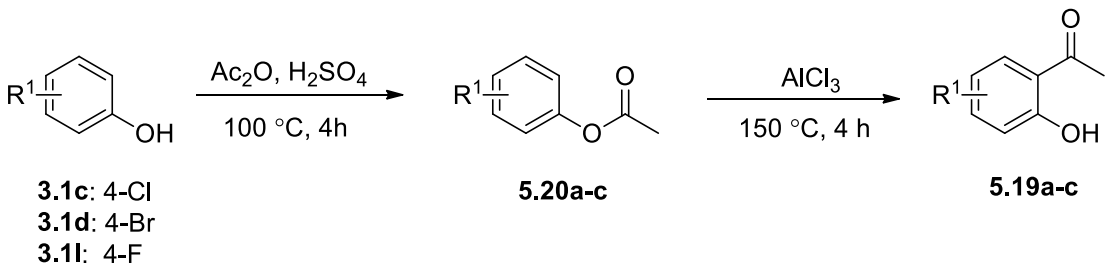

Scheme 5.11 Synthesis of 5′-halogenated 2′-hydroxyacetophenones (**5.19a-b**).

The halogenated phenols (**3.1c-d** and **3.1l**) were heated at 100 °C in Ac_2O containing catalytic amounts of sulphuric acid (H_2SO_4) for 3 hours.[17] After completion of the reaction (TLC), desired phenylacetate intermediates (**5.20a-c**) were achieved in excellent yields (95 – 97%) as colourless oils following a simple workup involving washing with distilled water. These intermediates were subjected to Fries rearrangement conditions by heating $AlCl_3$ in slight excess (1.5 equivalents) at 150 °C for 4 hours. [17] The initial fuming yellow powdery mixture turned into a uniform viscous material during the reaction that formed a brown solid upon cooling. The resultant solid was broken and excess $AlCl_3$ quenched with dilute HCl solution. The products were obtained as off-white solids in sufficient purity, as judged by ^{1}H NMR, to proceed to the next step after extraction with EtOAc, washing with brine, drying the extracts (Na_2SO_4) and removing the solvent *in vacuo* in excellent yields of 88 – 92%.

Successful Fries rearrangement was readily confirmed by the loss of symmetry in the NMR spectra of the products, which showed three aromatic proton signals integrating to a total of three protons in the ^{1}H NMR spectra and seven carbon peaks in the ^{13}C NMR spectrum of the 5′-halogenated 2′-hydroxyacetophenones (**5.19a-c**) (**Figure 5.16**).

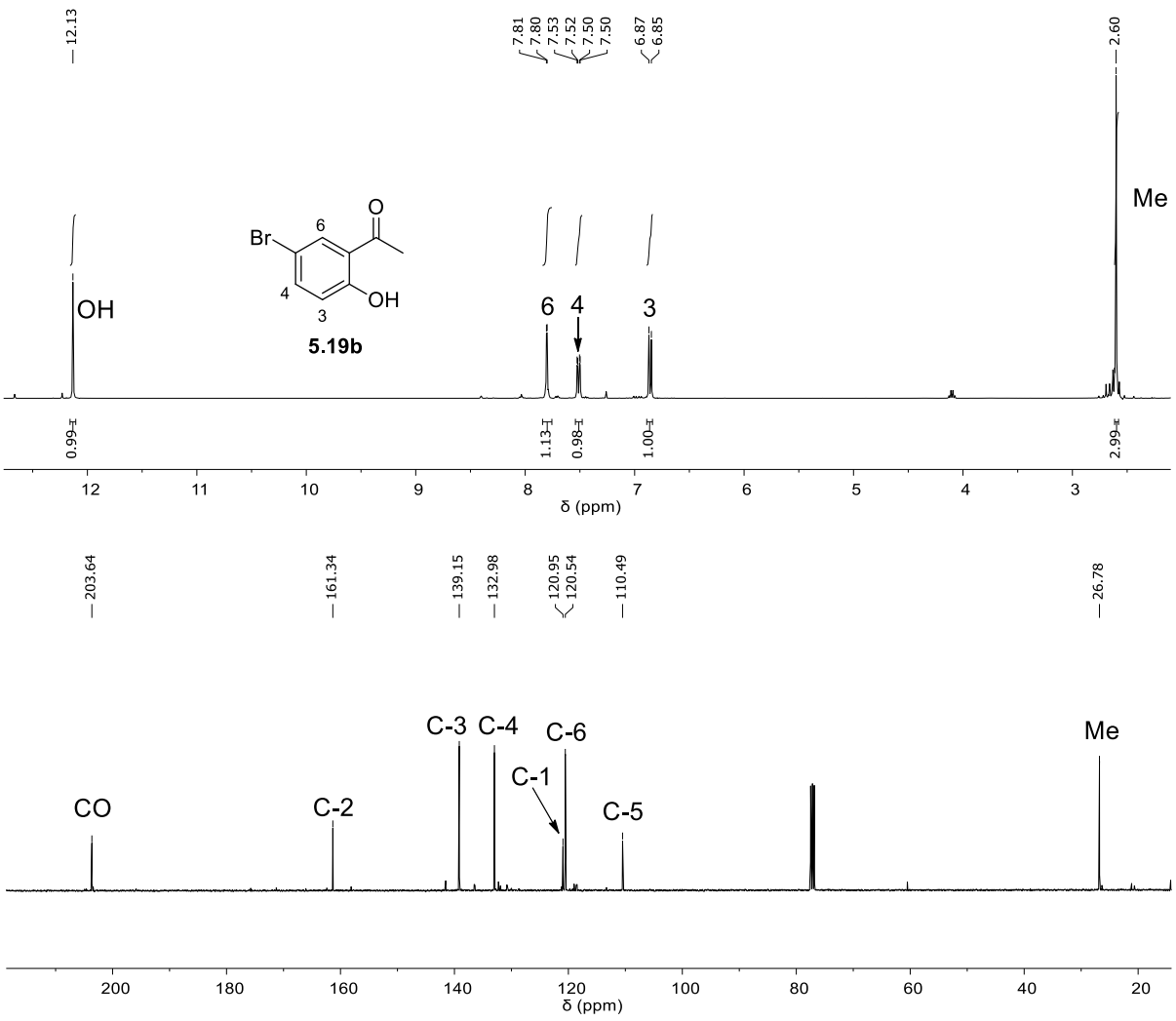

Figure 5.16 ^{1}H and ^{13}C NMR spectra of 5′-bromo-2′-hydroxyacetophenone **5.19b** in $CDCl_3$.

The desired 4-hydroxycoumarins were synthesized by cyclization of acetophenones **5.19a-c** with dimethyl carbonate (DMC) using sodium hydride (NaH) as a base (**Scheme 5.12**).[16c] Unsubstituted 4-hydroxycoumarin **5.9a** was not synthesized since it is commercially available.

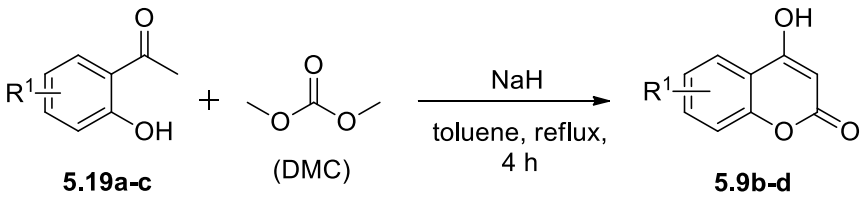

Scheme 5.12 Synthesis of 6-halogenated 4-hydroxycoumarins **5.9b-d**.

A solution of equimolar amounts of a relevant acetophenone **5.19a-c** and DMC in toluene was added slowly to a suspension of excess NaH (5.0 equivalents) in toluene on ice and stirred on ice for 30 minutes, which was then refluxed for 4 hours. After termination of the reaction, the products were precipitated out by acidification with HCl following quenching with water. The pure 4-hydroxycoumarin products **5.9b-d** were collected by filtration, air-dried and attained as off-white solids in 86 – 96% yields.

The structures of the formed 4-hydroxycoumarins **5.9b-d** were confirmed by melting point determination in addition to their spectral data. In all cases, the observed melting points were consistent with the literature values (**Table 5.1**).

Table 5.1 Melting point analysis of 5-halogenated 4-hydroxycoumarins (**5.9b-d**).

Compound	Observed melting point (°C)	Literature value (°C)	Reference
5.9b	231.4 – 234.8	232 – 235	Jeon and Kim[18]
5.9c	242.0 – 243.5	241 – 243	Jeon and Kim[18]
5.1d	238.8 – 240.7	240 – 241	Nolan et l.[19]

In order to synthesize the target 4-hydroxy-3-aminomethylcoumarins substituted with halogens at C-6 by reductive amination, the 5-halogenated 4-hydroxycoumarins had to be converted to corresponding 3-formylcouarin-4-ol derivatives. In the case of ferrocenyl 4-hydroxy-3-aminomethylcoumarins **5.13a-b**, the unsubstituted commercially available 4-hydroxycoumarin was transformed into 3-formylcoumarin-4-ol **5.14a** in two steps via Vilsmeier-Haack formylation followed by hydrolysis as previously described (**Scheme 5.7**). Although this strategy gave the desired compound in high yields without a purification step, the long reaction times (12 hours) were concerning. For expediency, a two-minute formylation procedure reported by Rad-Moghadam and Mohseni via microwave irradiation (mw) of 4-hydroxycoumarin with a conventional microwave was employed to synthesize the halogenated

3-formylcoumarin-4-ol **5.14b-d** (**Scheme 5.13**).[20] The method is catalysed by PTSA and proceeds via formation of a 3-(ethoxymethylene)chroman-2,4-dione intermediate (**5.14b′-d′**) using triethyl orthoformate ($CH(OEt)_3$) that is subsequently hydrolyzed into the desired 3-formylcoumarin-4-ol by a basic or acidic workup. Again, unsubstituted 3-formylcoumarin-4-ol **5.14a** was not synthesized under these conditions since it was already prepared by Vilsmeier-Haack formylation.

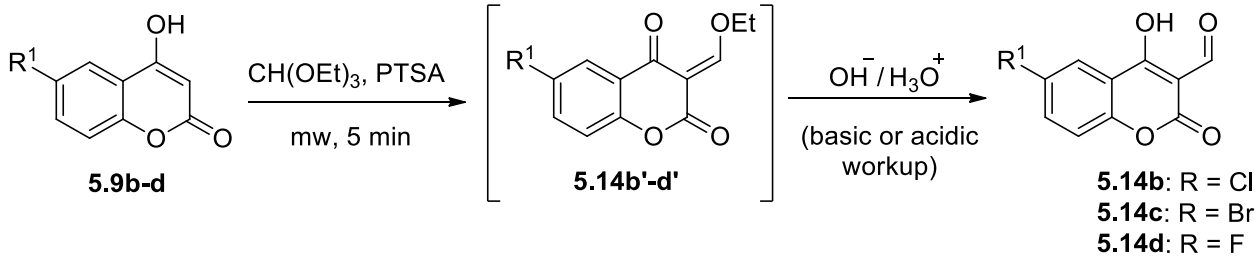

Scheme 5.13 Formylation of halogenated 4-hydroxycoumarins (**5.9b-d**) into corresponding 3-formylcoumarin-4-ols **5.14b-d** by microwave irradiation.

In a typical procedure, an appropriate 4-hydroxycoumarin (**5.9b-d**) and 10 % mol PTSA were placed in a 25 mL Erlenmeyer flask and thoroughly mixed with sufficient amount of $CH(OEt)_3$ to form a uniform paste. The mixture was irradiated at medium (3 minutes) and high (2 minutes) using a conventional kitchen microwave at which time the paste turned into a yellow suspension. After cooling the reaction mixture to room temperature, the product was precipitated by trituration with 2N HCl solution, and then collected by filtration and air-dried. The 3-formylcoumarin-4-ol products were obtained as light orange or yellow solids in 56 – 60% yields.

The structures of the products (**5.14b-d**) were confirmed by the appearance of the aldehyde group around δ 10.03 and 195.1 ppm, respectively, in the ^1H and ^{13}C NMR spectra of the compounds as illustrated in **Figure 5.17**.

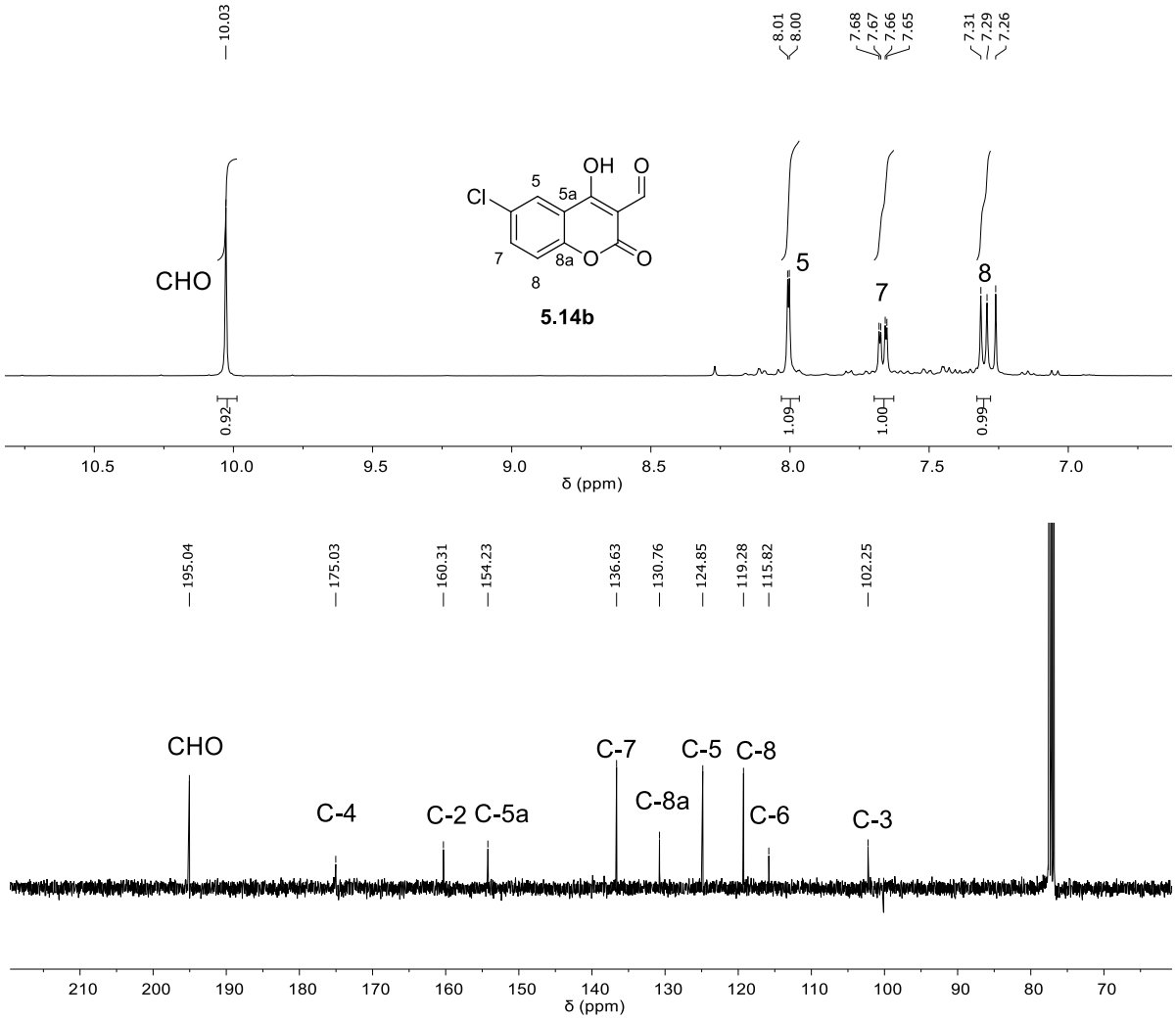

Figure 5.17 ^{1}H and ^{13}C NMR spectra of 6-chloro-3-formylcoumarin-4-ol **5.14b** in $CDCl_3$.

With the halogenated 3-formylcoumarin-4-ols (**5.14b-d**) at hand, synthesis of halogenated target ferrocenyl 3-aminomethylcoumarin-4-ol derivatives (**5.13c-e**) ensued employing reductive amination conditions in **Scheme 5.8** above. Due to the lack of activity of the plain ferrocenyl 3-aminomethylcoumarin-4-ol **5.13a** lacking the basic CH_2NMe_2 side chain when evaluated in the assays, only derivatives synthesized from the basic ferrocenyl amine **3.12b** and the corresponding aldehydes **5.14b-d** were pursued. The resultant compounds (**5.13c-e**) were obtained similarly to the non-halogenated 3-aminomethylcoumarin-4-ol **5.13b** (**Scheme 5.8**) in 64 – 84% yields (**Table 5.2**).

Table 5.2 Isolated product yields of non-halogenated (**5.13a-b**) and halogenated (**5.13c-d**) ferrocenyl 3-aminomethylcoumarin-4-ol derivatives via reductive amination.

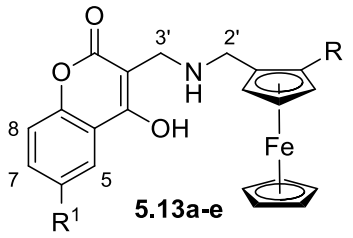

5.13a-e

Compound	R^1	R	Isolated yield (%)
5.13a	H	H	86
5.13b	H	CH_2NMe_2	68
5.13c	Cl	CH_2NMe_2	66
5.13d	Br	CH_2NMe_2	84
5.13e	F	CH_2NMe_2	64

The compounds were characterized in a similar manner to the non-halogenated variant **5.13a**. Using ferrocenyl 6-fluoro-3-aminomethylcoumarin-4-ol **5.13e** as an example, the spectral analysis of the compounds was performed as illustrated in **Figure 5.18**. The protons of the coumarin nucleus resonated in the same region as the 3-formyl (**5.15b-d**) and 4-hydroxy (**5.14b-d**) substrates with no changes in the peak multiplicities. Due to the $^{1}H - {}^{18}F$ coupling, the coumarin protons in **5.13e** were observed as doublet of doublets (J = 8.6, 2.9 Hz) and overlapping triplet of doublets and doublet of doublets at δ 7.85 and 7.18 – 7.13 ppm corresponding to protons 5, 7 and 8, respectively (**Figure 5.18**).

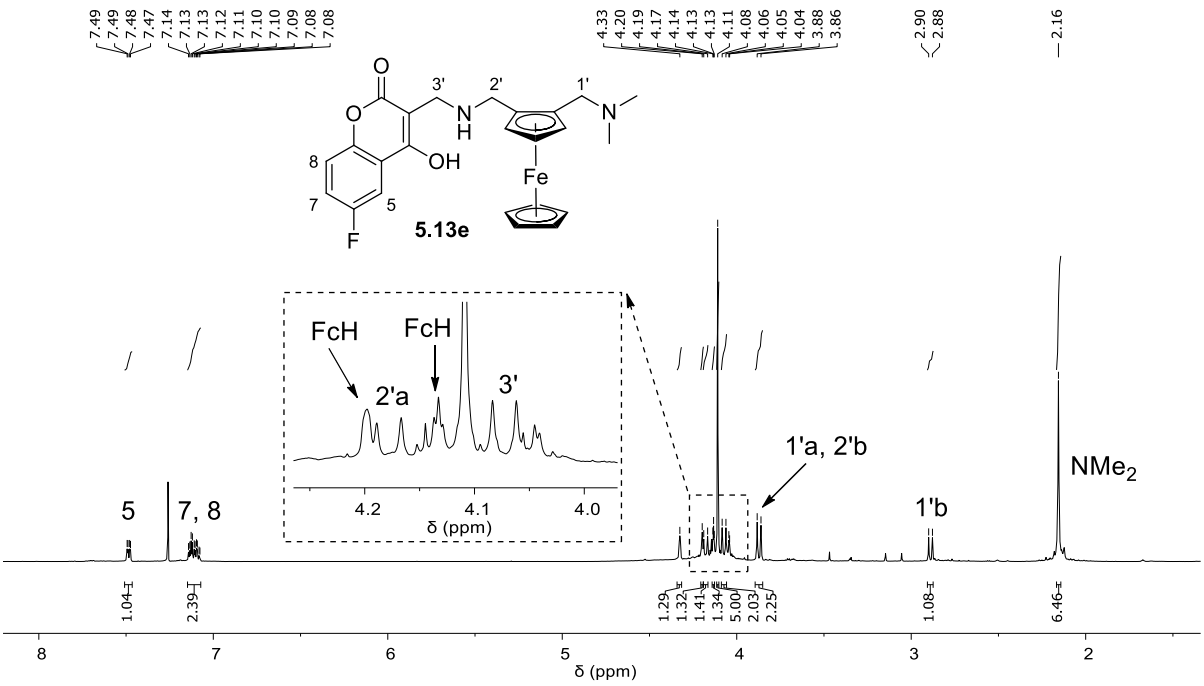

Figure 5.18 ^{1}H NMR spectrum of ferrocenyl 6-fluoro-3-aminomethylcoumarin-4-ol **5.13e** in $CDCl_3$.

Identification of the diastereotopic protons 1′a and 2′b at δ 3.87 ppm appearing as two overlapping doublets was facilitated by COSY NMR (**Figure 5.19**). Proton 1′b was easily identified as a 1H doublet at δ 2.89 ppm. The geminal coupling of proton 1′b and proton 1′a, overlapping with an unidentified proton at δ 3.87 ppm, was visible on the COSY NMR spectrum as a cross-peak at [2.89, 3.87] ppm (correlation *b*). Similarly, geminal coupling of protons 2′a and 2′b at [4.20, 3.87] ppm (correlation *a*) allowed spectral assignment of these protons.

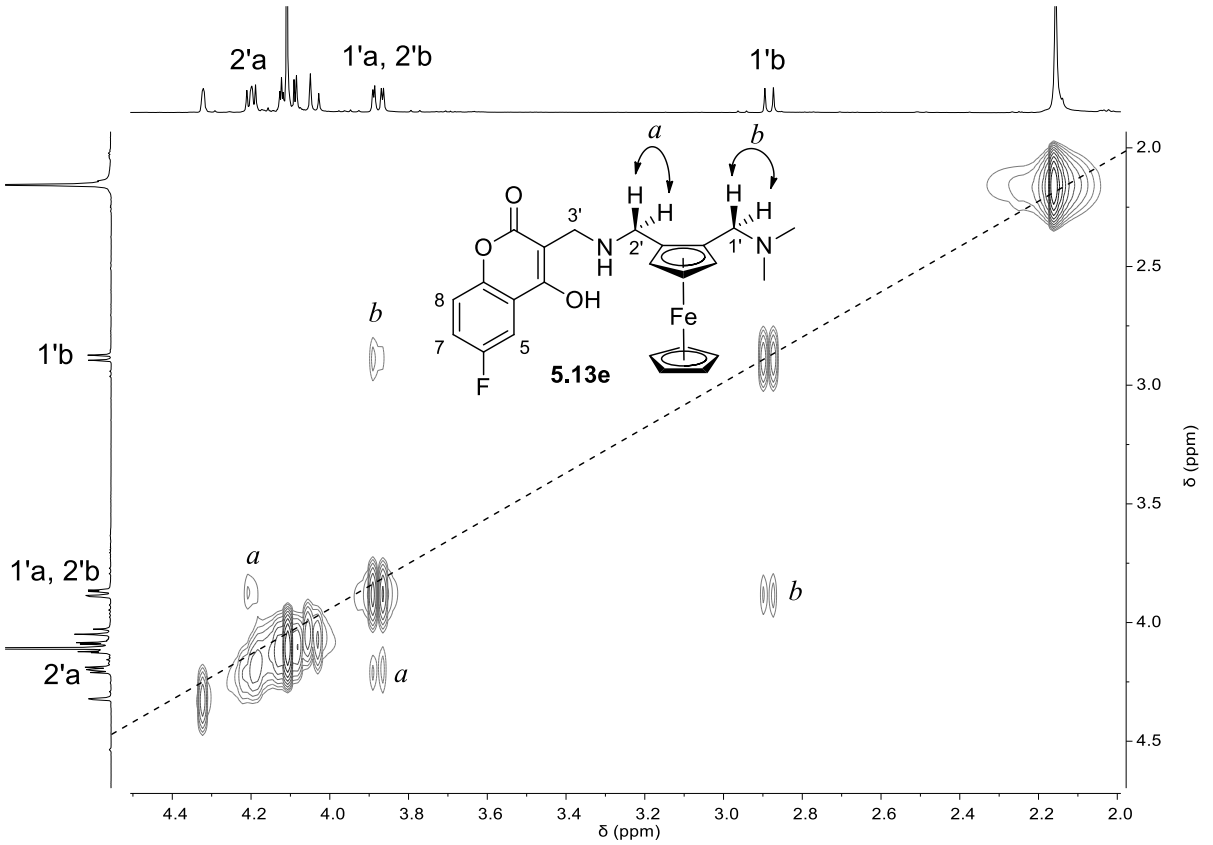

Figure 5.19 COSY NMR spectrum of compound **5.13e** in $CDCl_3$ showing the aliphatic region.

The HRMS spectral data of the synthesized ferrocenyl 3-aminomethylcoumarin-4-ol derivatives (**5.13a-e**) was consistent with the predicted results (**Table 5.3**).

Table 5.3 HRMS results of benzene annulated ferrocenyl coumarin derivatives (**5.13a-c**)

Compound	Expected mass $[M+H]^+$	Found $[M+H]^+$
5.13a	390.0793	390.0779
5.13b	447.1371	447.1371
5.13c	481.0976	481.1568
5.13d	404.0896	404.0952
5.13e	465.1279	465.1279

Having successfully prepared the appropriate acyclic substrates, i.e., ferrocenyl 3-aminomethylcoumarin-4-ols (**5.13a-e**), we were now in a position to undertake the synthesis of these coumarin-1,3-oxazines **5.10a-e** by cyclization with paraformaldehyde (**Scheme 5.14**).

To our disappointment, formation of the desired products under these conditions was unsuccessful, possibly due to the decrease in acidity (and nucleophilicity) of the coumarin OH group since it is attached to a non-aromatic pyrone ring instead of a benzene and no longer phenolic.[21] Addition of Lewis acids tested previously during the attempted Burke condensation also proved futile in yielding the desired products. In all cases, the starting materials were recovered unchanged.

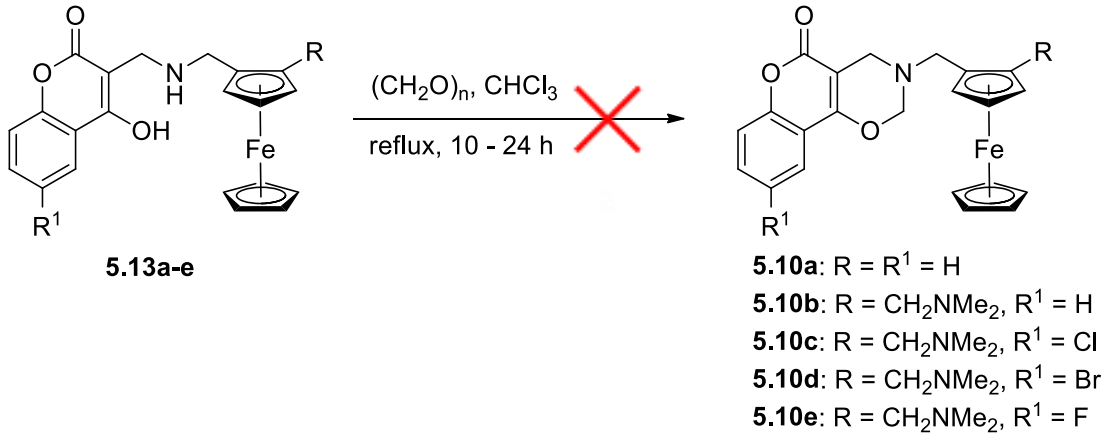

5.13a-e

5.10a: R = R^1 = H
5.10b: R = CH_2NMe_2, R^1 = H
5.10c: R = CH_2NMe_2, R^1 = Cl
5.10d: R = CH_2NMe_2, R^1 = Br
5.10e: R = CH_2NMe_2, R^1 = F

Scheme 5.14 Attempted synthesis of ferrocenyl coumarin-1,3-oxazines **5.10a-e** by cyclization of 3-aminomethylcoumarin-4-ols (**5.13a-e**).

At this point it was important to investigate the effect of the OH group and the ring to which it is attached on the reactivity of 3-aminomethyl-hydroxycoumarin substrates **5.13a-e** for cyclization into the desired coumarin-1,3-oxazine compounds **5.10a-e**. To achieve this, a phenolic coumarin bearing an OH group at C-7 on the benzene ring instead of the lactone, i.e. 7-hydroxycoumarin (**5.21**), was used as a tool compound to synthesize its corresponding coumarin-1,3-oxazine analogue. As with the halogenated 4-hydroxycoumarins (**5.9a-d**), commercially available 7-hydroxycoumarin (**5.21**) was first converted to its ortho-formylated variant (**5.22**) for subsequent reaction with amines **3.12a-b** to produce the acyclic 8-aminomethylcoumarin-7-ol derivatives (**5.23a-b**) of the target coumarin-1,3-oxazine products (**5.24a-b**) (**Scheme 5.15**).

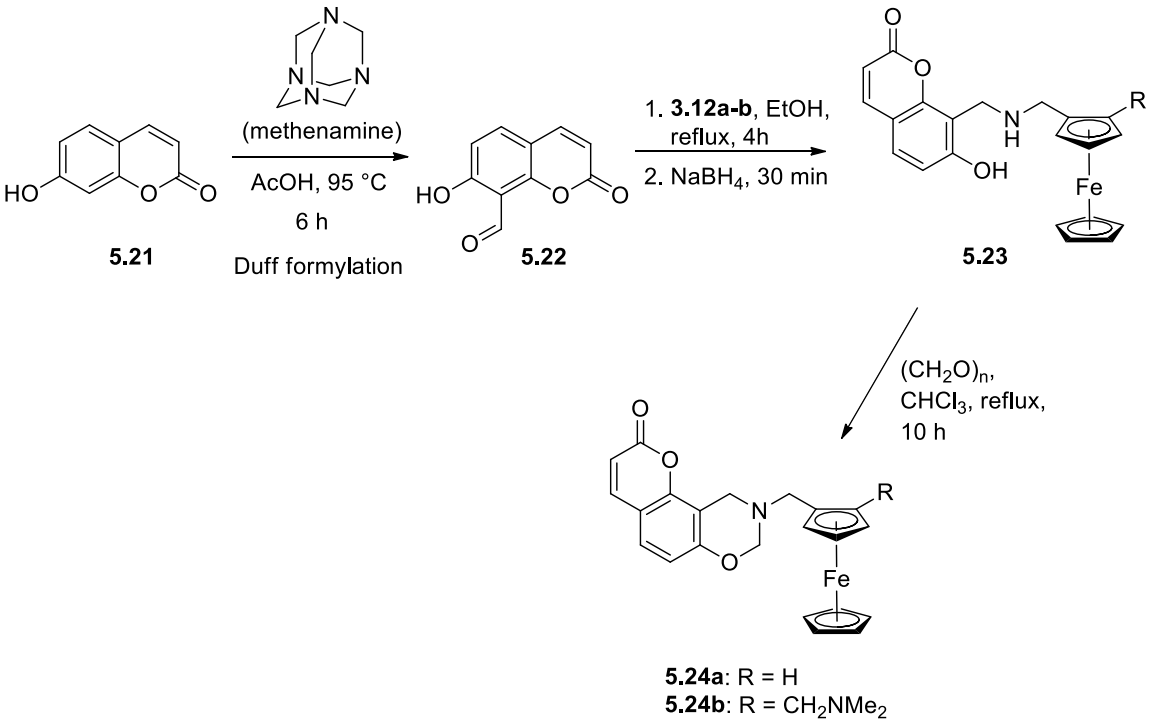

Scheme 5.15 Synthetic route to benzene-annulated ferrocenyl coumarin-1,3-oxazines **5.24a-b** via the two-step strategy.

The phenolic coumarin **5.21** could not be formylated by either of the procedures employed for formylation of the non-phenolic, pyrone-hydroxylated 4-hydroxycoumarins **5.9a-d** (**Schemes 5.7** and **5.13**). These observations were already highlighting the differences in the reactivity of these ring units, i.e. pyrone and benzene. The formylated product **5.22** was finally achieved by Duff formylation with methenamine (also known as hexamine) as a formyl carbon source (**Scheme 5.15**).[22]

Duff formylation proceeds via electrophilic aromatic substitution whereby methenamine is converted to an iminium ion intermediate in acidic medium that attacks the aromatic proton ortho to the OH group of the phenolic unit to subsequently effect the ortho-formylated product.[23] Formylation of 7-hydroxycoumarin **5.21** was performed by heating this phenolic substrate in glacial acetic acid (AcOH) for 6 hours at 95 °C, followed by an acidic workup with HCl after cooling the reaction mixture. The formylated product **5.22** was extracted with $CHCl_3$,

dried (Na_2SO_4) and obtained as a pale green solid in 22% yield after removing the solvent *in vacuo*. Identity of the product was determined by melting point and NMR. Both the observed melting point (M.p.: 175.4 – 177.2 °C, Lit.: 176–178 °C) and ^1H and ^{13}C NMR spectral data of the product were consistent with literature observations (**Figure 5.20**).[23]

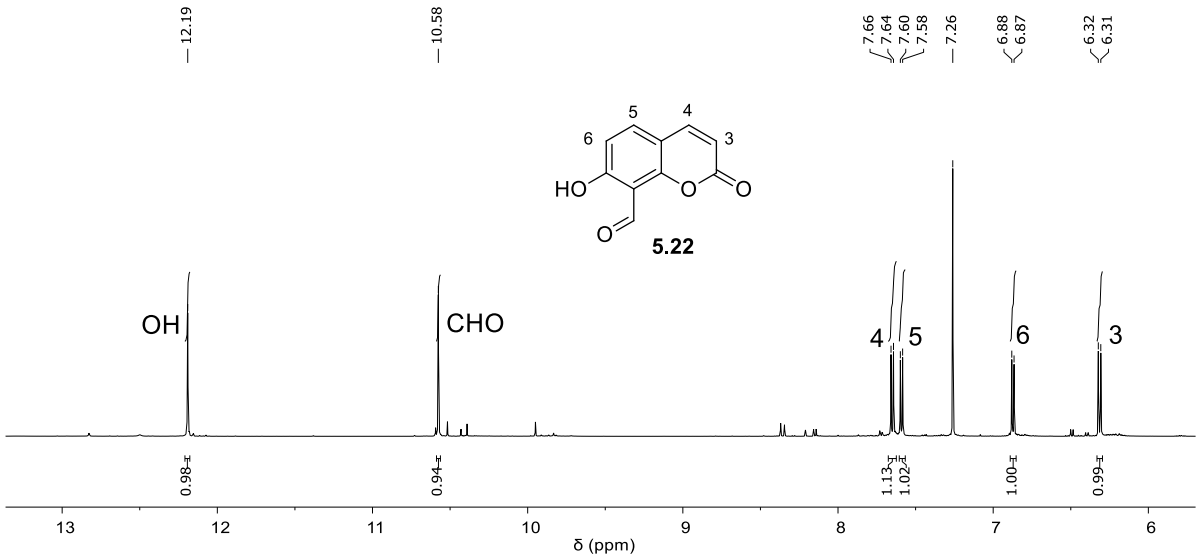

Figure 5.20 ^1H NMR spectrum of 8-formylcoumarin-7-ol **5.22** in $CDCl_3$.

The characteristic aldehyde peak resonated at δ 10.58 ppm as a singlet integrating to 1H, while the OH group was the most de-shielded signal in the spectrum at δ 12.19 ppm. Proton 4 was the most downfield coumarin signal due to being in meta position relative to the electron deficient lactone carbonyl at C-2. This was followed by proton 5 substituted meta to the tautomeric OH group at C-7, which can become ketone via keto-enol tautomerism, causing it to pull electron density from C-5.[24] Protons 3 and 6 were conveniently assigned by multiplet analysis as their *J*-coupling constants matched those of their respective coupling partners 4 and 5, respectively.

Reductive amination of 8-formylcoumarin-7-ol **5.22** with ferrocenyl amines **3.12a-b** employing the reaction conditions previously presented in **Scheme 5.8**. Both the plain (from amine **3.12a**) and the CH_2NMe_2 substituted (from amine **3.12b**) amination products (**5.23a-b**)

were attained as light brown semi-solids in good yields of 86 and 66%, respectively. The disappearance of the aldehyde peak (CHO, δ 10.58 ppm) and the appearance of the methylene (FcH, δ 4.20 – 4.13 ppm) and methylene protons 8′ and 1′ around δ 4.35 and 3.60 ppm, respectively, in the ^{1}H NMR spectra of product **5.23a-b** validated the successful conjugation of ferrocenyl amines **3.12a-b** and coumarin **5.22**. The coumarin protons resonated similarly to the 8-formylcoumarin-7-ol **2.22** substrate, with the exception of being more upfield (**Figure 5.21**).

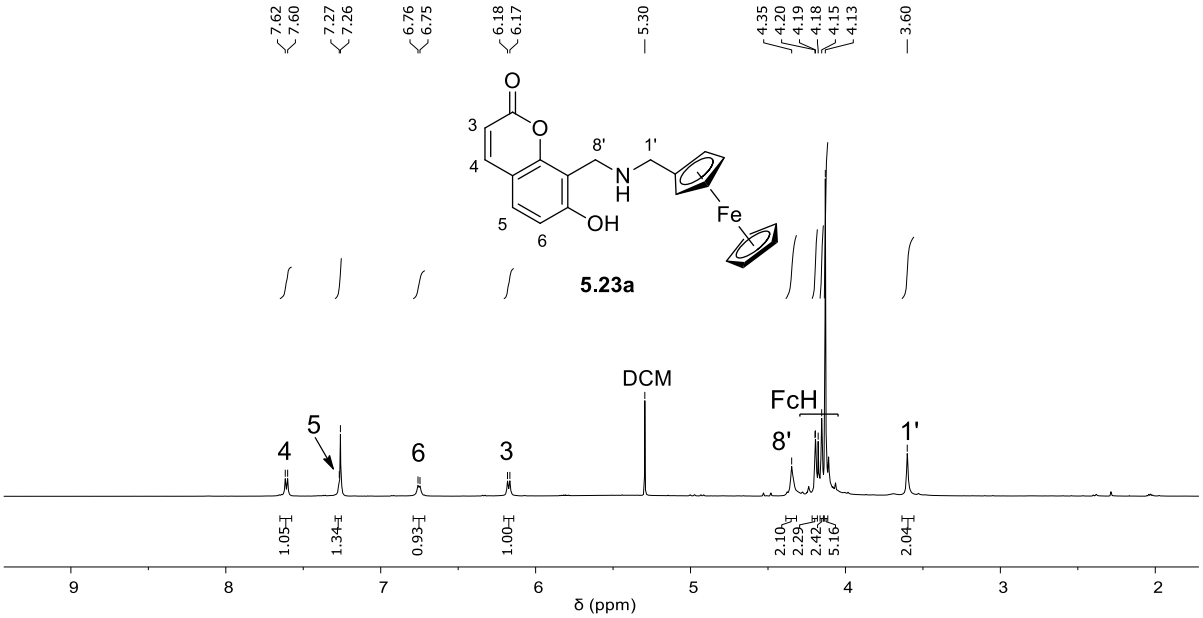

Figure 5.21 ^{1}H NMR spectrum of ferrocenyl 8-aminomethylcoumarin-7-ol **5.23a** in $CDCl_3$.

When subjected to cyclization with paraformaldehyde under conditions similar to the Burke condensation, ferrocenyl 8-aminomethylcoumarin-7-ol **5.23b** was easily transformed into its coumarin-1,3-oxazine variant **5.24** (**Scheme 5.16**). Complete cyclization of the non-cyclic substrate **5.23b** was achieved only after refluxing for 2 hours in $CHCl_3$.

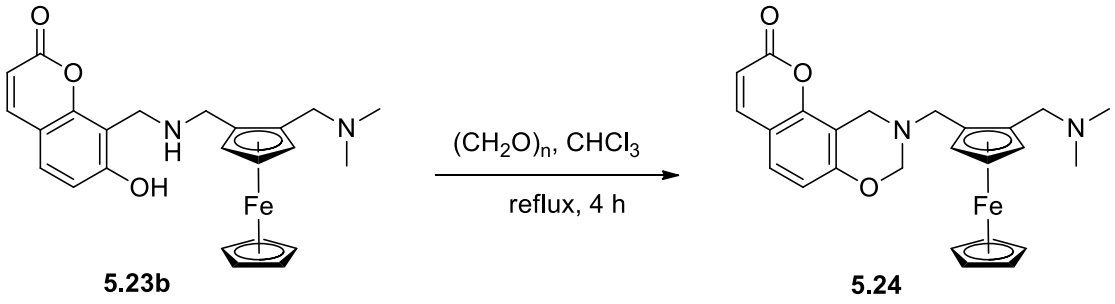

Scheme 5.16 Synthesis of benzene-annulated ferrocenyl coumarin-1,3-oxazine **5.24** by cyclization of 8-aminomethylcoumarin-7-ol **5.23b**.

The product was isolated by silica gel column chromatography in 70 % yield following a workup procedure employed the Burke condensation procedure.[25] It is clear from the demonstrated facile reactivity of the benzene-amended 8-aminomethylcoumarin-7-ol **5.23b** that the phenolic ring is more prone to cyclization with paraformaldehyde ($(CH_2O)_n$) than the pyrone OH group in 3-aminomethylcoumarin-4-ols (**5.14a-e**) (**Scheme 5.14**). Based on these findings, it could be argued that the acidity and, therefore, nucleophilicity of the OH group due to the ring to which it is attached (i.e., benzene or pyrone) on the coumarin nucleus is crucial in the cyclization of the acyclic aminomethyl-hydroxycoumarin substrates (**5.13a-e** and **5.23a-b**) into corresponding 1,3-oxazine products using paraformaldehyde. Thus, failure to synthesize the pyrone-annulated coumarin-1,3-oxazines (**5.10a-e**) by cyclization with $(CH_2O)_n$ via either Burke condensation (**Scheme 5.3**) or the two-step amine-mediated strategy (**Scheme 5.14**) was substantiated.

The chemical structure of the benzene-annulated ferrocenyl coumarin-1,3-oxazine **5.24** was confirmed by the characteristic 3,4-dihydro-2*H*-1,3-oxazine peaks at δ 4.96 and 4.22 – 4.12 ppm as a 2H singlet (H-8) and two 1H multiplets (H-10) overlapping with the ferrocenyl protons (FcH), respectively, in the ^{1}H NMR spectrum of the compound (**Figure 5.22**).[25-26] The methylene protons of the oxazine unit were observed at similar chemical shifts for the

ferrocenyl 3,4-dihydro-2*H*-1,3-benzoxazine derivatives presented in **Chapter 3** (**Schemes 3.7**, **3.10** and **3.16**).

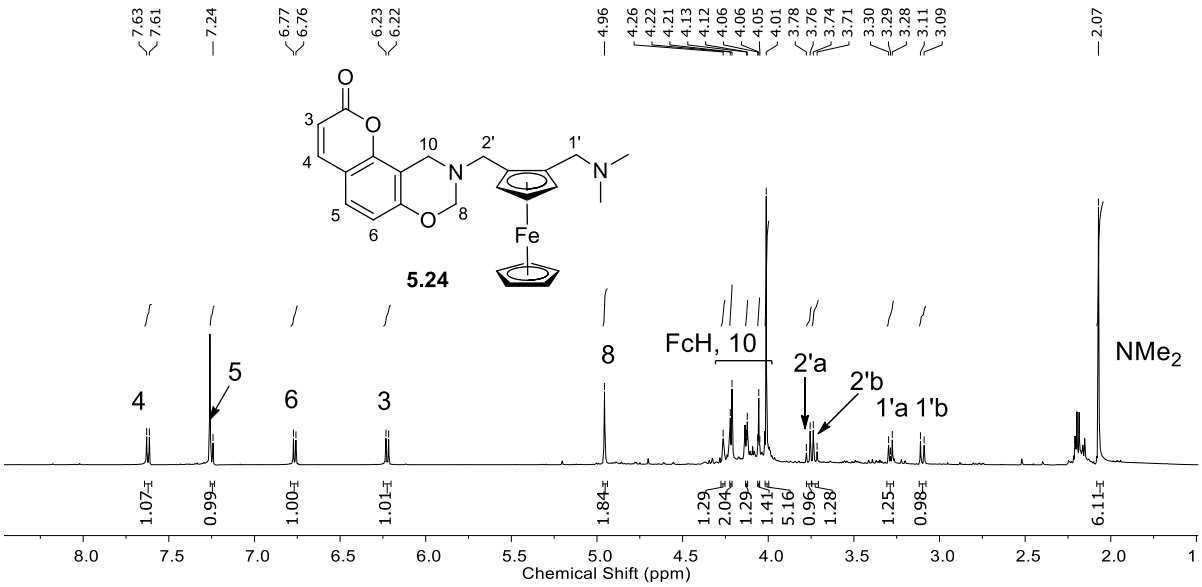

Figure 5.22 ^{1}H NMR spectrum of benzene-annulated ferrocenyl coumarin-1,3-oxazine **5.24** in $CDCl_3$.

Formation of the oxazine unit was further verified by the carbon signals at δ 83.0 and 57.5 ppm in the DEPT-135 NMR spectrum of the coumarin-1,3-oxazine (**Figure 5.23**), which are distinctive to the 1,3-oxazine methylene carbons as was observed for the ferrocenyl 1,3-benzoxazines in **Chapter 3**.[26]

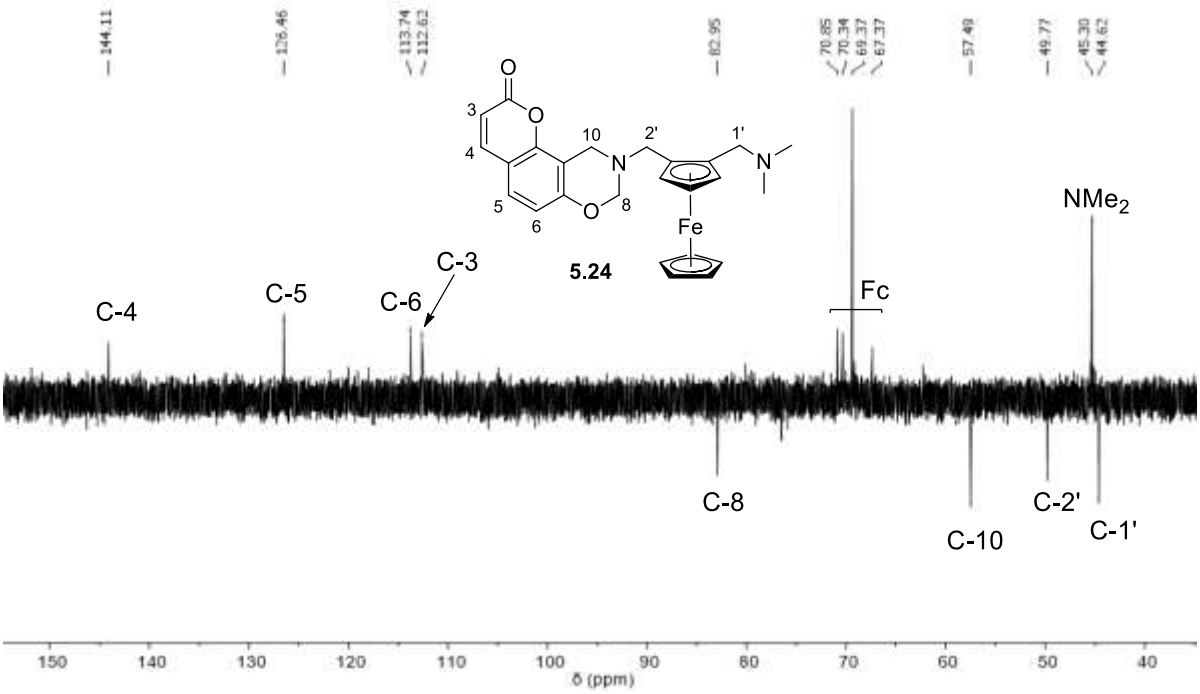

Figure 5.23 DEPT-135 NMR spectrum of benzene-annulated ferrocenyl coumarin-1,3-oxazine **5.24** in $CDCl_3$.

The NMR spectral data of the benzene-annulated derivatives **5.23a-b** and **5.24** was in agreement with the observed HRMS results, thus further corroborating the chemical structures of the compounds (**Table 5.4**).

Table 5.4 HRMS results of ferrocenyl 8-aminomethylcoumarin-7-ol derivatives (**5.23a-b**) and coumarin-1,3-oxazine **5.24**.

Compound	Expected mass $[M+H]^+$	Found $[M+H]^+$
5.23a	390.0793	390.0782
5.23b	447.1371	447.1367
5.24	459.1366	459.1363

In line with the objective of elucidating the overall SAR profile of the ferrocenyl 1,3-benzoxazine derivatives, the prepared acyclic aminomethyl-hydroxycoumarins **5.13a-e** and **5.23a-b** were converted into their cyclic carbamate coumarin-1,3-oxazin-2-one analogues

(**5.25a-e** and **5.26a-b**) bearing the less basic O-CO-linkage in place of the O-CH_2-N moiety as was done for the benzoxazine-2-one derivatives (**4.17a-d** and **4.18a-e**) in the preceding chapter (**Scheme 4.7**). The acyclic aminomethyl-hydroxycoumarins **5.13a-e** and **5.23a-b** were cyclized with CDI employing the reaction conditions as before (**Scheme 5.18**).

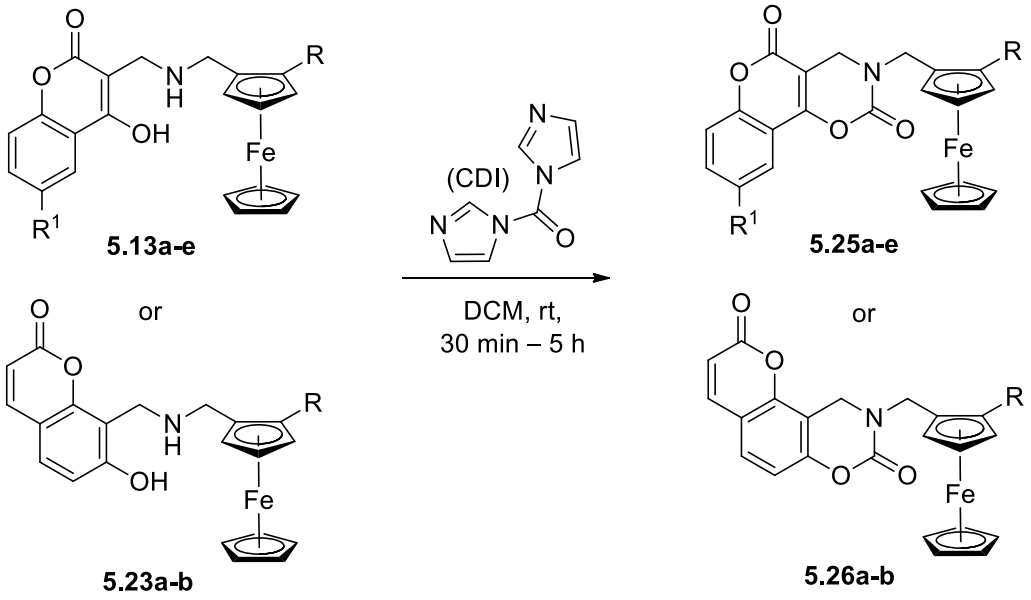

	R^1	Isolated yield (%)
R = H	**5.25a** : H	68
R = CH_2NMe_2	**5.25b** : H	75
	5.25c : 6-Cl	49
	5.25d : 6-Br	0
	5.25e : 6-F	36
R = H	**5.26a** : –	96
R = CH_2NMe_2	**4.26b** : –	90

Scheme 5.18 Synthesis of ferrocenyl coumarin-1,3-oxazin-2-one analogues **5.25a-e** and **5.26a-b**.

Except for 6-bromo-3-aminomethylcoumarin-4-ol **5.23d**, all the non-cyclic aminomethylcoumarinol substrates (**5.23a-c**,**e** and **5.23a-b**) were readily cyclized into their coumarin-1,3-oxazin-2-one analogues **5.25a-e** and **5.26a-b** in yields ranging between 36 and 96% (**Scheme 5.18**). The benzene-annulated 8-aminomethylcoumarin-7-ol substrates **5.23a-b** were completely converted to their corresponding products (**5.26a-b**) within 30 minutes of the

reaction (TLC) in excellent yields. On the other hand, the pyrone-conjugated counterparts (**5.23a-c**,**e**) required 5 hours of stirring to access the desired oxazine compounds (yields: 36 – 75%). The 6-bromo-3-aminomethylcoumarin-4-ol **5.23d** failed to cyclize under the conditions used. Collectively, these observations further underscore the difference in the reactivity of the OH groups as a result of the different ring units to which they are appended, i.e., phenolic OH > pyrone OH.

For both pyrone- and benzene-annulated coumarin-1,3-oxazines **5.25a-c**,**e** and **5.26a-b**, the incorporation of the O-CO-N carbamate unit was confirmed by the appearance of the carbamate carbonyl group between δ 149.0 and 148.0 ppm in the ^{13}C NMR spectra of the products as illustrated in **Figure 5.24**. This group was also observed in this region for the ferrocenyl 1,3-benzoxazin-2-one derivatives (**4.17a-d** and **4.18a-e**) in **Chapter 4** (**Figure 4.9**).

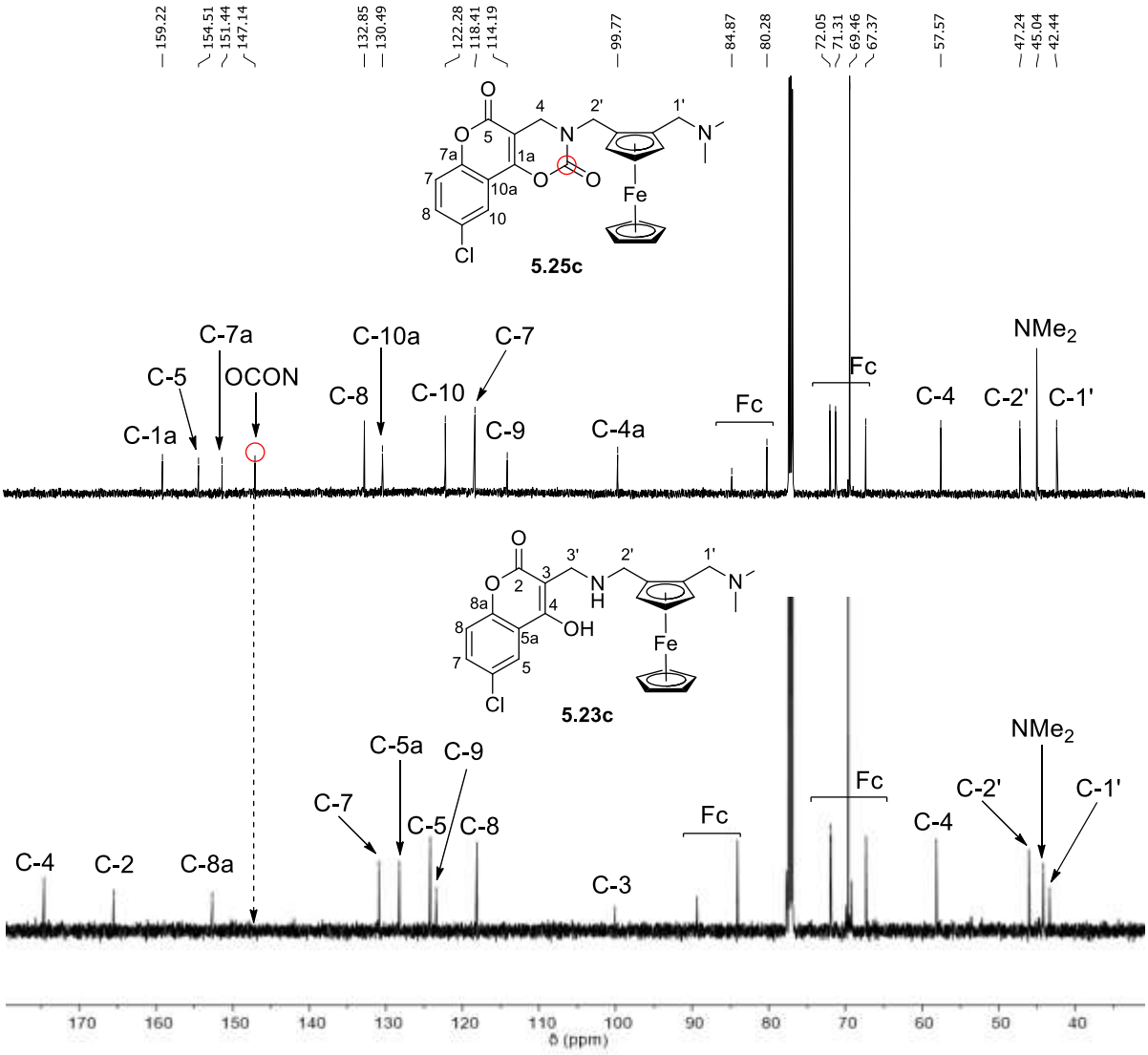

Figure 5.24 ^{13}C NMR spectrum of ferrocenyl coumarin-1,3-oxazin-2-one **5.25c** and its non-cyclic substrate **5.23c** in $CDCl_3$.

The ^{13}C NMR spectral data together with 2D HMBC were invaluable to verify the presence of the O-CO-N carbamate unit. The ^{1}H – ^{13}C correlation of protons 4 and 2′ with the carbonyl carbon of the O-CO-N unit at cross-peaks [4.99,147.3] (correlation *b*), [4.60,147.3] (correlation *b*), [4.50,147.3] (correlation *a*) and [4.32,147.3] ppm (correlation *a*) (**Figure 5.25**).

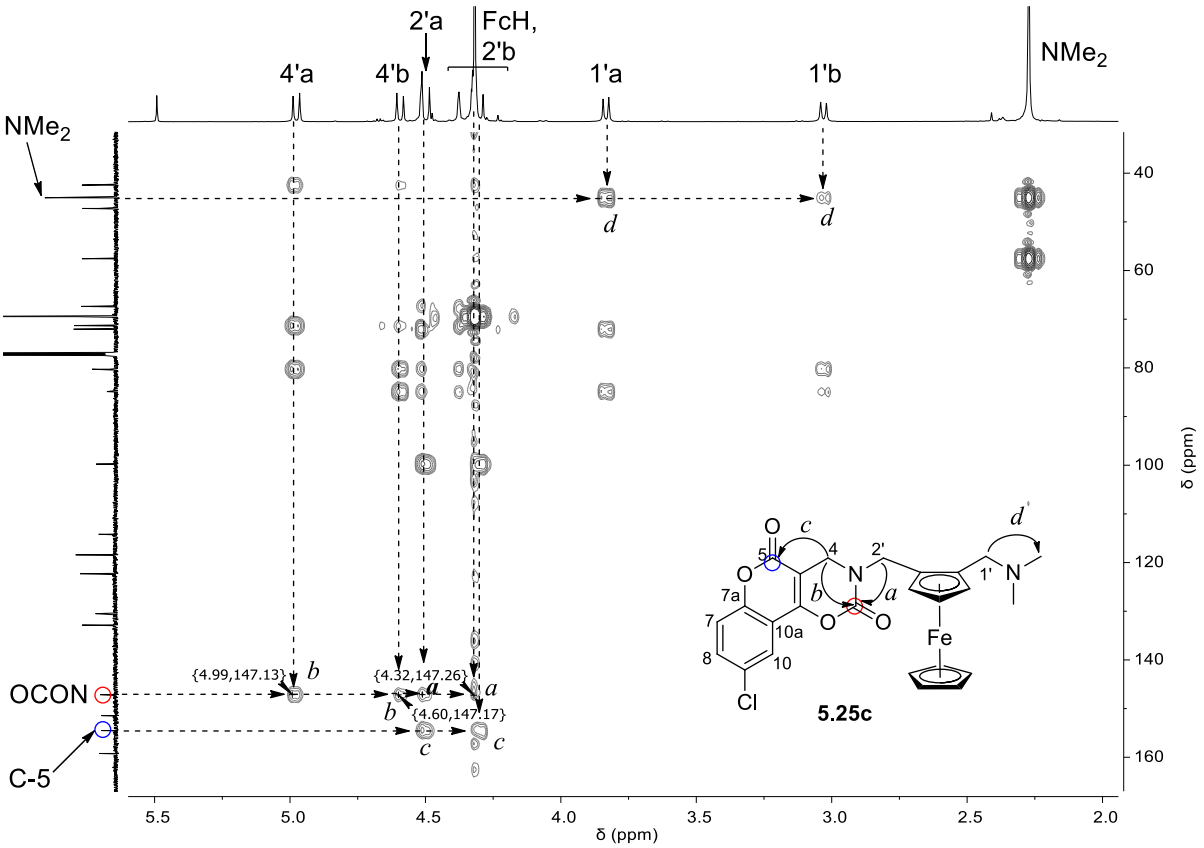

Figure 5.25 HMBC NMR spectrum of ferrocenyl coumarin-1,3-oxazin-2-one **5.25c** in $CDCl_3$ showing the aliphatic ^1H NMR region.

The NMR spectral data was complemented by the HRMS data. For all the synthesized compounds, the expected masses were in agreement with experimentally determined values The base peaks of the coumarin-1,3-oxazine products were observed as decarboxylated sodium chloride (NaCl) ions $[M - CO + NaCl + H_3]^+$ of the molecular masses [M] of the compounds (**Table 5.5**).

Table 5.5 HRMS results of ferrocenyl coumarin-1,3-oxazin-2-one derivatives (**5.25a-e** and **5.26a-b**).

Compound	Expected mass [M–CO+NaCl+H$_3$]	Found [M–CO+NaCl+H$_3$]$^+$
5.25a	416.0486[a]	416.0586[a]
5.25b	505.0952	505.1424
5.25c	539.1057	539.1057
5.25e	523.1338	523.1338
5.26a	390.0787[b]	390.0781[b]
5.26b	473.1164[a]	473.1159[a]

[a]Masses were obtained as $[M+H]^+$ ions. [b]Mass was obtained as $[M–CO+H_3]^+$ ion.

5.2. Biological evaluation results

The synthesized analogues with expanded ring units, i.e., naphthoxazines (**5.2a-b**), sesamyl-1,3-oxazine (**5.4**), aminomethylcoumarinols (**5.13a-e** and **5.23a-b**) and coumarin-1,3-oxazin-2-ones (**5.24**, **5.25a-c**,**e** and **5.26a-b**), were evaluated for potential antimalarial, antitrypanosomal and anticancer activity against 3D7 *P. falciparum* and 427 *T. b. brucei* strains and HCC70 triple-negative breast cancer cell line.

5.2.1. *In vitro* antiplasmodial activity

The conditions for the antiplasmodial biochemical screening assay with the 3D7 *P. falciparum* strains were the same as the preceding chapters and the activity was reported as mean IC_{50} values from experiments conducted in duplicate. In all cases, the standard deviation of the mean IC_{50} values was below 0.3, i.e., ± SD. The activities of the compounds are reported in **Table 5.6**. Generally, the ring-annulated derivatives were less active compared to the benzoxazines and their non-cyclic analogues in **Chapter 3** and **4**.

Table 5.5 *In vitro* antiplasmodial activity of ferrocenyl coumarin-1,3-oxazin-2-one derivatives (**5.25a-e** and **5.26a-b**) against the 3D7 *P. falciparum* strain.

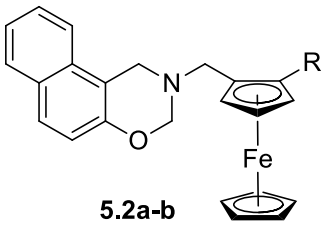

5.2a-b

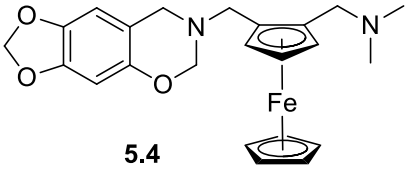

5.4

Compound	**R**	**IC_{50} (µM)**
		3D7
5.2a	–	3.49 (0.105[a])
5.2b	CH_2NMe_2	4.12 (0.178[a])
5.4	CH_2NMe_2	4.78

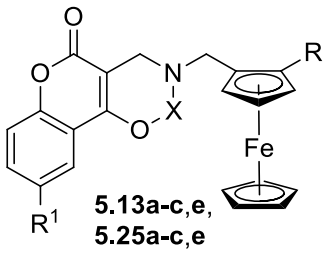

5.13a-c,e, 5.25a-c,e

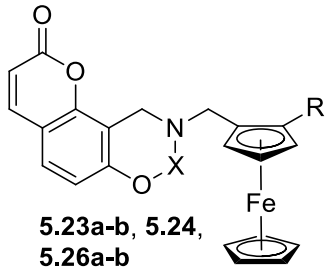

5.23a-b, 5.24, 5.26a-b

	X	**R**	**R^1**	
5.13a	H, H	H	H	[b]na
5.13b	H, H	CH_2NMe_2	H	[b]na
5.13c	H, H	CH_2NMe_2	Cl	5.7
5.13e	H, H	CH_2NMe_2	F	8.76
5.23a	H, H	H	–	9.1
5.23b	H, H	CH_2NMe_2	–	1.7
5.24	CH_2	CH_2NMe_2	–	1.0
5.25a	CO	H	H	[b]na
5.25b	CO	CH_2NMe_2	H	[b]na
5.25c	CO	CH_2NMe_2	Cl	[b]na
5.25e	CO	CH_2NMe_2	F	12.6
5.26a	CO	H	–	[b]na
5.26b	CO	CH_2NMe_2	–	7.3
Chloroquine	–	–	–	0.03

[a]Activity of the compound against the Dd2 strain. [b]na = not active.

Both the naphthoxazine (**5.2a-b**) and sesamyl-1,3-oxazine (**5.4**) compounds exhibited comparable activities (IC_{50} = 3.46 – 4.78 μM) that were lower than their benzoxazine counterparts **3.13a** (IC_{50} = 1.7 μM) and **3.16a** (IC_{50} = 1.09 1.7 μM) by approximately 4-fold (**Tables 3.2** and **5.5**). However, the naphthoxazines **5.2a-b**, which were also screened against the chloroquine-resistant Dd2 *P. falciparum* strain, were more active (**5.2a**, IC_{50} = 0.105 μM; **5.2b**, IC_{50} = 0.178 μM) (**Table 5.5**) than their benzoxazine partners **3.13a** (IC_{50} > 10 μM) and **3.16a** (IC_{50} = 2.23 μM) against this strain (**Tables 3.2**). This suggested that benzene ring annulation with naphthalene may be favourable for antiplasmodial activity against the resistant strain.

Within the acyclic ferrocenyl aminomethylcoumarinol derivatives (**5.13a-c**,**e** and **5.23a-b**), the phenolic analogues **5.23a-b** were active against the 3D7 strain, while their pyrone-substituted partners (**5.13a-b**) were not toxic towards the parasite (**Table 5.5**). This suggests that the phenolic OH group not only plays an important role in reactivity but is also essential for the pharmacological properties of the ferrocenyl aminomethylcoumarinol compounds investigated. Only the halogenated (6-Cl and 6-F) compounds were active within the 3-aminomethylcoumarin-4-ol series, further highlighting the beneficial effects of lipophilic EWGs for antiplasmodial activity as previously observed for 1,3-benzoxazines in **Chapter 3**. Notwithstanding, all the acyclic aminomethylcoumarinols were less potent than the α-amino-*o*-cresols in **Table 4.3**, except for the phenolic derivative **5.23b** (**Table 5.5**).

For the cyclic coumarin-1,3-oxazines (**5.24**, **5.25a-c**,**e** and **5.26a-b**), the benzene-annulated congener bearing the O-CH_2-N linkage exerted similar activity (IC_{50} = 1.0 μM) to its parental 1,3-benzoxazine compound (**3.16a**, IC_{50} = 1.09 μM) (**Tables 4.3** and **5.5**). On the other hand, replacement of this linkage with a carbamate O-CO-N unit was detrimental for activity as the majority of the compounds were not active against the *P. falciparum* parasite, excluding **5.25e** and **5.26b** (**Table 5.5**). Within the carbamate O-CO-N series, substitution of the benzene ring

with the coumarin nucleus was similarly unfavourable for activity since the coumarin-1,3-oxazin-2-one analogues (**5.25a-c**,**e** and **5.26a-b**) were generally non-toxic compared to the benzoxazine-2-one partners from **Chapter 3** (**Table 4.3**). The phenolic unit (**5.26b**, IC_{50} = 7.3 μM) still appeared to be better tolerated for antiplasmodial activity *vis-à-vis* its pyrone partner (**5.23b**, IC_{50} = na) (**Table 5.5**), further illustrating the pharmacophoric importance of this structural feature.

5.2.2. *In vitro* antitrypanosomal activity

Only the halogenated (**5.23c** and **5.23e**) and one benzene-annulated (**5.26b**) acyclic ferrocenyl aminomethylcoumarinol derivatives inhibited the growth of the *T. b. brucei* trypomastigotes in the coumarin series. The IC_{50} values of these compounds were: 5.00 (**5.23c**), 19.6 (**5.23e**) and 9.4 μM (**5.26b**). The phenolic coumarin-1,3-oxaizne (**5.24**) endowed with O-CH_2-N unit had not yet been tested for antitrypanosomal active at the time of writing the thesis. All the cyclic coumarin-1,3-oxazin-2-one hybrids (**5.25a-c**,**e** and **5.26a-b**) were not active. Again, the loss of activity upon incorporation of the carbamate unit could possibly be a result of the decrease in basicity of the nitrogen atom as previously observed (**Chapter 3**). Overall, the antitrypanosomal activity of the acyclic ferrocenyl aminomethylcoumarinols (**5.23c**, **5.23e** and **5.26b**) was less potent than that of the α-amino-*o*-cresols (**4.6c**,**f-h**). As before, it appears that replacing the benzene ring with a coumarin unit is not undesirable for the biological activity of the compounds. On the contrary, the naphthoxazine **5.2b** bearing the ferrocenyl CH_2NMe_2 chain was more potent (IC_{50} = 0.87 μM) than its 1,3-benzoxazine partner **3.16a** (IC_{50} = 1.2 μM) (**Table 3**). Thus, annulation with a naphthalene ring may be beneficial for trypanocidal effects of the compounds. The sesamyl-1,3-oxazine had not been assessed for trypanocidal activity at the time of compiling the thesis.

5.2.3. *In vitro* anticancer activity

Of all the ring-annulated derivatives presented in this chapter, only the plain ferrocenyl naphthoxazine **5.2a** inhibited the growth of the HCC70 cell line at the tested concentration range with an IC_{50} value of 14.1 μM. The rest of the compounds were not toxic to the cancer cells. The loss of activity upon expansion of the benzene ring by fusion with pyrone (for coumarin), dioxole (for sesamol) and phenyl (for naphthalene) ring units suggests that this structural modification is not compatible for anticancer activity of the ferrocenyl 1,3-benzoxazine scaffold.

5.2.4. Analysis of structure-activity relationships (SARs)

By studying the pharmacological influence of modifying the ferrocene and oxazine units of the investigated ferrocenyl 1,3-benzoxazine scaffold in **Chapters 3** and **4**, respectively, a refined SAR model was delineated (**Figure 4.16**). In the current chapter, the benzene ring of the explored scaffold has been annulated by fusion with phenyl, dioxole and pyrone to produce representative members of a novel class of ferrocenyl naphthoxazine (**5.2a-b**), sesamyl-1,3-oxazine (**5.4**), aminomethylcoumarinol (**5.13a-e**, **5.23a-b**) and coumarin-1,3-oxazine (**5.24**, **5.25a-c**,**e**, **5.26a-b**) compounds. Assessment of these compounds for biological activity generally revealed that benzene ring-annulation of the parental ferrocenyl 1,3-benzoxazine scaffold with these structural units is undesirable for biological activity. Regardless, the removal of the O-CH_2-N oxazine linkage was more tolerated for activity than its replacement with the O-CO-N carbamate unit as previously observed. Moreover, ferrocenyl naphthoxazines (**5.13a-b**) were the most potent in these modifications, followed by sesamyl-1,3-oxazine (**5.4**), aminomethylcoumarinols (**5.13a-e**, **5.23a-b**) and coumarin-1,3-oxazin-2-ones (**5.25a-c**,**e**, **5.26a-b**) for antimalarial activity. The ferrocenyl aminomethylcoumarinols (**5.13a-e**, **5.23a-b**) were the only modification that was tolerated for antitrypanosomal activity. However, all these

modifications did not improve the biological activity of the parental ferrocenyl 1,3-benzoxazine scaffold. Thus, the previous SAR model was further refined as below.

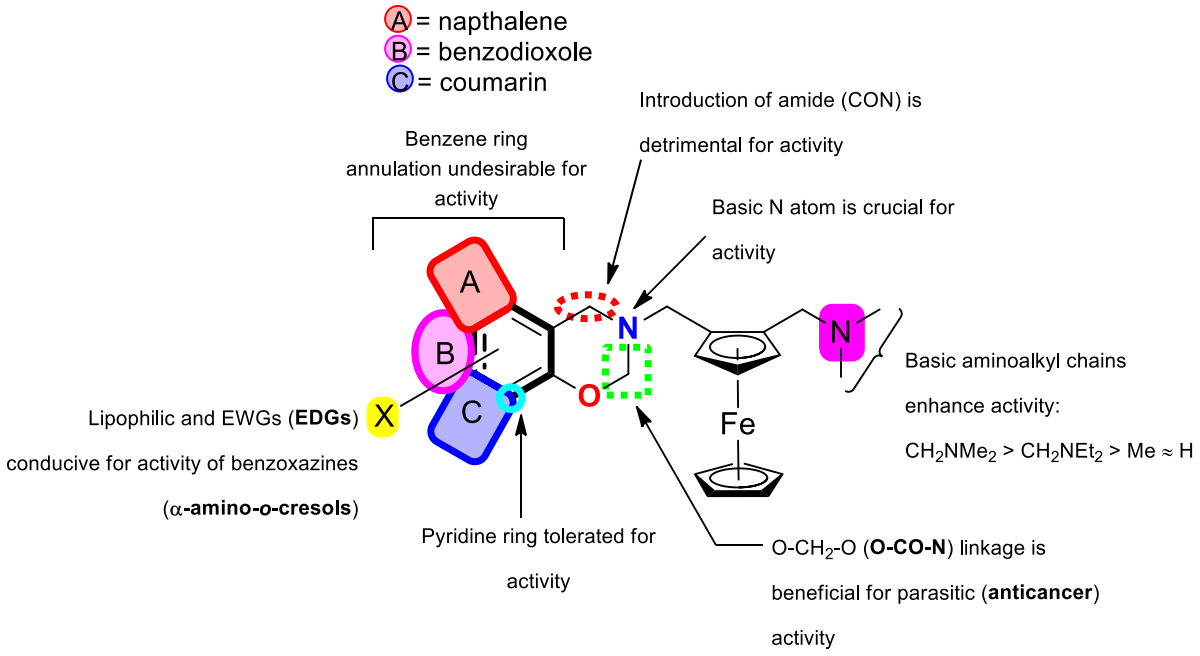

Figure 5.26 Updated SAR model incorporating benzene ring annulation.

5.2.5. Overall summary and conclusions

In order to further delineate the influence of benzene structural features of the pursued ferrocenyl 1,3-benzoxazine scaffold on the biological activity, compounds bearing expanded ring units, i.e., naphthalene, benzodioxole and coumarin, culminating in a novel class of ferrocenyl compounds were designed, synthesized and characterized by spectral techniques. Representative members of ferrocenyl naphthoxazines (**5.2a-b**) and sesamyl-1,3-oxazine (**5.4**) based on the 1,3-benzoxazine scaffold were prepared using the Burke protocol and obtained in modest to good yields. On the other hand, the acyclic ferrocenyl aminomethylcoumarinols (**5.13a-e**, **5.23a-b**) and their coumarin-1,3-oxazines (**5.24**, **5.25a-c**,**e**, **5.26a-b**) were accessed via reductive amination of formylated hydroxycoumarins employing the two-step strategy after the Burke condensation failed to furnish the desired compounds. The influence of the coumarin

subring units, i.e., benzene and pyrone, on the reactivity of the OH and NH_2 groups of the ferrocenyl aminomethylcoumarinols (**5.13a-e**, **5.23a-b**) for cyclization with $(CH_2O)_n$ into the desired coumarin-1,3-oxazine hybrid product was investigated. It was found that OH and NH_2 groups are more prone to cyclization if appended to the benzene subring of the coumarin nucleus than when contained on the pyrone unit. A ferrocenyl coumarin-1,3-oxazine (**5.24**) endowed with the O-CH_2-N linkage as the parental benzoxazine compounds was synthesized from its phenolic 8-aminomethylcoumarin-7-ol substrate (**5.26b**), while the coumarin-1,3-oxazin-2-ones (**5.25a-c**,**e**, **5.26a-b**) were formed by cyclization with CDI.

The biological screening results revealed that these modifications are not conducive for biological activity based on the inferior efficacies of these compounds relative to their ferrocenyl 1,3-benzoxazine counterparts. Consequently, the SAR model was revised to incorporate the pharmacological effects of expanding the benzene unit of the ferrocenyl 1,3-benzoxazine scaffold investigated in this study. The results of these modifications are summarized in the revised SAR analysis model in **Figure 5.26**.

References

(1) (a) Huang, M. H.; Wu, S. N.; Wang, J. P.; Lin, C. H.; Lu, S. I.; Liao, L. F.; Shen, A. Y. *Drug Dev. Res.* **2003**, *60*, 261; (b) Rokade, Y.; Sayyed, R. *Rasayan J. Chem* **2009**, *2*, 972; (c) Hassan, R. M.; Abd-Allah, W. H.; Salman, A. M.; El-Azzouny, A. A.-S.; Aboul-Enein, M. N. *Eur. J. Pharm. Sci.* **2019**, *139*, 105045; (d) Kaur, M.; Kohli, S.; Sandhu, S.; Bansal, Y.; Bansal, G. *Anticancer Agents Med. Chem.* **2015**, *15*, 1032; (e) Medina, F. G.; Marrero, J. G.; Macías-Alonso, M.; González, M. C.; Córdova-Guerrero, I.; García, A. G. T.; Osegueda-Robles, S. *Nat. Prod. Rep.* **2015**, *32*, 1472.

(2) (a) Urbański, T.; Radzikowski, C.; Ledochowski, Z.; Czarnocki, W. *Nature* **1956**, *178*, 1351; (b) Duffin, W.; Rollo, I. *Br. J. Pharmacol.* **1957**, *12*, 171; (c) Bajwa, G. S.; Hartman, K. E.; Joullie, M. M. *J. Med. Chem.* **1973**, *16*, 134; (d) Mathew, B. P.; Kumar, A.; Sharma, S.; Shukla, P.; Nath, M. *Eur. J. Med. Chem.* **2010**, *45*, 1502.

(3) Blackie, M. A. Doctoral Thesis, University of Cape Town, 2002.

(4) Khanna, G.; Saluja, P.; Khurana, J. M. *Aust. J. Chem.* **2017**, *70*, 1285.

(5) (a) Nofal, Z.; El-Zahar, M.; Abd El-Karim, S. *Molecules* **2000**, *5*, 99; (b) Zhang, M.-Z.; Zhang, R.-R.; Yin, W.-Z.; Yu, X.; Zhang, Y.-L.; Liu, P.; Gu, Y.-C.; Zhang, W.-H. *Mol. Divers.* **2016**, *20*, 611; (c) Nagamallu, R.; Gurunanjappa, P.; Kariyappa, A. K. *Pharm. Chem. J.* **2017**, *51*, 582; (d) Mathew, B. P.; Aggarwal, N.; Kumar, R.; Nath, M. *J. Sulfur Chem.* **2014**, *35*, 31.

(6) Mondal, A.; Rana, S.; Mukhopadhyay, C. *Tetrahedron Lett.* **2014**, *55*, 3498.

(7) (a) Mbaba, M.; Mabhula, A. N.; Boel, N.; Edkins, A. L.; Isaacs, M.; Hoppe, H. C.; Khanye, S. D. *J. Inorg. Biochem.* **2017**, *172*, 88; (b) Mbaba, M.; de la Mare, J.-A.; Sterrenberg, J. N.; Kajewole, D.; Maharaj, S.; Edkins, A. L.; Isaacs, M.; Hoppe, H. C.; Khanye, S. D. *J. Biol. Inorg. Chem.* **2019**, *24*, 139.

(8) (a) Jung, J.-C.; Park, O.-S. *Molecules* **2009**, *14*, 4790; (b) Bairagi, S. H.; Salaskar, P. P.; Loke, S. D.; Surve, N. N.; Tandel, D. V.; Dusara, M. D. *Int. J. Chem.* **2012**, *4*, 16; (c) Abdou, M. M.; El-Saeed, R. A.; Bondock, S. *Arab. J. Chem.* **2019**, *12*, 88.

(9) (a) Taylor, R. *Electrophilic aromatic substitution*; John Wiley & Sons: Hoboken, New Jersey, 1990; (b) McMurry, J. *Organic Chemistry. A biological approach*; Thomson Higher Education: Belmont, CA, United Sates, 2007.

(10) Traven, V. F.; Negrebetsky, V. V.; Vorobjeva, L. I.; Carberry, E. A. *Can. J. Chem.* **1997**, *75*, 377.

(11) Lohar, T.; Mane, A.; Kamat, S.; Salunkhe, R. *Polycyclic Aromat. Compd.* **2018**, 1.

(12) (a) Andreu, R.; Ronda, J. *Synth. Commun.* **2008**, *38*, 2316; (b) Kiskan, B.; Yagci, Y. In *Thermosets*; Elsevier, 2018.

(13) Milevskii, B.; Chibisova, T.; Solov'eva, N.; Anisimova, O.; Lebedev, V.; Ivanov, I.; Traven, V. *Chem. Heterocycl. Compd.* **2013**, *48*, 1781.

(14) Ollinger, P.; Wolfbeis, O. S.; Junek, H. *Monatsh. Chem.* **1975**, *106*, 963.

(15) Abdel-Magid, A. F.; Carson, K. G.; Harris, B. D.; Maryanoff, C. A.; Shah, R. D. *J. Org. Chem.* **1996**, *61*, 3849.

(16) (a) Shah, V.; Bose, J.; Shah, R. *J. Org. Chem.* **1960**, *25*, 677; (b) Park, S.-J.; Lee, J.-C.; Lee, K.-I. *Bull. Korean Chem. Soc.* **2007**, *28*, 1203; (c) Jung, J.-C.; Jung, Y.-J.; Park, O.-S. *Synth. Commun.* **2001**, *31*, 1195.

(17) Li, J.-S.; Fu, D.-M.; Xue, Y.; Li, Z.-W.; Li, D.-L.; Da, Y.-D.; Yang, F.; Zhang, L.; Lu, C.-H.; Li, G. *Tetrahedron* **2015**, *71*, 2748.

(18) Jeon, M.-K.; Kim, K. *Tetrahedron* **1999**, *55*, 9651.

(19) Nolan, K. A.; Doncaster, J. R.; Dunstan, M. S.; Scott, K. A.; Frenkel, A. D.; Siegel, D.; Ross, D.; Barnes, J.; Levy, C.; Leys, D. *J. Med. Chem.* **2009**, *52*, 7142.

(20) Rad-Moghadam, K.; Mohseni, M. *Monatsh. Chem.* **2004**, *135*, 817.

(21) McMurry, J. *Organic Chemistry. A biological approach*; Thomson Higher Education: Belmont, CA, United Sates, 2007.

(22) (a) Naik, R.; Thakor, V. *J. Org. Chem.* **1957**, *22*, 1626; (b) Al-Kawkabani, A.; Boutemeur-Kheddis, B.; Makhloufi-Chebli, M.; Hamdi, M.; Talhi, O.; Silva, A. M. *Tetrahedron Lett.* **2013**, *54*, 5111.

(23) Rahimi, S.; Khoee, S.; Ghandi, M. *Carbohydr. Polym.* **2018**, *201*, 236.

(24) Ivanov, I.; Panov, A.; Safronova, O.; Chibisova, T. *Russ. Chem. Bull.* **2008**, *57*, 1989.

(25) Burke, W. *J. Am. Chem. Soc.* **1949**, *71*, 609.

(26) Li, W.; Wei, T.; Gao, Y.; Xi, K.; Jia, X. *Polymer* **2012**, *53*, 1236.

Chapter 6: Synthesis and evaluation of ethyl carbamate and ethyl-spaced benzoxazine derivatives

Up to this point, the explored ferrocenyl 1,3-benzoxazine scaffold has been modified on the ferrocene unit, the oxazine unit and the benzene ring. Derivatives resulting from these modifications were evaluated for biological activity and SAR analysis of the scaffold owing to these modifications was performed to elucidate the influence of structural features of the scaffold. Herein, modifications of the methylene spacer linking the ferrocene and the benzoxazine units are presented. Lastly, exploratory studies towards the synthesis of the *N,N*-bis(2-hydroxybenzyl)ferrocenemethylamine derivatives, which formed as side products during the synthesis of the ferrocenyl 1,3-benzoaxazines carrying the basic CH_2NMe_2 side chain in **Chapter 3**, were undertaken.

6.1. Rationale: Modification of the benzoxazine-ferrocene spacer

One of the approached in the molecular hybridization strategy involves the use of a chemical motif that joins the chemical scaffolds being amalgamated to produce the desired hybrid compounds.[1] The nature of the linker influences the pharmacological properties of the resulting hybrid molecules.[1] For instance, increasing the alkyl linker between the 4-aminoquinoline and the ferrocene unit led to a reduction in antiplasmodial efficacies of ferroquine-type hybrid compounds assembled by Blackie et al. (**Figure 6.1**).[2]

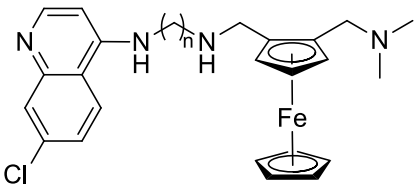

6.1a-d

	D10 IC_{50} (μM)
6.1a : n = 1	41.70
6.1b : n = 2	51.37
6.1c : n = 3	61.16
6.1d : n = 4	86.92

Decreasing activity

Figure 6.1 Influence of the linker in antiplasmodial activity of quinoline-ferrocene hybrid compounds.

In our case, the ferrocenyl methylene linker was modified by joining to a hydrolysable ethyl carbamate and ethylamine chains to produce representative ferrocenyl 1,3-benzoxazine derivatives containing these units. These modifications are summarized in **Figure 6.2**.

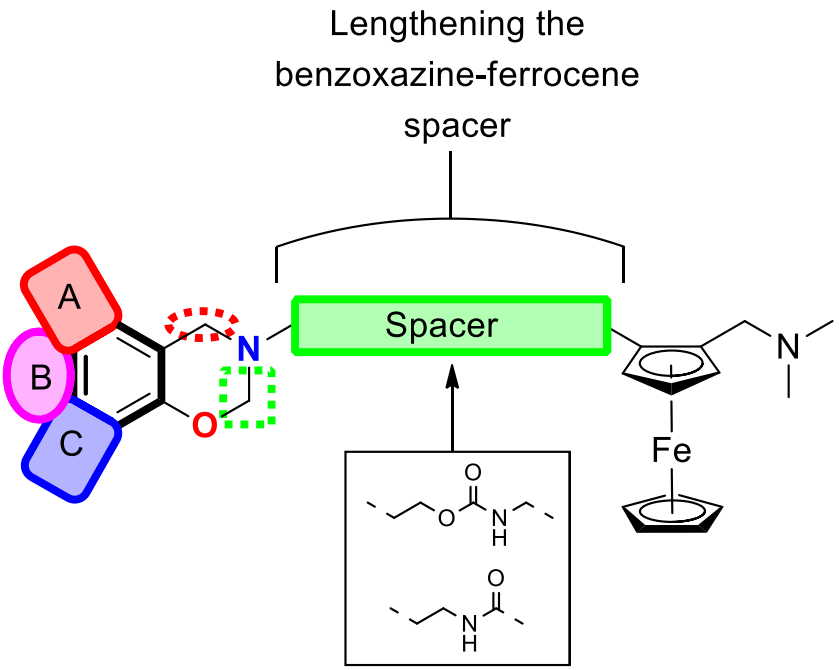

Figure 6.2 Modification of the benzoxazine-ferrocene spacer.

6.2. Synthesis and characterization of target compounds

In order to incorporate the ethyl carbamate linker between the benzoxazine and ferrocene units, 1,3-benzoxazine substrates carrying an ethanol moiety in position 3 were synthesized from phenols **3.1a**, **3.1d-e** and ethanolamine (**6.2**) using the Burke condensation (**Scheme 6.1**).[3]

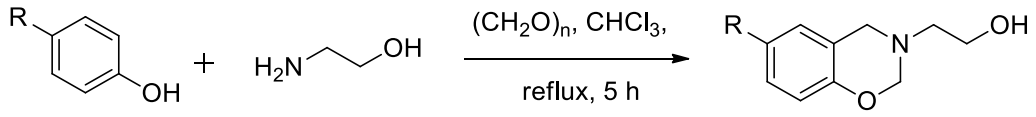

3.1a, **3.1d-e** **6.2** **6.3a-c**

	Yield (%)
6.3a : R = H	89
6.3b : R = Br	62
6.3c : R = OMe	98

Scheme 6.1 Synthesis of 1,3-benzoxazine 3-ethanols **6.2a-c**.

Unlike the reaction with the ferrocenyl amine **3.12b**, the complete conversion of phenols **3.1a** and **3.1d-e** with ethanolamine **6.2** was achieved within 5 hours of the reaction time (TLC) in 62 – 98% with no need for purification with silica gel column chromatography. The workup of the reaction was performed by extracting the formed benzoxazine products into the aqueous phase with 2N citric acid solution after which it was washed with diethyl ether. The products were isolated by basification with 1N NaOH solution and extracted with DCM, dried (Na_2SO_4) and attained as colourless viscous oils with sufficient purity to move to the next step. The structures of the formed 1,3-benzoxazine 3-ethanols were confirmed by the appearance of the characteristic 1,3-benzoxazine peaks around δ 4.88 and 4.02 ppm and the ethanol methylene proton as two 2H triplets at 3.69 and 2.96 ppm in the ^{1}H NMR spectra of the compounds (**Figure 6.3**).

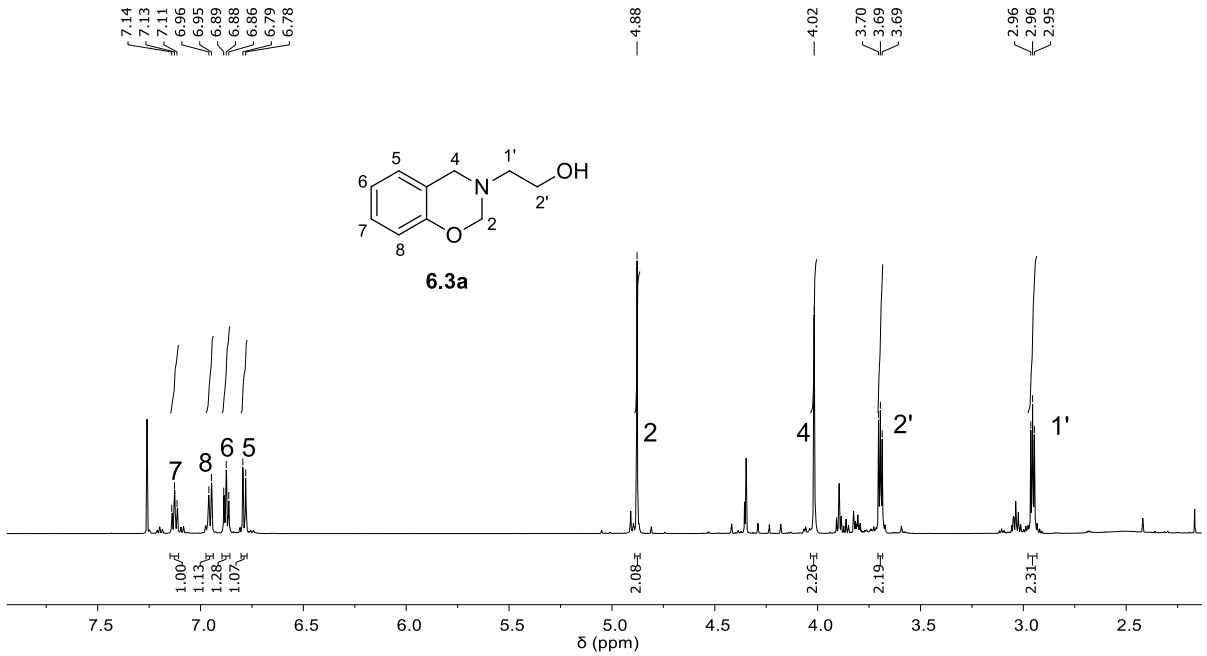

Figure 6.3 ^{1}H NMR spectrum of 1,3-benzoxazine 3-ethanol **6.3a** in $CDCl_3$.

Following the preparation of suitable benzoxazine 3-ethanols **6.3a-c**, ferrocenyl amine **3.12b** was conjugated to these substrates via a carbamate unit (O-CO-N) to produce target ferrocene ethyl carbamate benzoxazines **6.4a-c** (**Scheme 6.2**).[4] This was achieved by employing the CDI carbamate formation procedure used in the cyclization of ferrocenyl salicylamines (**4.17a-d** and **4.18a-e**) and salicylamide **4.16a** in **Chapter 4** into their corresponding benzoxazine products.[4]

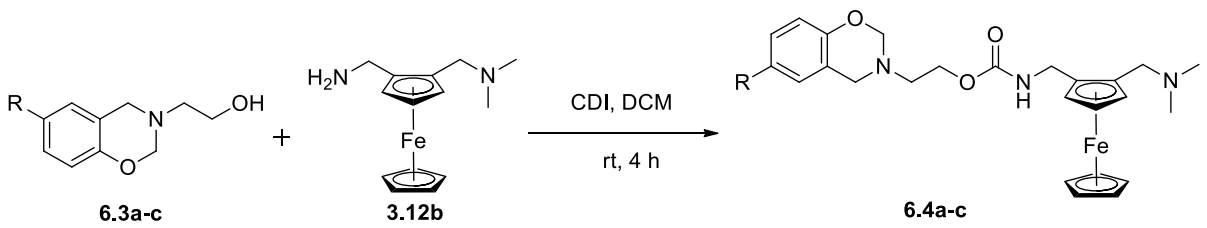

	Yield (%)
6.4a : R = H	76
6.4b : R = Br	80
6.4c : R = OMe	70

Scheme 6.2 Synthesis of target ferrocene ethyl carbamate benzoxazines **6.4a-c**.

The progress of the reaction was monitored by TLC. After completion of the reaction (TLC), the reaction mixture was successively washed with 1N HCl solution and water, dried over Na_2SO_4 and solvent removed under reduced pressure to afford the crude products.[4] Purification of the compounds by silica gel column chromatography led to degradation of the formed products into their constituent benzoxazine 3-ethanol starting materials **6.3a-c**. This challenge was overcome by subjecting the crude compound to column chromatography using basic alumina as the stationary phase and gradient elution with DCM and MeOH/DCM mixture. The pure compounds were obtained as brown semi-solids. Characterization of the achieved ferrocene ethyl carbamate benzoxazines was performed as described for compound **6.4c**.

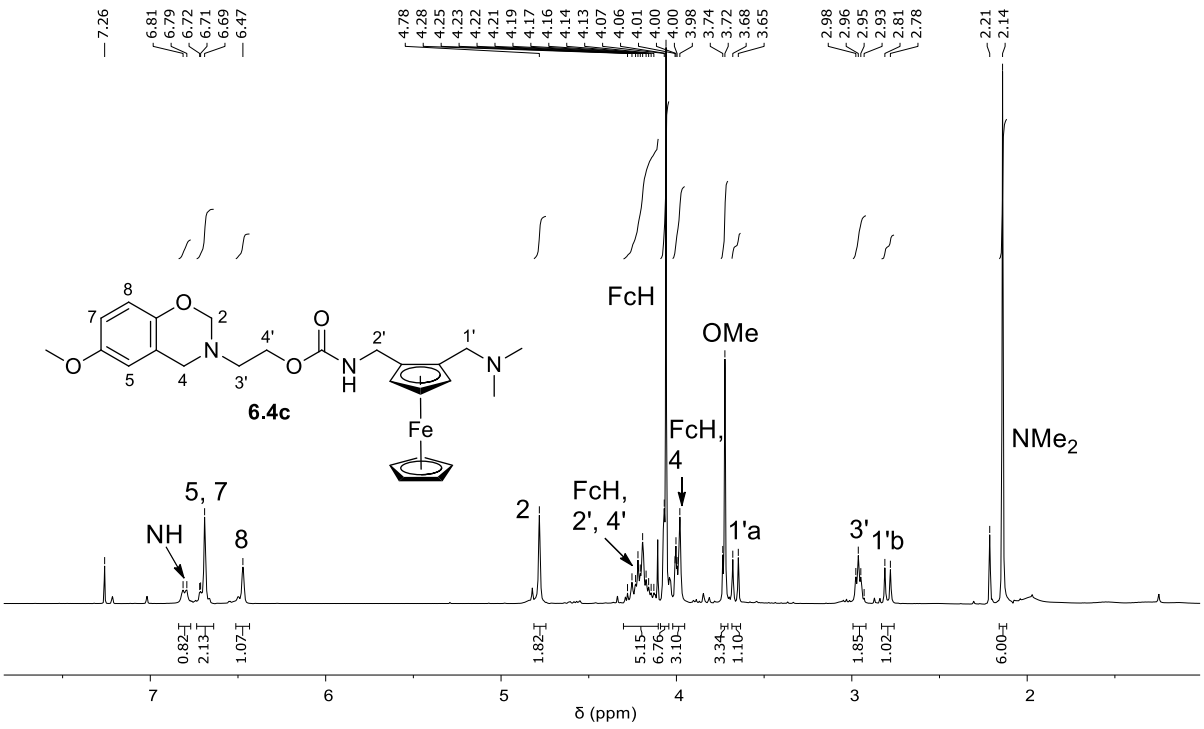

Figure 6.4 ^{1}H NMR spectrum of compound **6.4** in $CDCl_3$.

The proton signals of the benzoxazine 3-ethanol unit in the carbamate products were generally observed in similar regions as the 1,3-benzoxazine 3-ethanol substrates (**Figure 6.4**). However, proton 4′ attached to the oxygen of the carbamate unit was de-shielded from ~ δ 3.70 to the region 4.27 – 4.16 ppm upon coupling with the carbamate unit, owing to the presence of

electron deficient carbonyl (CO) group (**Figure 6.4**). Additionally, the ferrocene methylene proton (2′), resonated in the same region as proton 4′. This was identified by its H – H correlation (cross-peak *c*) with the amide NH group observed downfield at δ 6.80 ppm in the aromatic region in the COSY NMR spectrum of compound **6.4c** (**Figure 6.5**).

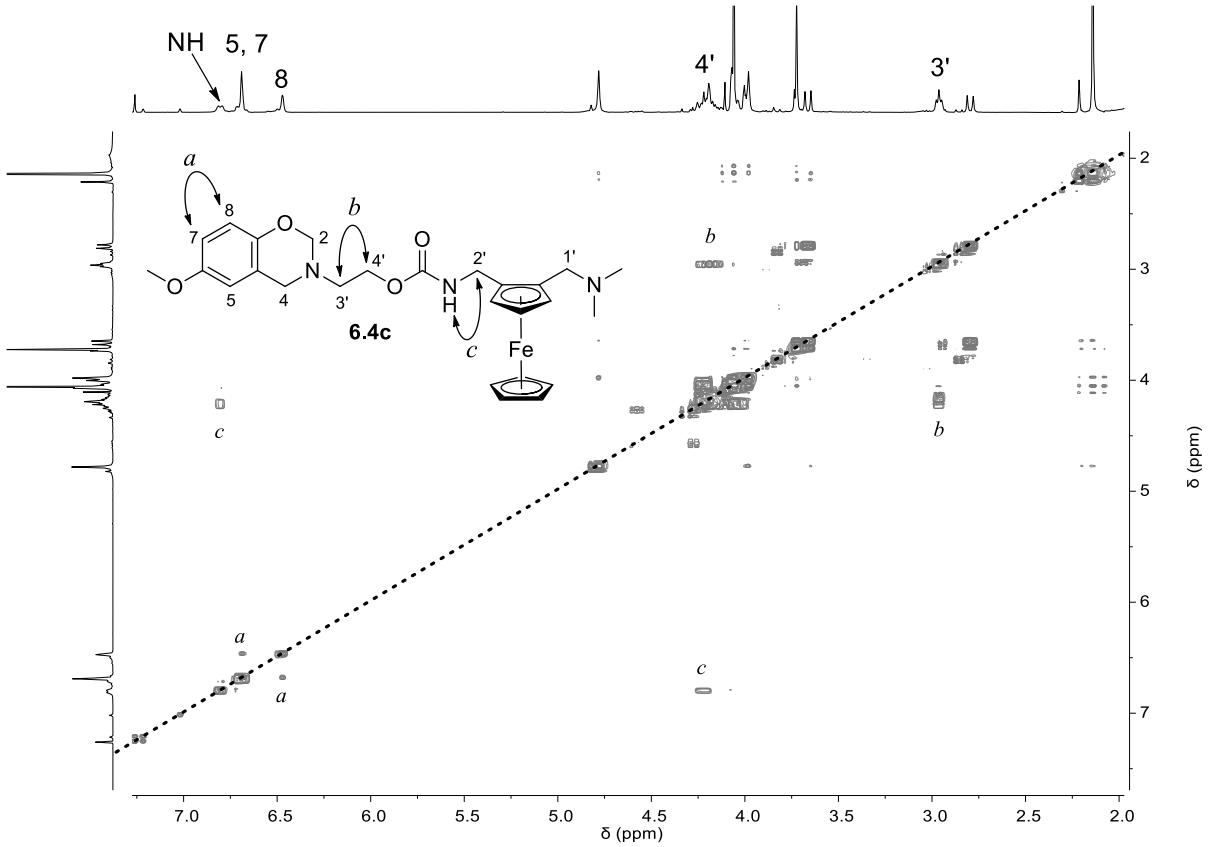

Figure 6.5 COSY NMR spectrum of compounds **6.4c** in $CDCl_3$.

Lastly, characterization of the compounds by NMR spectroscopic techniques was supported by the HRMS data. Carbon 2 of the oxazine O-CH_2-N unit was removed upon analysis of the compounds upon ionization during HRMS analysis, possibly due to its chemically labile nature.[5] As a result, in addition to their expected base peaks, all three ferrocene ethyl carbamate benzoxazine products **6.4a-c** were also observed as protonated molecular peak ions $[M+H]^+$ of their respective aminocresol fragments **6.4a′-c′** in the HRMS spectra (**Table 6.1**).

Table 6.1 HRMS results of the ferrocene ethyl carbamate benzoxazine products **6.4a-c**.

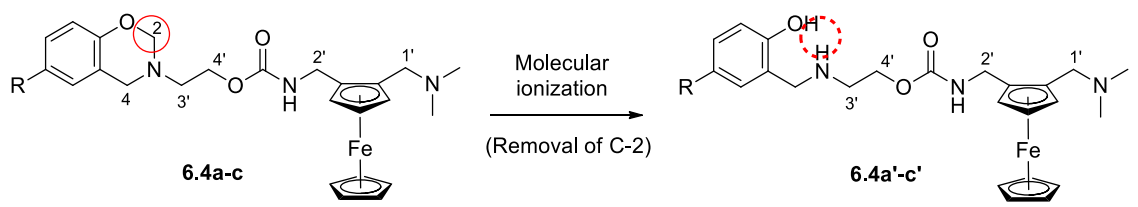

Compound	Predicted mass $[M+H]^+$	Found mass $[M+H]^+$
6.4a	478.1793	478.1790
6.4b	544.0898	544.0887
6.4c	508.1899	508.1902
6.4a′	488.1607[a]	488.1610[a]
6.4b′	544.0897	544.0905
6.4c′	496.1896	496.1898

[a]Mass observed as the molecular ion containing Na atom.

Fragmentation of the products into their corresponding aminocresol fragments is clearly illustrated by the HRMS spectrum of ferrocene ethyl carbamate benzoxazine **6.4a** (**Figure 6.6**).

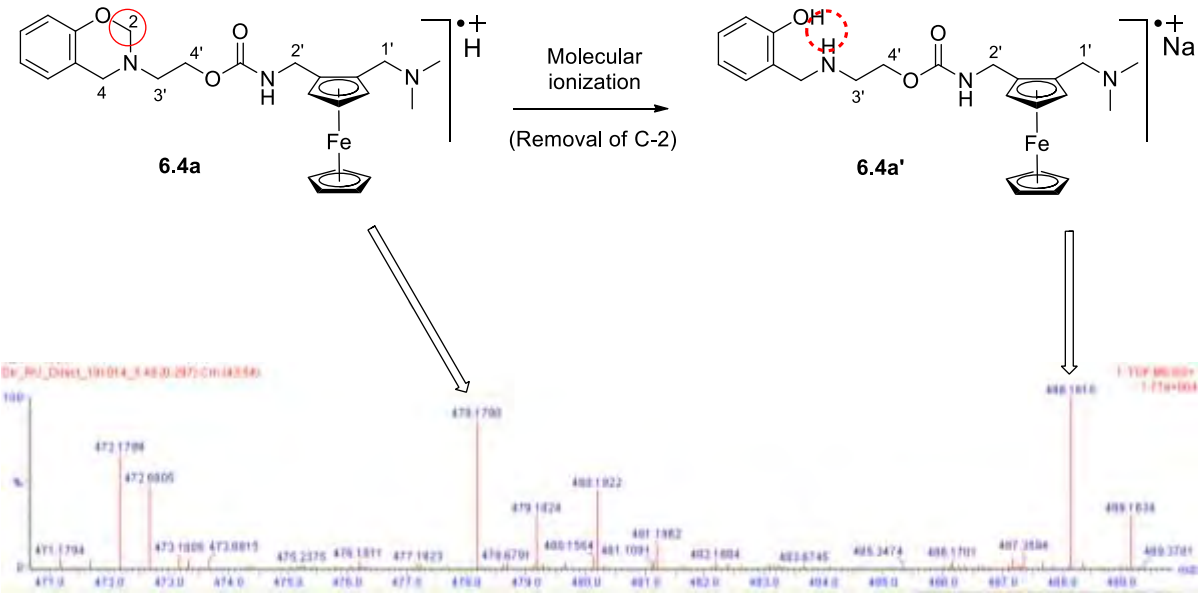

Figure 6.6 HRMS spectrum of compound **6.4a** showing its aminocresol fragment **6.4a′**.

Having synthesized the derivatives **6.4a-c** containing a hydrolysable ethyl carbamate spacer linking the ferrocene and benzoxazine units, we set out to prepare analogues bearing a non-hydrolysable ethylene (CH_2CH_2) linker as shown in **Figure 6.6**.[6]

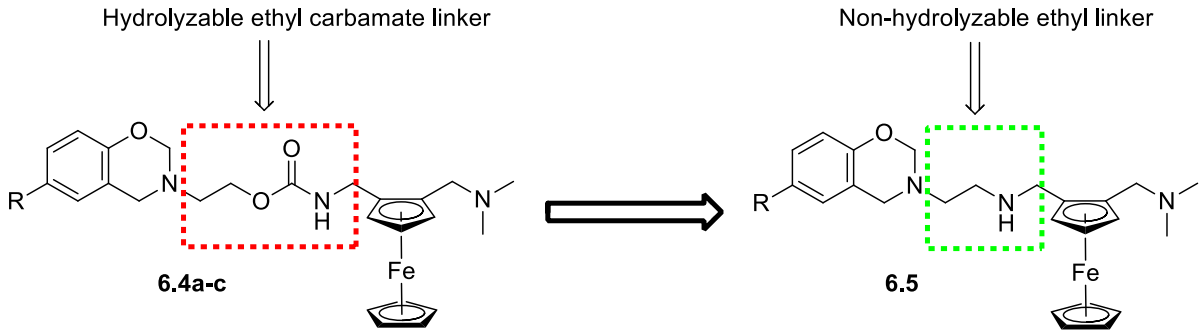

Figure 6.7 Replacement of the ethyl carbamate linker with an ethene spacer.

Initially, synthesis of the pursued compounds was proposed to be conducted by first attaching the ethylene chain to the ferrocene unit to produce a ferrocene ethylene amine (**6.9**) that would subsequently be subjected to Burke condensation with relevant phenolic substrates (**3.1**) to produce the desired compounds (**Scheme 6.3**).

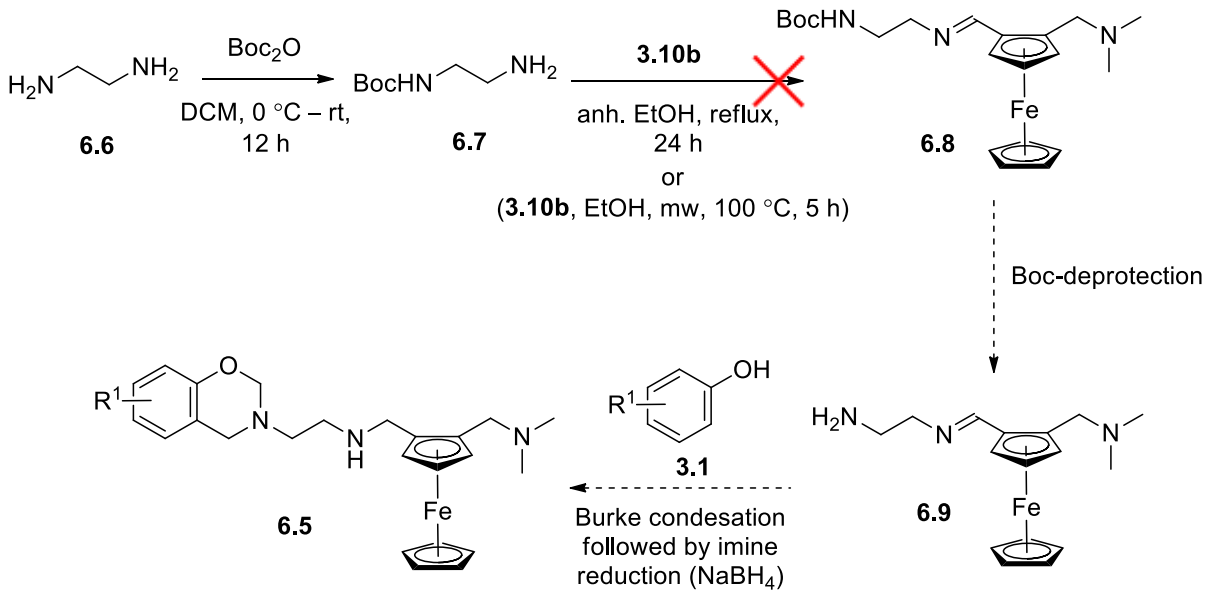

Scheme 6.3 Proposed route to target ferrocenyl benzoxazines containing an ethyl linker.

Starting from ethylene diamine (**6.6**), one of the amine groups was mono-protected with di-*tert*-butyl bicarbonate (Boc_2O) to avoid issues of selectivity.[7] The formation of the boc-protected Schiff base-type ferrocene ethyl amine **6.8** by coupling *N*-boc ethylenediamine **6.7** from the previous step with ferrocene carboxaldehyde **3.10** by reflux in anhydrous EtOH was unsuccessful.[8] It was hypothesized that ensuring complete absence of water from the reaction medium would facilitate the formation of the product since, being a condensation process, the reaction produces water. Therefore, fine molecular sieves (4 Å) were added to the reaction mixture to no avail. Adjusting the reaction conditions by employing microwave irradiation instead of heat failed to give the desired product, either. This step presented a stumbling block to accessing the desired compounds via this route.

The route for synthesis of the pursued compounds was revised by proposing attachment of the ethylene linker to the benzoxazine unit first and then coupling it to the ferrocene motif to produce the final compounds. Due to the sensitivity of the reaction to water and failure of the ferrocene carboxaldehyde **3.10b** to react with *N*-boc ethylenediamine **6.7**, we proposed replacing the aldehyde functional group with a carboxylic acid (**6.10**) and subjecting it to a less water-sensitive amidation transformation with 1,3-benzoxazine 3-ethylamines (**6.11a-b**) to subsequently effect 1,3-benzoxazine 3-ethylamido ferrocene products **6.12a-b** (**Scheme 6.4**).

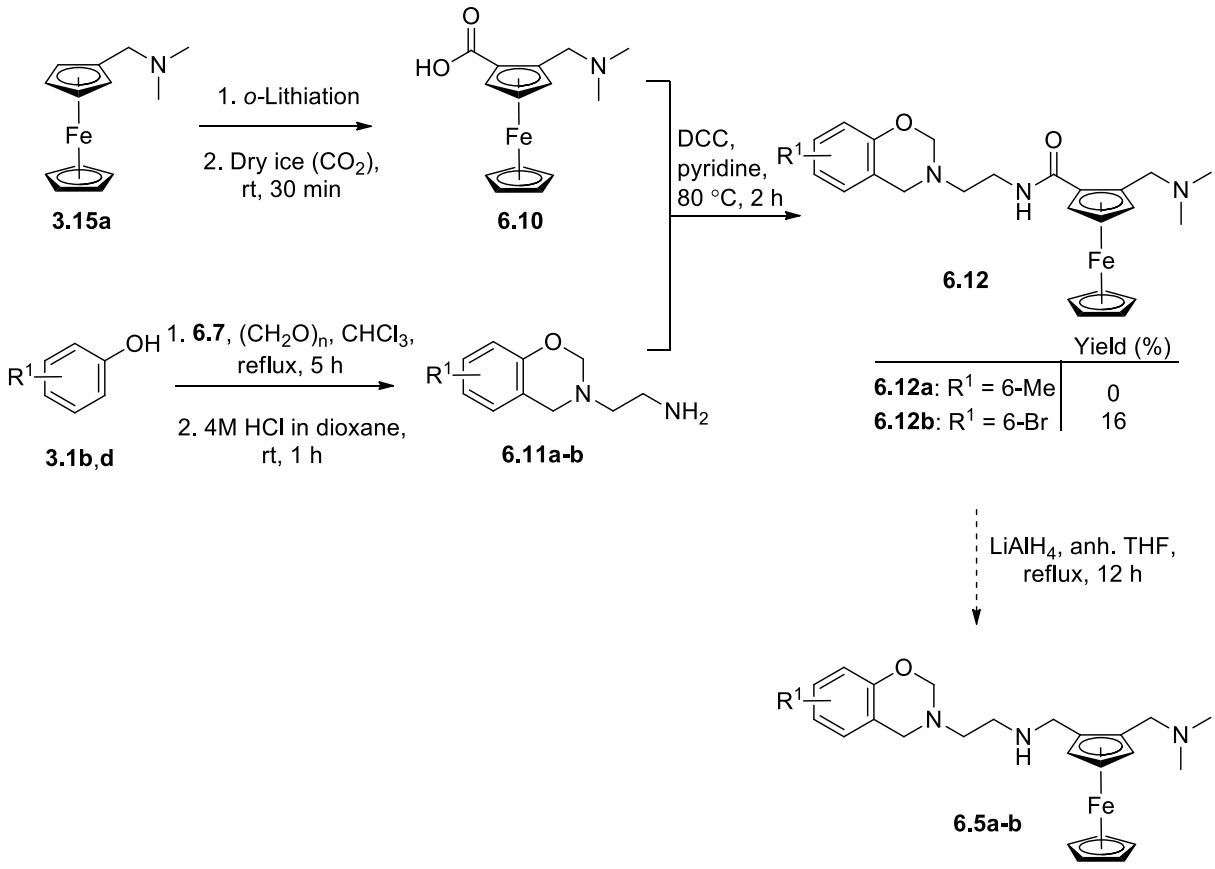

Scheme 6.4 Alternative route to synthesis of ferrocene ethylene-spaced 1,3-benzoxazine derivatives.

First, ferrocene carboxylic acid **6.10** was prepared by *ortho*-lithiation of *N,N*-dimethylaminomethylferrocene **3.15a** followed by carboxylation with dry ice (CO_2).[9] On the other hand, 1,3-benzoxazine 3-ethylamines **6.11a-b** were synthesized from 4-methyl and 4-bromophenol (**3.1b**,**d**) by Burke condensation with *N*-boc ethylenediamine **6.7** followed by boc-deprotection of the resultant 1,3-benzoxazine *N*-boc 3-ethylamine intermediates **6.11a′-b′** (not shown in **Scheme 6.4**).[10] These intermediates were characterized as illustrated in **Figure 6.8**.

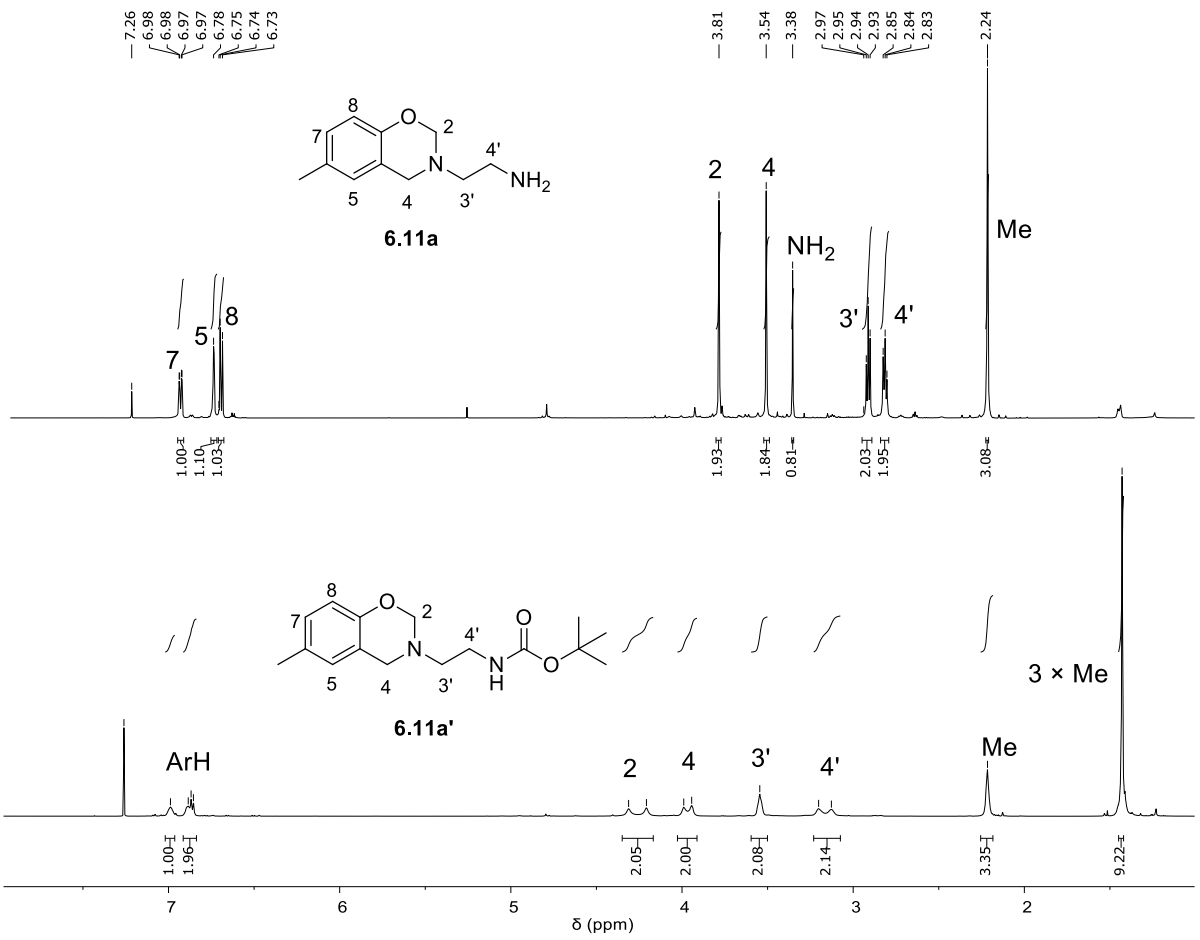

Figure 6.8 ^{1}H NMR spectrum of 5-methyl-1,3-benzoxazine 3-ethylamine **6.11a** and its *N*-boc intermediate **6.11a′** in $CDCl_3$..

The resulting 1,3-benzoxazine 3-ethylamines **6.11a-b** were subjected to the DCC amidation conditions with ferrocene carboxylic acid **6.10** by microwave irradiation (**Scheme 6.4**).[11] Only the brominated amide product (**6.12b**) was obtained in a poor yield of 16%, while the methyl congener could not be achieved under these conditions.

The brominated 1,3-benzoxazine 3-ethylamido ferrocene product **6.12b** was characterized by NMR and HRMS. The protons in the structure of the compound were assigned as shown in the ^{1} H NMR spectrum of the compound **6.12b** (**Figure 6.9**).

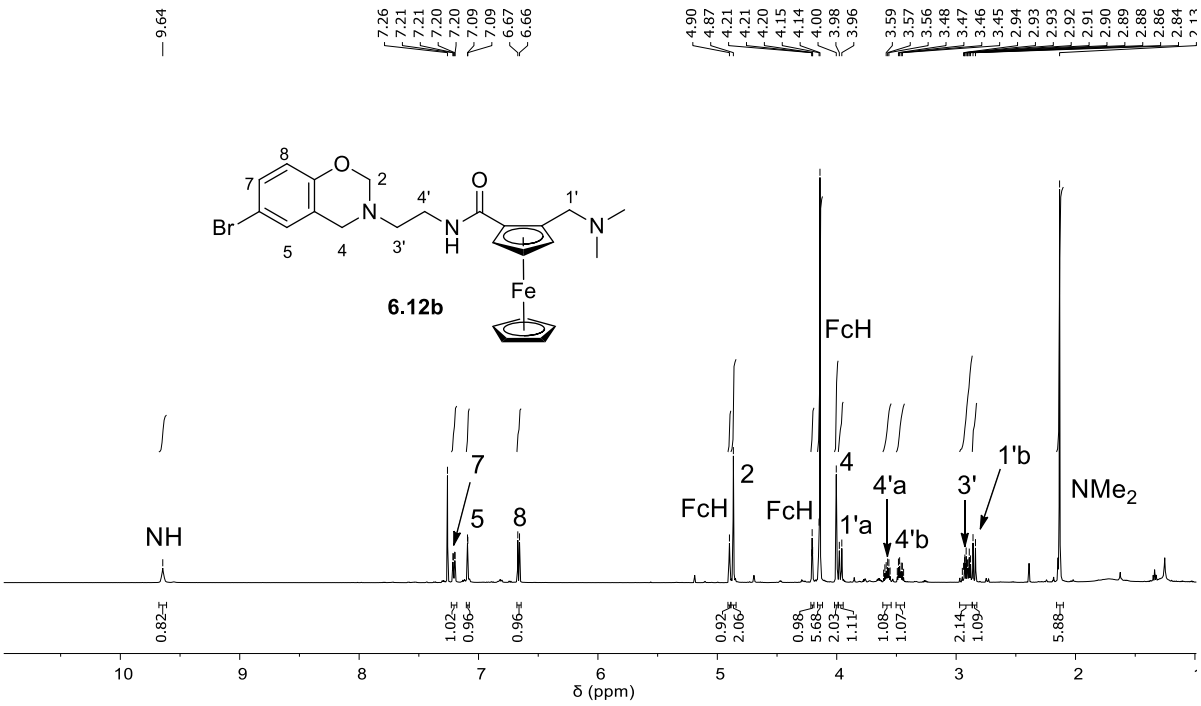

Figure 6.9 ^{1}H NMR spectrum of compound **6.12b** in $CDCl_3$.

The ethyl protons (3′ and 4′) were distinguished by COSY NMR (**Figure 6.10**). Proton 4′, which appeared as two 1H sextets (st) at δ 3.58 and 3.47 due to geminal coupling and its proximity to the neighbouring NH and proton 3′, was identified by its H – H correlation with the amide NH (cross-peak *a*) (**Figure 6.10**).

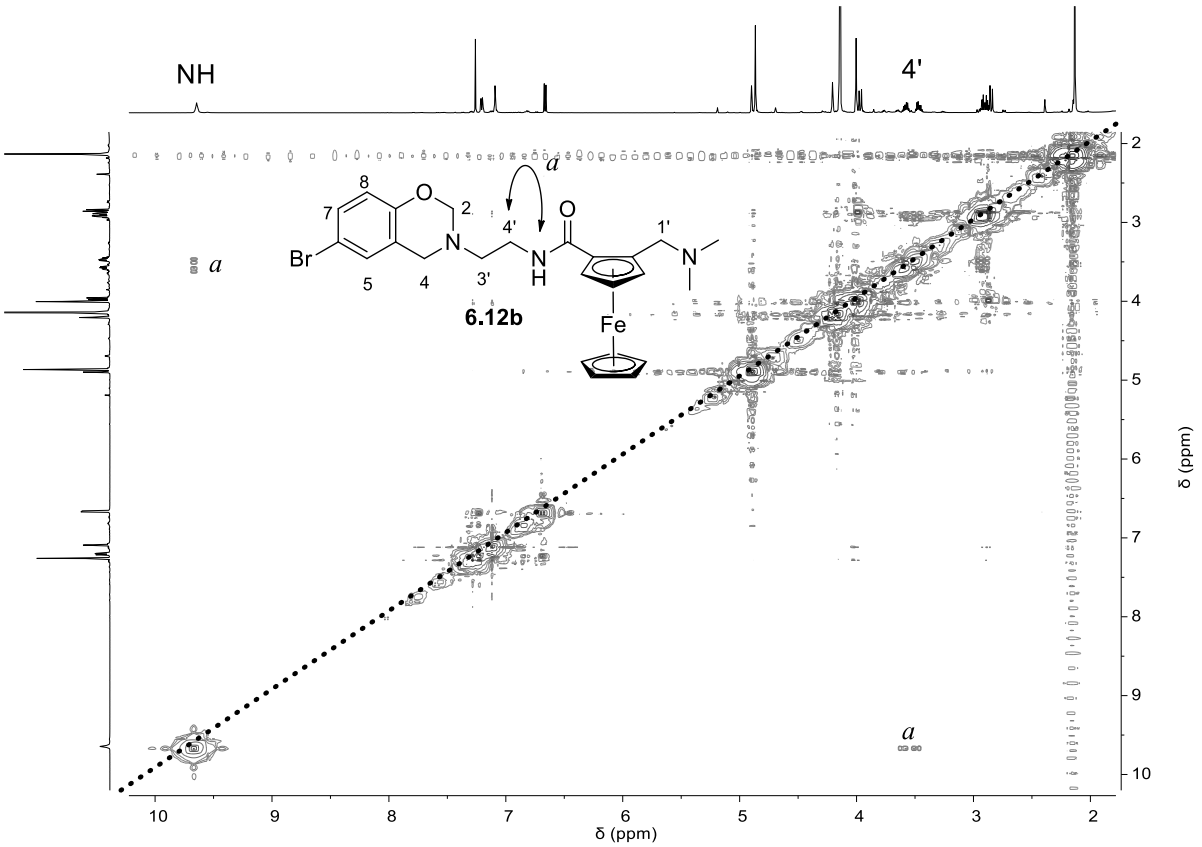

Figure 6.10 COSY NMR spectrum of compound **6.12b** in $CDCl_3$.

The assignment of carbons was facilitated by HSQC NMR displaying the DEPT-135 spectrum on the carbon (vertical) axis (**Figure 6.11**).

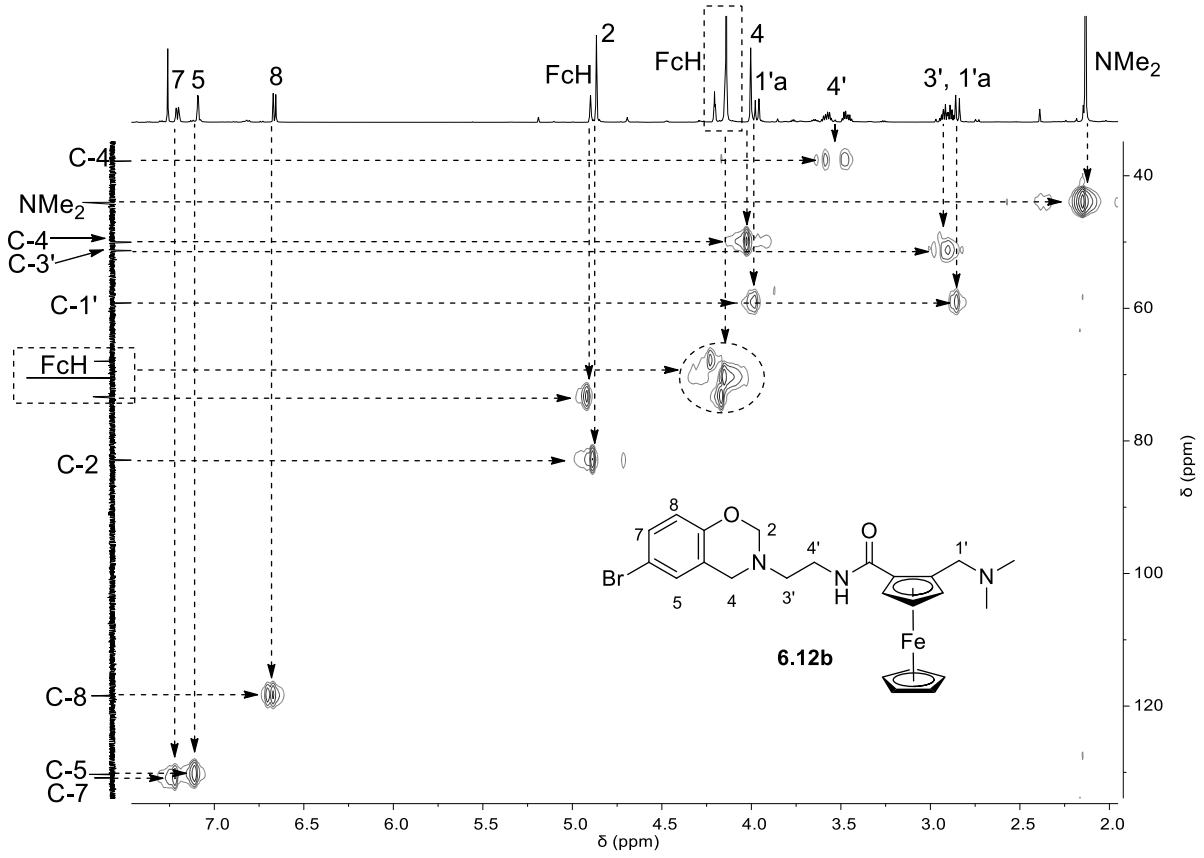

Figure 6.11 HSQC NMR spectrum of compound **6.12b** in $CDCl_3$ showing DEPT-135 spectrum on the vertical axis.

Due to time constraints, the conditions of this amidation transformation were not optimized to improve the product yields. Also, the formed brominated 1,3-benzoxazine 3-ethylamido ferrocene product **6.12b** was not reduced to the target ethylenediame congener **6.5b** owing to the small amount of the product obtained (16% yield).

6.3. Exploratory studies towards the synthesis of *N,N*-bis(2-hydroxybenzyl)ferrocenemethylamine derivatives

In the last part of the study, we undertook to explore the synthesis of the *N,N*-bis(2-hydroxybenzyl)ferrocenemethylamine derivatives that were formed as Mannich side products

during the Burke condensation of 4-methyl and 4-nitrophenols (**3.1b** and **3.1g**) into their respective ferrocenyl 1,3-benzoxazines **3.16b** and **3.16g** in **Chapter 3** (**Scheme 3.11**).

Based on the proposition that the formation of these side products takes place via the reaction of unreacted phenol substrates with the open-ring conformer of the forming benzoxazine product (**Scheme 3.12**) during Burke condensation, we proposed that reacting an already formed benzoxazine **3.16b**, supposedly exhibiting the open-ring iminium zwitterionic conformer **3.16b′**, with 4-methylphenol **3.1b** would result in the desired *N,N*-bis(2-hydroxybenzyl)ferrocenemethylamine product **3.16p** by electrophilic aromatic substitution (**Scheme 6.5**).[12] This approach failed to produce the desired compound after refluxing for 24 hours (TLC), and the ferrocenyl 1,3-benzoxazine **3.16b** substrate was recovered unchanged.

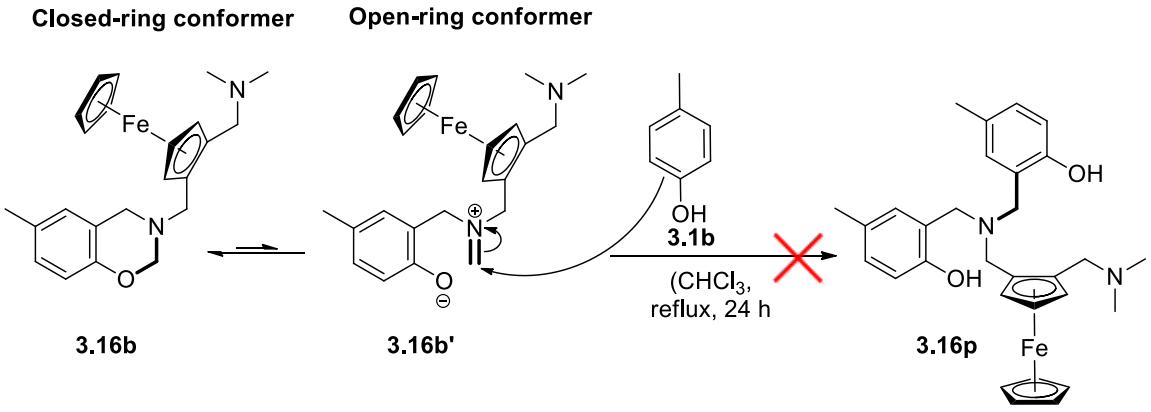

Scheme 6.5 Attempted synthesis of *N,N*-bis(2-hydroxybenzyl)ferrocenemethylamine **3.16p**.

An alternative route to synthesize the target compound **3.16p** by coupling 4-methyl α-amino-*o*-cresol **4.6b** to 5-methyl salicyaldehyde **6.13** by reductive amination with sodium triacetoxyborohydride ($Na(OAc)_3BH$) also failed to furnish the product (**Scheme 6.6**).[13]

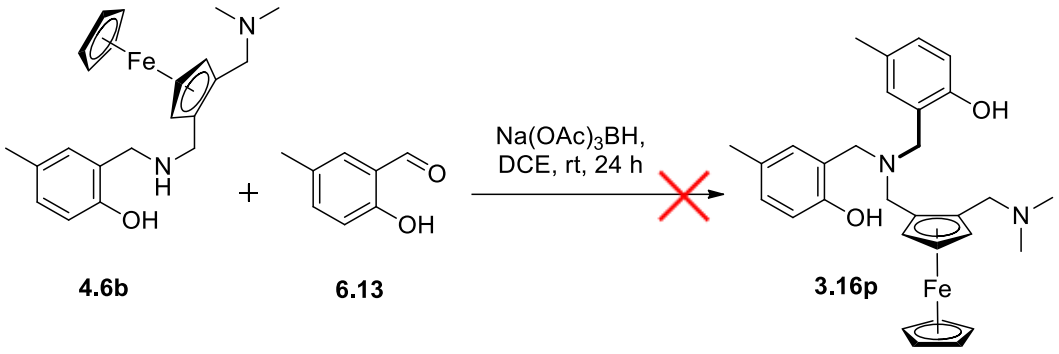

Scheme 6.6 Attempted synthesis of *N,N*-bis(2-hydroxybenzyl)ferrocenemethylamine **3.16p** via reductive amination.

At this point it was decided to increase the reactivity of the salicyaldehyde substrate (**6.13**) by converting it into its salicyl halide versions (**6.15a-b**) from the alcohol intermediate (**6.14**) that would then be reacted with aminocresol **4.6b** via nucleophilic substitution to the target compound **3.16p** (**Scheme 6.7**).[14] However, alcohol **6.14** formed unidentifiable polymeric materials under the bromination and chlorination conditions with phosphorus tribromide (PBr_3) and thionyl chloride (SO_2Cl), respectively (**Scheme 6.7**).[14]

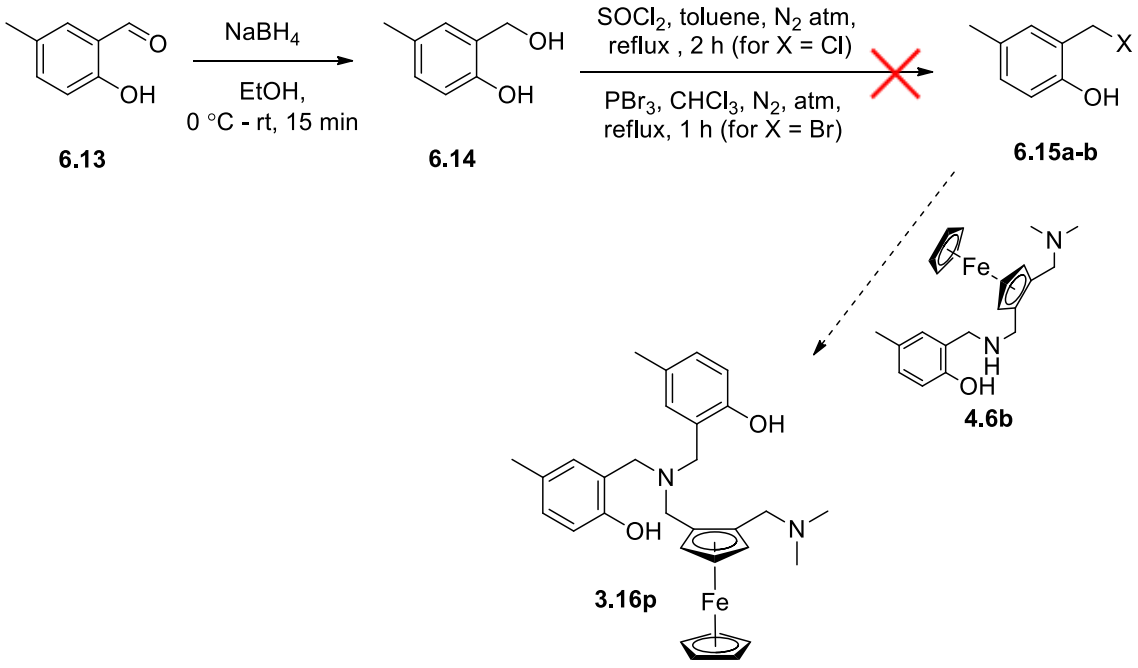

Scheme 6.7 Alternative synthesis of compound **3.16p** by nucleophilic substitution.

It was clear at this point that the reactivity of the salicylic substrate is crucial in the coupling reaction to aminocresol **4.6b** for the synthesis of the target compound. We reasoned that using a more electrophilic substrate would give better results. Thus, 5-chlorosalicylic acid **6.15** was coupled to aminocresol **4.6b** via various amidation protocols (**Scheme 6.8**).[11,15] Success was achieved with the amidation protocol reported by Chen et al. mediated by triethylphosphite ($P(OEt)_3$) and iodine.[15a] Briefly, 5-chlorosalicylic acid **6.14b** was treated with $P(OEt)_3$, iodine and triethylamine (Et_3N) at 0 °C and stirred for 30 minutes. Then, aminocresol **4.6b** was added to the above mixture and stirred for 3 hours, monitoring the reaction progress with TLC. The product was isolated in 70% yield by silica gel column chromatography purification of the crude product obtained following removal of the solvent after successive washing of the reaction mixture with aqueous NH_4Cl, NaOH and brine.[15a]

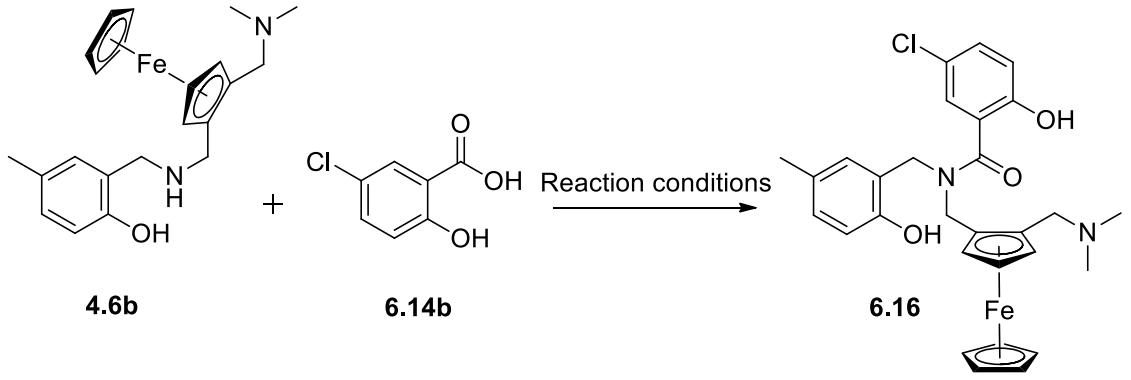

4.6b **6.14b** **6.16**

Reaction condtions	Yield (%)
EDCI•HCl, 30% pyridine/DCM, rt	0
DCC, pyridine, mw	0
T3P, pyridine/$CHCl_3$, reflux	0
1. SO_2Cl or $(COCl)_2$ then 2. **4.6b**	0
$P(OEt)_3/I_2$, Et_3N, DCM, rt	70

Scheme 6.8 Synthesis of compound **6.16** via amidation.

The chemical structure of the formed amidation product was confirmed by NMR and HRMS spectroscopy. The appearance of three salicylamide protons (3, 4 and 6) in the aromatic region of ^{1}H NMR spectrum of the product **6.16**, in addition to the cresol protons (3′, 4′ and 6′), verified successful coupling of salicylic acid **6.15** to the α-amino-*o*-cresol **4.6b** (**Figure 6.12**).

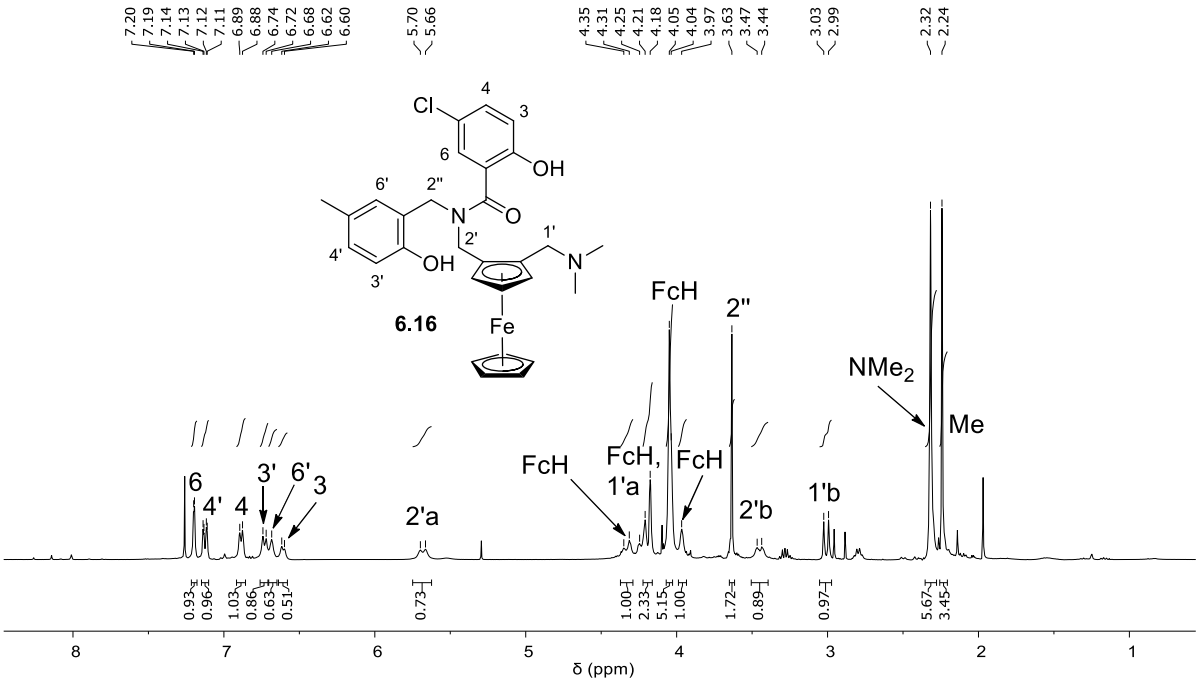

Figure 6.12 ^{1}H NMR spectrum of amide **6.16** in $CDCl_3$.

The assignment of protons was performed by multiplet analysis and COSY NMR (**Figure 6.13**). The methylene protons 2′ and 1′ were distinguished by the H – H correlations *a* and *b* at cross-peaks δ [5.68, 3.45] and [~4.21, 3.01] ppm due to geminal coupling, respectively (**Figure 6.13**).[2] The aromatic salicylamide protons 3 and 4 (blue dotted lines) and cresol protons 3′ and 4′ (red dotted lines) were assigned as shown in the COSY NMR spectrum of compound **6.16** (**Figure 6.13**).

Furthermore, the expected mass ($[M+H]^+$ = 547.1451 *m/z*) of amide **6.16** was in agreement with the observed mass $[M+H]^+$ = 547.1454 *m/z*.

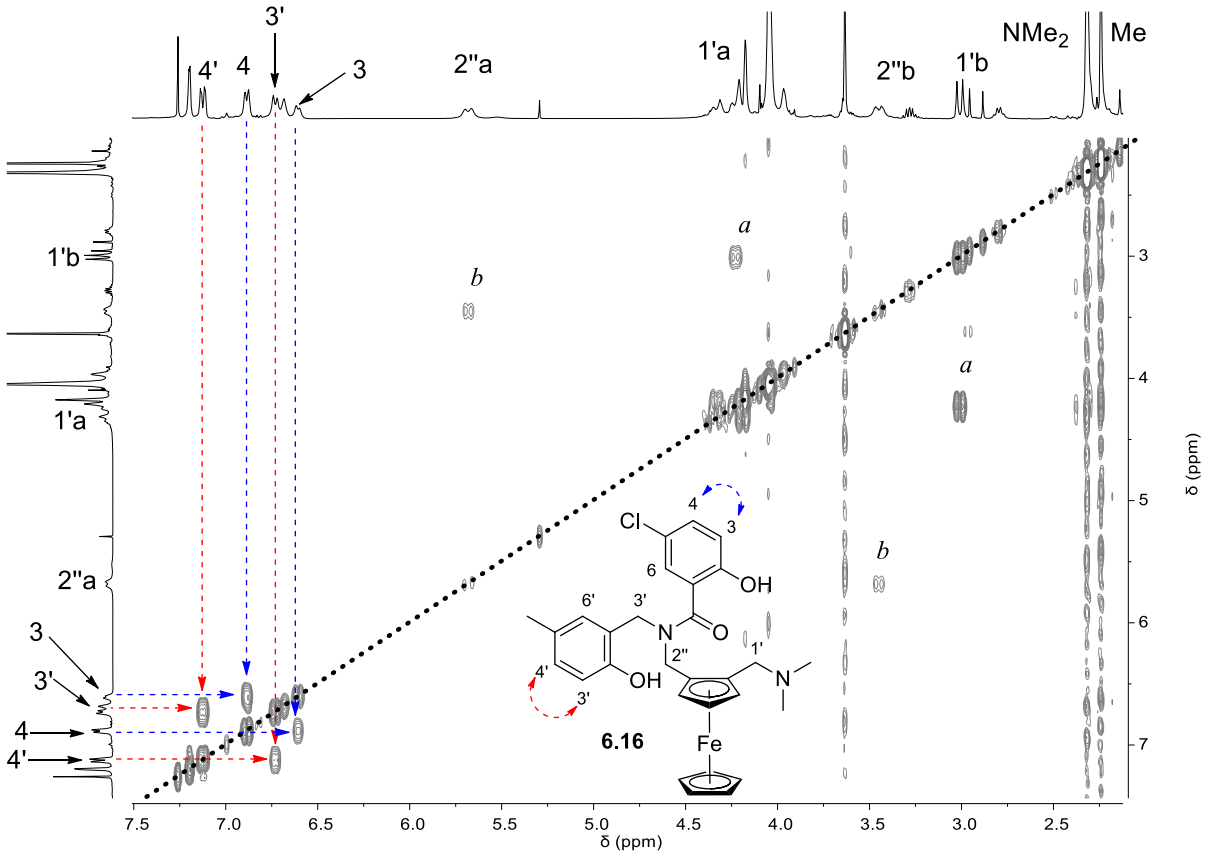

Figure 6.13 COSY NMR spectrum of amide **6.16** in $CDCl_3$.

Following successful formation of compound **6.16** achieved by coupling salicylic acid **6.15** to 4-methyl α-amino-*o*-cresol **6.4b**, this amide was reduced with $LiAlH_4$ in anhydrous THF to produce the target tertiary amine **6.17** (**Scheme 6.9**).[16] Complete reduction was achieved after 12 hours of the reaction (TLC). The product was attained in high purity by suction filtration after quenching of excess $LiAlH_4$ with distilled water and removal of solvent under reduced pressure.

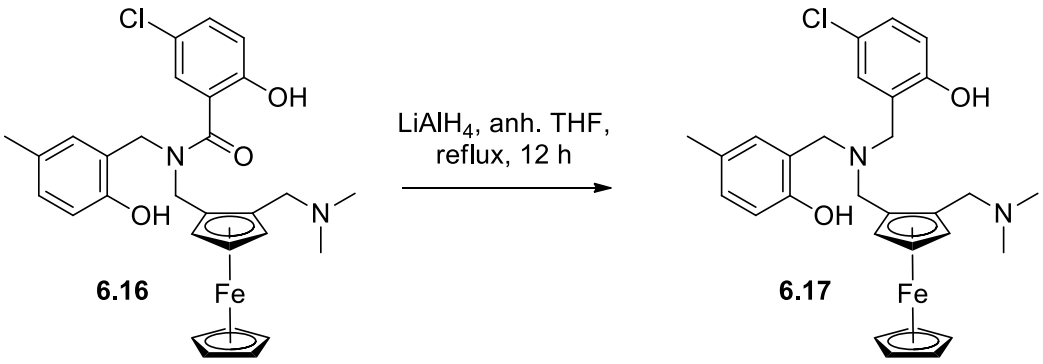

Scheme 6.9 Synthesis of ferrocenyl amine **6.17** via reduction of amide **6.16**.

The appearance of a new methylene signal (proton 2‴ at δ 3.83 ppm) in the ^{1}H NMR spectrum of the amine product **6.17** confirmed successful the reduction of amide **6.16** (**Figure 6.14**).

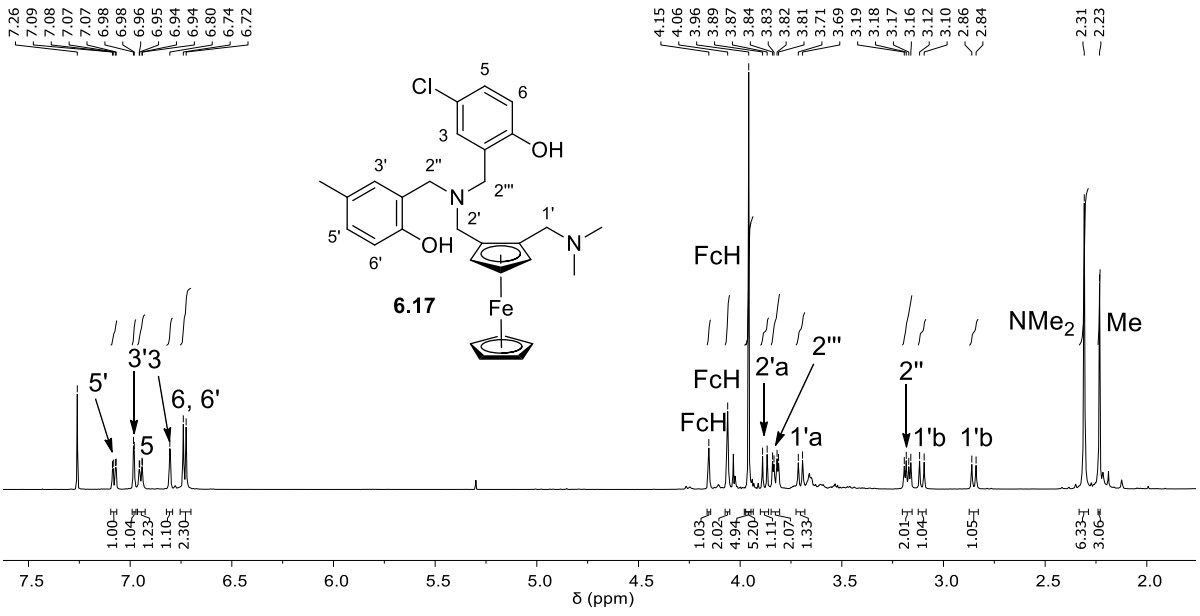

Figure 6.14 ^{1}H NMR spectrum of tertiary amine **6.17** in $CDCl_3$.

Furthermore, the amide carbonyl (CO) peak was not visible in the ^{13}C NMR spectrum of the product, thus, supporting the ^{1}H NMR data (**Figure 6.15**).

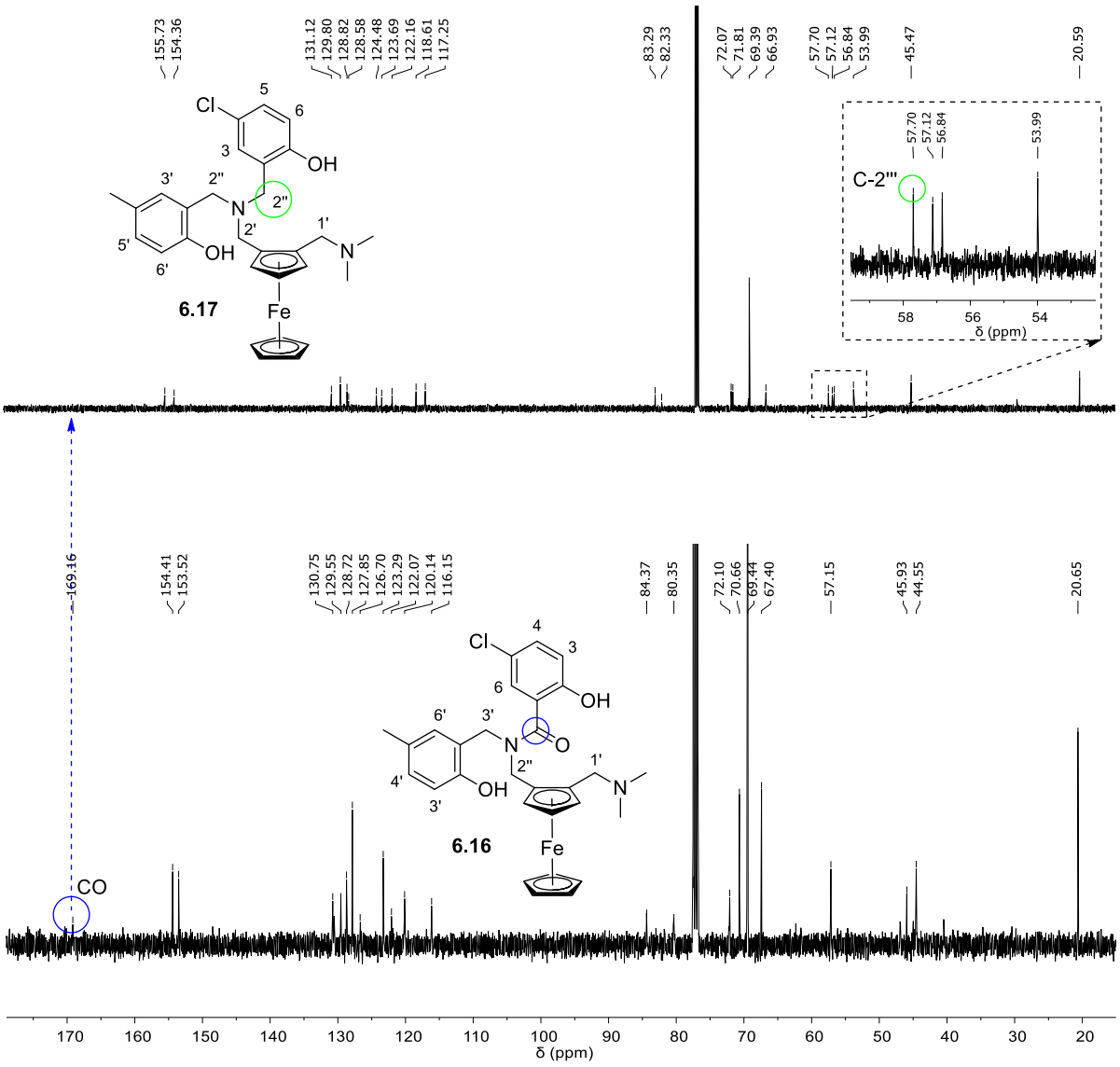

Figure 6.15 ^{13}C NMR spectrum of amine **6.17** and its corresponding amide precursor **6.16**.

The calculated mass of amine **6.17** ($[M]^+$ = 532.1580 *m/z*) was similar to that of its protonated molecular ion ($[M+H]^+$ = 533.1663 *m/z*) observed in the HRMS spectrum (**Figure 6.16**). Derivatives of the *N,N*-bis(2-hydroxybenzyl)ferrocenemethylamines, i.e., tertiary amines like **6.17**, could not be pursued further due to time constraints.

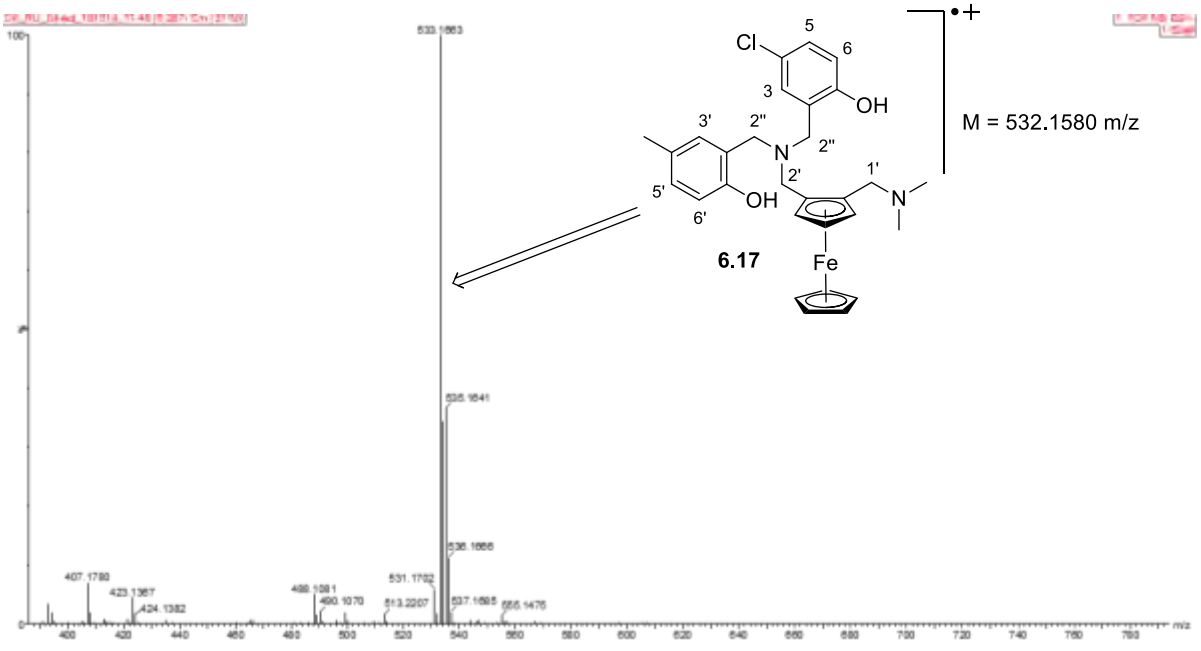

Figure 6.16 HRMS spectrum of amine **6.17**.

6.4. Biological evaluation results

The synthesized ferrocenyl 1,3-benzoxazines with a modified methyl linker (**6.4a-c**), tertiary amide **6.16** and amine **6.17** were evaluated for *in vitro* biological efficacy against the 3D7 *P. falciparum* strain and HCC70 triple-negative cancer cell lines. The results are presented in **Table 6.2** as IC_{50} values determined from experiments performed in duplicate. In all cases, the standard deviation (± SD) was below 1.0. Compound **6.12b** had not been synthesized by the time the biological screening of the compounds was conducted. Hence, its biological activity was not determined.

Table 6.2 *In vitro* biological activity of compounds **6.4a-c**, **6.16** and **6.17** against 3D7 *P. falciparum* strain and HCC70 breast cancer cell line.

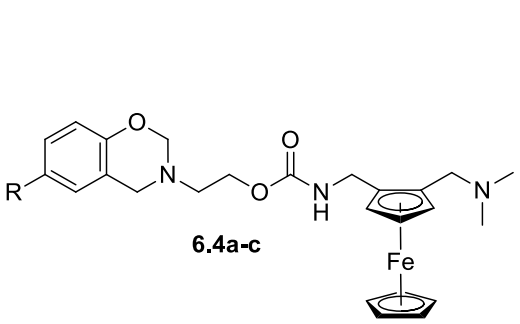

6.4a-c

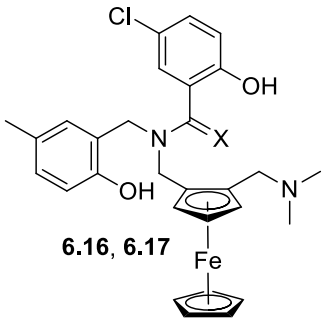

6.16, **6.17**

Compound	R or X	IC_{50} (μM)	
		3D7	**HCC70**
6.4a	H	0.89	33.8
6.4b	Br	1.84	18.4
6.4c	OMe	1.14	na
6.16	X = O	2.23	14.6
6.17	X = H, H	0.28	7.62
Chloroquine	–	0.03	–
Paclitaxel	–	–	0.0025

na = not active.

The 6-Br (**6.4b**) and 6-OMe (**6.4c**) ethyl carbamate analogues displayed antiplasmodial activity that was slightly lower than their parental methylene-spaced benzoxazine partners: **3.16d** (IC_{50} = 0.402 μM) and **3.16e** (IC_{50} = 0.407 μM) (**Tables 3.2** and **6.2**). Additionally, compound **6.4b** (IC_{50} = 18.4 μM) was comparable in activity to its non-ethyl carbamate variant **3.16c** (IC_{50} = 14.6 μM) against the HCC70 cancer cell line, whereas **6.4c** and its analogue **3.16e** were inactive (**Table 3.5**). On the other hand, while the plasmocidal activities of compound **6.4a** (IC_{50} = 0.89 μM) and its parental analogue **3.16a (**IC_{50} = 1.09 μM**)** were equivalent, replacing the methylene linker with the ethyl carbamate unit imparted anticancer activity to compound **6.4a**, i.e. HCC70 IC_{50} = na (**3.16a**) vs. 33.8 μM (**6.4a**) (**Tables 3.5** and **6.2**). Overall, it appears that the

incorporation of the ethyl carbamate moiety between the ferrocene and 1,3-benzoxazine units results in compounds displaying *in vitro* biological potencies that are similar to their parental methylene-spaced ferroceny l,3-benzoxazine derivatives explored in **Chapter 3**.

The chlorinated tertiary amine **6.17** and its amide precursor **6.16** had superior antiproliferative activity to the original methyl- and nitro- *N,N*-bis(2-hydroxybenzyl)ferrocenemethylamine side products **3.16p-q** (**Table 3.5** and **6.2**). More importantly, both the antiplasmodial and anticancer activity of these derivatives (**6.16** and **6.17**) increased upon reduction of amide **6.17** to tertiary amine **6.17** (**Table 6.2**). This seems to corroborate the previous assertion regarding the essential role of the basicity of the central nitrogen atom in the biological activity of ferrocenyl 1,3-benzoxazine derivatives explored in this study, as was observed by Chinnapattu et al. for their adamantane-based antiplasmodial compounds.[17]

6.5. Final SAR analysis model

The ferrocenyl 1,3-benzoxazine scaffold explored in this thesis comprises four key structural units, namely: ferrocene, benzene, oxazine and the methylene spacer (-CH_2-) joining the benzoxazine and ferrocene units. The preceding chapters explored the pharmacological effects resulting from structural modification of the ferrocene (**Chapter 3**), oxazine (**Chapter 4**) and benzene units (**Chapter 5**). An SAR analysis model summarizing these modifications was constructed (**Figure 5.26**). Through synthesis of representative derivatives (**6.4a-c**) of the ferrocenyl 1,3-benzoxazine scaffold containing a modified linker, i.e., ethyl carbamate, between the ferrocene and benzoxazine units, the pharmacological influence of altering the -CH_2- spacer was studied.

The ethyl carbamate compounds **6.4a-c** appeared to possess slightly lower, though related, *in vitro* antiplasmodial activities and favourable antiproliferative effects against the 3D7 *P. falciparum* strain and HCC70 breast cancer cell line, respectively, when compared to their

original non-carbamate analogues **3.16b**,**d-e** (**Table 3.2**, **3.5** and **6.2**). Notwithstanding, the activities of both the modified (**6.4a-c**) and native (**3.16b**,**d-e**) ferrocenyl 1,3-benzoxazines were overall comparable and were within the same concentration range. Therefore, from these observations we could conclude that increasing the length of the ferrocene-benzoxazine spacer with an ethyl carbamate unit is tolerated for biological activity of the ferrocenyl 1,3-benzoxazine compounds explored in this thesis. Consequently, a comprehensive SAR analysis model incorporating modifications of all four structural features of the ferrocenyl 1,3-benzoxine scaffold was drawn. The relationships of these modifications to pharmacological activity are illustrated in the final SAR analysis model of all the ferrocenyl 1,3-benzoxazine derivatives in **Figure 6.17**.

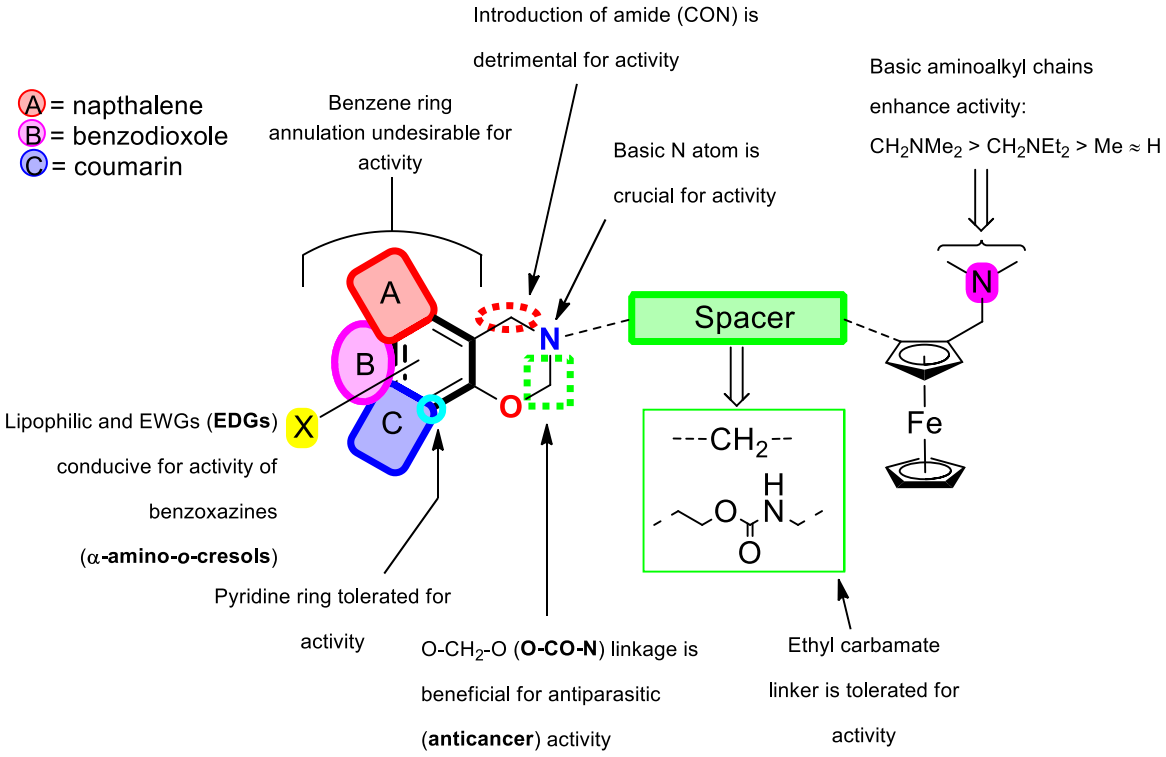

Figure 6.17 Final SAR analysis model of the ferrocenyl 1,3-benzoxazine derivatives.

6.6. Overall summary and conclusions

In this chapter, representative derivatives (**6.4a-c**) of the ferrocenyl 1,3-benzoxazine scaffold containing a modified linker (i.e., ethyl carbamate) between the ferrocene and benzoxazine units were prepared and fully characterized by NMR and HRMS spectroscopic techniques. Exploratory studies towards development of synthetic approaches to the ethylene-linked ferrocenyl 1,3-benzoxazine derivatives and tertiary amines based on the structural framework of *N,N*-bis(2-hydroxybenzyl)ferrocenemethylamine Burke condensation side products **3.16p-q** were undertaken. While only an advanced intermediate (**6.12b**) that is one step away from the final ethylene-linked ferrocenyl benzoxazine product (**6.6b**) could be achieved, a practical synthetic strategy for accessing the *N,N*-bis(2-hydroxybenzyl)ferrocenemethylamine derivatives was demonstrated via successful preparation of tertiary amine **6.17**.

The achieved compounds were evaluated for biological activity against the chloroquine-sensitive 3D7 *P. falciparum* strain and HCC70 triple-negative breast cancer cell line. The ethyl carbamate-spaced ferrocenyl 1,3-benzoxazine analogues **6.4a-c** displayed comparable, albeit lower, antiplasmodial and anticancer activity relative to their parental methylene-spaced counterparts (**3.16a**,**d-e**). On the other hand, the superior potency of the tertiary amine **6.17** to its corresponding amide **6.16** substantiated the crucial role of the basic central nitrogen atom (i.e., oxazine nitrogen for the benzoxazines) in the biological activity of the ferrocenyl 1,3-benzoxazine derivatives explored in this thesis. Lastly, amide **6.16** and amine **6.7** modelled on the *N,N*-bis(2-hydroxybenzyl)ferrocenemethylamine scaffold displayed anticancer potencies that were 5 times better than the original *N,N*-bis(2-hydroxybenzyl)ferrocenemethylamine side products **3.16p-q**. In conclusion, this finding presents the *N,N*-bis(2-hydroxybenzyl)ferrocenemethylamine structural framework as a promising bioactive scaffold, particularly for the generation of novel anticancer compounds and is worth further exploration.

References

(1) Fraga, C. A. M. *Expert Opin. Drug Dis.* **2009**, *4*, 605.

(2) Blackie, M. A. Doctoral Thesis, University of Cape Town, 2002.

(3) Burke, W. *J. Am. Chem. Soc.* **1949**, *71*, 609.

(4) D'Addona, D.; Bochet, C. G. *Tetrahedron Lett.* **2001**, *42*, 5227.

(5) Gemma, S.; Camodeca, C.; Brindisi, M.; Brogi, S.; Kukreja, G.; Kunjir, S.; Gabellieri, E.; Lucantoni, L.; Habluetzel, A.; Taramelli, D. *J. Med. Chem.* **2012**, *55*, 10387.

(6) Lazar, C.; Kluczyk, A.; Kiyota, T.; Konishi, Y. *J. Med. Chem.* **2004**, *47*, 6973.

(7) Feagin, T. A.; Shah, N. I.; Heemstra, J. M. *J. Nucleic Acids* **2012**, *2012*.

(8) Matsheku, A. C.; Chen, M. Y. H.; Jordaan, S.; Prince, S.; Smith, G. S.; Makhubela, B. C. *Appl. Organomet. Chem.* **2017**, *31*, e3852.

(9) Cullen, W.; Wickenheiser, E. *Can. J. Chem.* **1990**, *68*, 705.

(10) Nicolaou, K.; Bunnage, M. E.; Koide, K. *J. Am. Chem. Soc.* **1994**, *116*, 8402.

(11) Mu, F.; Lee, D. J.; Pryor, D. E.; Hamel, E.; Cushman, M. *J. Med. Chem.* **2002**, *45*, 4774.

(12) Li, W.; Wei, T.; Gao, Y.; Xi, K.; Jia, X. *Polymer* **2012**, *53*, 1236.

(13) Abdel-Magid, A. F.; Carson, K. G.; Harris, B. D.; Maryanoff, C. A.; Shah, R. D. *J. Org. Chem.* **1996**, *61*, 3849.

(14) (a) Xu, F.; Simmons, B.; Reamer, R. A.; Corley, E.; Murry, J.; Tschaen, D. *J. Org. Chem.* **2008**, *73*, 312; (b) Wong, Y.-L.; Mak, C.-Y.; Kwan, H. S.; Lee, H. K. *Inorg. Chim. Acta* **2010**, *363*, 1246.

(15) (a) Chen, P.-J.; Wang, H.-Y.; Peng, A.-Y. *RSC Advances* **2015**, *5*, 94328; (b) Mbaba, M.; Mabhula, A. N.; Boel, N.; Edkins, A. L.; Isaacs, M.; Hoppe, H. C.; Khanye, S. D. *J. Inorg. Biochem.* **2017**, *172*, 88; (c) Mbaba, M.; de la Mare, J.-A.; Sterrenberg, J. N.; Kajewole, D.; Maharaj, S.; Edkins, A. L.; Isaacs, M.; Hoppe, H. C.; Khanye, S. D. *J. Biol. Inorg. Chem.* **2019**, *24*, 139.

(16) Thiedemann, B.; Schmitz, C. M.; Staubitz, A. *J. Org. Chem.* **2014**, *79*, 10284.

(17) Chinnapattu, M.; Sathiyanarayanan, K. I.; Iyer, P. S. *Bioorg. Med. Chem. Lett.* **2015**, *25*, 952.

Chapter 7: Mechanistic studies towards the possible mode of action of ferrocenyl 1,3-benzoxazine derivatives

In the preceding chapters, various derivatives based on the ferrocenyl 1,3-benzoxazine scaffold were prepared, fully characterized by spectroscopic techniques and demonstrated to possess *in vitro* inhibitory activity against the triple-negative HCC70 breast cancer cell line, *P. falciparum* (3D7 and Dd2) strains and 427 *T. b. brucei* trypomastigotes. In line with the aims and objectives of the project, the current chapter presents experimental evidence to support a proposed mechanism by which the studied ferrocenyl 1,3-benzoxazines may exhibit biological activity. The studied possible biomolecular targets upon which the compounds were proposed to act are DNA binding interaction, DNA damage and hemozoin inhibition. Spectroscopic and cellular bioassays were employed to investigate the ability of the compounds to target the biomolecules or processes described above. Only representative compounds showing promising activity from each series were evaluated for mechanistic modality. These compounds were: benzoxazine **3.16c**, α-amino-*o*-cresol **4.6c** and 8-amimomethylcoumarin-7-ol **5.23b**. Lastly, computational docking simulations were performed to corroborate the experimentally determined results for DNA interaction.

7.1. Rationale

Benzoxazines belong to the phenolic class of Mannich bases. The ferrocenyl 1,3-benzoxazine derivatives explored in this project were assembled via the Mannich-type Burke condensation protocol. Mannich bases are reputable drug scaffolds with a broad spectrum of biological activities. For many years, Mannich base derivatives have been prolific subjects of research in

drug discovery as bioactive agents and their modes of action have been well studied.[1] Of the many mechanistic modalities of Mannich bases, DNA binding, including the disruption of the DNA replication machinery, is one of the most studied.[1] Examples of Mannich base compounds exhibiting biological activity by binding to DNA are shown in **Figure 7.1** with the Mannich base functionality in bold.[2]

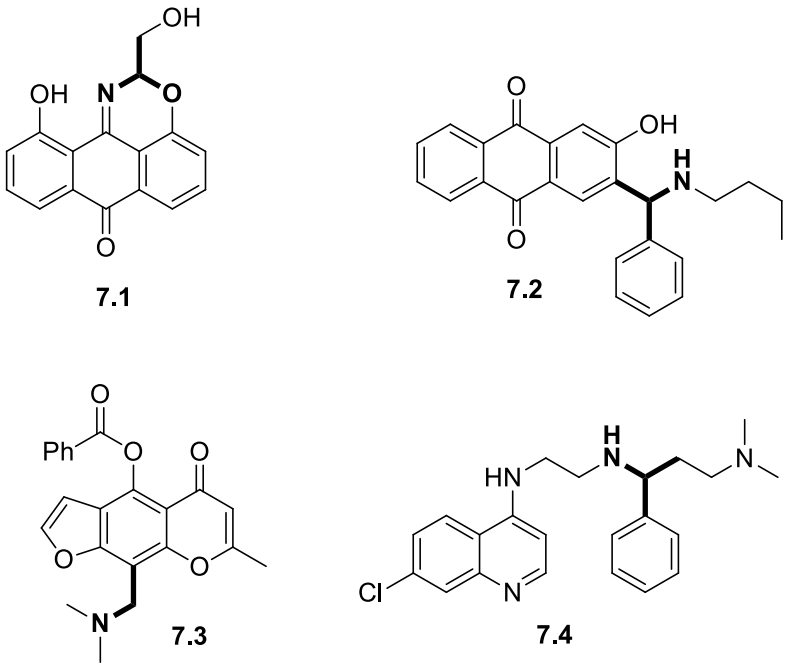

Figure 7.1 Some examples of bioactive Mannich base derivatives possessing DNA binding affinity featuring in literature.

As phenolic Mannich base derivatives, we hypothesized that the ferrocenyl 1,3-benzoxazine derivatives pursued in this study as described in previous chapters would display activity similar to other DNA-binding derivatives reported in literature.[2] In addition, the inhibition of hemozoin is a common target of many antimalarial compounds. Since the investigated ferrocenyl 1,3-benzoxazine compounds showed preferential selectivity for *P. falciparum* parasites, they were also investigated for hemozoin inhibition. Thus, representative compounds

from each series were investigated for DNA and hemozoin binding affinity to gain insight into their possible mode of action.

7.1.1. DNA binding affinity studies by UV-Vis DNA titration

UV-Vis spectroscopy is a versatile analytical tool in chemical biology to assess binding interactions. In UV-Vis DNA titration studies, a test compound is incubated with a DNA sample and the absorption is monitored.[3] In principle, when a small molecule binds to DNA, changes in the recorded spectrum are observed.[3] For instance, an increase in absorbance (i.e., hyperchromic effect) of the recorded spectra is attributed to external contact of the compound with DNA or uncoiling of the DNA double helix which exposes more nucleotide bases.[3] DNA absorbs strongly at a wavelength of 260 nm. In a typical DNA titration experiment, varying concentrations (30 – 100 μM) of test compounds **3.16c**, **4.6c** and **5.23b** were incubated with a 70 ng/μL mammalian calf thymus DNA sample of constant concentration and the absorbance was recorded at 260 nm after an incubation period of 15 minutes.[4] The ferrocenyl 1,3-benzoxazin-2-one **4.17b** was included in the assay for comparison. The results are depicted in **Figure 7.2**.

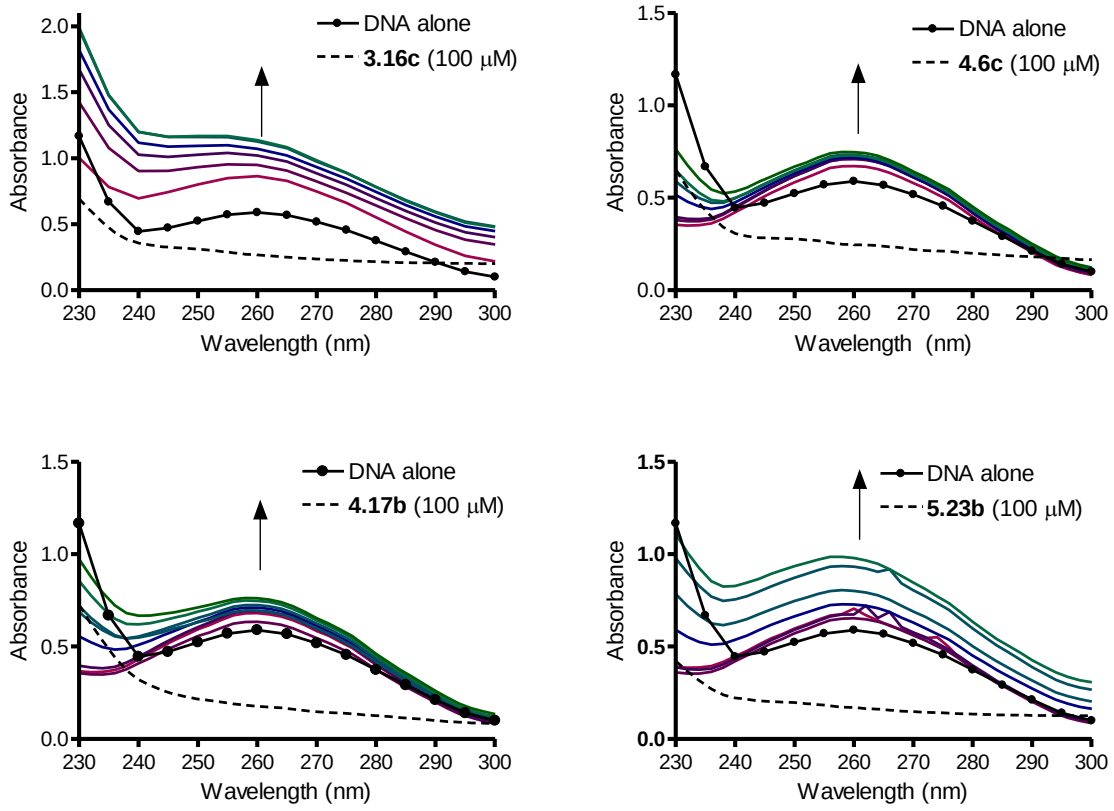

Figure 7.2 UV-Vis DNA titration experiment results showing hyperchromic effect with increasing concentration of each test compound.

In all cases, tested compounds elicited a dose-dependent hyperchromic response between 12 and 48% against the DNA sample at the tested concentrations in a linear fashion (**Figure 7.2**). The hyperchromic effect of the benzoxazine **3.16c** and 8-aminomethylcoumarin-7-ol **5.23b** was accompanied by a slight blue shift of ~ 4 nm at the absorbance maximum around 260 nm. The dose-dependent hyperchromic effect together with the slight blue shift, i.e., hypsochromic effect (~ 4 nm), of the DNA sample upon addition of compounds **3.16c** and **5.23b** are indicative of external interaction of the compounds with DNA via non-covalent associations as demonstrated in similar studies in literature.[3-4] On the other hand, the α-amino-*o*-cresol **4.6c** and its cyclic benzoxazine-2-one analogue **4.17b** did not show any significant hypsochromism or bathochromic effect (red shift) around the absorbance maximum. This suggested weaker interaction of the compounds with DNA.[3,5] Importantly, the absorbance of both unbound DNA

sample (70 ng/μL) and free compounds **3.16c**, **4.6c**, **4.17b** and **5.23b** at 100 μM was evidently lower at 260 nm compared to the test samples incubated with DNA (**Figure 7.2**). These results support the hypothesis that the investigated compounds possess DNA binding affinity.

Having verified that the compounds interact with DNA, we set out to quantify the binding strength of each compound in terms of the binding constant (K_b) by fitting the obtained data points into the reciprocal guest-host equation (1), which relates compound concentration [C] to absorbance of the DNA-compound complex (A_c):

$$\frac{1}{A_c - A_0} = \frac{1}{K_b(A_\infty - A_o)} \times \frac{1}{[C]} + \frac{1}{A_\infty - A_0} \qquad (1)$$

where A_0 and A_c represent the absorbance of unbound DNA and test samples containing a fixed amount of DNA with varying compound concentrations at 260 nm, respectively, while A_∞ is the hypothetical final absorbance of the DNA-compound complex.[4] The binding constants (K_b) were determined as the ratio of the intercept to slope of the linear plot of $1/(A_c - A_0)$ versus $1/[C]$ relating absorbance of the DNA-compound complex to compound concentration (**Figure 7.3**).[4]

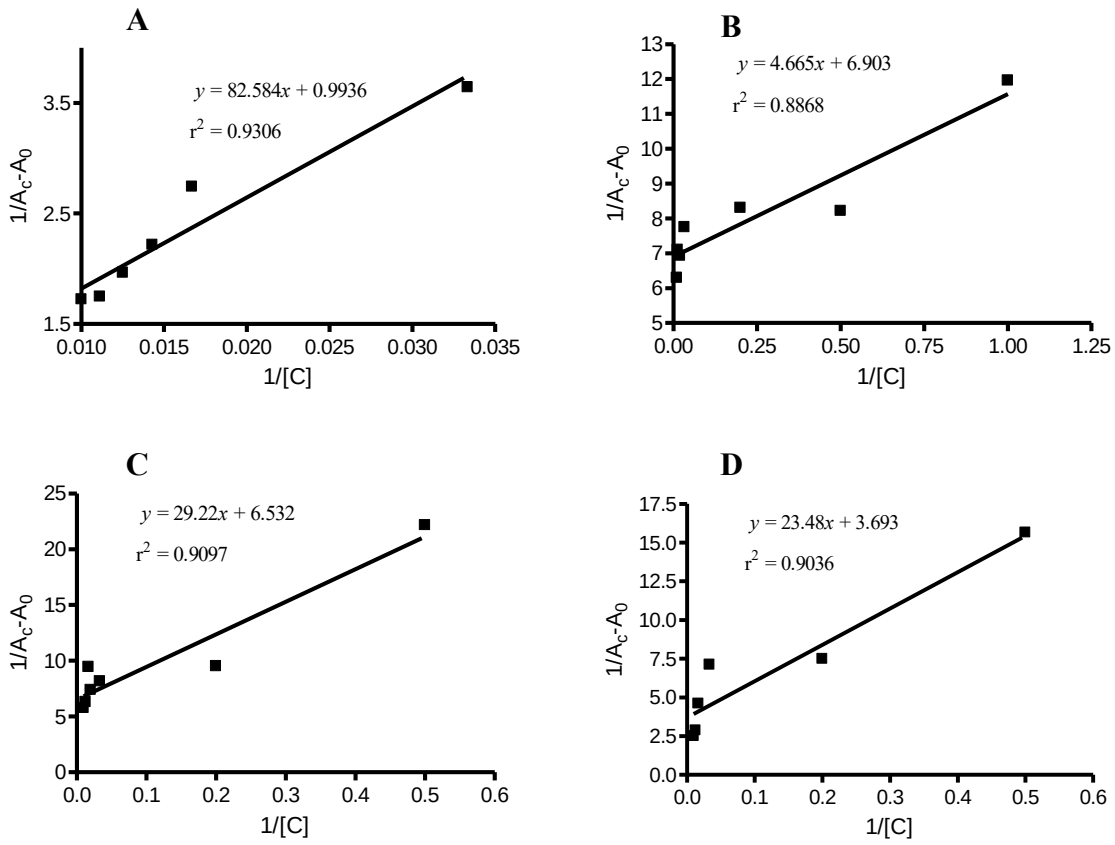

Figure 7.3 Linear guest-host reciprocal plot relating absorbance of the DNA-compound complex to compound concentration for (**A**) 1,3-benzoxazine **3.16c**, (**B**) α-amino-*o*-cresol **4.6c**, (**C**) 1,3-benzoxazin-2-one **4.17b** and (**E**) 8-aminomethylcoumarin-7-ol **5.23b**.[6]

The determined binding constants of the compounds are presented in **Table 7.1** alongside the anticancer activity against the HCC70 cell line.

Table 7.1 DNA binding constants of ferrocenyl 1,3-benzoxazine **3.16c**, α-amino-*o*-cresol **4.6c**, 1,3-benzoxazin-2-one **4.17b** and 8-aminomethylcoumarin-7-ol **5.23b**.

Compound	K_b (M^{-1})	HCC70 IC_{50} (μM)
3.16c	12.03×10^3	11.0
4.6c	1.480×10^6	6.67
4.17b	143.5×10^3	12.7
5.23b	2.760×10^3	na

na = not active

From the determined binding constants, the α-amino-*o*-cresol **4.6c** had the highest binding constant ($K_b = 1.480 \times 10^6$) followed by its benzoxazine-2-one analogue **4.17b** (143.5×10^3) despite having low hyperchromic shifts (12 – 14%) and not showing significant hypsochromic and bathochromic effects from the DNA titration spectra, implying weak DNA binding interactions (**Figure 7.2**).[3,5] The benzoxazine **3.6c** and 8-aminomethylcoumarin-7-ol **5.23b**, which showed substantial dose-dependent hyperchromic effects (36 – 48%) accompanied by a noticeable hypsochromic shift (~4 nm), had moderate binding constants of 12.03×10^3 and 2.760×10^3 M^{-1}, respectively (**Table 7.1**). The high binding affinity of the α-amino-*o*-cresol **4.6c** ($K_b = 1.480 \times 10^6$ M^{-1}) could be attributed to the exposed amino (NH) and hydroxyl (OH) groups, which can participate in hydrogen-bonding with the DNA bases or backbone residues to provide additional stabilization to the interactions within the formed DNA-compound complex. The binding constant of this compound against DNA seems to be linked to its anticancer activity ($IC_{50} = 6.67$ μM) evaluated on HCC70 breast cancer cells (**Tables 4.6** and **7.1**). This is further demonstrated by the decrease in both the binding constant ($K_b = 143.5 \times 10^3$ M^{-1}) and anticancer activity ($IC_{50} = 12.7$ μM) of the benzoxazine-2-one analogue (**4.17b**) of compound **4.6c** upon masking the NH and OH functional groups with a carbamate unit (O-CO-N) (**Table 7.1**). Compound **5.23b**, which was not active against the mammalian HCC70 cancer cell line, had the lowest DNA binding constant ($K_b = 2.760 \times 10^3$ M^{-1}), further emphasizing the association between DNA binding affinity of the compounds and their biological activity. Irrespective of the apparent contradiction between the expected binding constants based on spectral observations (**Figure 7.2**) and the determined values by the guest-host reciprocal plot (**Figure 7.3**), the DNA binding affinity of the compounds from both sets of data is unequivocal.

7.1.2. Competitive DNA binding affinity studies using fluorescence titration

Having demonstrated the affinity of the compounds for DNA binding interactions, the next step was to ascertain the mode by which the compounds interact with DNA. Depending on its size, structure and surface topology, a molecule can interact with the DNA double helix via three main modes namely binding to the major or minor groove, or by intercalation of the two DNA strands.[3] To assess the mode of binding of the compounds to DNA, qualitative competitive DNA binding studies were performed using a verified fluorescent DNA intercalator, methylene blue dye (**7.1**), and a DNA minor groove binder, Hoechst 33342 (**7.2**) (**Figure 7.4**).[7]

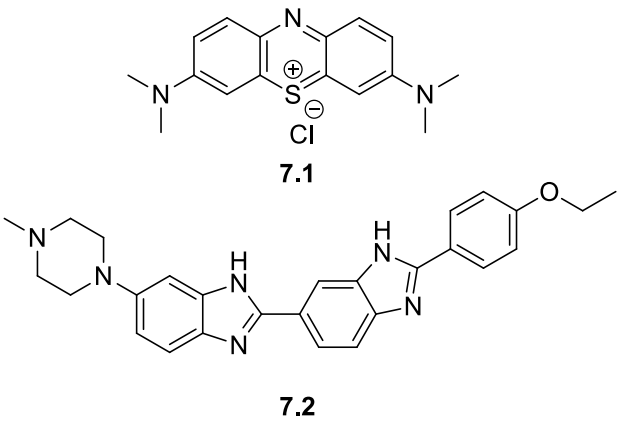

Figure 7.4 Chemical structures of methylene blue (**7.1**) and Hoechst 33342 (**7.4**).

In a typical assay, a fixed amount of calf thymus DNA (70 ng/μL) was combined with the appropriate dye (methylene blue or Hoechst 33342) in the presence (50 μM and 100 μM) and absence (DMSO) of the compound (**3.16c**, **4.6c** and **5.25b**) and fluorescence was monitored. Free methylene blue exhibits a strong fluorescence emission at 660 – 670 nm which decreases upon complexation with DNA due to reduced concentration of dye molecules in the medium.[7a] A strong DNA intercalator will amplify the fluorescence emission of the DNA-methylene blue complex since it competitively displaces the DNA-bound dye molecules and increases their accumulation in the medium. To verify the assay, a confirmed strong DNA cross-linker,

cisplatin, was employed as a positive control.[8] Cisplatin forms covalent bonds with the guanine bases of the DNA double helix, disrupting base-pairing of the strands.[9] It was employed as a positive control in the study because disruption of base-pairing interactions would interfere with DNA intercalation by an external compound, e.g. methylene blue, and prevent it from binding to DNA via this mode. This in turn would liberate the bound methylene blue molecules from the DNA adduct leading to intensification of fluorescence. The results of the competitive methylene blue assay are presented in **Figure 7.5**.

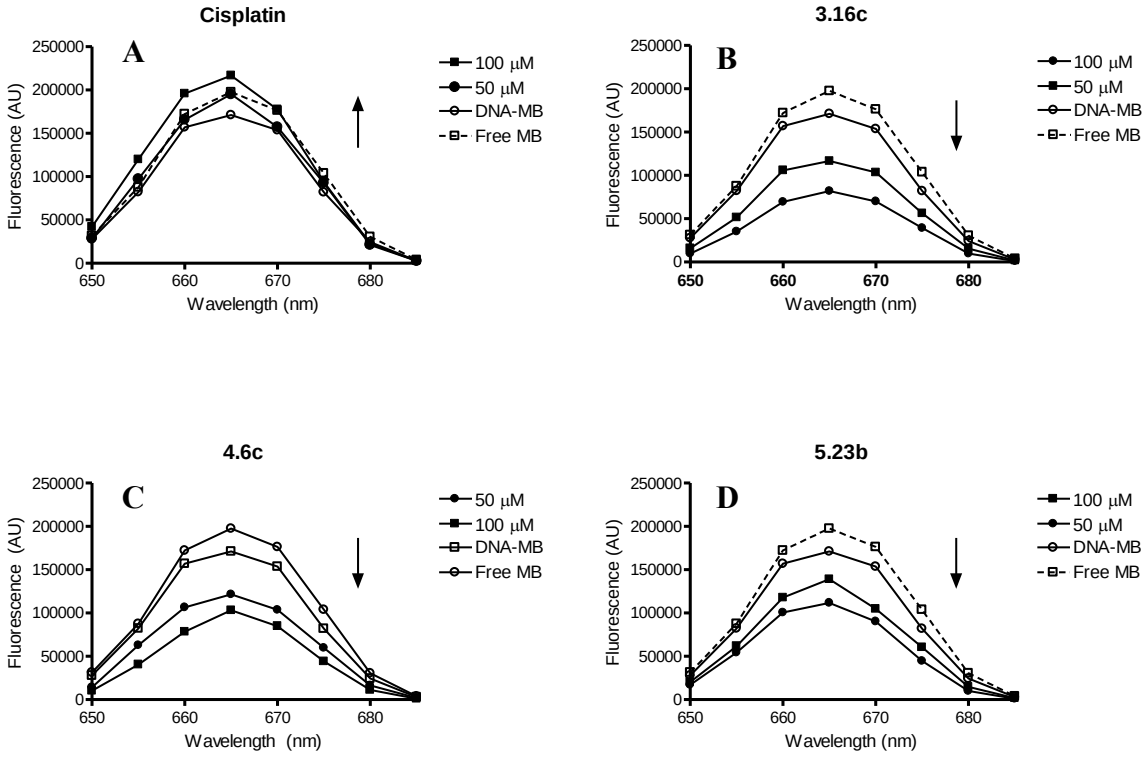

Figure 7.5 Results of the methylene blue assay for competitive DNA intercalation.

As illustrated in **Figure 7.5A**, cisplatin (–●–50 and –■–100 μM) intensified the fluorescence of the DNA-methylene blue adduct (–○–DNA-MB) in a dose-dependent manner by 31 – 36% around the maximum (665 nm), which was indicative of the exclusion of intercalated methylene blue molecules from the complex.

On the other hand, all the test compounds **3.16c**, **4.6c** and **5.23b** attenuated the fluorescence emission of the DNA-methylene blue complex (--□--DNA-MB) by approximately 45 – 60% (**Figure 7.5B-D**). The lower fluorescence of the test samples treated with the compounds (–●– 50 and –■–100 μM) compared to the DNA-methylene blue complex (--□--DNA-MB) suggests that the compounds do not compete with methylene blue for DNA interaction and can be confidently dismissed as DNA intercalators.

Attention was subsequently turned to investigating the compounds for possible DNA groove binding affinity by making use of a known DNA minor groove binder dye, Hoechst 33342.[7b] The Hoechst 33342 dye produces a strong fluorescence emission at 460 – 485 nm when bound to DNA.[10] In the presence of a competitive minor groove binder this emission gets quenched as the compound competitively replaces the DNA-bound dye molecules, thereby lowering fluorescence intensity of the DNA-Hoechst complex. The *N,N*-bis(2-hydroxybenzyl)ferrocenemethylamine **3.16p** was included in the assay for comparison. The results of the Hoechst 33342 assay for competitive DNA minor groove binding are illustrated in **Figure 7.6**.

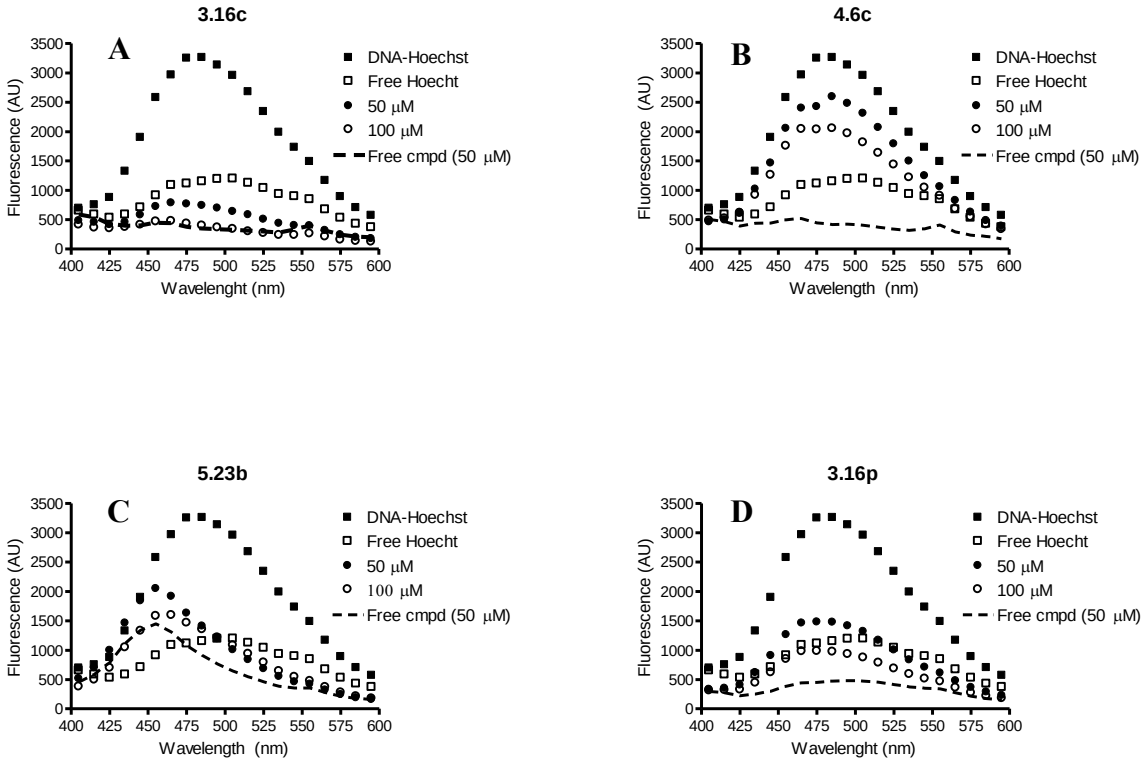

Figure 7.6 Results of competitive minor groove binding using Hoechst 33342.

In all instances, the intense band of the DNA-Hoechst complex (■DNA-Hoechst) was reduced upon addition of the test compounds (●50 and ○100 μM) (**Figure 7.6**). This reduction appeared to increase with the concentration of the compounds and was accompanied by a slight blue shift. For example, 50 μM of the benzoxazine **3.16c** resulted in 75% reduction of the DNA-Hoechst complex peak, while 100 μM completely attenuated the signal producing fluorescence that was comparable to the free compound without DNA (--Free cmpd (50 μM)) (**Figure 7.6A**). The observed quenching of the DNA-Hoechst adduct suggests that the compounds compete with the Hoechst 33342 dye molecules for binding to the DNA minor groove. The percentages by which the fluorescence of the complex was reduced by 100 μM of each compound are illustrated in **Table 7.2** alongside the binding constants (Kb) determined by UV-Vis and their inhibitory activity against the mammalian HCC70 cancer cell line.

Table 7.2 Percentage fluorescence quenching of compounds **3.16c**, **4.6c**, **4.17b** and **3.16p**.

Compound	Fluorescence quenching at 100 µM (%)	UV-Vis K_b (M^{-1})	HCC70 IC_{50} (µM)
3.16c	132	12.03×10^3	11.0
4.6c	49	1.480×10^6	6.67
4.17b	73	143.5×10^3	12.7
3.16p	100	–	111.3

There was no correlation between the capacity of the compounds to compete with Hoechst 33342 for DNA minor groove binding, as qualitatively assessed by percentage fluorescence quenching, and their experimental binding constants and biological activity against the HCC70 cancer cell line (**Table 7.2**). However, it is clear from the presented data that the tested compounds interact with DNA by binding to the minor groove. Thus, it was concluded that the investigated ferrocenyl 1,3-benzoxazine derivatives are DNA minor groove binders as demonstrated by the findings of this study.

7.1.3. DNA binding affinity studies for determining preferential binding between mammalian and malarial DNA

During the *in vitro* biological evaluation assay, it was noted that the investigated compounds possessed higher efficacy against the parasitic *P. falciparum* strains (3D7 and Dd2) than the mammalian HCC70 breast cancer cell line. For instance, compound **3.16c** from the ferrocenyl 1,3-benzoxazine series had sub-micromolar IC_{50} values of 0.261 and 0.599 µM against the 3D7 and Dd2 strains of the *P. falciparum* parasite compared to the low-micromolar activity of 11.0 µM against the mammalian HCC70 cell line (**Chapter 3**). Additionally, the compounds did not show significant toxicity effects when assessed for general cytotoxicity on the mammalian

HeLa cells. This suggested that the investigated ferrocenyl 1,3-benzoxazine derivatives are more selective for the parasitic *P. falciparum* cells than the mammalian cells.

To investigate the possible factors driving the observed selectivity of the compounds for the *P. falciparum* parasite over the mammalian cancer cell line, ferrocenyl 1,3-benzoxazine **3.16c** and α-amino-*o*-cresol **4.6c** were evaluated for preferential DNA binding affinity between the mammalian calf-thymus DNA and malarial DNA isolated from 3D7 *P. falciparum* parasites. Due to the low concentration of isolated 3D7 *P. falciparum* DNA, the Hoechst 3334-mediated minor groove binding assay was employed to assess the selectivity in DNA binding of the compounds for mammalian and malarial DNA since it more sensitive than the UV-Vis titration experiment. This was justified since the compounds had already been verified confirmed as DNA minor groove binders above. The assay was carried out as previously described with minor modifications. In the assay a DNA concentration of 2.5 ng/μL of either mammalian calf thymus DNA (CT) or 3D7 *P. falciparum* DNA (3D7) and Hoechst 33342 (1 μg/mL) were incubated with varying concentrations of the test compound (**3.16c** or **4.6c**): 0 (DMSO control), 5 and 15 μM. Fluorescence of the test samples was recorded after 15 minutes as before. The results of the assay are illustrated in **Figure 7.7**.

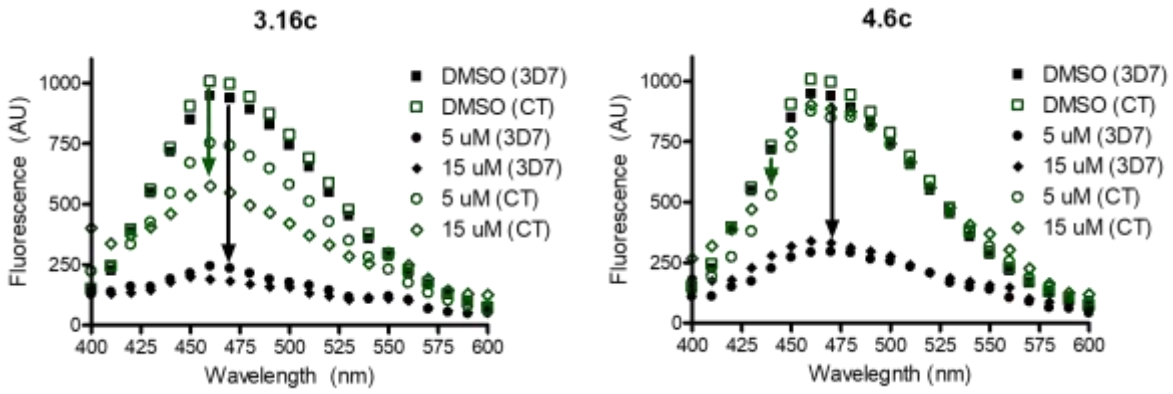

Figure 7.7 Results of the Hoechst assay for selective binding between mammalian (CT) and malarial (3D7) DNA.

Both compounds (**3.16c** and **4.6c**) showed a higher reduction in the fluorescence of the samples containing the malarial DNA [DMSO (3D7)] than the mammalian DNA [DMSO (CT)] (**Figure 7.7**). These results suggested that the compounds have higher binding affinity for the DNA isolated from the malaria parasite, 3D7 *P. falciparum*, than mammalian DNA. The percentage fluorescence quenching of the malarial (3D7) and calf thymus (CT) DNA samples by compounds **3.16c** and **4.6c** at 15 μM together with their *in vitro* antiplasmodial and anticancer activities are displayed in **Table 7.3**.

Table 7.3 Percentage fluorescence quenching of ferrocenyl 1,3-benzoxazine **3.16c** and α-amino-*o*-cresol **4.6c** against malarial (3D7) and calf thymus (CT) DNA.

Compound	% Fluorescence quenching at 15 μM		IC_{50} (μM)		
	3D7 DNA	CT DNA	3D7	Dd2	HCC70
3.16c	85	46	0.261	0.599	11.0
4.6c	74	11	1.6	nd	6.67

nd = not determined

The higher percentage fluorescence quenching by compounds **3.16c** and **4.6c** of the malarial DNA sample than the mammalian DNA at the tested concentration seems to be correlated to their higher antiplasmodial activities compared to the anticancer inhibitory effects (**Figure 7.7**). The demonstrated preferred binding affinity of the compounds for the malarial DNA *vis-à-vis* mammalian DNA could explain their higher selectivity for the *P. falciparum* parasites than the mammalian HCC70 cancer cell line.

In order to accurately quantify the differences in selective binding affinity of the compounds between mammalian and malarial DNA, a wider concentration range of compound **3.16c**, i.e., 0, 1, 2, 5, 10, 15 and 20 μM, were incubated with 2.5 ng/μL of calf thymus and 3D7 *P.*

falciparum DNA in the presence of Hoechst 33342, and the fluorescence was assessed as before. The treatment of mammalian and malarial DNA with compound **3.16c** produced a dose-dependent decrease in fluorescence of the test samples (**Figure 7.8A** and **7.8C**). The obtained data points were fitted into the Stern–Volmer equation (2), relating fluorescence quenching to compound concentration, to obtain the respective binding constants of compound for each DNA type (**Figure 7.8B** and **78D**):

$$\log \frac{F_o - F}{F} = n \times \log[C] + \log K_b \qquad (2)$$

where F_o is the fluorescence of the DNA-Hoechst complex not containing the compound (i.e., DMSO control), F is the fluorescence of the sample at varying compound concentration [C] and n is the binding stoichiometry.[11] The binding constant (K_b) of the compound was determined as the antilogarithm of the y-intercept of the obtained plot.

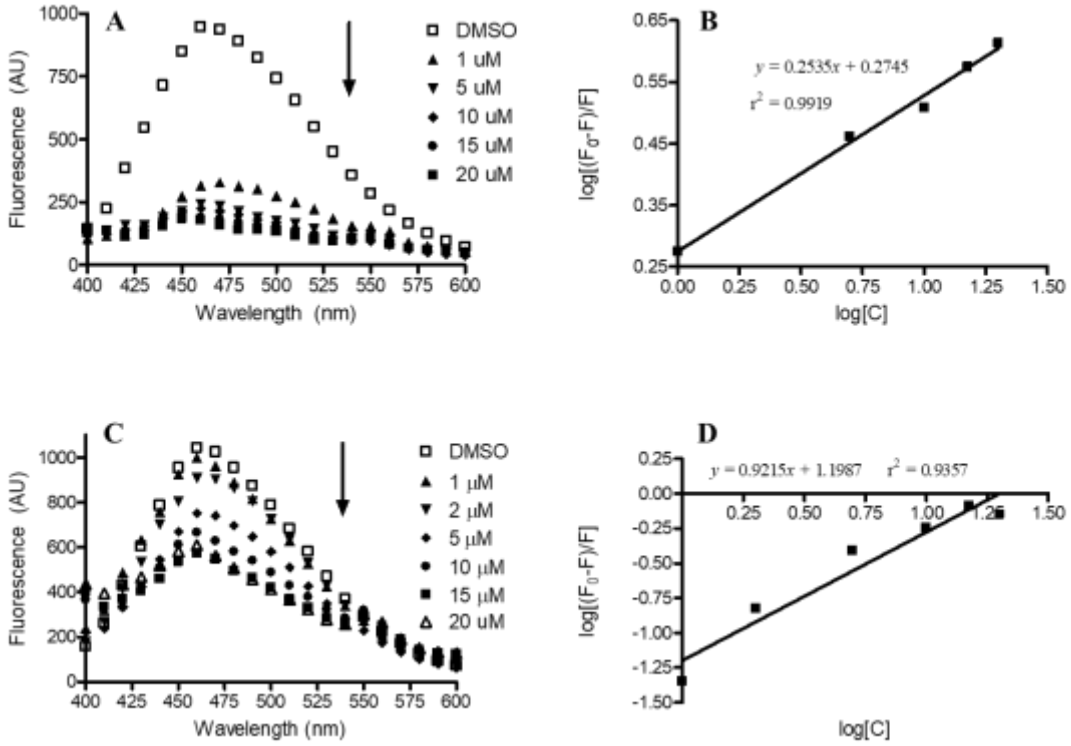

Figure 7.8 Results of selective DNA binding affinity of compound **3.16c** for (**A**) 3D7 *P. falciparum* malarial and (**C**) calf thymus mammalian DNA. Stern–Volmer plots relating fluorescence quenching of the 3D7 *P. falciparum* malarial (**B**) and calf thymus mammalian DNA (**D**) by compound **3.16c**.

As illustrated in **Figure 7.8A** and **7.8C**, compound **3.16c** caused a significant decrease in the fluorescence of the 3D7 *P. falciparum* malarial DNA sample relative to the mammalian calf thymus DNA sample. This is clearly demonstrated by the determined superior binding constant of **3.16c** against the malarial DNA, which was approximately 30 times higher than the binding constant on the mammalian DNA (**Table 7.4**).

Table 7.4 DNA binding constants of ferrocenyl 1,3-benzoxazine **3.16c** against malarial 3D7 *P. falciparum* DNA and mammalian calf thymus DNA determined by the Hoechst 33342 competitive fluorescence assay.

Compound	Binding constant (M^{-1})		IC_{50} (μM)		
	3D7 DNA	CT DNA	3D7	Dd2	HCC70
3.16c	1.88×10^{6}	63.3×10^{3}	0.261	0.599	11.0

The difference in the binding affinity of the tested compound for the malarial DNA than the mammalian DNA appears to be associated to biological activity of the compound. Compound **3.16c** showed *in vitro* antiplasmodial activity against the 3D7 *P. falciparum* strain that was ~42 times more potent than the anticancer efficacy on the HCC70 cancer cell line (**Table 7.4**). In addition to providing explanation for the observed selectivity of the compounds for the *P. falciparum* parasite over mammalian cells, these findings support the hypothesis that the investigated ferrocenyl 1,3-derivatives exert biological activity via DNA interactions, among other possible modes of action.

7.2. DNA damage studies the comet assay

Up to this point, spectroscopic models have been used to exhibit DNA binding as a possible mode by which the compounds elicit biological activity. It is important to note that the models employed above are based on an isolated DNA sample and are performed outside the cell, and do not take into account factors such as cell penetrating ability and lipophilicity of the compound and other pharmacological aspects that may interfere with DNA interaction inside an intact cell. With this in mind, it was considered prudent to validate the effects of DNA

binding interaction of compound **3.16c** by investigating its ability to cause DNA damage in intact HCC70 cells using the comet assay.

In the comet assay, live cells are treated with the compound being tested for DNA damage. After incubation, the cells are lysed and electrophorized on an agarose gel using an appropriate voltage. If the tested compound induces DNA damage, the DNA fragmentation induced by the treatment will result in a different migration pattern to intact DNA on the agarose gel, leading to a smear of DNA fragments which give rise to the comet-like appearance of cells with DNA damage after cell staining and visualization under a microscope. By examining shape and intensity of the visualized comet images showing the damaged DNA on the gel slides, the extent of DNA damage can be quantified using appropriate cell image analysis software such as ImageJ. The full procedure for the comet assay is described in the experimental section in **Chapter 9**.

In the current study, HCC70 cells were cultured similarly to the anticancer evaluation assay and incubated for six hours with the test compounds and DMSO (negative control), and one hour with the positive control hydrogen peroxide (H_2O_2). Compound **3.16f**, which is an inactive congener of **3.16c** bearing a neutrophilic NO_2 group in place of Cl at C-6, was included in the assay for comparison and to gain insights into the effects of lipophilicity on DNA damage, while H_2O_2 and DMSO were employed as positive and negative controls, respectively. Following incubation of cells with the test compounds, it was observed that **3.16c** significantly reduced cell growth, with **3.16f** exerting lower antiproliferative effects, which was in agreement with the previous observation regarding the anticancer potency of the compounds discussed in **Chapter 3**: **3.16c** > **3.16f** (**Table 3.2**). As a result, the culture treated with **3.16c** had the lowest average cell count compared to **3.16f** and the positive control H_2O_2. Similarly, upon visualizing the cells after electrophoresis and fluorescent staining, the sample of compound **3.16c** displayed more pronounced and intense comets *vis-à-vis* compound **3.16f** and

H_2O_2, whereas the DMSO sample contained almost completely intact nuclei, with only minimal shadow tails visible. The results of the comet assay are illustrated in **Figure 7.9**.

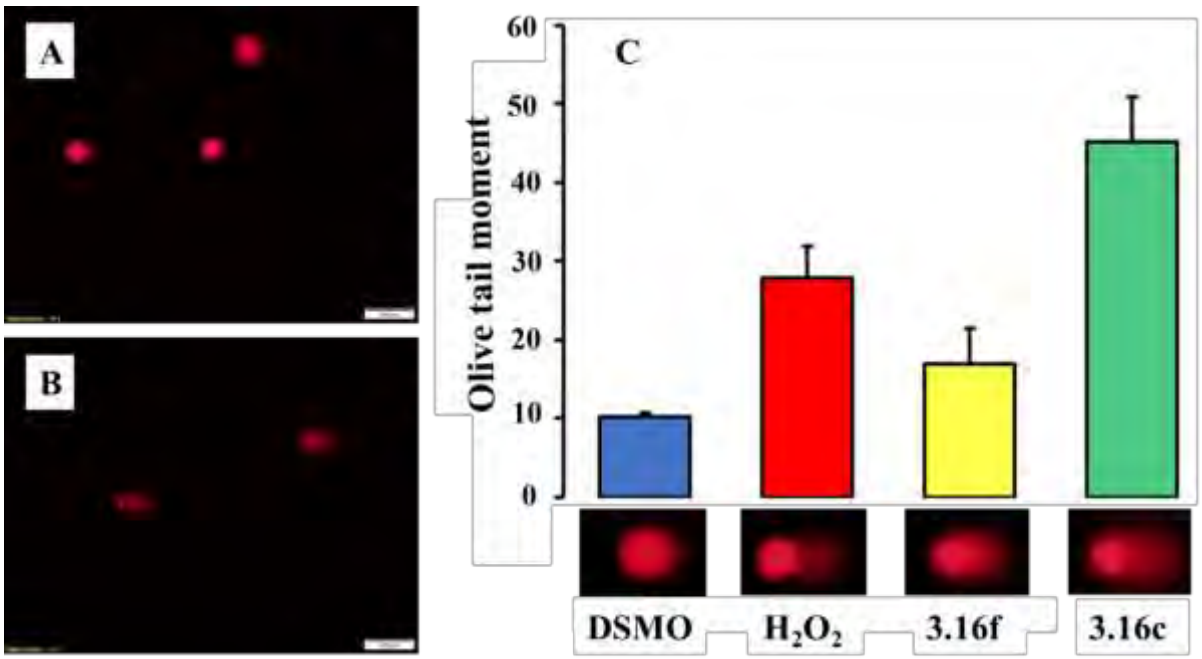

Figure 7.9 Assessment of DNA damage induced by novel benzoxazines in HCC70 breast cancer cells using the comet assay. (**A**) Comet images of DMSO and (**B**) **3.16c** treated cells showing corresponding DNA damage visualized at 10× magnification with an OLYMPUS BX60 fluorescence microscope fitted with a DP72 camera using a U-MWG green fluorescent filter cube (WG). (**C**) Bar graph of the average Olive tail moments of HCC70 cells treated with DMSO (negative control), H_2O_2 (positive control) and test compounds **3.16f** and **3.16c**. A total of 25 – 30 nuclei for each treatment were assessed and DNA damage was quantified using the Opencomet plugin in Image J. The data are presented as average Olive tail moments which is defined as the product of DNA percentage in comet tails and the distance between intensity-weighted centroids of tail and head.[12] The error bars represent standard deviation (±SD). Inset: cropped comet images of nuclei of HCC70 cells treated with the controls and test compounds.

As illustrated in **Figure 7.9**, the oxidative DNA damaging H_2O_2 positive control showed a higher average Olive tail moment value than DMSO by almost 3-fold, validating the assay. Compound **3.16c** exhibited the highest DNA damage with the most intense and defined comets (**Figure 7.9C**, inset) and displayed an Olive tail moment that was twice as high as that of **3.16f**. Looking at the preliminary structure-activity relationship trends of the anticancer activity of the compounds (**Table 3.2**), despite being structurally similar with both analogues containing electron-withdrawing groups (Cl and NO_2) which differ in lipophilicity, only the more lipophilic congener **4c** was efficacious against the cell line and caused significantly higher DNA damage compared to the lesser lipophilic **3.16f**. It seems reasonable to propose that the lack of activity of **3.16f** is a result of its low lipophilicity and limited ability to permeate the cells.[13] Being the most potent compound against the HCC70 cell line from the benzoxazine series **(Table 3.2**), the high DNA damaging ability of **3.16c** appeared to be linked to its observed anticancer activity. It is clear from these observations that the mechanism of action of compound **3.16c** likely involves DNA interaction with the minor groove resulting in DNA damage. Given that the representatives from other series of compounds investigated in the study exhibited DNA binding mode similar to compound **3.16c**, it seems reasonable to propose that their DNA binding affinity likely results in DNA damage as demonstrated by compound **3.16c**.

7.3. β-Hematin binding assay for hemozoin inhibition

During the asexual stages of the malaria in the human host, the parasite digests human haemoglobin to meet its iron needs for viability. Consumption of haemoglobin by the parasites leads to concomitant formation the haem complex, which is toxic to the parasite.[14] To counter the detrimental effects of the formed haem complex, the malaria parasite bio-crystallizes this complex into its non-toxic polymeric form known as hemozoin.[15] Several antimalarial drugs

are known to target this process by binding to the forming hemozoin crystal to prevent further detoxification of the haem complex, thereby leading to more accumulation of this toxic complex.[16] This leads to damage of the parasite, which eventually leads to its death. Hemozoin inhibition is the mechanism by which many antimalarial drugs exert biological activity.[17]

Given that the explored compounds possessed higher potency for the *P. falciparum* strains compared to the HCC70 cancer cell line, we directed our attention to the investigation of compounds for potential hemozoin inhibition activity using a synthetic form of the haem complex, β-hematin. The β-hematin inhibition assay was conducted according to the procedure developed by Egan and Ncokazi.[18] Briefly, a solution of β-hematin in HEPES and acetate buffers mimicking physiological conditions was treated with varying concentrations of the test compounds and hemozoin formation was induced by addition a detergent (NP-40). The samples were incubated for 6 hours after which the absorbance of the samples was recorded at the β-hematin maximum wavelength. The inhibition of hemozoin was quantified by fitting the obtained data points into the sigmoidal plot relating compound concentration to absorbance and was recorded as IC_{50} values, i.e., minimum compound concentration required to inhibit conversion of β-hematin into hemozoin by 50%. Full details of the assay are described in the experimental section in **Chapter 9**.

In the current study, compounds **3.16c**, **4.16c** and **5.23b** from the ferrocenyl 1,3-benzoxazine, α-amino-*o*-cresol and aminomethylcoumarinol series were investigated for potential hemozoin inhibition. These compounds emerged as most promising antiplasmodial analogues from their respective series in the *in vitro* screening assays. An established hemozoin-inhibiting antimalarial drug, chloroquine (CQ) was used a positive control in the assay, while DMSO served as the negative control. Commercially available hematin isolated from porcine was used as the source of the haem complex. The results of the study are illustrated in **Figure 7.10**.

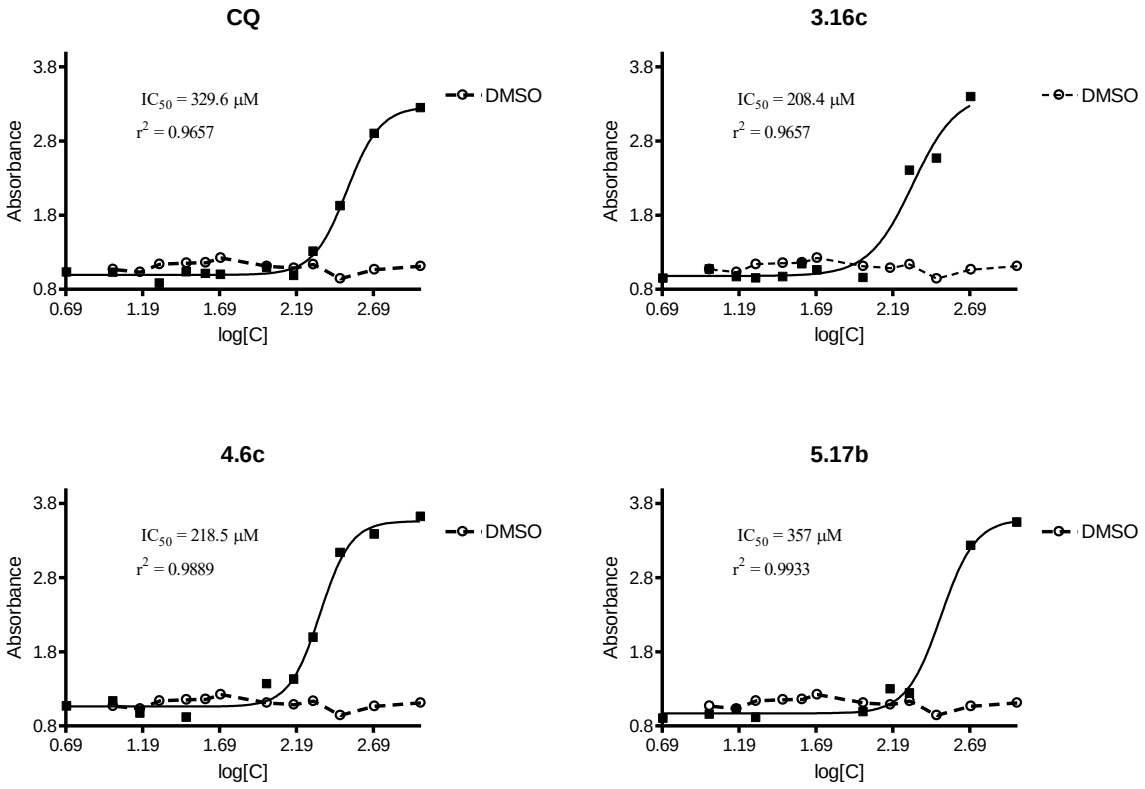

Figure 7.10 Hemozoin inhibition results for chloroquine (**CQ**), **3.16c**, **4.6c** and **5.23b**.

All the tested compounds exhibited IC_{50} values comparable to chloroquine for hemozoin inhibition (**Figure 7.10**). Compound **3.16c** which also emerged as the most promising member from the ferrocenyl 1,3-benzoxazine series possessed the most inhibition activity among the tested compounds. The order of increasing inhibition was: **3.16c** > **4.6c** > **CQ** > **5.23b**. When presented alongside the antiplasmodial activity of the compounds and chloroquine, there seemed to be a correlation between the observed hemozoin inhibition and antiplasmodial data of the compounds (**Table 7.4**). For instance, 8-aminomethylcoumarin-7-ol **5.23b** possessing the least potent hemozoin inhibitory activity (IC_{50} = 356 µM) was not active against the Dd2 *P. falciparum* strain, while benzoxazine **3.16c** displayed superior inhibitory activity against both hemozoin (IC_{50} = 208.4 µM) and the *P. falciparum* parasite (IC_{50} = 0.599 µM). These observations would imply that the attained hemozoin inhibition data is related to the antiplasmodial activity of the compounds. However, this fails to explain the lower hemozoin

inhibition activity of chloroquine (IC_{50} = 326.6 μM) relative to its potent antiplasmodial activity (IC_{50} = 0.188 μM) especially given that it is verified strong hemozoin inhibitor whose activity is directly linked to the inhibition of this complex.[19]

Table 7.4 Hemozoin inhibition results for compounds **3.16c**, **4.6c** and **5.23b**.

Compound	Hemozoin inhibition IC_{50} (μM)	Antiplasmodial activity IC_{50} (μM)	
		3D7	Dd2
3.16c	208.4	0.261	0.599
4.6c	218.5	1.6	0.689
5.23b	357	1.7	na
CQ	326.6	0.03	0.188

na = not active

Chloroquine usually displays IC_{50} values in the low to mid-micromolar range when assessed for hemozoin inhibitory activity using β-hematin isolated from bovine.[2a,18,20] In our case, β-hematin isolated from porcine was used in the assay. The difference in the type of β-hematin used in the assay could explain the lower hemozoin inhibitory activity of the chloroquine observed in the current study. Notwithstanding this fact, the inhibition assay conducted in the study clearly indicates that the compounds interact with β-hematin to prevent its polymerization into hemozoin despite the uncertainties in the correlation between these interactions and the observed antiplasmodial activities. Therefore, in addition to the experimentally determined DNA binding affinity of the compounds presented above, these findings about hemozoin inhibition provide an additional insight about mode of action by which the explored compounds exert biological activity. This could explain the higher selectivity of the compounds for the *P. falciparum* parasite, in which they can act by inhibiting

hemozoin formation in addition to DNA binding interactions, than the mammalian HCC70 cancer cell line.

7.4. Computer-aided docking simulations for DNA binding interactions

To support the experimental DNA binding affinity studies performed by UV-Vis and fluorescence spectroscopic titration techniques, the *(S)*-planar enantiomer of most promising compound **3.16c** was investigated for DNA binding interactions *in silico* against a B-DNA structure (PDB: 129D) as the receptor co-crystallized with the minor groove binder, Hoechst 33342. The *in silico* docking simulations were performed with AutoDock Vina in UCSF Chimera 1.13.1 and the interactions were visualized in Discovery Studio Visualizer (Dassault Systèmes BIOVIA, Discovery Studio 2019 Client, Sandiego: Dassault Systèmes, 2019).[21] The DNA receptor was prepared with Dock Prep in UCSF Chimera 1.13.1 by eliminating the crystallization waters and removing the bound co-ligand. The structure of ligand *(S)*-**3.16c** was constructed and minimized in Chem3D Pro 12.0 (minimum RMS gradient: 0.010) before further conformational optimization with default parameters in UCSF Chimera 1.13.1. Simulation parameters of the docking model were confirmed by re-docking the isolated Hoechst 33342 co-ligand structure into the prepared, uncomplexed DNA receptor, which fitted into the minor groove similarly to the original co-crystal structure, with a binding score of –10.2 kcal/mol (**Figure 7.11**).

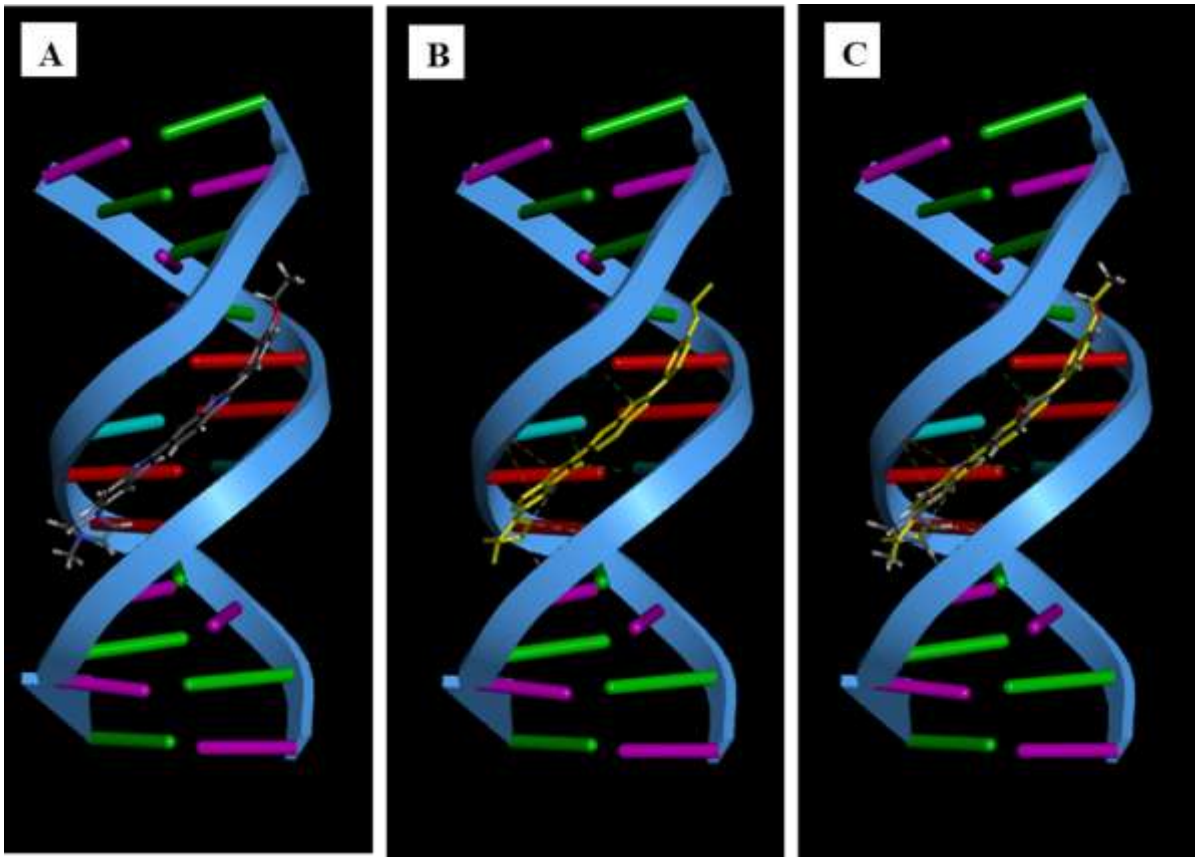

Figure 7.11 Images of Hoechst 33324 in the DNA minor groove. (**A**) Co-crystal structure of DNA with Hoechst 33342 in the minor groove as acquired from PDB before the docking simulation. (**B**) Structure of Hoechst 33342 re-docked to the DNA minor groove after the docking simulation. (**C**) Overlapping structures of both 'native' Hoechst 33324 and its computer generated re-docked conformer (yellow) in the DNA minor groove, respectively, before and after docking simulation.

All the predicted binding orientations of *(S)*-**3.16c** exclusively docked to the minor groove of the DNA receptor in the simulation (**Figure 7.12**) with binding scores of at least – 5.0 kcal/mol, symbolic of stable interactions.[22] This supports the experimental findings of compound **3.16c** as a DNA minor groove binder.

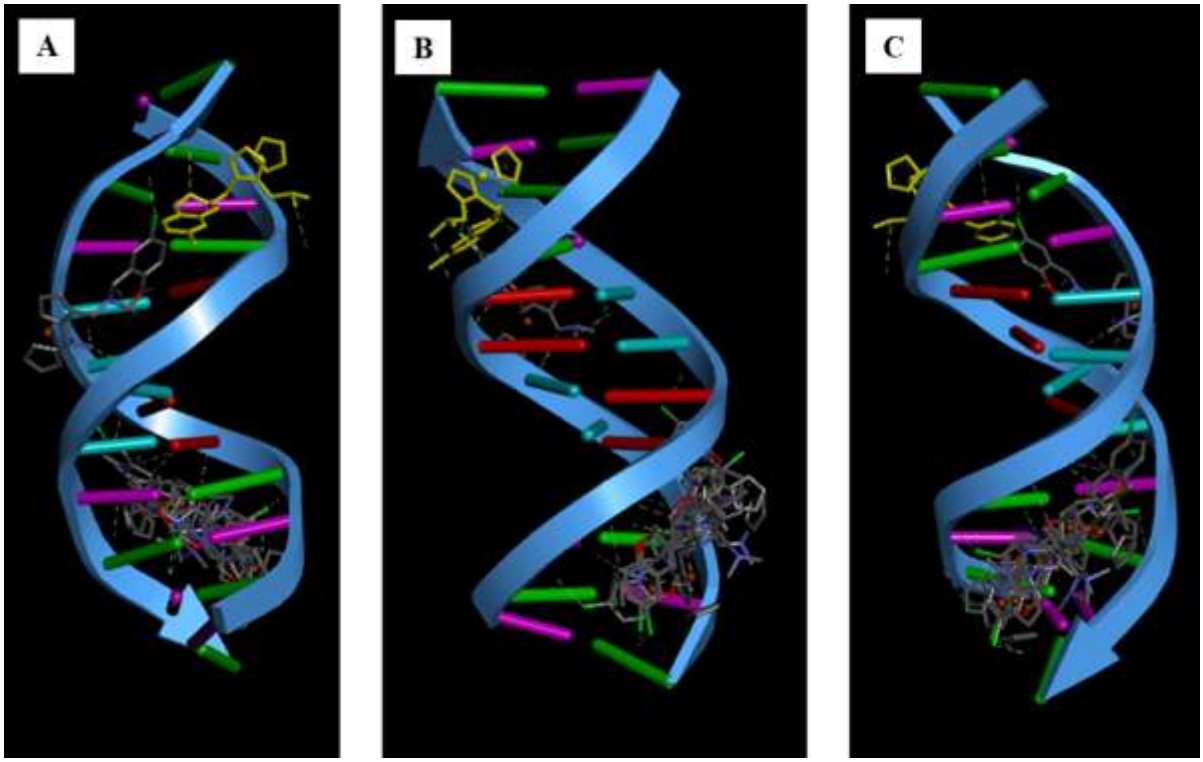

Figure 7.12 Predicted conformations of *(S)*-**3.16c** bound to the DNA minor groove in the docking simulation (**A-C**). The most stable conformation is highlighted in yellow. The receptor grid was placed across the entire DNA structure for the docking simulation.

The structure of the most stable conformation of *(S)*-**3.16c** bound to the DNA minor groove binder and showing the binding interactions is shown in **Figure 7.13**. The stabilizing interactions of the compound-DNA complex were predicted to be primarily non-covalent in the simulation, as shown by non-classical carbon hydrogen bonding (C-H···O) of the ligand with the cytosine oxygen from strand A (A: Cyst11) and deoxyadeninosine monophosphate (dAMP) residue in strand B (B: Ade17) of the DNA backbone through the oxazine unit (3.68 Å) and the ferrocenyl methyl(dimethylamine) sidechain (3.58 Å and 3.57 Å), respectively (**Figure 7.13C**).

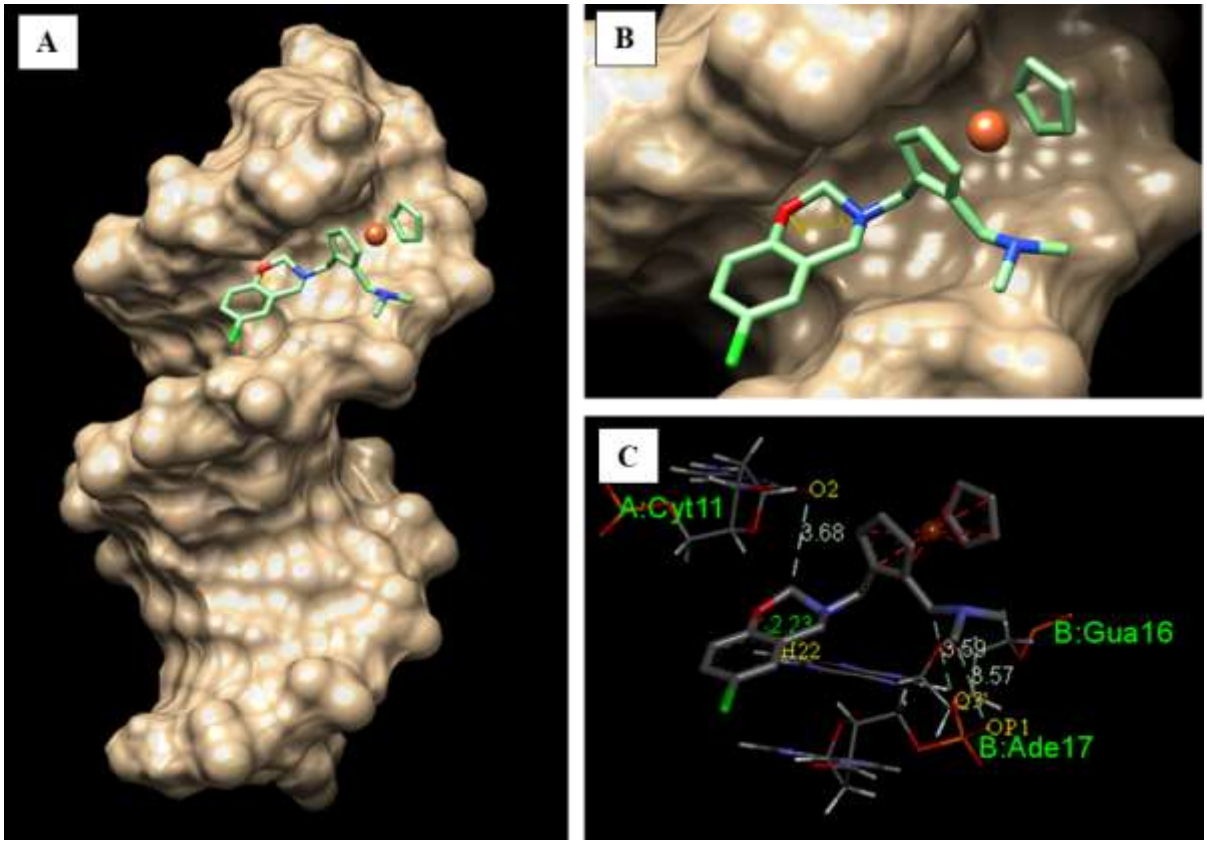

Figure 7.13 Simulated *(S)*-enantiomer of **3.16c** docked to the DNA minor groove. (**A**) Full view and (**B**) zoomed-in DNA surface images with **3.16c** in the minor groove. (**C**) Stick model of *(S)*-**3.16c** bound to the minor groove showing ligand-receptor interactions (dotted lines) with the DNA nucleotide residues.

Most importantly, this most stable DNA-ligand adduct with a binding score of – 7.5 kcal/mol exhibited classical hydrogen bonding (green dotted line: O1···H22; 2.23 Å) between the ligand oxazine oxygen and the guanine DNA base (B: Gua16) (**Figure 7.13C**), adding further stabilization to the adduct. Participation of both the oxazine oxygen and adjacent methylene carbon C2 of the O-CH_2-N linkage and the ferrocenyl CH_2NMe_2 sidechain in the ligand-receptor interactions further highlights the influence of these structural units on the biological activity of ferrocenyl 1,3-benzoxazines. Although inferior, the binding score of **3.16c** (– 7.5 kcal/mol) was in the same range as the re-docked co-crystallized ligand Hoechst 33342 (– 15

≤ *score* < – 5 kcal/mol) and both compounds were found to be exclusive minor groove binders in the simulation. These data validate compound **3.16c** as a DNA minor groove binder.

7.5. Overall summary and conclusions

As phenolic Mannich base derivatives, the ferrocenyl 1,3-benzoxazine derivatives explored in the study were proposed to exhibit similar pharmacological profile as other Mannich base compounds reported in literature. DNA interaction is one of the many mechanistic modalities by which Mannich bases elicit biological activity. Herein, we investigated the ferrocenyl 1,3-benzoxazine derivatives for DNA binding interactions using spectroscopic techniques: UV-Vis and fluorescence spectroscopy. All the tested compounds were found to possess DNA affinity by binding to the minor groove. The effects of DNA binding interactions of the compounds were investigated by assessing representative compound **3.16c** for its ability to induce DNA damage in HCC70 cancer cells using the comet assay, which was found to be the case. The spectroscopic DNA titration experimental results were supported by computational docking studies of compound **3.16c** to a B-DNA structure as the biomolecular receptor, which revealed minor groove binding.

Furthermore, compounds **3.16c** and **4.6c** were tested for selective binding between malarial and mammalian DNA. It was demonstrated that these compounds exhibited preferential binding for the DNA isolated from the 3D7 *P. falciparum* parasite over the mammalian calf thymus DNA. These findings corroborated the higher antimalarial efficacy of the compounds compared to the inhibition of the mammalian tumour cells, i.e., triple-negative HCC70 cancer cell line. In addition to DNA binding affinity, the compounds were found to block hemozoin formation as assessed by the detergent-mediated β-hematin binding assay, further supporting the preferred inhibitory activity of the compounds for the malaria parasite, *P. falciparum*. Collectively, these results appear to suggest that the ferrocenyl 1,3-benzoxazine derivatives

explored in this project may possess a dual mode of action for antiplasmodial activity involving DNA binding interactions and hemozoin inhibition.

In summary, using DNA binding experiments we have demonstrated that the anticancer activity of the explored compounds involves DNA binding interactions resulting in DNA damage. On the other hand, the antiplasmodial activity of the compounds was shown to be also associated with hemozoin inhibition in addition to DNA binding interactions.

References

(1) (a) Dimmock, J.; Kumar, P. *Curr. Med. Chem.* **1997**, *4*, 1; (b) Roman, G. *Eur. J. Med. Chem.* **2015**, *89*, 743.

(2) (a) Wenzel, N. I.; Chavain, N.; Wang, Y.; Friebolin, W.; Maes, L.; Pradines, B.; Lanzer, M.; Yardley, V.; Brun, R.; Herold-Mende, C. *J. Med. Chem.* **2010**, *53*, 3214; (b) Abdelhafez, O. M.; Abedelatif, N. A.; Badria, F. A. *Arch. Pharmacal Res.* **2011**, *34*, 1623; (c) Di Salvo, A.; Dugois, P.; Tandeo, D.; Peltekian, M.; Lin, P. K. T. *Eur. J. Med. Chem.* **2013**, *69*, 754.

(3) Sirajuddin, M.; Ali, S.; Badshah, A. *J. Photochem. Photobiol. B* **2013**, *124*, 1.

(4) (a) Shahabadi, N.; Hadidi, S. *Spectrochim. Acta A* **2012**, *96*, 278; (b) Saito, S. T.; Silva, G.; Pungartnik, C.; Brendel, M. *J. Photochem. Photobiol. B* **2012**, *111*, 59.

(5) Reddy, K. L.; Kumar, K. A.; Satyanarayana, S. *Synth. React. Inorg. M.* **2011**, *41*, 182.

(6) Mbaba, M.; Dingle, L. M. K.; Cash, D.; de Lamare, J.-A.; Laming, D.; Taylor, D.; Hoppe, H. C.; Edkins, A. L.; Khanye, S. D. **2019**. Repurposing of a polymer precursor: Synthesis and in vitro medicinal potential of ferrocenyl 1,3-benzoxazine derivatives Accepted manuscript: *Eur. J. Med. Chem*. https://doi.org/10.1016/j.ejmech.2019.111924

(7) (a) Vardevanyan, P.; Antonyan, A.; Parsadanyan, M.; Shahinyan, M.; Hambardzumyan, L. *J. Appl. Spectrosc.* **2013**, *80*, 595; (b) Bucevičius, J.; Lukinavičius, G.; Gerasimaitė, R. *Chemosensors* **2018**, *6*, 18.

(8) Gąsior-Głogowska, M.; Malek, K.; Zajac, G.; Baranska, M. *Analyst* **2016**, *141*, 291.

(9) Todd, R. C.; Lippard, S. J. *J. Inorg. Biochem.* **2010**, *104*, 902.

(10) Sandhu, L. C.; Warters, R. L.; Dethlefsen, L. A. *Cytometry A* **1985**, *6*, 191.

(11) Shahabadi, N.; Hadidi, S.; Taherpour, A. A. *Appl. Biochem. Biotechnol.* **2014**, *172*, 2436.

(12) Gyori, B. M.; Venkatachalam, G.; Thiagarajan, P.; Hsu, D.; Clement, M.-V. *Redox Biol.* **2014**, *2*, 457.

(13) Sagawa, N.; Shikata, T. *Phys. Chem. Chem. Phys.* **2014**, *16*, 13262.

(14) Foley, M.; Tilley, L. *Pharmacol. Ther.* **1998**, *79*, 55.

(15) Hempelmann, E. *Parasitol. Res.* **2007**, *100*, 671.

(16) Kumar, A.; Katiyar, S.; Agarwal, A.; Chauhan, P. *Curr. Med. Chem.* **2003**, *10*, 1137.

(17) Coronado, L. M.; Nadovich, C. T.; Spadafora, C. *Biochim. Biophys. Acta* **2014**, *1840*, 2032.

(18) (a) Ncokazi, K. K.; Egan, T. J. *Anal. Biochem.* **2005**, *338*, 306; (b) Lu, W.-J.; Wicht, K. J.; Wang, L.; Imai, K.; Mei, Z.-W.; Kaiser, M.; El Sayed, I. E. T.; Egan, T. J.; Inokuchi, T. *Eur. J. Med. Chem.* **2013**, *64*, 498.

(19) (a) Orjih, A. U.; Fitch, C. D. *Biochim. Biophys. Acta* **1993**, *1157*, 270; (b) Olafson, K. N.; Ketchum, M. A.; Rimer, J. D.; Vekilov, P. G. *Proc. Natl. Acad. Sci. U.S.A.* **2015**, *112*, 4946.

(20) Sandlin, R. D.; Carter, M. D.; Lee, P. J.; Auschwitz, J. M.; Leed, S. E.; Johnson, J. D.; Wright, D. W. *Antimicrob. Agents Chemother.* **2011**, *55*, 3363.

(21) (a) Vina, A. *J. Comput. Chem* **2010**, *31*, 455; (b) Pettersen, E. F.; Goddard, T. D.; Huang, C. C.; Couch, G. S.; Greenblatt, D. M.; Meng, E. C.; Ferrin, T. E. *J. Comput. Chem.* **2004**, *25*, 1605.

(22) Takahashi, O.; Masuda, Y.; Muroya, A.; Furuya, T. *SAR QSAR Environ. Res.* **2010**, *21*, 547.

Chapter 8: General summary, conclusions and recommendations

The 1,3-benzoxazine framework is an eminent chemical scaffold that is endowed with biological activities against a myriad of diseases and is largely represented in literature. On the other hand, introduction of the organometallic ferrocene unit into bioactive chemical moieties has been demonstrated to be an effective strategy for generation of novel bioactive compounds possessing appealing medicinal attributes. Despite the pharmacological relevance of the 1,3-benzoxazine motif, only a handful accounts of ferrocenyl 1,3-benzoxazines have been presented in literature solely for polymer applications. Motivated by the hybridization strategy of amalgamating ferrocene into bioactive chemical scaffolds in designing novel bioactive compounds, the present study sought to extensively explore the potential biological activity of 1,3-benzoxazine derivatives bearing the ferrocene unit. The general findings of the study and recommendations for prospective work are presented in this chapter.

8.1. General summary and conclusions

In this research project, the main objective was to explore the medicinal potential of novel compounds based on the ferrocenyl 1,3-benzoxazine scaffold. Thus, novel ferrocenyl 1,3-benzoxazine derivatives (**3.13a-i**, **3.16a-m** and **3.17a-f**) were designed, synthesized and evaluated for their *in vitro* biological activity against the *P. falciparum* strains, chloroquine sensitive (3D7) and multidrug resistant strain (Dd2) and HCC70 triple-negative breast cancer cell line. To examine the influence of structural features of this class of compounds responsible for biological activity, key strategic structural modifications were performed on the oxazine, benzene, ferrocene and the methylene linker units of the parent scaffold. These modifications culminated in the generation of novel ferrocenyl derivatives containing bioactive structural

motifs: i) aminocresol (**4.6a-i**, **4.7a-e**, **4.9a-d**) and salicylamide (**4.15a-e** and **4.16a-b**), ii) benzoxazinone (**4.17a-d**, **4.18a-e** and **4.24a**), iii) naphthalene (**5.2a-b**), benzodioxole (**5.4**) and coumarin (**5.13a-e**, **5.23a-b**, **5.24**, **5.25a-e** and **5.26a-b**), and iv) ethyl carbamates (**6.4a-c**).

Generally, all the compounds pursued in this study were more active against the protozoal parasites than the mammalian HCC70 cell line. The parental ferrocenyl 1,3-benzoxazines **3.13a-i**, **3.16a-m** and **3.17a-f** showed superior *in vitro* anticancer, antiplasmodial and trypanocidal activities to the other achieved series with IC_{50} values in the low and sub-micromolar range. All the compounds from this series showed higher selectivity for the chloroquine resistant Dd2 *P. falciparum* strain relative to the sensitive 3D7 strain. While compound **3.16l** containing a bulky NHBoc group at position 6 emerged as an antimalarial hit (IC_{50} = 0.05 μM (3D7) for **3.16l** vs. IC_{50} = 0.03 μM (Dd2) for chloroquine), compound **3.16c** showed overall superior activities across all three investigated diseases.

The results of the modified series are summarized below:

i) Despite being active in the same range, compounds from the aminocresol and salicylamide series were slightly less active than the parent 1,3-benzoxazines (**3.13a-i**, **3.16a-m** and **3.17a-f**). The basic ferrocenyl α-amino-*o*-cresols (**4.6a-i**, **4.7a-e** and **4.9a-d**) were more active than their salicylamide derivatives (**4.15a-e** and **4.16a-b**) against all three targeted diseases. The 4-bromo-amino-*o*-cresol **4.6c** was the most active compound from this series against the investigated diseases.

ii) The antiplasmodial and trypanocidal activity of the benzoxazinone derivatives (**4.17a-d**, **4.18a-e** and **4.24a**) drastically decreased upon replacement of the O-CH_2-N oxazine linkage with the O-CO-N carbamate unit. However, the presence of this moiety appeared to be conducive for anticancer activity against the triple-negative HCC70 breast cancer

cell line as shown by the higher activity of benzoxazinones (**4.17a-d**) compared to the parent benzoxazines (**3.16a-m**).

iii) Both naphthalene (**5.2a-b**) and benzodioxole (**5.4**) derivatives were less active against the 3D7 *P. falciparum* strain compared to their benzoxazine analogue (**3.16a**). This was also the case for the coumarin variants. Interestingly, the antiplasmodial efficacies of the naphthalene compounds (**5.2a-b**) were more potent compared to benzoxazine **3.16a** with IC_{50} values below 1 μM. Within this series, the naphthoxazines **5.2a-b** and the benzodioxole congener **5.4** were more potent than the coumarins (**5.13a-e**, **5.23a-b**, **5.24**, **5.25a-e** and **5.26a-b**) for antiplasmodial activity. On the other hand, coumarins **5.23c**,**e** and **5.26b** were the only compounds that exhibited antitrypanosomal activity in this series. Notwithstanding, the observed activity was lower than that of parent benzoxazines. Moreover, only naphthoxazine **5.2a** was active against the HCC70 cancer cell line with an IC_{50} value of 14.0 μM. Thus, modifications involving annulation of the benzene unit of the investigated 1,3-benzoxazine scaffold was found to be undesirable for activity.

iv) The benzoxazine derivatives containing the ethyl carbamate spacer (**6.4a-c**) demonstrated both antiplasmodial and anticancer activities that were comparable, albeit slightly lower, to the parental ferrocenyl 1,3-benzoxazine compounds. This suggested that the replacement of the methylene spacer with an ethyl carbamate linker of the ferrocenyl 1,3-benzoxazine scaffold pursued in this study is tolerated for biological activity of the compounds.

Lastly, mechanistic studies involving DNA interaction were conducted to gain insight into the possible mode of action of the compounds studied in this thesis. Using the most promising compound **3.16c** and representative compounds from other series, the studies revealed that the activity of the compounds involves DNA interaction leading to DNA damage. Moreover, compound **3.16c** displayed preferential binding for DNA isolated from 3D7 *P. falciparum*

parasite over the mammalian DNA from calf thymus. Furthermore, the β-hematin binding assay revealed that the compounds presented herein may act by inhibiting the hemozoin pathway of the malaria parasite. Collectively, these data supported the selectivity of the compounds for the malaria parasite, *P. falciparum*, over cancer cells.

In conclusion, by grafting ferrocene into the 1,3-benzoxazine scaffold, a novel class of compounds based on the structural architecture of a polymer precursor, i.e., ferrocenyl 1,3-benzoxazine, has been successfully synthesized, fully characterized and demonstrated to possess *in vitro* anticancer and antiprotozoal activities through DNA interaction and hemozoin inhibition. The presented data suggest that ferrocenyl 1,3 benzoxazines are a class of compounds with a great scope for further exploration as potential anticancer and antimalarial agents.

8.2. Recommendations for future work

This study has demonstrated the pharmacological potential of novel compounds based on the 1,3-benzoxazine scaffold as a polymer precursor. Several hit compounds with appealing antiplasmodial, antitrypanosomal and anticancer activity were identified, and these have to undergo hit validation before being declared leads. To further elaborate the pharmacological profile of these compounds the following studies are recommended for future work: i) *in silico* and *in vitro* ADME assessment of the compounds including stability studies and identification of metabolites and ii) *in vivo* evaluation of the identified lead compounds. Since the possible mode of active of the compounds was demonstrated to involve DNA interaction, additional mechanistic elucidation studies pertaining DNA interaction such as inhibition of the DNA replication machinery are also required.

Lastly, novel ferrocenyl tertiary amines were identified as side products and shown to possess potent biological efficacies. A practical synthetic route to accessing a representative derivative

of this class of compounds was developed but due to time constraints, additional analogues of these compounds could not be pursued further. Thus, synthesis and pharmacological evaluation of the identified novel ferrocenyl tertiary amines is recommended for further exploration.

Chapter 9: Experimental

9.1. General details and instrumentation

All chemicals and solvents used in this study were sourced from Merck (South Africa) and used without further purification. In the case reactions requiring anhydrous condition, the solvents were dried following established solvent drying protocols according to literature methods.[1]

The progress of the reactions was monitored by analytical thin layer chromatography (TLC) using Merck F254 silica gel plates (supported on aluminium sheets) and the plates were visualised under ultraviolet (UV 254 and 366 nm) light and in iodine flask. Where necessary, the crude compounds were purified by column chromatography using Merck Kieselgel 60 Å: 70 – 230 (0.068 – 0.2 mm) silica gel mesh or activated basic Brockmann alumina (Al_3O_4).

The ^{1}H and ^{13}C NMR spectra were recorded on Bruker Biospin 300, 400 or 600 MHz spectrometers, and were referenced internally using residual solvent signals of deuterated DMSO-*d*$_6$: 2.50 ppm for ^{1}H and 39.5 ppm for ^{13}C NMR, or deuterated chloroform $CDCl_3$: 7.26 ppm for ^{1}H and 77.2 ppm for ^{13}C NMR at room temperature. The spectra were processed using MestReNova software. The chemical shifts were reported in parts per million (ppm) and the *J*-coupling constants in Hertz (Hz). The abbreviations used to describe signal multiplicities are: s = singlet, br s = broad singlet, d = doublet, t = triplet, q = quartet, and m = multiplet.

The high-resolution mass spectrometry (HRMS) data were acquired on Waters Synapt G2 Mass Spectrometer (Central Analytical Facility, University of Stellenbosch) using electron impact (EI) ionization in the positive ionization mode, and the IR spectra were recorded on PerkinElmer Spectrum 100 FT-IR Spectrometer in the mid-IR range (640 – 4000 cm^{-1}). Only the HRMS data of compound **4.15c** was recorded in the negative ionization mode (ESI^-). The

HPLC purity of the compounds was determined using a reverse-phase Luna® LC column (5 µM C18, 100 Å, 250 × 4.6 mm i.d.) on an Agilent 1100 Series HPLC instrument fitted with a G1315B diode-array detector (DAD), G1311A quaternary pump, G1322A degasser and a G1328B manual injector. The compounds were run by isocratic elution for a total running time of 8 minutes. The melting points were determined using Reichert melting point apparatus and were uncorrected. The calf thymus DNA was sourced from Thermo Fischer Scientific (South Africa). The UV-Vis and fluorescent spectra for DNA binding assays were recorded on a SpectraMax M3 microplate reader and the comets were visualized with an OLYMPUS BX60 fluorescence microscope mounted with a DP72 camera using a U-MWG green fluorescent filter cube (WG).

9.2. Experimental details

Synthesis of ferrocenecarboxaldehyde oxime (3.10a)[2]

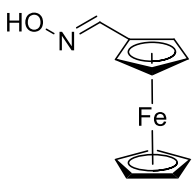

3.11a

Hydroxylamine hydrochloride (1.04 g, 14.9 mmol) was added to a solution of an appropriate ferrocenecarboxaldehyde (2.00 g, 9.34 mmol) in EtOH (50 mL) in a 100 mL round bottom flask followed by addition of aqueous NaOH solution (1.23 g, 30.8 mmol) in 10 mL in distilled water. The mixture was refluxed for 2 hours under nitrogen atmosphere after which it was cooled to room temperature. The reaction mixture was bubbled with CO_2 gas with stirring for 30 minutes. Following the addition of distilled water (50 mL), the product was extracted with DCM (3 × 30 mL), dried (Na_2SO_4) and the solvent removed under reduced pressure to give a dark orange hygroscopic semi-solid. The solid was dried in the freeze dryer overnight to afford a dark orange hygroscopic solid. Yield: 2.08 g (97%). ^{1}H NMR (300 MHz, $CDCl_3$) δ 8.69 (s, 1H, OH), 7.99 (s, 1H, CHN), 4.56 – 4.52 (m, 2H, FcH), 4.38 – 4.34 (m, 2H, FcH), 4.22 (s, 5H, FcH); ^{13}C NMR (75 MHz, $CDCl_3$) δ 150.1, 77.2, 70.2 (2C), 69.4 (5C), 67.7 (2C).

Synthesis of ferrocene methylamine (3.12a)[2]

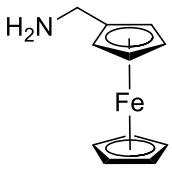

3.12a

To a solution of ferrocenecarboxaldehyde oxime (2.00 g, 8.73 mmol) in anhydrous THF (50 mL) on ice was added lithium aluminium hydride (1.09 g, 28.8 mmol) portion wise. The reaction mixture was refluxed for 15 hours under nitrogen gas after which it was allowed to cool to room temperature. Following the dilution of the mixture with Et_2O (20 mL), brine (30 mL) was slowly added to quench the reaction. The product was extracted with Et_2O (3 × 50 mL) and dried with K_2CO_4. The solvent was removed under reduced pressure to afford the product. Orange viscous oil Yield: 1.73 g (92%). ^{1}H NMR (400 MHz, $CDCl_3$) δ 4.16 (br s, 2H, FcH), 4.14 (s, 5H, FcH), 4.11 (br s, 2H, FcH), 3.54 (s, 2H, CH_2); ^{13}C NMR (100 MHz, $CDCl_3$) δ 91.1, 68.4 (2C), 67.7 (5C), 67.2 (2C), 41.5.

General procedure for synthesis of ferrocenyl 1,3-benzoxazines (3.13a-k)[3]

A suspension of ferrocene methylamine **3.12a** (1.0 eq.) and paraformaldehyde (1.0 eq.) in $CHCl_3$ (15 mL) was refluxed for 30 minutes followed by addition of a substituted phenol **3.1a-i** (1.0 eq.). The reaction mixture was further heated under reflux for 6 – 10 hours. After reflux, the reaction solution was cooled to room temperature and diluted with $CHCl_3$ (50 mL) and successively washed with 1N NaOH solution (50 mL) and distilled water (50 mL). The organic layer was dried (Na_2SO_4) and the solvent removed under reduced pressure to give a crude product which was purified by silica gel chromatography (1:9 EtOAc/Hex) to produce the desired compound.

3-Ferrocenemethyl-3,4-dihydro-*2H*-1,3-benzoxazine (3.13a)

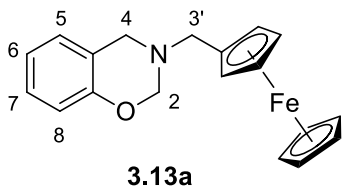

3.13a

Light orange solid. Yield: 61.1 mg (20%). M.p: 127.8 – 128.2 °C. ^{1}H NMR (300 MHz, $CDCl_3$) δ 7.15 (t, J = 7.7 Hz, 1H, H_7), 6.96 (d, J = 7.4 Hz, 1H, H_8), 6.89 (t, J = 7.4 Hz, 1H, H_6), 6.81 (d, J =

8.2 Hz, 1H, H_5), 4.84 (s, 2H, H_2), 4.22 (s, 2H, FcH), 4.15 (s, 2H, FcH), 4.10 (s, 5H, FcH), 3.99 (s, 2H, H_4), 3.72 (s, 2H, $H_{3'}$); ^{1}H NMR (300 MHz, $CDCl_3$) δ 7.15 (t, J = 7.7 Hz, 1H, H_6), 6.96 (d, J = 7.4 Hz, 1H, H_5), 6.89 (t, J = 7.4 Hz, 1H, H_7), 6.81 (d, J = 8.2 Hz, 1H, H_8), 4.84 (s, 2H, H_2), 4.22 (s, 2H, FcH), 4.15 (s, 2H, FcH), 4.10 (s, 5H, FcH), 3.99 (s, 2H, H_4), 3.72 (s, 2H, $H_{3'}$); ^{13}C NMR (75 MHz, $CDCl_3$) δ 154.2, 127.7, 127.6, 120.6, 120.0, 116.4, 83.6, 81.5, 69.8 (2C), 68.6 (5C), 68.3 (2C), 51.0, 49.6; HRMS (ESI$^+$) *m/z* calcd for $C_{19}H_{19}FeNO$ $[M]^+$: 333.0816, Found 333.0797; HPLC purity > 99% (t_R = 4.49 min).

6-Methyl-3-ferrocenemethyl-3,4-dihydro-*2H*-1,3-benzoxazine (3.13b)

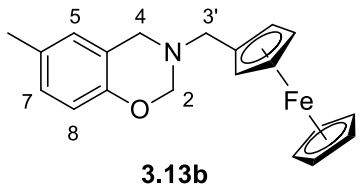

3.13b

Dark orange solid. Yield: 120.2 mg (37%). M.p.: 99.4 – 100.2 °C. ^{1}H NMR (300 MHz, $CDCl_3$) δ 6.96 (dd, J = 8.9, 1.9 Hz, 1H, H_7), 6.77 (br s, 1H, H_5), 6.72 (d, J = 8.2 Hz, 1H, H_8), 4.81 (s, 2H, H_2), 4.23 (t, J = 1.8 Hz, 2H, FcH), 4.15 (t, J = 1.7 Hz, 2H, FcH), 4.10 (s, 5H, FcH), 3.95 (s, 2H, H_4), 3.71 (s, 2H, $H_{3'}$), 2.27 (s, 3H, Me); ^{13}C NMR (75 MHz, $CDCl_3$) δ 152.0, 129.9, 128.4, 128.0, 119.7, 116.2, 83.7, 81.5, 70.0 (2C), 68.7 (5C), 68.4 (2C), 51.0, 49.6, 20.8; HRMS (ESI$^+$) *m/z* calcd for $C_{20}H_{21}FeNO$ $[M]^+$: 347.0973, Found 347.0950; HPLC purity > 99% (t_R = 5.01 min).

6-Chloro-3-ferrocenemethyl-3,4-dihydro-*2H*-1,3-benzoxazine (3.13c)

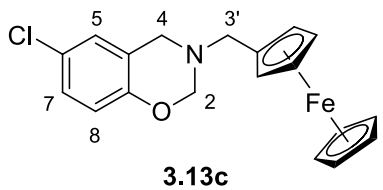

3.13c

Dark brown solid. Yield: 225.6 mg (66%). M.p.: 124.8 – 125.7 °C. ^{1}H NMR (400 MHz, $CDCl_3$) δ 7.10 (d, J = 8.7 Hz, 1H, H_7), 6.94 (s, 1H, H_5), 6.75 (d, J = 8.6 Hz, 1H, H_8), 4.82 (s, 2H, H_2), 4.21 (s, 2H, FcH), 4.16 (s, 2H, FcH), 4.11 (s, 5H, FcH), 3.94 (s, 2H, H_4), 3.69 (s, 2H, $H_{3'}$); ^{13}C NMR (100 MHz, $CDCl_3$) δ 152.9, 127.8, 127.3, 125.2, 121.5, 117.9, 83.3, 81.8, 69.9 (2C), 68.7 (5C), 68.5 (2C), 51.1, 49.3; HRMS (ESI$^+$) *m/z* calcd for $C_{19}H_{19}ClFeNO$ $[M+H]^+$: 368.0500, Found 368.0505; HPLC purity > 99% (t_R = 5.03 min).

6-Bromo-3-ferrocenemethyl-3,4-dihydro-*2H*-1,3-benzoxazine (3.13d)

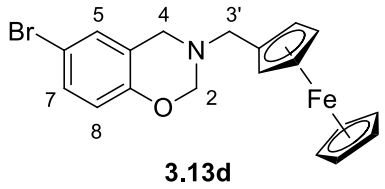

3.13d

Dark orange solid. Yield: 142.9 mg (37%). M.p.: 118.9 – 120.1 °C ^{1}H NMR (300 MHz, $CDCl_3$) δ 7.21 (dd, J = 8.6, 2.3 Hz, 1H, H_7), 7.05 (d, J = 2.3 Hz, 1H, H_5), 6.67 (d, J = 8.7 Hz, 1H, H_8), 4.79 (s, 2H, H_2), 4.18 (t, J = 1.8 Hz, 2H, FcH), 4.13 (t, J = 1.8 Hz, 2H, FcH), 4.08 (s, 5H, FcH), 3.91 (s, 2H, H_4), 3.66 (s, 2H, $H_{3'}$); ^{13}C NMR (75 MHz, $CDCl_3$) δ 153.3, 130.7, 130.2, 122.0, 118.3, 112.5, 83.2, 81.7, 69.9 (2C), 68.7 (5C), 68.5 (2C), 51.0, 49.2; HRMS (ESI^+) *m/z* calcd for $C_{19}H_{18}BrFeNO$ $[M]^+$: 410.9921, Found 410.9891; HPLC purity > 99% (t_R = 5.43 min).

6-Methoxy-3-ferrocenemethyl-3,4-dihydro-*2H*-1,3-benzoxazine (3.13e)

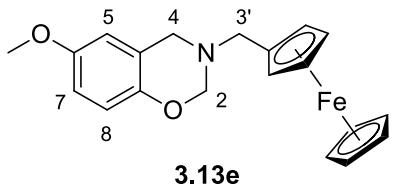

3.13e

Beige solid. Yield: 140.6 mg (42%). M.p.: 93.0 – 94.6 °C. ^{1}H NMR (300 MHz, $CDCl_3$) δ 6.78 6.70 (m, 2H, H_7, H_8), 6.51 (d, J = 2.7 Hz, 1H, H_5), 4.78 (s, 2H, H_2), 4.22 (br s, 2H, FcH), 4.15 (br s, 2H, FcH), 4.10 (s, 5H, FcH), 3.96 (s, 2H, H_4), 3.76 (s, 3H, OMe), 3.71 (s, 2H, $H_{3'}$); ^{13}C NMR (75 MHz, $CDCl_3$) δ 153.7, 148.2, 120.6, 117.1, 113.7, 112.3, 83.7, 81.6, 70.0 (2C), 68.7 (5C), 68.4 (2C), 55.8, 51.1, 49.9; HRMS (ESI^+) *m/z* calcd for $C_{20}H_{21}FeNO_2$ $[M]^+$: 363.0922, Found 363.0894; HRMS (ESI^+) *m/z* calcd for $C_{20}H_{21}FeNO_2$: 363.0922, Found 363.0894 $[M]^+$; HPLC purity > 98% (t_R = 4.23 min).

6-Nitro-3-ferrocenemethyl-3,4-dihydro-*2H*-1,3-benzoxazine (3.13f)

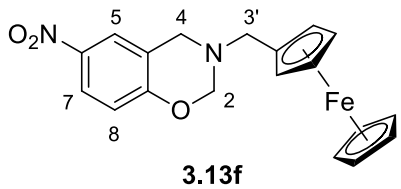

3.13f

Light brown semi-solid. Yield: 33.9 mg (19%). ^{1}H NMR (300 MHz, $CDCl_3$) δ 8.05 (dd, J = 9.0, 2.6 Hz, 1H, H_7), 7.92 (d, J = 2.6 Hz, 1H, H_5), 6.86 (d, J = 8.9 Hz, 1H, H_8), 4.93 (s, 2H, H_2), 4.19 – 4.18 (m, 2H, FcH), 4.16 – 4.15 (m, 2H, FcH), 4.10 (s, 5H, FcH), 4.03 (s, 2H, H_4), 3.68 (s, 2H, $H_{3'}$); ^{13}C NMR (75 MHz, $CDCl_3$) δ 160.1, 141.1, 124.1, 124.0, 120.1, 117.0, 82.7,

69.9 (2C), 68.7 (7C), 51.2, 49.2; HRMS (ESI$^+$) *m/z* calcd for $C_{19}H_{18}FeN_2O_3$ $[M+H]^+$: 379.0740 Found 379.0745; HPLC purity > 96% (t_R = 4.00 min).

7-Methyl-3-ferrocenemethyl-3,4-dihydro-*2H*-1,3-benzoxazine (3.13g)

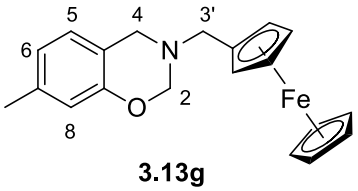

3.13g

Dark brown solid. Yield: 189.2 mg (59%). M.p.: 117.0 – 118.1 °C. ^{1}H NMR (300 MHz, $CDCl_3$) δ 6.85 (d, J = 7.6 Hz, 1H, H_5), 6.75 – 6.69 (m, 1H, H_6), 6.65 (d, J = 2.3 Hz, 1H, H_8), 4.82 (s, 2H, H_2), 4.22 (t, J = 1.8 Hz, 2H, FcH), 4.15 (t, J = 1.8 Hz, 2H, FcH), 4.10 (s, 5H, FcH), 3.96 (s, 2H, H_4), 3.71 (s, 2H, $H_{3'}$), 2.31 (s, 3H); ^{13}C NMR (75 MHz, $CDCl_3$) δ 154.0, 137.8, 127.6, 121.6, 116.9, 114.2, 83.7, 81.6, 70.0 (2C), 68.7 (5C), 68.4 (2C), 50.9, 49.4, 21.4; HRMS (ESI$^+$) *m/z* calcd for $C_{20}H_{22}FeNO$ $[M+H]^+$: 348.1051, Found 348.1031; HPLC purity > 99% (5.01 min).

7-Bromo-3-ferrocenemethyl-3,4-dihydro-*2H*-1,3-benzoxazine (3.13h)

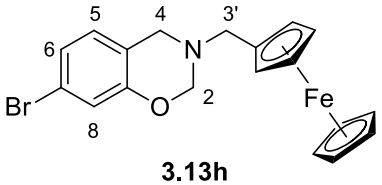

3.13h

Light brown solid. Yield: 156.1 mg (41%). M.p: 148.2 – 148.6 °C. ^{1}H NMR (300 MHz, $CDCl_3$) δ 7.04 – 6.94 (m, 2H, H_6, H_8), 6.81 (d, J = 7.9 Hz, 1H, H_5), 4.82 (s, 2H, H_2), 4.19 (t, J = 1.8 Hz, 2H, FcH), 4.15 (t, J = 1.8 Hz, 2H, FcH), 4.10 (s, 5H, FcH), 3.91 (s, 2H, H_4), 3.68 (s, 2H, $H_{3'}$); ^{13}C NMR (75 MHz, $CDCl_3$) δ 155.1, 129.0, 123.7, 120.6, 119.6, 119.0, 83.3, 81.8, 69.9 (2C), 68.7 (5C), 68.5 (2C), 51.0, 49.2; HRMS (ESI$^+$) *m/z* calcd for $C_{19}H_{18}BrFeNO$ $[M]^+$: 410.9921, Found 410.9889; HPLC purity > 99% (t_R = 5.43 min).

7-Fluoro-3-ferrocenemethyl-3,4-dihydro-*2H*-1,3-benzoxazine (3.13i)

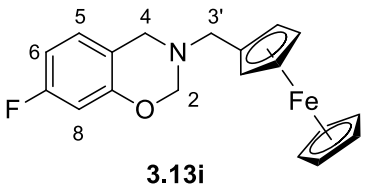

3.13i

Dark brown solid. Yield: 153.6 mg (46%). M.p.: 109.1 – 109.7 °C. ^{1}H NMR (300 MHz, $CDCl_3$) δ 6.92 – 6.84 (m, 1H, H_5), 6.61 (td, J = 8.5, 2.5 Hz, 1H, H_6), 6.54 (dd, J = 10.2, 2.5 Hz, 1H, H_8), 4.82 (s, 2H, H_2), 4.21 (t, J = 1.7 Hz, 2H, FcH), 4.15 (t, J = 1.7 Hz, 2H, FcH), 4.10 (s, 5H, FcH),

3.94 (s, 2H, H_4), 3.69 (s, 2H, $H_{3'}$); ^{13}C NMR (75 MHz, $CDCl_3$) δ ^{13}C NMR (75 MHz, $CDCl_3$) δ 162.1 (d, J = 243.7 Hz), 155.1 (d, J = 12.0 Hz), 128.5 (d, J = 9.6 Hz), 115.5 (d, J = 3.1 Hz), 107.7 (d, J = 21.5 Hz), 103.6 (d, J = 24.1 Hz), 83.4, 81.8, 69.9 (2H), 68.7 (5C), 68.5 (2C), 50.9, 49.1; HRMS (ESI$^+$) *m/z* calcd for $C_{19}H_{19}FFeNO$ $[M+H]^+$: 352.0800, Found 352.0800; HPLC purity > 99% (t_R = 4.43 min).

5-Bromo-3-ferrocenemethyl-3,4-dihydro-*2H*-1,3-benzoxazine (3.13j)

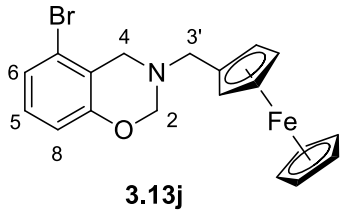

3.13j

Brown solid: 98.8 mg (26%). M.p.: 62.8 – 64.5 °C. ^{1}H NMR (400 MHz, $CDCl_3$) δ 7.13 (dd, J = 7.9, 1.1 Hz, 1H, H_6), 7.02 (t, J = 8.1 Hz, 1H, H_7), 6.78 (dd, J = 8.2, 1.1 Hz, 1H, H_8), 4.80 (s, 2H, H_2), 4.23 (t, J = 1.8 Hz, 2H, FcH), 4.16 (t, J = 1.8 Hz, 2H, FcH), 4.11 (s, 5H,FcH), 3.97 (s, 2H, H_4), 3.69 (s, 2H, $H_{3'}$); ^{13}C NMR (100 MHz, $CDCl_3$) δ 155.6, 128.5, 124.5, 123.3, 120.2, 115.7, 83.3, 81.5, 70.0 (2C), 68.7 (5C), 68.5 (2C), 51.4, 50.8; HRMS (ESI$^+$) *m/z* calcd for $C_{19}H_{19}BrFeNO$: 411.9921, Found 411.9922 $[M+H]^+$; HPLC purity > 99% (t_R = 5.59 min).

5-Fluoro-3-ferrocenemethyl-3,4-dihydro-*2H*-1,3-benzoxazine (3.13k)

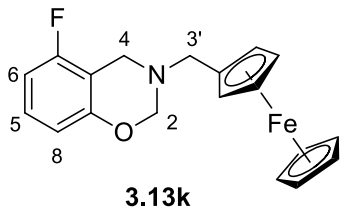

3.13k

Light yellow solid. Yield: 47.5 mg (15%). M.p.: 57.2 – 58.0 °C. ^{1}H NMR (300 MHz, $CDCl_3$) δ 7.10 (dd, J = 15.1, 8.2 Hz, 1H, H_6), 6.67 – 6.58 (m, 2H, H_7, H_8), 4.82 (s, 2H, H_2), 4.24 (t, J = 1.8 Hz, 2H, FcH), 4.17 (t, J = 1.8 Hz, 2H, FcH), 4.11 (s, 5H, FcH), 4.03 (s, 2H, H_4), 3.70 (s, 2H, $H_{3'}$); ^{13}C NMR (75 MHz, $CDCl_3$) 160.5(d, J = 243.3 Hz), 155.4(d, J = 8.1 Hz), 127.7 (d, J = 10.4 Hz), 112.0 (d, J = 3.1 Hz), 108.2 (d, J = 22.0 Hz), 106.9 (d, J = 21.3 Hz), 83.2, 81.4, 69.8 (2C), 68.6 (5C), 68.4 (2C), 51.1, 44.3; HRMS (ESI$^+$) *m/z* calcd for $C_{19}H_{19}FFeNO$ $[M+H]^+$: 352., Found 352.0800; HPLC purity > 99% (t_R = 4.59 min).

Synthesis of ((*N*,*N*-dimethylamino)methyl)ferrocenecarboxaldehyde (3.10b)[2]

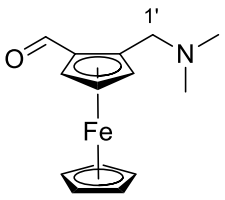

3.10a

A solution of *tert*-butyllithium (7.41 mL, 12.6 mmol) in pentane was added dropwise with caution to a solution of (dimethylaminomethyl)ferrocene **3.15a** (2.00 mL, 10.1 mmol) in anhydrous Et_2O stirred under nitrogen gas at room temperature. The reaction was further stirred for 30 minutes during which time an orange suspension formed. After 30 minutes DMF (0.972 mL, 12.6 mmol) was added dropwise to the suspension and allowed to stir for another 30 minutes to produce a red solution. The reaction was quenched with distilled water (20 mL) and kept at room temperature for 10 minutes with stirring. The reaction solution was diluted with Et_2O (30 mL) and the product extracted with the same solvent (3 × 25 mL). The organic extracts were combined, dried (Na_2SO_4) and the solvent was removed under reduced pressure to afford a brown liquid residue. The residue was purified by silica gel column chromatography (7:2:1 Et_2O/Hex/Et_3N) to yield the desired product as a brown semi-solid. Yield: 2.29 g (85%). ^{1}H NMR (400 MHz, $CDCl_3$) δ 10.08 (s, 1H, CHO), 4.76 – 4.75 (m, 1H, FcH), 4.60 – 4.59 (m, 1H, FcH), 4.54 – 4.53 (m, 1H, FcH), 4.20 (s, 5H, FcH), 3.82 (d, J = 13.0 Hz, 1H, $H_{1',a}$), 3.33 (d, J = 13.0 Hz, 1H, $H_{1',b}$), 2.19 (s, 6H, NMe_2); ^{13}C NMR (100 MHz, $CDCl_3$) δ 193.3, 86.6, 77.9, 76.0, 72.0, 70.5, 70.3 (5C), 56.6 , 44.9 (2C).

Synthesis of 2-((*N*,*N*-dimethylamino)methyl)ferrocenecarboxaldehyde oxime (3.11b)[2]

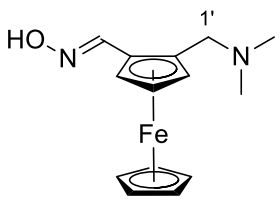

3.11b

Oxime **3.11b** was synthesized from ((*N*,*N*-dimethylamino)methyl)ferrocenecarboxaldehyde **3.10b** according to the procedure described for the preparation of ferrocenecarboxaldehyde oxime **3.11a**. Light-brown semi-solid. Yield: 2.10 g (91%). ^{1}H NMR (400 MHz, $CDCl_3$) δ 8.02 (s, 1H, CHN), 4.56 – 4.52 (m, 1H, FcH), 4.37 (br s, 1H, FcH), 4.30 – 4.28 (m, 1H, FcH), 4.13 (s, 5H, FcH), 3.94 (d, J = 13.1 Hz,

1H, $H_{1'a}$), 3.41 (d, J = 13.1 Hz, 1H, $H_{1'b}$), 2.29 (s, 6H, NMe_2); ^{13}C NMR (100 MHz, $CDCl_3$) δ 148.2, 81.1, 72.8, 70.0, 69.9 (5C), 69.1, 68.2, 56.8, 44.2 (2C).

Synthesis of 2-((*N,N*-dimethylamino)methyl)ferrocenemethylamine (3.12b)

Ferrocenyl amine **3.12b** was synthesized from 2-((*N,N*-dimethylamino)methyl)ferrocenecarboxaldehyde oxime **3.11b** following the method described for the synthesis of ferrocenemethylamine **3.12a**.

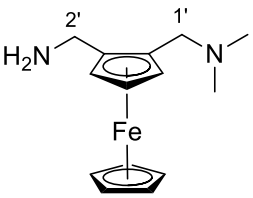

3.12b

Dark brown viscous oil. Yield: 1.77 g (93%). ^1H NMR (400 MHz, $CDCl_3$) δ 4.13 – 4.12 (m, 1H, FcH), 4.10 – 4.09 (m, 1H, FcH), 4.03 (s, 5H, FcH), 4.01 – 4.00 (m, 1H, FcH), 3.65 (d, J = 14.1 Hz, 1H, $H_{2'a}$), 3.60 (d, J = 12.6 Hz, 1H, $H_{1'a}$), 3.45 (d, J = 13.7 Hz, 1H, $H_{2'b}$), 2.87 (d, J = 12.6 Hz, 1H, $H_{1'b}$), 2.13 (s, 6H, NMe_2); ^{13}C NMR (100 MHz, $CDCl_3$) δ 90.3, 83.2, 71.0 , 68.9 (5C), 68.4, 66.0, 58.1, 45.1 (2C), 40.5.

Synthesis of ferrocenyl 1,3-benzoxazine derivatives (3.16a-o)

Ferrocenyl 1,3-benzoxazines **3.16a-o** were synthesized following the Burke protocol described for the preparation of the unsubstituted ferrocenyl 1,3-benzoxazines **3.13a-k**.

3-(2-((*N,N*-Dimethylamino)methyl)ferrocenemethyl)-3,4-dihydro-*2H*-1,3-benzoxazine (3.16a)

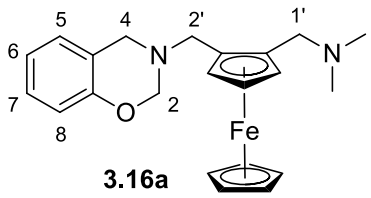

3.16a

Light brown viscous oil. Yield: 123.4 mg (43%). ^1H NMR (400 MHz, $CDCl_3$) δ 7.14 (t, J = 7.3 Hz, 1H, H_7), 6.94 (d, J = 6.7 Hz, 1H, H_8), 6.88 (t, J = 7.7 Hz, 1H, H_6), 6.81 (d, J = 8.2 Hz, 1H, H_5), 4.91 (d, J = 9.9 Hz, 1H, H_{2a}), 4.88 (d, J = 9.9 Hz, 1H, H_{2b}),4.25 (t, J = 1.8 Hz, 1H, FcH), 4.23 (t, J = 1.9 Hz, 1H, FcH), 4.12 (t, J = 2.5 Hz, 1H, FcH), 4.04 (br s, 2H, H_4), 4.01 (s, 5H, FcH), 3.76 (s, 2H, $H_{2'}$), 3.29 (d, J = 12.9 Hz, 1H, $H_{1'a}$), 3.20 (d, J = 12.9 Hz, 1H, $H_{1'b}$), 2.16 (s,

6H, NMe_2); ^{13}C NMR (100 MHz, $CDCl_3$) δ 154.4, 128.0, 127.6, 120.6 (2C), 116.4, 84.3, 83.9, 82.4, 70.7, 70.3, 69.4 (5C), 67.2, 57.4, 49.4, 49.4, 45.5 (2C); HRMS (ESI^+) *m/z* calcd for $C_{22}H_{27}FeN_2O$ $[M+H]^+$: 391.1473, Found 391.1466; HPLC purity > 97% (t_R = 3.21 min).

6-Methyl-3-(2-((*N*,*N*-dimethylamino)methyl)ferrocenemethyl)-3,4-dihydro-*2H*-1,3-benzoxazine (3.16b)

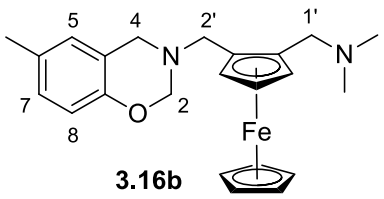

3.16b

Light brown viscous oil. Yield: 87.8 mg (30%). ^1H NMR (400 MHz, $CDCl_3$) δ 6.94 (d, J = 8.2 Hz, 1H, H_7), 6.76 (s, 1H, H_5), 6.72 (d, J = 8.2 Hz, 1H, H_8), 4.88 (d, J = 9.9 Hz, 1H, H_{2a}), 4.84 (d, J = 9.9 Hz, 1H, H_{2b}), 4.25 (t, J = 1.8 Hz, 1H, FcH), 4.24 (t, J = 1.9 Hz, 1H, FcH), 4.12 (t, J = 2.4 Hz, 1H, FcH), 4.01 (s, 5H, FcH), 4.00 (br s, 2H, H_4), 3.75 (s, 2H, $H_{2'}$), 3.29 (d, J = 12.9 Hz, 1H, $H_{2'a}$), 3.21 (d, J = 12.9 Hz, 1H, $H_{1'b}$), 2.26 (s, 3H, Me), 2.17 (s, 6H, NMe_2); ^{13}C NMR (100 MHz, $CDCl_3$) δ 152.1, 129.7, 128.3, 128.2, 120.2, 116.1, 84.2, 83.9, 82.4, 70.7, 70.3, 69.4 (5C), 67.2, 57.3, 49.4 (2C), 45.5 (2C), 20.8; HRMS (ESI^+) *m/z* calcd for $C_{22}H_{29}FeN_2O$ $[M+H]^+$: 405.1628, Found 405.1628; HPLC purity > 98% (t_R = 2.87 min).

6-Chloro-3-(2-((*N*,*N*-dimethylamino)methyl)ferrocenemethyl)-3,4-dihydro-*2H*-1,3-benzoxazine (3.16c)

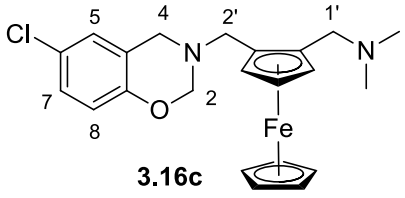

3.16c

Light brown viscous oil. Yield: 156.3 mg (50%). ^1H NMR (600 MHz, $CDCl_3$) δ 7.08 (dd, J = 8.7, 2.5 Hz, 1H, H_7), 6.91 (d, J = 2.4 Hz, 1H, H_5), 6.74 (d, J = 8.6 Hz, 1H, H_8), 4.88 (2H, H_2), 4.25 – 4.23 (m, 2H, FcH), 4.12 (t, J = 2.4 Hz, 1H, FcH), 4.02 (s, 5H, FcH), 3.99 (d, J = 4.1 Hz, 2H, H_4), 3.74 (d, J = 13.3 Hz, 1H, $H_{2'a}$), 3.71 (d, J = 13.4 Hz, 1H, $H_{2'b}$), 3.30 (d, J = 12.8 Hz, 1H, $H_{1'a}$), 3.13 (d, J = 12.9 Hz, 1H, $H_{1'b}$), 2.15 (s, 6H, NMe_2); ^{13}C NMR (150 MHz, $CDCl_3$) δ 153.0, 127.8, 127.6, 125.1, 122.0, 117.8, 83.6, 82.8, 70.9, 70.4, 69.5, 69.4 (5C), 67.3,

57.4, 49.5, 48.8, 45.4 (2C); HRMS (ESI$^+$) *m/z* calcd for $C_{22}H_{26}ClFeN_2O$: 425.1083 $[M+H]^+$, Found 425.1077; HPLC purity > 99% (t_R = 3.56 min).

6-Bromo-3-(2-((*N*,*N*-dimethylamino)methyl)ferrocenemethyl)-3,4-dihydro-*2H*-1,3-benzoxazine (3.16d)

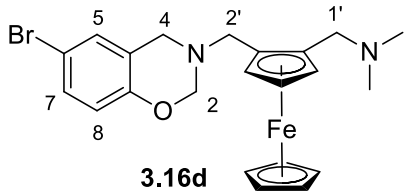

3.16d

Light brown sticky solid. Yield: 173.2 mg (50 %). ^{1}H NMR (400 MHz, $CDCl_3$) δ 7.22 (dd, J = 8.6, 2.3 Hz, 1H, H_7), 7.05 (d, J = 1.9 Hz, 1H, H_5), 6.69 (d, J = 8.7 Hz, 1H, H_8), 4.26 – 4.22 (m, 2H, H_2), 4.17 (s, 1H, FcH), 4.13 (t, J = 2.3 Hz, 1H, FcH), 4.04 (s, 1H, FcH), 4.02 (s, 5H, FcH), 3.99 (s, 2H, H_4), 3.72 (d, J = 2.8 Hz, 2H, $H_{2'}$), 3.30 (d, J = 12.8 Hz, 1H, $H_{1'a}$), 3.13 (d, J = 12.8 Hz, 1H, $H_{1'b}$), 2.15 (s, 6H, NMe_2); ^{13}C NMR (1z00 MHz, $CDCl_3$) δ 153.4, 130.7, 130.5, 122.5, 118.2, 112.4, 84.1, 83.6, 82.8, 70.9, 70.4, 69.4 (5C), 67.4, 57.4, 49.4, 48.6, 45.4 (2C); HRMS (ESI$^+$) *m/z* calcd for $C_{22}H_{26}BrFeN_2O$ $[M+H]^+$: 469.0572, Found 469.0569; HPLC purity > 97% (t_R = 3.59 min).

6-Methoxy-3-(2-((*N*,*N*-dimethylamino)methyl)ferrocenemethyl)-3,4-dihydro-*2H*-1,3-benzoxazine (3.16e)

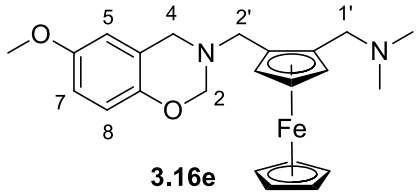

3.16e

Light brown sticky solid. Yield: 109.0 mg (35%). ^{1}H NMR (300 MHz, $CDCl_3$) δ 6.74 – 6.72 (m, 2H, H_7, H_8), 6.50 (d, J = 2.1 Hz, 1H, H_5), 4.86 (d, J = 9.9 Hz, 1H, H_{2a}), 4.81 (d, J = 9.9 Hz, 1H, H_{2b}), 4.26 – 4.25 (m, 1H, FcH), 4.24 – 4.22 (m, 1H, FcH), 4.12 (t, J = 2.5 Hz, 1H, FcH), 4.01 (s, 7H, H_4, FcH), 3.75 (s, 5H, $H_{2'}$, OMe), , 3.31 (d, J = 12.9 Hz, 1H, $H_{1'a}$), 3.21 (d, J = 12.9 Hz, 1H, $H_{1'b}$), 2.17 (s, 6H, NMe_2); ^{13}C NMR (75 MHz, $CDCl_3$) δ 153.5, 148.2, 121.0, 117.0, 113.6, 112.5, 84.0, 83.8, 82.3, 70.7, 70.4, 69.4 (5C), 67.2, 57.3, 55.8, 49.5, 49.4, 45.4 (2C); HRMS (ESI$^+$) *m/z* calcd for $C_{23}H_{29}FeN_2O_2$ $[M+H]^+$: 421.1573, Found 421.1573; PLC purity > 83% (t_R = 2.73 min).

6-Nitro-3-(2-((*N*,*N*-dimethylamino)methyl)ferrocenemethyl)-3,4-dihydro-*2H*-1,3-benzoxazine (3.16f)

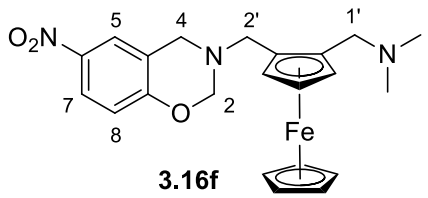

3.16f

Brown viscous oil. Yield: 108.0 mg (66%). ^{1}H NMR (600 MHz, $CDCl_3$) δ 8.03 (dd, J = 9.0, 2.7 Hz, 1H, H_7), 7.87 (d, J = 2.6 Hz, 1H, H_5), 6.85 (d, J = 9.0 Hz, 1H, H_8), 5.01 (d, J = 4.9 Hz, 2H, H_2), 4.23 (s, 1H, FcH), 4.22 – 4.21 (m, 1H, FcH), 4.12 (t, J = 2.4 Hz, 1H, FcH), 4.121 – 4.10 (m, 1H, H_{4a}), 4.05 – 4.04 (m, 1H, H_{4b}), 4.01 (s, 5H, FcH), 3.74 (d, J = 13.3 Hz, 1H,$H_{2'a}$), 3.69 (d, J = 13.3 Hz, 1H, $H_{2'b}$), 3.30 (d, J = 12.8 Hz, 1H, $H_{1'a}$), 3.01 (d, J = 12.8 Hz, 1H, $H_{1'b}$), 2.11 (s, 6H, NMe_2); ^{13}C NMR (150 MHz, $CDCl_3$) δ 160.2, 140.9, 124.6, 123.8, 120.7, 116.8, 84.3, 83.9, 83.2, 71.2, 70.4, 69.4 (5C), 67.5, 57.4, 49.7, 48.3, 45.4 (2C); HRMS (ESI^+) *m/z* calcd for $C_{22}H_{26}FeN_3O_3$ $[M+H]^+$: 436.1324, Found 436.1324; HPLC purity > 94% (t_R = 2.37 min).

7-Methyl- and 5-methyl-(2-((*N*,*N*-dimethylamino)methyl)ferrocenemethyl)-3,4-dihydro-*2H*-1,3-benzoxazine (3.16g)

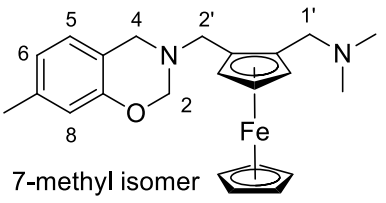

7-methyl isomer

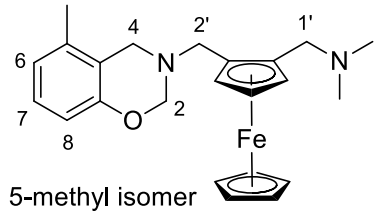

5-methyl isomer

3.16g

Light brown viscous oil. Yield: 87.8 mg (30%). **5-Methyl isomer:** ^{1}H NMR (600 MHz, $CDCl_3$) δ 7.05 (t, J = 7.8 Hz, 1H, H_7), 6.83 (d, J = 7.6 Hz, 1H, H_6), 6.73 (d, J = 7.4 Hz, 1H, H_8), 4.90 – 4.86 (m, 2H, H_2), 4.26 – 4.25 (m, 2H, H_4), 4.12 – 4.11 (m, 2H, FcH), 4.02 (s, 6H, FcH), 3.77 (br s, 2H, $H_{2'}$), 3.33 – 3.31 (m, 2H, $H_{1'}$), 2.31 (s, 3H, Me), 2.18 (s, 6H, NMe_2). **7-Methyl isomer:** ^{1}H NMR (600 MHz, $CDCl_3$) δ 6.70 (d, J = 8.4 Hz, 1H, H_5), 6.68 (d, J = 8.5 Hz, 1H, H_6), 6.65 (br s, 1H, H_8), 4.85 – 4.80 (m, 2H, H_2), 4.25 – 4.21 (m, 2H, H_4), 4.13 (t, J = 2.4 Hz, 1H, FcH), 4.01 – 3.99 (m, 7H, FcH), 3.75 (br s, 2H, $H_{2'}$), 3.24 – 3.21 (m, 2H, $H_{1'}$), 2.16 (s, 6H, NMe_2); HRMS

(ESI$^+$) *m/z* calcd for $C_{22}H_{29}FeN_2O$: 405.1629 $[M+H]^+$, Found 405.1628; HPLC purity: 37% (t_R = 3.30 min) and 63% (t_R = 5.46 min).

7-Bromo-3-(2-((*N*,*N*-dimethylamino)methyl)ferrocenemethyl)-3,4-dihydro-*2H*-1,3-benzoxazine (3.16h)

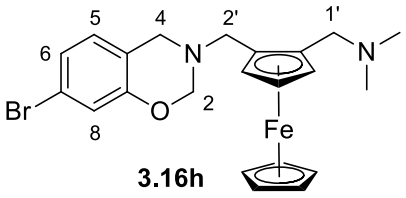

3.16h

Dark brown sticky solid. Yield: 37.8 mg (11%). ^{1}H NMR (400 MHz, $CDCl_3$) δ 7.00 – 6.98 (m, 2H, H_6, H_8), 6.79 (d, J = 7.8 Hz, 1H, H_5), 4.91 – 4.84 (m, 2H, H_2), 4.26 (t, J = 1.8 Hz, 1H, FcH), 4.21 (t, J = 1.8 Hz, 1H, FcH), 4.12 (t, J = 2.6 Hz, 1H, FcH), 4.01 (s, 5H, FcH), 3.97 (s, 2H, H_4), 3.71 (d, J = 3.3 Hz, 2H, $H_{2'}$), 3.31 (d, J = 12.9 Hz, 1H, $H_{1'a}$), 3.20 (d, J = 12.8 Hz, 1H, $H_{1'b}$), 2.16 (s, 6H, NMe_2); ^{13}C NMR (100 MHz, $CDCl_3$) δ 155.2, 129.2, 123.6, 120.4, 119.5, 119.4, 83.9, 83.5, 82.6, 70.9, 70.4, 69.4 (5C), 67.3, 57.3, 49.4, 48.9, 45.3 (5C); HRMS (ESI$^+$) *m/z* calcd for $C_{22}H_{26}BrFeN_2O$ $[M+H]^+$: 469.0578, Found 469.0579; HPLC purity > 89% (t_R = 2.85 min).

7-Fluoro-3-(2-((*N*,*N*-dimethylamino)methyl)ferrocenemethyl)-3,4-dihydro-*2H*-1,3-benzoxazine (3.16i)

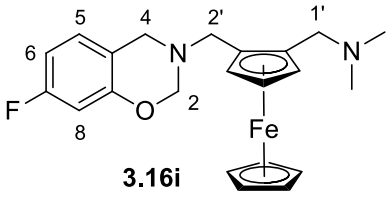

3.16i

Dark brown semi-solid. Yield: 37.7 mg (13%). ^{1}H NMR (600 MHz, $CDCl_3$) δ 6.88 – 6.85 (m, 1H, H_5), 6.59 (td, J = 8.4, 2.5 Hz, 1H, H_6), 6.53 (dd, J = 10.2, 2.5 Hz, 1H, H_8), 4.89 (d, J = 9.9 Hz, 1H, H_{2a}), 4.87 (d, J = 9.9 Hz, 1H, H_{2b}), 4.24 (d, J = 1.9 Hz, 1H, FcH), 4.22 (d, J = 1.8 Hz, 1H, FcH), 4.12 (t, J = 2.4 Hz, 1H, FcH), 4.01 (s, 5H, FcH), 3.99 (s, 2H, H_4), 3.74 (d, J = 13.3 Hz, 1H, $H_{2'a}$), 3.71 (d, J = 13.4 Hz, 1H, $H_{2'b}$), 3.29 (d, J = 12.9 Hz, 1H, $H_{1'a}$), 3.17 (d, J = 12.9 Hz, 1H, $H_{1'b}$), 2.15 (s, 6H, NMe_2); ^{13}C NMR (150 MHz, $CDCl_3$) δ 160.7 (d, J = 243.4 Hz), 155.6 (d, J = 8.2 Hz), 127.6 (d, J = 10.2 Hz), 112.0 (d, J = 3.0 Hz), 108.8 (d, J = 22.0 Hz), 106.9 (d, J = 21.3 Hz), 103.7, 84.2, 83.7, 82.7, 70.8, 70.3, 69.5 (5C), 69.4, 57.4, 49.4, 48.9,

45.4 (2C); HRMS (ESI$^+$) *m/z* calcd for $C_{22}H_{26}FFeN_2O$: 409.1373 $[M+H]^+$, Found 409.1370; HPLC purity > 92% (t_R = 2.49 min).

5-Bromo-3-(2-((*N*,*N*-dimethylamino)methyl)ferrocenemethyl)-3,4-dihydro-*2H*-1,3-benzoxazine (3.16j)

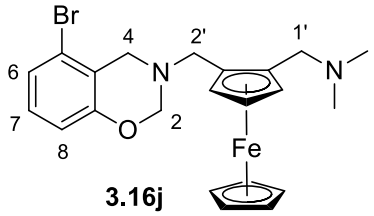

3.16j

Light brown sticky solid. Yield: 80.2 mg (23%). ^{1}H NMR (400 MHz, $CDCl_3$) δ 7.11 (d, J = 7.9 Hz, 1H, H_6), 7.01 (t, J = 8.1 Hz, 1H, H_7), 6.78 (d, J = 8.1 Hz, 1H, H_8), 4.85 (d, J = 9.9 Hz, 1H, H_{2a}), 4.81 (d, J = 9.9 Hz, 1H, H_{2b}), 4.27 (s, 1H, FcH), 4.24 (s, 1H, FcH), 4.13 (t, J = 2.6 Hz, 1H, FcH), 4.05 – 4.01 (m, 7H, H_{4a}, FcH), 3.95 – 3.91 (m, 1H, H_{4b}), 3.73 (d, J = 2.5 Hz, 2H, $H_{2'}$), 3.31 (d, J = 12.8 Hz, 1H, $H_{1'a}$), 3.25 (d, J = 12.9 Hz, 1H, $H_{1'b}$), 2.17 (s, 6H, NMe_2); ^{13}C NMR (100 MHz, $CDCl_3$) δ 155.8, 128.4, 124.5, 123.3, 120.6, 115.8, 84.0, 83.5, 82.1, 70.7, 70.4, 69.4 (5C), 67.3, 57.3, 50.8, 49.7, 45.4 (2C); HRMS (ESI$^+$) *m/z* calcd for $C_{22}H_{26}BrFeN_2O$ $[M+H]^+$: 469.0582, Found 469.0582; HPLC purity > 98% (t_R = 3.31 min).

5-Fluoro-3-(2-((*N*,*N*-dimethylamino)methyl)ferrocenemethyl)-3,4-dihydro-*2H*-1,3-benzoxazine (3.16k)

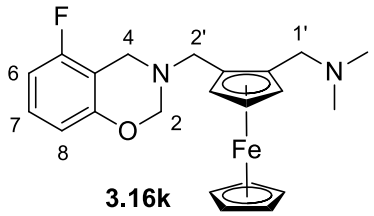

3.16k

Light brown semi-solid. Yield: 43.4 mg (14%). ^{1}H NMR (600 MHz, $CDCl_3$) δ 7.08 (q, J = 8.0 Hz, 1H, H_6), 6.62 (d, J = 8.3 Hz, 1H, H_7), 6.59 (d, J = 8.5 Hz, 1H, H_8), 4.89 (d, J = 9.9 Hz, 1H, H_{2a}), 4.86 (d, J = 9.9 Hz, 1H, H_{2b}), 4.26 – 4.24 (m, 2H, FcH), 4.12 (t, J = 2.4 Hz, 1H, FcH), 4.05 (d, J = 6.1 Hz, 2H, H_4), 4.02 (s, 5H, FcH), 3.75 (d, J = 13.4 Hz, 1H, $H_{2'a}$), 3.73 (d, J = 13.4 Hz, 1H, $H_{2'b}$), 3.31 (d, J = 12.9 Hz, 1H, $H_{1'a}$), 3.18 (d, J = 12.9 Hz, 1H, $H_{1'b}$), 2.14 (s, 6H, NMe_2); ^{13}C NMR (150 MHz, $CDCl_3$) δ 160.7 (d, J = 243.4 Hz), 155.6 (d, J = 8.2 Hz), 127.6 (d, J = 10.2 Hz), 112.0 (d, J = 3.0 Hz), 108.8 (d, J = 22.0 Hz),

106.9 (d, J = 21.3 Hz), 83.6, 82.4, 70.7, 70.3, 69.4 (5C), 67.2, 57.4, 49.6, 45.3 (2C), 44.1 (2C); HRMS (ESI$^+$) *m/z* calcd for $C_{22}H_{26}FFeN_2O$ $[M+H]^+$: 409.1379, Found 409.1382; HPLC purity > 92% (t_R = 2.50 min).

6-*N*-Boc-amino-3-(2-((*N*,*N*-dimethylamino)methyl)ferrocenemethyl)-3,4-dihydro-*2H*-1,3-benzoxazine (3.16l)

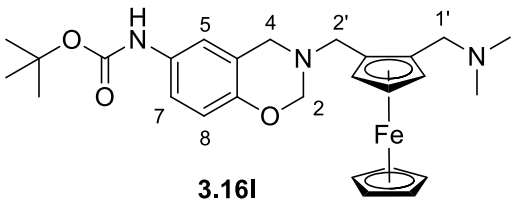

3.16l

Brown sticky solid. Yield: 62.0 mg (39%). ^{1}H NMR (600 MHz, $CDCl_3$) δ 7.12 (br s, 1H, NH), 6.97 (dd, J = 8.7, 2.4 Hz, 1H, H_7), 6.73 (d, J = 8.7 Hz, 1H, H_8), 6.34 (s, 1H, H_5), 4.85 (d, J = 9.8 Hz, 1H, H_{2a}), 4.82 (d, J = 9.8 Hz, 1H, H_{2b}), 4.25 (br s, 1H, FcH), 4.22 (br s, 1H, FcH), 4.11 (t, J = 2.4 Hz, 1H, FcH), 4.01 (d, J = 3.4 Hz, 7H, H_4, FcH), 3.72 (s, 2H, $H_{2'}$), 3.29 (d, J = 12.9 Hz, 1H, $H_{1'a}$), 3.23 (d, J = 12.9 Hz, 1H, $H_{1'b}$), 2.17 (s, 6H, NMe_2), 1.51 (s, 9H, Bu^t); ^{13}C NMR (150 MHz, $CDCl_3$) δ 193.4, 186.9, 153.3, 150.4, 131.2 (2C), 120.8, 116.6, 84.1, 83.8, 82.3, 70.7, 70.4, 69.4 (5C), 67.2, 57.3, 49.8, 49.4, 45.4 (2C), 28.5 (3C); HRMS (ESI$^+$) *m/z* calcd for $C_{27}H_{36}FeN_3O_3$ $[M+H]^+$: 506.2096, Found 506.2096; HPLC purity > 96% (t_R = 5.05 min).

5,7,8-Trichloro-3-(2-((*N*,*N*-dimethylamino)methyl)ferrocenemethyl)-3,4-dihydro-*2H*-1,3-benzoxazine (3.16m)

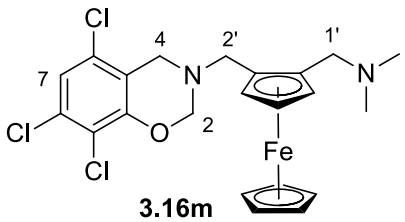

3.16m

Brown semi-solid. Yield: 56.6 mg (39%) ^{1}H NMR (600 MHz, $CDCl_3$) δ 7.37 (s, 1H, H_6), 4.97 (s, 2H, H_2), 4.25 (s, FcH), 4.22 (s, FcH), 4.16 – 4.11 (m, FcH, FcH), 4.03 (s, 7H, H_4, FcH), 3.76 (d, J = 13.2 Hz, 1H, $H_{2'a}$), 3.70 (d, J = 13.3 Hz, 1H, $H_{2'b}$), 3.30 (d, J = 12.7 Hz, 1H, $H_{1'a}$), 3.07 (d, J = 12.6 Hz, 1H, $H_{1'b}$), 2.11 (s, 6H, NMe2); ^{13}C NMR (150 MHz, $CDCl_3$) δ 149.8, 129.8, 128.4, 123.7, 121.9, 120.1, 84.5, 83.4,

83.1, 70.8, 70.3, 69.4 (5C), 67.3, 57.5, 49.9, 48.5, 45.4 (2C); HRMS (ESI^+) *m/z* calcd for $C_{22}H_{24}Cl_3FeN_2O$ $[M+H]^+$: 493.0305, Found 493.0305; HPLC purity > 92% (t_R = 3.98 min).

6-Chloro-3-(2-methylferrocene)methyl-3,4-dihydro-*2H*-1,3-benzoxazine (3.16n)

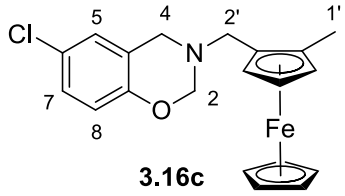

3.16c

Light brown viscous oil. Yield: 19.7 mg (6%). ^1H NMR (400 MHz, $CDCl_3$) δ 7.10 (dd, J = 8.7, 2.4 Hz, 1H, H_7), 6.94 (d, J = 2.3 Hz, 1H, H_5), 6.74 (d, J = 8.7 Hz, 1H, H_8),), 4.84 (d, J = 9.9 Hz, 1H, H_{2a}), 4.77 (d, J = 10.0 Hz, 1H, H_{2b}), 4.12 (br s, 1H, FcH), 4.10 (br s, 1H, FcH), 4.02 (d, J = 2.5 Hz, 1H, FcH), 4.00 (s, 5H, FcH), 3.94 – 3.91 (m, 2H, H_4), 3.79 (d, J = 12.8 Hz, 1H, $H_{2'a}$), 3.67 (d, J = 12.9 Hz, 1H, $H_{2'b}$), 1.95 (s, 3H, Me); ^{13}C NMR (100 MHz, $CDCl_3$) δ 152.9, 127.8, 127.4, 125.2, 121.6, 117.8, 84.3, 82.2, 81.8, 70.1, 69.7 (5C), 69.3, 66.2, 49.5, 49.3, 13.3; HRMS (ESI^+) *m/z* calcd for $C_{20}H_{21}ClFeNO$ $[M]^+$: 381.0583, Found 381.0580; HPLC purity > 94% (t_R = 2.38 min).

6-Nitro-3-(2-methylferrocene)methyl-3,4-dihydro-*2H*-1,3-benzoxazine (3.16o)

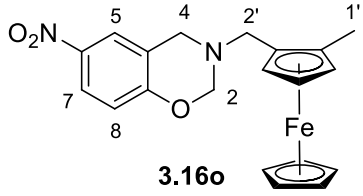

3.16o

Brown solid. Yield: 19.0 mg (7%). M.p.: 103.9 – 105.2 °C. ^1H NMR (600 MHz, $CDCl_3$) δ 8.05 (dd, J = 9.0, 2.7 Hz, 1H, H_7), 7.92 (d, J = 2.6 Hz, 1H, H_5), 6.86 (d, J = 9.0 Hz, 1H, H_8), 4.95 (d, J = 10.0 Hz, 1H, H_{2a}), 4.89 (d, J = 10.0 Hz, 1H, H_{2b}), 4.11 (br s, 1H, FcH), 4.10 – 4.09 (m, 2H, 2H, H_4), 4.04 (br s, 1H, FcH), 4.03 (t, J = 2.4 Hz, 1H, FcH), 4.00 (s, 5H, FcH), 3.79 (d, J = 12.9 Hz, 1H, $H_{2'a}$), 3.66 (d, J = 12.9 Hz, 1H, $H_{2'b}$), 1.94 (s, 3H, Me); ^{13}C NMR (150 MHz, $CDCl_3$) δ 160.2, 142.6, 124.2, 124.0, 120.3, 117.0, 84.3, 82.8, 81.6, 70.2, 69.7, 69.4 (5C), 66.4, 49.7, 49.3, 13.3; HRMS (ESI^+) *m/z* calcd for $C_{20}H_{21}FeN_2O_3$ $[M+H]^+$: 393.1623, Found 393.1623; HPLC purity > 98% (t_R = 1.91 min).

N,N-Bis(2-hydroxybenzyl)ferrocenemethylamines 3.16p-q

Compounds **3.16p-q** were isolated as side products from the Burke condensation of ferrocenyl amine **3.12b** and 4-methylphenol (**3.1b**) and 4-nitrophenol (**3.1g**).

N,N-bis(2-hydroxy-5-methyl-benzyl)ferrocenemethylamine 3.16p

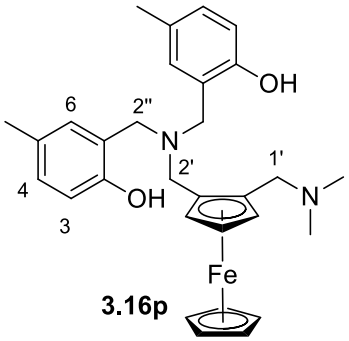

3.16p

Brown semi-solid. Yield: 43.4 mg (39%). ^{1}H NMR (300 MHz, $CDCl_3$) δ 6.94 (dd, J = 8.2, 2.2 Hz, 2H, H_4), 6.81 (d, J = 2.2 Hz, 2H, H_6), 6.72 (d, J = 8.1 Hz, 2H, H_6), 4.14 (s, 1H, FcH), 4.10 (t, J = 2.0 Hz, 1H, FcH), 4.05 (t, J = 2.5 Hz, 1H, FcH), 3.94 (s, 5H, FcH), 3.91 – 3.79 (m, 4H, $H_{2''}$), 3.69 (d, J = 12.5 Hz, 1H, $H_{2'a}$), 3.20 (d, J = 12.5 Hz, 1H, $H_{2'b}$), 3.13 (d, J = 13.4 Hz, 1H, $H_{1'a}$), 2.82 (d, J = 13.4 Hz, 1H, $H_{1'b}$), 2.29 (s, 6H, 2 × Me), 2.24 (s, 6H, NMe_2); ^{13}C NMR (75 MHz, $CDCl_3$) δ 154.5 (2C), 131.0 (2C), 129.5 (2C), 128.4 (2C), 122.6 (2C), 117.1 (2C), 83.6, 82.7, 72.0, 71.8, 69.4 (5C), 66.8, 57.8, 57.1 (2C), 53.8, 45.5 (2C), 20.6 (2C); HRMS (ESI$^+$) *m/z* calcd for $C_{30}H_{37}FeN_2O_2$ $[M+H]^+$: 513.2204, Found 513.2208.

N,N-Bis(2-hydroxy-5-nitro-methyl-benzyl)ferrocenemethylamine 3.16q

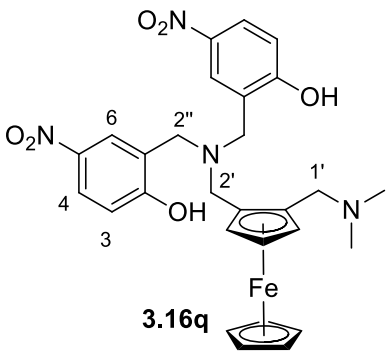

3.16q

Brown semi-solid. Yield: 19.8 mg (23%). ^{1}H NMR (600 MHz, $CDCl_3$) δ 8.11 – 7.86 (m, 4H, H_3, H_4), 6.87 – 6.71 (m, 2H, H_6), 4.18 – 4.16 (m. 4H, $H_{2''}$), 4.07 (s, 6H, FcH), 4.02 (s, 2H, FcH), 3.83 (d, J = 13.0 Hz, 1H, $H_{2'a}$), 3.71 (td, J = 12.9, 12.4, 5.7 Hz, 1H, $H_{2'b}$), 3.45 (d, J = 12.8 Hz, 1H, $H_{1'a}$), 2.84 (d, J = 12.8 Hz, 1H, $H_{1'b}$), 2.15 (s, 6H, NMe_2); ^{13}C NMR (151 MHz, $CDCl_3$) δ 126.4, 125.5, 124.5, 124.0, 117.7, 116.1, 83.7, 81.1, 71.9, 71.2, 69.5 (2C), 66.8, 58.2 (2C), 49.4, 45.5, 44.6 (2C); HRMS (ESI$^+$) *m/z* calcd for $C_{28}H_{31}FeN_4O_6$ $[M+H]^+$: 575.1515, Found 575.1508.

Synthesis of ferrocene methanol (3.20)

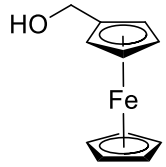

3.20

$NaBH_4$ (0.350 g, 9.30 mmol) was added to a solution of ferronecarboxaldehyde **3.10a** (2.00g, 9.30 mmol) and the reaction mixture stirred at room temperature for 30 minutes. After complete disappearance of the aldehyde **3.10a**, the reaction mixture was diluted with distilled water (25 mL) and stirred at room temperature for 5 minutes. The product was extracted with DCM (2 × 25 mL) and the combined organic layers were dried over Na_2SO_4 and filtered. The solvent was removed under reduced pressure to produce the pure ferrocene methanol product as an orange solid **3.20**. Yield: 1.80 (90%). M.p.: 76.9 – 78.0 °C. ^{1}H NMR (400 MHz, $CDCl_3$) δ 4.12 (br s, 4H, FcH), 4.03 (s, 5H, FcH), 3.68 (s, 2H, CH_2); ^{13}C NMR (100 MHz, $CDCl_3$) δ 93.4, 69.6 (2C), 67.8 (5C), 67.2 (2C), 48.9.

Synthesis of *N,N*-dethylaminomethylferrocene (3.15b)[4]

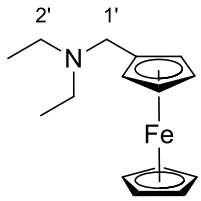

3.15b

A solution of excess diethylamine **3.19** (10 mL) in DCE (20 mL) was added to a stirring suspension of $AlCl_3$ (0.960 g, 7.20 mmol) in DCE (25 mL) on ice. A solution of ferrocene methanol **3.20** (0.800 g, 3.70 mmol) was then slowly added to the reaction mixture over 10 minutes. The reaction mixture was removed from ice and then heated at 50 – 60 °C for 6 hours. After completion of the reaction (TLC), distilled water (15 mL) was added to quench unreacted $AlCl_3$. The product was extracted with DCM (3 × 25 mL), dried (Na_2SO_4) and the solvent removed i *in vacuo*. The resulting crude product was dissolved in pentane (25 mL), washed with distilled water, dried (Na_2SO_4) and the solvent removed under reduced pressure. The pure compound was obtained as an orange oil. Yield: 0.820 g (82%). ^{1}H NMR (600 MHz, $CDCl_3$) δ 4.15 (s, 2H, H, FcH), 4.11 (s, 5H, FcH), 4.10 – 4.09 (m, 2H, FcH), 3.50 (s, 2H, $H_{1'}$), 2.43 (q, J = 7.1 Hz, 4H, $H_{2'}$),

1.03 (t, J = 7.1 Hz, 6H, Me_2); ^{13}C NMR (150 MHz, $CDCl_3$) δ 83.1, 70.3 (2C), 68.6 (5C), 67.9 (2C), 52.0 (2C), 46.3 (2C), 12.1 (2C).

Synthesis of ((*N,N*-diethylamino)methyl)ferrocenecarboxaldehyde (3.10b)

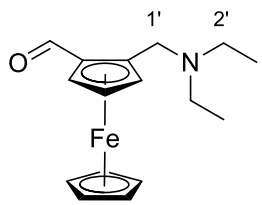

3.10b

The same protocol described for the synthesis of ((*N,N*-diethylamino)methyl)ferrocenecarboxaldehyde **3.10a** was employed to access compound **3.10b** from *N,N*-diethylaminomethylferrocene **3.15b**.[2] Brown viscous oil. Yield: 1.40 g (75%). ^{1}H NMR (600 MHz, $CDCl_3$) δ 10.13 (s, 1H, CHO), 4.77 (s, 1H, FcH), 4.61 (s, 1H, FcH), 4.54 (t, J = 2.5 Hz, 1H, FcH), 4.22 (s, 5H, FcH), 3.90 (d, J = 13.7 Hz, 1H, $H_{1'a}$), 3.52 (d, J = 13.7 Hz, 1H, $H_{1'b}$), 2.51 (dq, J = 14.3, 7.1 Hz, 2H, $H_{2'a}$), 2.44 (dq, J = 14.0, 7.1 Hz, 2H, $H_{2'b}$), 1.01 (t, J = 7.1 Hz, 6H, Me_2); ^{13}C NMR (151 MHz, $CDCl_3$) δ 193.5, 88.3, 77.9, 75.8, 71.8, 70.3 (5C), 69.8, 50.5, 46.4 (2C), 12.0 (2C).

Synthesis of ((*N,N*-diethylamino)methyl)ferrocenecarboxaldehyde oxime (3.11c)

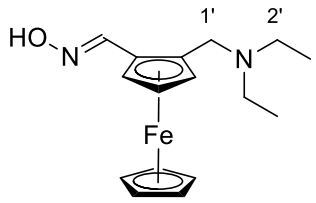

3.11c

The same protocol described for the synthesis of ((*N,N*-diethylamino)methyl)ferrocenecarboxaldehyde oxime **3.11a** was used to prepare oxime **3.11c** from ((*N,N*-diethylamino)methyl)ferrocenecarboxaldehyde **3.10b**.[2] Orange viscous oil. Yield: 1.85 g (85 %). ^{1}H NMR (400 MHz, $CDCl_3$) δ 8.04 (s, 1H, CHN), 4.51 (s, 1H, FcH), 4.39 (s, 1H, FcH), 4.30 (t, J = 2.5 Hz, 1H, FcH), 4.15 (s, 5H, FcH), 3.74 – 3.63 (m, 2H, $H_{1'}$), 2.78 – 2.75 (m, 2H, $H_{2'a}$), 2.57 – 2.47 (m, 2H, $H_{2'b}$), 1.11 (t, J = 7.2 Hz, 6H, Me_2); ^{13}C NMR (100 MHz, $CDCl_3$) δ 148 .5, 100.1 (2C), 76.3, 72.8, 70.0 (5C), 69.1, 50.7, 46.0 (2C), 11.3 (2C).

Synthesis of 2-((*N*,*N*-diethylamino)methyl)ferrocenemethylamine (3.12c)

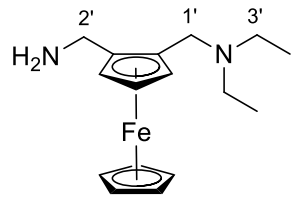

3.12c

Ferrocenyl amine **3.12c** was synthesized from 2-((*N*,*N*-diethylamino)methyl)ferrocenecarboxaldehyde oxime **3.11c** following the method described for the synthesis of ferrocenemethylamine **3.12a**.[2] Dark brown viscous oil. Yield: 1.35 g (75%). ^{1}H NMR (600 MHz, $CDCl_3$) δ 4.10 (s, 1H, FcH), 4.09 (s, 1H, FcH), 4.04 (s, 5H, FcH), 3.99 (t, J = 2.2 Hz, 1H, FcH), 3.76 (d, J = 12.9 Hz, 1H, $H_{2'a}$), 3.69 (d, J = 12.9 Hz, 1H, $H_{2'b}$), 3.40 (d, J = 13.9 Hz, 1H, $H_{1'a}$), 3.00 (d, J = 13.9 Hz, 1H, $H_{1'b}$), 2.59 (dq, J = 14.4, 7.2 Hz, 2H, $H_{3'a}$), 2.28 (dq, J = 13.8, 7.0 Hz, 2H, $H_{3'b}$), 0.98 (t, J = 7.1 Hz, 6H, Me_2); ^{13}C NMR (150 MHz, $CDCl_3$) δ 90.7, 84.1, 71.2, 68.9 (5C), 68.6, 65.6 (2C), 52.1, 46.3, 41.0, 11.8 (2C).

Synthesis of ferrocenyl 1,3-benzoxazine derivatives (3.17a-f)

Ferrocenyl 1,3-benzoxazines **3.17a-f** were synthesized via the Burke protocol using ferrocenyl amine **3.12c** and phenols **3.1b-d**,**f**,**n** following the conditions described for the synthesis of benzoxazines **3.13a-k**.[3]

6-Methyl-3-(2-((*N*,*N*-diethylamino)methyl)ferrocenemethyl)-3,4-dihydro-*2H*-1,3-benzoxazine (3.17a)

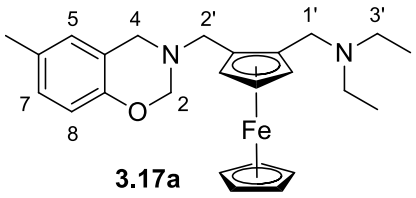

3.17a

Brown viscous oil. Yield: 102.0 mg (52%). ^{1}H NMR (600 MHz, $CDCl_3$) δ 6.96 – 6.93 (m, 1H, H_7), 6.75 (br s, 1H, H_5), 6.71 (d, J = 8.3 Hz, 1H, H_8), 4.88 – 4.82 (m, 2H, FcH), 4.86 (d, J = 9.8 Hz, 1H, H_{2a}), 4.84 (d, J = 9.8 Hz, 1H, H_{2b}), 4.10 (t, J = 2.4 Hz, 1H, FcH), 4.02 (s, 5H, FcH), 4.01 – 3.95 (m, 2H, H_4), 3.77 (d, J = 13.9 Hz, 2H, $H_{2'}$), 3.46 (d, J = 13.4 Hz, 1H, $H_{1'a}$), 3.34 (d, J = 13.5 Hz, 1H, $H_{1'b}$), 2.53 (dq, J = 14.2, 7.1 Hz, 2H, $H_{3'a}$), 2.44 (dq, J = 14.1, 7.1 Hz, 2H, $H_{3'a}$), 2.26 (s, 3H, Me), 0.96 (t, J = 7.1 Hz, 6H, Me_2); ^{13}C NMR (150 MHz, $CDCl_3$) δ 152.1, 129.7, 128.2, 128.2, 120.3, 116.2, 85.0, 84.0, 82.4, 70.8, 70.2, 69.3 (5C), 66.9, 51.0,

49.5, 49.5, 46.3 (2C), 20.7, 11.6 (2C); HRMS (ESI^+) *m/z* calcd for $C_{25}H_{33}FeN_2O$ $[M+H]^+$: 433.1937, Found 433.2012.

6-Methoxy-3-(2-((*N*,*N*-diethylamino)methyl)ferrocenemethyl)-3,4-dihydro-*2H*-1,3-benzoxazine (3.17b)

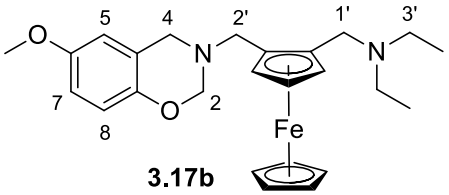

3.17b

Brown viscous oil. Yield: 130.52mg (65%). ^1H NMR (400 MHz, $CDCl_3$) δ 6.78 – 6.69 (m, 2H, H_7, H_8), 6.49 (d, J = 2.6 Hz, 1H, H_5), 4.85 (d, J = 9.8 Hz, 1H, H_{2a}), 4.81 (d, J = 9.8 Hz, 1H, H_{2b}), 4.24 - 4.23 (m, 2H, FcH), 4.09 (t, J = 2.4 Hz, 1H, FcH), 4.02 (s, 5H, FcH), 4.00 (s, 2H, H_4), 3.76 (s, 2H, $H_{2'}$), 3.75 (s, 3H, Me), 3.47 (d, J = 13.5 Hz, 1H, $H_{1'a}$), 3.33 (d, J = 13.4 Hz, 1H, $H_{1'b}$), 2.52 (dq, J = 13.9, 7.1 Hz, 2H, H $H_{3'a}$), 2.42 (dq, J = 13.9, 7.0 Hz, 2H, $H_{3'b}$), 0.95 (t, J = 7.1 Hz, 6H, Me_2); ^{13}C NMR (100 MHz, $CDCl_3$) δ 153.5, 148.3, 121.2, 117.1, 113.6, 112.4, 85.0, 84.0, 82.4, 70.8, 70.2, 69.3, 66.9 (5C), 55.8, 51.0, 49.6, 49.6, 46.3 (2C), 11.6 (2C); HRMS (ESI^+) *m/z* calcd for $C_{25}H_{33}FeN_2O_2$ $[M+H]^+$: 449.1891, Found 449.1887.

6-Chloro-3-(2-((*N*,*N*-diethylamino)methyl)ferrocenemethyl)-3,4-dihydro-*2H*-1,3-benzoxazine (3.17c)

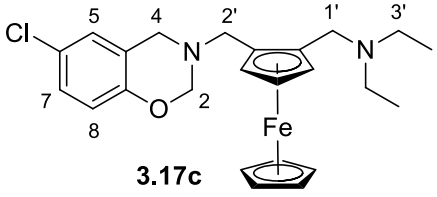

3.17c

Brown viscous oil. Yield: 186.5 mg (79%). ^1H NMR (600 MHz, $CDCl_3$) δ 7.07 (dd, J = 8.7, 2.5 Hz, 1H, H_7), 6.91 (d, J = 2.4 Hz, 1H, H_5), 6.73 (d, J = 8.7 Hz, 1H, H_8), 4.87 (s, 2H, H_2), 4.24 – 4.22 (m, 2H, FcH), 4.10 (t, J = 2.4 Hz, 1H, FcH), 4.02 (s, 5H, FcH), 3.98 (s, 2H, H_4), 3.75 (d, J = 13.2 Hz, 1H, $H_{2'a}$), 3.72 (d, J = 13.3 Hz, 1H, $H_{2'b}$), 3.45 (d, J = 13.4 Hz, 1H, $H_{1'a}$), 3.27 (d, J = 13.4 Hz, 1H, $H_{1'b}$), 2.55 – 2.49 (m, 2H, $H_{3'a}$), 2.40 (dq, J = 14.0, 7.0 Hz, 2H, $H_{3'b}$), 0.93 (t, J = 7.1 Hz, 6H, Me_2); ^{13}C NMR (150 MHz, $CDCl_3$) δ 153.1, 127.6, 127.6,

125.1, 122.2, 117.8, 85.1, 83.7, 82.8, 70.9, 70.2, 69.4 (5C), 67.0, 51.0, 49.7, 49.0, 46.4 (2C), 11.5 (2C); HRMS (ESI$^+$) *m/z* calcd for $C_{24}H_{30}ClFeN_2O$ $[M+H]^+$: 45231318, Found 453.1411.

6-Bromo-3-(2-((*N*,*N*-diethylamino)methyl)ferrocenemethyl)-3,4-dihydro-*2H*-1,3-benzoxazine (3.17d)

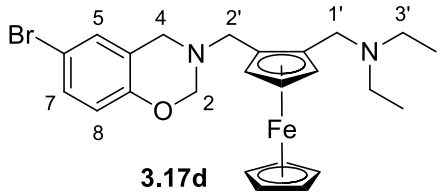

3.17d

Brown viscous oil. Yield: 64.0 mg (50%). ^{1}H NMR (600 MHz, $CDCl_3$) δ 7.21 (dd, J = 8.7, 2.4 Hz, 1H, H_7), 7.05 (d, J = 2.3 Hz, 1H, H_5), 6.69 (d, J = 8.7 Hz, 1, H_8), 4.87 (s, 2H, H_2), 4.24 – 4.22 (m, 2H, FcH), 4.10 (t, J = 2.4 Hz, 1H, FcH), 4.02 (s, 5H, FcH), 3.97 (br s, 2H, H_4), 3.75 (d, J = 13.3 Hz, 1H, $H_{2'a}$), 3.72 (d, J = 13.3 Hz, 1H, $H_{2'a}$), 3.45 (d, J = 13.4 Hz, 1H, $H_{1'a}$), 3.26 (d, J = 13.4 Hz, 1H, $H_{1'b}$), 2.53 (dq, J = 14.3, 7.2 Hz, 2H, $H_{3'a}$), 2.43 – 2.37 (m, 2H, $H_{3'b}$), 0.93 (t, J = 7.1 Hz, 6H, Me_2); ^{13}C NMR (151 MHz, $CDCl_3$) δ 153.6, 130.5, 130.4, 122.7, 118.3, 112.4, 85.1, 83.7, 82.8, 70.9, 70.2, 69.3 (2C), 67.0, 51.0, 49.6, 48.8, 46.3 (2C), 11.5 (2C); HRMS (ESI$^+$) *m/z* calcd for $C_{24}H_{29}BrFeN_2O$ $[M]^+$: 496.0813, Found 496.1887.

6-Fluoro-3-(2-((*N*,*N*-diethylamino)methyl)ferrocenemethyl)-3,4-dihydro-*2H*-1,3-benzoxazine (3.17e)

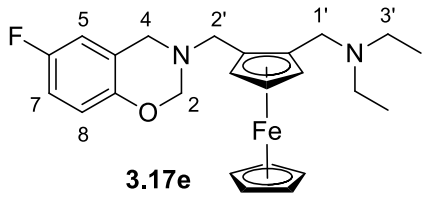

3.17e

Brown viscous oil. Yield: 59.8 mg (54%). ^{1}H NMR (600 MHz, $CDCl_3$) δ 6.82 (td, J = 8.6, 2.9 Hz, 1H, H_7), 6.75 (dd, J = 8.9, 4.8 Hz, 1H, H_5), 6.64 (dd, J = 8.5, 2.9 Hz, 1H, H_8), 4.86 (d, J = 9.8 Hz, 1H, H_{2a}), 4.83 (d, J = 9.8 Hz, 1H, H_{2b}), 4.23 – 4.22 (m, 2H, FcH), 4.09 (t, J = 2.3 Hz, 1H, FcH), 4.02 (s, 5H, FcH), 3.99 (s, 2H, H_4), 3.75 (d, J = 1.5 Hz, 2H, H_2), 3.46 (d, J = 13.4 Hz, 1H, $H_{1'a}$), 3.29 (d, J = 13.5 Hz, 1H, $H_{1'b}$), 2.52 (dq, J = 14.2, 7.1 Hz, 2H, $H_{3'a}$), 2.41 (dq, J = 14.0, 7.0 Hz, 2H, $H_{3'b}$), 0.94 (t, J = 7.1 Hz, 6H, Me_2); ^{13}C NMR (150 MHz, CDl_3) δ 156.9 (d, J = 238.8 Hz), 150.4 (d, J = 1.9 Hz), 121.7 (d, J = 6.5 Hz), 117.4 (d, J = 7.6 Hz), 114.2 (d, J = 23.0 Hz), 113.8 (d, J = 22.6 Hz); 85.0, 83.8, 82.6, 70.9, 70.2, 69.3 (5C), 66.9,

51.0, 49.7, 49.2, 46.3 (2C), 11.5 (2C); HRMS (ESI^+) *m/z* calcd for $C_{24}H_{30}FFeN_2O$ $[M+H]^+$: 437.1613, Found 437.1696.

6-Nitro-3-(2-((*N*,*N*-diethylamino)methyl)ferrocenemethyl)-3,4-dihydro-*2H*-1,3-benzoxazine (3.17f)

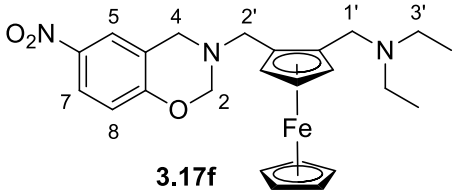

3.17f

Yellow semi-solid. Yield: 66.3 mg (46%). ^1H NMR (600 MHz, $CDCl_3$) δ 8.03 (dd, J = 8.9, 2.7 Hz, 1H, H_7), 7.89 (d, J = 2.6 Hz, 1H, H_5), 6.85 (d, J = 9.0 Hz, 1H, H_8), 5.00 – 4.97 (m, 2H, H_2), 4.22 (t, J = 2.2 Hz, 1H, FcH), 4.10 (t, J = 2.5 Hz, 1Hm FcH), 4.07 – 4.03 (m, 3H, H_4, FcH), 4.02 (s, 5H, FcH), 3.77 (d, J = 13.3 Hz, 1H, $H_{2'a}$), 3.71 (d, J = 13.3 Hz, 1H, $H_{2'b}$), 3.46 (d, J = 13.3 Hz, 1H, $H_{1'a}$), 3.22 (d, J = 13.3 Hz, 1H, $H_{1'b}$), 2.57 – 2.48 (m, 2H, $H_{2'a}$), 2.37 (d, J = 13.6, 2H, $H_{2'b}$), 0.92 (t, J = 7.1 Hz, 6H, Me_2); ^{13}C NMR (151 MHz, $CDCl_3$) δ 160.2, 140.9, 124.2, 123.7, 120.7, 116.8, 83.7, 83.2, 71.1, 70.1, 69.4 (5C), 69.3, 67.0, 50.9, 49.8, 48.7, 46.2 (2C), 11.2 (2C); HRMS (ESI^+) *m/z* calcd for $C_{24}H_{30}FeN_3O_3[M+H]^+$: 464.1648, Found 464.1642.

General procedure for synthesis of α-amino-*o*-cresols (4.6a-i and 4.7a-e)[5]

To a solution of ferrocenyl amine **3.12a-b** (1.0. eq.) in EtOH (5 mL) was added an appropriate salicyaldehyde **4.5a-i** or aldehyde **4.8a-c** (1.0 eq.) and the resulting suspension was refluxed for 4 hours. After 4 hours, the reaction mixture was allowed to cool to room temperature followed by addition of sodium borohydride (2.0 eq.). The reaction mixture was stirred at room temperature for 15 minutes and then refluxed for another 15 minutes. Following cooling to room temperature, 2N HCl solution was added to extract the product into the aqueous phase and washed with EtOAc (25 mL). The aqueous layer was basified with 1N NaOH solution (pH 8) and the product extracted with DCM (2 × 25 mL). The collected organic layers were combined, dried (Na_2SO_4) and the solvent was removed under reduced pressure to afford the

desired compound in high purity. In some cases the product was purified by column chromatography on basic alumina using gradient elution (DCM → 1:9 MeOH/DCM) to furnish the pure compound.

_N_-2-((_N_,_N_-Dimethylamino)methyl)ferrocenemethyl α-amino-_o_-cresol (4.6a)

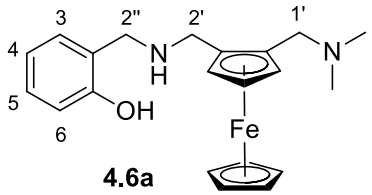

4.6a

Brown semi-solid. Yield: 175.0 mg (95%). ^{1}H NMR (600 MHz, $CDCl_3$) δ 7.17 (t, J = 7.7 Hz, 1H, H_5), 6.94 (d, J = 7.2 Hz, 1H, H_6), 6.84 (d, J = 8.0 Hz, 1H, H_3), 6.77 (t, J = 7.4 Hz, 1H, H_4), 4.11 (d, J = 2.5 Hz, 2H, $H_{2''}$), 4.05 (t, J = 2.5 Hz, 1H, FcH), 4.02 (s, 5H, FcH), 3.86 (d, J = 7.9 Hz, 2H, FcH), 3.79 (d, J = 13.5 Hz, 1H, $H_{1'a}$), 3.73 (d, J = 12.6 Hz, 1H, $H_{2'a}$), 3.34 (d, J = 13.5 Hz, 1H, $H_{1'b}$), 2.77 (d, J = 12.6 Hz, 1H, $H_{2'b}$), 2.12 (s, 6H, NMe_2); ^{13}C NMR (150 MHz, $CDCl_3$) δ 159.1, 128.5, 128.5, 122.6, 118.8, 116.4, 84.6, 84.1, 71.3, 70.7, 69.1 (5C), 66.0, 58.4, 50.8, 45.9, 45.0 (2C); ; IR (ATR, cm^{-1}) v = 3219 (O-H), 1653 (N-H), 1271 (C-N); HRMS (ESI^+) *m/z* calcd for $C_{21}H_{27}FeN_2O$ $[M+H]^+$: 379.1465, Found 379.1467; HPLC purity > 99% (t_R = 2.97 min).

_N_-2-((_N_,_N_-Dimethylamino)methyl)ferrocenemethyl 4-methyl-α-amino-_o_-cresol (4.6b)

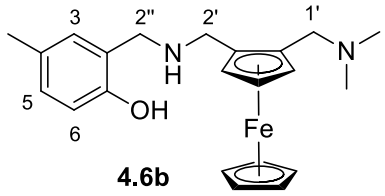

4.6b

Brown semi-solid. Yield: 86.5 mg (63%). ^{1}H NMR (600 MHz, $CDCl_3$) δ 6.97 (dd, J = 8.1, 1.6 Hz, 1H, H_5), 6.76 (br s, 1H, H_3), 6.74 (d, J = 8.1 Hz, 1H, H_6), 4.14 – 4.10 (m, 2H, FcH), 4.05 (t, J = 2.4 Hz, 1H, FcH), 4.02 (s, 5H, FcH), 3.82 (d, J = 6.0 Hz, 2H, $H_{2''}$), 3.78 (d, J = 13.5 Hz, 1H, $H_{1'a}$), 3.72 (d, J = 12.6 Hz, 1H, $H_{2'a}$), 3.34 (d, J = 13.5 Hz, 1H, $H_{2'b}$), 2.76 (d, J = 12.6 Hz, 1H, $H_{1'b}$), 2.25 (s, 3H, Me), 2.12 (s, 6H, NMe_2); ^{13}C NMR (150 MHz, $CDCl_3$) δ 152.7, 131.4, 129.1, 128.0, 126.1, 115.0, 85.2, 71.1, 70.3, 69.0 (5C), 66.1, 58.0, 52.6, 47.2, 45.8, 43.9 (2C); 20.3; HRMS (ESI^+) *m/z* calcd for $C_{22}H_{29}FeN_2O$ $[M+H]^+$: 393.1631, Found 393.1632; HPLC purity > 99% (t_R = 3.04 min).

_N_-2-((_N_,_N_-Dimethylamino)methyl)ferrocenemethyl 4-bromo-α-amino-_o_-cresol (4.6c)

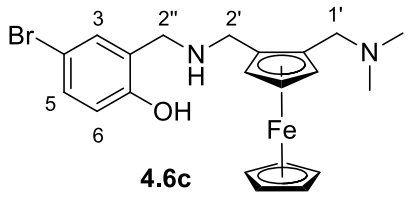

4.6c

Brown viscous oil. Yield: 138.0 mg (41%). ^{1}H NMR (600 MHz, $CDCl_3$) δ 7.24 (d, J = 7.6 Hz, 1H, H_5), 7.05 (br s, 1H, H_3), 6.72 (d, J = 8.5 Hz, 1H, H_6), 4.12 (s, 2H, FcH), 4.07 – 4.06 (m, 1H, FcH), 4.03 (s, 5H, FcH), 3.84 – 3.79 (m, 3H, $H_{2'a}$, $H_{2''}$), 3.75 (d, J = 12.6 Hz, 1H, $H_{1'a}$), 3.31 (d, J = 13.5 Hz, 1H, $H_{2'b}$), 2.77 (d, J = 12.6 Hz, 1H, $H_{1'b}$), 2.13 (s, 6H, NMe_2); ^{13}C NMR (150 MHz, $CDCl_3$) δ 158.3, 131.3, 131.1, 124.5, 118.3, 110.4, 84.1, 83.9, 71.5, 70.8, 69.2 (5C), 66.1, 58.4, 50.2, 45.9, 44.9 (2C); HRMS (ESI^+) *m/z* calcd for $C_{21}H_{26}BrFeN_2O$ $[M+H]^+$: 457.0578, Found 457.0573; HPLC purity > 82 % (t_R = 3.06 min).

_N_-2-((_N_,_N_-Dimethylamino)methyl)ferrocenemethyl 4-methoxy-α-amino-_o_-cresol (4.6d)

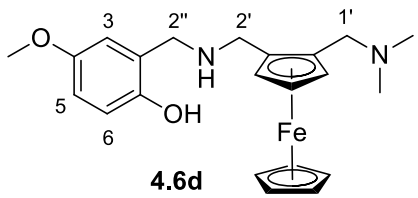

4.6d

Yellow semi-solid. Yield: 98.8 mg (50%). ^{1}H NMR (600 MHz, $CDCl_3$) δ 7.26 (s, 1H, H_5), 6.92 – 6.85 (m, H_3, H_6), 4.12 – 4.00 (m, 8H, FcH), 3.84 (br s, 2H, $H_{2''}$), 3.63 – 3.64 (m, 2H, $H_{2'}$), 2.90 – 2.74 (m, 1H, $H_{1'}$), 2.13 (s, 6H, NMe_2); HRMS (ESI^+) *m/z* calcd for $C_{21}H_{26}FeN_3O_3$ $[M+H]^+$: 407.1858, Found 407.1864.

_N_-2-((_N_,_N_-Dimethylamino)methyl)ferrocenemethyl 4-nitro-α-amino-_o_-cresol (4.6e)

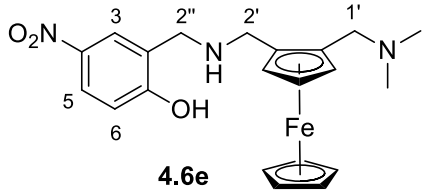

4.6e

Yellow semi-solid. Yield: 98.8 mg (55%). ^{1}H NMR (600 MHz, $CDCl_3$) δ 8.10 – 8.05 (m, 1H, H_5), 7.87 (d, J = 2.8 Hz, 1H, H_3), 6.71 (d, J = 9.0 Hz, 1H, H_8), 4.16 (br s, 1H, FcH), 4.15 (br s, 1H, FcH), 4.11 (s, 1H, FcH), 4.06 – 4.02 (m, 7H, FcH, $H_{2''}$), 3.89 (d, J = 13.6 Hz, 1H, $H_{2'a}$), 3.79 (d, J = 13.6 Hz, 1H, $H_{2'b}$), 3.39 (d, J = 12.7 Hz, 1H, $H_{1'a}$), 2.79 (d, J = 12.7 Hz, 1H, $H_{1'b}$), 2.13 (s, 6H, NMe_2); ^{13}C NMR (151 MHz, $CDCl_3$) δ 159.6, 140.3, 128.9, 124.8, 123.9, 115.4, 83.9 (2C), 71.7, 71.0, 69.4, 69.2 (5C), 66.4, 58.2, 44.7, 44.6 (2C); HRMS (ESI^+)

m/z calcd for $C_{21}H_{26}FeN_3O_3$ $[M+H]^+$: 423.1245, Found 423.1986; HPLC purity > 93% (t_R = 4.83 min).

_N_-2-((_N_,_N_-Dimethylamino)methyl)ferrocenemethyl 6-methoxy-α-amino-_o_-cresol (4.6f)

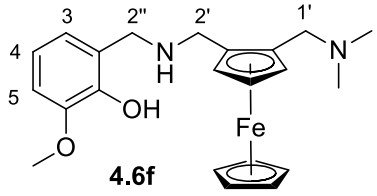

4.6f

Light brown viscous oil. Yield: 228.8 mg (76%). ^{1}H NMR (600 MHz, $CDCl_3$) δ 6.82 (d, J = 7.9 Hz, 1H, H_5), 6.75 (t, J = 7.8 Hz, 1H, H_4), 6.67 (d, J = 7.5 Hz, 1H, H_3), 4.17 (br s, 1H, FcH), 4.13 (br s, 1H, FcH), 4.06 (t, J = 2.4 Hz, 1H, FcH), 4.03 (s, 5H, FcH), 3.93 (d, J = 6.0 Hz, 1H, $H_{2"a}$), 3.91 (d, J = 6.0 Hz, 1H, $H_{2"b}$), 3.88 (s, 3H, OMe), 3.85 (d, J = 14.0 Hz, 1H, $H_{2'a}$), 3.77 (d, J = 12.7 Hz, 1H, $H_{1'a}$), 3.43 (d, J = 14.0 Hz, 1H, $H_{2'b}$), 2.81 (d, J = 12.7 Hz, 1H, $H_{1'b}$), 2.12 (s, 6H, NMe_2); ^{13}C NMR (150 MHz, $CDCl_3$) δ 148.0, 147.8, 122.1, 120.9, 118.5, 110.8, 83.8, 83.6, 71.4, 71.0, 69.1 (5C), 66.1, 58.2, 56.0, 49.6, 45.7, 44.8 (2C); HRMS (ESI^+) *m/z* calcd for $C_{22}H_{29}FeN_2O_2$ $[M+H]^+$: 409.1578, Found 409.1581; HPLC purity > 82 % (t_R = 3.23 min).

_N_-2-((_N_,_N_-Dimethylamino)methyl)ferrocenemethyl 6-nitro-α-amino-_o_-cresol (4.6g)

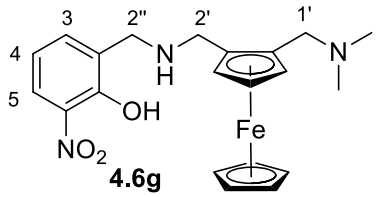

4.6g

Light yellow sticky solid. Yield: 48.2 mg (38%). ^{1}H NMR (600 MHz, $CDCl_3$) δ 7.90 (d, J = 8.2 Hz, 1H), H_5, 7.06 (d, J = 6.6 Hz, 1H, H_3), 6.32 (t, J = 7.6 Hz, 1H, H_4), 4.48 (d, J = 13.1 Hz, 1H, $H_{2'a}$), 4.27 (s, 1H, FcH), 4.19 (d, J = 9.2 Hz, 1H, FcH), 4.16 (s, 1H, FcH), 4.12 (s, 5H, FcH), 4.10 – 4.06 (m, 1H, $H_{2'b}$), 3.85 – 3.75 (m, 2H, $H_{2"}$), 3.65 (d, J = 12.9 Hz, 1H, $H_{1'a}$), 3.37 (d, J = 6.7 Hz, 1H, exch D_2O, NH), 2.88 (d, J = 12.8 Hz, 1H, $H_{1'b}$), 2.17 (s, 6H, NMe_2); ^{13}C NMR (150 MHz, $CDCl_3$) δ 135.3, 127.3, 126.6, 125.8, 122.9, 111.6, 83.7, 77.4, 71.9, 71.8, 69.7 (5C), 67.1, 57.7, 47.5, 45.4, 44.3 (2C); HRMS (ESI^+) *m/z* calcd for $C_{21}H_{25}FeN_3O_3$ $[M+H]^+$: 424.1324, Found 424.1324; HPLC purity > 94% (t_R = 4.43 min).

_N_-2-((_N_,_N_-Dimethylamino)methyl)ferrocenemethyl 4,6-dibromo-α-amino-_o_-cresol (4.6h)

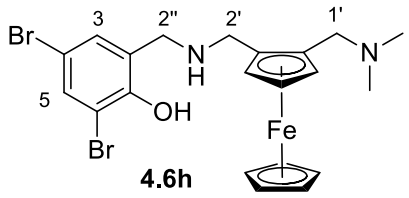

4.6h

Red sticky solid. Yield: 170.1 mg (83%). ^{1}H NMR (600 MHz, $CDCl_3$) δ 7.50 (s, 1H, H_5), 6.96 (s, 1H, H_5), 3 4.16 (s, 2H, FcH) 4.10 (s, 1H, FcH), 4.05 (s, 5H, FcH), 3.98 – 3.91 (m, 2H, $H_{2''}$), 3.82 – 3.77 (m, 2H, $H_{2'a}$, $H_{1'a}$), 3.37 (d, J = 13.0 Hz, 1H, $H_{2'b}$), 2.85 (d, J = 12.3 Hz, 1H, $H_{1'b}$), 2.18 (s, 6H, NMe_2); ^{13}C NMR (150 MHz, $CDCl_3$) δ 156.3, 133.9, 130.3, 124.3, 112.0, 109.0, 83.0, 82.7, 71.7, 71.2, 69.3 (5C), 66.7, 58.1, 49.7, 45.6, 44.6 (2C); HRMS (ESI^+) *m/z* calcd for $C_{21}H_{25}Br_2FeN_2O$ $[M+H]^+$: 534.9683, Found 534.9680; HPLC purity > 92% (t_R = 7.18 min).

_N_-2-((_N_,_N_-Dimethylamino)methyl)ferrocenemethyl 6-bromo-4-nitro-α-amino-_o_-cresol (4.6i)

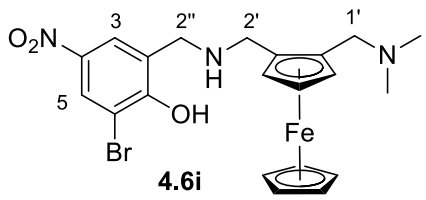

4.6i

Light orange solid. Yield: 58.6 mg (23%). ^{1}H NMR (600 ^{1}H NMR (600 MHz, $CDCl_3$) δ 8.46 (d, J = 2.8 Hz, 1H, H_5), 7.82 (d, J = 2.8 Hz, 1H, H_3), 4.32 (d, J = 13.6 Hz, 1H, $H_{2'a}$), 4.27 – 4.26 (m, 1H, FcH), 4.24 (t, J = 1.8 Hz, 1H, FcH), 4.21 (t, J = 2.5 Hz, 1H, FcH), 4.12 (s, 5H, FcH), 3.89 (d, J = 7.5 Hz, 1H, $H_{2''a}$), 3.87 (d, J = 7.5 Hz, 1H, $H_{2''b}$), 3.72 (d, J = 13.6 Hz, 1H, $H_{2''b}$), 3.64 (d, J = 13.1 Hz, 1H, $H_{1'a}$), 2.90 (d, J = 13.0 Hz, 1H, $H_{1'b}$), 2.12 (s, 6H, Me_2); ^{13}C NMR (150 MHz, $CDCl_3$) δ 159.6, 142.0, 129.6, 126.2, 123.5, 111.1, 83.7, 77.4, 71.9, 71.8, 69.7 (5C), 67.1, 57.7, 47.5, 45.4, 44.3 (2C); HRMS (ESI^+) *m/z* calcd for $C_{21}H_{25}BrFeN_3O_3$ $[M+H]^+$: 502.0418, Found 502.0420; HPLC purity > 97% (t_R = 3.88 min).

_N_-2-Ferrocenemethyl α-amino-_o_-cresol (4.7a)

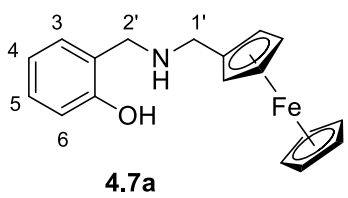

4.7a

Brown solid. Yield: 293.5 mg (98%). M.p.: 116.5 – 119.0 °C. ^{1}H NMR (600 MHz, $CDCl_3$) δ 7.19 (br s, 1H, H_5), 7.00 (d, J = 7.3 Hz, 1H, H_6), 6.86 (d, J = 7.9 Hz, 1H, H_3), 6.79 (br s, 1H, H_4), 4.17 (s, 2H, FcH), 4.15 (s, 2H, FcH), 4.13 (s, 5H, FcH), 4.01 (s, 2H, $H_{2'}$), 3.57 (s, 2H, $H_{1'}$); ^{13}C NMR (150 MHz, $CDCl_3$) δ 158.6, 128.8, 128.5, 122.4, 119.1, 116.5, 85.1, 68.6 (5C), 68.5 (2C), 68.2 (2C), 52.0, 47.5; HRMS (ESI^+) *m/z* calcd for $C_{18}H_{20}FeNO$ $[M+H]^+$: 322.0889, Found 322.0900; HPLC purity > 95% (t_R = 2.37 min).

_N_-2-Ferrocenemethyl 4-bromo-α-amino-_o_-cresol (4.7b)

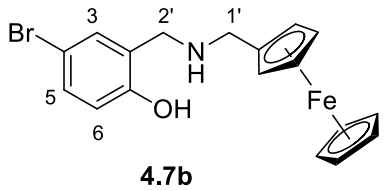

4.7b

Light orange solid. Yield: 180.0 mg (97%). M.p.: 106.5 – 107.2 °C. ^{1}H NMR (600 MHz, $CDCl_3$) δ 7.24 (br s, 1H, H_5), 7.10 (br s, 1H, H_3), 6.72 (br s, 1H, H_6), 4.15 (s, 4H, FcH), 4.12 (s, 5H, HcH), 3.95 (s, 2H, $H_{2'}$), 3.54 (s, 2H, $H_{1'}$); ^{13}C NMR (150 MHz, $CDCl_3$) δ 157.8, 131.5, 131.2, 124.4, 118.4, 110.8, 84.7, 68.7 (5C), 68.5 (5C), 68.4 (2C), 51.4, 47.5; IR (ATR, cm^{-1}) ν = 3219 (O-H), 1653 (N-H), 1271 (C-N); HRMS (ESI^+) *m/z* calcd for $C_{18}H_{19}BrFeNO$ $[M+H]^+$: 399.9994, Found 400.001; HPLC purity > 91% (t_R = 5.03 min).

_N_-2-Ferrocenemethyl 6-nitro-α-amino-_o_-cresol (4.7c)

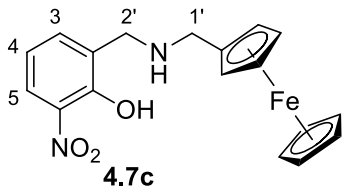

4.7c

Light green semi-solid. Yield: 130.0 mg (96%). ^{1}H NMR (400 MHz, $CDCl_3$) δ 8.10 (d, J = 7.7 Hz, 1H, H_5), 7.42 (d, J = 7.0 Hz, 1H, H_3), 6.69 (t, J = 7.5 Hz, 1H, H_4), 4.59 (s, 2H, $H_{2'}$), 4.24 – 4.15 (m, 9H, FcH), 4.01 (s, 2H, $H_{1'}$); ^{13}C NMR (100 MHz, $CDCl_3$) δ 139.6, 138.3, 131.6, 120.0, 114.4, 110.1, 81.8, 69.0 (7C), 68.5 (2C), 54.4, 47.5; HRMS (ESI^+) *m/z* calcd for $C_{18}H_{19}FeN_2O_3$ $[M+H]^+$: 367.0745, Found 367.0753; HPLC purity > 87% (t_R = 3.99 min).

_N_-2-Ferrocenemethyl 4,6-dibromo-α-amino-_o_-cresol (4.7d)

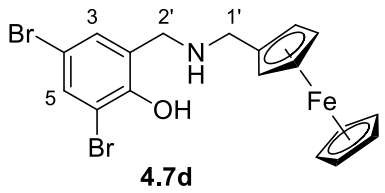

4.7d

Brown semi-solid. Yield: 314.8 mg (71%). ^{1}H NMR (600 MHz, $CDCl_3$) δ 7.55 (br s, 1H, H_3), 7.05 (br s, 1H, H_5), 4.18 (s, 2H, FcH), 4.16 (s, 2H, FcH), 4.13 (s, 5H, FcH), 3.96 (s, 2H, $H_{2'}$), 3.56 (s, 2H, $H_{1'}$); ^{13}C NMR (150 MHz, $CDCl_3$) δ 156.3, 133.9, 130.3, 124.3, 112.0, 109.0, 84.9, 68.8 (5C), 68.3 (2C), 68.0 (2C), 57.9, 48.0; HRMS (ESI$^+$) *m/z* calcd for $C_{18}H_{18}Br_2FeNO$ $[M+H]^+$: 477.9105, Found 477.9099; HPLC purity > 85% (t_R = 6.99 min).

_N_-2-Ferrocenemethyl 4,6-dibromo-α-amino-_o_-cresol (4.7e)

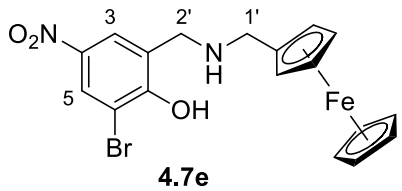

4.7e

Light brown semi-solid. Yield: 241.8 mg (82%). ^{1}H NMR (600 MHz, DMSO-d_6) δ 8.49 (d, J = 2.9 Hz, 1H, H_5), 8.41 (d, J = 2.9 Hz, 1H, H_3), 4.63 (s, 2H, $H_{2'}$), 4.33 (t, J = 1.8 Hz, 2H, FcH), 4.27 (s, 5H, FcH), 4.24 (t, J = 1.8 Hz, 2H, FcH), 4.21 (s, 2H, $H_{1'}$); ^{13}C NMR (150 MHz, DMSO) δ 166.8, 132.8, 132.3, 131.1, 118.0, 111.5, 81.7, 68.4 (5C), 68.2 (2C), 67.6 (2C), 57.9, 49.7; HRMS (ESI$^+$) *m/z* calcd for $C_{18}H_{19}BrFeN_2O_3$ $[M+H]^+$: 444.9845, Found 444.9872; HPLC purity > 86% (t_R = 2.05 min).

***N*-((*N*,*N*-Dimethylamino)methyl)ferrocenemethyl)methyl benzylamine (4.9c)**

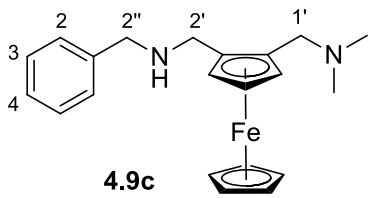

4.9c

Brown semi-solid. Yield: 384 mg (97%). ^{1}H NMR (600 MHz, $CDCl_3$) δ 7.32 – 7.31 (m, 4H, H_2, H_3), 7.26 – 7.23 (m, 1H, H_4), 4.19 (s, 1H, FcH), 4.10 (s, 1H, FcH), 4.04 (s, 1H, FcH), 4.02 (s, 5H, FcH), 3.84 – 3.78 (m, 2H, $H_{2''}$), 3.70 (d, J = 13.1 Hz, 1H, $H_{2'a}$), 3.64 (d, J = 12.6 Hz, $H_{2'b}$), 3.37 (d, J = 13.1 Hz, 1H, $H_{1'a}$), 2.81 (d, J = 13.0 Hz, 1H, $H_{1'b}$), 2.09 (s, 6H, NMe_2); ^{13}C NMR (150 MHz, $CDCl_3$) δ 139.5, 128.4 (2C), 128.3 (2C), 127.0 (2C), 85.3, 71.1, 70.3, 69.0 (5C), 66.1, 58.0, 52.6, 46.9, 44.9 (2C); HRMS (ESI$^+$) *m/z* calcd for $C_{21}H_{27}FeN_2$ $[M+H]^+$: 363.1524, Found 363.1527; HPLC purity > 87% (t_R = 4.59 min).

_N_-((_N_,_N_-Dimethylamino)methyl)ferrocenemethyl)methyl 2-methoxybenzylamine (4.9c)

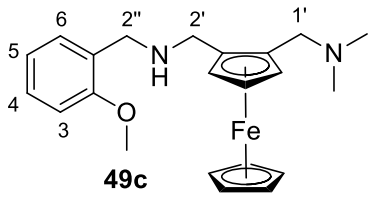

49c

Orange viscous oil. Yield: 45 mg (34%). ^{1}H NMR (400 MHz, $CDCl_3$) δ 6.81 – 6.70 (m, 3H, H_3, H_4, H, H_5), 6.55 – 6.51 (m, 1H, H_6), 4.11 – 4.09 (m, 4H, $H_{2''}$, FcH), 4.04 (br s, H, FcH), 4.02 (s, 5H, FcH), 3.80 (dd, J = 14.0, 10.5 Hz, 2H, $H_{2'}$), 3.74 (s, Hz, 3H, OMe), 3.32 (d, J = 13.4 Hz, 1H, $H_{1'a}$), 2.76 (d, J = 12. Hz, 1H, $H_{1'b}$), 2.11 (s, 6H, NMe_2); ^{13}C NMR (100 MHz, $CDCl_3$) δ 157.7, 129.9, 120.5 (2C), 110.3 (2C), 84.0, 83.6, 70.8, 69.4, 69.1 (5C), 69.0, 66.2, 57.9, 55.4, 50.4, 45.0 (2C); HRMS (ESI$^+$) *m/z* calcd for $C_{22}H_{29}FeN_2O$ $[M]^+$: 393.1622, Found 393.1623; HPLC purity > 95% (t_R = 5.12 min).

_N_-((_N_,_N_-Dimethylamino)methyl)ferrocenemethyl)methyl 2-nitrobenzylamine (4.9c)

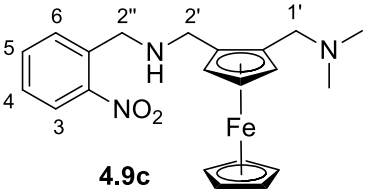

4.9c

Brown semi-solid. Yield: 124.2 mg (59%). ^{1}H NMR (600 MHz, $CDCl_3$) δ 7.94 (d, J = 8.1 Hz, 1H, H_3), 7.66 (d, J = 7.7 Hz, 1H, H_4), 7.58 (t, J = 7.5 Hz, 1H, H_4), 7.39 (t, J = 7.7 Hz, 1H, H_5), 4.19 (br s, 1H, FcH), 4.12 – 4.10 (m, 1H, FcH), 4.02 (br s, 1H, FcH), 4.05 – 3.99 (m, 7H, FcH, $H_{2''}$), 3.76 (d, J = 12.9 Hz, 1H, $H_{2'a}$), 3.61 (d, J = 12.6 Hz, 1H, $H_{1'a}$), 3.37 (d, J = 12.9 Hz, 1H, $H_{2'b}$), 2.83 (d, J = 12.6 Hz, 1H, $H_{1'b}$), 2.09 (s, 6H, NMe_2); ^{13}C NMR (150 MHz, $CDCl_3$) δ 149.1, 136.1, 133.2, 130.8, 127.7, 124.7, 86.2, 83.6, 71.1, 69.9, 69.0 (5C), 66.2, 53.6, 50.0, 47.7, 45.0 (2C); HRMS (ESI$^+$) *m/z* calcd for $C_{21}H_{26}FeN_3O_2$ $[M+H]^+$: 408.1367, Found 408.1369; HPLC purity > 92% (t_R = 7.18 min).

Synthesis of *N*-((*N*,*N*-dimethylamino)methyl)ferrocenemethyl)methyl 2-aminobenzylamine (4.9d)[6]

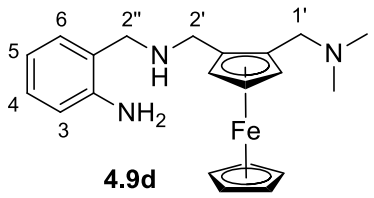

4.9d

A mixture of 2-nitrobenzylamine **4.9c** (95.0 mg), zinc dust (126.0 mg) and ammonium chloride (25.0 mg) in methanol (10 mL) was refluxed for 12 hours. Following reflux, the solids were removed through a small pad of silica gel and filtrate collected and concentrated *in vacuo*. The resulting residue was re-dissolved in EtOAc (25 mL) and then successively washed with saturated $NaHCO_3$ solution and water. The collected organic layer was dried (Na_2SO_3) and the solvent removed under reduced pressure to afford the desired compound as a yellow semi-solid in high purity. Yield: 86.0 mg (98%). ^{1}H NMR (600 MHz, $CDCl_3$) δ 8.69 (d, J = 9.0 Hz, 1H, H_3), 7.65 (d, J = 8.4 Hz, 1H, H_4), 7.45 – 7.39 (m, 1H, H_5), 7.20 – 7.16 (m, 1H, H_6), 6.55 (d, J = 15.1 Hz, 1H, $H_{2''a}$), 5.34 (d, J = 15.1 Hz, 1H, $H_{2''b}$), 4.78 (d, J = 13.0 Hz, 1H, $H_{2'a}$), 4.25 – 4.24 (m, 6H, FcH), 4.21 (br s, 1H, FcH), 4.17 (t, J = 2.5 Hz, 1H, FcH), 4.13 – 4.10 (m, 1H, $H_{2'b}$), 3.08 (d, J = 13.0 Hz, 1H, $H_{1'a}$), 2.71 – 2.70 (m, 1H, $H_{1'b}$), 2.29 – 2.20 (m, 6H, NMe_2); ^{13}C NMR (150 MHz, $CDCl_3$) δ 129.6, 127.3, 123.6, 121.5, 120.3, 117.5, 82.6, 79.4, 73.6, 70.0, 69.8 (5C), 69.4, 58.4, 51.8, 49.2, 43.3 (2C); HRMS (ESI^+) *m/z* calcd for $C_{21}H_{28}FeN_3$ $[M+H]^+$: 378.1633, Found 378.1629; HPLC purity > 83% (t_R = 4.11 min).

Synthesis of *N*-ferrocenyl salicylamides 4.15a-e and 4.16a-b

Method A: Amidation with phosphorus trichloride[7]

Phosphorus trichloride (16 μL, 0.184 mmol) was added to a suspension of amine **3.12b** (100.0 mg, 0.367 mmol) and salicylic acid **4.14a** (50.7 mg, 0.367 mmol) in chlorobenzene (20 mL) on ice. The reaction mixture was refluxed for 5 hours after which the resulting dark brown solution was cooled to room temperature. Unreacted PCl_3 was quenched by addition of distilled

water (25 mL) and the product extracted with $CHCl_3$. An emulsion formed after addition of $CHCl_3$. Thus, saturated brine (20 mL) was added to facilitate separation of the layers. The collected organic layers were combined, dried (Na_2SO_4) and the solvents removed under reduced pressure. The remaining volume of chlorobenzene was removed by freeze-drying the crude product overnight. The resultant brown paste was subjected to silica gel column chromatography (1:2:7 Et_3N/EtOac/Hex) to afford the product (**4.15a**) as a light brown semi-solid. Yield: 13.0 mg (9%).

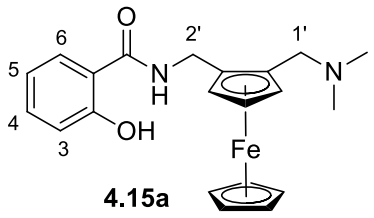

4.15a

^{1}H NMR (400 MHz, $CDCl_3$) δ 7.33 – 7.14 (m, 2H, H_3, H_4), 6.90 (t, J = 8.2 Hz, 1H, H_5), 6.69 (br s, 1H, H_6), 4.68 (d, J = 13.1 Hz, 1H, $H_{2'a}$), 4.24 – 4.16 (m, 2H, FcH), 4.06 (s, 6H, FcH), 3.83 – 3.80 (m, 1H, $H_{2'b}$), 3.10 – 3.04 (m, 1H, $H_{1'a}$) 2.82 (q, J = 12.1 Hz, 1H, $H_{1'b}$), 2.19 (s, NMe_2); ^{13}C NMR (100 MHz, $CDCl_3$) δ 169.1, 161.8, 133.6, 125.7, 118.3, 118.2, 114.8, 83.9, 71.3, 70.4, 69.6, 69.3 (5C), 66.0, 44.8, 38.3, 29.7 (2C); IR (ATR, cm^{-1}) v = 2925 (N-H, amide), 1758 (C=O, amide); HRMS (ESI$^+$) *m/z* calcd for $C_{21}H_{25}FeN_2O_2$ $[M+H]^+$: 393.1290, Found 393.1295; HPLC purity > 80% (t_R = 4.09 min).

Method B: Amidation with *N,N'*-dicyclohexylcarbodiimide (DCC)[8]

A suspension of ferrocenyl amine **3.12b** (100.0 mg, 0.367 mmol), salicylic acid **4.14a** (50.7 mg, 0.367 mmol) and DDC (90.9 mg, 0.440 mmol) in pyridine (15 mL) was stirred at room temperature for 24 hours. A heavy white precipitate of the urea side product was observed at the termination of the reaction. The reaction mixture was diluted with EtOAc (25 mL) and filtered through celite, eluting the product with 25 mL of the solvent. The filtrate was successively washed with 1N HCl solution (25 mL) and brine (25 mL), dried (Na_2SO_4) and the solvent removed *in vacuo* to afford the crude product, which still contained the urea precipitate. Filtration (celite) of the crude product and removal of the solvent was repeated as necessary

until all the urea precipitate was removed. The obtained crude product was purified by silica gel column chromatography (1:2:7 Et_3N/EtOAc/Hex) to furnish the pure compound **4.15a** as a light brown semi-solid in 48% yield (69.0 mg).

Method C: DCC amidation using microwave irradiation

A suspension of ferrocenyl amine **3.12b** (100.0 mg, 0.367 mmol), salicylic acid **4.14a** (50.7 mg, 0.367 mmol) and DDC (90.9 mg, 0.440 mmol) pyridine (15 mL) was heated in a monowave microwave reactor at 80 °C for 2 hours. After completion of the reaction, the formed dark brown suspension was put on ice for 10 minutes, diluted with EtOAc (25 mL) and then filtered through celite to remove the urea precipitate. The crude product was obtained after drying the collected filtrate under reduced pressure and then subjected to silica gel column chromatography to afford the pure salicylamide product **4.15a** (1:2:7 Et_3N/EtOAc/Hex). Yield: 92% (132.0 mg).

The other salicylamides **4.15b-e** were synthesized by microwave irradiation following Method C above.

***N*-(*N*,*N*-Dimethylamino)methyl)ferrocenemethyl-5-chlorosalicylamide (4.15b)**

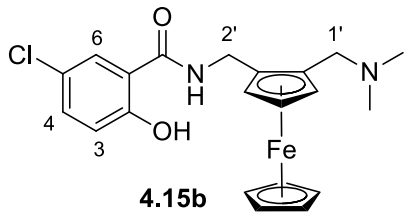

4.15b

Light yellow semi-solid. Yield: 149.0 mg (95%). ^{1}H NMR (600 MHz, $CDCl_3$) δ 7.26 – 7.25 (m, 2H, H, H_4, H_6), 6.88 (d, J = 9.0 Hz, 1H, H_3), 4.71 (d, J = 14.4 Hz, 1H, $H_{2'a}$), 4.24 (br s, 1H, FcH), 4.21 (d, J = 14.4 Hz, 1H, $H_{2'b}$), 4.14 (br s, 1H, FcH), 4.11 (s, 5H, FcH), 4.05 (t, J = 2.4 Hz, 1H, FcH), 3.86 (d, J = 12.7 Hz, 1H, $H_{1'a}$), 2.89 (d, J = 12.7 Hz, 1H, $H_{1'b}$), 2.29 (s, 6H, NMe_2); ^{13}C NMR (150 MHz, $CDCl_3$) δ 168.0, 160.4, 133.4, 125.8, 123.0, 119.9, 115.8, 83.8, 83.7, 71.6, 70.5, 69.4 (5C), 66.1, 58.4, 44.7 (2C), 38.7; HRMS (ESI^+) *m/z* calcd for $C_{21}H_{24}ClFeN_2O_2$ $[M+H]^+$: 427.0876, Found 427.0874; HPLC purity > 93% (t_R = 4.09 min).

***N*-(*N*,*N*-Dimethylamino)methyl)ferrocenemethyl-5-nitrosalicylamide (4.15c)**

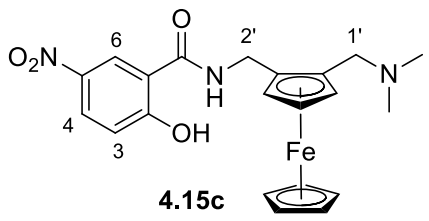

4.15c

Yellow semi-solid. Yield: 125.1 mg (78%). ^{1}H NMR (600 MHz, $CDCl_3$) δ 7.56 – 7.53 (m, 2H, H_4, H_6), 6.72 (d, J = 9.3 Hz, 1H, H_3), 4.70 (d, J = 14.4 Hz, 1H, $H_{2'a}$), 4.23 (br s, 1H, FcH), 4.19 (d, J = 14.4 Hz, 1H, $H_{2'b}$), 4.14 (br, 1H, FcH), 4.11 (s, 5H, FcH), 4.05 (t, J = 2.4 Hz, 1H, FcH), 3.84 (d, J = 12.7 Hz, 1H, $H_{1'a}$), 2.87 (d, J = 12.7 Hz, 1H, $H_{1'b}$), 2.33 (s, 6H, NMe_2); ^{13}C NMR (150 MHz, $CDCl_3$) δ 168.0, 137.6, 128.9 (2C), 124.2, 120.1, 114.7, 83.9, 81.9, 71.4, 70.6, 69.5 (5C), 66.8, 58.4, 44.2 (2C), 38.4; HRMS (ESI^+) *m/z* calcd for $C_{21}H_{24}FeN_3O_4$ $[M+H]^+$: 438.1116, Found 438.1120; HPLC purity > 97% (t_R = 2.83 min).

***N*-(*N*,*N*-Dimethylamino)methyl)ferrocenemethyl-4-fluorosalicylamide (4.15d)**

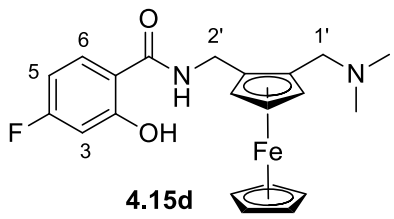

4.15d

Light orange semi-solid. Yield: 123.4 mg (82%). ^{1}H NMR (600 MHz, $CDCl_3$) δ 7.26 – 7.19 (m, 1H, H_6), 6.61 (dd, J = 10.5, 2.3 Hz, 1H, H_6), 6.46 (td, J = 8.6, 2.3 Hz, 1H, H_5), 4.71 (d, J = 14.4 Hz, 1H, $H_{2'a}$), 4.25 (s, 1H, FcH), 4.12 (s, 1H, FcH), 4.10 (s, 5H, FcH), 4.04 (s, 1H, FcH), 3.85 (d, J = 12.7 Hz, 1H, $H_{1'a}$), 2.88 (d, J = 12.7 Hz, 1H, $H_{1'b}$), 2.23 (s, 6H, NMe_2); ^{13}C NMR (150 MHz, $CDCl_3$) δ 169.6, 165.9 (d, J = 251.7 Hz), 164.0 (d, J = 13.6 Hz), 127.6 (d, J = 11.1 Hz), 111.6, 106.1 (d, J = 22.6 Hz), 104.9 (d, J = 23.3 Hz), 83.9 (2C), 71.4, 70.5, 69.4 (5C), 66.2, 58.2, 44.8 (2C), 38.4; HRMS (ESI^-) *m/z* calcd for $C_{21}H_{23}FeN_2O_2$ $[M+H]^-$: 409.1015, Found 409.1010; HPLC purity > 99% (t_R = 3.88 min).

_N_-(_N_,_N_-Dimethylamino)methyl)ferrocenemethyl-2-hydroxynicotinamide (4.15e)

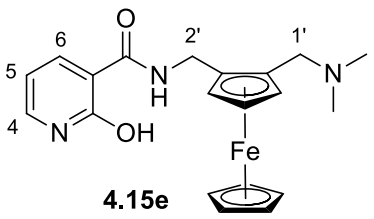

4.15e

Light brown semi-solid. Yield: 99.6 mg (69%). ^{1}H NMR (600 MHz, $CDCl_3$) δ 9.84 (s, 1H, NH), 8.56 (d, J = 7.1 Hz, 1H, H_6), 7.30 – 7.25 (m, 1H, H_4), 6.41 (t, J = 6.8 Hz, 1H, H_5), 4.49 (dd, J = 15.0, 5.7 Hz, 1H, $H_{2'a}$), 4.31 (dd, J = 15.0, 3.8 Hz, 1H, $H_{2'b}$), 4.24 (br s, 1H, FcH), 4.23 (br s, 1H, FcH), 4.16 (s, 5H, FcH), 4.10 (t, J = 2.1 Hz, 1H, FcH), 3.51 (d, J = 13.0 Hz, 1H, $H_{1'a}$), 3.31 (d, J = 13.0 Hz, 1H, $H_{1'b}$), 2.20 (s, 6H, NMe_2); ^{13}C NMR (151 MHz, $CDCl_3$) δ 163.8, 163.5, 145.3, 138.1, 121.3, 107.7, 85.3, 82.4, 70.7, 69.3, 68.5(2C), 67.1, 57.1, 44.8 (2C), 37.7; HRMS (ESI$^+$) *m/z* calcd for $C_{20}H_{24}FeN_3O_2$ $[M+H]^+$: 394.1218, Found 394.1221; HPLC purity > 98% (t_R = 3.50 min).

_N_-Ferrocenemethylsalicylamide (4.16a)

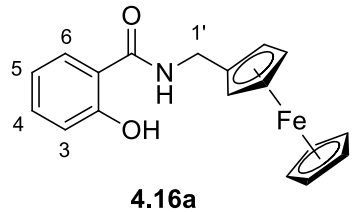

4.16a

Orange semi-solid. Yield: 218.2 mg (70%). ^{1}H NMR (400 MHz, $CDCl_3$) δ 12.37 (br s, 1H, OH), 7.40 (t, J = 8.4 Hz, 1H, H_4), 7.32 (d, J = 8.0 Hz, 1H, H_6), 7.00 (d, J = 8.3 Hz, 1H, H, H_3), 6.84 (t, J = 7.9 Hz, 1H, H_5), 6.49 (br s, 1H, NH), 4.32 (d, J = 5.1 Hz, 2H, $H_{1'}$), 4.26 – 4.25 (m, 2H, FcH), 4.21 (s, 5H, FcH), 4.20 – 4.18 (m, 2H, FcH); ^{13}C NMR (100 MHz, $CDCl_3$) δ 169.4, 161.8, 134.4, 125.3, 118.8 (2C), 114.3, 84.1, 68.7 (2C), 68.6 (7C), 39.2; HRMS (ESI$^+$) *m/z* calcd for $C_{18}H_{17}FeNO_2$ $[M]^+$: 335.0609, Found 335.0601; HPLC purity > 99% (t_R = 2.14 min).

_N_-Ferrocenemethylthiosalicylamide (4.16b)

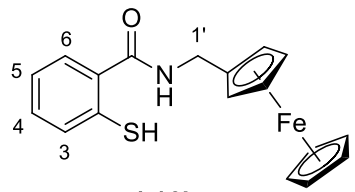

4.16b

Brown semi-solid. Yield: 222.1 mg (68%). ^{1}H NMR (600 MHz, $CDCl_3$) δ 8.02 (d, J = 7.8 Hz, 1H, H_6), 7.55 (t, J = 7.4 Hz, 1H, H_4), 7.46 (d, J = 8.0 Hz, 1H, H_3), 7.36 (t, J = 7.4 Hz, 1H, H_5), 4.82 (s, 2H, $H_{1'}$), 4.33 (s, 2H, FcH), 4.21 (s, 5H, FcH), 4.19 (s,

2H, FcH); ^{13}C NMR (150 MHz, $CDCl_3$) δ 164.9, 140.4, 131.7, 126.8, 125.5, 124.9, 120.4, 82.1, 69.6 (2C), 69.0 (7C), 43.6; HRMS (ESI^+) *m/z* calcd for $C_{18}H_{17}FeNOS$ $[M]^+$: 351.0380, Found 351.0269; HPLC purity > 99% (t_R = 3.37min).

Synthesis of ferrocenyl 1,3-benzoxazin-2-ones 47.17a-d and 4.18a-e

Method A: Cyclization with triphosgene[8]

Triphosgene (77.2 mg, 0.264 mmol) was added portion-wise to a stirring solution of ferrocenyl α-amino-*o*-cresol **4.6a** (100.0 mg, 0.264 mmol) in 50% pyridine/DCM on ice. The reaction mixture was stirred at room temperature for 5 hours. After the reaction, the reaction mixture was diluted with 2% HCl aqueous solution (15 mL) and the product extracted with DCM (2 × 25 mL), dried (Na_2SO_4) and the solvent removed under reduced pressure. The resultant crude product was purified by silica gel column chromatography (1:9 MeOH/DCM). The product was obtained as a yellow semi-solid. Yield: 20.3 mg (19%).

3-(2-((*N*,*N*-dimethylamino)methyl)ferrocenemethyl)-3,4-dihydro-*2H*-1,3-benzoxazin-2-one (4.17a)

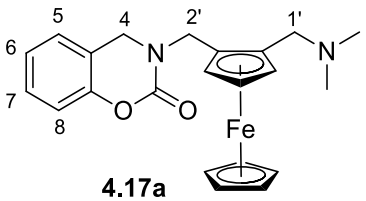

4.17a

^{1}H NMR (600 MHz, $CDCl_3$) δ 7.19 (t, J = 7.8 Hz, 1H, H_7), 7.02 (t, J = 7.5 Hz, 1H, H_6), 6.98 (d, J = 8.2 Hz, 1H, H_8), 6.95 (d, J = 7.6 Hz, 1H, H_5), 4.64 (d, J = 14.6 Hz, 1H, H_{4a}), 4.47 (d, J = 14.2 Hz, 1H, H_{4b}), 4.41 (d, J = 14.9 Hz, 1H, $H_{2'a}$), 4.34 – 4.32 (m, 2H, FcH, $H_{2'b}$), 4.27 – 4.24 (m, 1H, FcH), 4.13 (s, 1H, FcH), 4.11 (s, 5H, FcH), 3.64 (d, J = 12.6 Hz, 1H, $H_{1'a}$), 3.02 – 3.01 (m, $H_{1'b}$), 2.10 (s, 6H, NMe_2); ^{13}C NMR (150 MHz, $CDCl_3$) δ 151.0, 149.9, 128.6, 125.5, 124.0, 118.2, 116.1, 81.5 (2C), 71.6, 70.9 (5C), 69.5, 67.4, 57.4, 53.6, 46.4, 45.7, 44.8 (2C); HRMS (ESI^+) *m/z* calcd for $C_{22}H_{25}FeN_2O_2$ $[M+H]^+$: 405.1265, Found 405.1260.

Method B: Cyclization with 1,1'-carbonyldiimidazole (CDI)[9]

CDI (1.2 eq.) was added to a solution of a relevant ferrocenyl α-amino-*o*-cresol (**4.6** and **4.7**) (1.0 eq.) in DCM. The resultant reaction mixture was stirred at room temperature for 1 – 2 hours. After completion of the reaction (TLC), unreacted CDI was quenched by addition of 0.5N NaOH solution (15 mL) and the product extracted with DCM (2 × 25 mL). The combined organic layers were washed with distilled water (25 mL), dried (Na_2SO_4) and solvent removed under reduced pressure to furnish the desired carbamate product **4.17a-d** and **4.18a-e** in high purity.

3-(2-((*N*,*N*-dimethylamino)methyl)ferrocenemethyl)-3,4-dihydro-*2H*-1,3-benzoxazin-2-one (4.17a)

Compound **4.17a** was achieved in 60% yield via Method B.

5-Bromo-3-(2-((*N*,*N*-dimethylamino)methyl)ferrocenemethyl)-3,4-dihydro-*2H*-1,3-benzoxazin-2-one (4.17a)

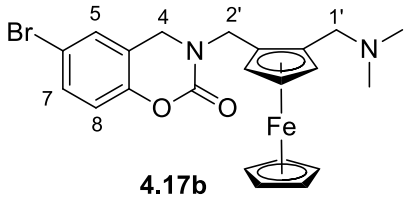

4.17b

Light brown sticky solid. Yield: 71.75 mg (45%). ^{1}H NMR (600 MHz, $CDCl_3$) δ 7.31 (dd, J = 8.7, 2.0 Hz, 1H, H_7), 7.09 (s, 1H, H_5), 6.87 (d, J = 8.7 Hz, 1H, H_8), 4.72 – 4.65 (m, 1H, FcH), 4.42 – 4.26 (m, 5H, FcH, H_4, $H_{2'}$), 4.15 (br s, 1H, FcH), 4.12 (s, 5H, FcH), 3.70 – 3.60 (m, 1H, $H_{1'a}$), 3.15 – 3.06 (m, 1H, $H_{1'b}$), 2.14 (s, 6H, NMe_2); ^{13}C NMR (150 MHz, $CDCl_3$) δ 150.4, 148.9, 131.6, 128.3, 120.2, 117.9, 116.4, 81.1 (2C), 71.9, 70.9, 70.8, 69.6 (5C), 67.7, 57.2, 46.5, 45.3, 44.5 (2C); HRMS (ESI^+) *m/z* calcd for $C_{22}H_{24}BrFeN_2O_2$ $[M+H]^+$: 483.0371, Found 483.0368.

6,8-Dibromo-3-(2-((*N*,*N*-dimethylamino)methyl)ferrocenemethyl)-3,4-dihydro-*2H*-1,3-benzoxazin-2-one (4.17c)

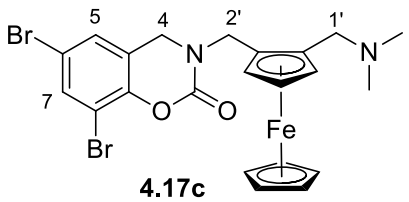

4.17c

Orange semi-solid. Yield: 126.0 mg (68%). ^{1}H NMR (600 MHz, $CDCl_3$) δ 7.55 (d, J = 1.9 Hz, 1H, H_7), 6.99 (d, J = 1.5 Hz, 1H, H_5), 4.59 (d, J = 14.5 Hz, 1H, H_{4a}), 4.47 (d, J = 14.5 Hz, 1H, H_{4b}), 4.40 (d, J = 15.4 Hz, 1H, $H_{2'a}$), 4.29 (s, 1H, FcH), 4.26 (d, J = 15.4 Hz, 1H, $H_{2'b}$), 4.16 (s, 1H, FcH), 4.10 (s, 6H, FcH), 3.61 (d, J = 12.6 Hz, 1H, $H_{1'a}$), 2.82 (d, J = 12.6 Hz, 1H, $H_{1'b}$), 2.04 (s, 6H, NMe_2); ^{13}C NMR (150 MHz, $CDCl_3$) δ 149.6, 146.5, 134.4, 127.3, 121.8, 116.2, 110.7, 84.6, 81.0, 71.8, 70.9, 69.5 (5C), 67.3, 57.6, 46.4, 45.2, 45.0 (2C); HRMS (ESI^+) *m/z* calcd for $C_{22}H_{22}Br_2FeN_2O_2$ $[C_{22}H_{23}BrFeN_2O_2+Na]^+$: 506.1441, Found 506.1441.

8-Methoxy-3-(2-((*N*,*N*-dimethylamino)methyl)ferrocenemethyl)-3,4-dihydro-*2H*-1,3-benzoxazin-2-one (4.17d)

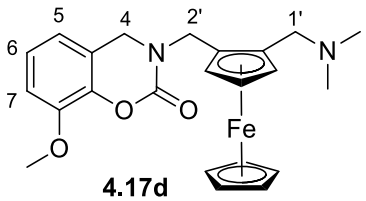

4.17d

Orange viscous oil. Yield: 125.0 mg (81%). ^{1}H NMR (600 MHz, $CDCl_3$) δ 6.94 (t, J = 7.9 Hz, 1H, H_6), 6.77 (d, J = 8.1 Hz, 1H, H_7), 6.51 (d, J = 7.7 Hz, 1H, H_5), 4.58 (d, J = 14.5 Hz, 1H, H_{4a}), 4.52 (d, J = 14.5 Hz, 1H, H_{4b}), 4.40 (d, J = 14.9 Hz, 1H, $H_{2'a}$), 4.32 – 4.28 (m, 2H, FcH, $H_{2'b}$), 4.18 (s, 1H, FcH), 4.09 (s, 6H, FcH), 3.85 (s, 3H, OMe), 3.58 (d, J = 12.7 Hz, 1H, $H_{1'a}$), 2.94 (d, J = 12.7 Hz, 1H, $H_{1'b}$), 2.08 (s, 6H, NMe_2); ^{13}C NMR (150 MHz, $CDCl_3$) δ 150.6, 147.2, 139.3, 124.0, 119.3, 116.8, 111.0, 84.6, 81.5, 71.4, 70.8, 69.4 (5C), 67.2, 57.5, 56.1, 46.3, 45.7, 45.0 (2C); HRMS (ESI^+) *m/z* calcd for $C_{23}H_{27}FeN_2O_3$ $[M+H]^+$: 435.1371, Found 435.1369.

3-Ferrocenemethyl-3,4-dihydro-*2H*-1,3-benzoxazin-2-one (4.18a)

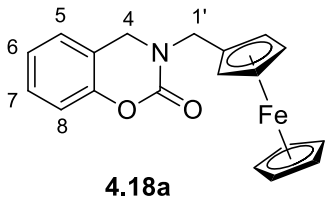

4.18a

Yellow solid: 81.8 mg (31%). ^{1}H NMR (400 MHz, $CDCl_3$) δ 7.28 – 7.19 (m, 1H, H_7), 7.05 (br s, 2H, H_6, H_8), 7.00 (d, J = 7.9 Hz, 1H, H_5), 4.42 – 4.36 (m, 6H, FcH, H_4), 4.26 (br s, 5H, FcH, $H_{1'}$); ^{13}C NMR (100 MHz, $CDCl_3$) δ 150.5, 149.6, 128.8, 125.6, 124.1, 117.3, 116.2, 86.3, 70.2 (2C), 69.3 (5C), 69.2 (2C), 48.5, 46.5; HRMS (ESI$^+$) *m/z* calcd for $C_{19}H_{18}FeNO_2$ $[M+H]^+$: 348.0687, Found 348.0666.

6-Bromo-3-ferrocenemethyl-3,4-dihydro-*2H*-1,3-benzoxazin-2-one (4.18b)

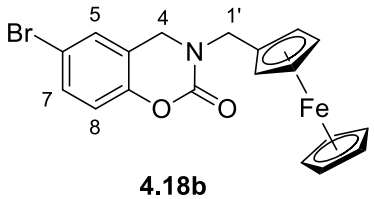

4.18b

Light yellow solid. Yield: 95.8 mg (98%). M.p: 88.0 – 88.9 °C. ^{1}H NMR (600 MHz, $CDCl_3$) δ 7.32 (d, J = 7.1 Hz, 1H, H_7), 7.17 (s, 1H, H_5), 6.87 (d, J = 8.7 Hz, 1H, H_8), 4.44 (s, 2H, FcH), 4.30 (br s, 2H, H_4), 4.29 (s, 2H, FcH), 4.19 – 4.18 (m, 7H, FcH, $H_{1'}$); ^{13}C NMR (150 MHz, $CDCl_3$) δ 150.0, 148.9, 132.0, 128.5, 119.4, 118.1, 116.6, 80.8, 69.8 (2C), 69.0 (2C), 68.9 (5C), 48.6, 45.9; IR (ATR, cm^{-1}) ν = 1702 (C=O, carbamate), 1239 (C-O), 1192 (C-N, carbamate), HRMS (ESI$^+$) *m/z* calcd for $C_{19}H_{17}BrFeNO_2$ $[M+H]^+$: 425.9787, Found 425.9573.

6,8-Dibromo-3-ferrocenemethyl-3,4-dihydro-*2H*-1,3-benzoxazin-2-one (4.18c)

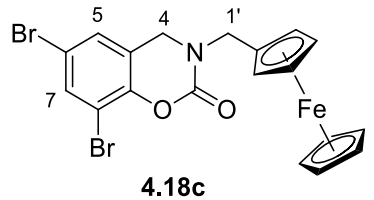

4.18c

Light yellow semi-solid. Yield: 150.0 mg (77%). ^{1}H NMR (600 MHz, $CDCl_3$ δ 7.58 (s, 1H, H_7), 7.11 (s, 1H, H_5), 4.43 (s, 2H, FcH), 4.33 – 4.27 (m, 4H, FcH, H_4), 4.20 – 4.19 (m, 7H, FcH, $H_{1'}$); ^{13}C NMR (150 MHz, $CDCl_3$) δ 149.1, 146.3, 134.9, 127.6, 120.5, 116.5, 111.0, 80.6, 69.9 (2C), 69.1 (2C), 69.0 (5C), 48.6, 46.0; HRMS (ESI$^+$) *m/z* calcd for $C_{19}H_{16}Br_2FeNO_2$ $[M+H]^+$: 503.8806, Found 503.8858.

6-Methoxy-3-ferrocenemethyl-3,4-dihydro-*2H*-1,3-benzoxazin-2-one (4.18d)

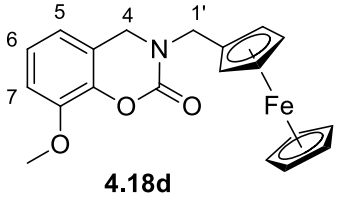

4.18d

Brown semi-solid. Yield: 95.0 mg (89%). ^{1}H NMR (600 MHz, $CDCl_3$) δ 6.98 (t, J = 8.0 Hz, 1H, H_6), 6.79 (d, J = 8.2 Hz, 1H, H_7), 6.59 (d, J = 7.7 Hz, 1H, H_5), 4.45 (s, 2H, FcH), 4.30 (s, 4H, FcH, H_4), 4.17 (s, 5H, FcH), 4.16 (s, 2H, $H_{1'}$), 3.85 (s, 3H, OMe); ^{13}C NMR (150 MHz, $CDCl_3$) δ 150.1, 147.3, 139.2, 124.2, 118.3, 116.9, 111.3, 81.2, 69.8 (2C), 68.8 (5C), 68.7 (2C), 56.1, 48.4, 46.4; HRMS (ESI^+) *m/z* calcd for $C_{20}H_{20}FeNO_3$ $[M+H]^+$: 378.0787, Found 378.0781.

6-Nitro-3-ferrocenemethyl-3,4-dihydro-*2H*-1,3-benzoxazin-2-one (4.18e)

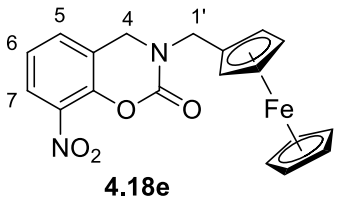

4.18e

Dark brown semi-solid. Yield: 94.7 mg (71%). ^{1}H NMR (600 MHz, $CDCl_3$) δ 7.79 (d, J = 7.9 Hz, 1H, H_7), 7.28 (d, J = 7.5 Hz, 1H, H_5), 7.16 (t, J = 7.9 Hz, 1H, H_7), 4.46 (s, 2H, H_4), 4.37 (s, 2H, FcH), 4.31 (s, 2H, FcH), 4.19 (s, 5H, FcH), 4.14 (s, 2H, $H_{1'}$); ^{13}C NMR (150 MHz, $CDCl_3$) δ 148.3, 143.1, 137.7, 130.3, 124.8, 123.7, 120.5, 80.4, 69.9 (2C), 69.1 (2C), 69.0 (5C), 48.8, 46.0; HRMS (ESI^+) *m/z* calcd for $C_{19}H_{17}FeN_2O_4$ $[M+H]^+$: 393.0538, Found 393.0523.

Synthesis of 3-ferrocenemethyl-3,4-dihydro-*2H*-1,3-benzoxazin-2,4(3*H*)-dione (4.24a)

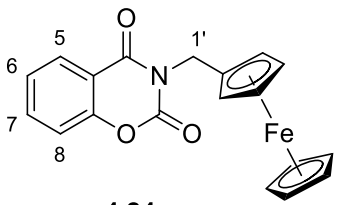

4.24a

Benzoxazine **4.24a** was synthesized according to Method C of the synthesis of benzoxazine-2-ones (**4.17a-4.17d** and **4.18a-e**) by cyclization of salicylamide **4.16a** with CDI. Yellow solid. Yield: 31.0 mg (63%). M.p.: 124.8 – 126.8 °C. ^{1}H NMR (600 MHz, $CDCl_3$) δ 8.06 (dd, J = 7.9, 1.3 Hz, 1H, H_5), 7.65 (t, J = 7.8 Hz, 1H, H_7), 7.33 (t, J = 7.6 Hz, 1H, H, H_6), 7.23 (d, J = 8.3 Hz, 1H, H_8), 4.98 (s, 2H, $H_{1'}$), 4.47 (t, J = 1.5 Hz, FcH), 4.20 (s, 5H, FcH), 4.12 (t, J = 1.5 Hz, 2H, FcH); ^{13}C NMR (150 MHz, $CDCl_3$) δ 160.4, 152.7, 148.2, 136.1, 128.2, 125.5, 116.5, 114.5, 81.5, 70.6 (2C), 68.8 (5C), 68.6 (2C), 41.9; HRMS (ESI^+) *m/z* calcd for $C_{19}H_{15}FeO_3$ $[M]^+$: 361.0401, Found 361.0404.

Synthesis of 6-chloro-3-(2-((*N*,*N*-dimethylamino)methyl)ferrocenemethyl)-3,4-dihydro-*2H*-1,3-benzoxazin-2,4(3*H*)-dione (4.23b)[10]

Excess oxalyl chloride (0.5 mL) was added to a suspension of salicylamide **4.15b** (0.100 g, 0.298 mmol) in toluene (20 mL). The reaction mixture was refluxed for 4 hours after which the volatiles were removed under reduced pressure for produce a dark brown material. The attained substance was subjected to silica gel column chromatography (1:9 MeOH/DCM) to afford the pure compound **4.23b** as a yellow semi-solid. Yield: 10.8 mg (8%).

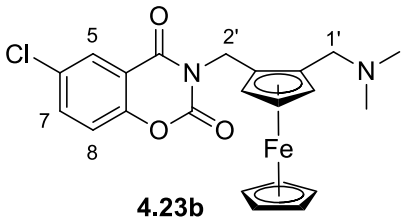

4.23b

^{1}H NMR (600 MHz, $CDCl_3$) δ 8.02 (d, J = 2.5 Hz, 1H, H_5), 7.63 (dd, J = 8.8, 2.5 Hz, 1H, H_7), 7.21 (d, J = 8.8 Hz, 1H, H_8), 5.17 (d, J = 14.1 Hz, 1H, $H_{2'a}$), 4.97 (d, J = 14.1 Hz, 1H, $H_{1'b}$), 4.55 (s, 1H, FcH), 4.36 (dd, J = 12.3, 8.3 Hz, 1H, FcH), 4.30 (s, 1H, $H_{1'a}$), 4.18 (s, 5H, FcH), 4.17 (t, J = 2.4 Hz, 1H, FcH), 3.24 – 3.19 (m, 1H, $H_{1'b}$), 1.25 (s, 6H, NMe_2); ^{13}C NMR (151 MHz, $CDCl_3$) δ 160.1, 151.0, 148.1, 136.6, 131.5, 127.7, 118.2, 115.4, 86.9, 80.3, 71.4, 70.4, 69.3 (5C), 68.8, 59.3, 40.8, 29.9 (C2).

Synthesis of 3-((*N*,*N*-dimethylamino)methyl)ferrocenemethyl)methyl-3,4-dihydroquinazoline (4.30)[11]

A suspension of 2-aminobenzylamine **4.9d** (86.0 mg, 0.228 mmol) and 4-toluenesulphonic acid monohydrate (2.18mg, 0.05 mmol) in ethyl orthoformate (2 mL) was stirred at 100 °C for 2 hours. After completion of the reaction (TLC), the reaction mixture was diluted with $CHCl_3$ (20 mL), quenched with 1N HCl aqueous solution (10 mL) and shaken vigorously in a separating funnel. The aqueous layer was collected, washed with chloroform (5 mL) and then basified to pH 10 – 12 with saturated sodium hydroxide solution. The product was extracted with $CHCl_3$ (2 × 20 mL), washed with water (2 × 10 mL), dried (Na_2SO_4) and solvent removed

under reduced pressure to afford the desired quinazoline **4.30** in high purity as a yellow viscous oil.

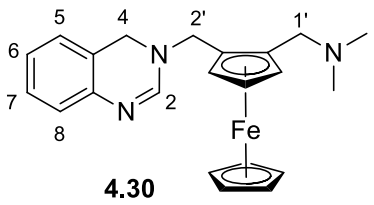

4.30

Yield: 19.0 mg (22%). ^{1}H NMR (400 MHz, $CDCl_3$) δ 7.51 (s, 1H, H_2), 7.15 – 7.09 (m, 2H, H_7, H_8), 6.98 (t, J = 7.5 Hz, 1H, H_6), 6.80 (d, J = 7.5 Hz, 1H, H_5), 4.53 (q, J = 14.3 Hz, 2H, $H_{4'}$), 4.35 (t, J = 13.4 Hz, 1H, $H_{2'a}$), 4.24 (s, 1H, FcH), 4.22 (s, 1H, FcH), 4.15 – 14.14 (m, 1H, $H_{2'b}$), 4.10 (s, 5H, FcH), 4.01 (s, 1H, FcH), 3.59 (d, J = 12.8 Hz, 1H, $H_{1'a}$), 2.98 (d, J = 12.8 Hz, 1H, $H_{1'b}$), 2.13 (s, 6H, NMe_2); ^{13}C NMR (100 MHz, $CDCl_3$) δ 150.5, 139.2, 128.6, 125.8, 125.1, 123.0, 119.8, 84.3, 80.6, 71.8, 70.1, 69.5 (5C), 67.4, 57.8, 51.7, 46.5, 45.0 (2C); HRMS (ESI^+) *m/z* calcd for $C_{22}H_{26}FeN_3$ $[M+H]^+$: 388.1476, Found 388.1423.

Synthesis of ferrocenyl naphthoxazines 5.2a-b

Naphthoxazines **5.2a-b** were synthesized according to the Burke procedure described for the preparation of 1,3-benzoxazines **3.13a-k** and **3.16a-o** using 2-naphthol and **5.1** ferrocenyl amines **3.12a-b**.

2-(2-((*N,N*-Dimethylamino)methyl)ferrocenemethyl)-2,3-dihydro-*1H*-naphtho[1,2-e][1,3]oxazine (5.2a)

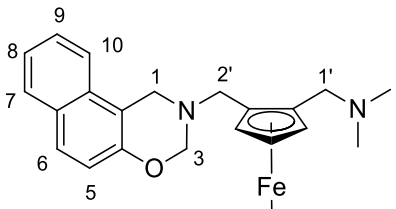

5.2a

Light brown semi-solid. Yield: 72.3 mg (22%). ^{1}H NMR (600 MHz, $CDCl_3$) δ 7.77 (d, J = 7.7 Hz, 1H, H_7), 7.66 (d, J = 8.6 Hz, 1H, H_6), 7.58 (d, J = 8.1 Hz, 1H, H_{10}), 7.48 – 7.43 (m, 1H, H_9), 7.36 (d, J = 6.9 Hz, 1H, H_8), 7.06 (d, J = 8.6 Hz, 1H, H_5), 4.97 – 4.92 (m, 2H, H_3), 4.40 – 4.38 (m, 1H, FcH), 4.33 – 4.31 (m, 2H, H_1), 4.28 (s, 1H, FcH), 4.16 (s, 1H, FcH), 4.02 (s, 5H, FcH), 3.82 (s, 2H, $H_{2'}$), 3.43 (d, J = 12.8 Hz, 1H, $H_{1'a}$), 3.32 (d, J = 12.3 Hz, 1H, $H_{1'b}$), 2.15 (s, 6H, NMe_2); ^{13}C NMR (150 MHz, $CDCl_3$) δ 151.9, 132.2, 129.2, 128.7, 128.0, 126.5, 123.6, 121.5, 118.6, 112.1, 83.9, 82.1, 71.0, 70.9, 70.5, 69.5

(5C), 67.6, 57.1, 49.9, 47.0, 44.7 (2C); HRMS (ESI$^+$) *m/z* calcd for $C_{26}H_{29}FFeN_2O$ $[M+H]^+$: 441.1624, Found 441.1465; HPLC purity > 93% (t_R = 3.06 min).

2-Ferrocenemethyl-2,3-dihydro-*1H*-naphtho[1,2-e][1,3]oxazine (5.2b)

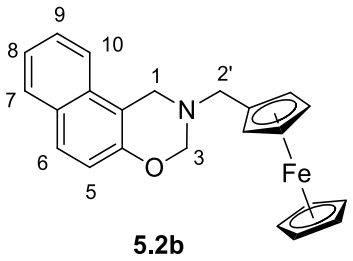

5.2b

Dark brown solid. Yield: 126.6 mg (71%). M.p.: 104.6 – 106.1 °C. ^{1}H NMR (600 MHz, $CDCl_3$) δ 7.79 (d, J = 7.8 Hz, 1H, H_7), 7.67 (d, J = 8.9 Hz, 1H, H_6), 7.60 (dq, J = 9.3, 0.8 Hz, 1H, H_{10}), 7.48 (ddd, J = 8.3, 6.8, 1.3 Hz, 1H, H_9), 7.37 (ddd, J = 8.0, 6.8, 1.1 Hz, 1H, H_8), 7.07 (d, J = 8.9 Hz, 1H, H_5), 4.92 (s, 2H, H_3), 4.34 (s, 2H, H_1), 4.24 (t, J = 1.8 Hz, 2H. FcH), 4.16 (t, J = 1.8 Hz, 2H, FcH), 4.09 (s, 5H, FcH), 3.78 (s, 2H, $H_{2'}$); ^{13}C NMR (150 MHz, $CDCl_3$) δ 152.0, 132.1, 129.1, 128.8, 128.1, 126.7, 123.6, 121.2, 118.7, 111.7, 83.8, 81.5, 70.1 (2C), 68.7 (5C), 68.5 (2C), 51.7, 47.2; IR (ATR, cm^{-1}) ν = 1221 (C-O), 1187 (C-N); HRMS (ESI$^+$) *m/z* calcd for $C_{23}H_{22}FeN_2O_3$ $[M+H]^+$: 384.1051, Found 384.1025; HPLC purity > 99% (t_R = 5.46 min).

Synthesis of sesamoxazine 5.4

Compound **5.4** was synthesized via the Burke condensation using sesamol **5.3** and ferrocenyl amine **3.12b** as previously described.

7-(2-((*N,N*-Dimethylamino)methyl)ferrocenemethyl)-7,8-dihydro-6*H*-[1,3]dioxolo[4',5':4,5]benzo[1,2-e][1,3]oxazine (5.4)

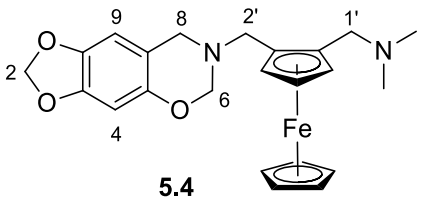

5.4

Brown semi-solid. Yield: 135.5 mg (85%). ^{1}H NMR (400 MHz, $CDCl_3$) δ 6.39 (s, 1H, H_9), 6.38 (s, 1H, H_4), 5.87 (s, 2H, H_2), 4.85 – 4.77 (m, 2H, H. H_6), 4.25 (br s, 1H, FcH), 4.22 (br s, 1H, FcH), 4.12 – 4.11 (m, 1H, FcH), 4.02 (s, 5H, FcH), 3.93 (br s, 2H, H_8), 3.73 (s, 2H, H, $H_{2'}$), 3.30 (d, J = 12.9 Hz, 1H, $H_{1'a}$), 3.19 (d, J = 12.9 Hz, 1H, $H_{1'b}$), 2.16 (s, 6H, NMe_2); ^{13}C NMR (100 MHz, $CDCl_3$) δ 148.8, 146.6, 141.5, 111.7, 106.9, 100.8, 98.5, 84.2, 83.9, 82.4,

70.7, 70.3, 69.4 (5C), 67.2, 57.4, 49.3, 49.3, 45.4 (2C); HRMS (ESI^+) *m/z* calcd for $C_{23}H_{27}FeN_2O_3$ $[M+H]^+$: 435.1366, Found 435.1370.

Synthesis of 4-chloro-3-formylcoumarin (5.15)

$POCl_3$ (1.00 mL, 12.12 mmol) was added to a DMF (1.00 mL, 12.92 mmol) on ice and the resulting solution was heated at 50 °C for 30 minutes. After 30 minutes, a solution of 4-hydroxycoumarin **5.9a** (1.00 g, 6.17 mmol) in DMF (1 mL) was added to the above reaction mixture at the same temperature and then heated at 60 °C for 12 hours. After cooling to room temperature, the reaction was quenched with ice-water (5 – 7 mL) until no fuming was observed. The resulting yellow precipitate was filtered, washed with cold water (3 × 5 mL) and air-dried to afford 4-chloro-3-formylcoumarin **5.15** as a yellow solid. Yield: 1.28 g (75% yield).

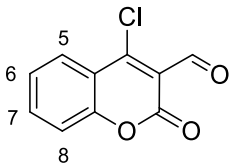

5.15

^{1}H NMR (600 MHz, $CDCl_3$) δ 10.37 (s, 1H, CHO), 8.13 (d, J = 8.1 Hz, 1H, H_8), 7.74 (t, J = 7.8 Hz, 1H, H_7), 7.45 (t, J = 7.7 Hz, 1H, H_6), 7.39 (d, J = 8.3 Hz, 1H, H_5); ^{13}C NMR (150 MHz, $CDCl_3$) δ 186.9, 158.5, 153.6, 153.4, 135.8, 127.8, 125.7, 118.5, 118.3, 117.3.

Synthesis of 3-formylcoumarin-4-ol (5.14a)

In a 50 mL round bottom flask, a suspension of 4-chloro-3-formylcoumarin **5.15** (1.00 g, 4.82 mmol) in 5% K_2CO_3 aqueous solution (30 mL) was heated open at 100 °C for 1 hour. The solution was cooled to room temperature and then kept on ice for 15 minutes. The resulting suspension was acidified (aqueous HCl) to pH 1 and the formed precipitate was filtered, washed with distilled water (5 × 10 mL) and air-dried to obtain the product as an off-white solid. Yield: 1.35 g (64%).

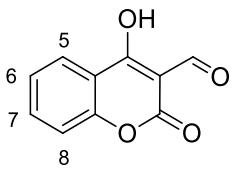

5.14a

^{1}H NMR (600 MHz, $CDCl_3$ δ 10.04 (s, 1H, CHO), 8.05 (d, J = 7.9 Hz, 1H, H_8), 7.73 (t, J = 7.8 Hz, 1H, H_8), 7.38 (t, J = 7.6 Hz, 1H, H_6), 7.34 (d, J =

8.4 Hz, 1H, H_5); ^{13}C NMR (150 MHz, $CDCl_3$) δ 195.1, 176.1, 160.9, 155.9, 136.7, 125.6, 125.0, 117.7, 114.7, 102.1.

Synthesis of ferrocenyl 3-aminomethylcoumarin-4-ols (5.13a-b)

Ferrocenyl 3-aminomethylcoumarin-4-ols **5.13a-b** were prepared according the procedure employed for the synthesis of α-amino-*o*-cresols **4.6a-i** and **4.7a-e** using 3-formylcoumarin-4-ol **5.15** and ferrocenyl amines **3.12a-b**.

3-((Ferrocenemethyl)aminomethyl)-coumarin-4-ol (5.13a)

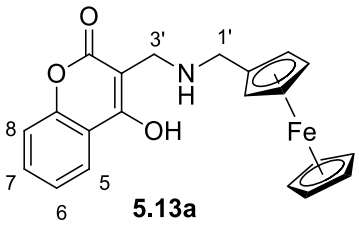

5.13a

Light brown semi-solid: 235.2 mg (86%). ^1H NMR (600 MHz, DMSO-d_6) δ 7.83 – 7.81 (m, 2H, H_5, H_7), 7.34 (t, J = 7.4 Hz, 1H, H_6), 7.10 – 7.03 (m, 2H, H_5, H_8), 4.16 (s, 2H, FcH), 4.13 (s, 2H, FcH), 4.10 (s, 5H, FcH), 4.02 (s, 2H, $H_{1'}$), 3.55 (s, 2H, $H_{1'}$); ^{13}C NMR (150 MHz, DMSO-d_6) δ 173.1, 165.0, 153.9, 129.4, 124.7, 123.6, 121.5, 115.5, 95.1, 88.9, 68.2 (5C), 67.4 (2C), 66.8 (2C), 46.9, 44.2; HRMS (ESI^+) *m/z* calcd for $C_{21}H_{20}FeNO_3$ $[M+H]^+$: 390.0793, Found 390.0779.

3-((2-((*N*,*N*-Dimethylamino)methyl)ferrocenemethyl)aminomethyl)-coumarin-4-ol (5.13b)

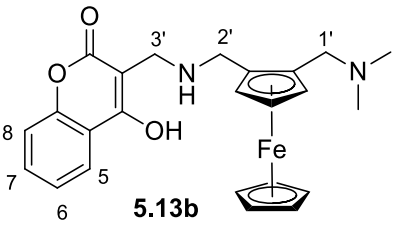

5.13b

Brown semi-solid: 350.2 mg (68%). ^1H NMR (600 MHz, $CDCl_3$ δ 7.83 (dd, J = 7.7, 1.1 Hz, 1H, H_5), 7.40 (td, J = 7.7, 1.4 Hz, 1H, H_7), 7.17 (d, J = 7.8 Hz, 1H, H_8), 7.14 (t, J = 7.5 Hz, 1H, H_6), 4.34 (s, 1H, FcH), 4.19 (br s, 1H, FcH), 4.20 – 4.17 (m, 2H, $H_{3'a}$, FcH),), 4.13 (t, J = 2.4 Hz, 1H, FcH), 4.11 (s, 5H, FcH), 4.09 (d, J = 8.8 Hz, 2H, $H_{2'}$), 3.90 – 3.89 (m, 2H, $H_{1'a}$, $H_{3'b}$), 2.88 (d, J = 13.0 Hz, 1H, $H_{1'b}$), 2.16 (s, 6H, NMe_2); ^{13}C NMR (150 MHz, $CDCl_3$) δ 176.1, 165.8, 154.4, 131.1, 124.5, 122.8, 122.0, 116.6, 100.1,

88.8, 84.1, 72.0 (2C), 69.7 (5C), 67.3, 58.1, 45.7, 44.2, 43.7 (2C); HRMS (ESI^+) *m/z* calcd for $C_{24}H_{27}FeN_2O_3$ $[M+H]^+$: 447.1371, Found 447.1371.

General procedure for the synthesis of phenyl acetates 5.20a-c

A suspension of an appropriate phenol **3.1c-d**,**l** (1.0 eq.) and Ac_2O (1.25 eq.) and concentrated H_2SO_4 (1 drop) was stirred at 100 °C for 4 hours. The reaction mixture was cooled to room temperature, diluted with EtOAc (50 mL) and extracted. The organic extract was washed with distilled water (3 × 50 mL), dried (Na_2SO_4). The product was obtained as a sweet-smelling colourless oil with sufficient purity after removing the solvent under reduced pressure.

4-Chlorophenyl acetate (5.20a)

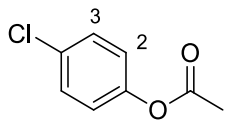

5.20a

Colourless oil. Yield: 1.84 g (98%). ^1H NMR (400 MHz, $CDCl_3$) δ 7.42 – 7.39 (m, 2H, H_3), 7.17 – 7.13 (m, 2H, H_2), 2.26 (s, 3H); ^{13}C NMR (100 MHz, $CDCl_3$) δ 168.8, 146.7, 139.4 (2C), 123.2 (2C), 113.1, 21.1.

4-Bromophenyl acetate (5.20b)

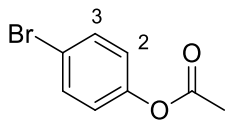

5.20b

Colourless oil. Yield: 1.78 g (90%). ^1H NMR (400 MHz, $CDCl_3$) δ 7.51 – 7.44 (m, 2H, H_3), 7.02 – 6.95 (m, 2H, H_2), 2.28 (s, 3H, Me); ^{13}C NMR (100 MHz, $CDCl_3$) δ 169.2, 149.8, 132.5 (2C), 123.5 (2C), 119.0, 21.1.

4-Fluorophenyl acetate (5.20c)

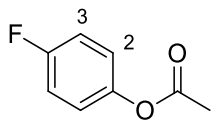

5.20c

Colourless oil. Yield: 1.64 g (98%). ^1H NMR (400 MHz, $CDCl_3$) δ 7.21 – 7.16 (m, 2H, H_2), 7.06 – 7.03 (m, 2H, H_3), 2.26 (s, 3H, Me); ^{13}C NMR (100 MHz, $CDCl_3$) δ 168.9, 160.01 (d, J = 252.1 Hz), 146.7 (d, J = 3.1 Hz), 123.8 (d, J = 8.1 Hz, 2C), 116.3 (d, J = 20.0 Hz, 2C), 21.09.

General procedure for the synthesis of halogenated 2′-hydroxyacetophenones (5.19a-c)

A suspension of a substituted phenylacetate **5.20a-b** (1.0 eq.) and aluminium chloride (1.5 eq.) was stirred at 150 °C. After 4 hours, the reaction was cooled to room temperature and quenched with dilute HCl after which the solid mass was broken up with a spatula. The product was extracted with ethyl acetate (2 × 25 mL), washed with brine, dried (Na_2SO_4) and the solvent removed *in vacuo* to give the desired compound.

5′-Chloro-2′-hydroxyacetophenone (5.19a)

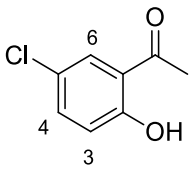

5.19a

Off-white solid. Yield: 0.896 g (88%). ^{1}H NMR (600 MHz, $CDCl_3$) δ 7.74 (d, J = 1.9 Hz, 1H, H_6), 7.31 (dd, J = 8.9, 1.9 Hz, 1H, H_4), 6.90 (d, J = 8.9 Hz, 1H, H_5), 2.60 (s, 3H); ^{13}C NMR (150 MHz, CDl_3) δ 203.6, 160.1, 135.7, 129.9, 125.5, 122.1, 119.6, 26.7.

6′-Chloro-2′-hydroxyacetophenone (5.19b)

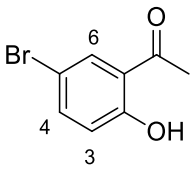

5.19b

Off-white solide. Yield: 0.968 g (92%). ^{1}H NMR (400 MHz, $CDCl_3$) δ 12.13 (s, 1H, OH), 7.80 (d, J = 2.4 Hz, 1H, H_6), 7.51 (dd, J = 8.9, 2.4 Hz, 1H, H_4), 6.86 (d, J = 8.9 Hz, 1H, H_3), 2.60 (s, 3H, Me); ^{13}C NMR (100 MHz, $CDCl_3$) δ 203.6, 161.3, 139.2, 133.0, 120.9, 120.5, 110.5, 26.8.

6′-Fluoro-2′-hydroxyacetophenone (5.19c)

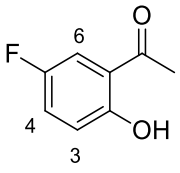

5.19c

Light yellow solid. Yield: 0.908 g (89%). ^{1}H NMR (600 MHz, $CDCl_3$) δ 7.26 (dd, J = 8.0, 1.9 Hz, 1H, H_6), 7.13 (td, J = 8.2, 1.9 Hz, 1H, H_4), 6.92 (dd, J = 8.4, 4.9 Hz, 1H, H_3), 2.61 (s, 3H, Me); ^{13}C NMR (150 MHz, $CDCl_3$) δ 203.56 (d, J = 2.9 Hz), 159.4, 157.4 (d, J = 252.1 Hz), 123.0 (d, J = 20.0 Hz), 122.9 (d, J = 7.9 Hz), 124.7 (d, J = 7.9 Hz), 117.9 (d, J = 20.0 Hz), 29.7.

General procedure for the synthesis of 4-hydroxycoumarins (5.13c-e)

A solution of a relevant 2′-hydroxyacetophenone (**5.19b-d**) (1.0 eq.) and dimethyl carbonate (1.5 eq.) in toluene (15 mL) was added slowly to sodium hydride (5.0 eq.) stirred in toluene (20 mL) on ice. The reaction mixture was stirred for 30 minutes on ice and then refluxed for 4 hours. After refluxing, the reaction was quenched with water and acidified with HCl. The formed solid was collected by filtration and successively washed with toluene (2 × 10 mL) and distilled water (3 × 10 mL). The solid was air-dried to obtain the desired compound.

6-Chloro-4-hydroxycoumarin (5.9b)

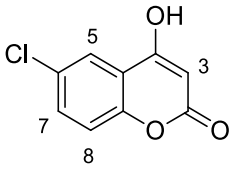

5.9b

White solid. Yield: 1.98 g (86%). M.p.: 231.4 – 234.8 °C (Lit. 232 – 235 °C).[12] ^{1}H NMR (600 MHz, DMSO-d_6) δ 13.00 (br s, 1H, OH), 7.74 (s, 1H, H_5), 7.65 (d, J = 8.6 Hz, 1H, H_7), 7.39 (d, J = 7.2 Hz, 1H, H_8), 5.72 (s, 1H, H_3); ^{13}C NMR (151 MHz, DMSO-d_6) δ 164.7, 161.6, 152.2, 132.4, 128.1, 122.4, 118.6, 117.4, 91.8.

6-Bromo-4-hydroxycoumarin (5.9b)

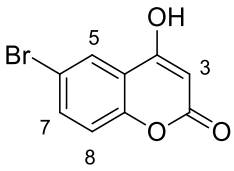

5.9c

Off-white solid. Yield: 1.95 g (96%). M.p.: 242.0 – 243.5 °C (Lit. 241 – 243 °C).[12] ^{1}H NMR (400 MHz, DMSO-d_6) δ 12.98 (br s, 1H, OH), 7.88 (d, J = 2.4 Hz, 1H, H_5), 7.78 (dd, J = 8.8, 2.5 Hz, 1H, H_7), 7.34 (d, J = 8.8 Hz, 1H, H_8), 5.68 (s, 1H, H_3); ^{13}C NMR (100 MHz, DMSO) δ 164.6, 161.5, 152.6, 135.2, 125.4, 118.9, 117.9, 115.8, 91.7.

6-Fluoro-4-hydroxycoumarin (5.9b)

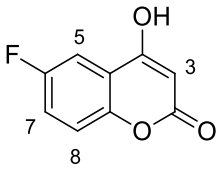

5.9d

Off-white solid. Yield: 0.857 g (88%). M.p.: 238.8 – 240.7 °C (Lit. 240 – 241 °C).[13] ^{1}H NMR (500 MHz, $CDCl_3$) δ 7.57 (dd, J = 8.0, 2.5 Hz, 1H, H_5), 7.33 – 7.26 (m, 2H, H_5), 5.76 (s, 1H, H_3); ^{13}C NMR (150 MHz, $CDCl_3$) δ 162.1 (d, J = 3.1 Hz), 161.9, 158.8, 152.1 (d, J = 3.1 Hz), 120.6 (d, J = 20.0 Hz), 117.4 (d, J = 8.1 Hz), 113.5 (d, J = 8.1 Hz), 112.1 (d, J = 20.0 Hz), 90.9.

Synthesis of halogenated 3-formylcoumarin-4-ols (5.14b-d)[14]

A substituted 4-hydroxycouamarin (1.00 g) and 4-toluenesulphonic acid monohydrate (ca. 10 mg) were placed in a 25 mL Erlenmeyer flask and thoroughly mixed with triethyl orthoformate (1.5 mL) using a spatula. The flask was covered with a watch glass and irradiated in a Russell Hobbs conventional microwave oven for 3 minutes (medium) and 2 minutes (high). After cooling the resulting orange suspension to room temperature, excess triethyl orthoformate was quenched by addition of water (5 mL) to precipitate out the product. The formed precipitate was collected by filtration, triturated in distilled water (10 mL), filtered and then successively washed with water (2 × 15 mL) and methanol (5 mL) and air-dried to produce the desired product.

6-Chloro-3-formylcoumarin-4-ol (5.14b)

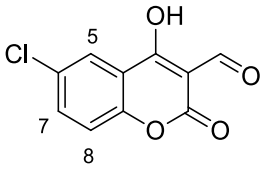

5.14b

Light orange solid. Yield: 0.535 g (59%). ^{1}H NMR (400 MHz, $CDCl_3$) δ 10.03 (s, 1H, CHO), 8.01 (d, J = 2.4 Hz, 1H, H_5), 7.67 (dd, J = 8.9, 2.4 Hz, 1H, H_7), 7.30 (d, J = 8.9 Hz, 1H, H_8); ^{13}C NMR (100 MHz, $CDCl_3$) δ 195.0, 175.0, 160.3, 154.2, 136.6, 130.8, 124.8, 119.3, 115.8, 102.3.

6-Bromo-3-formylcoumarin-4-ol (5.14c)

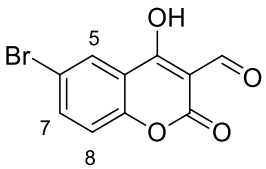

5.14c

Light orange solid. Yield: 0.915 g (60%). ^{1}H NMR (600 MHz, $CDCl_3$) δ 10.02 (s, 1H, CHO), 8.16 (d, J = 2.4 Hz, 1H, H_5), 7.80 (dd, J = 8.9, 2.4 Hz, 1H, H_7), 7.25 (d, J = 7.0 Hz, 1H, H_8); ^{13}C NMR (150 MHz, $CDCl_3$) δ 195.0, 175.0, 160.2, 154.7, 139.4, 128.0, 119.5, 117.9, 116.3, 102.3.

6-Fluoro-3-formylcoumarin-4-ol (5.14d)

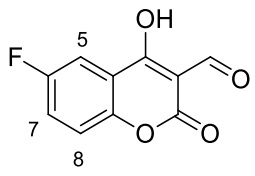

5.14d

Light yellow solid. Yield: 882.0 mg (60%). ^{1}H NMR (400 MHz, $CDCl_3$) δ 10.04 (s, 1H, CHO), 7.70 (dd, J = 7.6, 3.0 Hz, 1H, H_5), 7.49 – 7.42 (m, 1H, H_7), 7.35 (dd, J = 9.1, 4.2 Hz, 1H, H_8); ^{13}C NMR (100 MHz, $CDCl_3$) δ 195.1, 175.3 (d, J = 2.9 Hz), 160.2, 159.0 (d, J = 247.0 Hz), 124.5 (d, J = 24.7 Hz), 119.6 (d, J = 8.0 Hz), 115.6 (d, J = 8.7 Hz), 110.9 (d, J = 25.1 Hz), 102.2, 77.2.

Synthesis of 8-formylcoumarin-7-ol (5.22)[15]

A suspension of 7-hydroxycoumarin **5.21** (5.00 g, 30.8 mmol) and methenamine (10.07 g, 71.9 mmol) in glacial acetic acid (36 mL) was stirred at 95 °C for 6 hours. After 6 hours, the resultant orange solution was acidified by addition of 75 mL dilute aqueous HCl solution (8.4:10 conc. HCl/H_2O) and refluxed for 30 minutes after which it was allowed to cool to room temperature and diluted with distilled water (300 mL). The product was extracted with $CHCl_3$ (3×150 mL), washed with brine and dried (Na_2SO_4). The solvent was removed *in vacuo* to yield the product as a light green solid in sufficient purity to use in subsequent steps.

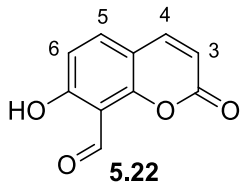

5.22

Light yellow solid. Yield: 1.26 g (22%). M.p.: 175.4 – 177.2 °C (Lit. 174 – 176 °C).[15] ^{1}H NMR (600 MHz, $CDCl_3$) δ 12.19 (s, 1H, OH), 10.58 (s, 1H, CHO), 7.65 (d, J = 9.6 Hz, 1H, H_4), 7.59 (d, J = 8.8 Hz, 1H, H_5), 6.87 (d, J = 8.8 Hz, 1H, H_6), 6.31 (d, J = 9.6 Hz, 1H, H_3); ^{13}C NMR (150 MHz, $CDCl_3$) δ 193.0, 165.6, 159.3, 156.8, 143.5, 136.1, 114.8, 113.5, 111.0, 108.8.

Synthesis of halogenated 4-aminomethycoumarin-4-ols (5.13c-e) and 8-aminomethylcoumarin-7-ols (5.3a-b)

Aminomethylcoumarinols **5.13c-e** and **5.23a-b** were prepared according the procedure employed for the synthesis of α-amino-*o*-cresols **4.6a-i** and **4.7a-e** using formylcoumarinols (**5.13b-d** and **5.22**) ferrocenyl amines **3.12a-b**.

3-((2-((*N*,*N*-Dimethylamino)methyl)ferrocenemethyl)aminomethyl)-6-chloro-4-hydroxycoumarin (5.13c)

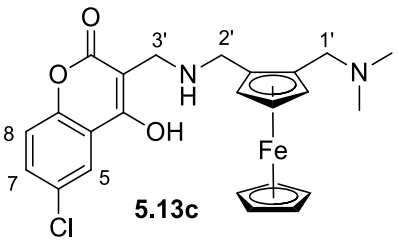

5.13c

Light brown semi-solid. Yield: 174.4 mg (66%). ^{1}H NMR (600 MHz, $CDCl_3$) δ 7.75 (d, J = 2.5 Hz, 1H, H_5), 7.31 (dd, J = 8.7, 2.6 Hz, 1H, H_7), 7.09 (d, J = 8.7 Hz, 1H, H_4), 4.31 (br s, 1H, FcH), 4.21 (d, J = 13.3 Hz, 1$H_{3'a}$), 4.19 (br s, 1H, FcH), 4.11 (d, J = 4.7 Hz, 6H, FcH), 4.06 – 4.01 (m, 2H, $H_{2'}$), 3.88 (d, J = 13.0 Hz, 1H, $H_{1'a}$), 3.85 (d, J = 13.3 Hz, 1H, $H_{3'b}$), 2.87 (d, J = 13.0 Hz, 1H, $H_{1'b}$), 2.15 (s, 6H, NMe_2); ^{13}C NMR (150 MHz, $CDCl_3$) δ 174.6, 165.5, 152.7, 130.9, 128.2, 124.2, 123.4, 118.1, 100.1, 89.4, 84.1, 72.0, 71.9, 69.6 (5C), 67.3, 58.1, 46.0, 44.2 (2C), 43.3; HRMS (ESI^+) *m/z* calcd for $C_{24}H_{26}ClFeN_2O_3$ $[M+H]^+$: 481.0976, Found 481.1568.

3-((2-((*N*,*N*-Dimethylamino)methyl)ferrocenemethyl)aminomethyl)-6-bromo-4-hydroxycoumarin (5.13d)

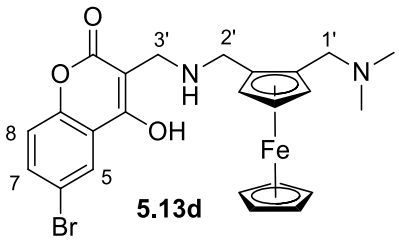

5.13d

Light brown semi-solid. Yield: 60.5 mg (35%). ^{1}H NMR (400 MHz, $CDCl_3$) δ 7.96 (d, J = 2.0 Hz, 1H, H_5), 7.45 (dd, J = 8.7, 2.1 Hz, 1H, H_7), 7.04 (d, J = 8.7 Hz, 1H, H_8), 4.33 (s, 1H, FcH), 4.17 (s, 1H, FcH), 4.12 (t, J = 2.3 Hz, 1H, FcH), 4.09 (s, 5H, FcH), 4.05 – 4.02 (m, 2H, $H_{3'}$), 3.86 (dd, J = 18.1, 13.1 Hz, 2H, $H_{2'}$), 3.60 – 3.52 (m, 1H, $H_{1'a}$), 2.86 (d, J = 13.0 Hz, 1H, $H_{1'b}$), 2.14 (s, 6H, NMe_2); ^{13}C NMR (100 MHz, $CDCl_3$) δ 190.7, 175.1, 165.4, 153.2, 133.7, 127.3, 123.9, 118.5, 115.7, 89.0, 83.9, 71.9, 71.9, 69.6 (5C), 67.3, 58.0, 45.7, 44.1 (2C), 43.3; HRMS (ESI^+) *m/z* calcd for $C_{24}H_{26}BrFeN_2O_3$ $[M+H]^+$: 404.0896, Found 404.0952.

3-((2-((*N*,*N*-dimethylamino)methyl)ferrocenemethyl)aminomethyl)-6-fluoro-4-hydroxycoumarin (5.13e)

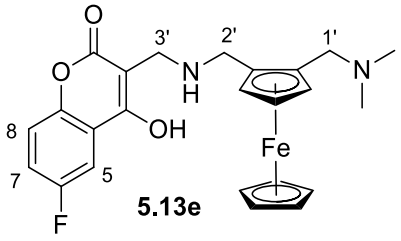

5.13e

Light brown semi-solid. 109.0 (64%). ^{1}H NMR (600 MHz, $CDCl_3$) δ 7.48 (dd, J = 8.6, 2.9 Hz, 1H, H_5), 7.14 – 7.09 (m, 2H, H_7, H_8), 4.33 (br s, 1H, FcH), 4.20 (br s, 1H, FcH), 4.18 (d, J = 13.4 Hz, 1H, $H_{2'a}$), 4.13 (t, J = 2.4 Hz, 1H, FcH), 4.11 (s, 5H, FcH), 4.07 (d, J = 13.0 Hz, 2H, $H_{3'}$), 3.87 (d, J = 13.1 Hz, 2H, $H_{1'a}$, $H_{2'b}$), 2.89 (d, J = 13.0 Hz, 1H, $H_{1'b}$), 2.16 (s, 6H, NMe_2); ^{13}C NMR (150 MHz, $CDCl_3$) δ 174.9, 165.8, 159.3, 157.7, 150.3, 123.2 (d, J = 7.9 Hz), 118.3 (d, J = 24.8 Hz), 118.0 (d, J = 7.9 Hz), 109.9 (d, J = 23.8 Hz), 89.2, 84.1, 72.0, 71.9, 69.6 (5C), 67.3, 58.1, 46.0, 44.2 (2), 43.5; HRMS (ESI$^+$) *m/z* calcd for $C_{24}H_{26}FFeN_2O_3$ $[M+H]^+$: 465.1279, Found 465.1279.

3-((Ferrocenemethyl)aminomethyl)-4-hydroxycoumarin (5.23a)

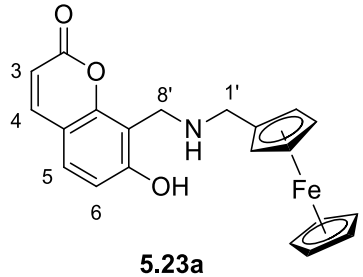

5.23a

Light brown semi-solid: 235.2 mg (86%). ^{1}H NMR (600 MHz, DMSO-d_6) δ 7.83 – 7.81 (m, 2H, H_5, H_7), 7.34 (t, J = 7.4 Hz, 1H, H_6), 7.10 – 7.03 (m, 2H, H_6, H_8), 4.16 (s, 2H, FcH), 4.13 (s, 2H, FcH), 4.10 (s, 5H, FcH), 4.02 (s, 2H, $H_{3'}$), 3.55 (s, 2H, $H_{1'}$); ^{13}C NMR (150 MHz, DMSO-d_6) δ 173.1, 165.0, 153.9, 129.4, 124.7, 123.6, 121.5, 115.5, 95.1, 88.9, 68.2 (5C), 67.4 (2C), 66.8 (2C), 46.9, 44.2; HRMS (ESI$^+$) *m/z* calcd for $C_{21}H_{20}FeNO_3$ $[M+H]^+$: 390.0793, Found 390.0782.

9-(2-((*N*,*N*-Dimethylamino)methyl)ferrocenemethyl)-9,10-dihydro-2*H*,8*H*-chromeno[8,7-*e*][1,3]oxazine-2,8-dione (5.23b)

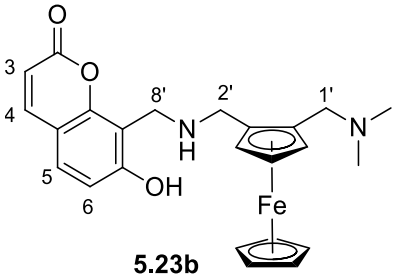

5.23b

Light brown semi-solid. Yield: 121.6 mg (56%). ^{1}H NMR (600 MHz, $CDCl_3$) δ 7.59 (d, J = 9.3 Hz, 1H, H_3), 7.23 (d, J = 8.4 Hz, 1H, H_6), 6.72 (d, J = 8.4 Hz, 1H, H_5), 6.10 (d, J =

9.3 Hz, 1H, H_4), 4.22 (br s, 1H, FcH), 4.18 (br s, 1H, FcH), 4.13 – 4.12 (m, 2H, $H_{8'}$), 4.09 (br s, 1H, FcH), 4.04 (s, 5H, FcH), 3.91 (d, J = 13.2 Hz, 1H, $H_{2'a}$), 3.79 (d, J = 12.7 Hz, 1H, $H_{1'a}$), 3.42 (d, J = 13.2 Hz, 1H, $H_{2'b}$), 2.80 (d, J = 12.6 Hz, 1H, $H_{1'b}$), 2.15 (s, 6H, NMe_2); ^{13}C NMR (150 MHz, $CDCl_3$) δ 161.9, 153.6, 144.7, 128.1, 115.1, 110.2, 110.1, 107.4, 100.1, 84.2, 82.6, 69.9, 69.5, 69.2 (5C), 69.0, 58.4, 46.4, 44.9 (2C), 44.6; HRMS (ESI^+) *m/z* calcd for $C_{24}H_{27}FeN_2O_3$ $[M+H]^+$: 447.1371, Found 447.1371.

Synthesis of benzene-annulated ferrocenyl coumarin-1,3-oxazine (5.24)

Coumarin-1,3-oxazine was synthesized by cyclization of 8-aminomethylcoumarin-7-ol **5.23b** with paraformaldehyde according to the Burke procedure.[3]

9-(2-((*N,N*-Dimethylamino)methyl)ferrocenemethyl)-9,10-dihydrochromeno[8,7-e][1,3]oxazin-2(8*H*)-one (5.24)

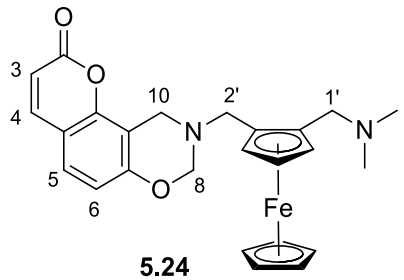

5.24

Light yellow semi-solid. Yield: 94.3 mg (68%). ^{1}H NMR (600 MHz, $CDCl_3$) δ 7.62 (d, J = 9.4 Hz, 1H, H_3), 7.24 (s, 1H, H_6), 6.76 (d, J = 8.5 Hz, 1H, H_5), 6.22 (d, J = 9.4 Hz, 1H, H_4), 4.96 (s, 2H, H_8), 4.26 (br s, 1H, H, H_{10a}), 4.22 – 4.21 (m, 2H, FcH, H_{8b}), 4.12 (t, J = 2.5 Hz, 1H, FcH), 4.06 (s, 1H, FcH), 4.01 (s, 5H, FcH), 3.77 (d, J = 13.3 Hz, 1H, $H_{2'a}$), 3.73 (d, J = 13.3 Hz, 1H, $H_{2'b}$), 3.31 – 3.27 (m, 1H, $H_{1'a}$), 3.10 (d, J = 12.9 Hz, 1H, $H_{2'b}$), 2.07 (s, 6H, NMe_2); ^{13}C NMR (150 MHz, $CDCl_3$) δ 161.3, 158.0, 152.8, 144.1, 126.5, 113.7, 112.6, 112.2, 108.7, 84.4, 83.3, 82.9, 70.8, 70.3, 69.4 (5C), 67.4, 57.5, 49.8, 45.3 (2C), 44.6; HRMS (ESI^+) *m/z* calcd for $C_{25}H_{27}FeN_2O_3$ $[M+H]^+$: 459.1366, Found 459.1363.

Synthesis of ferrocenyl coumain-1,3-oxazin-2-ones (5.25a-c,e and 5.26a-b)

Coumarin-1,3-oxazin-2-ones **5.25a-c**,**e** and **5.26a-b** were prepared by cyclizing their corresponding aminomethylcoumarinols **5.13a-c**,**e** and **5.23a-b** with CDI following the reaction conditions for the synthesis of 1,3-benzoxazin-2-ones (**4.17a-d** and **4.18a-e**).

3-(2-((*N,N*-Dimethylamino)methyl)ferrocenemethyl)-3,4-dihydro-2*H*,5*H*-chromeno[3,4-*e*][1,3]oxazine-2,5-dione (5.25a)

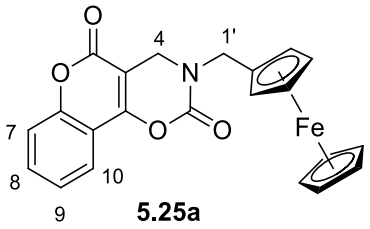

5.25a

Light brown semi-solid. Yield: 41.0 mg (68%). ^{1}H NMR (600 MHz, $CDCl_3$) δ 7.86 (dd, J = 8.1, 1.4 Hz, 1H, H_7), 7.59 (td, J = 8.4, 1.4 Hz, 1H, H_8), 7.35 – 7.33 (m, 2H, H_9, H_{10}), 4.47 (s, 2H, H, H_4), 4.34 (br s, 2H, FcH), 4.20 – 4.19 (m, 9H, FcH, $H_{1'}$); ^{13}C NMR (150 MHz, $CDCl_3$) δ 159.8, 155.9, 153.2, 147.1, 133.1, 124.9, 122.8, 117.0, 113.0, 98.2, 80.1, 70.0 (2C), 69.2 (2C), 68.9 (5C), 49.3, 43.3; HRMS (ESI^+) *m/z* calcd for $C_{22}H_{18}FeNO_4$ $[M+H]^+$: 416.0586, Found 416.0586.

3-(2-((*N,N*-Dimethylamino)methyl)ferrocenemethyl)-3,4-dihydro-2*H*,5*H*-chromeno[3,4-*e*][1,3]oxazine-2,5-dione (5.25b)

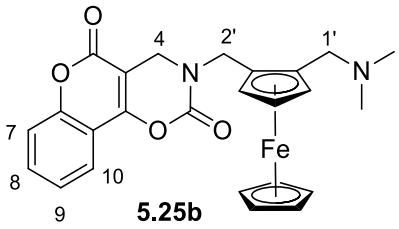

5.25b

Light brown semi-solid. Yield: 37.3 mg (75%). ^{1}H NMR (600 MHz, $CDCl_3$) δ 7.88 (d, J = 7.8 Hz, 1H, H_7), 7.58 (t, J = 7.6 Hz, 1H, H_8), 7.33 – 7.33 (m, 2H, H_9, H_{10}), 4.81 (d, J = 14.5 Hz, 1H, H_{4a}), 4.38 (d, J = 14.5 Hz, 1H, H_{4b}), 4.32 (d, J = 12.1 Hz, 2H,), 4.32 (d, J = 12.1 Hz, 1H, $H_{2'a}$), 4.28 (s, 1H, FcH), 4.21 (br s, 1H, FcH), 4.14 – 4.13 (m, 7H, $H_{2'b}$, FcH), 3.66 (d, J = 12.4 Hz, 1H, $H_{1'a}$), 2.90 (br s, 1H, $H_{1'b}$), 2.10 (s, 6H, NMe_2); ^{13}C NMR (150 MHz, $CDCl_3$) δ 159.8, 155.6, 153.2, 147.6, 132.8, 124.8, 122.7, 117.0, 113.1, 98.8, 88.5, 80.5, 72.0, 71.3, 69.5 (5C), 67.5, 57.5, 47.2 (2C), 44.9, 42.5; HRMS (ESI^+) *m/z* calcd for $C_{24}H_{27}ClFeN_2O_3Na$ $[M–CO+NaCl+H_3]^+$: 505.0952, Found 505.1424.

3-(2-((*N,N*-Dimethylamino)methyl)ferrocenemethyl)-9-chloro-3,4-dihydro-2*H*,5*H*-chromeno[3,4-*e*][1,3]oxazine-2,5-dione (5.25c)

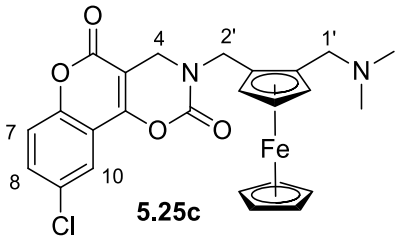

5.25c

Light brown semi-solid. Yield: 17.3 mg (49%). ^{1}H NMR (600 MHz, $CDCl_3$) δ 8.06 (d, J = 2.4 Hz, 1H, H_{10}), 7.71 (dd, J = 8.8, 2.4 Hz, 1H, H_8), 7.47 (d, J = 8.9 Hz, 1H, H_7), 4.98 (d, J = 14.5 Hz, 1H, H_{4a}), 4.59 (d, J = 14.5 Hz, 1H, H_{4b}), 4.51 – 4.49 (m, 2H, FcH, $H_{2'a}$), 4.38 (br s, 1H, FcH), 4.33 – 4.32 (m, 7H, FcH, $H_{2'b}$), 3.83 (d, J = 12.5 Hz, 1H, $H_{1'a}$), 3.03 (d, J = 12.6 Hz, 1H, $H_{1'b}$), 2.27 (s, 6H, NMe_2); ^{13}C NMR (150 MHz, $CDCl_3$) δ 159.2, 154.5, 151.4, 147.1, 132.9, 130.5, 122.3, 118.4, 114.2, 99.8, 84.9, 80.3, 72.1, 71.3, 69.5 (5C), 67.4, 57.6, 47.2, 45.0 (2C), 42.4; HRMS (ESI$^+$) *m/z* calcd for $C_{24}H_{26}Cl_2FeN_2O_3Na$ $[M–CO+NaCl+H_3]^+$: 539.1057, Found 539.1057.

3-(2-((*N,N*-Dimethylamino)methyl)ferrocenemethyl)-9-fluoro-3,4-dihydro-2*H*,5*H*-chromeno[3,4-*e*][1,3]oxazine-2,5-dione (5.25e)

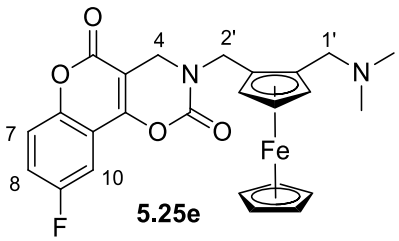

5.25e

Light brown semi-solid. Yield: 16.6 mg (36%). ^{1}H NMR (600 MHz, $CDCl_3$) δ 7.56 (dd, J = 8.0, 2.8 Hz, 1H, H_{10}), 7.33 – 729 (m, 2H, H_7, H_{18}), 4.79 (d, J = 14.5 Hz, 1H, H_{4a}), 4.39 (d, J = 14.5 Hz, 1H, H_{4b}), 4.34 – 4.29 (m, 2H, $H_{2'a}$, FcH), 4.18 (s, 1H, FcH), 4.15 – 4.09 (m, 7H, $H_{2'b}$, FcH), 3.64 (d, J = 12.6 Hz, 1H, $H_{1'a}$), 2.84 (d, J = 12.6 Hz, 1H, $H_{1'b}$), 2.07 (s, 6H); ^{13}C NMR (150 MHz, $CDCl_3$) δ 159.5, 158.2, 154.8, 149.3, 147.2, 120.4 (d, J = 24.6 Hz), 118.7 (d, J = 8.3 Hz), 114.1 , 108.6 (d, J = 25.9 Hz), 99.8, 84.9, 80.3, 72.1, 71.3, 69.5 (5C), 67.4, 57.6, 47.3, 45.0 (2C), 42.5; HRMS (ESI$^+$) *m/z* calcd for $C_{24}H_{26}ClFFeN_2O_3Na$ $[M–CO+NaCl+H_3]^+$: 523.1338, Found 523.1338.

9-Ferrocenemethyl-9,10-dihydro-2*H*,8*H*-chromeno[8,7-*e*][1,3]oxazine-2,8-dione (5.26a)

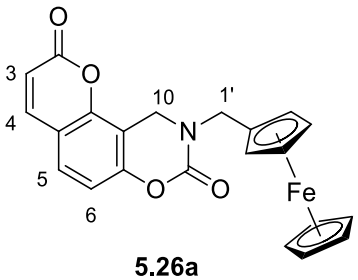

5.26a

Light brown semi-solid. Yield: 146.0 mg (96%). M.p.: 145.4 – 148.0 °C. ^{1}H NMR (400 MHz, DMSO-d_6/Acetone-d_6) δ 8.03 (d, J = 9.3 Hz, 1H, H_3), 7.66 (d, J = 8.4 Hz, 1H, H_6), 7.01 (d, J = 8.2 Hz, 1H, H_5), 6.41 (d, J = 9.4 Hz, 1H, H_4), 4.57 (s, 2H, H_{10}), 4.47 (s, 2H, $H_{1'}$), 4.40 (s, 2H, FcH), 4.23 (s, 5H, FcH), 4.19 (s, 2H, FcH); ^{13}C NMR (100 MHz, DMSO-d_6/Acetone-d_6) δ 159.3, 151.6, 150.1, 148.2, 144.1, 128.7, 114.8, 114.2, 112.0, 105.8, 81.4, 69.4, 68.5, 68.2, 47.9, 42.0; HRMS (ESI$^+$) *m/z* calcd for $C_{21}H_{20}FeNO_3$ $[M–CO+H_3]^+$: 390.0787, Found 390.0781.

9-(2-((*N*,*N*-dimethylamino)methyl)ferrocenemethyl)-9,10-dihydro-2*H*,8*H*-chromeno[8,7-*e*][1,3]oxazine-2,8-dione (5.26b)

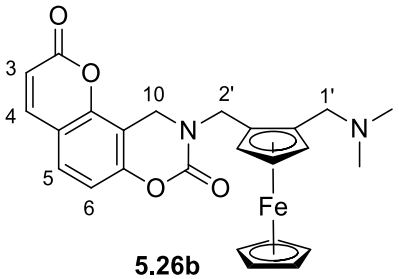

5.26b

Light yellow solid. Yield: 62.2 mg (90%). M.p.: 105.3 – 108.6 °C. ^{1}H NMR (400 MHz, $CDCl_3$) δ 7.63 (d, J = 9.6 Hz, 1H, H_3), 7.34 (d, J = 8.5 Hz, 1H, H_6), 6.91 (d, J = 8.5 Hz, 1H, H_5), 6.31 (d, J = 9.6 Hz, 1H, H_4), 4.73 – 4.68 (m, 2H, H_{10}), 4.55 – 4.48 (m, 2H, $H_{2'}$), 4.39 (br s, 1H, FcH), 4.29 (br s, 1H, FcH), 4.16 (t, J = 2.4 Hz, 1H, FcH), 4.13 (s, 5H, FcH), 3.83 – 3.70 (m, 1H, $H_{1'a}$), 3.15 – 3.03 (m, 1H, $H_{1'b}$), 2.19 (s, 6H, NMe_2); ^{13}C NMR (100 MHz, $CDCl_3$) δ 160.0, 152.3, 150.5, 149.4, 143.3, 127.9, 114.9, 114.8, 112.7, 106.5, 80.9 (2C), 71.9, 71.2, 69.5 (5C), 67.8, 57.2, 46.9, 44.4 (2C), 41.9; HRMS (ESI$^+$) *m/z* calcd for $C_{24}H_{25}FeN_2O_4$ $[M+H]^+$: 473.1164, Found 473.1159.

Synthesis of 1,3-benzoxazine 3-ethanols (6.3a-c)

The 1,3-benzoxazine 3-ethanols **6.3a-c** were synthesized from ethanolamine **6.2** and phenols **31a** and **3.1c-d** according to the Burke procedure previously described for the preparation of ferrocenyl 1,3-benzoxazine derivatives **3.13a-k** with minor modifications.[3] After completion

of the reaction (TLC), 2N citric acid (25 mL) was added to reaction mixture to extract the product into the aqueous phase. The aqueous phase was washed with diethyl ether (2 × 25 mL) and the pH was adjusted to 8 using 1N NaOH solution. The product was extracted with DCM (3 × 25 mL), dried (Na_2SO_4) and the solvent removed *in vacuo* to furnish the title compound in sufficient purity to use in the next step.

3,4-Dihydro-2*H*-1,3-benzoxazin-3-ethanol (6.3a)

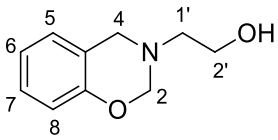

6.3a

Colourless oil. Yield: 898.5 mg (89%).^{1}H NMR (600 MHz, $CDCl_3$) δ 7.13 (t, J = 7.7 Hz, 1H, H_7), 6.95 (d, J = 7.6 Hz, 1H, H_8), 6.88 (t, J = 7.4 Hz, 1H, H_6), 6.79 (d, J = 8.2 Hz, 1H, H_5), 4.88 (s, 2H, H_2), 4.02 (s, 2H, H_4), 3.70 (t, J = 5.4 Hz, 2H, $H_{2'}$), 2.96 (t, J = 5.4 Hz, 2H, $H_{1'}$); ^{13}C NMR (150 MHz, $CDCl_3$) δ 154.1, 128.0, 127.7, 120.9, 119.9, 116.7, 82.9, 59.2, 53.5, 50.0.

6-Bromo-3,4-dihydro-2*H*-1,3-benzoxazin-3-ethanol (6.3b)

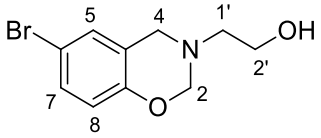

6.3b

Colourless oil. Yield: 586.3 mg (62%). ^{1}H NMR (400 MHz, $CDCl_3$) δ 7.22 (dd, J = 8.6, 2.3 Hz, 1H, H_7), 7.05 (d, J = 1.9 Hz, 1H, H_5), 6.69 (d, J = 8.7 Hz, 1H, H_8), 4.88 (s, 2H, H_2), 4.02 (s, 2H, H_4), 3.71 – 3.68 (m, 2H, $H_{2'}$), 2.98 – 2.93 (m, 2H, $H_{1'}$); ^{13}C NMR (150 MHz, $CDCl_3$) δ 146.0, 132.0, 131.0, 121.8, 118.5, 112.7, 85.6, 63.8, 53.4, 49.6.

6-Methoxy-3,4-dihydro-2*H*-1,3-benzoxazin-3-ethanol (6.3b)

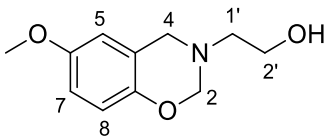

6.3c

Colourless oil. Yield: 1.02 g (98%). ^{1}H NMR (600 MHz, $CDCl_3$) δ 6.72 (s, 1H, H_5), 6.71 – 6.70 (m, 1H, H_7), 6.50 – 6.49 (m, 1H, H_8), 4.82 (s, 2H, H_2), 3.98 (s, 2H, H_4), 3.73 (s, 3H, OMe), 3.70 – 3.67 (m, 2H, $H_{2'}$), 2.96 – 2.92 (m, 2H, $H_{1'}$); ^{13}C NMR (150 MHz, $CDCl_3$) δ 153.7, 148.0, 120.4, 117.3, 114.0, 112.2, 82.7, 59.3, 55.8, 53.5, 50.2.

Synthesis of ferrocene ethyl carbamate derivatives (6.4a-c)

Ferrocene ethyl carbamate derivatives **6.4a-c** were synthesized following the CDI cyclization procedure for the synthesis of ferrocenyl 1,3-benzoxazin-2-ones (**4.17a-d** and **4.18a-e**) (Method B).[9] Instead of NaOH, the reaction solution was washed with 1N HCl (20 mL) and distilled water (20 mL). After the removal of the solvent under reduce pressure, the obtained crude product was subjected to column chromatography using basic alumina (DCM → 1:9 MeOH/DCM) to afford the desired compound.

3,4-Dihydro-*2H*-1,3-benzoxazin-3-ethanol-2-((*N*,*N*-dimethylamino)methyl)ferrocenemethyl carbamate (6.4a)

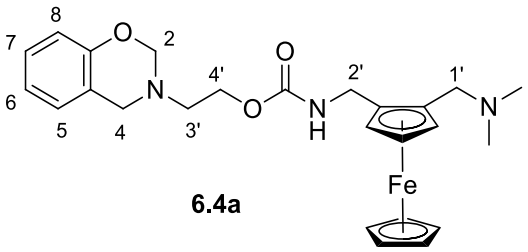

6.4a

Brown semi-solid. Yield: 86.5 mg (76%). ^{1}H NMR (400 MHz, $CDCl_3$) δ 7.10 (t, J = 7.9 Hz, 1H, H_7), 6.95 – 6.90 (m, 1H, H_8), 6.87 – 6.84 (m, 1H, H_6), 6.84 – 6.82 (m, 1H, NH), 6.78 – 6.74 (m, 1H, H_5), 4.88 – 4.84 (m, 2H, H_2), 4.27 – 4.16 (m, 4H, $H_{2'}$, $H_{4'}$), 4.07 – 4.06 (m, 7H, FcH), 4.01 (br s, 3H, H_4, FcH), 3.67 (d, J = 12.4 Hz, 1H, $H_{1'a}$), 2.99 – 2.94 (m, 2H, $H_{3'}$), 2.80 (d, J = 12.6 Hz, 1H, $H_{1'b}$), 2.22 – 2.15 (m, 6H, NMe_2); ^{13}C NMR (100 MHz, $CDCl_3$) δ 156.4, 155.2, 127.8, 127.7, 120.7, 120.1, 116.6, 85.0, 83.1, 71.0, 69.8, 69.4, 69.2 (5C), 66.1, 62.9, 58.1, 50.8, 50.7, 44.8 (2C), 39.8; HRMS (ESI$^+$) *m/z* calcd for $C_{25}H_{32}FeN_3O_3$ $[M+H]^+$: 478.1793, Found 478.1790.

6-Bromo-3,4-Dihydro-*2H*-1,3-benzoxazin-3-ethanol-2-((*N*,*N*-dimethylamino)methyl)ferrocenemethyl carbamate (6.4b)

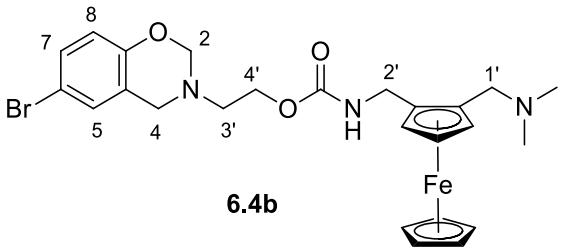

6.4b

Brown semi-solid. Yield: 98.6 mg (80%). ^{1}H NMR (600 MHz, $CDCl_3$) δ 7.22 – 7.18 (m, 1H, H_7), 7.10 – 7.02 (m, 1H, H_5), 6.88 – 6.86 (m, 1H, NH), 6.68 – 6.63 (m, 1H, H_8), 4.86 – 4.81

(m, 2H, H_2), 4.28 – 4.10 (m, 4H, $H_{2'}$, $H_{4'}$), 4.06 (s, 6H, FcH), 4.01 (t, J = 2.2 Hz, 1H, FcH), 3.98 – 3.97 (m, 2H, FcH, H_{4a}), 3.71 – 3.63 (m, 2H, H_{4b}, $H_{1'a}$), 2.95 – 2.91 (m, 2H, $H_{3'}$), 2.80 (d, J = 12.6 Hz, 1H, $H_{1'b}$), 2.17 – 2.16 (m, 6H, NMe_2); ^{13}C NMR (150 MHz, $CDCl_3$) δ 156.4, 153.3, 130.8, 130.2, 122.1, 118.4, 112.5, 85.0, 83.2, 71.1, 69.8, 69.2 (5C), 66.1, 62.9, 59.2, 58.1, 53.6, 50.8, 50.4, 44.8 (2C); HRMS (ESI$^+$) *m/z* calcd for $C_{25}H_{31}BrFeN_3O_3$ $[M+H]^+$: 544.0898, Found 544.0887.

6-Methoxy-3,4-Dihydro-*2H*-1,3-benzoxazin-3-ethanol-2-((*N,N*-dimethylamino)methyl)ferrocenemethyl carbamate (6.4c)

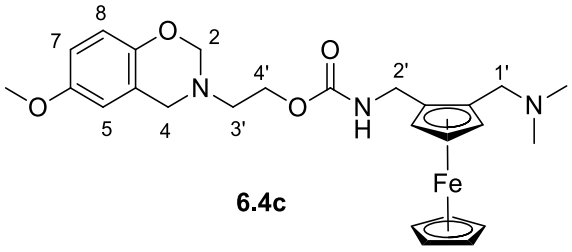

6.4c

Brown semi-solid. Yield: 70.6 mg (75%). ^{1}H NMR (400 MHz, $CDCl_3$) δ 6.80 (d, J = 8.6 Hz, 1H, NH), 6.81 – 6.69 (m, 2H, H_7, H_5), 6.47 (s, 1H, $H_{8'}$), 4.78 (s, 2H, H_2), 4.28 – 4.13 (m, 5H, $H_{2'}$, $H_{4'}$, FcH), 4.07 – 4.06 (m, 6H, FcH), 4.02 – 3.95 (m, 3H, H_4, FcH), 3.72 (s, 3H, OMe), 3.66 (d, J = 12.6 Hz, 1H, $H_{1'a}$), 2.95 (q, J = 7.5, 6.6 Hz, 2H, $H_{3'}$), 2.80 (d, J = 12.6 Hz, 1H, $H_{1'b}$), 2.14 (s, 6H, NMe_2); ^{13}C NMR (100 MHz, $CDCl_3$) δ 156.4, 153.6, 148.1, 120.6, 117.2, 113.8, 112.2, 85.0, 83.8, 82.9, 71.0, 69.7, 69.2 (5C), 66.0, 62.9, 58.1, 55.8, 50.9, 50.8, 44.8 (2C), 39.8; HRMS (ESI$^+$) *m/z* calcd for $C_{26}H_{33}FeN_3O_4$ $[M+H]^+$: 508.1899, Found 508.1902.

Synthesis of *N*-boc ethylene diamine (6.7)[16]

A solution of di-*tert*-butyl bicarbonate (2.00g, 9.16 mmol) in DCM (20 mL) was slowly added to a stirring solution of excess ethylene diamine **6.6** (3 mL) in DCM (100 mL) over 1 hour on ice. The reaction mixture was removed form ice and stirred at room temperature for 12 hours after which the solvent was removed under reduced pressure. The resultant sticky material was reconstituted in saturated K_2O_3 solution (50 mL) and the product extracted with DCM (3 × 50

mL). The collected organic layers were dried (Na_2SO_4) and the solvent removed *in vacuo* to afford the pure compound as a colourless oil. Yield: 1.44 g (98%).

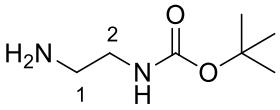

6.7

^{1}H NMR (600 MHz, $CDCl_3$) δ 4.91 (s, 1H. NH), 3.16 (q, J = 5.4 Hz, 2H, H_2), 2.78 (t, J = 5.9 Hz, 2H, H_1), 1.43 (s, 9H, 3 × Me), 1.32 (s, 2H, NH_2); ^{13}C NMR (150 MHz, $CDCl_3$) δ 156.3, 79.3, 43.5, 42.0, 28.5 (3C).

Synthesis of ((*N*,*N*-dimethylamino)methyl)ferrocenecarboxylic acid (6.10)[17]

A solution of t*ert*-butyllithium (7.41 mL, 12.6 mmol) in pentane was added dropwise with caution to a stirring solution of (dimethylaminomethyl)ferrocene **3.15a** (2.00 mL, 10.1 mmol) in anhydrous Et_2O under nitrogen gas at room temperature. The reaction was further stirred for 30 minutes during which time an orange suspension formed. After 30 minutes, the solution was bubbled with CO_2 gas for 30 minutes. The resulting yellow precipitate was collected by removing the solvent under reduced pressure. The precipitate was subjected to flash silica gel column chromatography to furnish the desired compound as an orange semi-solid (4:1 MeOH/DCM). Yield: 1.00 g (35%).

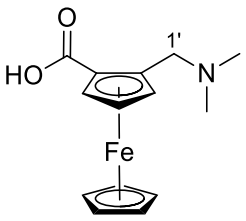

6.10

^{1}H NMR (400 MHz, $CDCl_3$) δ 4.96 – 4.91 (m, 1H, FcH), 4.11 (br s, 7H, FcH), 3.30 – 3.26 (m, 1H, $H_{1'a}$), 2.40 (d d, J = 12.6 Hz, 1H, $H_{1'b}$), 17 (s, 6H, NMe_2); ^{13}C NMR (100 MHz, $CDCl_3$) δ 173.6, 79.0, 75.6, 72.0, 71.0, 69.9 (5C), 69.1, 56.8, 44.2 (2C).

Synthesis of *N*-boc 1,3-benzoxazine 3-ethylamines (6.11a′-b′)

The 1,3-benzoxazine 3-ethylamines **6.11a′-b′** were synthesized via Burke condensation by reacting *N*-boc ethylenediame with phenols **3.1b** and **3.1d** as described for the synthesis of 1,3-benzoxazine 3-ethanols **6.4a-c**.

_N_-Boc 6-methyl-3,4-dihydro-2_H_-1,3-benzoxazin-3-ethylamine (6.11a′)

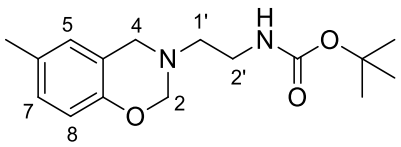

6.11'a

Colourless oil. Yield: 753.0 mg (89%). ^{1}H NMR (600 MHz, $CDCl_3$) δ 6.99 (s, 1H, H_5), 6.91 – 6.84 (m, 2H, H_7, H_8), 4.31 – 4.21 (m, 2H, H_2), 3.99 – 3.94 (m, 2H, H_4), 3.55 (br s, 2H, $H_{1'}$), 3.20 – 3.13 (m, 2H, $H_{2'}$), 2.22 (s, 3H, Me), 1.43 (s, 9H, NMe_2); ^{13}C NMR (150 MHz, $CDCl_3$) δ 154.6, 153.1, 130.9, 130.8, 130.7, 129.0, 116.5, 81.0, 66.5, 55.3, 51.1, 43.2, 28.4, 20.5 (3C).

_N_-Boc 6-bromo-3,4-dihydro-2_H_-1,3-benzoxazin-3-ethylamine (6.11b′)

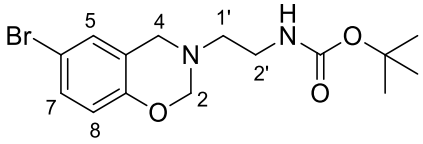

6.11'b

Colourless oil. Yield: 596.5 mg (78%). ^{1}H NMR (300 MHz, $CDCl_3$) δ 7.21 (dd, J = 8.6, 2.3 Hz, 1H, H_7), 7.05 (br s, 1H, H_5), 6.67 (d, J = 8.7 Hz, 1H, H_8), 4.45 – 4.39 (m, 2H, H_2), 4.02 – 3.99 (m, 2H, H_4), 3.55 (br s, 2H, $H_{1'}$), 3.20 – 3.13 (m, 2H, $H_{2'}$), 2.22 (s, 3H, Me), ^{13}C NMR (150 MHz, $CDCl_3$) δ 153.3, 130.8, 130.2, 122.1, 118.4, 112.5, 81.0, 66.5, 55.3, 51.7, 43.7, 29.8, 20.9 (3C).

Synthesis of 1,3-benzoxazine 3-ethylamines (6.11a-b)[18]

An appropriate *N*-boc 1,3-benzoxazine 3-ethylamine (**6.11a′-b′**) was stirred in 4M HCl solution in dioxane (1 mL) for 1 hour at room temperature. After completion of the reaction (TLC), the solvent was removed *in vacuo* to afford a hydrochloride salt of the formed amine as an off white solid. The obtained material was dissolved in 1N NaOH (10 mL) and then extracted with DCM (3 × 25 mL), dried and solvent removed *in vacuo* to afford the pure amine (**6.11a-b**).

6-Methyl-3,4-dihydro-2*H*-1,3-benzoxazin-3-ethylamine (6.11a)

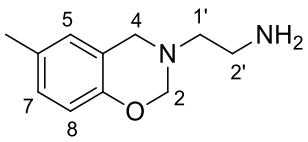

6.11a

Colourless oil. Yield: 450.0 mg (98%). ^{1}H NMR (600 MHz, $CDCl_3$) δ 6.97 (dd, J = 8.2, 1.8 Hz, 1H, H_7), 6.78 (br s, 1H, H_5), 6.73 (d, J = 8.2 Hz, 1H, H_8), 3.81 (s, 2H, H_2), 3.54 (s, 2H), 3.38 (s, 1H), 2.94 (t, J = 6.7 Hz, 2H, $H_{1'}$), 2.84 (t, J = 6.7 Hz, 2H, $H_{2'}$), 2.24 (s, 3H, Me); ^{13}C NMR (150 MHz, $CDCl_3$) δ 155.5, 129.3, 128.8, 128.2, 121.6, 115.9, 75.9, 74.2, 51.6, 50.5, 20.6.

6-Bromo-3,4-dihydro-2*H*-1,3-benzoxazin-3-ethylamine (6.11b)

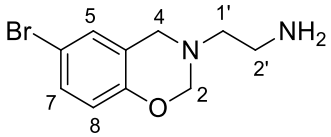

6.11b

Colourless oil. Yield: 298.8 mg (83%). ^{1}H NMR (300 MHz, $CDCl_3$) δ 7.21 (dd, J = 8.6, 2.3 Hz, 1H, H_7), 7.05 (br s, 1H, H_5), 6.67 (d, J = 8.7 Hz, 1H, H_8), 4.45 – 4.39 (m, 2H, H_2), 4.02 – 3.99 (m, 2H, H_4), 3.55 (br s, 2H, $H_{1'}$), 2.89 – 2.78 (m, 2H, $H_{2'}$); ^{13}C NMR (150 MHz, $CDCl_3$) δ 154.8, 132.0, 131.7, 124.4, 117.3, 116.4, 82.0, 55.5, 52.6, 40.0.

Synthesis of ferrocene ethylene-spaced 1,3-benzoxazine derivative (6.12b)

Compound **6.12b** was accessed via microwave-assisted DCC amidation of benzoxazine 3-ethylamine **6.11b** (100.0 mg, 0.389 mmol) and ferrocene carboxylic acid **6.10** (112.0 mg, 0.389) as described for the synthesis of salicylamides **4.15a-e** and **4.16a-b** (Method B).

***N*-(2-(6-Bromo-2*H*-benzo[*e*][1,3]oxazin-3(4*H*)-yl)ethyl)-2-((*N*,*N*-dimethylamino)methyl)ferrocenecarboxamide (6.12b)**

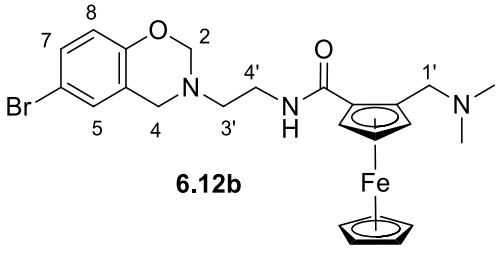

6.12b

Light brown semi-solid. Yield: 32.8 mg (16%). ^{1}H NMR (600 MHz, $CDCl_3$) δ 9.64 (s, 1H, NH), 7.21 (dd, J = 8.7, 2.2 Hz, 1H, H_7), 7.09 (d, J = 1.7 Hz, 1H, H_5), 6.66 (d, J = 8.7 Hz, 1H, H_8), 4.90 (s, 1H, FcH), 4.87 (s, 2H, H_2), 4.21 (t, J = 2.3 Hz, 1H, FcH), 4.14 (s, 5H, FcH), 4.00 (s, 2H, H_4), 3.97 (d, J =

12.4 Hz, 1H, $H_{1'a}$), 3.58 (dq, J = 12.4, 6.1 Hz, 1H, $H_{4'a}$), 3.47 (dq, J = 11.9, 5.9 Hz, 1H, $H_{4'b}$), 2.97 – 2.86 (m, 2H, $H_{3'}$), 2.85 (d, J = 12.4 Hz, 1H, $H_{1'b}$), 2.13 (s, 6H, NMe_2); ^{13}C NMR (150 MHz, $CDCl_3$) δ 170.6, 153.4, 130.8, 130.3, 122.1, 118.4, 112.6, 82.9, 80.5, 79.6, 73.4, 73.3, 70.5 (5C), 68.0, 59.2, 51.3, 50.0, 44.0 (2C), 37.8; HRMS (ESI$^+$) *m/z* calcd for $C_{24}H_{29}BrFeN_3O_2$ $[M+H]^+$: 526.0787, Found 526.0902.

_N_-(2-Hydroxy-4-methylbenzyl)-_N_-(_N,N_-dimethylamino)methyl)ferrocenemethyl-5-chlorosalicylamide (6.16)[19]

Iodine (92.0 mg, 0.378 mmol), 5-chlorosalicylic acid (65.2 mg, 0.378 mmol) and Et_3N (80 µL, 0.567 mmol) were successively added to a solution of $P(OEt)_3$ at room on ice and the resulting brown mixture was for 30 minutes. A solution of 4-methyl α-amino-*o*-cresol (**4.6b**) was slowly added to the stirring reaction mixture. The reaction mixture was removed from ice and stirred at room temperature for 12 hours at which time an intense spot of the product was observed. The resultant dark brown reaction mixture was diluted with DCM (25 mL) and successively washed with saturated ammonium chloride solution (15 mL), 5% NaOH solution (15 mL) and brine (15 mL). The organic layer was dried (Na_2SO_4) and the solvent removed *in vacuo* to afford a brown crude product, which was subjected to silica gel column chromatography (1:2:7 Et_3N/EtOAc/Hex). The title compound was obtained as a light brown semi-solid.

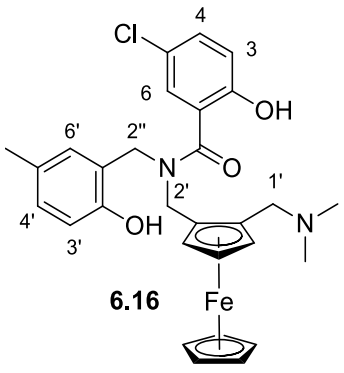

6.16

Light brown semi-solid. Yield: 145.6 mg (70%). ^{1}H NMR (400 MHz, $CDCl_3$) δ 7.20 (d, J = 2.2 Hz, 1H, H_6), 7.13 (dd, J = 8.7, 2.3 Hz, 1H, $H_{4'}$), 6.89 (d, J = 7.3 Hz, 1H, H_4), 6.73 (d, J = 8.6 Hz, 1H, $H_{3'}$), 6.68 (br s, 1H, $H_{6'}$), 6.61 (d, J = 7.3 Hz, 1H, H_3), 5.68 (d, J = 13.6 Hz, 1H, $H_{2"a}$), 4.39 – 4.29 (m, 1H, FcH), 4.25 – 4.18 (m, 2H, FcH, $H_{1'a}$), 4.05 (s, 5H, FcH), 3.97 (s, 1H, FcH), 3.63 (s, 2H, $H_{2'}$), 3.45 (d, J = 12.0 Hz, 1H, $H_{2"b}$), 3.01 (d, J = 12.7 Hz, 1H, $H_{1'b}$), 2.32 (s,

6H, NMe_2), 2.24 (s, 3H, Me); ^{13}C NMR (100 MHz, $CDCl_3$) δ 169.2, 154.4, 153.5, 130.8 (2C), 129.5, 128.7, 127.9, 126.7, 123.3, 122.1, 120.1, 116.1, 84.4, 80.3, 72.1, 70.7, 69.4 (5C), 67.4 (2C), 57.2, 45.9, 44.5 (2C), 20.7; HRMS (ESI^+) *m/z* calcd for $C_{29}H_{32}ClFeN_2O_3$ $[M+H]^+$: 547.1451, Found 547.1454.

_N_-(2-Hydroxy-4-methylbenzyl)-_N_-((_N_,_N_-dimethylamino)methyl)ferrocenemethyl)-5-chloro-2-hydroxybenzylamine (6.17)

Excess $LiAlH_4$ (31.3 mg, 0.825 mmol) was added portion wise to a solution of tertiary benzamide **6.16** (90.0 mg, 0.165 mmol) in anhydrous THF (15 mL) on ice. The solution was refluxed under nitrogen for 12 hours after which unreacted $LiAlH_4$ was quenched by slow addition of brine (5 mL). The separated organic layer was collected by decantation and the sedimented clumpy solid was washed with THF (2 × 25 mL). The organic layers were combined, washed with brine (10 mL) and dried (Na_2SO_4). Following filtration and removal of the solvent *in vacuo* the pure product was obtained as light brown semi-solid.

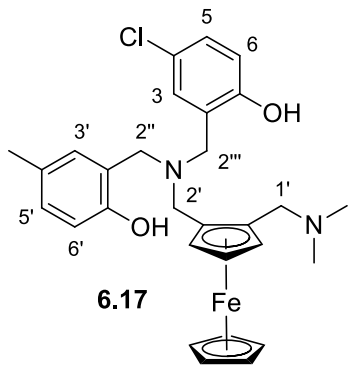

6.17

Light brown semi-solid. Yield: 51.0 mg (58%). ^1H NMR (600 MHz, $CDCl_3$) δ 7.08 (dd, J = 8.6, 2.4 Hz, 1H, $H_{5'}$), 6.98 (d, J = 2.4 Hz, 1H, $H_{3'}$), 6.95 (d, J = 8.1 Hz, 1.2 Hz, 1H, H_5), 6.80 (br s, 1H, H_3), 6.74 – 6.72 (m, 2H, H_6, $H_{6'}$), 4.15 (s, 1H, FcH), 4.06 (s, 2H, FcH), 3.96 (s, 5H, FcH), 3.88 (d, J = 13.4 Hz, 1H, $H_{2'a}$), 3.83 (dd, J = 13.3, 4.2 Hz, 2H, $H_{2'''}$), 3.70 (d, J = 12.5 Hz, 1H, $H_{1'a}$), 3.18 (dd, J = 13.3, 5.9 Hz, 2H, $H_{2''}$), 3.11 (d, J = 13.4 Hz, 1H, $H_{2'b}$), 2.85 (d, J = 12.6 Hz, 1H, $H_{1'b}$), 2.31 (s, 6H, NMe_2), 2.23 (s, 3H, Me); ^{13}C NMR (150 MHz, $CDCl_3$) δ 155.7, 154.4, 131.1, 129.8 (2C), 128.8, 128.6, 124.5, 123.7, 122.2, 118.6, 117.3, 83.3, 82.3, 72.1, 71.8, 69.4 (5C), 66.9, 57.7, 57.1, 56.8, 54.0, 45.5 (2C), 20.6; HRMS (ESI^+) *m/z* calcd for $C_{29}H_{34}ClFeN_2O_2$ $[M+H]^+$: 533.1658, Found 533.1663.

9.3. Biological evaluation assays

9.3.1. 3D7 Plasmodium falciparum antiplasmodial assay

The 3D7 strain *P. falciparum* parasites were cultured in a RPMI1640 medium supplemented with 25 mM HEPES (Lonza, Switzerland), 0.5% (w/v) Albumax II (Thermo Fisher Scientific, Waltham, MA), 22 mM glucose, 0.65 mM hypoxanthine, 0.05 mg/mL gentamicin and 2 – 4 % (v/v) human erythrocytes and maintained at 37 □C under an atmosphere of 5% CO_2, 5% O_2 and 90% N_2. The cultures were treated with serial dilutions of the test compounds and chloroquine (control) for 48 hours and the plasmocidal activities and IC_{50} value determined using a parasite lactate dehydrogenase (pLDH) assay as previously described.[20]

9.3.2. Dd2 Plasmodium falciparum antiplasmodial assay

P. falciparum parasites of the chloroquine-resistant Dd2 strain were cultured and maintained in a medium containing Albumax II (Thermo Fisher Scientific, South Africa) according to a modified procedure by Trager and Jensen.[21] Cultures were kept below 4% haematocrit and were diluted to 1% parasitemia upon reaching the trophozoite stage. The test compounds and controls (chloroquine and artemisinin) were dissolved in DMSO to a final concentration of 10 μM and serial dilutions were prepared from this solution and incubated for 48 hours with the parasites seeded in 96-well plates under an atmosphere containing 4% CO_2 and 3% O_2 in nitrogen at 37 °C. Antiplasmodial activity of each compound against the strain was determined in triplicate as previously described [22] following the parasite lactate dehydrogenase (pLDH) procedure by Makler et al.

9.3.3. Antitrypanosomal assay

Trypanosoma brucei brucei 427 trypomastigotes were grown in a 5% CO_2 incubator kept at 37 °C in IMDM medium (Lonza, Switzerland) supplemented with 10% fetal serum, HMI-9

supplement,[23] hypoxanthine and penicillin/streptomycin. Following 24-hour incubation of the parasites seeded in 96-well plates with varying concentrations of test compounds and pentamidine (positive control), resazurin was added to a final concentration of 50 μM. Incubation was continued for a further 24 hours and fluorescence read at excitation and emission wavelengths of 560 nm and 590 nm, respectively. Readings were converted to percentage viability relative to untreated controls and plotted against Log[compound] to determine IC_{50} values by non-linear regression analysis.[24]

9.3.4. HCC70 breast cancer cell line toxicity assay

The HCC70 human triple-negative breast cancer cells were cultured in RPMI media containing 10% (v/v) foetal bovine serum (FBS), 1 mM L-glutamine, 100 U/mL penicillin, 100 μg/mL streptomycin and 12.5 μg/mL amphotericin (PSA) and were maintained at 37 °C in a 9% CO_2 atmosphere. The cytotoxicity of the compounds and the positive control (paclitaxel) against the cell line was performed spectrophotometrically in triplicate using the resazurin assay as previously described with minor modifications.[25] HCC70 cells were seeded at 5×10^3 cells/well in a 96-well plate and allowed to adhere overnight, after which cells were treated with DMSO or a range of concentrations of either paclitaxel (positive control) or the benzoxazine compounds for 72 hours. Thereafter, cell viability was determined by adding 0.009 mM resazurin in phosphate buffered saline (PBS) and incubating for an additional 2 – 4 hours. Reduction of resazurin to resorufin by viable cells was assessed by fluorescence readings (excitation 560 nm, emission 590 nm) in a SpectraMax M3 microplate plate reader (Molecular Devices, San Jose, CA, USA). IC_{50} values were calculated by non-linear regression using GraphPad Prism 4 software (San Diego, CA, USA).

9.3.5. UV-Vis DNA titration assay

Varying concentrations from 1 to 100 μM were prepared from a 20 mM stock solution in DMSO of a test compound (**3.16c**, **4.6c**, **4.17b** and **5.23b**) using milli-Q water. Calf thymus DNA (70 ng/μL) was added and the samples were allowed to equilibrate at room temperature for 15 minutes before absorbance was monitored between 230 and 290 nm on a SpectraMax M3 microplate plate reader (Molecular Devices, San Jose, CA, USA). Controls included a 100 μM sample of the test compounds lacking calf thymus DNA and a sample of calf thymus DNA alone (70 ng/μL) in milli-Q water. The absorbance was recorded similarly to the above test samples. To visualize the affinity of the compounds for DNA binding, the concentration-dependent response of test samples was plotted as spectra depicting absorbance measured over wavelengths from 230 to 290 nm. To quantify DNA binding affinity of the compound, the binding constant (K_b) was determined as the ratio of intercept to slope of the reciprocal guest-host plot correlating absorbance to compound concentration.[26]

9.3.6. Competitive DNA binding assays

A solution of methylene blue (1.5 μg/ml; DNA intercalator) or Hoechst 33342 dye (1 μg/ml; DNA minor groove binder) was added to solutions of the test compound **3.16c**, **4.6c** or **5.25b** (50 and 100 μM) containing 70 ng/μL calf thymus DNA in milli-Q water. Samples were kept at room temperature in the dark for 10 minutes before fluorescence spectra (excitation 665 nm, emission 650 – 750 nm for methylene blue, and excitation 350 nm, emission 400 – 600 nm for Hoechst 33342) were acquired. Cisplatin (100 μM) was employed as a positive control in the DNA intercalation study with methylene blue dye, whilst DMSO, prepared similarly to the test samples, served as a negative control in both assays. Samples containing either methylene blue or Hoechst 33342 dye and the appropriate test compound (50 or 100 μM) without DNA were included as additional controls.

9.3.7. Selective DNA binding assay between malarial and mammalian DNA

The selective binding assay was carried out as described for the Hoechst assay above using varying concentrations of compound **3.16c** (0, 1, 5, 10, 15 and 20 μM) and calf-thymus DNA and DNA isolated from the 3D7 *P. falciparum*. Isolation of malarial DNA was accomplished according to literature methods using 3D7 *P. falciparum* trophozoites cultured as described for the 3D7 antiplasmodial evaluation assay as the DNA source.[27] The *Quick*-DNA Microprep Kit (#D3024/D3025) was used for the isolation.[27] The binding constants were determined by fitting the obtained data points into the Stern–Volmer equation relating fluorescence of the DNA-compound complex to the concentration of the compound.[28]

9.3.8. Comet assay

HCC70 cells were seeded at 4×10^5 cells/well in a 6-well plate and allowed to adhere overnight after which they were treated with the test compounds **3.16c** and **3.16f** (55.0 μM) for 6 hours or H_2O_2 (20.0 μM) for 1 hour as the positive control. The negative control sample was prepared by treating the cells with the same amount of DMSO (0.27% v/v) as the test samples. The cells were diluted to a final density of 2×10^4 cells/mL from which 400 μL was pipetted and dispersed in 1 mL low-gelling agarose gel (1% w/v) kept at 40 °C, to give a final cell density of 5714 cells/mL. The dispersed cells in agarose gel (1 mL) were layered on slides pre-coated with agarose gel (1% w/v) and allowed to set at room temperature. Cells were lysed by incubating the slides at 4 °C for 1 hour in an alkaline lysis solution (100 mM Na_2EDTA, 0.1% [w/v] sodium lauryl sarcosinate, 1.2 M NaCl, 0.26 M NaOH), rinsed with the electrophoresis solution (2 mM Na_2EDTA, 0.03M NaOH) and then electrophoresed for 25 minutes at 40 mA and 20 V in the same solution. After electrophoresis, the slides were rinsed with distilled water and stained with 10μg/mL propidium iodide in PBS at room temperature in the dark for 20 minutes. The stained slides were kept at 4 °C in the dark for 18 hours after rinsing with distilled water.

The comets were visualized on a fluorescence microscope using U-MWG wide green filter cube (WG) at 10× magnification. The captured comet images were processed in Image J with the Open Comet plugin to quantify DNA damage.[29] A total of 25 – 30 nuclei were assessed for Olive tail moment in each treatment.

9.3.9. β-Hematin binding assay

Hemozoin binding was performed according the procedure reported by Egan and colleagues with minor modifications.[30] A 25 μM stock solution of β-hematin was prepared dissolving 25 mg of hemin (from porcine) in 947 μL of DMSO and sonicating the resulting suspension for 1 minute to ensure complete dissolution. A volume of 178 μM of hematin solution was added to 20 mL of 1 M acetate buffer (pH 4.8) and thoroughly mixed to give a final concentration of 220 μM hematin solution. Varying concentrations (1 – 1000 μM) of the test compounds (**3.16c**, **4.16c** and **5.23b)** in DMSO were placed in 96-well plate, keeping the total volume of DMSO below 10 μL in each well. A sample of chloroquine was prepared similarly and used as a positive control in the assay, while DMSO was used as a negative control. The samples were treated with 100 μL of the 220 μM hematin solution in acetate 20 μL and 30 μM NP-40 detergent was added to induce hemozoin formation. This was followed by addition of 70 μL of deionised water to give a final volume of 200 μM in each well. The plate was incubated at 37 °C for 6 hours with gently shaking. After 6 hours, the analysis of hemozoin formation was carried out according to the pyridine-ferrichrome method by Ncokazi and Egan by adding to each well a solution of 50% pyridine (v/v), 20% acetone (v/v), 10% distilled water and 20% 200 mM HEPES buffer (pH 7.4).[31] The plate was further incubated for 10 minutes with gently shaking after which 50 μL acetone was added to facilitate hemozoin dispersion. Absorbance of was measured at 605 nm for each well and the plotted against a logarithm of the corresponding

concentration on Graph-Pad Prism. Sigmoidal non-linear regression analysis was performed to quantify hemozoin inhibition of each compound in terms IC_{50} values.

9.3.10. Computational DNA docking studies

Computational docking studies were performed with the AutoDock Vina plugin in UCSF Chimera 1.13.1 using a DNA co-crystal structure with Hoechst 33342 obtained from the Protein Data Bank as a receptor (PDB: 129D). The ligand structures of *(S)*-**3.16c** and Hoechst 33342 were drawn and minimized in Chem3D Pro 12.0 applying minimum RMSD gradient of 0.010. Both the DNA receptor and ligands were prepared by employing Dock Prep in Chimera for the docking simulation applying the AMBER ff14SB forcefield and assigning Gasteiger charges computed using ANTECHAMBER.[32] Following removal of crystallization waters and conformational optimization, the Hoechst 33342 co-ligand was removed from the DNA receptor which was now ready for docking. Docking scores were obtained in kcal/mol and the ligand-receptor interactions were visualized in Biovia Discovery Studio Visualizer (Dassault Systèmes BIOVIA, Discovery Studio 2019 Client, Sandiego: Dassault Systèmes, 2019).

References

(1) Furniss, B. S.; Hannaford, A. J.; Smith, P. W. G.; Tatchell, A., R *Vogel's Text Book of Practical Organic Chemistry*; 5 ed.; Longmann Scientific & Technical: New York, United States, 1989.

(2) Biot, C.; Glorian, G.; Maciejewski, L. A.; Brocard, J. S.; Domarle, O.; Blampain, G.; Millet, P.; Georges, A. J.; Abessolo, H.; Dive, D. *J. Med. Chem.* **1997**, *40*, 3715.

(3) Burke, W. *J. Am. Chem. Soc.* **1949**, *71*, 609.

(4) (a) Sturm, T.; Weissensteiner, W.; Spindler, F.; Mereiter, K.; López-Agenjo, A. M.; Manzano, B. R.; Jalón, F. A. *Organometallics* **2002**, *21*, 1766; (b) Weißenbacher, M.; Sturm, T.; Kalchhauser, H.; Kratky, C.; Weissensteiner, W. *Monatsh. Chem.* **2002**, *133*, 991.

(5) Abdel-Magid, A. F.; Carson, K. G.; Harris, B. D.; Maryanoff, C. A.; Shah, R. D. *J. Org. Chem.* **1996**, *61*, 3849.

(6) Saikia, B. *Synlett* **2011**, *17*, 2597.

(7) Waisser, K.; Hladuvková, J.; Gregor, J.; Rada, T.; Kubicová, L.; Klimešová, V.; Kaustová, J. *Arch. Pharm.* **1998**, *331*, 3.

(8) Mu, F.; Lee, D. J.; Pryor, D. E.; Hamel, E.; Cushman, M. *J. Med. Chem.* **2002**, *45*, 4774.

(9) D'Addona, D.; Bochet, C. G. *Tetrahedron Lett.* **2001**, *42*, 5227.

(10) Hernandez, A. G.; Grooms, G. M.; El-Alfy, A. T.; Stec, J. *Synthesis* **2017**, *49*, 2163.

(11) Gemma, S.; Camodeca, C.; Brindisi, M.; Brogi, S.; Kukreja, G.; Kunjir, S.; Gabellieri, E.; Lucantoni, L.; Habluetzel, A.; Taramelli, D. *J. Med. Chem.* **2012**, *55*, 10387.

(12) Jeon, M.-K.; Kim, K. *Tetrahedron* **1999**, *55*, 9651.

(13) Nolan, K. A.; Doncaster, J. R.; Dunstan, M. S.; Scott, K. A.; Frenkel, A. D.; Siegel, D.; Ross, D.; Barnes, J.; Levy, C.; Leys, D. *J. Med. Chem.* **2009**, *52*, 7142.

(14) Rad-Moghadam, K.; Mohseni, M. *Monatsh. Chem.* **2004**, *135*, 817.

(15) Al-Kawkabani, A.; Boutemeur-Kheddis, B.; Makhloufi-Chebli, M.; Hamdi, M.; Talhi, O.; Silva, A. M. *Tetrahedron Lett.* **2013**, *54*, 5111.

(16) Feagin, T. A.; Shah, N. I.; Heemstra, J. M. *J. Nucleic Acids* **2012**, *2012*.

(17) Cullen, W.; Wickenheiser, E. *Can. J. Chem.* **1990**, *68*, 705.

(18) Nicolaou, K.; Bunnage, M. E.; Koide, K. *J. Am. Chem. Soc.* **1994**, *116*, 8402.

(19) Chen, P.-J.; Wang, H.-Y.; Peng, A.-Y. *RSC Advances* **2015**, *5*, 94328.

(20) Mbaba, M.; Mabhula, A. N.; Boel, N.; Edkins, A. L.; Isaacs, M.; Hoppe, H. C.; Khanye, S. D. *J. Inorg. Biochem.* **2017**, *172*, 88.

(21) Trager, W.; Jensen, J. B. *Science* **1976**, *193*, 673.

(22) Oderinlo, O. O.; Tukulula, M.; Isaacs, M.; Hoppe, H. C.; Taylor, D.; Smith, V. J.; Khanye, S. D. *Appl. Organomet. Chem.* **2018**, *32*, e4385.

(23) Hirumi, H.; Hirumi, K. *J. Parasitol.* **1989**, 985.

(24) Beteck, R. M.; Legoabe, L. J.; Isaacs, M.; Khanye, S. D.; Laming, D.; Hoppe, H. C. *Medicina* **2019**, *55*, 206.

(25) Mbaba, M.; de la Mare, J.-A.; Sterrenberg, J. N.; Kajewole, D.; Maharaj, S.; Edkins, A. L.; Isaacs, M.; Hoppe, H. C.; Khanye, S. D. *J. Biol. Inorg. Chem.* **2019**, *24*, 139.

(26) Shahabadi, N.; Hadidi, S. *Spectrochim. Acta A* **2012**, *96*, 278.

(27) Wu, H.; de Gannes, M. K.; Luchetti, G.; Pilsner, J. R. *Biotechniques* **2015**, *58*, 293.

(28) Shahabadi, N.; Hadidi, S.; Taherpour, A. A. *Appl. Biochem. Biotechnol.* **2014**, *172*, 2436.

(29) Gyori, B. M.; Venkatachalam, G.; Thiagarajan, P.; Hsu, D.; Clement, M.-V. *Redox Biol.* **2014**, *2*, 457.

(30) Lu, W.-J.; Wicht, K. J.; Wang, L.; Imai, K.; Mei, Z.-W.; Kaiser, M.; El Sayed, I. E. T.; Egan, T. J.; Inokuchi, T. *Eur. J. Med. Chem.* **2013**, *64*, 498.

(31) Ncokazi, K. K.; Egan, T. J. *Anal. Biochem.* **2005**, *338*, 306.

(32) (a) Maier, J. A.; Martinez, C.; Kasavajhala, K.; Wickstrom, L.; Hauser, K. E.; Simmerling, C. *J. Chem. Theory Comput.* **2015**, *11*, 3696; (b) Wang, J.; Wang, W.; Kollman, P. A.; Case, D. A. *J. Mol. Graphics Modell.* **2006**, *25*, 247.